Temperature Programming of the Second Dimension in Comprehensive Two-Dimensional Gas Chromatography (GC×GC)

by

Hei-Yin John Chow

A thesis

presented to the University of Waterloo

in fulfillment of the

thesis requirement for the degree of

Doctor of Philosophy

in

Chemistry

Waterloo, Ontario, Canada, 2022

Examining Committee Membership

The following served on the Examining Committee for this thesis. The decision of the Examining Committee is by majority vote.

External Examiner	Robert Synovec Professor Department of Chemistry University of Washington
Supervisor	Tadeusz Górecki Professor Department of Chemistry University of Waterloo
Internal Member	Wojciech Gabryelski Professor Department of Chemistry University of Guelph
Internal Member	Scott Hopkins Professor Department of Chemistry University of Waterloo
Internal – External Member	Ken Stark Professor Department of Kinesiology and Health Sciences University of Waterloo

Author's Declaration

This thesis consists of material all of which I authored or co-authored: see Statement of Contributions included in the thesis. This is a true copy of the thesis, including any required final revisions, as accepted by my examiners.

I understand that my thesis may be made electronically available to the public.

Statement of Contributions

Parts of Chapter 1 are based on book chapters written by the author of this thesis. Only sections written by the author were used. All other chapters were solely the work of the author. Chapters 1 to 4 of this thesis are based on the following publications:

Chapter 1:

Boswell, H., Chow, H. Y. J., & Gorecki, T. (2020). Chapter 4 - Modulators. In N. H. Snow (Ed.), *Separation Science and Technology* (pp. 89-140) Academic Press. doi:10.1016/B978-0-12-813745-1.00004-0

Chow, H. Y. J., Boswell, H., & Górecki, T. (2023). Comprehensive Two-Dimensional Gas Chromatography. In E. Barry, & T. Brettell (Eds.), *Modern Practice of Gas Chromatography* (5th ed.) John Wiley and Sons. In print.

Chapter 2:

Chow, H. J., & Górecki, T. (2017). Temperature Programming of the Second Dimension in Comprehensive Two-Dimensional Gas Chromatography. *Analytical Chemistry, 89*(16), 8207-8211. doi:10.1021/acs.analchem.7b02134

Chapter 3:

Chow, H. Y. J., & Górecki, T. (2022). Second dimension temperature programming system for comprehensive two-dimensional gas chromatography with true temperature control. *Journal of Chromatography Open, 2*, 100062. doi:10.1016/j.jcoa.2022.100062

Chapter 4:

Chow, H. Y. J., & Górecki, T. (2023). Second dimension temperature programming system for comprehensive two-dimensional gas chromatography. part 1: precise temperature control based on column electrical resistance. *Analytical Chemistry*. In revision.

Chow, H. Y. J., & Górecki, T. (2023). Second dimension temperature programming system for comprehensive two-dimensional gas chromatography. part 2: technical improvements and compatibility with flow modulation and time-of-flight mass spectrometry. *Analytical Chemistry*. In revision.

Abstract

Comprehensive two-dimensional gas chromatography (GC×GC) is a mature separation technique that is now over three decades old. It separates all sample components using two GC columns with different selectivities, connected in series through a special interface called a modulator to provide two dimensions of separation. Early research and development of this technique focused on the modulator, the most critical component in a GC×GC system. The modulator facilitates the collection and transfer of effluent from the first dimension (^{1}D) to the second dimension (^{2}D) column. As the modulator development matured with various designs being commercialized, research focus shifted towards chemometrics and applications. However, a fundamental issue that has not been resolved thus far in GC×GC is the general elution problem in ^{2}D due to the nearly isothermal conditions in this dimension during a single separation. This thesis details the development, testing, and application of a ^{2}D temperature programming system for GC×GC to overcome this problem.

Every stage of development for the ^{2}D temperature programming system is described, from the proof-of-concept to the final design. The proof-of-concept system in Chapter 2 focused on the heating and cooling aspects of ^{2}D temperature programming. It featured a ballistic heating system that synchronized the heating and cooling of the ^{2}D column to the modulation period. Although the final temperature offset could be pre-calibrated, the system did not feature any real temperature control. Despite its simplicity, ballistic heating eliminated wraparound peaks while maintaining the separation of weakly retained compounds in the ^{2}D.

The first prototype of a true ^{2}D temperature programming system, detailed in Chapter 3, featured an Arduino microcontroller for PID temperature control. The temperature difference between the ^{2}D column and the GC oven was measured directly using two thermocouples connected differentially. Although ^{2}D temperature programming with the prototype improved the peak capacity by 48 %, the fragility of the thermocouple attachment was an issue for commercial designs.

The final version of the ^{2}D temperature programming system (^{2}DTPS), described in Chapter 4, tackled the robustness and user-friendliness of the system, building upon the core functions from the prior designs. The temperature measurement system was completely redesigned to determine the ^{2}D column temperature based on the ^{2}D column electrical resistance. The column connections and column cage were also redesigned to incorporate longer ^{2}D columns and provide a more secure connection to the column for heating and resistance measurement. A real time clock and remote port were also added to allow the ^{2}DTPS to be a completely standalone device for any GC×GC system. A Windows Forms application was written to control and monitor the ^{2}DTPS. System compatibility was tested with both thermal and flow modulators, as well as a flame ionization detector (FID) and time-of-flight mass spectrometer (TOFMS).

Finally, the ^{2}DTPS was applied to the characterization of renewable hydrocarbon samples from a local Ontario company in Chapter 5. Samples from various points in the production process were characterized to help with product development. The GC×GC separation with the ^{2}DTPS was optimized with both a normal and a reverse column set, as well as two detectors, an FID and a TOFMS. The ^{2}DTPS improved the signal-to-noise ratio and peak capacity for the characterization of the samples.

Acknowledgements

Acknowledgements are the most difficult to write, especially when there are many people that have helped me over the years. It is difficult to put into words my gratitude for their support and expertise they have all contributed. Nevertheless, I will try my best to thank each and every person.

First and foremost, I would like to thank Dr. Tadeusz Górecki for being my supervisor, from CHEM 494 to being a part of his research group. I would not have considered graduate studies or doing a PhD if it was not for your encouragement. Thank you for guiding me throughout this research and giving me the freedom to learn and build the various instruments in this thesis. It allowed me to rediscover the fun and frustration of coding. I am truly grateful your door was always open to chat, to discuss results, and to talk about the problems I was facing with coding or the electronics. I probably visited too much throughout the day. Thank you to the other members of the group, Haleigh Boswell, Faten Salim, and Alshymaa Aly for their help. Haleigh, in particular, taught me how to maintain the GC and allowed me to be self-sufficient in the lab.

I would like to thank the members of my committee, Dr. Wojciech Gabryelski, Dr. Scott Hopkins, and Dr. Terry McMahon for their guidance and the time and effort spent reading my thesis. Thank you to Dr. Robert Synovec for being my external member and Dr. Ken Stark for being my internal-external member.

I would like to thank everyone from the Science Technical Services department for their help throughout this research. Their support in electronics, machining, and vacuum servicing was invaluable during my time in Waterloo. During the development of the ^{2}DTPS, I visited the electronics shop often to consult on the design and borrowed a spare desk and their equipment to solder everything together. Thank you Zhenwen Wang and Krunomir Dvorski for being so patient and allowing me to work there. The ^{2}DTPS could not have been built without them. Thank you to Hiruy Haile for assisting in the machining work and ideas for some of the physical aspects of the instrumentation built. Thank you to Jacek for building the electronics early on in my research.

Thank you to Stacey Lavery for allowing me to have such a wonderful experience as a teaching assistant. I truly learned a lot during my time in your lab, rotating to a different instrumentation experiment every term. As you found out later on, I met my wife on the very first day as your teaching assistant. Do not worry, we did not date until after the course. She still complains I gave her the lowest mark out of all the teaching assistants.

Lastly, I would like to thank my family and friends for their support over the years. In particular, thank you to my wife, Vera Quan, for being so patient with me. Even though writing this thesis took a long time, you still encouraged me that it was all worth it. You have been there through many of my presentations, listening to me practice repeatedly until you could practically do it yourself. I know it was not easy supporting us and our many pets, and I will always be grateful for that.

Table of Contents

List of Figures

List of Tables

List of Abbreviations

1D	One Dimensional
^{1}D	First Dimension
$^{1}R_s$	First Dimension Resolution (Resolution in the ^{1}D of GC×GC)
$^{1}t_r$	First Dimension Retention Time
$^{1}W_b$	First Dimension Peak Width at the Base
$^{1}\sigma$	Standard Deviation of a ^{1}D Gaussian Peak
2D	Two Dimensional
^{2}D	Second Dimension
^{2}DTPS	Second Dimension Temperature Programming System
^{2}FWHM	Second Dimension Full Width at Half Maximum
$^{2}R_s$	Second Dimension Resolution (Resolution in the ^{2}D of GC×GC)
$^{2}W_b$	Second Dimension Peak Width at the Base
ANOVA	Analysis of Variation
CFT	Capillary Flow Technology
CPU	Central Processing Unit
DPGM	Dynamic Pressure Gradient Modulation
DS	Deans Switching
E	Seebeck Voltage
ECD	Electron Capture Detector
EI	Electron Ionization
EIC	Extracted Ion Chromatogram
FA	Fatty Acid
FAEE	Fatty Acid Ethyl Ester
FAME	Fatty Acid Methyl Ester
FFA	Free Fatty Acid
FID	Flame Ionization Detector
FPD	Flame Photometric Detector
F-ratio	Fisher Ratio
GC	Gas Chromatography
GC×GC	Comprehensive Two-Dimensional Gas Chromatography

GC-GC	Heat-Cut Multidimensional Gas Chromatography
GPIO	General Purpose Input/Output
GPU	Graphics Processing Unit
HCA	Hierarchical Cluster Analysis
HPLC	High Performance Liquid Chromatography
HR-TOFMS	High-Resolution Time-of-Flight Mass Spectrometry
HS-SPME	Headspace Solid-Phase Microextraction
IDE	Integrated Development Environment
IO	Input/Output
IR	Infrared
IRMS	Isotope-Ratio Mass Spectrometry
k	Retention factor
LC×LC	Comprehensive Two-Dimensional Liquid Chromatography
LMCS	Longitudinally Modulated Cryogenic System
LSB	Least Significant Bit
m	Components
MDGC	Multidimensional Gas Chromatography
MMM	Multi-Mode Modulator
MMS	Multi-Mode Source
M_R	Modulation Ratio
MS	Mass Spectrometry
N	Number of Theoretical Plates
n_c	Peak Capacity
NCD	Nitrogen Chemiluminescence Detector
NCI	Negative Chemical Ionization
NPD	Nitrogen Phosphorus Detector
NPM	Negative Pulsed Flow Method
OS	Operating System
PC	Principal Component
PCA	Principal Component Analysis
PCI	Positive Chemical Ionization
PDMS	Polydimethylsiloxane

PEG	Polyethylene Glycol
P_M	Modulation Period
PPM	Positive Pulsed Flow Method
Pw	Pulse Width
PWM	Pulse Width Modulation
QC	Quality Control
QMS	Quadrupole Mass Spectrometer
QqQMS	Triple-Quadrupole Mass Spectrometer
RAM	Random-Access Memory
RFF	Reverse Fill/Flush
$R_{s,2D}$	Two-dimensional resolution (Resolution between two peaks on a GC×GC chromatogram
RTD	Resistance temperature detector
S/N	Signal-to-Noise
SCD	Sulfur Chemiluminescence Detector
SPS	Samples per Second
SRAM	Static Random-Access Memory
SSM	Solid State Modulator
T	Temperature
TCD	Thermal Conductivity Detector
TDM	Thermal Desorption Modulator
TiM	Thermal Independent Modulator
TOFMS	Time-of-Flight Mass Spectrometry
UART	Universal Asynchronous Receiver-Transmitter
VUV	Vacuum Ultraviolet
W_b	Peak Width at Base
W_b	Peak Width at the Base
α	Seebeck Coefficient
µGC×µGC	Comprehensive Two-Dimensional Microscale Gas Chromatography
µTM	Microfabricated Thermal Modulator

1 Introduction[i]

Gas chromatography (GC) was introduced by James and Martin in 1952. In their seminal paper, they described the separation of volatile fatty acids by gas-liquid partition chromatography [1]. Due to the shift from coal to petroleum as the predominant fuel source, GC was rapidly adopted by the petroleum industry for the separation of the complex petroleum-derived samples [2]. Early work in GC utilized packed columns, and it was not until Golay's work in 1958 that the superior separation capabilities of capillary columns were demonstrated [3]. The following decades focused on the development of the capillary column, with key innovations including the introduction of fused-silica columns and cross-linked stationary phases [2]. As GC continued to develop, the concept of peak capacity (n_c) was defined, in 1967, as the maximum number of resolvable peaks in a separation if one assumes the peaks elute side by side at the stated resolution [4]. However, real samples will never elute with evenly distributed components (m), so peak capacity is the ideal maximum number of resolvable peaks. For randomly distributed peaks, described using Poisson statistics, Giddings stated that "to resolve 98 % of the components, n_c must exceed m by a factor of 100" [5, 6]. A recent innovation in GC which significantly increases peak capacity is comprehensive two-dimensional gas chromatography (GC×GC), introduced in 1991 by Liu and Phillips [7].

1.1 Multidimensional Gas Chromatography

Coelutions of analytes with the matrix or with other analytes in a complex sample are difficult to resolve on a single stationary phase in GC. No matter how many theoretical plates are added by increasing

[i] This chapter is based on the following book chapters that have been written by the author:
H. Boswell, H-Y. Chow, T. Górecki, "Modulators", in: N. Snow (Ed.), "Basic Multidimensional Gas Chromatography", part of the "Separation Sciences and Technology" series edited by S. Ahuja, Elsevier, 2020, p. 89-140.
H.-Y. Chow, H. Boswell, T. Górecki, "Comprehensive Two-Dimensional Gas Chromatography", in: E. Barry and T. Brettell (Ed.), "Modern Practice of Gas Chromatography", 5th Ed., John Wiley and Sons, in print.
Only sections written by the author were used.

the length of the column or reducing its inner diameter, compounds with identical retention indices on a given stationary phase will not be resolved. Changing the stationary phase may separate analytes that were unresolved, but this leads to the same problem where previously resolved analytes could end up co-eluting. This limitation of selectivity in a single stationary phase led to the idea of multidimensional gas chromatography (MDGC). MDGC involves the sequential separation of sample components on different stationary phases to achieve increased selectivity. Compounds that could not be separated on a given stationary phase are introduced to a second column with different selectivity for additional separation. Two forms of MDGC includes heart-cut MDGC (GC-GC) and GC×GC [8].

1.1.1 Heart-Cut Multidimensional Gas Chromatography

GC-GC is a mature technique, with its first appearance in 1958 [8]. The general layout of a GC-GC system is presented in Figure 1-1A. For most of the run, the sample is analyzed on column A with the interface device directing the effluent to detector A. For specific portions of effluent that contain unresolved compounds of interest, the interface device switches the flow to column B. After transferring the unresolved portion of effluent, the interface switches back, completing the heart-cut procedure. The transferred portions of unresolved effluent undergo separation on a stationary phase with a different selectivity (column B) for separation and detection (detector B). In the representation shown in Figure 1-1B, previously unresolved regions of interest in the first dimension (^{1}D) chromatogram are “heart-cut” and resolved in the second dimension (^{2}D) chromatogram. The secondary benefit of heart-cut 2DGC is the increased peak capacity achieved from the addition of the second column. The total peak capacity of GC-GC is the peak capacity in the first column plus the peak capacity of the second column times the number of heart-cuts made [Total peak capacity = ^{1}D peak capacity + (^{2}D peak capacity × number of heart-cuts)]. A more detailed discussion of GC-GC can be found in a review paper by Tranchida et al. [9].

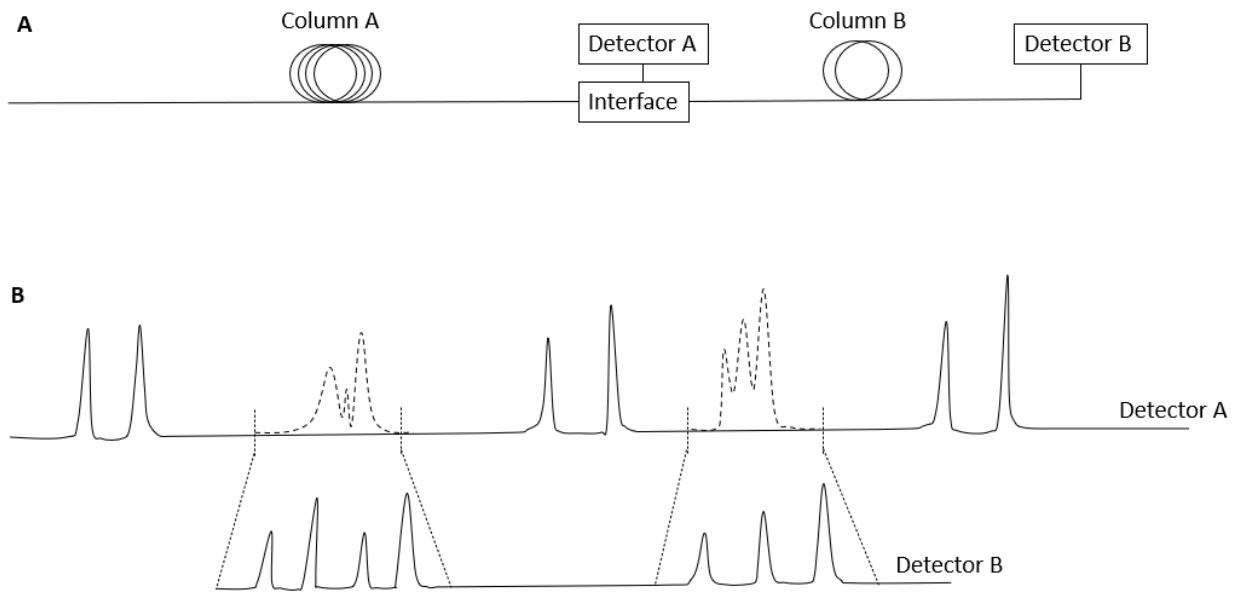

Figure 1-1: A general schematic of a GC-GC system, with an interface to switch the Column A effluent between Detector A and Column B (A) and an example of the detector signals from GC-GC (B). The signal between the dashed lines in (B) represents the portion of the effluent diverted to the second column. Based on Ref. [10].

1.1.2 Comprehensive Two-Dimensional Gas Chromatography

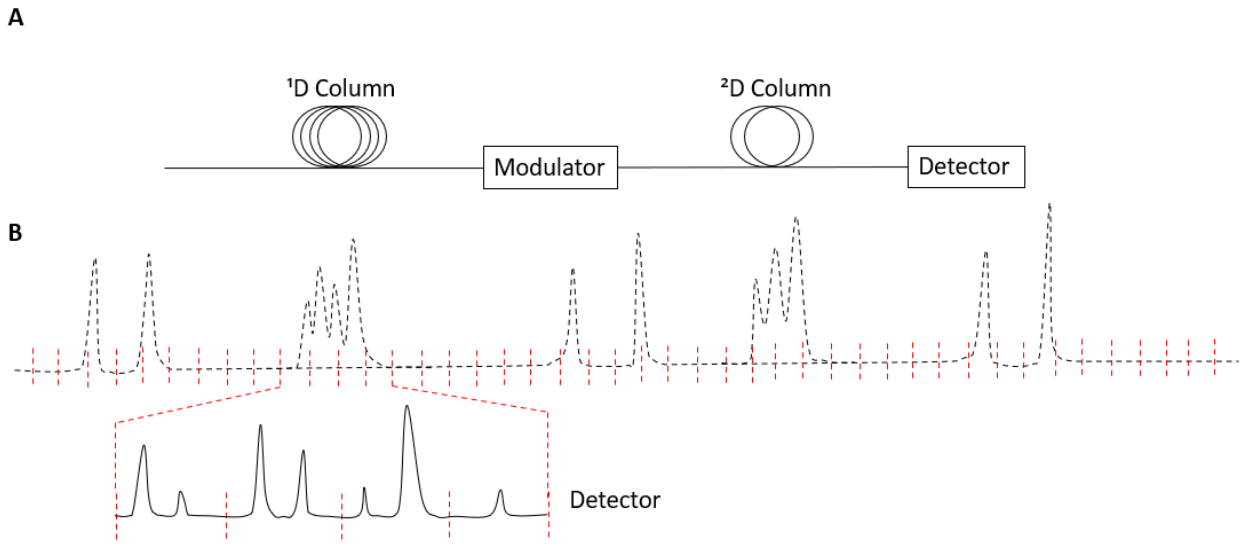

Figure 1-2: Basic schematic of a GC×GC system (A) and an example of the detector signal (solid black chromatogram) from the GC×GC separation (B). The original chromatogram shown in black dashed lines, represents the effluent from the ¹D column. The red dashed lines that evenly divides the effluent, represents the consecutive fractions transferred to the ²D column for further separation and subsequent detection. The resulting signal from just four out of the numerous fractions is shown. Based on Ref. [10].

GC×GC is a comprehensive separation technique that subjects the whole sample through two dimensions of separation without loss of separation in either dimension. The general schematic of a

GC×GC setup is shown in Figure 1-2A. The interface, known as the modulator in GC×GC, transfers effluent from the ^{1}D column to the ^{2}D column as discrete pulses at regular intervals known as the modulation period. This is illustrated in (Figure 1-2B), where the fractions of effluent transferred from the ^{1}D column are represented by the regions between the red dashed lines. Each fraction is further separated by the ^{2}D column and then measured by the detector, producing a single chromatogram made of consecutive ^{2}D separations. Hence, the advantage of increased selectivity in GC-GC is applied to all components in the sample rather than just select fractions. Transforming the chromatogram consisting of consecutive ^{2}D separations into the contour plot that is commonly shown in GC×GC work requires the use of specialized software. Multiple software packages exist, designed to handle and manipulate GC×GC data. They include GCImage (GC Image LLC, Lincoln, NE, USA), ChromaTOF (LECO Corporation, St. Joseph, MI, USA), ChromSpace (SepSolve Analytical, Peterborough, UK), ChromSquare 2 (Chromaleont srl, Messina, Italy), HyperChrom (Thermo Fisher Scientific, Waltham, MA, USA), GC×GC-Analyzer (MsMetrix, Utrecht, Netherlands), AnalyzerPro XD (SpectralWorks Ltd., Cheshire, UK), Canvas (JnX Technologies, Shanghai, China), and GasPedal (Decodon, Greifswald, Germany) [11, 12]. The software divides the chromatogram into individual “slices” (Figure 1-3A) and realigns them along the ^{1}D and ^{2}D planes (Figure 1-3B). A contour plot is then generated from the top-down view of the aligned chromatogram, where the peak height is represented by a color scale (Figure 1-3C). The benefit of GC×GC, in addition to the increase in selectivity and the multiplicative increase in peak capacity, is the unique distribution pattern of analytes. Compounds with similar physical and chemical properties will elute within a similar region, providing additional insight into the compound classes present within complex samples.

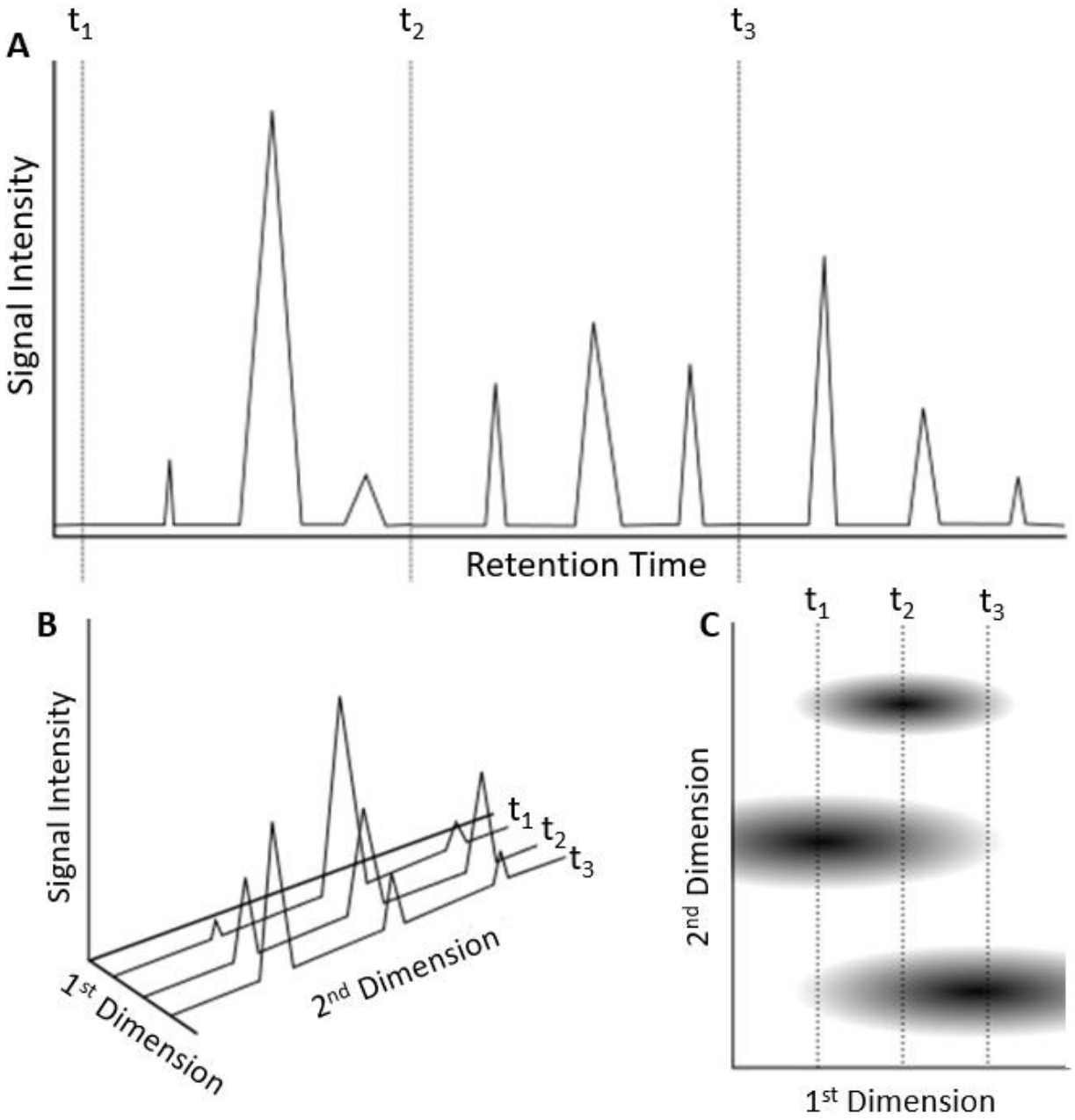

Figure 1-3: Transformation of a linear detector signal from a GC×GC separation to a 2D chromatogram. The linear data, represented by the standard GC chromatogram, is divided into modulation period wide sections (A), reassembled side-by-side (B), and represented by the top-down view in the form of a 2D chromatogram (C). Based on Ref. [10].

Although the schematic in Figure 1-2A of a GC×GC system appears simpler, the process of transferring effluent to the ^{2}D column while maintaining separation in both dimensions is difficult [10]. This demanding process is accomplished by the modulator, which is often regarded as the "heart" of a GC×GC system [13, 14]. The collection or sampling of the ^{1}D column effluent and its reinjection into the ^{2}D column is done on-

line with minimal disturbance to the separation process in the ^{1}D. The entire process from sampling to reinjection is completed in seconds, resulting in many individual "slices" across the chromatogram, as shown in Figure 1-2B. This places a huge demand on the modulator, which must maintain adequate performance while performing hundreds of reinjections per run and possibly over a million reinjections a year (6 s modulation period, 8 hours/day, 5 days/week, 52 weeks/year). Being critical to the success of GC×GC, the modulator has been the focus of instrumental development for over three decades and will be discussed in more detail in section 1.2 [13, 14]. The other areas of GC×GC research gaining more attention in recent years as the technology has matured are chemometrics and the application of GC×GC in a variety of fields.

1.1.2.1 Data Analysis and Chemometrics

The term chemometrics was first coined in the 1970s [15, 16], where the fundamental idea was to draw useful information from data obtained in chemical analyses. Data processing and chemometrics is becoming an area of increased attention due to the significant volume of data produced, especially when dealing with GC×GC coupled with [high-resolution (HR)] time-of-flight mass spectrometry (TOFMS) data and large data sets [17]. In many cases, only a few compounds of importance may be discovered through chemometrics [18]. This may seem odd, when GC×GC chromatograms are typically producing hundreds if not thousands of peaks per sample, but it is precisely due to chemometrics that we are able to filter out compounds unrelated to the research question or response. Without GC×GC, these compounds of significance may not be discoverable due to insufficient separation with traditional 1D techniques.

Before the data can be processed by the different chemometric tools available, the raw signal needs to be cleaned [17]. These functions are typically provided with the software packages used in GC×GC, such as baseline correction, smoothing, deconvolution (for MS data), and identification. In addition, retention times can shift and signal intensity can change from sample to sample over time, so pre-processing including peak alignment and signal correction/normalization is necessary [17]. Peak alignment can be

accomplished with the integrated peak table or on the entire (global) chromatogram [19]. LECO Corp.'s ChromaTOF Statistical Compare, for example, performs peak table alignment, relying on the retention times (^{1}D and ^{2}D) and the mass spectrum of each integrated peak [20]. Changes in signal intensity between samples unrelated to changes in concentration needs to be corrected to reduce unrelated variation. These variations in signal intensity could be due the sample preparation process. This can be done with internal standards for targeted analysis, or pooled quality control (QC) samples for untargeted analysis [21]. Sum-normalization can also be performed when an internal standard is not available [22]. This is where the signal is divided by the total peak area of a baseline corrected chromatogram. This is useful for correcting injection volume variations where the total peak area would reflect the injection volumes. Artifacts where a single peak/compound is integrated as multiple peaks also need to be removed, particularly because some commercial software work with the peak tables for their chemometric functions. However, manual removal and combining of peaks are subject to user bias, where one analyst may exclude a peak while another may include it or combine with another peak. In addition, this can be extremely laborious for large datasets.

After pre-processing, chemometric methods (not unique to GC×GC) can be applied for data analysis. This includes Fisher ratio (F-ratio), principal component analysis (PCA), and hierarchical cluster analysis (HCA). These are just some of the more common chemometric methods applied to GC×GC data analysis as this area of research develops. F-ratio is a popular feature selection tool calculated as the between-class variance divided by the within-class variance [23]. Since F-ratio analysis is sensitive to retention time shifts, peak alignment is important prior to analysis. F-ratio can be applied at the pixel-level for every data point in the GC×GC chromatogram, to peak tables (aligned), or to rectangular regions (bins or tiles) of the chromatogram [24]. The resulting F-ratio is compared to an F critical value to identify significant compounds. Since classification of the samples is necessary, this is a supervised method where prior knowledge of the samples is needed [24].

PCA is a common tool applied to GC×GC datasets, for data reduction, class separation, and feature selection [24]. PCA takes a 2D data array (rows: samples, columns: variables) and constructs principal components (PCs) which accounts for the greatest variation in the data [22]. When plotted on a scores plot, related samples (i.e. of the same class) will cluster together in the plot. The loadings plot displays the variables which have the greatest influence on each component [24]. Since PCA is a visualization of the variance, retention time alignment, mean-centering, and scaling are critical pre-processing steps necessary before applying PCA to the data set [24].

HCA is another pattern recognition method like PCA but simpler. It clusters samples based on their similarities, creating a dendrogram and heatmap where similar samples would be grouped closer together and dissimilar chromatograms being farther apart. The method of measuring similarity can vary and will result in differences in clustering, however, the Euclidian method is commonly cited [17, 22, 23]. More detailed reviews dedicated to chemometrics and data handling in GC×GC have been published [17, 19].

1.1.2.2 Applications

Application of GC×GC started in the petrochemical research area. Over time, they have spread to other fields like environmental analysis, food, forensics, and metabolomics. Detailed reviews of GC×GC application in each area have been published [25, 26, 27, 28, 29]. Recent publications involving the application of GC×GC from a variety of areas will be briefly described.

The analysis of organic pollutants in environmental matrices is a challenging task, involving complex samples with a large number of compounds with significant variations in concentrations [25]. Due to the increased separation capabilities and peak capacity of GC×GC, sample preparation can be simplified while the grouping of related chemical species in combination with MS aids in their identification. A particular strength of GC×GC is the discovery of emerging pollutants in untargeted analysis, which may have similar toxicities and environmental fate as pollutants being monitored today. Fernando et al. explored the use

of GC×GC coupled to a high-resolution time-of-flight mass spectrometer (HR-TOFMS) for the screening and semi-quantitation of halogenated contaminants in the Great Lakes' top predator fish [30]. Mass spectral filtering was applied to identify chlorinated and brominated compounds. Authentic standards were used when available, while other compounds were tentatively identified based on their MS spectral library match and accurate mass (<5 ppm). The most abundant class of pollutants found were halogenated methoxyphenols, accounting for over 60 % of the total halogenated pollutant concentration. This class of pollutants was not monitored by the United States Environmental Protection Agency's Great Lakes Fish Monitoring and Surveillance Program and demonstrates the effectiveness of the technique as a screening tool for complex samples.

The analytical information gained from food analysis by GC×GC-TOFMS can be used for purposes like qualitative profiling, fingerprinting for sample classification, or targeted analysis for the quantification of contaminants [26]. Using headspace solid-phase microextraction (HS-SPME) in combination with GC×GC-TOFMS, Sudol et al. studied the geographical differences in wine aroma for five Grillo wines produced with the same method from different regions of Sicily [31]. Tile-based F-ratio analysis was performed using ChromaTOF, generating 220 hits following manual artifact and redundancy removal. This was followed by one-way analysis of variation (ANOVA) at a p-value of 0.01 for further data reduction to distinguish true positives (187 hits) from the false positive hits (33 hits). PCA was then applied to the true positive hits, where 85.76 % of the variance was captured along both principal component (PC) axes, with clustering for each wine and without overlap of the clusters.

Although the application of GC×GC in forensics science is still in its early stages due to the lack of standardized methods, its use has been explored in a variety of areas [27]. Kates et al. explored the use of GC×GC in arson investigations for the identification of ignitable liquid residue [32]. 456 samples from wildfires suspected of arson were analyzed by the standard gas chromatography-mass spectrometry (GC-MS) method, while select samples (164) were further analyzed by GC×GC-TOFMS. Samples were classified

as either positive, tentative, or negative for ignitable liquid residue based on the ASTM 1618 method for GC-MS analysis, while extracted ion chromatograms were also checked for the GC×GC analysis. Background samples were used to establish a threshold level for ignitable liquid residue-related compounds for GC×GC analysis, which was not possible with GC-MS due to coelutions. The enhanced separation of ignitable liquid residue compounds from natural interferences and lower detection limits accomplished by GC×GC-TOFMS allowed for reduced uncertainty in sample classification. Of the 164 samples analyzed by both GC-MS and GC×GC-TOFMS, 46 %, 27 %, and 27 % were classified as positive, tentative, and negative by the GC-MS method, respectively. For the GC×GC-TOFMS method, the results were 75 %, 6 %, and 19 %, respectively. The reduced number of tentative results highlight the effectiveness of GC×GC-TOFMS in determining the presence of ignitable liquid residues in complex wildfire debris samples.

Metabolomics is the comprehensive analysis of the metabolites in a biological system [28]. This involves the detection, identification, and quantitation of individual metabolites with large disparities in concentrations. It requires software to handle and process the large amount of raw data produced, and chemometrics to extract pertinent information from the data. The capability of GC×GC to separate complex samples while coupled to an MS provides a powerful tool for untargeted analysis in metabolite profiling or the discovery of biomarkers. Barberis et al. utilized GC×GC-TOFMS to discover potential biomarkers in exhaled breath condensates for the development of a non-invasive approach to the diagnosis and monitoring of COVID-19 [33]. Eight potential biomarkers were found to differentiate between healthy volunteers and COVID-19 patients. However, they were not suitable for differentiating between COVID-19 patients and patients with cardiopulmonary edema. Mack et al. studied volatile organic compounds in human urine to identify biomarkers of coffee consumption [34]. Acidified urine samples were extracted by HS-SPME followed by GC×GC coupled with a quadrupole mass spectrometer (QMS). Six different normalization methods were compared to correct for unequal concentrations of urine

samples. ANOVA was performed to screen for volatiles differentiating the coffee consumers from non-consumers. This was followed by Spearman's correlation coefficient, which identified 6 potential markers for coffee consumption.

Overall, these applications have demonstrated the effectiveness of GC×GC as a separation technique, as its peak capacity and enhanced selectivity were leveraged to tackle the challenges of complex matrices. The combination of the technique with MS or HR-TOFMS provided a powerful tool for untargeted analysis. The grouping of compounds with similar physical and chemical properties on the 2D space, in addition to the improved separation for a cleaner mass spectra, allowed for more confident tentative identification of unknowns.

1.2 GC×GC Modulators

The modulator is the single unique component that can transform a standard GC into a GC×GC system. The invention of the first modulator by John Phillips and co-workers made GC×GC possible. Over the next three decades following the report on the first modulator [7] many unique designs have been presented, some of which are now obsolete. These modulators can be broadly classified into two categories: thermal modulators and flow modulators.

1.2.1 Thermal Modulator

Thermal modulation relies on cooling and/or heating, relative to the GC oven temperature, for the effective adsorption and desorption of analytes in the modulation device. Essentially, the trapping and remobilization of the analytes are accomplished by manipulating their retention factors. Based on the various designs published, the trapping function has been accomplished using a highly adsorptive interface (thick stationary phase or sorbent), intense cooling, or a combination of the two. The major advantage of thermal modulation over flow modulation is the focusing effect from the reconcentration of the analyte bands during trapping. This leads to signal-to-noise (S/N) improvements of up to an order

of magnitude [35]. Several of the early thermal modulators started out as either injection devices or devices meant to improve S/N prior to detection [36, 37, 38, 39]. For thermal modulation, rapid remobilization of the trapped analytes was necessary to produce narrow reinjection bands into the ^{2}D column. Historically, this was accomplished through heating or rapid equilibration with the ambient GC oven temperature, possible thanks to the low thermal mass of the capillary columns.

1.2.1.1 Heater Designs

Heater designs rely on the passive sorption of analytes through the use of thick liquid stationary phases or adsorbent phases at or below ambient temperature, while using active heating for the rapid desorption of the trapped analytes. One of the inherent limitations of heater designs with trapping carried out at the oven temperature is the upper temperature limit of the trapping phase being used for modulation. Since additional heating is provided for desorption, this limits the maximum GC oven temperature to the maximum operational temperature of the trapping phase minus the differential temperature applied [40]. This limitation becomes less severe if trapping is carried out below the oven temperature.

1.2.1.1.1 Thermal Desorption Modulator

The first thermal desorption modulator (TDM) developed by Phillips and co-workers was originally developed as a sample introduction device in multiplex and high-speed gas chromatography [36, 37, 38, 41]. It was not until 1991 that this device was adapted into a dual-stage thermal desorption modulator to perform the first GC×GC separation [42]. The dual-stage thermal desorption modulator was constructed from the head of the ^{2}D column that was looped outside the oven and maintained at room temperature. A thin film of electrically conductive gold paint coated this 15 cm segment of ^{2}D column that was divided into two equal-length stages by three electrical leads. Modulation was accomplished by alternating the heating between the two stages. Analytes eluting from the ^{1}D column were trapped and focused by the ^{2}D column stationary phase coating (Figure 1-4A). Direct resistive heating of the first stage of the

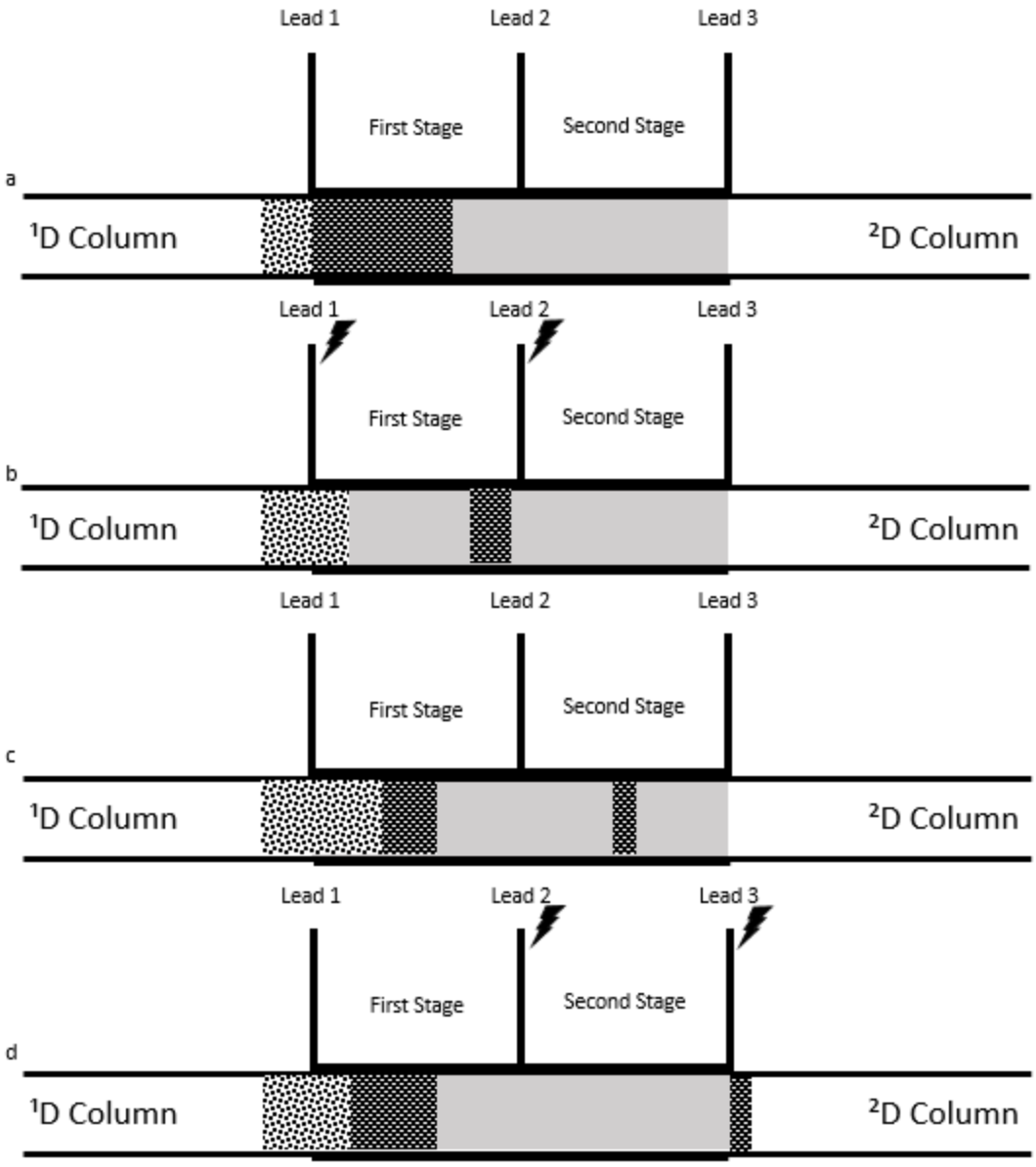

Figure 1-4: Modulation process of the original TDM. The TDM was constructed from the head of the ^{2}D column and divided into two stages by three electrical leads. (A) Analytes from the ^{1}D column are trapped and focused in the first stage. (B) Electrical current is applied to leads 1 and 2 to resistively heat the first stage and remobilize the analytes. (C) The remobilized analytes are trapped and focused in the second stage. (D) Electrical current is applied to leads 2 and 3 to resistively heat the second stage and inject the analytes into the ^{2}D column. Based on Ref. [7]

modulator remobilized the analytes (Figure 1-4B), which were then immediately trapped and focused once again in the second stage (Figure 1-4C). As the first stage cooled down and began to trap the next fraction of the analytes, the second stage was resistively heated, injecting the trapped analytes as a narrow band into the ^{2}D column (Figure 1-4D). Although successful in accomplishing the first GC×GC separation, the design was not very robust due to frequent burnouts and the delicate nature of the thin

conductive films [43]. A later modification to the design, by the same group, utilized an approximately three times longer first stage and a shorter second stage to minimize breakthrough [44]. The TDM was revisited by Hantao and coworkers, with updated materials, a simple design, and inexpensive commercial components [45].

1.2.1.1.2 Rotating Thermal Modulator ("Sweeper")

The rotating thermal modulator (Figure 1-5) was the first commercially available device (Zoex Corporation, Lincoln, NE, USA). Its initial design was introduced in 1996 as a more reliable and rugged version of the preceding thermal desorption modulator [46]. The final version was presented in 1999, detailing its construction, performance, and reliability over the two years of development [43]. The rotating thermal modulator, commonly referred to as the "sweeper" [47], utilized a slotted heater that rotated around a shaft to heat the modulator [43]. Analytes from the ^{1}D column would accumulate at the head of the modulator capillary coated with a thick film of the stationary phase (Figure 1-5A). The slotted heater would rotate and heat the upstream portion of the modulator column, remobilizing the trapped analytes (Figure 1-5B). The remobilized analytes would then be continuously refocused in the downstream portion of the modulator column that was still at oven temperature (Figure 1-5C). As the slotted heater rotated over the downstream portion of the modulator column, the focused fraction of the analytes was ultimately injected into the ^{2}D column (Figure 1-5D). In order to produce sufficiently narrow modulated peaks, the temperature difference between the heater and the modulator capillary had to be at least 100 °C [48]. This limited the maximum GC oven temperature during the separation and reduced the volatility range of compounds that could be modulated. Although five seemingly identical prototypes were constructed, only two worked reliably over the two years [43]. Following the introduction of cryogenic modulators, the usage of the sweeper declined, and it was discontinued.

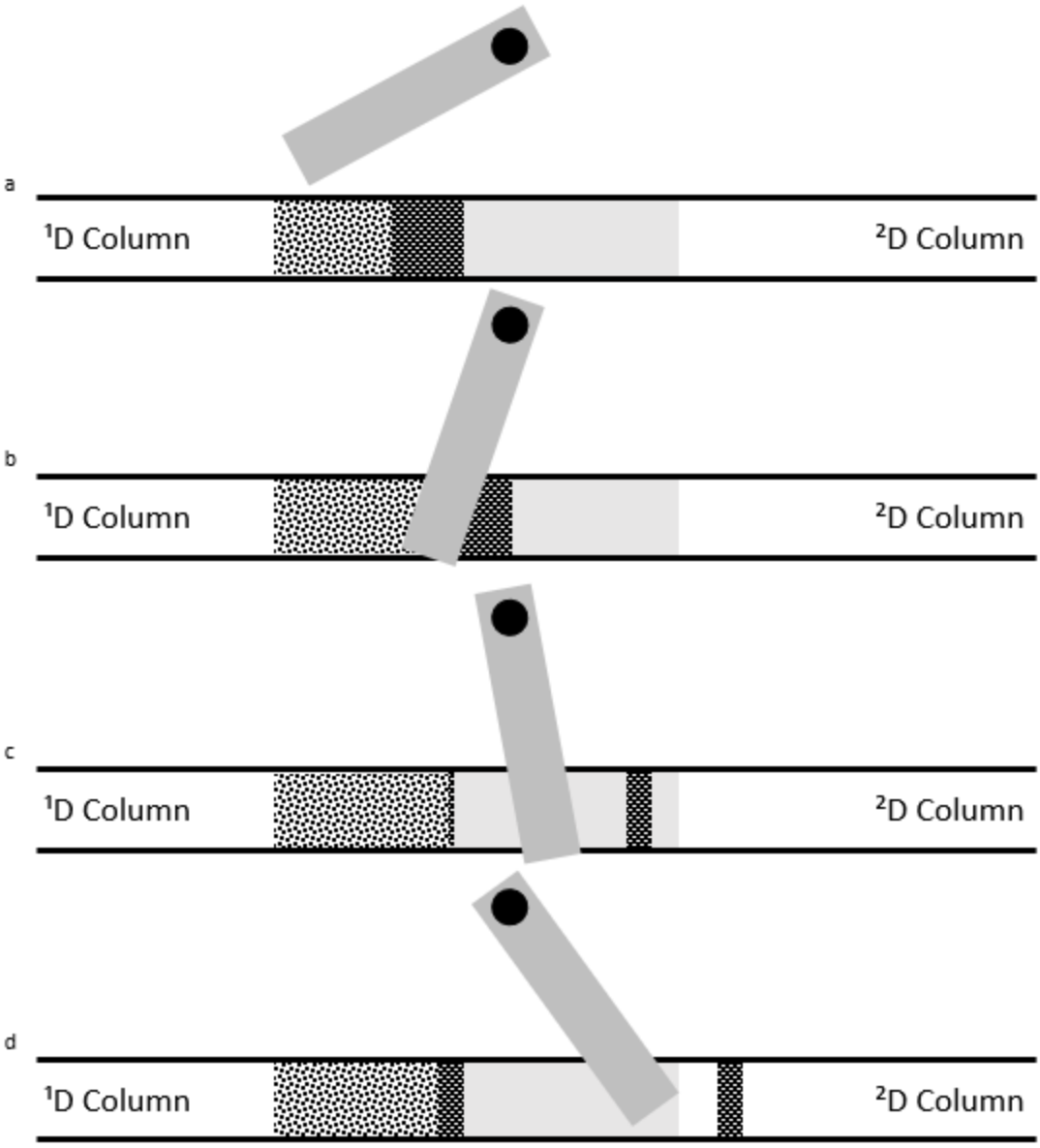

Figure 1-5: Modulation process of the rotating thermal modulator. (A) Analytes from the ¹D column accumulate at the head of the modulator column. (B) The rotating slotted heater heats the upstream portion of the modulator column, remobilizing the accumulated analytes in the heated region. (C) The remobilized analytes are refocused in the downstream portion of the modulator column. (D) The slotted heater continues to rotate and reaches the downstream portion of the modulator column, remobilizing and injecting the focused band of analytes into the ²D column. Based on Ref. [46].

1.2.1.2 Cryogenic Designs

Cryogenic modulators use cryogens to provide cooling in order to trap the analytes at temperatures significantly lower than the oven temperature. Analytes are then remobilized once the cooled section of the modulator is brought back to or close to the GC oven temperature. Although the use of cryogens

added a consumable cost to the system, it provided the best performance while overcoming the previous temperature limitations of the heater designs.

1.2.1.2.1 Longitudinally Modulated Cryogenic System (LMCS)

The Longitudinally Modulated Cryogenic System (LMCS) was first detailed in 1997 by Marriott and Kinghorn [49] and has been applied to various modes of gas chromatography [49, 50, 51]. It was used for GC×GC in 1998 in the separation of a kerosene sample as the first cryogenic modulator [52]. The LMCS (Figure 1-6) utilized a cryogenically cooled trap that moved longitudinally along the head of the ^{2}D column to trap and release analytes [49, 53]. The trap was constructed using two stainless steel tubes of differing lengths and inner diameters. The two tubes were sealed together at the ends to create a cavity, with the inner tube left open to let the GC column through. One inlet port and two outlet ports on the outer tube were used to pass through a flow of liquid CO_2. Analytes were first trapped at the segment of the column cooled by the trap in the top position. In the next step, the cooled segment of the column was exposed to the GC oven temperature via the longitudinal movement of the trap to the bottom position. The focused band of analytes would then be remobilized at or close to the GC oven temperature and re-trapped at the second trap position. The movement of the trap back to its original (top) position allowed the trapped band to remobilize again and enter the ^{2}D column, while preventing any potential analyte breakthrough. The longitudinal movement of the trap was driven by a pneumatic, electrical or stepper motor actuator through a modulator arm connected to the trap. Owing to the low thermal mass of the capillary column, it responded rapidly to the change in temperature from the movement of the trap [49]. Compared to the sweeper, the LMCS produced equivalent results in terms of peak widths and symmetry [54]. However, analyte remobilization for the LMCS system could suffer at lower oven temperatures if a slow temperature program was used [54]. This was described for high-boiling analytes where severe band broadening was observed [55]. In terms of robustness, ice buildup in the trap could cause column breakage. A dry nitrogen purge later incorporated into the design largely eliminated the problem [56].

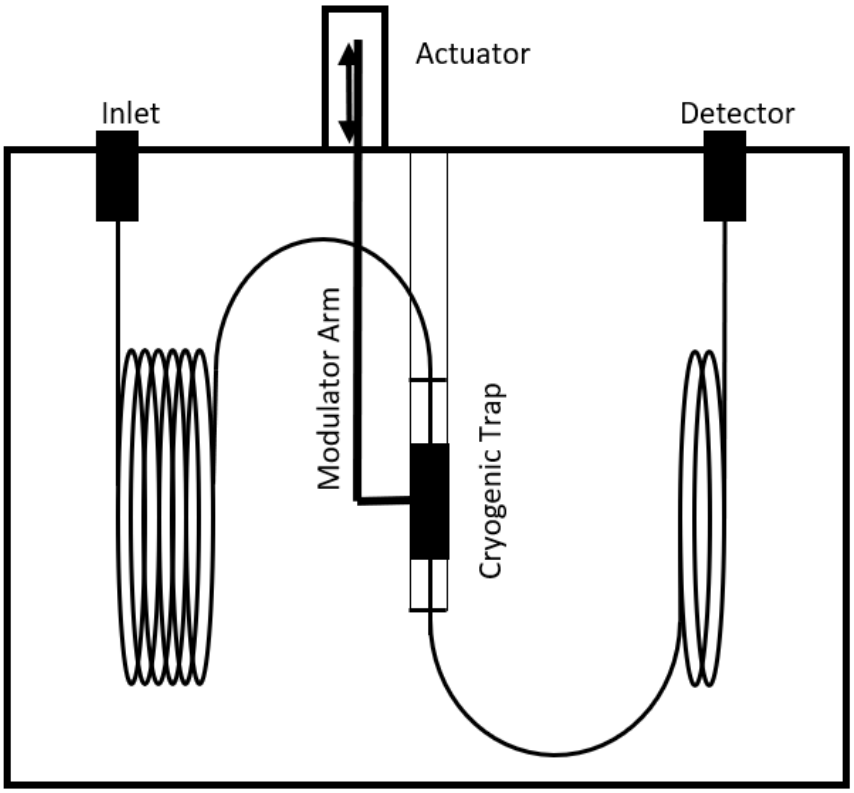

Figure 1-6: Schematic diagram of the LMCS. Based on Ref. [53].

1.2.1.2.2 Dual Stage Jet Modulators

The dual stage quad jet modulator introduced by Ledford in 2000 was one of the most widely adopted thermal modulator designs [57]. As shown in Figure 1-7, it utilized two hot jets and two cold jets to provide dual stage modulation [58]. These jets were positioned to provide a transverse gas flow onto the head of the ^{2}D column where modulation occurred [59]. Gas for the cold jets was cooled in a heat exchanger which utilized liquid nitrogen for cooling [59]. An electric heater provided heating for the gas flowing to the hot jets [59]. Analytes eluting from the ^{1}D column were trapped and focused at the first trapping stage provided by the upstream cold jet (Figure 1-7A). The upstream hot jet was then pulsed, remobilizing the trapped analytes to the second stage where the downstream cold jet would re-focus the band of analytes and prevent any breakthrough (Figure 1-7B). Following the heat pulse, the upstream cold jet would re-engage, allowing the upstream cold spot to start trapping the next fraction of the analytes (Figure 1-7C). The re-focused band of the analytes in the second stage was remobilized and injected into the ^{2}D column

when the downstream hot jet engaged while the upstream cold jet remained on to prevent breakthrough (Figure 1-7D). This design was commercialized by Zoex Corporation as the KT2001 modulator [60], while LECO Corp. designed its own dual stage quad jet modulator under license from the Zoex Corporation [61]. This modulator is available in both a liquid nitrogen variant with a modulation range of C_4 to C_{40}, and a consumable-free variant with a modulation range of C_8 to C_{40} [62]. The consumable-free variant uses a closed loop chiller instead of liquid nitrogen to cool the heat exchanger [62].

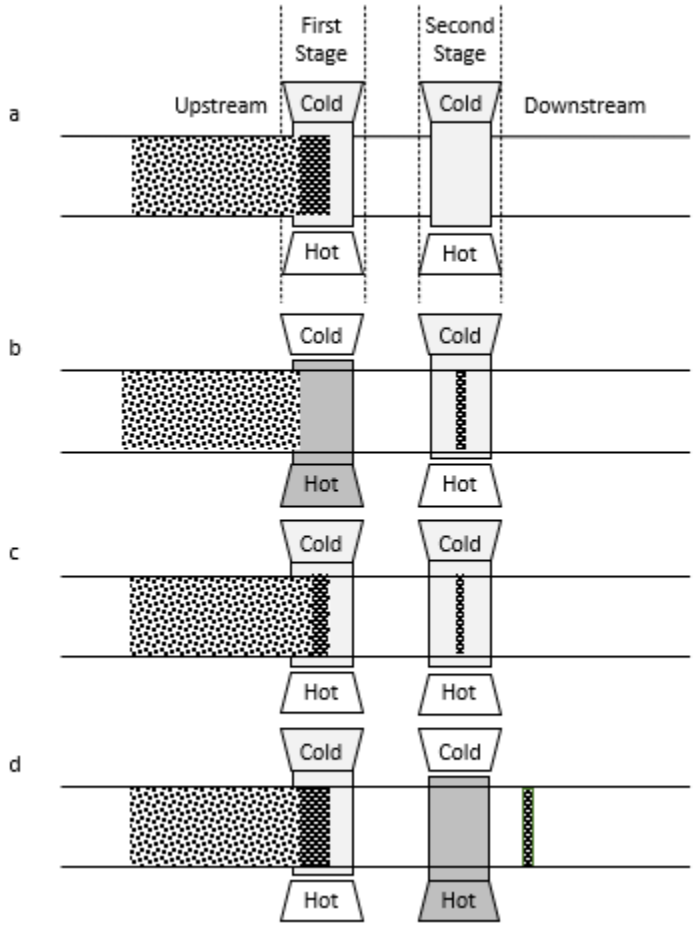

Figure 1-7: Modulation process of the dual stage quad jet thermal modulator. (A) The upstream cold jet traps the analytes in the first stage. (B) The upstream hot jet is pulsed, to remobilize the analytes while the downstream cold jet re-focuses the band. (C) The upstream cold jet reforms the cold spot and traps the next fraction of analytes. (D) The downstream hot jet injects the focused band into the ^{2}D column. Based on Ref. [58]

In 2001, Beens et al. developed a simplified dual stage modulator based on Ledford's design, which used liquid CO_2 jets for trapping and the ambient GC oven heat for remobilization [63]. This design

was further simplified in 2003 into a single-jet/single-stage modulator that relied on a single liquid CO_2 jet for modulation [64]. Performance of the single stage system was found to be comparable to the previous dual stage system [64]. The original Beens modulator was commercialized by Thermo Fisher Scientific under license from Zoex Corporation [65].

1.2.1.2.3 Dual Jet Loop Modulator

Ledford later designed a dual stage jet modulator using a single cold and hot jet, known as the "loop modulator" [66]. Shown in Figure 1-8, the gas forced from each jet passes through two segments of a looped capillary, providing dual stage modulation while eliminating two jets from the previous design. The cold jet, which runs continuously, creates two cold spots, one in the upstream and one in the downstream portion of the loop (Figure 1-8A). The hot jet is activated periodically, momentarily diverting the path of the cold jet gas away from the loop and heating the cold spots to remobilize the trapped analytes (Figure 1-8B). This also helps defrost the tip of the cold jet. Analytes from the ^{1}D column are trapped by the cold jet at the upstream cold spot. Activation of the hot jet remobilizes the trapped analytes into the looped capillary. As the analytes travel through the loop, the hot jet is deactivated, allowing the cold spots to re-form from the cold jet. When the analytes in the loop reach the downstream cold spot, they are refocused together with potential breakthrough. At the same time, the next fraction of the analytes eluting from the 1D column is trapped at the upstream cold spot. The subsequent activation of the hot jet injects the refocused band of analytes into the ^{2}D column and releases the trapped analytes from the upstream cold spot into the loop [67]. This modulator type is commercially available from the Zoex Corporation [68]. It is available with liquid nitrogen cooling (model ZX1) or as a consumable-free modulator using a refrigeration unit (model ZX2). Both modulators can be bought separately to be installed in existing GCs, or as a part of a complete GC×GC system. It is important to note that the cryogen-free ZX2 modulator is only rated for modulating C7 and higher, similar to LECO Corp.'s cryogen-free quad jet modulator [69], while the ZX1 is stated to be able to modulate from C_2 and higher [70].

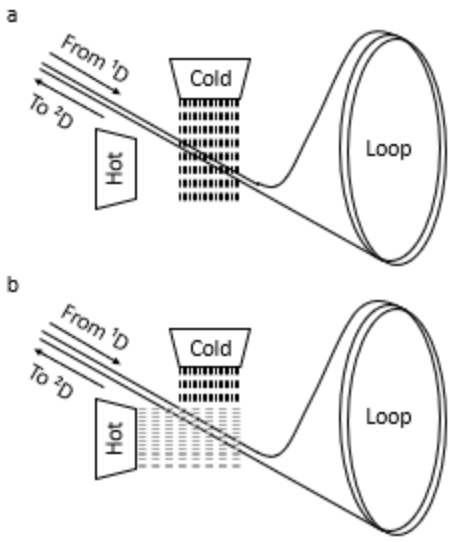

Figure 1-8: Modulation process of the dual jet loop modulator. Each jet blows at two segments of the looped capillary column to provide dual stage modulation using only two jets. (A) The cold jet creates a cold spot in the upstream and downstream portion of the column simultaneously. (B) The hot jet is periodically activated to remobilize the trapped analytes in each section of the column. Based on Ref. [67]

1.2.1.2.4 Liquid Nitrogen Jet Modulator

Unlike the previously described jet modulators, which use cooled nitrogen gas for the modulation, the liquid nitrogen modulators use liquid nitrogen for direct cooling [71, 72, 73]. The benefit of such modulators is the capability to efficiently trap highly volatile compounds such as propane, as well as highly concentrated bands of volatile solvents like methylene chloride and CS_2 [71, 72, 73]. Pursch et al. described a dual jet modulator which used liquid nitrogen delivered directly from a Dewar for modulation [71]. A three-way solenoid valve alternated between liquid nitrogen cooling and warm nitrogen gas heating (oven temperature) for dual stage modulation. Liquid nitrogen consumption was reported to be about 30 L to 40 L per day with peaks width at half height of 66 ms for butane [71]. Harynuk and Górecki also reported a liquid nitrogen modulator at around the same time [72]. The design was based on the loop modulator introduced by Ledford et al. at Pittcon in 2002 [66]. This system used high pressure nitrogen from an in-house supply line that was cooled through a heat exchanger using liquid nitrogen. Although this was similar to the cooling method of previous cryogenic modulators, the higher pressure from the lines in combination with the low temperatures produced liquid nitrogen within the coils in the heat

exchanger. This near-boiling liquid nitrogen was then passed through a phase separator, with only the liquid phase directed to the cold jet for modulation. The excess liquid nitrogen and cold gaseous liquid nitrogen that were separated, were used to cool the valves and connectors of the interface. Two jets of compressed air at oven temperature were directed towards the cold spots to rapidly warm the capillary and blow away any remaining droplets of liquid nitrogen.

The Górecki group introduced a new liquid nitrogen modulator in 2016, eliminating the capillary loop from their previous design and creating a single stage cryogenic modulator [73]. The liquid nitrogen delivery system was simplified, using liquid nitrogen from a pressurized Dewar. A piece of deactivated fused silica tubing was used as the modulator capillary and a restriction was made in the middle of the modulator capillary using a 3-4 mm plug of compressed fused silica wool. Two hot air jets were used, one to defrost the cryojet nozzle using oven temperature air, and another that was temperature controlled for analyte desorption. The hot air jet for desorption was maintained at a temperature offset from the oven temperature. Both hot air jets were turned on when the cold jet turned off. The restriction within the modulator capillary served to prevent breakthrough from single stage modulation by increasing the surface area of the cold spot. At the trapping temperature, carrier gas viscosity decreased to the point where the plug offered very little restriction to the flow. At the desorption temperature, gas viscosity increased and reduced the flow to near zero preventing breakthrough while still allowing for desorption of the trapped analytes.

1.2.1.3 Other Designs

Early thermal modulators (heater design) lacked robustness but were inexpensive to run and simple in design. Commercial cryogenic modulators improved on robustness and performance, but required large amounts of cryogens, increasing the running costs. Other designs for thermal modulation eliminated cryogens without significant compromises to the performance and robustness, or looked to miniaturize the modulator device.

1.2.1.3.1 Single-Stage Consumable Free Modulator

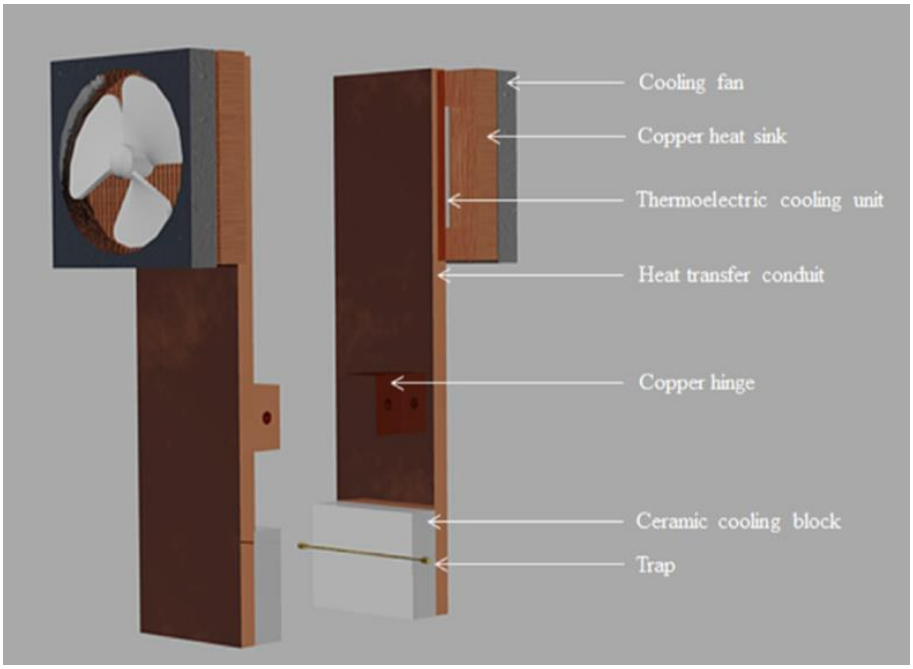

Figure 1-9: Schematic diagram of the single-stage modulator [74]. Reprinted from Journal of Chromatography A, Vol. 1391, A. M. Muscalu, M. Edwards, T. Górecki and E. J. Reiner, Evaluation of a single-stage consumable-free modulator for comprehensive two-dimensional gas chromatography: Analysis of polychlorinated biphenyls, organochlorine pesticides and chlorobenzenes, 93 – 101, 2015, with permission from Elsevier.

The Górecki group has created several different designs for a consumable-free modulator [75, 76, 74, 77, 78]. Early designs utilized a 15 cm segment of flattened Silcosteel® capillary packed with a microsorbent bed that looped outside the GC oven to trap analytes with the help of forced air convection [75, 76]. Reinjection of these focused band of analytes was accomplished through resistive heating, by a capacitive discharge pulse [75, 76]. The single-stage consumable-free modulator was introduced by the Górecki group in 2015 [74]. This design, shown in Figure 1-9, utilized a specially coated stainless steel capillary trap that could be passively or actively cooled [74]. Analytes were focused in the trap with the aid of cooling from the compression of the trap between two ceramic cooling blocks. The ceramic cooling blocks were cooled through a copper heat transfer conduit that was passively cooled by two heat sinks or actively cooled with the addition of a thermoelectric cooling unit between the heat transfer conduit and the heat sink. Just as before [75, 76], the band of focused analytes was injected into the ^{2}D column by resistive heating using capacitive discharge [74]. The performance was comparable to the commercial

LECO Corp's LN_2 dual-stage quad-jet modulator when using a routine accredited method for the analysis of polychlorinated biphenyls, organochlorine pesticides, and chlorobenzenes [74].

1.2.1.3.2 Microfabricated Thermal Modulator

In order to develop a comprehensive two-dimensional microscale gas chromatography system (μGC×μGC), a dual stage microfabricated thermal modulator (μTM) was developed in 2010 [79]. The two stages of the μTM were made of microchannels etched onto a silicon wafer and doped with boron. The walls of the microchannels were dynamically coated with polydimethylsiloxane (PDMS), and Pyrex glass was anodically bonded to the wafer to seal the microchannels. Microheaters and temperature sensors were patterned onto the Pyrex glass, and microfabricated silicon spacers were used to create an air gap between the thermoelectric cooler and the μTM. Both stages were cooled by the thermoelectric cooler while heating alternated to provide dual-stage modulation. In the work from 2010 to 2013, the focus was on the optimization of the modulator dimensions and parameters, using relatively simple *n*-alkane mixtures (C_7 – C_{10}) [79, 80, 81, 82]. In 2016, temperature programming was incorporated into the μTM, to adjust the minimum and maximum temperature of the two stages over the course of the separation. The modulator was tested using an Agilent 6890 with a standard sized GC×GC setup and a gasoline sample [83].

1.2.1.3.3 Solid State Modulator

The Solid State Modulator (SSM) previously available commercially from J&X Technologies [84] was introduced in 2016 as the thermal independent modulator (TiM), as seen in Figure 1-10 [85]. The TiM operated outside the GC oven and featured thermally independent heating and cooling stages [85]. Two heated areas (entry and exit zones) could be temperature programmed from ambient to greater than 350 °C for remobilization, while the trapping zone in the middle could be programmed from -50 °C to 50 °C. The heated zones used micathermic heaters to heat the aluminum chambers, while the cooling zone utilized a pair of three-stage thermoelectric coolers. Temperature for each zone was monitored using

resistive temperature detectors. Dual stage modulation was accomplished by mechanically moving the modulator column back and forth in a fashion opposite to Marriott's LMCS system, in which the cold trap was moved along the column [49]. Analytes from the ^{1}D column were trapped in the segment of column exposed to the cooled zone. Remobilization of analytes in the first stage was accomplished by moving the column towards the heated entry zone, thereby exposing the trapped analytes to the elevated temperature. This movement also exposed the downstream segment of the modulator column to the cooling units. The remobilized analytes would then reach the newly cooled zone for the second stage of trapping. Moving the column towards the exit zone exposed the trapped analytes once again to an elevated temperature and injected the band into the ^{2}D column. This simultaneously exposed the upstream segment of the column to the first stage of trapping once again. Volatility range was reported to be from C_6 to C_{24}, while peak widths at half height of 120 ms were reported for aromatic compounds [85]. The modulation range of the SSM has been updated from the TiM to range from C_2 to C_{40}+ depending on the modulator column installed [86].

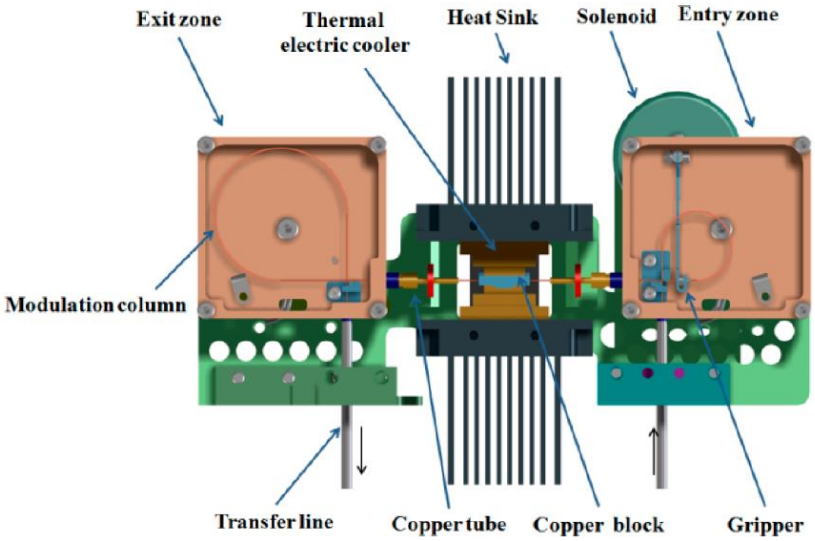

Figure 1-10: Schematic diagram of the TiM [85]. Reprinted (adapted) with permission from Analytical Chemistry, 88, J. Luong, X. Guan, S. Xu, R. Gras and R. A. Shellie, Thermal Independent Modulator for Comprehensive Two-Dimensional Gas Chromatography, 8428-8432, 2016. Copyright (2016) American Chemical Society.

1.2.1.3.4 Stop-Flow GC×GC

Stop-flow GC×GC was a unique system that would stop the flow from the ^{1}D column for a brief time, allowing for extended modulation periods without sacrificing the sampling rate of the ^{1}D effluent. This allowed the ^{2}D separation time to be lengthened, improving the ^{2}D resolution. By stopping the ^{1}D flow, one could sample the ^{1}D effluent more often without reducing the time available for the separation in the ^{2}D. This allowed for the optimization of both dimensions separately without compromise.

The original stop-flow GC×GC system was presented in 2004 by Harynuk and Górecki [87] using a 6-port high temperature Valco valve (VICI, Houston, TX, USA) placed in-line with the column assembly (Figure 1-11). The ^{1}D column was connected directly to the GC injector, while a bypass column (uncoated tubing) with precisely matched pneumatic resistance was connected to the carrier gas supply line before the GC injector. Only 3 ports of the valve were used, connecting the outlets of the ^{1}D column, the bypass column, and the inlet of the ^{2}D column. In the sampling state, the effluent from the ^{1}D column flowed through the valve to a single jet liquid nitrogen modulator described in section 1.2.1.2.4 [72]. After a set period (sample time), the collected fraction was reinjected into the ^{2}D column, following which the valve switched to the stop state, halting the flow in the ^{1}D column. In the stop state, the carrier gas continued uninterrupted with flow from the bypass column to the ^{2}D column. The performance of the stop-flow system was tested with a mixture of C_5 – C_{13} *n*-alkanes. ^{1}D separation resulted in peak widths at the base of around 6 s. With a 2 s sampling time and a 4 s bypass time, each peak was sampled 3 - 4 times, with a ^{2}D separation of 6 s. This significantly improved the resolution in the ^{1}D, while ^{2}D resolution was the same as with a 6 s modulation period. Although the design was successful in demonstrating the effectiveness of stop-flow GC×GC, the system suffered from the short life span of rotary valves operating at high duty cycles at high temperature. In addition, the polymers used in the valve tended to off-gas, resulting in artifact peaks.

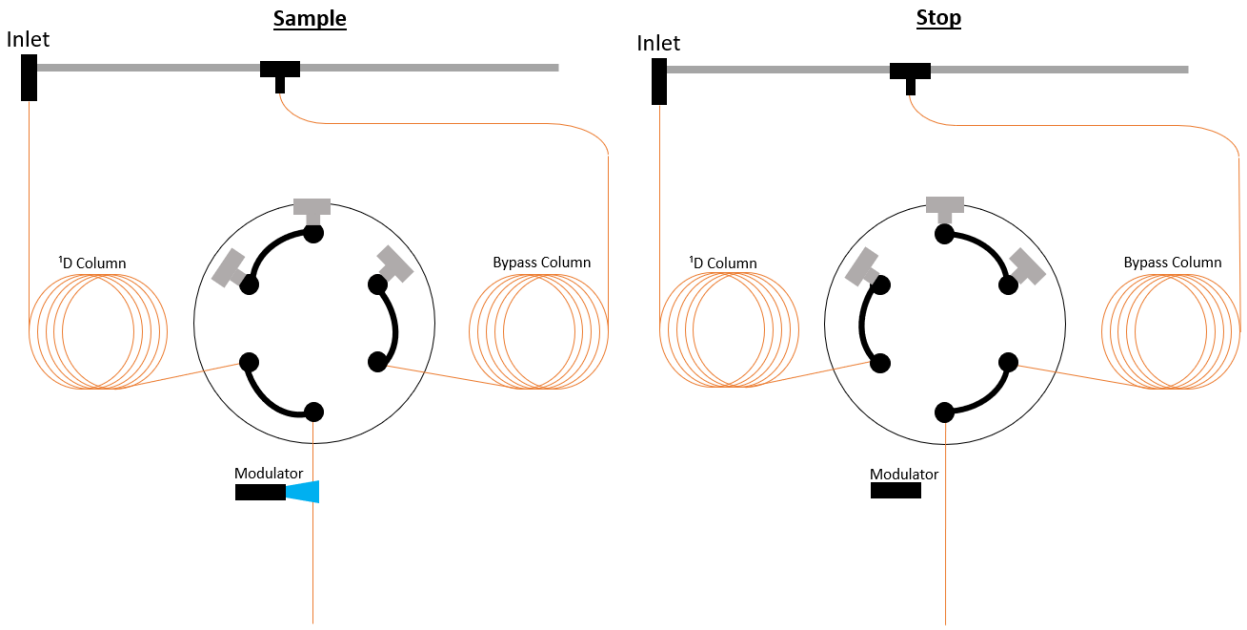

Figure 1-11: Schematic diagram of the stop-flow GC×GC design utilizing a six-port valve to achieve stop-flow conditions in the ¹D. Based on Ref. [87].

In 2008, the stop-flow system was revisited [88]. Based on the work of Veriotti and Sacks in 2001 [89], the inline rotary valve was replaced with a solenoid valve placed outside the GC oven for pneumatic flow stopping. This eliminated the previous complications encountered when using an in-line valve within the GC. An auxiliary flow was supplied from an unused on-column injector through a solenoid valve to a 4-port junction (one end capped) connecting the ¹D column and a 100 µm fused-silica capillary restrictor connected to the modulator. The modulator used for the experiments was one of the early designs of the single-stage consumable free modulators referenced in 1.2.1.3.1 [78]. By applying an appropriate pressure/duration of the auxiliary gas, the flow from the ¹D column could be temporarily stopped for a brief period. The restrictor was needed to reduce the auxiliary flow needed for stop-flow conditions. With this system, a 3 s stop-flow period with a 6 s modulation was used, resulting in 3 s of sampling for the modulator. This effectively doubled the sampling frequency of each ¹D peak while maintaining the separation time in the ²D. During the stop-flow period, the auxiliary flow resulted in an elevated second dimension flow rate, allowing the use of longer ²D columns. A comparison of conventional GC×GC with stop-flow GC×GC was done with a modulation period of 6 s using a diesel sample. ¹D separation improved

with stop-flow GC×GC due to the greater sampling frequency, resulting in narrower ^{1}D peaks. ^{2}D peaks on the order of 100 ms were achieved for stop-flow GC×GC compared to 200 ms from conventional GC×GC. Although a longer column was used for stop-flow GC×GC, the increased flow rates led to narrower peaks, improved resolution, and increased sensitivity.

1.2.2 Flow Modulators

Cryogenic modulators have been the most popular due to their ability to produce narrow peaks with minimal breakthrough. Recently, though, flow modulators have been gaining in popularity due to their simplicity and cryogen-free modulation, making them inexpensive and easy to maintain once set up and optimized [90]. Many different flow modulators designs have been published and they tend to be made of similar components, consisting of valves (solenoid or diaphragm), unions, and capillary tubing (bleed or storage). Overall, flow modulators can generally be divided into either diverting flow or full transfer flow modulators, with some designs capable of performing both types of modulation.

1.2.2.1 Diverting Flow Modulators

Diverting flow modulators are so-called low duty cycle modulators, where only a portion of the total ^{1}D column effluent is diverted to the ^{2}D column while the rest is vented through a bleed or restrictor column. Typically, a majority of the effluent is exhausted and only a small fraction of the ^{1}D column effluent is transferred in very short pulses at regular intervals (modulation period). These short transfers produce very narrow injection bands onto the ^{2}D column, which results in narrow ^{2}D peaks. In addition, since none of the ^{1}D column effluent is collected or re-concentrated, modulation periods would have to be shorter than what may be used with thermal modulation, to ensure peaks are not lost in-between injections onto the ^{2}D column. The biggest concern, however, with low duty cycle flow modulators would be the loss in sensitivity, as a majority of the sample is vented.

1.2.2.1.1 Diaphragm Valve Modulators

The low duty cycle diaphragm valve modulator by Synovec's group represented the first flow modulator used in GC×GC [91]. It consisted of a six-port diaphragm valve with low dead volume fittings, where only four ports were used for the ^{1}D and ^{2}D column, the auxiliary gas, and the vent. The diaphragm valve modulator functioned within the GC oven, briefly diverting flow from the ^{1}D column to the ^{2}D column every half second, with most the effluent from the ^{1}D column vented outside. The GC×GC chromatogram was vastly different from its thermal modulator counterparts, with some runs having modulation periods under 1 s. The main limitation was the low operational temperature limit of the diaphragm valve of 175 °C. This limited the analysis to volatile compounds. The other limitation was the low duty cycle, where only 10 % of the sample was analyzed in both dimensions, reducing the sensitivity of the analysis. The working temperature of the diaphragm valve modulator was increased to 250 °C in 2003, and further increased in 2015 to 325 °C [92, 93].

In 2000, Seeley's group developed the differential flow modulator, with which approximately 80 % of the sample was separated and analyzed in both dimensions [94]. A six-port diaphragm valve was used, connected to the ^{1}D column, ^{1}D column exhaust, sample loop, auxiliary gas flow, and ^{2}D column. In the collection stage, the ^{1}D column effluent flowed through the sample loop to the ^{1}D column exhaust. Transfer of the effluent from the sample loop to the ^{2}D column occurred when the valve was switched to the inject position. Here, the auxiliary flow was kept at least 20 times higher than the ^{1}D flow, compressing the contents in the sample loop to 5 % of the collection time. Injection of the effluent contained in the sample loop to the ^{2}D column by the ^{2}D flow was in the direction opposite to collection. The 0.045 s injection band widths observed were comparable to those reported for cryogenic modulators. However, this modulator was still limited to the analysis of volatile compounds due to the temperature limits of the diaphragm valve. This was the preceding work to differential flow modulators described in section 1.2.2.2.1.

1.2.2.1.2 Deans Switch

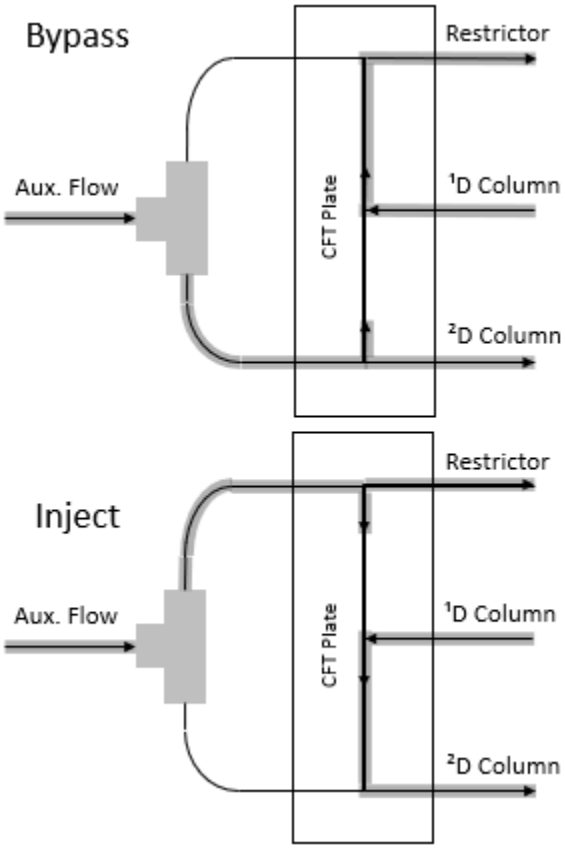

Figure 1-12: Schematic diagram of the low duty cycle Deans switch modulator in the bypass and inject states. Gas flow is represented by the greyed areas over the pathways, with the direction of flow represented by the arrows. Based on Ref. [95].

Deans switching (DS) is a flow switching technique utilizing differential pressures to direct fluid flow in the direction of lower pressure [96]. This microfluidic flow switching technique was invented in the 1960s [97] and adopted for GC-GC [98]. It was not until 2007 that the DS was adapted as a modulator for GC×GC use by Seeley [95], using Agilent's capillary flow technology (CFT) platform. The DS was assembled using Agilent's 5-port microfluidic DS manifold and a three-port solenoid valve. A general schematic of flows is presented in Figure 1-12. The ^{1}D column was connected to the center port of the manifold, with its flow directed to one of two capillary columns: the ^{2}D column or the restrictor column. The two ports on the opposite end of the manifold were connected to the solenoid valve. In the bypass state [Figure 1-12A], a high auxiliary flow was directed towards the ^{2}D column, splitting the flow between ^{2}D column and the central T connected to the ^{1}D column. This ^{1}D flow combined with the auxiliary flow and travelled

towards the restrictor column. The DS was periodically switched to the inject state [Figure 1-12B], in which the auxiliary flow was directed towards the restrictor column, splitting the flow between the restrictor column and the central T. The auxiliary flow was combined with the ^{1}D flow and was directed to the ^{2}D column. Sharp peaks were produced by switching to the inject state for only 5 – 10 % of the modulation period.

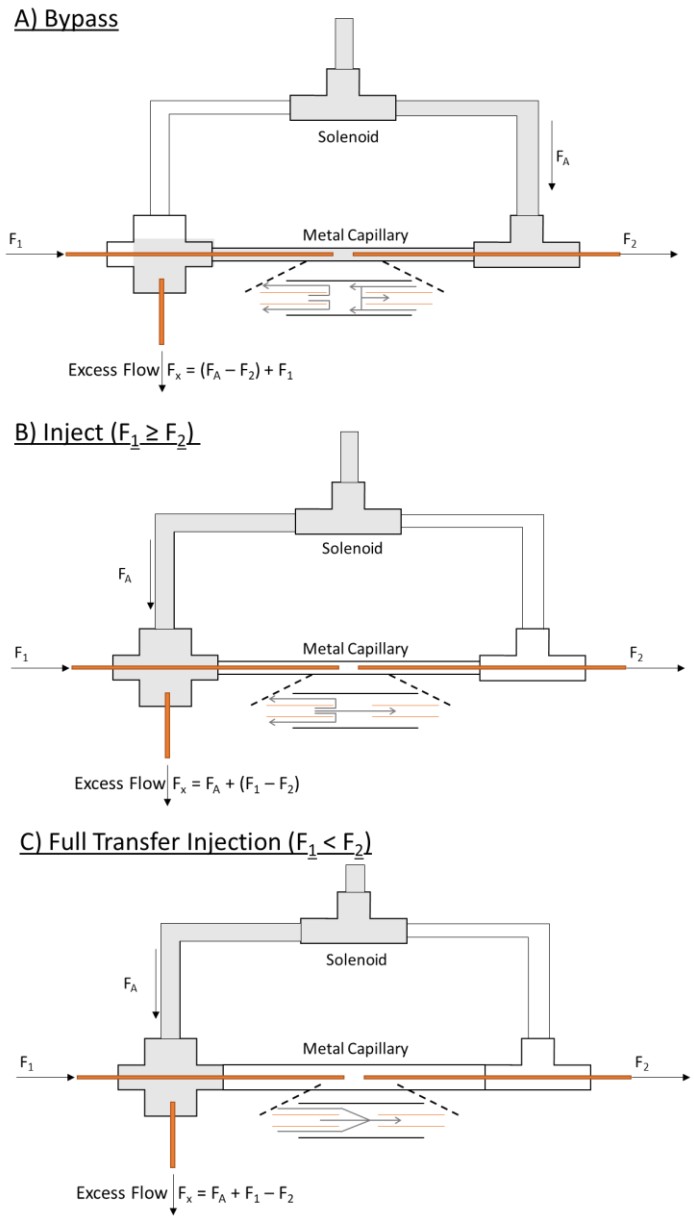

Figure 1-13: Schematic diagram of the high-speed Deans switch modulator. Solid lines extending into the metal capillary represent the ^{1}D and ^{2}D columns. Auxiliary gas flow is represented by the greyed areas, with the direction of flow (F_A, F_1, F_2, and F_x) indicated by the arrows. Based on Ref. [99].

In 2013, Seeley [99] redesigned the DS specifically for GC×GC, focusing on reducing the time needed to switch between DS states while keeping the ^{2}D flow rates low for compatibility with mass spectrometers. This high speed Deans switch modulator, shown in Figure 1-13, was assembled using a solenoid valve, a cross union, and a T-union. The solenoid valve was connected to the two unions that were joined together with a deactivated metal capillary. The ^{1}D and ^{2}D columns were inserted through the cross unions and into the metal capillary, with a small gap in between. The remaining port, labelled as the excess flow port, was connected to a flow restrictor column. In the bypass state [Figure 1-13A], the auxiliary flow was directed towards the T-union so that the ^{1}D effluent (F_1) was directed towards the excess flow port. This resulted in F_A providing the flow for the ^{2}D column with the difference in flow ($F_A - F_2$) directing F_1 towards the excess flow port ($F_x = F_1 + F_A - F_2$). In the inject state [Figure 1-13B], F_A was directed towards the cross union allowing F_1 to flow towards the ^{2}D column. If $F_1 > F_2$, the excess was combined with F_A at the excess flow port. If $F_1 < F_2$, then a portion of the F_A combined with F_1, diluting the effluent going into the ^{2}D column.

1.2.2.1.3 Multi-Mode Modulator

An update to the low-duty cycle flow modulator from 2013 [99] is the multi-mode modulator (MMM) by Seeley, which adds the capabilities of full-transfer modulation [100]. Minimal changes to the original 2013 design (Figure 1-13A/B) were needed to allow for full transfer modulation. The physical change was an increase in the size of the joining capillary, while achieving full transfer modulation required an increase in the F_A to direct all of the F_1 into the ^{2}D column. With these changes, the MMM was capable of performing GC-GC, low-duty cycle modulation, and full transfer modulation. With the new modifications, when $F_1 < F_2$, full transfer modulation (Figure 1-13C) occurred as a portion of F_A was directed towards the ^{2}D column to supplement F_2. This also swept the effluent contained in the annular region to the ^{2}D column to ensure full transfer. Although this design makes it both a diverting flow and a full transfer flow modulator, only the low-duty cycle setup was commercialized by LECO Corp. as the FLUX modulator [101].

1.2.2.2 Full Transfer Flow Modulators

Unlike the diverting flow modulators which are low duty cycle, full transfer flow modulators modulate the whole sample like thermal modulators. To accomplish this, the ^{1}D column effluent is typically stored in a sample loop. Before the column is overfilled, the loop content is transferred rapidly to the ^{2}D column for further separation. Thus, unlike thermal modulators which concentrate the analyte band, full transfer flow modulators simply reinject the plug of effluent collected in the sample loop. This is typically done at high flow rates to try to compress the injection band and reduce re-injection band width.

1.2.2.2.1 Differential Flow Modulators

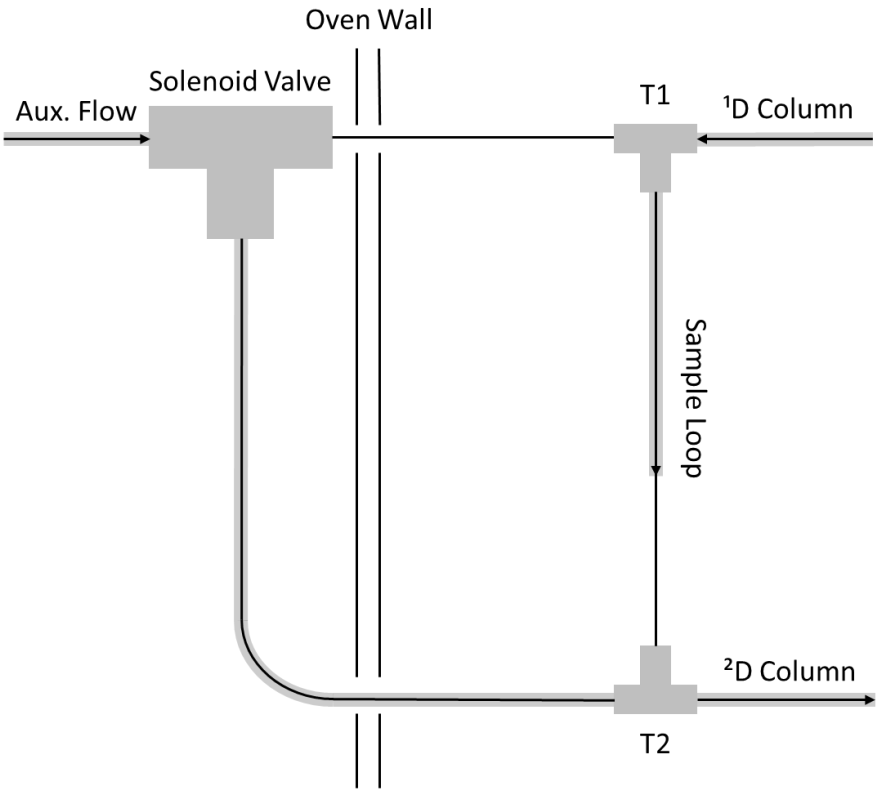

Figure 1-14: Schematic diagram of the simple fluidic modulator. Solid lines connected to the T unions (T1 and T2) and solenoid valve represent columns. Greyed areas over the solid lines represent the gas flow, with the direction of flow indicated by arrows. Based on Ref. [102].

The first differential flow modulator was reported in 2000 utilizing the temperature limited diaphragm valve [94]. In 2004, Bueno and Seeley [102] described a full transfer flow modulator that utilized no valves within the oven or in the sample path, eliminating the temperature limitation and the risk of pressure and

flow fluctuations during switching. The components used within the oven were non-moving and made with materials suitable for a wide range of temperatures. This design was simplified in 2006 by Seeley et al. [103] as the "simple fluidic modulator" (Figure 1-14). The solenoid valve, positioned outside the GC oven, normally directed auxiliary flow (20 mL/min) to T2 as the ^{1}D flow (1 mL/min) filled the sample loop between the two T-unions. Before the ^{1}D effluent reached T2, the solenoid valve was switched to direct the auxiliary flow towards T1. Due to the significant difference in pressure between the auxiliary flow and the ^{1}D flow, the sample loop was flushed in a fraction of the fill time. Furthermore, a longer fused silica column was used between T2 and the solenoid valve to create greater flow resistance compared to the column to T1. This increased the pressure at the solenoid valve during the fill state, creating a pressure pulse when switching to the flush state. This pressure pulse temporarily stopped the ^{1}D flow into the sample loop, minimizing peak tailing. These modulators were characterized by their extended operational temperature range, simple and inexpensive design, and high duty cycle. In 2008, Poliak et al. published a paper on their pulsed flow modulator with a near identical design [104]. It was stated that they worked independently and the focus of their design was directed towards GC-MS with supersonic molecular beams [104].

In 2016, the design of the simple fluidic modulator was brought back with some slight modifications [105]. Rather than using two different length transfer lines to create a difference in pressure between the pathways to the T-unions, two 2-way solenoid valves along with individual miniature pressure regulators, pressure sensors, and a control unit were used. This allowed independent settings for the flow through the two transfer lines of equal dimensions. The advantage was that adjusting the flow rate for the injection pulse or ^{2}D flow required no adjustment in dimensions of the transfer lines. This made optimizing the flow modulator much easier.

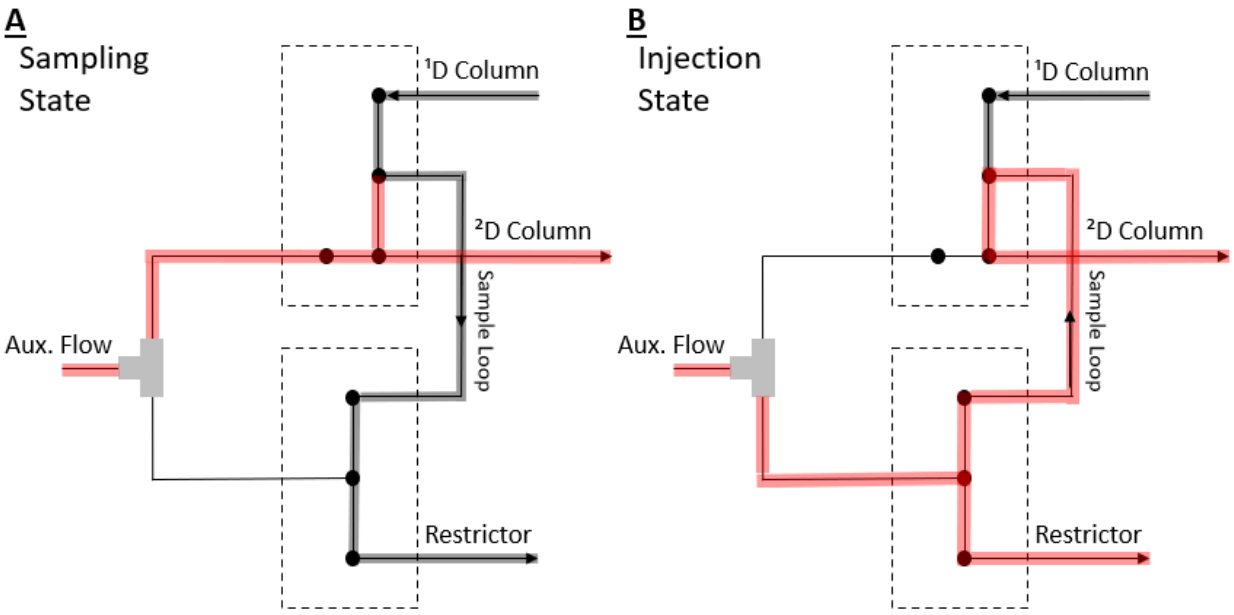

Figure 1-15: Schematic diagram of the reverse fill/flush differential flow modulator, assembled using Agilent's CFT plates. Flow pathways are indicated by the solid lines. Auxiliary gas flow (light grey) and ¹D column gas flow (dark grey) is represented by the shaded areas. The direction of flow is indicated by the arrows. The sample loop, represented by the connection between the two plates, is filled and flushed in opposite directions. Based on Ref. [106].

In 2012, Griffith et al. [106] described a reverse fill/flush (RFF) differential flow modulator, based on the Seeley's simplified differential flow modulator [103], and constructed with Agilent's capillary flow technology (CFT) plates. The purpose of the RFF flow modulator was to reduce the tailing of second dimension peaks. Shown in Figure 1-15, the RFF was constructed using a 2-way non-purged splitter and a 2-way purged splitter CFT plates connected with a sample loop made from fused silica tubing and Silcosteel® tubing (Restek Corporation, Bellefonte, PA, USA). A 3-way solenoid valve directed auxiliary flow to one of two CFT plates. In the sampling state [Figure 1-15A], auxiliary flow was directed to the 2-way purged splitter, where the ²D flow was maintained by the auxiliary flow while the ¹D effluent was directed to the sample loop. In the injection state [Figure 1-15B], the auxiliary flow was directed to the 2-way non-purged CFT plate, flushing the contents of the accumulation loop in the reverse direction to the ²D column. The forward fill/flush (FFF) differential flow modulator was constructed using the same CFT plates, with the ¹D column replacing the restrictor column and the original first dimension column position blocked. When comparing the FFF and the RFF designs, it was found that the RFF design significantly reduced tailing

in the ^{2}D. Further testing of the RFF design by Duhamel et al. in 2015 and Krupcik et al. in 2016 confirmed the findings that the RFF design reduced tailing or band broadening [107, 108]. Commercial versions of the RFF flow modulator are available from Agilent as their second generation CFT with an integrated collection channel, and from SepSolve with their INSIGHT^{TM} flow modulator with an adjustable sample loop.

1.2.2.2.2 Low Flow – Flow Modulation

Hyphenation of flow modulated GC×GC to MS was first reported in 2003 by Sinha et al. [109] using TOFMS. This was accomplished using the low duty cycle diaphragm valve modulator and limiting the flow in the ^{2}D column to the maximum operational flow limit of 10 mL/min for the TOFMS. In general, hyphenation with a mass spectrometer is difficult due to the high gas flows generated with flow modulation. Flows could be reduced by splitting the flow post modulation to a vent or at the exit of the ^{2}D column to another detector, but this reduces sensitivity. In 2013, Seeley reduced the ^{2}D flow to 2 mL/min, making it compatible with most mass spectrometers, but this was accomplished with the low duty cycle DS [99].

In 2014, Tranchida et al. [110] set out to achieve a low-flow, full transfer flow modulator for compatibility with common mass spectrometers. The modulator was based on their 2011 design [111], utilizing a 7-port valve and an accumulation loop. Originally, this was a low duty cycle modulator with a majority of the effluent vented through the waste port. This was modified by blocking the waste port and careful adjustment of the auxiliary flow rate and injection period to achieve full transfer of the effluent between the ^{1}D and ^{2}D column. Optimization of the linear velocity within the loop was needed to prevent peak breakthrough. This occurs when the analyte elutes from the loop before the injection pulse. Injection period also needed to be optimized, with longer injection periods risking the ^{1}D effluent flowing into the loop before the end of injection. The fundamental principle that converted their original design to a low flow high duty cycle modulator was the reduction of injection flow rates by proportionally increasing the

injection period (24 mL/min with 100 ms injection to 6 mL/min with 400 ms injection). In 2016, Tranchida et al. attempted to further reduce the ^{2}D flow rate to approximately 4 mL/min for compatibility with more mass spectrometers [112]. The modulator combined the simplified differential flow modulator design by Seeley et al. from 2006 [103] and the flow reduction principle tested in 2014 [110]. A 4 mL/min flow rate in the ^{2}D column was accomplished during the sampling period (4500 ms) and a 5 mL/min flow during injection (700 ms) for a modulation period of 5.2 s. Peak width at half height was reported to be about 290 ms for nonane on an SLB-35ms ^{2}D column.

1.2.2.2.3 Pulsed Flow Modulator

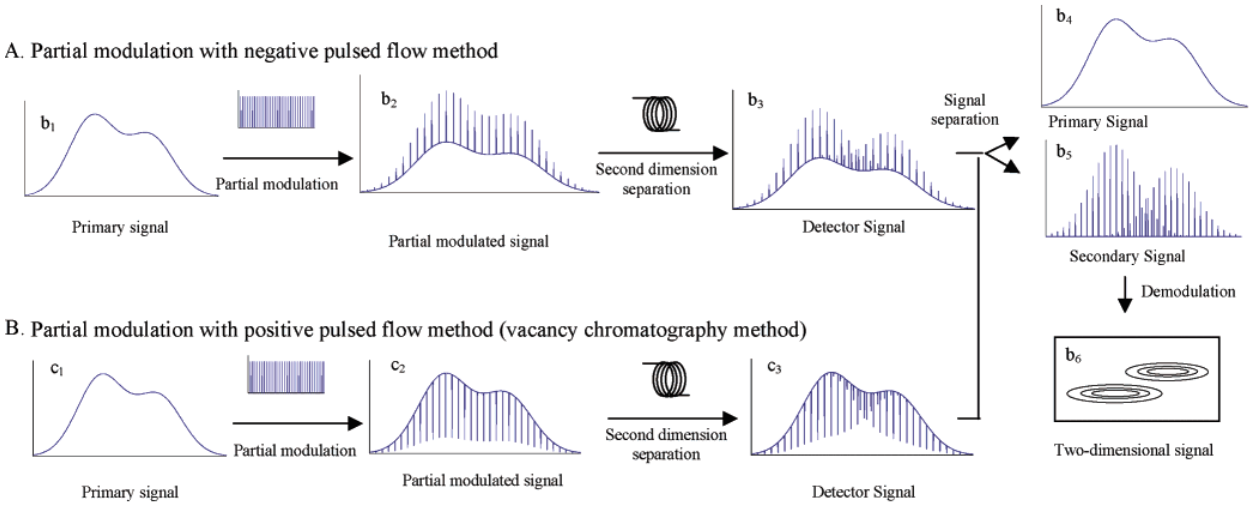

Figure 1-16: Schematic diagram of the partial modulation process for negative pulsed flow (A) and positive pulsed flow (B), as well as signal processing to separate the ^{1}D and ^{2}D signal [113]. Reprinted from Analytical Chemistry, 76, Cai and Stearns, Partial Modulation Method via Pulsed flow Modulator for Comprehensive Two-Dimensional Gas Chromatography, 6064-6076, 2004 with permission from the publisher.

The pulsed flow modulator was introduced by Cai and Stearns in 2004 as a partial modulation method where only a fraction of the first-dimension separation was modulated [113]. Unlike other flow modulation techniques, the pulsed flow modulator does not use a sample loop and all of the sample is delivered to the ^{2}D column. This modulator functions by supplying either a high or low flow of carrier gas at the junction between the ^{1}D and ^{2}D columns, using a Y-connector. Two methods of modulation were possible with this technique, either positive or negative pulsed flow (Figure 1-16). With the positive pulsed flow method (PPM) (Figure 1-16A), the modulator supplies a low flow of carrier gas for a majority of the

separation with periodic pulses of high flow carrier gas. When the high flow pulse occurs, it results in a sudden and rapid decrease in the concentration of the analyte band from the ^{1}D column, seen as a negative peak by the detector. These negative peaks are separated on the ^{2}D column just like in other modulation techniques; this approach is known as vacancy chromatography. With the negative pulsed flow method (NPM) (Figure 1-16B), the modulator supplies a high flow of carrier gas for most of the separation with periodic pulses of low flow carrier gas. This results in a constant dilution of the effluent from the ^{1}D column, with a relatively high concentration plug of effluent being introduced to the ^{2}D column when the low flow pulse occurs. This was seen as a positive peak superimposed on top of the unmodulated separation. For both the PPM and NPM, the resulting signal was separated into the ^{1}D and ^{2}D signal, where the ^{2}D signal was further processed into a GC×GC chromatogram (Figure 1-16). Decoupling the ^{1}D and ^{2}D signals involved a differential equation and a deviation equation to distinguish the modulated peaks. The modulated peaks were then reconnected at the base with straight lines and the data was smoothed to obtain the ^{1}D signal. The ^{1}D signal was then subtracted from the raw signal to get the ^{2}D signal. This provided a chromatogram of the unmodulated separation (rather than a reconstruction using the modulated peaks) and a GC×GC chromatogram. However, since only some of the sample was modulated, the sensitivity was lower compared to traditional modulation techniques. Furthermore, due to the additional processing involved in generating the modulated peaks, the chromatographic peaks were not produced in the traditional sense and were described as “apparent” chromatographic peaks [114]. The only critical component in this setup was the fast solenoid valve needed to rapidly switch between the high and low flow to generate the sharp flow pulses. Since it was placed outside the GC oven, the overall design was simple and there were no temperature limits as the sample did not pass into the valve. Reproducibility was tested with a *n*-alkane mix (C_1-C_6), where the average RSD was 0.074 % for first dimension retention time and 0.070 % for second dimension retention time [113]. The modulated peak area reproducibility was found to be 20 % for C_1 and 0.61 % for C_6 [113].

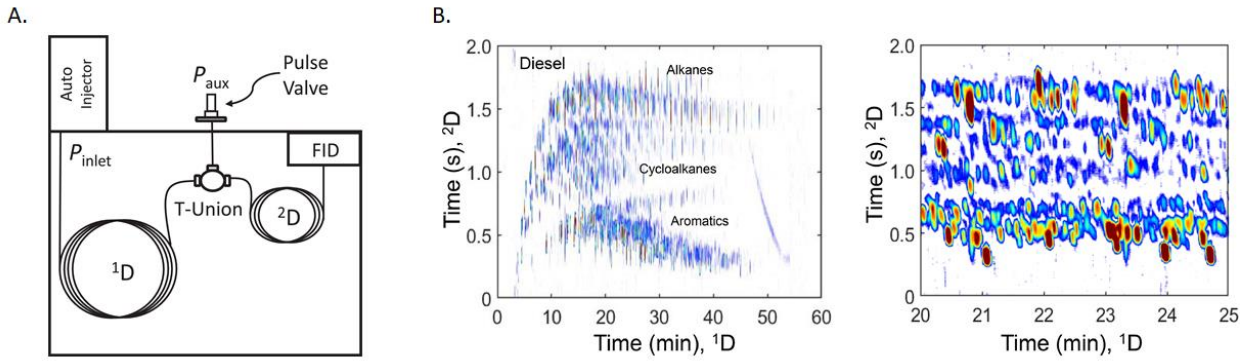

Figure 1-17: Schematic diagram of the pulsed flow modulator for dynamic pressure gradient modulation (A). A separation of diesel using dynamic pressure gradient modulation for a reverse column set, with a zoom in of the region between 20 min and 25 min (B) [115]. Reprinted from Journal of Chromatography A, 1609, Timothy J. Trinklein, Derrick V. Gough, Cable G. Warren, Grant S. Ochoa, Robert E. Synovec, Dynamic pressure gradient modulation for comprehensive two-dimensional gas chromatography, 460488, Copyright (2020), with permission from Elsevier.

The pulsed flow modulator was further explored by Synovec's group for shorter modulation periods of 500 ms or less using a commercial pulse valve [114, 116]. Unlike the 2-position valve used by Cai and Stearns [113] which provides high or low flow, the pulse valve delivers high flow or no flow. This eventually evolved into dynamic pressure gradient modulation (DPGM), a full modulation technique [115]. The fundamental components and operation of the modulator remained the same for DPGM, but the pulse width (Pw), the duration the auxiliary gas flow was OFF, was in-between the NPM and PPM modes (Figure 1-17A). In addition, the auxiliary pressure from the pulse valve was large enough to generate stop-flow conditions described first by the Górecki group [88]. Careful adjustment of the pulse width and auxiliary pressure was necessary to achieve full modulation. While the auxiliary pressure was on, it had to be sufficiently high to stop the flow of effluent from the ^{1}D column. When the auxiliary pressure was off, the effluent from the ^{1}D column was allowed to flow to the ^{2}D column for the modulation injection. DPGM with full modulation was tested using a 90 component mixture and diesel sample with an FID detector. The peak areas of the modulated and unmodulated (Pw = 0, auxiliary flow always on) peaks for pristane and 1-propanol, from the 90 component mixture, were compared and in agreement, validating the system's 100 % duty cycle. Diesel was also separated with the system using a 2.0 s modulation period and 150 ms pulse width, where the average peak widths at base were 168 ms for the second dimension and 5

s for the first dimension for a 60 min separation (Figure 1-17B). The setup also was later shown to be compatible with the TOFMS, utilizing a 4 mL/min second dimension flow to separate a 90 component mixture [117, 118].

The quasi-stop-flow modulator by Guan et al. was very similar in design to the DPGM technique, utilizing the same principles for modulation [119]. For this modulator, a 3-way solenoid valve was used rather than a 2-way pulse valve, and was installed between the inlet and the junction connecting the ^{1}D and ^{2}D columns (Figure 1-18A). This eliminated the need for an additional electronic pressure controller (EPC) for low-cost modulation. This modulator is commercially available as the QFM1200 (J&X Technologies, Shanghai, China) and from arc (Minnesota, USA) [120, 121].

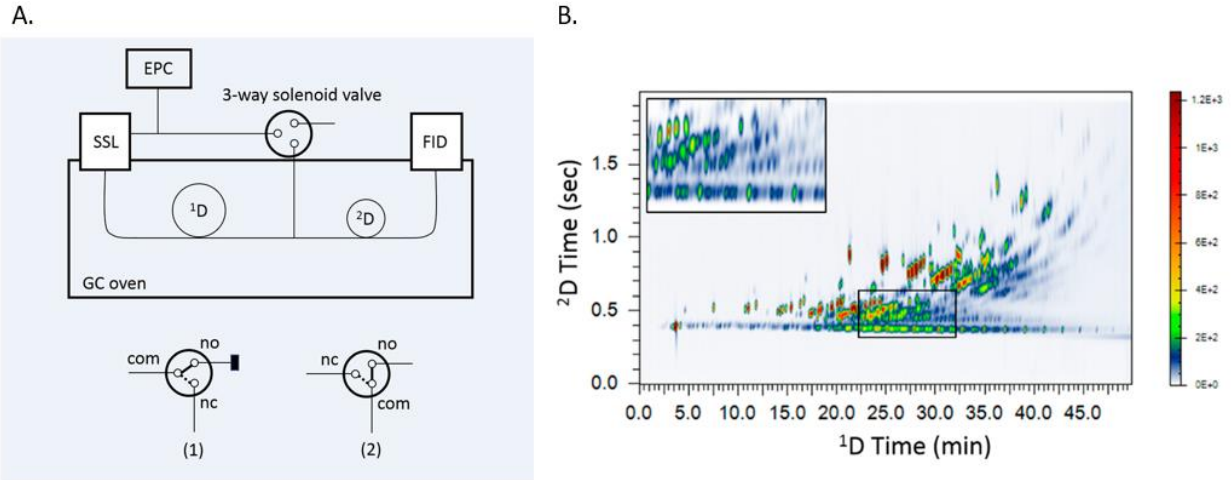

Figure 1-18: Schematic diagram of the quasi-stop flow modulator setup (A). A separation of a light oil cycle sample with quasi-stop-flow modulation (B) [119]. Reprinted (adapted) with permission from Analytical Chemistry, 92, Xiaosheng et al., Quasi-Stop-Flow Modulation Strategy for Comprehensive Two-Dimensional Gas Chromatography, 6251-6256, Copyright (2020) American Chemical Society.

1.3 GC×GC Method Optimization

Although a GC×GC instrument can be assembled relatively easily using common GC components and a modulator, its optimization is much more complicated. In addition to having an extra column and modulator to optimize, many parameters are interconnected. Figure 1-19 illustrates how each parameter can affect other parameters in GC×GC using thermal modulation. This makes optimization a balancing act

to get the best separation out of both dimensions [122]. The key parameters to consider in optimization includes the stationary phase combination, column dimensions, carrier gas flow rates, temperature program, modulator parameters, and detector.

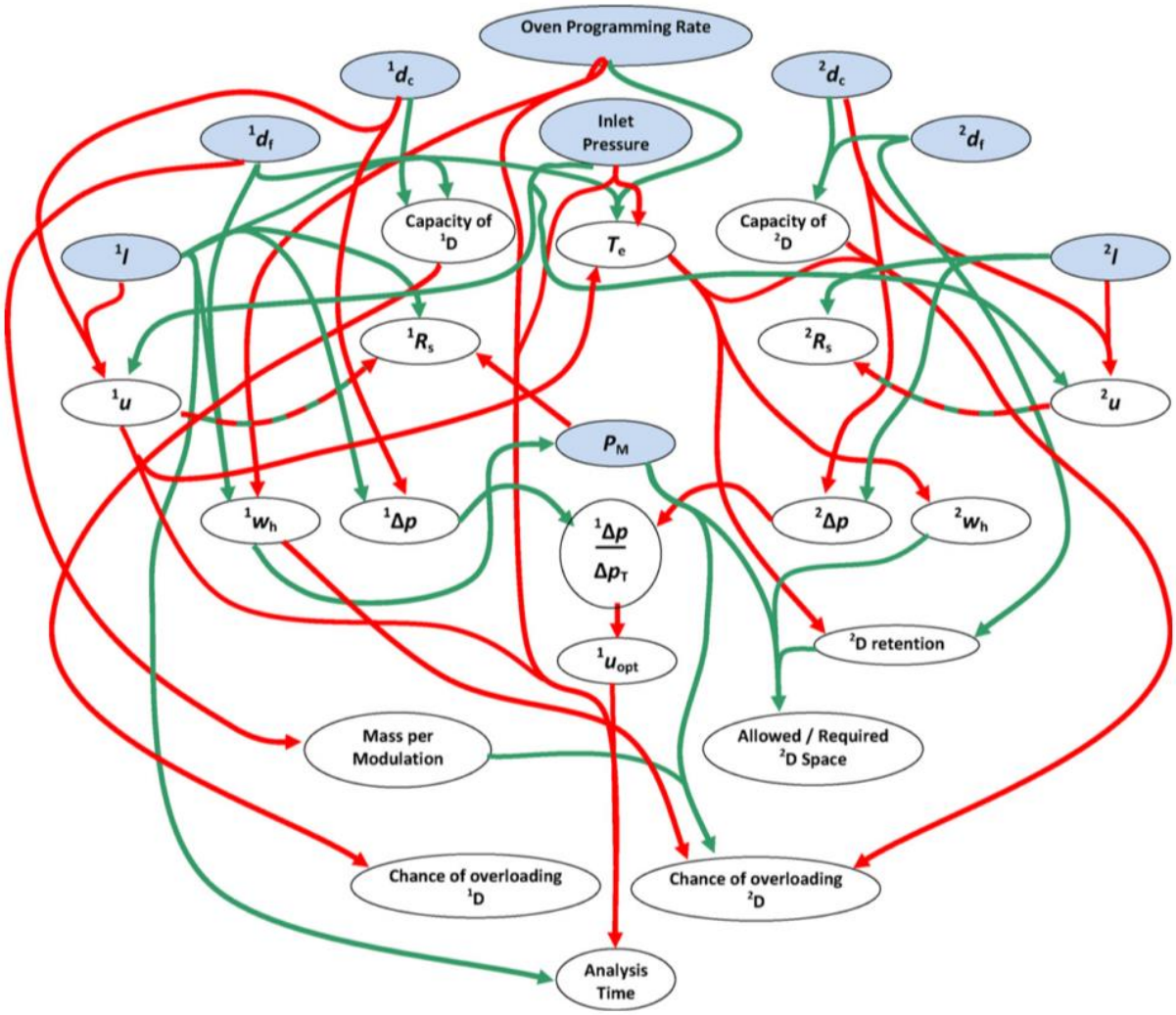

Figure 1-19: Schematic diagram of the interconnected parameters in GC×GC. Individual parameters are within ovals, with user-controlled parameters in blue. Green arrows point to parameters which increase with the input parameters while red arrows point to parameters which decrease as the input parameters increase [122]. Reprinted from Journal of Chromatography A, 1255, A. Mostafa, M. Edwards and T. Górecki, Optimization aspects of comprehensive two-dimensional gas chromatography, 38-55, Copyright (2012), with permission from Elsevier.

1.3.1 Column Configuration

The column set used for a GC×GC separation will likely depend on what is already available in the lab. In the separation of petrochemicals, the "standard" or "normal" column set as well as the "reverse"

column set are typically used. The normal column set is the combination of a non-polar ^{1}D column, typically a 100 % PDMS or a 5 % diphenyl/95 % PDMS, and a polar or mid-polarity ^{2}D column like a polyethylene glycol (PEG) or 50 % diphenyl/50 % PDMS. The reverse column set reverses the polarity of the ^{1}D and ^{2}D, utilizing a polar or mid-polarity ^{1}D column and a non-polar ^{2}D column. In the separation of diesel, this can lead to improved separation of alkanes (linear and branched) and naphthenes (cycloalkanes) in the ^{2}D compared to the "normal" setup, which is better for separating the aromatics in the ^{2}D [123]. Other stationary phases are available and may be more suitable depending on the analytes of interest. Stefanuto et al. utilized a reverse column set with a trifluoropropylmethyl polysiloxane stationary phase in the ^{2}D for its selectivity and peak shape for the separation of alcohols and esters [124]. Literature search of GC×GC separations with similar sample compositions should provide a good starting point for the choice of stationary phase combination and order.

Column length, to a degree, depends on the modulator used, where the Insight flow modulator by SepSolve which utilizes a large flow in the ^{2}D requires longer columns (2 - 10 m) to make up for the loss in efficiency due to the high linear gas velocity. For thermal modulators which utilize a single column train and flow rate, ^{2}D column lengths are typically 0.3 - 1 m. Early works in GC×GC typically utilized a narrower ^{2}D column to achieve fast and efficient separations within the modulation period [122]. However, if the ^{2}D column becomes overloaded, which is much more likely with narrow-bore columns, it becomes less efficient than 0.25 mm and 0.32 mm columns when those are not overloaded [125]. Klee et al. demonstrated that a peak capacity gain for a GC×GC system of nearly 9 times over a GC analysis with the same analysis time and detection limit was possible [126]. This requires narrow reinjection pulses from the modulator, identical diameters for the ^{1}D and ^{2}D columns, a long ^{1}D column, and optimal conditions for flow rate and temperature programming rate.

1.3.2 Modulator Parameters

For GC×GC systems with thermal modulators, optimizing the flow rate is not too different from GC, particularly when column diameters are identical between the ^{1}D and ^{2}D columns. A good starting point is using a flow rate with optimal linear velocity for the ^{1}D, which can then be adjusted from there based on the separation. For differential flow modulators, an additional consideration is the flow ratio between ^{2}D and ^{1}D. Since flow modulators do not have a focusing effect like thermal modulators, re-injection of the stored effluent from the sample loop results in analyte plugs which retain the shape of the ^{1}D peak, leading to skewed peaks [127]. The analyte plug width [Eq. (1.1)] depends on the modulation period (P_M) and the flow ratio (ratio of flush and fill rates in the modulator).

$$Plug\ width\ \cong \frac{P_M}{Flow\ Ratio} \tag{1.1}$$

Whether it is thermal or flow modulation, the main parameter to consider is the modulation period as this factor affects both the ^{1}D resolution and ^{2}D separation space. For the ^{1}D separation to be maintained, the modulator needs to sample the effluent from the ^{1}D column with sufficient frequency to not lose the resolution already achieved. One of the most referenced papers devoted to sampling rate in multidimensional chromatography is Murphy et al. from 1998 [128]. Although the study was dedicated to comprehensive two-dimensional liquid chromatography (LC×LC), it was just as applicable to GC×GC. The paper concluded that each separated ^{1}D peak needs to be sampled at least three times. This sampling rate, that is so critical in maintaining the ^{1}D resolution, is well known in GC×GC as the modulation ratio (M_R) [129]. M_R is calculated with Eq. (1.2), where W_b is the peak width at the base, P_M is the modulation period, and $^1\sigma$ is the standard deviation of a ^{1}D Gaussian peak [129].

$$M_R = \frac{W_b}{P_M} = \frac{4 \cdot {}^1\sigma}{P_M} \tag{1.2}$$

Over sampling the ^{1}D effluent is also undesirable since it reduces the duration of the ^{2}D separation and lowers the ^{2}D peak capacity. The M_R for typical GC×GC separations should be 2 to 4 [130].

1.3.3 Temperature Programming Rate

Since the ^{2}D separation is very fast, it is always practically isothermal [122]. In GC×GC, both columns can be placed in the same oven, or a secondary oven can be used to house the ^{2}D column. The disadvantage of a single oven system is the dependency of the ^{2}D separation temperature on the ^{1}D elution temperature. A slow temperature programming rate results in wider ^{1}D peaks, easing the restriction on the modulation period for longer ^{2}D separation. However, it also leads to longer analysis times and lower elution temperatures from the ^{1}D. In single oven setups, the stronger interaction with the ^{2}D stationary phase at lower temperature increases the risk of peak wraparound. This risk is alleviated, however, with the use of a secondary oven, which can be kept at a temperature higher than that of the primary oven. An interesting effect of temperature programming is that with each modulation period, the isothermal separation in the ^{2}D occurs at a slightly higher temperature. With a fast-enough rate, this might result in a noticeable downward trend in the elution pattern of the analytes.

1.3.4 Detectors

With some flow modulators, peaks as narrow as 16 ms at the base are possible [131]. Proper detection thus requires detectors with low time constants, low internal volumes, and high data acquisition rates [122]. This is necessary to prevent detector-induced band broadening and for proper peak reconstruction with at least 10 points per peak required for quantitative analysis. For example, a 100 ms wide peak requires at least a 100 Hz data acquisition rate. An additional consideration is the high ^{2}D flow with differential flow modulators. This makes pairing with mass spectrometers more difficult due to their limited maximum operational flow rates [110, 112]. The solution to the high flow rates is usually the use of a splitter for dual detection (flame ionization detector/MS) where only a portion of the flow is diverted

to the mass spectrometer for identification. The ideal detector should accurately reconstruct the elution profile without affecting the chromatographic separation [132].

The earliest detector used with GC×GC, since its inception with the TDM [7], was the flame ionization detector (FID). Characterized as a universal detector and a workhorse in GC, it is one of the few detectors that easily meets the data acquisition rate requirements, as it can operate at up to 500 Hz. In addition, it has a low dead volume and low time constant, as well as a detection limit in the low pg C/s and a wide linear dynamic range of 10^7. Furthermore, its simplicity, reliability, and stability made it a popular detector for many GC×GC methods [133, 134, 135, 136]. Selective detectors have also been coupled with GC×GC, including the electron capture detector (ECD) [74, 132, 137, 138], flame photometric detector (FPD), sulfur chemiluminescence detector (SCD), nitrogen chemiluminescence detector (NCD) [139], and nitrogen phosphorus detector (NPD) [132, 140, 141]. The vacuum ultraviolet (VUV) detector has also been used with the ability to simultaneously collect VUV absorption data between 115 – 240 nm at a data acquisition rate of 100 Hz [142]. Groger et al. reported the first use of the VUV detector with GC×GC [143]. The high sensitivity from the larger absorption cross section compared to IR, fast detection, and most importantly, the structural information for isomeric differentiation makes this a highly sensitive and selective detector for GC×GC.

With the complexity of samples that are analyzed by GC×GC, utilization of reference materials for peak assignment is impractical when thousands of components are separated. To characterize the individual peaks and their structures, the power of mass spectrometers is necessary [144]. GC×GC coupled with MS (GC×GC-MS) provides a third dimension of analysis, with substantially more qualitative information. The advantage of GC×GC-MS over GC-MS lies in the improved resolution achieved through the two dimensions of chromatographic separation and band compression from the modulator [144]. Furthermore, the higher purity of analytes that enter the mass spectrometer and group type separation of compounds provide greater confidence with identification [144]. The type of mass spectrometer most

used with GC×GC is TOFMS. The clear advantage of a TOFMS compared to other available MS is their very high data acquisition speed [144]. Early hyphenation of TOFMS to GC×GC used low-resolution TOFMS (LR-TOFMS), combining high acquisition rate, spectral deconvolution ability and high sensitivity. Combining the separation power of GC×GC and extracted ion chromatograms (EIC), much of the overlap between peaks and matrix interferences can be reduced for both targeted and untargeted analysis of complex samples [145, 146, 147, 148, 149, 150, 151, 152, 153]. The combination of GC×GC with HR-TOFMS provides a full spectrum of higher resolution and mass accuracy at the cost of reduced data acquisition rates. The LECO Pegasus GC-HRT 4D is one commercially available GC×GC-HR-TOFMS system with acquisition rates of up to 200 Hz. A downside to the TOFMS is high cost.

QMS was first coupled with GC×GC by Frysinger and Gaines in 1999 [154]. However, early QMS detectors did not have the acquisition rates needed for quantitative GC×GC. This is due to the operating principle of the QMS, where only one m/z passes through the quadrupole at a time. Thus, the spectra generation rate is dependent on the scan speed, the interscan delay and the mass range desired. Another consideration with using a QMS is the possibility of spectral skewing when ion concentrations change in the ion source during a single scan. This is due to the narrow peaks generated by GC×GC, resulting in concentration changes during a scan, which in turn leads to inconsistent ion ratios [155]. Although the TOFMS and QMS have been the dominant instruments used with GC×GC, other mass spectrometers like the triple-quadrupole MS (QqQMS) [104, 156, 157, 158, 159], and isotope-ratio MS (IRMS) [160, 161] have also been used.

Other technological advances related to GC×GC-MS concern the ion source. Markes International (Llantrisant, UK) has patented and released a tandem ionization source for their TOFMS, providing simultaneous acquisition at 70 eV and soft electron ionization (EI) [162]. LECO Corp. has also released a Multi-Mode Source™ (MMS™) which provides EI, positive chemical ionization (PCI) and negative chemical

ionization (NCI) without needing any hardware changes [163]. Both sources provide additional information for greater confidence in compound identification.

1.4 General Elution Problem

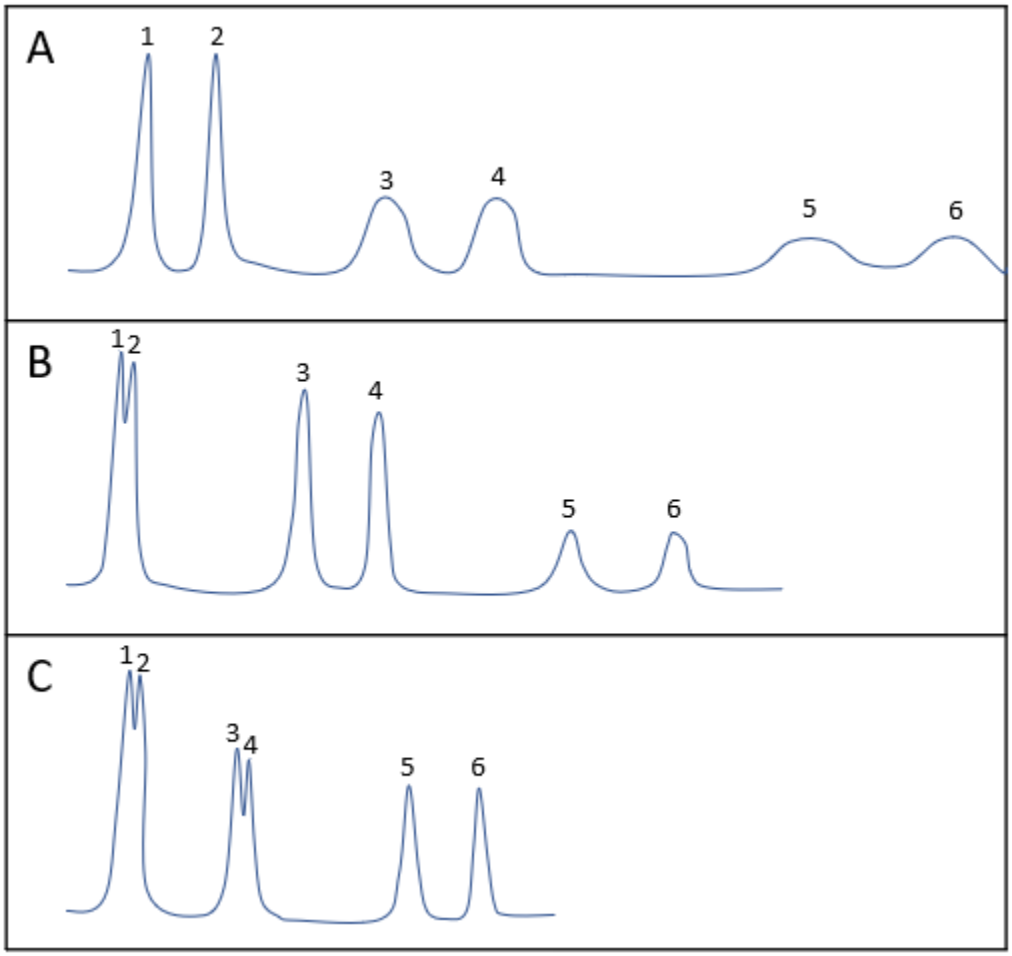

Figure 1-20: Example of a separation of a mixture containing compounds with a wide range of retention factors. Each peak pair (1 & 2, 3 & 4, 5 & 6) has significantly different retention factors and requires a different set of conditions (A, B, C) for optimal separation of each pair. Separation A is optimized for the weakly retained compounds (1, 2), resulting in peak broadening for the more retained compounds (3, 4, 5, 6). Separation B is optimized for peaks 3 and 4, resulting in coelution of peaks 1 and 2, and the broadening of peaks 5 and 6. Separation C, optimized for peaks 5 and 6, results in coelution of peaks 1 & 2, and 3 & 4.

The general elution problem, described in the 1960s, is where no single set of conditions is sufficient for the separation of a sample containing analytes with a wide range of retention factors (*k*) [164]. The retention factor of a component is dependent on the amount of time a component is retained by the column. Shown in Figure 1-20 is an illustration of the general elution problem for a simple 6 component

mixture. Each pair of components, 1 & 2, 3 & 4, 5 & 6, represents very different *k*, and are optimally separated under different conditions (A, B, and C). The separation condition (A), optimal for peaks 1 & 2, results in significant peak broadening for the more strongly retained peaks of 3 - 6, while the optimal condition for peaks 5 & 6 (C) results in coelution for peaks 1 - 4.

Thus, it has long been recognized that complex samples containing a wide range of retention factors, require some form of *k* programming for optimized separation [165]. This is typically accomplished by gradient elution in high performance liquid chromatography (HPLC) or temperature programming in GC. In 1962, Giddings reasoned that a majority of an analyte's movement through a column occurs near its elution temperature [166]. Under typical operating conditions, the fraction of the analyte in the vapour phase doubles for approximately every 30 °C increase in temperature (20 °C to 40 °C depending on GC temperature and boiling point) [166]. Thus, it could be imagined that at low temperatures at the start of a temperature program, high boiling point compounds are essentially stationary at the head of the column. It is not until the temperature is near an analyte's elution temperature that it starts migrating at a noticeable rate. It is because of this that one can achieve near constant peak width in a temperature programmed separation, thus improving peak capacity.

1.4.1 Temperature Programming Systems

Temperature programming systems can essentially be broken down into the three areas: heating, measurement, and control. For a GC oven, heating is accomplished by a heating element and the hot air is circulated with a fan. The result is a convection oven for uniform heating of a GC column. A temperature sensor is used to provide feedback to a controller which handles the temperature control. The downsides of a traditional GC oven are its large size, slow heating rates, and high power consumption. To combat these issues, the GC oven sizes have decreased over time and research on resistively heated GC columns

has been explored. Detailed reviews on the developments of resistive heating for GC columns have been published [167, 168].

1.4.1.1 Resistively Heated GC Columns for Rapid Temperature Programming

Resistive heating of the column rather than the GC oven can significantly reduce the space and power needed to heat the column. This is especially important for portable instruments which have size constraints and run on batteries. In order to resistively heat a column, three main approaches have been developed: coaxial, collinear, and direct resistive heating.

The coaxial design resistively heats a conductive tube in which the fused silica column is housed. Erhmann et al. designed and compared a coaxial and collinear column heater to a standard GC oven (HP 5890) [169]. The coaxial heater resistively heated a stainless steel tube with silver plating. The plating was used to reduce the electrical resistance of the tube. A capillary column and sensor wire were inserted into the stainless steel tube and the whole assembly was inserted into Teflon tubing for insulation. A computer set the operational parameters while a microcontroller maintained the set temperature or temperature program via pulse width modulation to adjust the heating. In the preliminary evaluation of the coaxial and collinear designs, it was found that like other cladded designs, the silver plating tended to peel off due to the different thermal expansion coefficients of the materials. This led to hot spots which damaged the insulation of the sensor wire, and ultimately the approach was abandoned. The EZ Flash system from Thermedics Detection Inc. (Chemsford, MA, USA) was the first coaxial resistive heating system designed to upgrade a standard GC to a fast GC [170]. A standard GC column was inserted into a 5 m or 10 m metal tube, which was resistively heated, and the temperature was determined based on the electrical resistance of the metal tube. The system could be heated at rates of up to 1200 °C/min, and the temperature was measured every 10 ms for temperature control. Both coaxial designs described thus far relied on the heated inlet and detector from a standard GC, and both were installed inside the GC oven. As a slight departure from the typical setup, Fialkov et al. designed a low thermal mass fast GC which

utilized the coaxial design, but the column was situated outside the GC oven [171]. The low thermal mass design utilized a 0.53 mm i.d. MXT guard column (Restek Corporation) for resistive heating, in which a standard GC column was inserted. The whole device was mounted on top of the GC, on the detector plate, where the inlet and outlet of the assembly were situated at the inner edge of the GC oven wall. The GC inlet and detector were connected to the inlet and outlet of the device, respectively, through the GC oven, which essentially served as a heated transfer line. A temperature calibration table made by measuring the temperature (via thermocouple) and the current was used to determine the column temperature based on the current.

The collinear design uses a heating wire which is wrapped around the fused silica column and resistively heated. The collinear design is the more common design used in commercial fast GC systems. Agilent currently provides the LTM Series II system which is installed on the outside of an Agilent 7890/8890 GC, making use of the instrument's injector and detectors [172]. This system has been demonstrated for both fast GC analysis and for use in GC×GC for a ^{2}D temperature offset [173]. Valco provides a Fast GC column and fan modules that are built to order, based on the user's needs. Columns of 1 m × 0.1 mm to 30 m × 0.53 mm can be requested [174]. Due to the design of these column bundles, where heater wire and temperature sensors need to be integrated into a tightly wrapped insulated bundle, changing columns and adjusting column dimensions becomes much more difficult as these must be done by the manufacturer. However, one benefit of these fast GC systems is a tightly integrated heating, temperature measurement, and cooling system optimized by the factory to minimize user mistakes.

Direct resistive heating uses a column coated with a conductive layer or a column made of a conductive material for heating. Hail and Yost resistively heated a commercial aluminum-clad capillary column for use as a compact GC probe for GC-MS [175]. The 2.3 m aluminum clad column was covered with a glass braid insulation and wrapped around a PTFE spool, where the ends were connected to a DC power supply. The temperature was determined from the column resistance using a resistance vs

temperature curve. The system provided average heating rates of 8.7 °C/s and cooling rates of 2.7 °C/s. However, the low resistance of the aluminum made precise temperature measurements difficult at low temperatures. In addition, it was found that the difference in thermal expansion of the aluminum and fused silica caused the coating to rupture after a few temperature cycles [169]. The thermal desorption modulator by Phillips also utilized a direct resistive heating design, in which an electrical pulse was applied to a gold film painted on a capillary column [7]. This idea has also been applied by Phillips in fast temperature programming for GC analysis, where electrically conductive paint was used on a fused silica capillary column [176]. However, painting a fused silica column results in more problems in robustness. In addition to the difference in thermal expansion coefficients, the coating uniformity was a significant issue, causing frequent burnouts. Nickel clad columns have also been explored by Stearns et al. for direct resistive heating gas chromatography [177]. Nickel was chosen due to the large temperature coefficient of resistance, to allow for more accurate temperature monitoring based on resistance. Compared to a standard GC oven, the nickel clad column resulted in a 4.4 % decrease in theoretical plates number. This was attributed to the unevenness of the heating, which could be due to the material non-uniformity, the structure of the column bundle, and/or the column mounting system. Straying away from the metal-coated columns, Xu et al. used a commercial stainless steel column for direct resistive heating [178]. Stainless steel columns eliminate the issue of incompatibility of the thermal expansion coefficients between the conductive metal layer and the fused silica column. This improves the ruggedness of the system but introduces other issues. Compared to nickel or aluminum, stainless steel has a lower temperature coefficient of resistance. This results in a smaller electrical resistance change with temperature (Ω/°C), making temperature measurements based on resistance more difficult. This was likely why a 0.003” type k thermocouple was used for temperature measurement. The system was capable of 10 °C/s heating rate; however, even a short 2.2 m column required 50 V to achieve a 5 °C/s heating rate.

1.4.1.2 Methods of Temperature Measurement

Modern GC ovens use a resistance temperature detector (RTD) to measure the temperature of the air circulating inside. An RTD consists of a resistor whose resistance changes with temperature in a predictable manner. In order to measure the resistance, a current needs to be passed through the resistor, which can lead to errors due to self-heating. In addition, depending on the wire configuration (2, 3, or 4 wire), the resistance of the lead wires and connections can also contribute to the overall resistance resulting in measurement errors. The most popular and accurate RTD is the Pt100, which uses platinum wire with a resistance of 100 Ω at 0 °C. Other materials can be used for RTDs, like nickel and copper, but platinum is the most popular since it can withstand high temperatures, has excellent stability, and resists corrosion or oxidation. In addition, the temperature vs. resistance curve is fairly linear over a very wide temperature range (-200 to 650 °C) [179].

A thermocouple consists of two dissimilar metals joined together at two ends (junctions). When one junction is heated or cooled, a net electromotive force is generated, creating an electric current in the circuit. This is known as the Seebeck effect [180]. By opening the circuit to measure the potential difference (Seebeck voltage), one can determine the differential temperature based on the metals used and the voltage produced [181]. The magnitude of the electromotive force can be represented by Eq.(1.3), where E is the Seebeck voltage, α is the Seebeck coefficient for the material, and T is the temperature [182].

$$dE = \alpha_{A,B} dT \tag{1.3}$$

The popularity of the thermocouple is due to its simplicity, low cost, and robustness, with a variety of probes to suit the situation and many combinations of metals for different temperature ranges to be measured. One advantage of thermocouples over an RTD, besides cost, is its response time or time constant (time required for a 63.2 % step change in temperature at specified conditions). For an exposed 0.001“ diameter thermocouple, its time constant for air at room temperature and atmospheric pressure

is 0.003 s [183]. However, RTDs are generally more accurate than thermocouples which have a nonlinear temperature vs resistance relationship [184]. Consequently, for applications like a GC oven which operates at temperatures compatible with both the RTD and thermocouples, the RTD is preferred due to its accuracy and stability. Due to the extensive use of thermocouples in this research, its theory of operation is explained in greater detail.

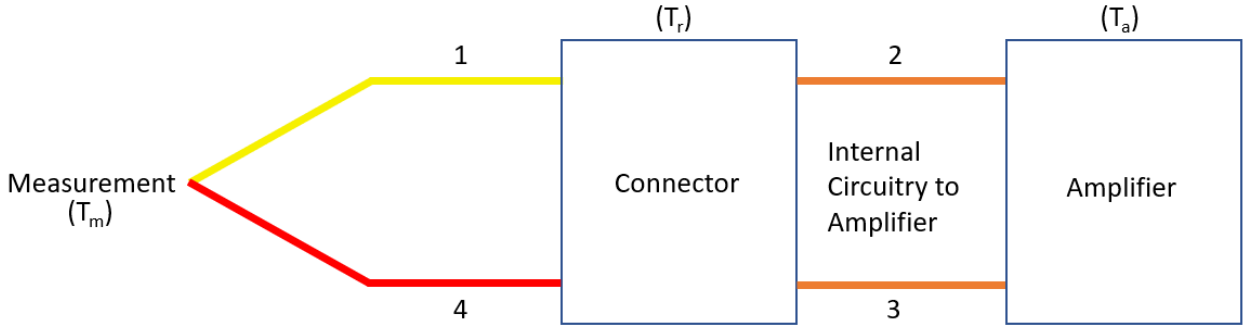

Figure 1-21: Basic K-type thermocouple configuration. Wiring: copper (orange), chromel (yellow), alumel (red).

A simple configuration of a K-type thermocouple is shown in Figure 1-21. This circuit consists of three different metals, chromel, alumel, and copper, forming three junctions. The net electromotive force can be represented by Eq.(1.4).

$$E = \int_{T_r}^{T_m} \alpha_{chromel}\, dT + \int_{T_a}^{T_r} \alpha_{copper}\, dT + \int_{T_r}^{T_a} \alpha_{copper}\, dT + \int_{T_m}^{T_r} \alpha_{alumel}\, dT$$

$$E = \int_{T_r}^{T_m} \alpha_{chromel}\, dT + \left(\int_{T_a}^{T_r} \alpha_{copper}\, dT - \int_{T_a}^{T_r} \alpha_{copper}\, dT \right) - \int_{T_r}^{T_m} \alpha_{alumel}\, dT$$

$$E = \int_{T_r}^{T_m} \alpha_{chromel}\, dT - \int_{T_r}^{T_m} \alpha_{alumel}\, dT$$

$$E = \int_{T_r}^{T_m} \alpha_{chromel,alumel}\, dT, \qquad where\ \alpha_{chromel,alumel} = \alpha_{chromel} - \alpha_{alumel} \tag{1.4}$$

The electromotive force due to the copper wiring which connects to the amplifier from the connector has no effect on the net electromotive force. This is due to the Law of Intermediate Metals [180]. This is where any number of dissimilar metals can be introduced to the circuit without an effect on the net

electromotive force, as long as the junctions are at the same temperature. In all likelihood, the internal circuitry composed of the metal wiring and soldering are in such close proximity, that the temperature is uniform. This is how a measurement device for thermocouples do not affect the electromotive force.

It is important to remember that thermocouples are not a measurement of the absolute temperature, but always a differential measurement between two points. In order to determine the measurement temperature, the reference temperature needs to be known. This is accomplished by cold junction compensation or reference junction compensation. Cold junction compensation is accomplished by submerging the connections at T_r into an ice bath (0 °C) allowing the absolute temperature of T_m to be measured. Reference junction compensation is accomplished using another temperature measurement device, such as a thermistor, diode, or RTD, to compensate for the reference junction temperature.

Infrared (IR) sensors have also been used in flow field thermal gradient GC for column temperature measurement [185]. The thermal gradient GC used a coaxial resistive heating design with a commercial fused silica GC column inserted into a fixed stainless steel capillary, where IR sensors were used to monitor its temperature. IR sensors use a lens to focus the IR energy from an object onto a detector, which converts it into an electrical signal proportional to the temperature [186]. The advantage of IR sensors, as demonstrated by the flow field thermal gradient GC, is when a contact-less measurement is desired. Thermocouples and RTDs require direct contact with the object, which can affect the temperature of the object due to the change in thermal mass or other conditions due to the attachment.

Thermistors are very similar to RTDs, in which the temperature is measured based on the resistance. However, unlike RTDs which use pure materials, thermistors use semiconductors which have resistance greater than conductors but lower than insulators [187]. One application of thermistors remotely related to GC is the thermal conductivity detector (TCD), which measures the thermal conductivity of the carrier gas [188, 189]. This detector is typically used for detecting permanent gases. Although thermistors are

highly accurate, they have limited temperature ranges, making them unsuitable for GC column temperature measurements.

1.4.1.3 Microcontrollers and Single-Board Computers

For electronics projects, two platforms popular among students, hobbyists, or professionals in the industry are Arduino and Raspberry Pi. Although the two platforms are comparable in size and can control different electronic components, deciding on the appropriate one to use depends on the project as well as the existing user's familiarity with either platform.

The Arduino is an open-source electronics platform featuring easy to use microcontrollers (Arduino boards) and software written in the Arduino programing language [190]. Various Arduino boards are available, where each board features a microcontroller and varying amounts of static random-access memory (SRAM), flash memory, operating voltage (3.3 or 5 V), and a set of general purpose input/output (GPIO) pins. The overall size and cost of each board vary, and they may also have some unique built-in components like the Arduino Nano 33 BLE Sense which has many embedded sensors [191]. The Arduino programming language is based on Wiring, which is also an open-source programming framework [190, 192].

The Raspberry Pi is a single board computer, which comprises of all essential computer components including the central processing unit (CPU), graphics processing unit (GPU), storage, random-access memory (RAM), input/output (IO), and operating system (OS). The Raspberry Pi runs on a Linux-based OS and is used like a traditional computer, with a mouse, keyboard, and display. It also includes many features like WiFi and Bluetooth, and significantly more RAM and processing power compared to an Arduino. A microcontroller (RP2040) has also been released recently to compete with the Arduino, the Raspberry Pi Pico. It is a microcontroller with an Arm® processor, 26 GPIO pins, serial peripheral interface (SPI), inter-

integrated circuit (I2C), and universal asynchronous receiver-transmitter (UART) connections, and 16 pulse width modulation (PWM) channels [193].

Both the Arduino and Raspberry Pi are very popular, and each platform has its own advantages. The Arduino is generally less expensive and much simpler to use compared to the Raspberry Pi computers. It was built to be interfaced with various sensors, motors, LEDs, buttons, and other electronic components, and designed to complete a single or a few tasks repeatedly. Additional functionality can be added to the Arduino, such as WiFi, motor driver, or an SD card reader through the use of Arduino Shields (boards which plug into the Arduino pin headers). Some Arduino boards may have WiFi or other functionality built in. The Raspberry Pi computer is a more powerful device that runs on an operating system, allowing one to use multiple applications or develop their own applications. Although the strength of the Raspberry Pi computer is in providing an inexpensive platform for software development, it also has a set of 40 GPIO pins which can connect to electronic components. The combination of software and electronics is what allows the Raspberry Pi computer to accomplish more complex projects.

The release of the new Raspberry Pi Pico board with the recently designed microcontroller chip, the RP2040 (Jan 21, 2021), made the distinction between choosing a Raspberry Pi or Arduino somewhat blurred [194]. The Raspberry Pi Pico ($4 USD, April 13, 2022) is a recent product that is less expensive than the comparable Arduino Nano Every ($12.90 USD, April 13, 2022) [194, 195]. It can be programmed in C/C++ or MicroPython (Python 3 for microcontrollers). This product provided users with an inexpensive option when one did not want to develop on the Arduino platform, while providing a microcontroller than had more processing power than the ATMega4809 in the Arduino Nano Every. However, since the RP2040 design was licensed to other manufacturers, Arduino released their own RP2040 based microcontroller board (Arduino Nano RP2040 Connect) which is compatible with the RP2040 ecosystem of software and the Arduino programming language. This gave users even more choices for processing power,

programming language, and board specifications (number of analog and digital pins, input voltage, communication, connectivity).

1.4.1.3.1 Arduino Sketch

Since the Arduino was utilized in the ²D temperature programming system design for sections 3 and 4, the basics of an Arduino program are discussed. An Arduino program, known as a sketch, is typically written in the Arduino Integrated Development Environment (IDE). A sketch consists of variables and functions; variables are the storage space for values, while functions are blocks of code that are reusable throughout a program. Libraries to be included (`#include`) and global (accessed throughout the program) variables are defined at the beginning of a sketch, with or without a value. The body of a function is encapsulated between `{}`, and is executed when the function is called. In addition, comments can be included within the sketch to describe the function or purpose of areas of code. All text following a `//` for that line are comments. The two basic functions in an Arduino sketch are `setup()` and `loop()`. As the name implies, `setup()` sets up the Arduino and defines its initial state when it first boots. This is where the I/O pins are defined as input or output, variables could be given their initial values, and libraries are initialized. The `setup()` function is only executed once in the sketch upon boot. After `setup()` is completed, the `loop()` function is called. The body of code within the `loop()` function is called repeatedly until the Arduino is either RESET or powered OFF. Both the `setup()` and `loop()` functions must be in the sketch, whether or not they are used. Libraries are sets of code that provide new functions or are used to run specific components (e.g. thermocouple sensors, LCD screen, etc.). Some libraries are standard with the Arduino software and provide basic functions like controlling the I/O pins, while others can be downloaded through the software's library manager or imported in compressed .zip format. After a sketch is written, it is compiled to turn the code into machine language, combined with the standard Arduino libraries, and an Intel hex file is generated and written to the Arduino board.

1.5 Thesis Objective

The focus of instrument development in GC×GC has primarily been on the development of new modulators. This is understandable, as it is the core component of any GC×GC system and the foundation of the ^{2}D separation, being equivalent to an autosampler/inlet of the ^{2}D. However, just like how an autosampler and inlet is important in a GC system, the GC oven is also a critical component in the separation technique. It is this area of instrument development in GC×GC which has largely been neglected. The only device analogous to the GC oven for the ^{2}D column is the secondary oven. Although the secondary oven is significantly smaller than a standard GC oven, the thermal mass is still relatively large. This results in heating and cooling rates similar to a GC oven, allowing a user to set the ^{2}D column at a temperature offset from the ^{1}D column. However, due to the short duration of the ^{2}D separation in GC×GC, the ^{2}D column is still effectively isothermal within the timespan of a modulation period.

The problem that arises with isothermal separations is the general elution problem discussed in section 1.4. Although it can be argued that the effluent being re-injected into the ^{2}D column contains pre-separated fractions with similar *k*, optimal stationary phase combinations which maximize the 2D separation space often result in the components being injected into the ^{2}D to have very different *k*. This can result in wraparound peaks which can co-elute with separated peaks in the subsequent modulation period. This phenomenon is analogous to carry-over in GC, where compounds that have not eluted in the previous separation are eluting in the subsequent separation as a “ghost” peak.

The typical solution to this issue is to reduce the ^{2}D column length, use a faster GC temperature program to achieve a higher elution temperature, increase the flow rate, change stationary phase (to reduce retention), or apply a positive temperature offset to the ^{2}D column with a secondary oven (Figure 1-22B). Each solution, however, suffers from the general elution problem, which tends to compromise the separation of the less retained compounds. The thesis objective is the development of a ^{2}D temperature

programming system (²DTPS) for GC×GC, which can increase peak capacity and eliminate wraparound peaks, as shown in Figure 1-22C.

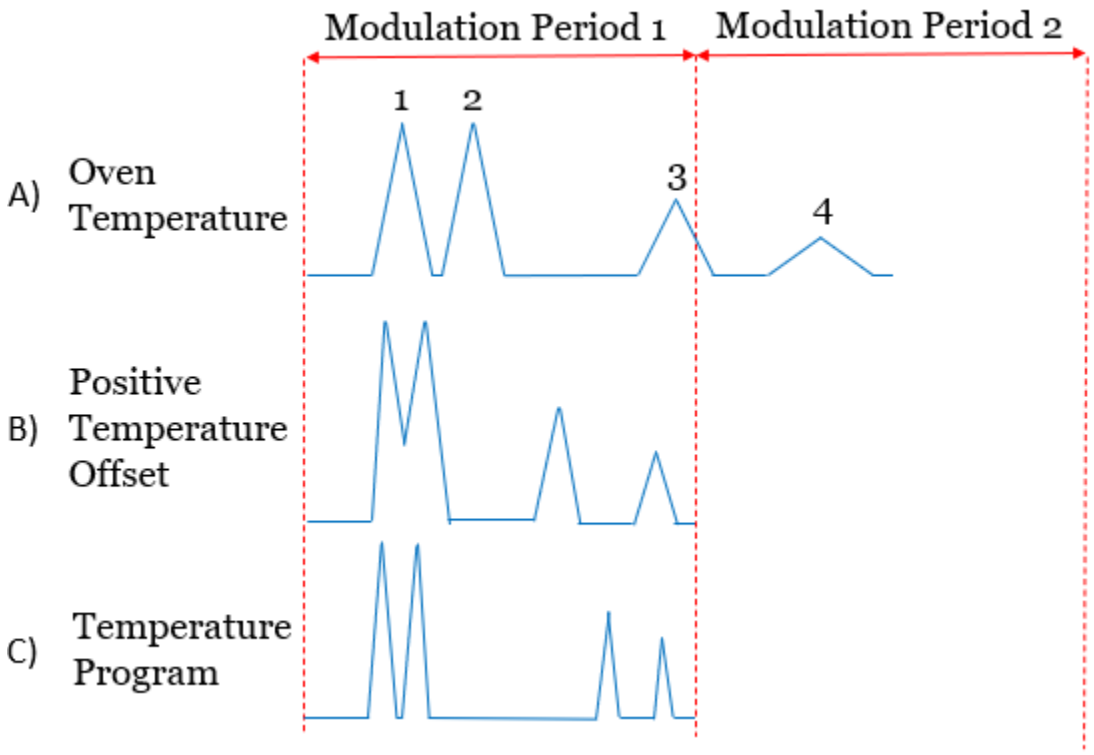

Figure 1-22: Separation of a single fraction injected into the ²D column under three conditions. (A) At oven temperature optimal for peaks 1 and 2. (B) At a positive temperature offset which eliminates wraparound peaks, but results in coelution of peaks 1 and 2. (C) Temperature programming separation to maximize peak capacity within the limited separation space.

During this process, different areas of focus were addressed in a straightforward step by step manner as the ²DTPS evolved from a proof of concept to its final design. The first area of focus was the heating and cooling system, to develop a device that can reliably heat and cool the column at temperature programming rates suitable for the short duration of the ²D separation. Following this proof-of-concept design was the addition of temperature control through the use of an Arduino which acted as a PID controller. This design was finally improved upon to create a more robust temperature measurement and control system that was more tightly integrated with software to improve the overall user experience. Throughout the development, diesel was a common sample of choice due to the abundance of components in the sample which uniformly cover the 2D separation space to provide a visual diagnostic.

Most components in diesel are relatively non-polar and their elution pattern is primarily affected by temperature, the parameter of focus when developing this ^{2}DTPS. Any errors in the ^{2}D temperature profile, whether random or systemic, would be noticed in the GC×GC chromatogram. The ^{2}DTPS envisioned should be capable of accomplishing all three ^{2}D temperature profiles illustrated in Figure 1-23, where more than one ^{2}D temperature program can be used in a single GC×GC separation for optimal 2D separation.

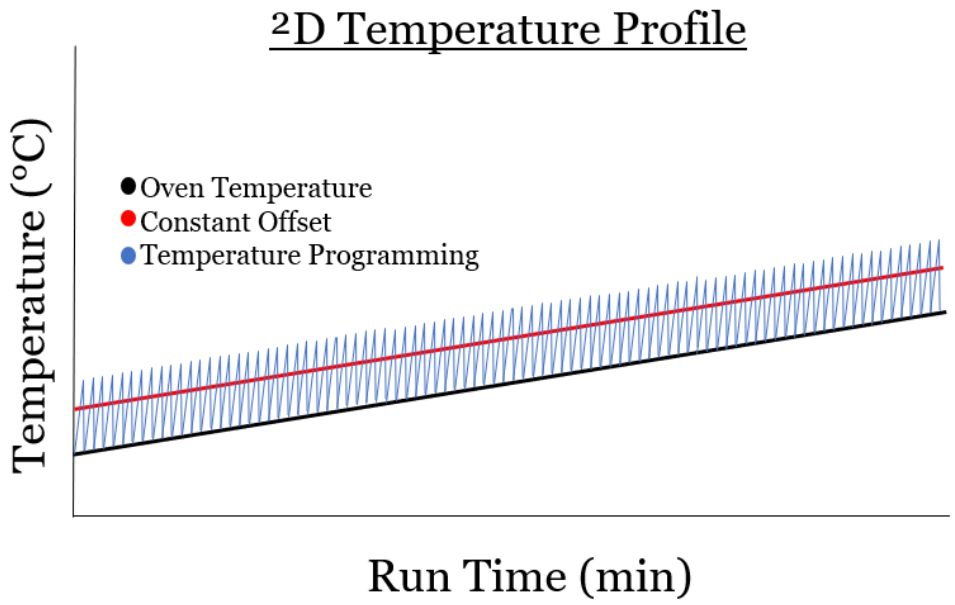

Figure 1-23: ^{2}D column temperature profile over the course of a GC×GC separation at oven temperature (black), with a positive constant temperature offset (red), and with temperature programming (blue).

2 Proof of Concept – Ballistic Heating System for the ^{2}D in GC×GC[ii]

The secondary oven has been the primary method of applying a positive temperature offset to the ^{2}D column in GC×GC. Typical constant temperature offsets of 0 °C – 40 °C [196, 197, 198, 199, 200, 201, 202, 203, 204, 205] [206, 207, 208, 209, 210, 211] have been applied, and in some cases, this temperature offset can change over the course of a run [212]. Thus, it can be expected that with temperature programming, higher temperature offsets would need to be achieved in order to compensate for the time the column was at a lower temperature compared to a constant temperature offset. Depending on the type of modulator used, modulation periods are typically between 2 - 6 s, with flow modulators typically having shorter modulations periods and thermal modulators having longer modulation periods. Therefore, it is expected that heating rates on the order of at least 10 °C/s would be needed, ruling out the use of standard GC ovens that rely on air convection. Resistive heating of the column is a technology that has been researched extensively in GC. It provides greater power efficiency, faster temperature programming, and significantly reduces the size of the GC, allowing for the miniaturization of the instrument. All of these factors are critical in designing a ^{2}DTPS with adequate performance for GC×GC.

Each of the three approaches to resistive heating, described in section 1.4.1.1, has its own benefits and limitations when used for ^{2}D temperature programming. The coaxial design has the advantage of allowing users to use standard GC columns; however, the large thermal mass of the resistively heated conductive tubing inevitably results in slower cooling. The collinear design, that is more common in commercial fast GC systems, lack the flexibility of column changes. Any changes in dimensions and stationary phase would need to be done by the manufacturer and makes method development much more difficult. The main benefit, however, would be a working temperature programming system that

[ii] This Chapter is based on the letter published in Analytical Chemistry by the author [265]:
Chow, H.-Y. J.; Górecki, T. Anal. Chem. 2017, 89, 8207-8211

can probably be adapted for ^{2}D temperature programming. The direct resistive heating approach is promising, due to the simplicity of the design. Both the nickel- and aluminum-clad columns utilized the column's electrical resistance for temperature measurement rather than a separate temperature sensor. Metal cladded columns, however, do have risks of the metal cladding being damaged over time from repetitive temperature cycling, due to the different thermal expansion coefficients of the metal and the fused silica capillary [175]. This may be even more pronounced in ^{2}D temperature programming, which demands more frequent and rapid temperature cycling compared to fast GC separations. Stainless steel columns as used by Xu et al. [178] are the easiest to implement and test, as the columns are commercially available in many geometries and with many different stationary phases. For the proof of concept, this design allowed testing with minimal additional equipment to demonstrate the potential of ^{2}D temperature programming.

2.1 Experimental

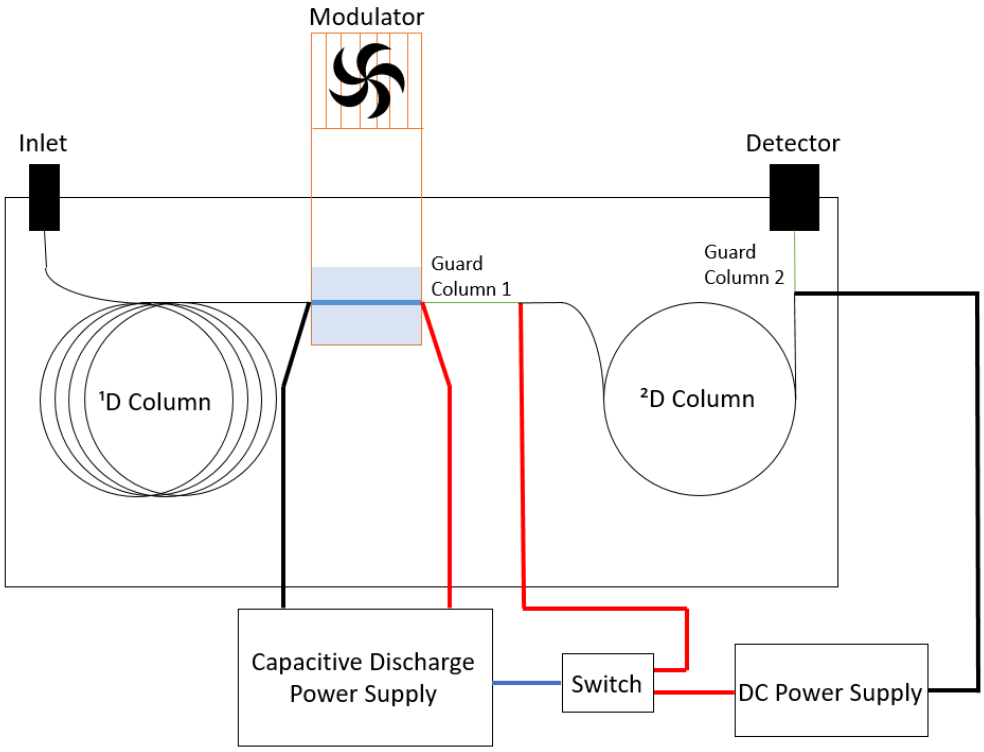

Figure 2-1: GC×GC setup used for temperature programming of the second dimension. The capacitive discharge power supply periodically heats the modulator and controls the timing of the DC power supply providing constant current for the ^{2}D column.

A diagram of the GC×GC setup used for the proof-of-concept experiments is presented in Figure 2-1. An Agilent 6890A GC was equipped with a single-stage consumable-free modulator developed at the University of Waterloo detailed in section 1.2.1.3.1 [74]. This modulator will be referred to as the Waterloo Modulator from here on. Analytes were trapped and focused using an actively cooled stainless steel capillary trap (coated) and injected into the ^{2}D column by rapid resistive heating using capacitive discharge. Voltage and timing of the discharge were controlled and set manually on the capacitive discharge power supply. The power supply was equipped with two channels for discharge, either of which could be used with the modulator. A DC power supply (QW-MS305D, Wuxi Qiaowei Electronics Co., Ltd, China) was used to provide constant current to a stainless steel ^{2}D column for resistive heating. The

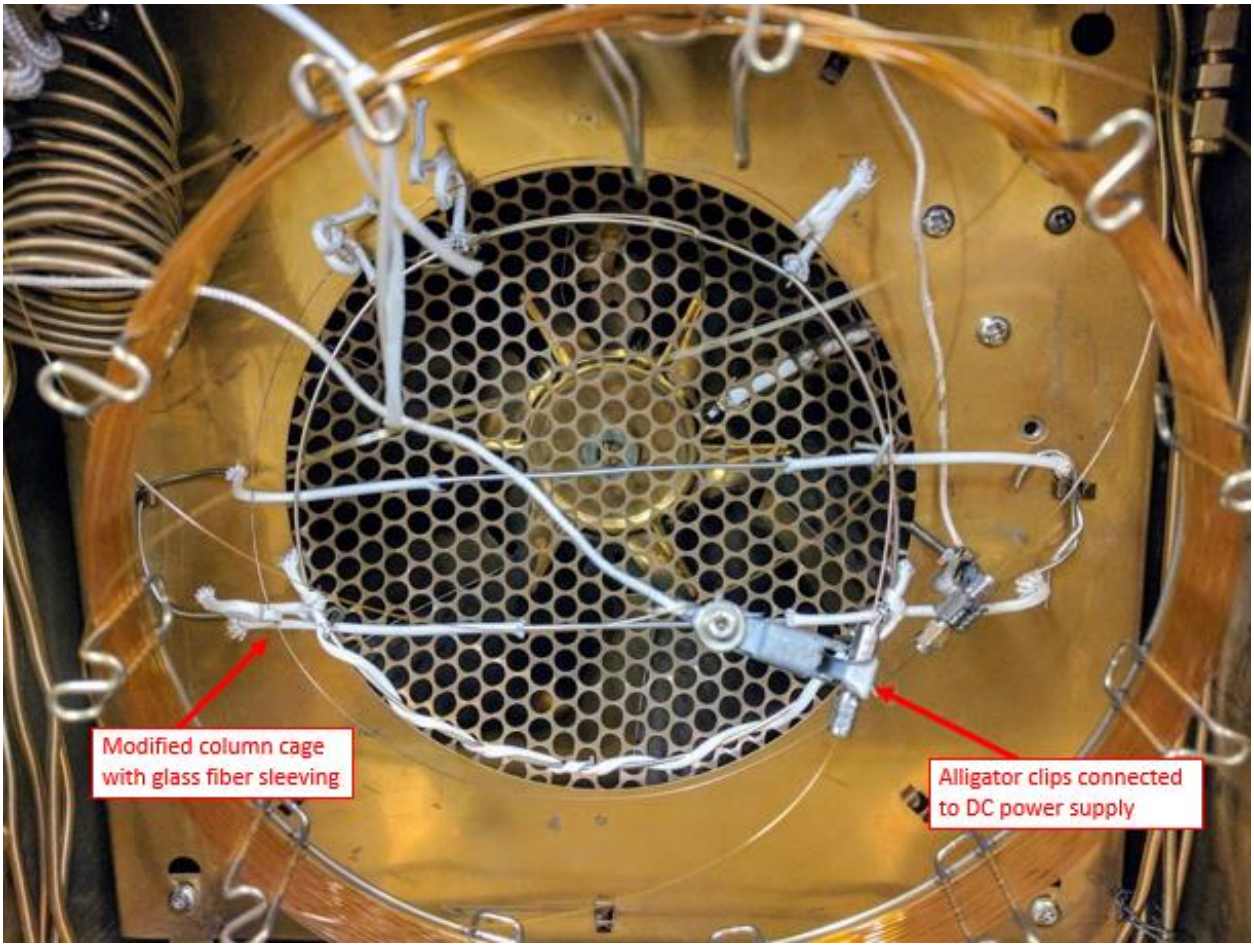

Figure 2-2: 0.50 m x 0.25 mm x 0.25 µm MXT-Wax column mounted in front of GC oven fan, connected to a DC power supply using alligator clips.

heating rate and maximum temperature offset achieved were a function of the current supplied. A switch was connected to the DC power supply to turn it on and off using the discharge signal from capacitive discharge power supply. The ^{2}D column was mounted directly in front of the GC oven fan using a modified GC column cage that was covered with glass fiber sleeving for electrical insulation (Figure 2-2). Fused-silica guard columns were connected before and after the ^{2}D column as electrical insulators to isolate the heating to the ^{2}D column. All column connections were made using SilTite mini unions (Trajan Scientific Americas Inc., Austin, TX, USA). Alligator clips were used to connect the DC power supply to the ^{2}D column.

2.1.1 ^{2}D Column Temperature Measurement

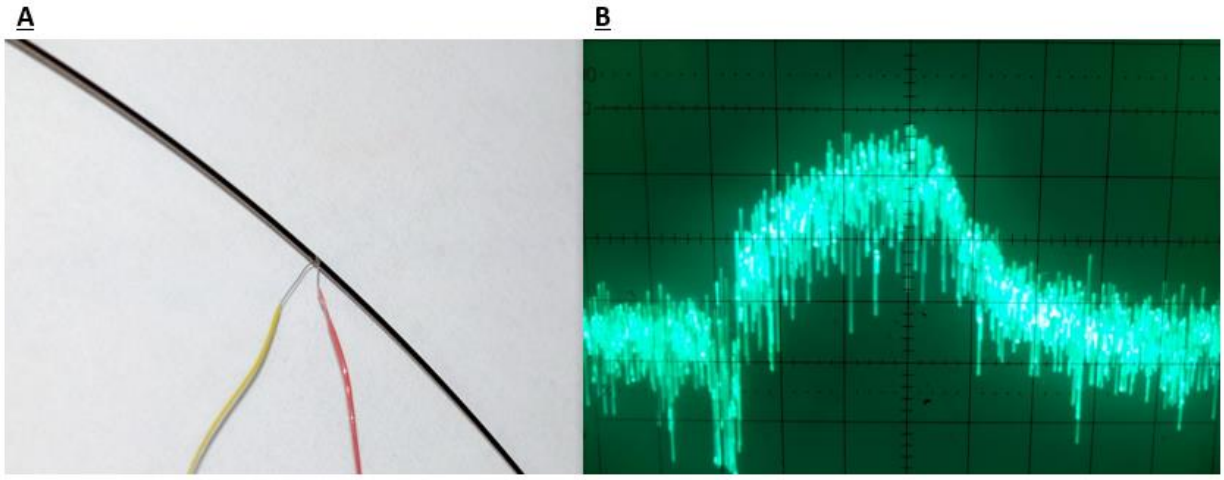

*Figure 2-3:MXT-WAX column with a 0.003" µm K-type thermocouple spot-welded to the surface (A). Oscilloscope readout of the thermocouple signal following a 100x gain amplification (**x-axis: 1 s/div., y-axis: 50 mV/div**) of the 0.50 mm MXT-WAX column being heated then cooled in the GC oven (B).*

A 0.003" type K thermocouple (OMEGA Engineering Inc., Norwalk, CT, United States) was spot-welded to the ^{2}D column (Figure 2-3A) and connected to a HAMEG HM208 oscilloscope (HAMEG Instruments, Mainhausen, Germany) through a 100x gain amplifier. The signal (mV) change over time was measured with carrier gas flowing through the column. Before a GC run, the discharge power supply was manually started to simulate a separation. The signal (Figure 2-3B) from the thermocouple was monitored, and the constant current from the DC power supply was adjusted in order to achieve the desired temperature

offset. Cooling time was also monitored to ensure the column can cool back to oven temperature within one modulation period.

2.1.2 ^{2}D Ballistic Heating

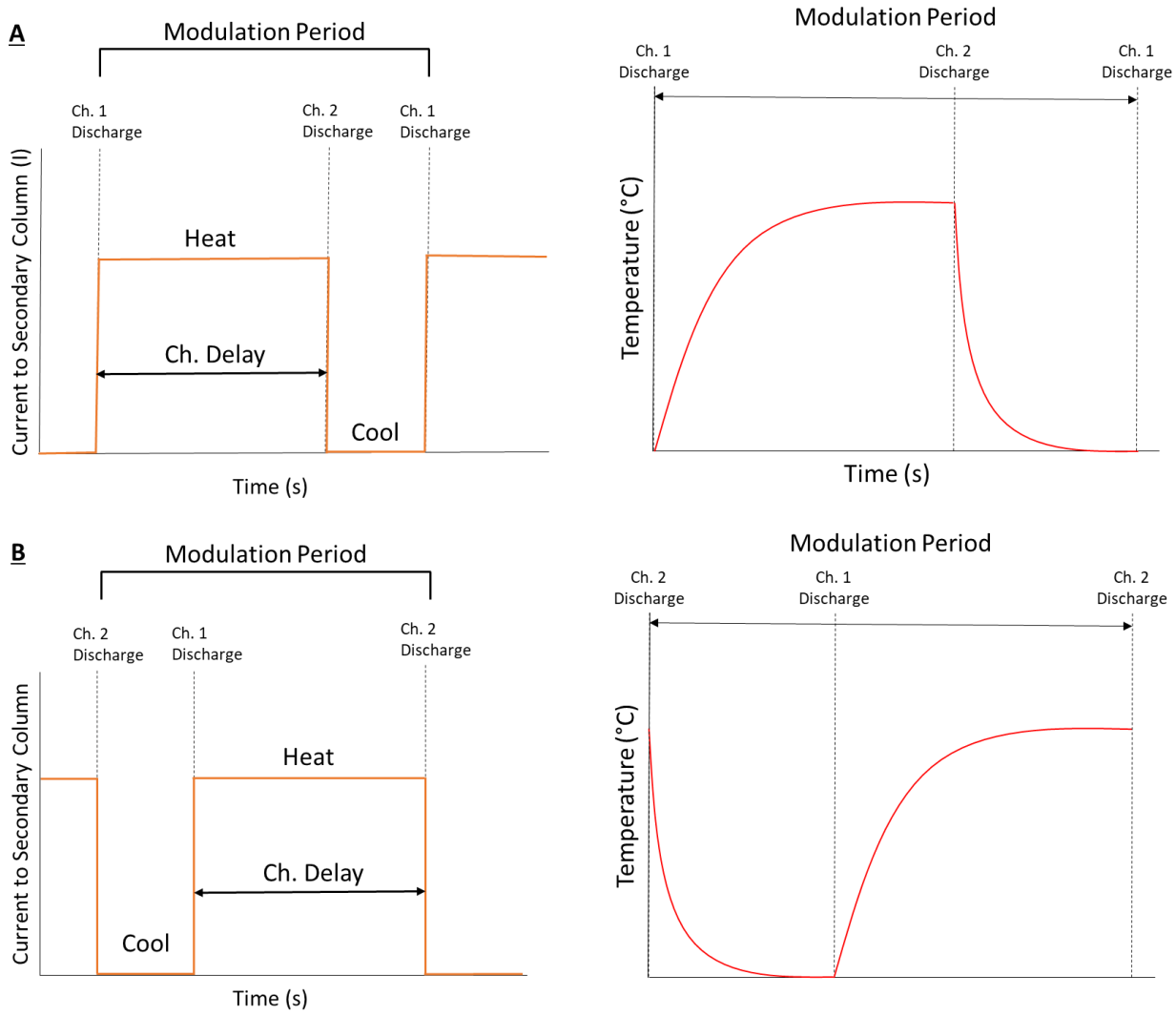

Figure 2-4: Current vs time profile for the ^{2}D column in relation to the modulation period and channel discharge of the capacitive discharge power supply (LEFT) and the corresponding temperature vs time profile (Right). Configuration 1 (A). Configuration 2 (B)

Re-injection of trapped analytes into the ^{2}D column (the beginning of the modulation period) and heating of the ^{2}D column were controlled by the timing of the discharge from channel 1 and channel 2 of the capacitive discharge power supply. Available settings for timing included the modulation period and the channel delay. The channel delay was the delay after which channel 2 would discharge after channel

1 discharged. Discharge from channel 1 turned the remote switch ON, allowing current from the DC power supply to be delivered to the ^{2}D column. Discharge from channel 2 turned the switch OFF and allowed the ^{2}D column to cool back to the oven temperature through forced air convection provided by the GC oven fan. Two different configurations were tested, with the modulator connected to channel 1 or channel 2 (Figure 2-4). In configuration 1 (Figure 2-4A), with the modulator connected to channel 1, the resistive heating applied to the ^{2}D column was synchronized with the start of the modulation period. The duration of the heating was determined by the channel delay, and the remaining time left in the modulation period allowed the column to cool. In configuration 2 (Figure 2-4B), with the modulator connected to channel 2, the onset of cooling (heating turned off) was synchronized with the start of the modulation period. The channel delay determined the duration of cooling, and the ^{2}D column was then heated for the rest of the modulation period.

2.1.3 ^{2}D Constant Temperature Offset

By connecting the modulator to channel 1 on the capacitive discharge power supply and turning channel 2 off, the switch remained in the ON state throughout the GC×GC run. This provided constant current to the ^{2}D column, which kept it at a constant positive temperature offset similar to the use of a secondary oven. The magnitude of the current supplied to the ^{2}D column controlled the temperature offset.

2.1.4 Experimental Conditions

For the comparison between configuration 1 and constant temperature offset separations, diesel fuel was analyzed using an Rxi-5ms (30 m x 0.25 mm x 0.25 µm) ^{1}D column and MXT-WAX (0.75 m x 0.25 mm x 0.50 µm and 0.49 m x 0.25 mm x 0.50 µm) ^{2}D columns. 1.0 µL of diesel fuel was injected with a 300:1 split ratio. Hydrogen was used as the carrier gas at a constant flow of 2.5 mL/min. The oven temperature program started at 40 °C and increased to 200 °C (10 min hold) at a rate of 5 °C/min

for a total runtime of 42 min. The modulation period was 5 s and an FID was used with nitrogen as the makeup gas.

For the comparison between configuration 2 and constant temperature offset separations, diesel was analyzed using an Rxi-5ms (30 m x 0.25 mm x 0.25 µm) ^{1}D column with an MXT-WAX (0.49 m x 0.25 mm x 0.50 µm) and an MXT-65 (0.50 m x 0.18 mm x 0.20 µm) ^{2}D columns. For both setups, 1.0 µL of diesel fuel was injected with a 300:1 split ratio and the FID was used. For the MXT-WAX ^{2}D setup, a constant flow rate of 1.2 mL/min (H_2) was used. The oven temperature program started at 40 °C and increased to 200 °C (10 min hold) at a rate of 5 °C/min for a total runtime of 42 min. The modulation period was 5 s. For the MXT-65 ^{2}D column setup, a constant flow of 2.0 mL/min (H_2) was used. The oven temperature program started at 50 °C and increased to 250 °C at a rate of 3 °C/min for a total runtime of 66.67 min. A modulation period of 4 s was used. Other instrumental parameters remained the same.

For the MXT-WAX column, 20 °C, 30 °C, and 40 °C temperature offsets were achieved by applying constant current of approximately 1.00 A, 1.25 A, and 1.45 A, respectively. For the MXT-65 column, 20 °C, 30 °C, and 40 °C temperature offsets were achieved by applying constant current of approximately 0.75 A, 1.00 A, and 1.10 A, respectively. These values were approximate as they depended on the electrical resistance of the entire circuit, which could vary slightly due to the nature of the alligator clip contacts. Thus, the DC power supply output would be adjusted slightly while monitoring the oscilloscope to ensure the desired temperature offset was achieved.

2.2 Results and Discussion

2.2.1 Heating and Cooling Times

Rapid heating and cooling rates are critical to the success of the ^{2}DTPS due to the short time available in a modulation. The resistive heating system needs to be capable of achieving a satisfactory temperature offset in a reasonable amount of time (1 to 4 s). The cooling rate also needs to be as short as possible to

restore the ^{2}D column to the initial conditions quickly. Thus, the time required to heat and cool the ^{2}D column was measured for various temperature increases (20 °C, 30 °C, 40 °C) and at different oven temperatures (50 °C, 100 °C, 150 °C, 200 °C, 250 °C). For the MXT-WAX column, measurements were taken up to an oven temperature of 200 °C due to the upper-temperature programming limit of 250 °C for the stationary phase. For the MXT-65 column, the temperature range for the stationary phase was 50 °C to 300 °C. The MXT-WAX and MXT-65 columns were tested due to their difference in inner diameter, 0.25 mm and 0.18 mm, respectively. For the MXT-WAX column, three column lengths were tested (1.0 m, 0.75 m, and 0.50 m). These different parameters (oven temperature, temperature offset, column length, column inner diameter) should cover the main changes in GC conditions related to the ^{2}D column temperature programming.

Heating and cooling times, as well as the current applied for heating, are found in Table A – 1 and Table A – 2 of Appendix A. An example of the oscilloscope signal obtained from the thermocouple following a 100x amplification was shown in Figure 2-3B. Due to the direct spot-welding of the bare thermocouple wires to the metal column, electrical noise originating from the power supply was picked up by the thermocouple. However, direct attachment of the thermocouple was necessary to minimize the time constant when measuring the heating and cooling times. Due to the significant amount of noise, the time required for the column to reach about 90 % of the final temperature (around the start of the plateau) was recorded, since identifying the exact point at which the column has equilibrated to the desired temperature offset was extremely difficult. Looking at the oscilloscope signal in Figure 2-3B, cooling followed a typical exponential profile, being very rapid in the initial portion of the cooling period and becoming slower as the column temperature approached the oven temperature. Similarly, the temperature increase was very rapid for the initial duration of the heating, followed by a plateau in temperature as the column reached a steady-state between heat generation and heat dissipation. This

result is consistent with previous studies which showed similar results for the heating and cooling profile [175, 177].

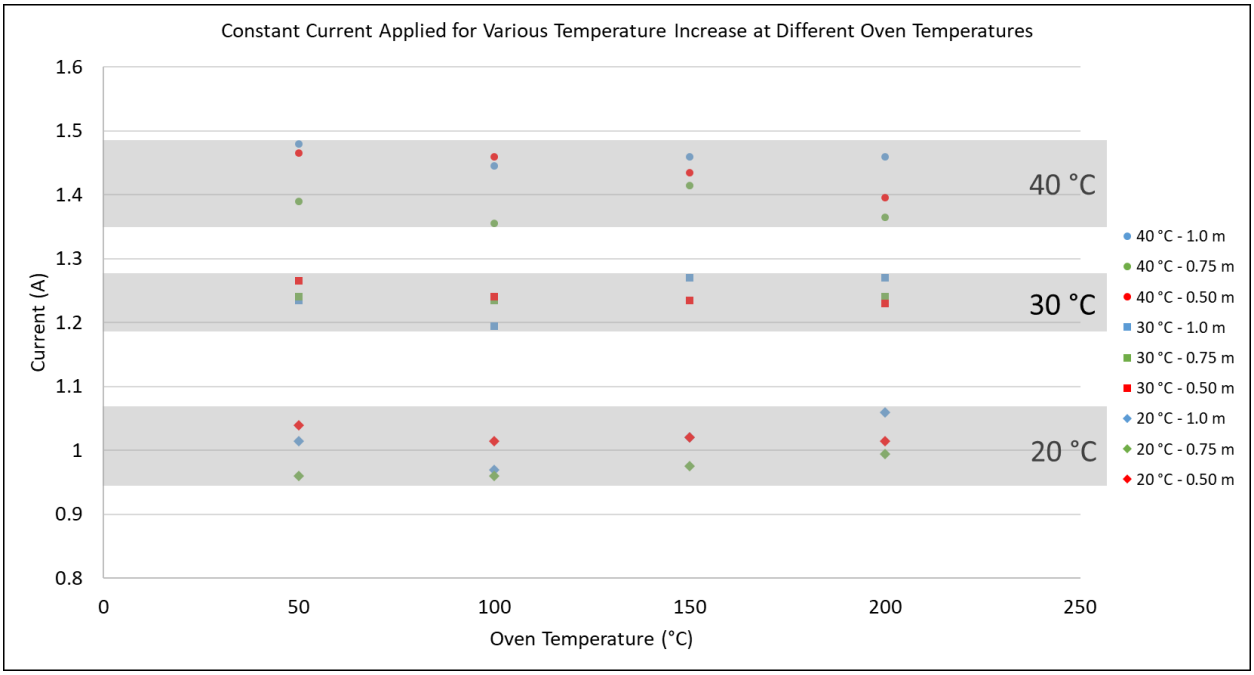

Figure 2-5: Constant current applied for each temperature increase (40 °C, 30 °C, and 20 °C) and different oven temperatures (50 °C, 100 °C, 150 °C, 200 °C) for the MXT-WAX (0.25 mm x 0.25 µm).

As shown in Figure 2-5, the general trend of requiring higher current to achieve a higher temperature increase was confirmed. Since the DC power supply was set to constant current mode, the power applied to the column increased proportionally to the column's electrical resistance [Eq. (2.1)].

$$Power = I^2R \qquad (2.1)$$

Therefore, the current applied for a desired temperature increase should remain constant if the column material remains uniform, the cross-sectional area is identical, the heatsink effect of the connectors is negligible, and the resistance at the alligator clip connections is consistent. However, there was a spread of 0.11 A at 100 °C for the 40 °C increase, 0.05 A at an oven temperature of 100 °C for the 30 °C increase, and 0.08 A at 50 °C for the 20 °C increase. This was likely due to the alligator clip connection between the DC power supply and the SilTite unions, since the three lengths of column were cut from the same column. It seems unlikely that there were significant differences in the material uniformity or cross-

sectional area over 2.25 m of the column length. The resistance of stainless steel increases with temperature, so the power applied to the column would increase as the oven temperature was increased. However, the current applied to the column remained fairly consistent at the different oven temperatures tested. This may indicate that this resistance change was negligible or more power was needed at higher oven temperatures to reach the target temperature increase.

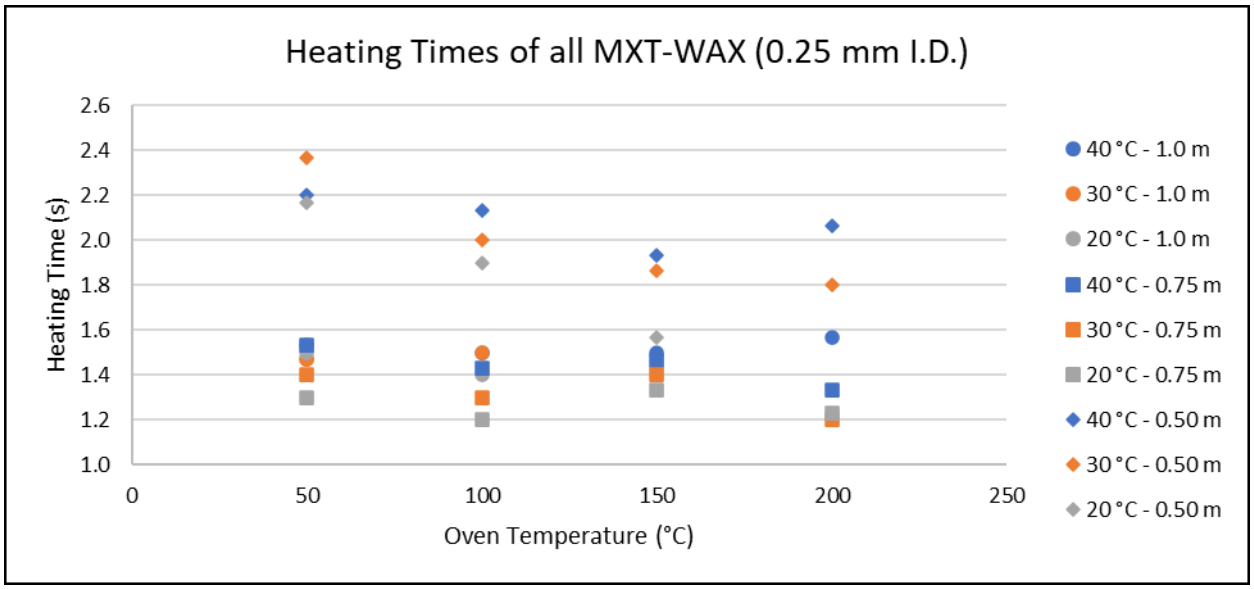

Figure 2-6: Heating times for the 0.25 mm I.D. MXT-WAX column at oven temperatures of 50 °C to 200 °C, for temperature increases of 20 °C to 40 °C.

Figure 2-6 shows the heating times for various lengths of the MXT-WAX column at different oven temperatures and for different temperature increases. Due to the fragile nature of the thermocouple connection to the column, the thermocouple was spot-welded after the column was installed onto the column cage. For the 1.0 m x 0.25 mm MXT-WAX column, heating times were nearly identical for all temperature increases and oven temperatures. Due to the amount of noise in the measurement, the differences were negligible and difficult to notice. For the 0.75 m x 0.25 mm MXT-WAX column, there were greater differences in heating times between the various temperature increases than for the 1.0 m x 0.25 mm column. The difference was about 100 ms between each temperature increase at each oven temperature, except at 200 °C where the heating time was nearly the same between the

temperature increase of 20 °C and 30 °C. In addition, the measurements had larger standard deviations compared to the 1.0 m column. When the column length was reduced to 0.50 m, the heating time increased 200 ms to 1000 ms when compared to the 0.75 m column. In addition, the standard deviation continued to increase compared to the 1.0 m and 0.75 m columns.

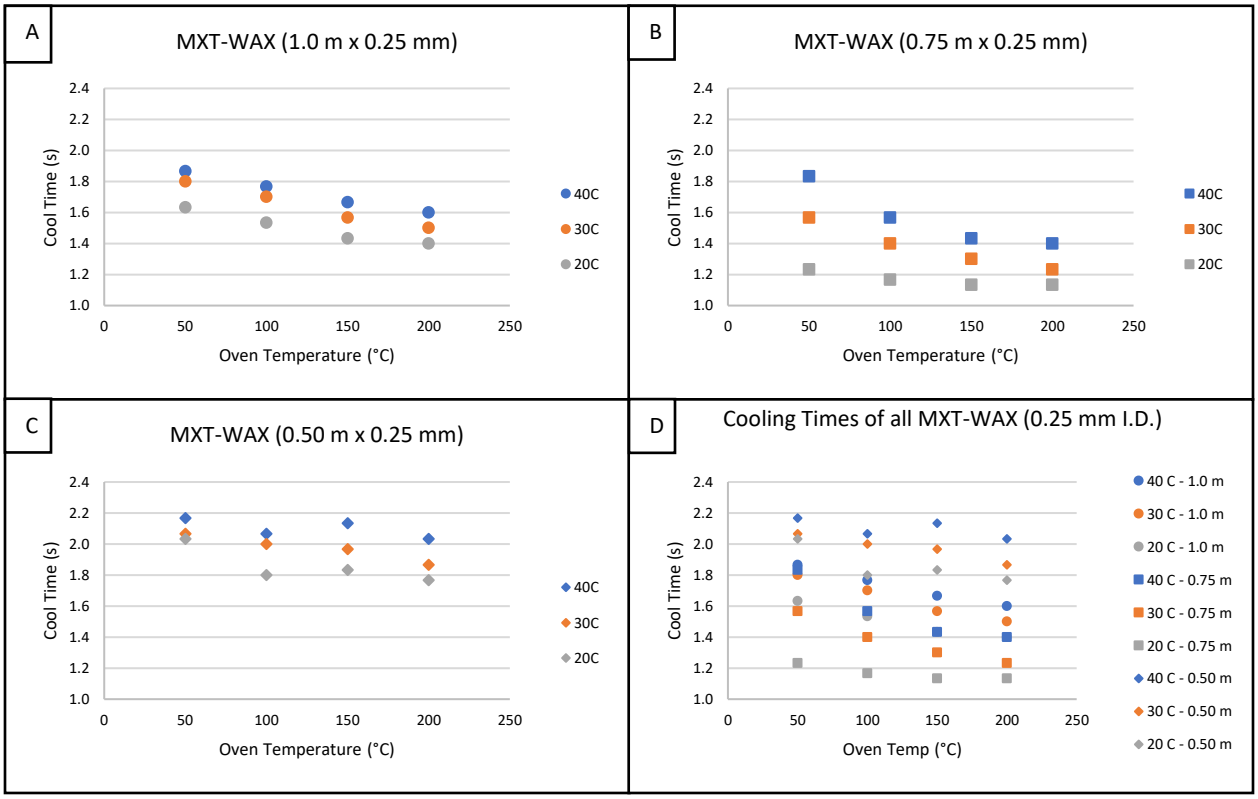

Figure 2-7: Cooling times for the 0.25 mm I.D. MXT-WAX column at oven temperatures of 50 °C to 200 °C, for temperature increases of 20 °C to 40 °C. (A) 1.0 m x 0.25 mm x 0.50 µm MXT-WAX. (B) 0.75 m x 0.25 mm x 0.50 µm MXT-WAX. (C) 0.50 m x 0.25 mm x 0.50 µm MXT-WAX. (D) Summary of all results.

Figure 2-7 shows the cooling times for the various lengths of MXT-WAX column (0.25 mm x 0.50 µm). For the 1.0 m and the 0.75 m columns, there was a general trend of shorter cooling times as the oven temperature increased. This was not as evident for the 0.50 m column, for which the cooling times remained more consistent. However, as was the case for the heating times, there was a noticeable increase in cooling time for the 0.50 m column compared to the 1.0 m and 0.75 columns. Hot or cold spots at the thermocouple junction with the column could have affected the temperature measurements. This may have developed during the spot-welding of the thermocouple to the column and was unlikely to be

due to a manufacturing defect resulting in inconsistency in the column material's uniformity. Another possibility would be due to differences in the positioning of the column in front of the GC oven. As seen in Figure 2-2, although the column cage was secured in front of the GC fan, slight deviations may cause changes in the air flow over the column, affecting the heating and cooling. The most likely possibility could be the SilTite mini-union connectors acting as heatsinks. Since the unions were not heated, the heat at the ends of the column would be efficiently transferred to the connectors. As the column length was reduced, a larger portion of the column would be affected by the connectors, making it more difficult to reach a steady state. The best solution to this would be to attach the thermocouple to the center of the column (lengthwise), but due to the difficulties with spot-welding the thermocouple, it was always attached at the bottom of the first coil facing towards the GC oven door. This position was naturally closer to one of the SilTite mini-unions, which made it more difficult to measure the heating and cooling times accurately.

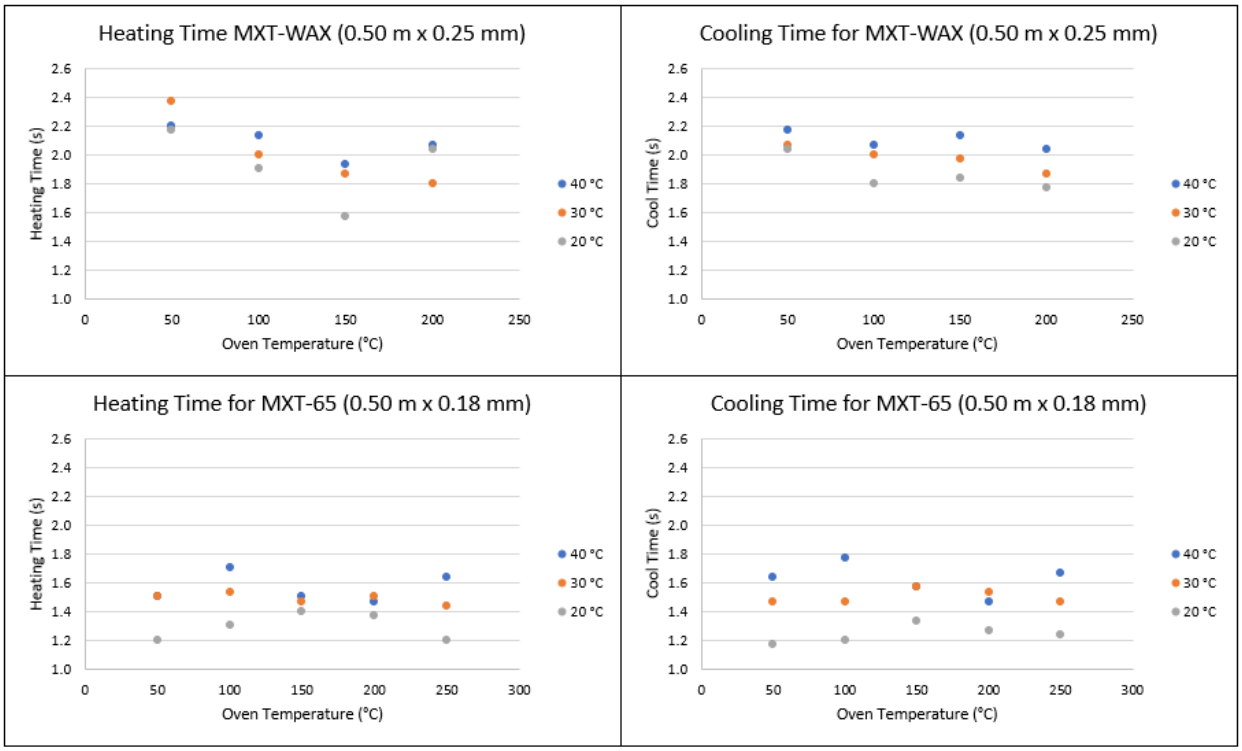

Figure 2-8: Heating and cooling times for an MXT-WAX (0.49 m x 0.25 mm) and MXT-65 (0.50 m x 0.18 mm) column.

Figure 2-8 illustrates the heating and cooling times for the MXT-WAX (0.49 m x 0.25 mm x 0.50 µm) and MXT-65 (0.49 m x 0.18 mm x 0.20 µm) columns. These two column dimensions were compared separately from the other column dimensions due to the impact of the SilTite min-union's heatsink effect. The MXT-65 column, with the 0.18 mm I.D., had a lower thermal mass compared to the MXT-WAX column, resulting in shorter heating and cooling times.

Although the measurements were not very reliable and no conclusive relationship between the column dimensions and heating/cooling times could be determined, the results were still useful in determining the approximate heating and cooling durations for the different column dimensions. Overall, the MXT-WAX column took around 2 s to heat and cool for the various temperature increases and oven temperatures. For the MXT-65 column, it took around 1.5 s to heat and cool under the same conditions. Based on the cooling time required for each column, the appropriate cooling duration was estimated for different modulation period durations. The cooling duration was determined in consideration of the heating duration needed to eliminate or minimize the impact of wraparound peaks.

2.2.2 Ballistic Heating: Heating followed by cooling within one modulation period (Configuration 1)

Diesel fuel was analyzed to evaluate the ballistic heating system for the ^{2}D of GC×GC. The separation of diesel using a 0.75 m x 0.25 mm x 0.50 µm MXT-WAX ^{2}D column is shown in Figure 2-9 with detailed experimental conditions in section 2.1.4. The structure of the chromatogram was similar to the chromatogram previously described using the same stationary phase combination for GC×GC separation [213]. With the thick film 0.50 µm WAX stationary phase, there was great separation within the band of saturated hydrocarbons. However, the more polar aromatic compounds had excessive retention on the column, resulting in broad wraparound peaks. In addition, the group of 2-ring aromatic hydrocarbons had so much retention that they coeluted with analytes from the following modulation period and could not

be labeled. This was a great starting point, as a sort of “stress test” for the ballistic heating system, to compare ballistic heating with a constant temperature offset in the ^{2}D.

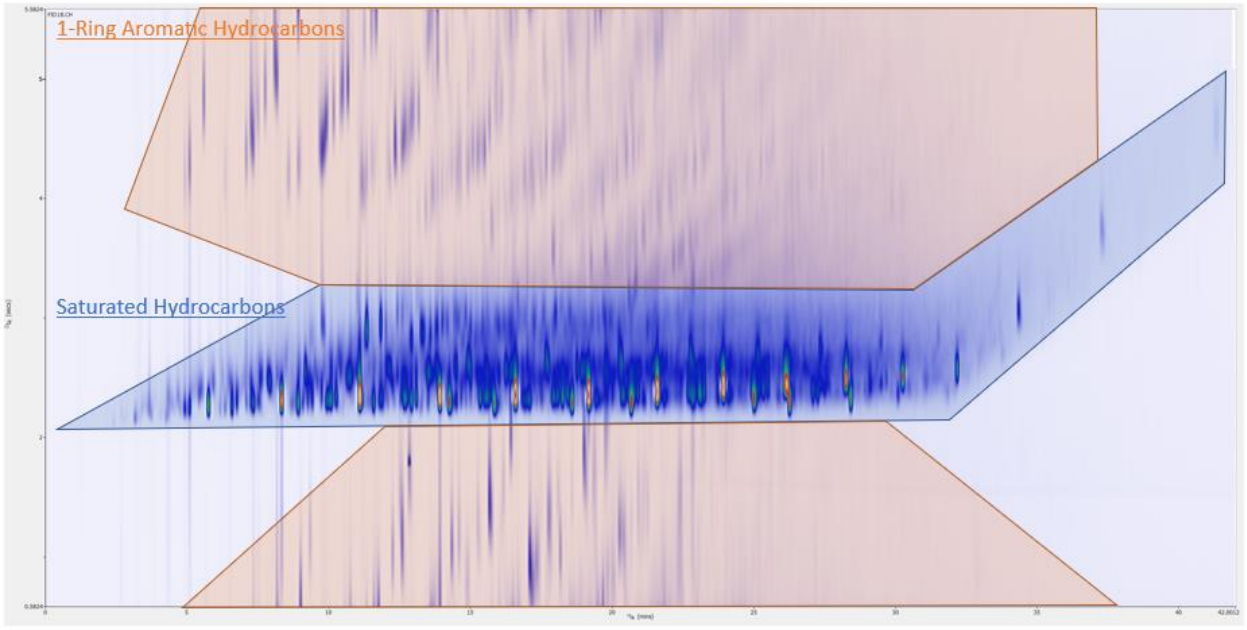

Figure 2-9: Separation of 1.0 µL of diesel (300:1 split) on ^{1}D: Rxi-5ms (30 m x 0.25 mm x 0.25 µm) and ^{2}D MXT-WAX (0.75 m x 0.25 mm x 0.50 µm). A carrier gas (H_2) flow rate of 2.5 mL/min was used with an oven temperature program of 40 °C to 200 °C (10 min hold) at a rate of 5 °C/min. Modulation period was 5 s and an FID with nitrogen as a makeup gas was used. Blue region: saturated hydrocarbons; Orange region: 1-ring aromatic hydrocarbons. ***X-axis: 0 – 42 min. Y-axis: 0 – 6 s.***

Initial testing started with configuration 1, where the ^{2}D column heating was synchronized with the start of the modulation period and then the column was cooled back to oven temperature in the final seconds of the modulation period. In theory, this temperature profile with respect to the modulation period should be similar to a complete GC run, which includes the cooling of the GC oven back to the initial temperature. With ballistic heating, it was expected that there would be an improvement in resolution and peak capacity compared to the constant offset separations, even though there was no control over the rate of temperature increase.

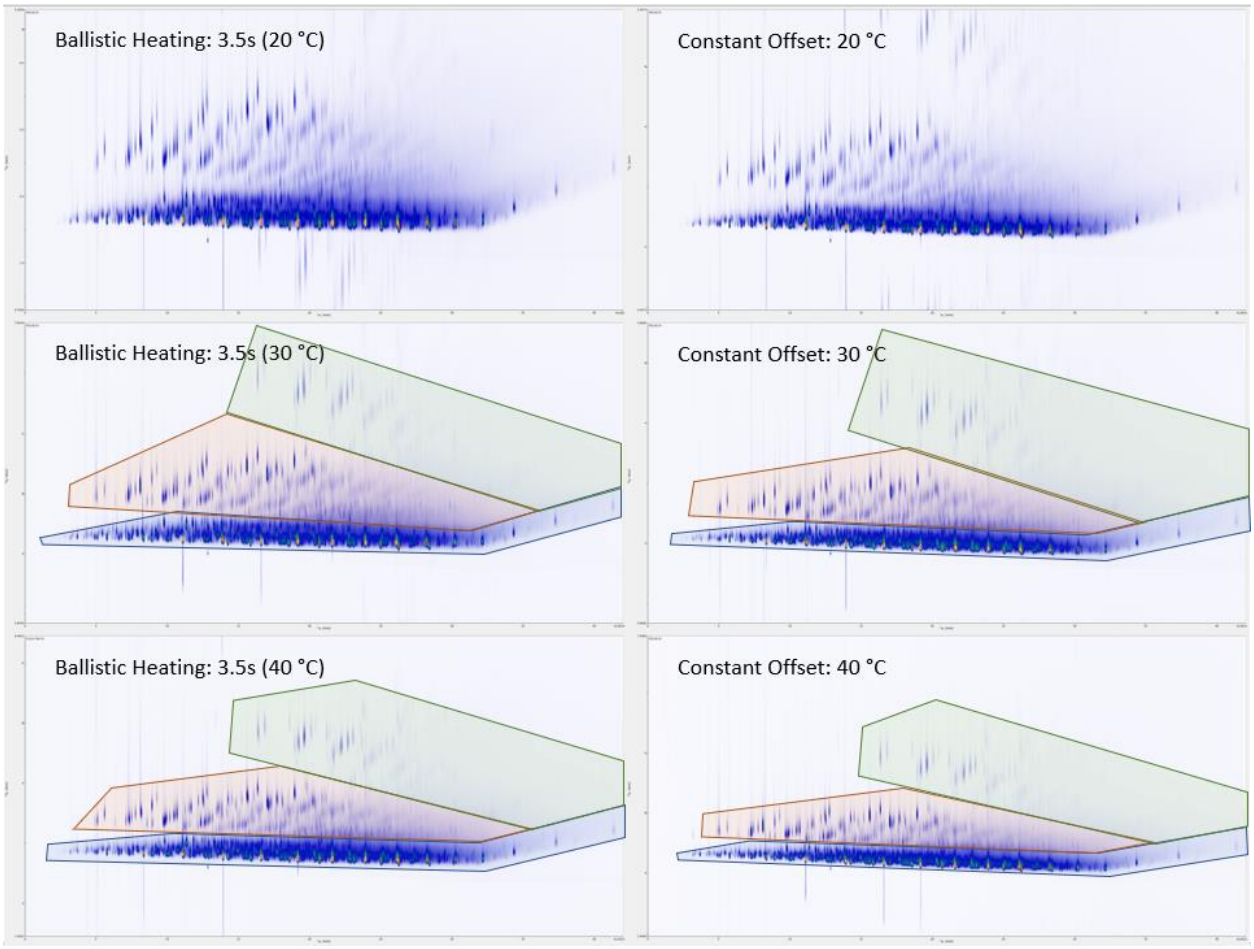

Figure 2-10: Comparison of ballistic heating (configuration 1) and constant temperature offset in the ²D using the ballistic heating system with an MXT-WAX (0.75 m x 0.25 mm x 0.50 µm) column. Blue region: saturated hydrocarbons, orange region: 1-ring aromatic hydrocarbons, green region: 2-ring aromatic hydrocarbons. ***X-axis: 0 – 42 min. Y-axis: 0 – 6 s****.*

Comparing the ballistic heating separations to the constant offset separations with the same final temperature offsets (Figure 2-10), there was only a slight improvement in the separation between the saturated hydrocarbons. Since the constant offset separations were practically isothermal in the ²D, the temperature offset had the effect of reducing the retention of all analytes in the ²D. As the temperature offset was increased, from 20 °C to 40 °C, wraparound peaks were eliminated, but the group of saturated hydrocarbons co-eluted more due to reduced retention on the ²D column. This was an issue experienced in all GC×GC separations due to the general elution problem. With the ballistic heating separations, a constant current was applied for the first 3.5 s of the modulation period. The column was then cooled back to oven temperature in the final 1.5 s of the modulation period. Although 1.5 s does not allow the

column to fully cool to oven temperature, the temperature offset at the start of the next modulation period was no more than 5 - 10 °C depending on the offset value applied. With the ballistic heating separations, it was noticed that the separation between the saturated hydrocarbons was slightly improved compared to the constant offset separation. In addition, the rest of the compounds did have longer retention times in the second dimension compared to the constant offset separations, which indicated that less heating was experienced overall with the separation. However, the slight improvement was disappointing when taking into consideration the added complexity of the system. The problem with synchronizing the heating with the start of the modulation period, was that the weakly retained compounds (saturated hydrocarbons) were experiencing the ballistic heating as they entered and were separating in the ^{2}D column. This resulted in an unnecessary reduction in the retention for the saturated hydrocarbons. For the more strongly retained compounds (2-ring aromatic hydrocarbons, green region in Figure 2-10), the ballistic heating separation at 20 °C was not sufficient as wraparound peaks co-eluting with peaks in the subsequent modulation period were observed. This indicated that these compounds experienced ballistic heating, rapid cooling, and then ballistic heating again before eluting. The rapid cooling that these compounds experienced likely contributed to the significant band broadening that was observed. This was a stark contrast to the more gradual increase in peak width that was seen with the constant offset separation. Both the ballistic heating and constant offset separations at 30 °C and 40 °C were significantly better than the 20 °C separations. For the ballistic heating separations, the 2-ring aromatic hydrocarbons eluted near the end of the heating period or during the early portions of cooling, where the column temperature was still elevated. Peak widths for the 2-ring aromatic hydrocarbons were better, but the overall separation was still very similar to the constant offset separations.

Configuration 1 of the ballistic heating system was also tested with the 0.49 m x 0.25 mm x 0.50 µm MXT-WAX using diesel and is found in Figure A – 1 in Appendix A. The overall separation was nearly identical as the stationary phase combination was the same. The retention time was shorter in the ^{2}D for

the 0.49 m MXT-WAX, particularly for the more retained aromatic hydrocarbons for the 20 °C ballistic heating separation. For the 30 °C and 40 °C separations, differences in the separation were harder to notice without the side-by-side comparison. In particular, the separation for the band of saturated hydrocarbons was nearly identical for all three ballistic heating temperature offsets for both column lengths.

2.2.3 Ballistic Heating: Cooling followed by heating within one modulation period (Configuration 2)

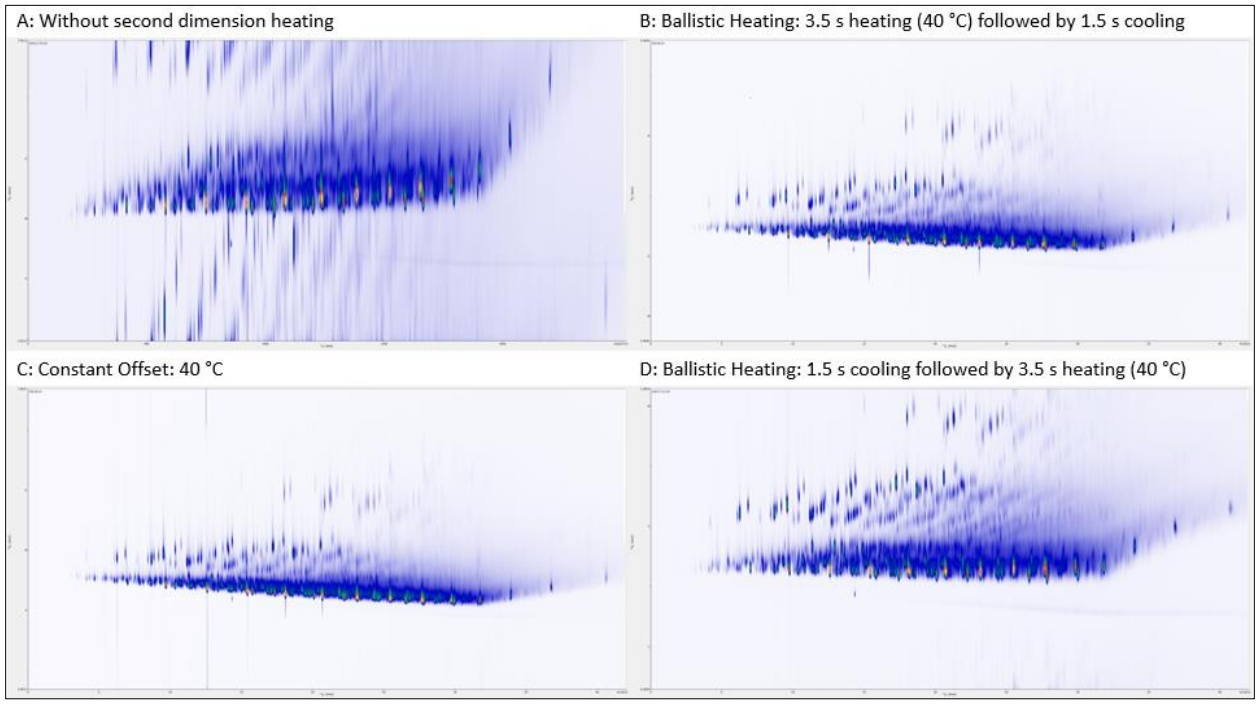

Figure 2-11: GC×GC separation of diesel using a ^{1}D: Rxi-5ms (30 m x 0.25 mm x 0.25 µm) and ^{2}D: MXT-WAX (0.49 m x 0.25 mm x 0.50 µm) column set. A: Standard GC×GC separation; B: Ballistic heating with 3.5 s of heating to a 30 °C offset followed by 1.5 s of cooling (configuration 1); C: Constant temperature offset of 40 °C; D: Ballistic heating with 1.5 s of cooling followed by 3.5 s of heating to 30 °C above the oven temperature (configuration 2). ***X-axis: 0 – 41.8 min. Y-axis: 0 – 5 s****.*

Configuration 2 of the ballistic heating system delayed the heating of the ^{2}D column for 1.5 s to allow the column to cool at the start of the modulation period, followed by 3.5 s of heating. Diesel was separated on a 0.49 m x 0.25 mm x 0.50 µm MXT-WAX column without additional ^{2}D heating, where the saturated hydrocarbons eluted between 2 - 3 s in the ^{2}D (Figure 2-11A). Comparing configuration 1 (Figure 2-11B) and configuration 2 (Figure 2-11D), the overall retention times of all compounds in the ^{2}D were

longer for configuration 2. The separation between the saturated hydrocarbons improved significantly compared to both configuration 1 (Figure 2-11B) and the constant offset separation (Figure 2-11C), but was still slightly worse compared to the separation without ^{2}D heating (Figure 2-11A). Most importantly, the ^{2}D peak widths for configuration 2 separation were very consistent through the entire separation, indicating an effective temperature program. This was not the case for configuration 1, where the saturated hydrocarbon peaks were much narrower than the aromatic hydrocarbon peaks in the ^{2}D.

Although the temperature offset and the duration of the heating and cooling were identical for configurations 1 and 2, the timing of each event was switched within the modulation period. The dead time in the ^{2}D, as indicated by the faint bleed line, was about 1.3 - 1.6 s (changes over the course of the temperature program). By the end of the dead time, configuration 1 would have nearly reached the final temperature offset, while configuration 2 would have nearly reached oven temperature. In configuration 1, the temperature change was so rapid for the ballistic heating that for most of the separation time these compounds were being separated under near isothermal conditions at the final temperature offset. This explains why the separation was so similar to the constant offset separation. For configuration 2, the compounds were experiencing a mix of cooling and heating. The rapidly cooling column at the start of the modulation period would result in lower average column temperature compared to the rapidly heated column of configuration 1, due to the non-linear temperature profile. In addition, following the capacitive discharge of the modulator, the compounds need to travel through the guard column before reaching the ^{2}D column. During this time the cooling was the fastest, which helped start the ^{2}D separation at a lower initial temperature (still elevated compared to the GC oven). As the column continued to cool, the first band of peaks was separated at close to oven temperature. When the ballistic heating started, the first band of peaks would have already traversed through most of the ^{2}D column, so their separation was less affected compared to configuration 1. For the more retained compounds, like the third band of peaks, these compounds were likely to be near the head of the ^{2}D column due to their much stronger retention.

The ballistic heating helped mobilize these compounds and allow them to separate and elute closer to their ideal elution temperatures, just like in temperature programming.

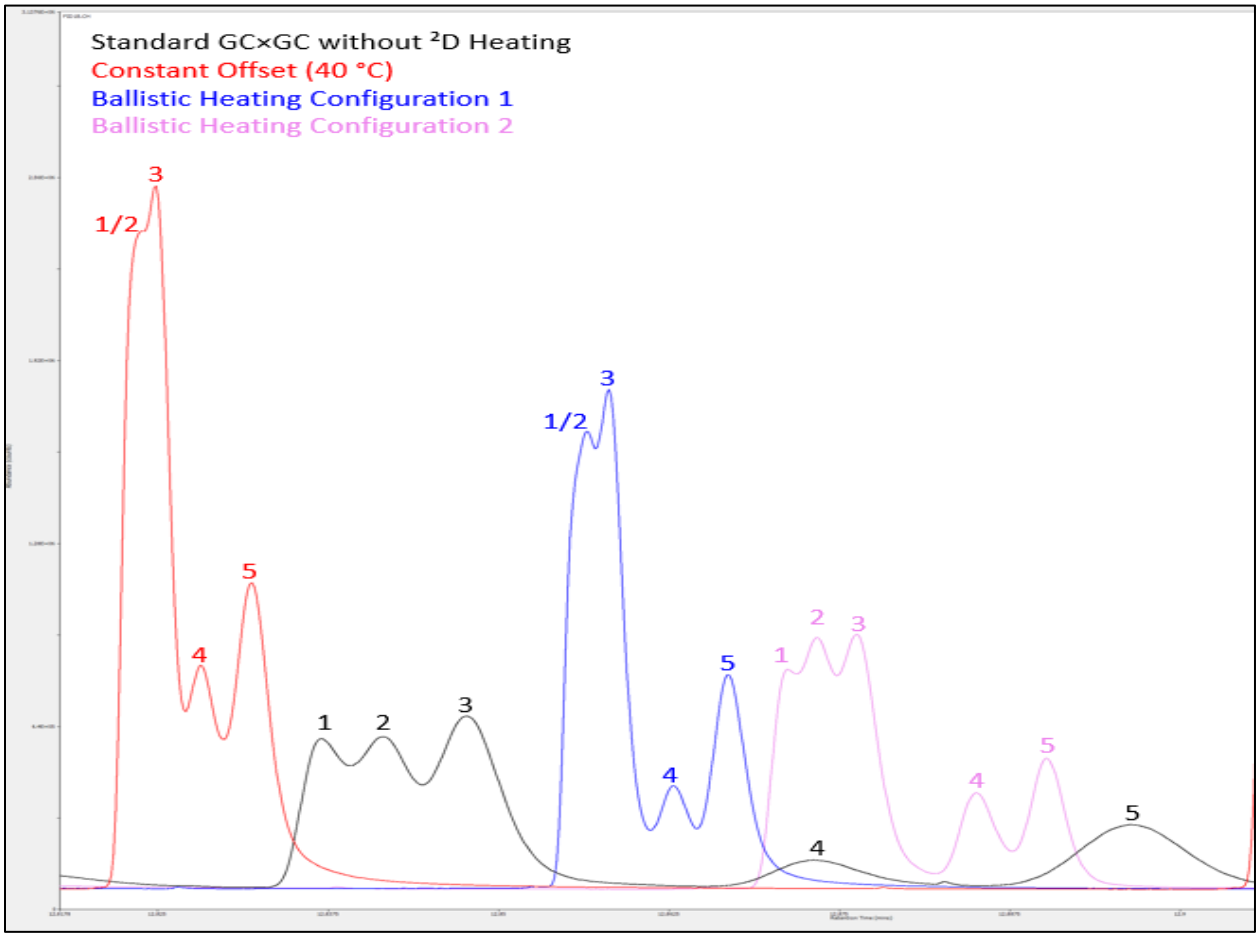

Figure 2-12: A comparison of raw GC signals for the GC×GC separation of diesel using an Rxi-5ms (30 m x 0.25 mm x 0.25 µm) and MXT-WAX (0.49 m x 0.25 mm x 0.50 µm). ***X-axis: 12.8178 – 12.9354 min. Y-axis: 0 – 3.1376 × 10⁶.***

Figure 2-12 compares the raw GC-FID signal before GC×GC processing for a single modulation period (at around 12.81 min.) for the four separations from Figure 2-11. For the separation without any additional heating of the ²D column, 5 distinct peaks were observed, getting progressively broader with increasing retention time, illustrating the general elution problem. Among the four separations, the separation without any heating had the reasonable separation between the early eluting peaks (peaks 1 - 3). For the constant offset separation, peaks 1 - 3 were almost co-eluting as a single peak, and all five peaks were not baseline-resolved. With configuration 1 of the ballistic heating system, the separation was similar to the

constant offset separation. Peaks 1 - 5 were not completely resolved, but there was an improvement in separation between peaks 1/2 and peak 3, and between peak 3 and peak 4. The greatest improvement was with configuration 2 of the ballistic heating system, where five distinct peaks were observed and there was partial separation between peak 1 and peak 2. Peak widths for peak 4 and peak 5 in this configuration were also quite similar, being 175 ms and 181 ms at half height, respectively. Compared to the separation without ^{2}D heating, there was an improvement in S/N without significantly compromising the peak resolution that was observed with the constant offset separation.

2.2.3.1 Retention Time Reproducibility

Improvements in resolution and peak capacity had to be demonstrated to justify designing a ^{2}D temperature programming system. However, retention time reproducibility was an important specification for the ballistic heating system since this is relied upon for peak identification. With the MXT-65 ^{2}D column installed, five replicate injections of diesel were completed and the relative standard deviations (RSD) of the retention times of 10 peaks were calculated to determine the run-to-run reproducibility. Of these 10 peaks, five were early eluting peaks and five were late eluting peaks in the ^{2}D. This was completed for both ballistic heating (configuration 2) and for a standard GC×GC separation without ^{2}D heating. A constant offset separation was not included in the comparison since the results should be similar to the ballistic heating separation, as the same system was used. The data is found in Table A – 3 and Table A – 4 of Appendix A, for the ballistic heating and standard GC×GC separation, respectively. For both types of separation, the ^{1}D retention time's average RSD for the 10 peaks were 0.0 %. This was expected, as the ^{1}D retention time RSD demonstrates the reproducibility of the GC system itself, and this value was consistent with the expected characteristics of Agilent 6890 Plus GC [214]. The ^{2}D retention time RSD for the standard GC×GC separation was 0.1 - 1.2 %, with an average of 0.6 %. For the ballistic heating system, the RSD was 0.2 - 2.0 %, with an average of 0.7 %. Comparing the results, the ^{2}D retention time RSD for the standard GC×GC separation represented the modulator reproducibility,

while for the ballistic heating system, it was a combination of the ballistic heating and the modulator. Student's t-test was performed for both the ^{1}D and ^{2}D retention time RSDs, comparing the two systems. It was found that the differences were not statistically significant at the 95 % probability level. This showed that the ballistic heating system had a negligible effect on retention time reproducibility.

2.2.3.2 GC×GC Separation and Integration Comparison

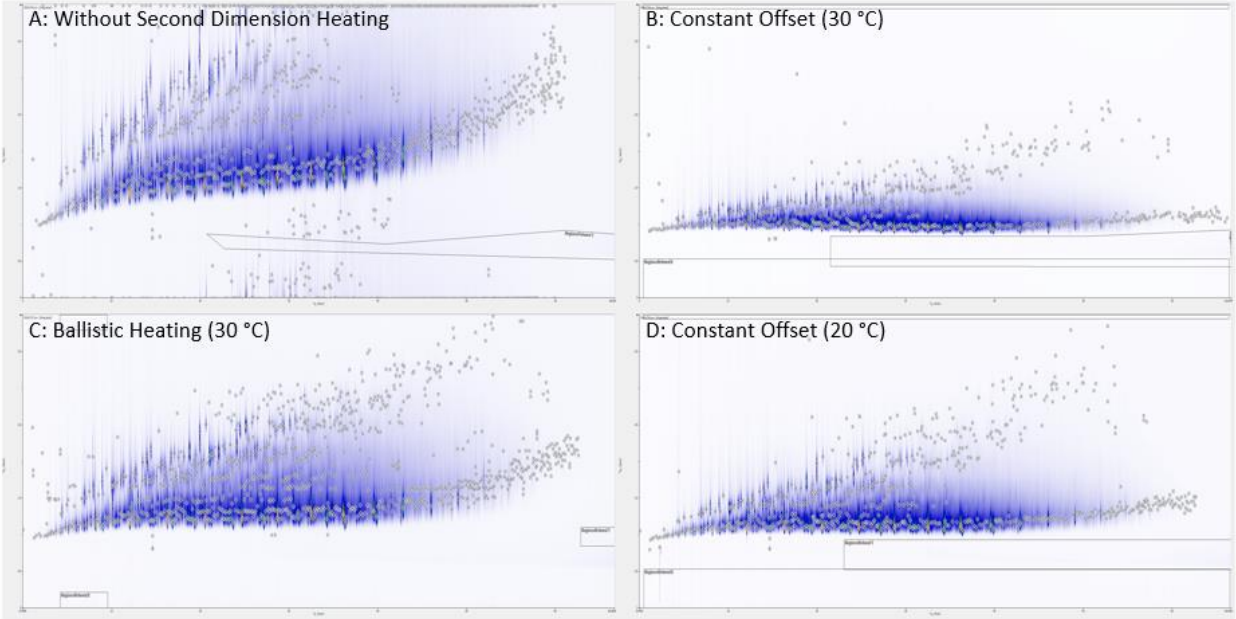

Figure 2-13: GC×GC separation of diesel using a ^{1}D Rxi-5ms (30 m x 0.25 mm x 0.25 µm) and ^{2}D MXT-65 (0.50 m x 0.18 mm x 0.20 µm) column set. A: Standard GC×GC separation; B: Constant temperature offset of 30 °C; C: Ballistic heating with 1.5 of cooling followed by 2.5 s of heating to 30 °C above the oven temperature (configuration 2); D: Constant temperature offset of 20 °C. Integrated peaks are denoted by markers on the chromatogram. ***X-axis: 0 – 66.6 min. Y-axis: 0 – 4 s****.*

The 2D resolution ($R_{s,2D}$) for five peak pairs was compared for four separations using the MXT-65 ^{2}D column: standard GC×GC separation (Figure 2-13A), constant offset of 30 °C (Figure 2-13B), ballistic heating to 30 °C offset - configuration 2 (Figure 2-13C), and constant offset of 20 °C (Figure 2-13D). The peak pairs chosen were separated enough for the calculation of peak widths for all four separations. This meant that peak pairs that were separated in the ballistic heating and the standard GC×GC separations, but not in the constant offset separation, were not considered. In addition, since this was a comparison of ^{2}D heating profiles, the ^{1}D retention time ($^{1}t_R$) was similar for the two peaks, where they would have co-eluted in a 1D separation. This would place a much higher weight on the ^{2}D resolution ($^{2}R_s$) in the $R_{s,2D}$

calculation. GC separation conditions and columns were identical for all four separations. The GC conditions were optimized for the standard separation without any additional heating to make full use of the separation space, while the ballistic heating temperature offset was optimized to eliminate wraparound peaks. The 20 °C constant temperature offset and ballistic heating separation had similar elution times in the ^{2}D for the late eluting compounds, while the 30 °C constant temperature offset had an identical temperature offset to the ballistic heating separation. ^{1}D resolution (^1R_s), ^2R_s, $R_{s,2D}$, and ^{2}D peak width at the base (^2W_b) can be calculated as follows [128]:

$$^1R_s = \frac{\triangle\ ^1t_r}{^1W_{b,\ avg}} \tag{2.2}$$

$$^2R_s = \frac{\triangle\ ^2t_r}{^2W_{b,\ avg}} \tag{2.3}$$

$$R_{s,2D} = \sqrt{(\ ^1R_s)^2 + (\ ^2R_s)^2} \tag{2.4}$$

$$^2W_b = 1.699 \cdot\ ^2FWHM \tag{2.5}$$

where the ^1W_b, and ^{2}FWHM are the ^{1}D peak width at base, ^{2}D peak width at base, and ^{2}D full width at half maximum, respectively. Since the ChromSpace software provides ^1W_b but not ^2W_b, the ^2R_s calculation involved manual measurement of the FWHM for the largest sub-peak. The ^2W_b was estimated according to Eq. (2.5). Among the four separations, the standard separation had the best resolution (average: 1.805) between the peak pairs selected, as it made full use of the separation space (including the ^{2}D dead time) without allowing the wraparound peaks to co-elute with peaks in the subsequent modulation period. Any ^{2}D heating applied would result in a loss of separation under these GC×GC conditions, but the trade-off was an improvement in the S/N. This improvement was particularly noticeable for the most strongly retained peaks shown in Figure 2-14, calculated using Eq. (2.6), where the S/N improved by 257 %. Using the standard separation as the benchmark, the average $R_{s,2D}$ of the peak pairs decreased by 12 % (average:

1.581), 26 % (average: 1.343), and 35 % (average: 1.178) for the ballistic heating, 20 °C constant offset, and 30 °C constant offset separations, respectively (Table A – 5 of Appendix A).

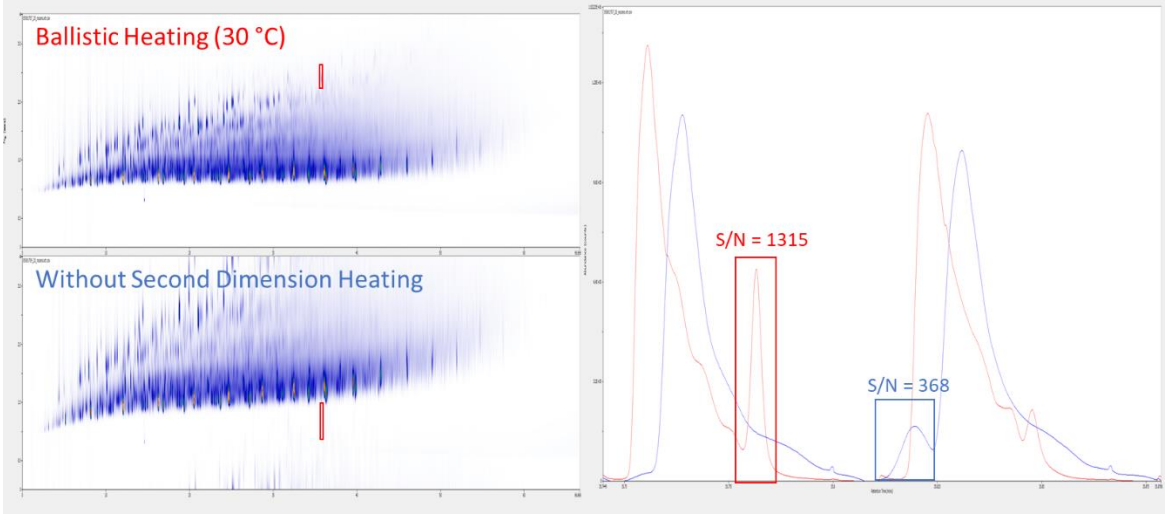

Figure 2-14: Comparison of S/N between the GC×GC separation without ²D heating and with ballistic heating (30 °C).

$$\frac{S}{N} = \frac{(Height - Average\ Noise)}{(Max\ noise - Min\ noise)} \tag{2.6}$$

For the standard GC×GC separation, a total of 1130 peaks were integrated (excluding bleed peaks), although this number was inflated due to the elution of peaks during the modulator discharge (Figure 2-15). The discharge created a pressure pulse which was detected by the FID as a sharp rise in the baseline. For the other separations with a lack of wraparound peaks, no peaks would be integrated since the default peak filter (minimum height: 10000, minimum area: 10000, minimum width: 0.001) would have filtered it out. However, this sudden pressure pulse in conjunction with an eluting peak can artificially create an additional peak which passes the peak filter setting (Figure 2-15A). In other cases, the pressure pulse could affect the peak shape and shift the retention time of the peak without integrating the same peak twice (Figure 2-15B). Manually combing through each peak would be too difficult so all peaks were included and will result in an inflated number. Bleed peaks were removed by specifying a region of the chromatogram to be ignored. Comparing the ballistic heating (30 °C) and constant offset (20 °C) separations, although the elution time of the late eluting peaks were similar, the ballistic heating separation had a more even

distribution of peaks along the 2D space. This had a direct impact on the peak capacity, where the number of peaks integrated (excluding bleed) for ballistic heating was 1046 peaks while the constant offset (20 °C) had 690 peaks. The constant offset of 30 °C was clearly too high as all peaks eluted between 0.9 s and 2.7 s, with only 578 peaks integrated.

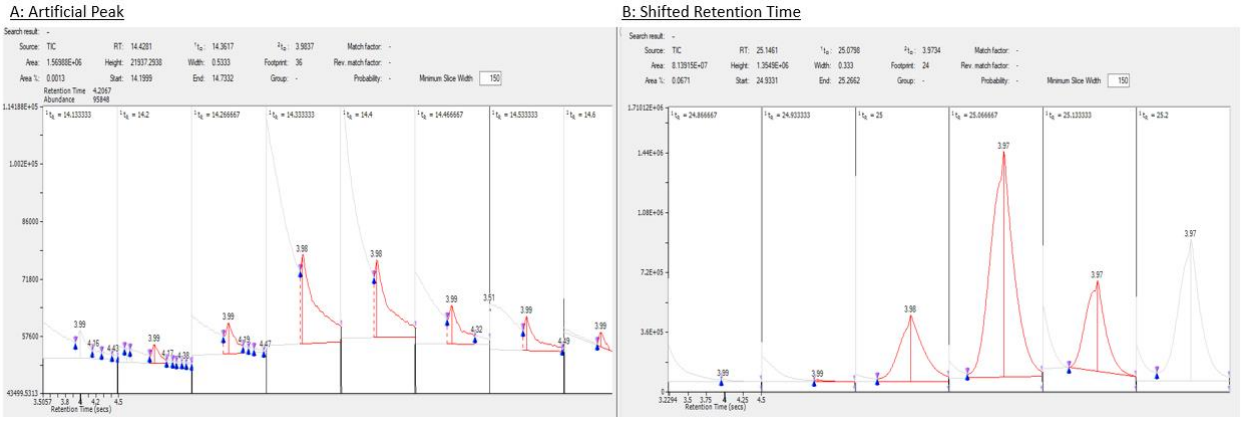

Figure 2-15: Raw GC signal of the sub-peaks of a GC×GC peak eluting during the modulator pulse discharge. A: Generation of an artificial peak; B: Shift of peak maximum affecting retention time.

Comparing these separations to the ones obtained previously with the MXT-WAX column (0.49 m x 0.25 mm x 0.50 µm; Figure 2-11), the MXT-65 column (0.50 m x 0.18 mm x 0.20 µm; Figure 2-13) had shorter ^{2}D retention times due to the lower polarity and thinner stationary phase. This made the MXT-65 column more suitable for the standard GC×GC separation, as there were fewer issues with wraparound peaks co-eluting with peaks in subsequent separations (Figure 2-11A). However, due to the similar nature of the stationary phases in the Rxi-5ms and the MXT-65 columns, both of which are bonded, cross-linked, diphenyl dimethyl polysiloxane stationary phases with differing phenyl content, there was less orthogonality between the two dimensions. This was demonstrated by the band of early eluting peaks, positioned more diagonally along the GC×GC chromatogram for the MXT-65 column (Figure 2-13A). Although the MXT-WAX column provides greater orthogonality, the strong retention of the compounds in the ^{2}D results in significant peak wraparounds, which require either a faster GC temperature programming rate, or a larger constant temperature offset. This provided a better scenario to

demonstrate the merits of the ballistic heating system, which was able to eliminate wraparound peaks without significant loss of separation to the band of early eluting peaks. In addition, the chromatogram was more structured as a result, with clear distinctions between the three bands of peaks (saturated hydrocarbons, 1-ring aromatics, 2-ring aromatics). This was not seen with the MXT-65 column, where the band of early eluting peaks could only be distinguished from the other peaks due to the large differences in concentration.

2.3 Conclusions

It was demonstrated that ballistic heating of the ^{2}D in GC×GC could successfully eliminate (or at least significantly reduce) wraparound peaks, while maintaining better separation of early eluting compounds compared to constant temperature offset. Even with this simple design and lack of precise heating control, ballistic heating significantly improved the ^{2}D separation compared to a constant temperature offset. Resistive heating and passive cooling relying on the forced convection within the GC oven were sufficient in providing the heating and cooling rates needed for ^{2}D temperature programming in GC×GC. Improvements to the design can be made to gain finer control over the heating rate to further improve the ^{2}D separation. Building upon what was learned, the next design (prototype) focused on temperature control, in order to achieve true ^{2}D temperature programming.

3 Prototype - ^{2}DTPS in GC×GC (Version 1.0)[iii]

The proof-of-concept design from section 2 utilized direct resistive heating to ballistically heat a commercial stainless-steel capillary column in the ^{2}D. To achieve true temperature programming, the previous design was updated with the addition of an Arduino microcontroller (Arduino, MA, USA) and a differential thermocouple system to directly measure the difference between the GC oven and ^{2}D column temperature for ease of method development. This was the first demonstration of a temperature programming system for the ^{2}D of GC×GC with full control of the heating rate and temperature offset. As such, it provides significant advantages over the previously described ballistic heating system and is an important milestone.

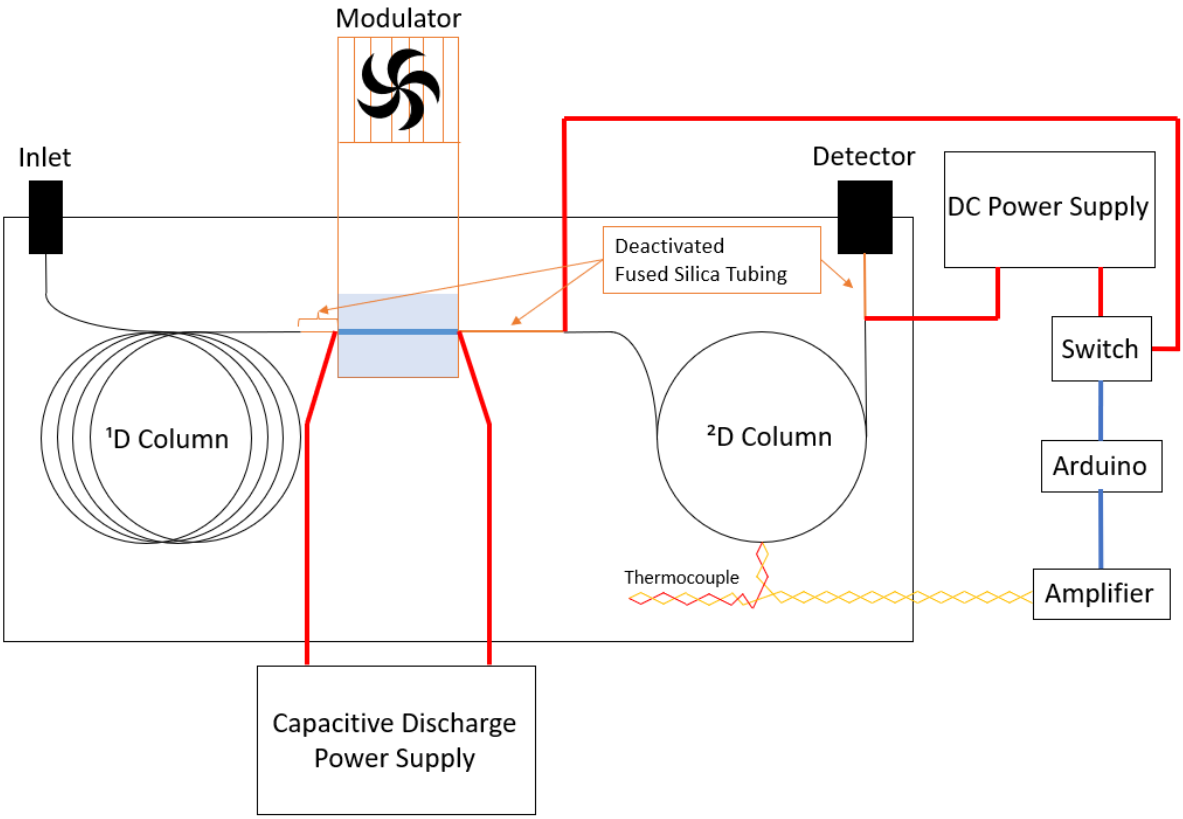

Figure 3-1: GC×GC setup used for the Arduino based ^{2}DTPS utilizing a thermocouple for differential temperature measurement and the Arduino for PID control.

[iii] This Chapter is based on the article published in Journal of Chromatography Open by the author: Chow, H.-Y. J.; Górecki, T. J. Chromatogr. Open 2022, 2, 100062

The layout of the whole GC×GC system with the prototype ²DTPS installed is shown in Figure 3-1. The temperature measurements provided by the differentially connected thermocouples were passed through an amplifier to the Arduino microcontroller. Using that data, the Arduino controlled the switch that was used previously for the ballistic heating setup. However, rather than turning the switch ON and OFF once during the modulation period, the Arduino controlled the heating through PWM to adjust the average amount of power over time that was supplied to the ²D column.

3.1 Temperature Measurement and Calibration

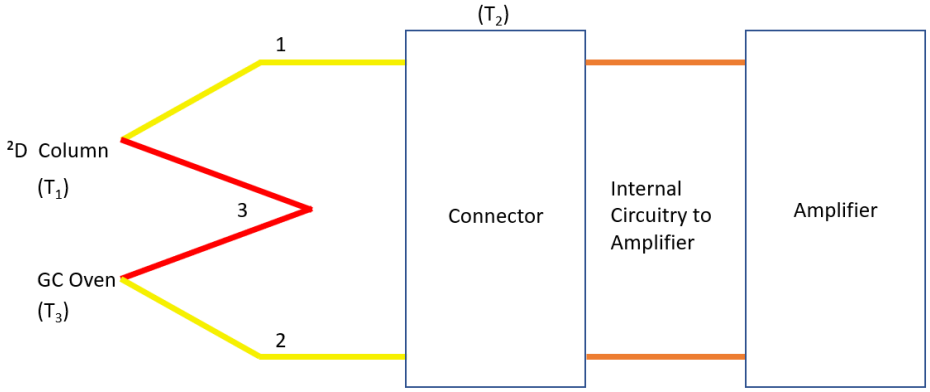

Figure 3-2: Differential temperature measurement between the ²D column and GC oven. Wiring: copper (orange), chromel (yellow), alumel (red).

Measurement of the temperature offset of the ²D column relative to the GC oven was accomplished using two thermocouples connected differentially (Figure 3-2). In this configuration, the Seebeck voltage that was measured through the amplifier was determined by the difference in temperature between the ²D column (T_1) and the GC oven (T_3). This is shown in Eq.(3.1).

$$E = \int_{T_2}^{T_1} \alpha_{chromel}\, dT + \int_{T_3}^{T_2} \alpha_{chromel}\, dT + \int_{T_1}^{T_3} \alpha_{alumel}\, dT$$

$$E = \int_{T_3}^{T_1} \alpha_{chromel}\, dT - \int_{T_3}^{T_1} \alpha_{alumel}\, dT$$

$$E = \int_{T_3}^{T_1} \alpha_{chromel,alumel}\, dT \qquad (3.1)$$

An instrumentation amplifier with a gain of approximately 185 was used to amplify the thermocouple voltage generated from the temperature difference between the ^{2}D column and GC oven. The Arduino Uno analog pins had 10 bits (2^{10} = 1024 = 0 – 1023) of resolution, being mapped to 0 - 5 V. This meant that the resolution of the system was 0.0049 V/unit. For a k-type thermocouple, a 1 °C temperature difference at the measurement junction (reference junction at 0 °C) produces 0.039 mV [215]. With a gain of 185, this produced 0.0072 V, which was just above the resolution of the Arduino Uno following amplification of the signal. To account for any sources of error, the system was calibrated using the cold junction compensation method. This involved submerging the thermocouple junction that was normally left hanging inside the GC oven into an ice bath. The thermocouple junction for the ^{2}D column remained attached and the GC oven was set to a series of temperatures from 35 °C to 100 °C in increments of 5 °C, for approximately 1 min at each temperature. The voltage from the amplifier was connected to the analog pins of the Arduino, where the readout (after conversion to mV), was collected through serial communication in the Arduino IDE software's Serial Monitor. This data was then copied to Excel (Microsoft Corporation, WA, USA) where the voltages were averaged at each temperature, and a linear curve was fitted to the temperature versus voltage data.

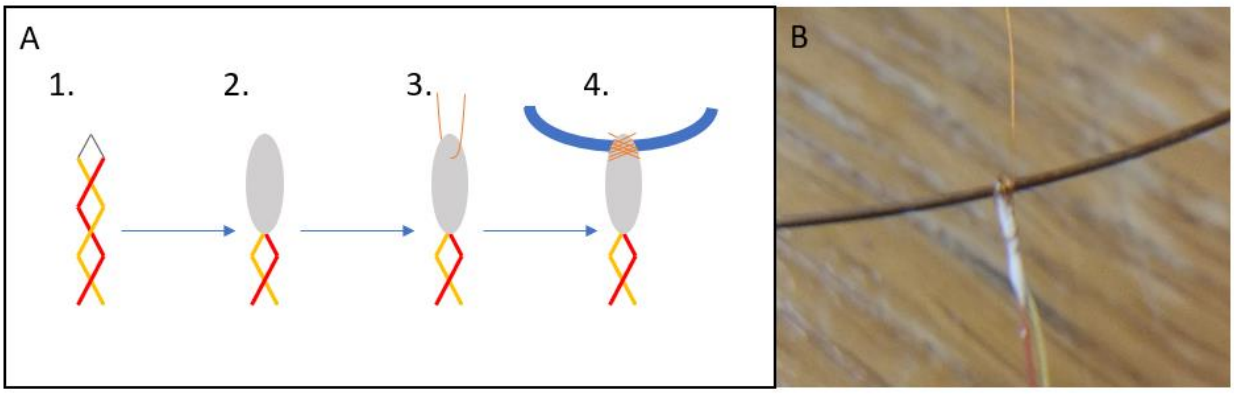

Figure 3-3: Procedure for the attachment of thermocouple to the ^{2}D column (A). Example of an attached thermocouple (B).

The k-type thermocouple (0.003”, perfluoroalkoxy insulation) was attached to the ^{2}D column using OMEGABOND OB-600 (OMEGA Engineering Inc.), an electrically insulating and thermally conductive cement, and a 46 gauge wire (Figure 3-3). The procedure was as follows:

1. 0.003” chromel and alumel thermocouple wires were spot-welded together to form the junction. Excess thermocouple wire beyond the junction was trimmed off.
2. The exposed (bare wire) junction was dipped in the OB-600 cement.
3. A 46 gauge wire was threaded through the first loop of the twisted junction that was coated in the cement. The cement was allowed to cure at 80 °C in the GC oven for 30 min.
4. After the cement was cured, the thermocouple was tied to the ^{2}D column using the 46 gauge wire.

Unlike the ballistic heating setup where the thermocouple was spot-welded to the column directly, the cement was used to eliminate the electrical noise being passed from the DC power supply. This noise made it extremely difficult to acquire an accurate measurement without significant digital filtering which would result in slow response times. This was not as much of an issue with the ballistic heating setup, because the thermocouple signal was measured with an oscilloscope when the temperature was constant. This provided a stable signal, although slightly noisy, to determine the temperature as well as the achieved temperature offset when the power supply was on. For the Arduino system, noise was a significant issue since frequent temperature measurements were needed to adjust the heating. Noise would affect the data sent to the Arduino resulting in erroneous adjustment of the heating, and consequently inaccurate temperature programming.

3.2 ^{2}D Temperature Control

PWM is a type a digital signal that is typically used to drive or control analog devices. In this design, it was used to control the heating to the ^{2}D column. PWM yields a square wave signal that fluctuates between ON (5 V on the Arduino Uno) and OFF (0 V). This signal was used to control the modified switch

from the ballistic heating system. Although the Arduino has dedicated PWM pins (3, 9, 10, 11) of 490 Hz and 980 Hz (5, 6), the built in PWM function (`analogWrite()`) was not used for greater control over the pulse width. For this prototype, a frequency of 40 Hz was used. This was sufficient for generating a smooth temperature program ramp that tracked the ^{2}D temperature program accurately. Lower frequencies were found to result in an oscillating signal, while higher frequencies displayed no noticeable improvement in temperature control. To adjust the average power over time from the DC power supply, the duty cycle was adjusted by changing the heating duration (pulse width) within a set time window (period). For example, a 40 Hz frequency has a window size of 25 ms. A 50 % duty cycle to deliver 50 % of the DC power supply's power output would require the heating duration to be 12.5 ms.

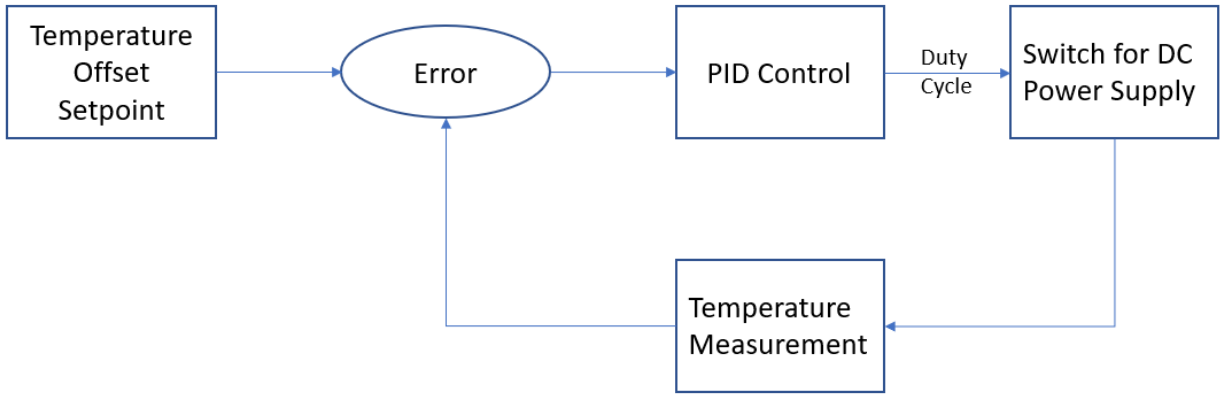

Figure 3-4: PID temperature control process.

For temperature control, the Arduino acted as a proportional, integral, derivative (PID) controller. A PID controller is a feedback loop system (Figure 3-4), where the controller calculates the error between a setpoint (desired temperature offset) and measured variable (actual temperature offset) and provides an output (heating duration within a set time window) based on the proportional, integral, and derivative terms as shown in Eq.(3.2) [216].

$$u(t) = K_p e(t) + K_i \int_0^t e(t)dt + K_d \frac{de}{dt} \tag{3.2}$$

K_p, K_i, and K_d are the gain values for the proportional, integral, and derivative terms, respectively. The proportional term calculates an output proportional to the instantaneous error. The larger the error, the larger the output. However, as the error becomes smaller, the output eventually becomes insufficient to correct the error and results in a steady state with a constant offset from the setpoint. This steady state error can be reduced with a larger proportional gain, but that can lead to instability and oscillations. The integral term sums the error over time, eliminating the steady state offset error that would be seen with a proportional only controller. The output from the derivative term is proportional to the rate of change of the error. As the error decreases (input is getting closer to the setpoint), the derivative term reduces the correction factor, preventing overshoot. However, the derivative term is susceptible to noise, due to the sudden changes in error.

3.3 Code

Two separate Arduino sketches were created for the prototype ^{2}DTPS, one for the calibration of the thermocouple signal and another for the ^{2}D temperature programming.

3.3.1 Sketch: Thermocouple Calibration

```
#define thermocouple A4

void setup()
{
  pinMode(thermocouple, INPUT);
  Serial.begin(9600);
}
void loop()
{
  float voltage = analogRead(thermocouple) * 5 / 1023.000 * 1000;
  Serial.println(voltage);
}
```

The sketch for the thermocouple calibration only has one purpose, to read the signal (mV) from the thermocouple through the amplifier and print the data through the serial port. The data was then transferred to Excel for linear regression, where the slope (mV versus temperature) was used for the ^{2}D temperature programming sketch. The signal from analog pin `A4` (defined as a constant variable labeled

thermocouple) was read using the function `analogRead()`. This 10-bit reading mapped to 0 – 5 V was then converted to mV and stored in the variable, `voltage`. This variable was then printed (`Serial.println(voltage)`) to the serial port of the Arduino IDE's Serial Monitor.

3.3.2 Sketch: ^{2}D Temperature Programming

The complete sketch for ^{2}D temperature programming is found in Appendix B under B: ^{2}D Temperature Programming Sketch – Prototype (Version 1.0). The sketch for ^{2}D temperature programming can be broken down as follows:

```
#include libraries
Declare global variables and their initial values

void setup()
{
  Initialize pin modes
  Initialize PID settings
  Initialize array values to 0 for the running average functions
  Set Serial communication baud rate
}

void loop()
{
  while(run has not started)
  {
Take a running average of the thermocouple signal to zero the signal
Check to see if discharge box started
  }
  switch(state)
 {


  case 0: delay the heating


  case 1: linear temperature ramp


  case 2: cool column


  }
}

Define functions
```

When the Arduino was first powered on, it was initialized with all the defined global variables and the settings within `setup()`. After it entered the `loop()`, it proceeded to the `while(condition)` function,

which was a loop that continued for as long as the condition was true. In this case, the condition was that the discharge box has not discharged, meaning the run has not started. Within the `while()` loop, it was taking a running average (25 data points) of the thermocouple signal to be used to zero the mV reading.

After the GC run started and the discharge box has discharged, the program exited the `while()` loop and would never enter it again until the Arduino was reset. The next set of code was the `switch(state)` function which specified the set of code to execute depending on the value of `state` (0, 1, or 2), initially set to `0`. `Case 0` was to delay the heating for a set amount of time (global variable defined before `setup()`). At the end of the body of code within a `case`, the value of `state` was incremented by 1 (`state = state + 1`) and the `break` function was used. This exited the `switch()` function and the `loop()` was repeated. At this point, the previous `while()` loop condition was false, so the system would proceed directly to the `switch()` function, entering `case 1` (linear temperature ramp). This process repeated, cycling through the three available cases: `0` (delay heating), `1` (linear temperature ramp), and `2` (Cool column).

Within each `case` were multiple variables to keep track of the elapsed time (since the Arduino powered ON), `millis()`, and the window time. The `initTime` variable stored the value returned by the `millis()` function at the beginning of each `case`. This was the timestamp for when that segment of the temperature program started. The `cycleTime` variable was passed the duration of that portion of the temperature program in ms (i.e., 2500 ms for a linear temperature ramp duration). The `diffTimeMS` variable was passed the elapsed time since the start of the `case`. Within each `case` was a `while()` loop which ran for as long as the elapsed time (`diffTimeMS`) was less than the duration of `cycleTime` for that `case`. The `diffTimeMS` variable value was recalculated at the end of the `while()` loop. The bulk of the temperature programming and temperature monitoring lies within this `while()` loop. Once the `diffTimeMS` was equal to or had exceeded the `cycleTime`, the program would exit the `while()` loop,

the `state` value was incremented, the `break` function was used, and the program moved on to the next `case` (segment of temperature program).

The following lines of code present the `tempRead()` function for reading the thermocouple temperature:

```
float tempRead(void)
{
   float voltage = analogRead(thermocouple) * 5 / 1023.000 * 1000;
   float temperature = (voltage – zero) / 7.657643
   return temperature;
}
```

The `tempRead()` function was defined as a `float` since it returned a floating point value (temperature). The `void` within the brackets of the function indicated that it required no input values. When this function was called, it executed the body of code, and returned the value stored in the `temperature` variable. The first line used the `analogRead()` function to read the analog signal from the analog pin (`thermocouple = A4`). This value was converted into mV by multiplying the analog value by 5 V/1023 units*1000 mV/V.

Due to the complexity of the circuit, which included all the components and wiring from the connector to the ADC on the Arduino, the reading was zeroed to eliminate the minor contributions of electromotive force from these components. The `zero` value was calculated before the start of the run while the Arduino was idling. The temperature was then calculated using the slope (mV/°C) from the calibration curve generated using data from the Thermocouple Calibration sketch (section 3.3.1).

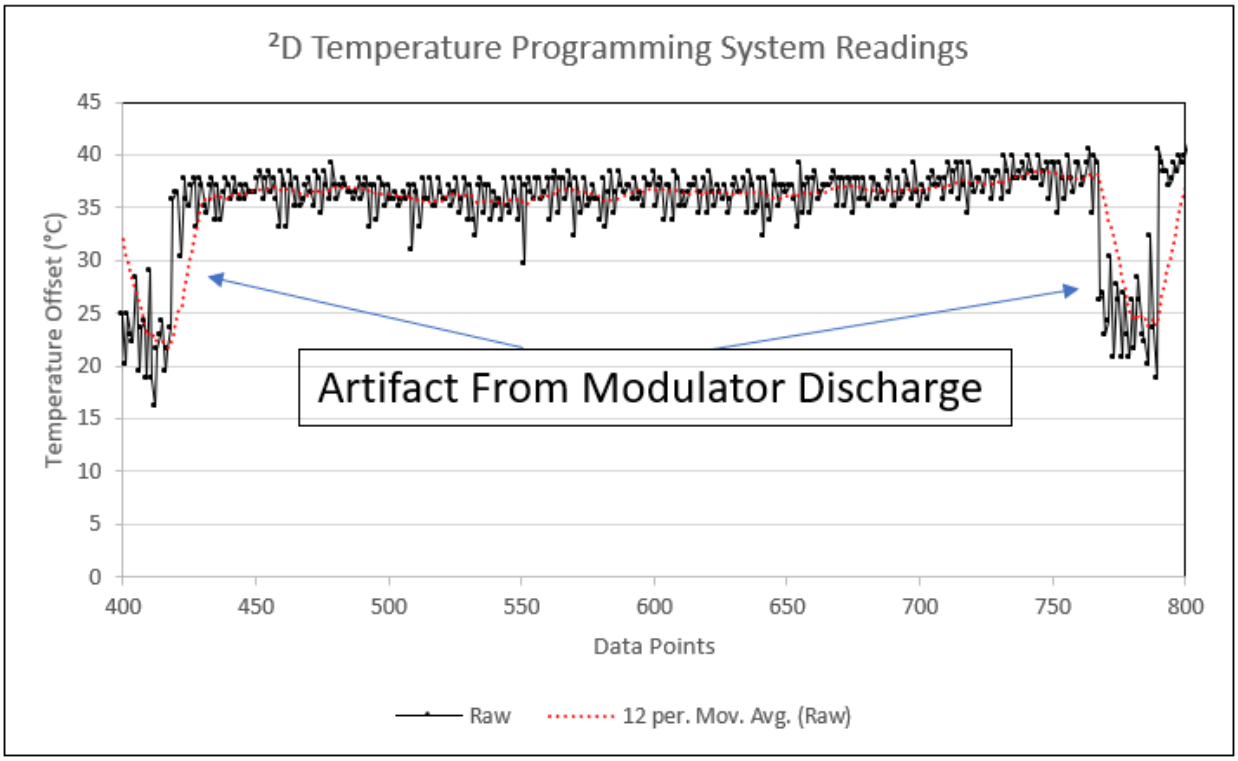

Figure 3-5: Raw readings from the ²DTPS measured by the k-type thermocouple. A drop in the signal was observed due to electromagnetic interference caused by the modulator discharge.

Temperature offset readings from the ²DTPS are shown in Figure 3-5. Even with the use of the insulating cement, there was still a significant amount of noise in the readings. This noise had a significant impact on the PID system, particularly for the derivative term in the calculation. To reduce the noise, the thermocouple readings were filtered using a running average of 12 points with the following code (function):

```
float movingAverage(float temperature)
{
  totalTemp = totalTemp - tempReading[index];
  tempReading[index] = temperature;
  totalTemp = totalTemp+ tempReading[index];
  index = index + 1;

  if (index >= period)
  {
    index = 0;
  }
  averageTemp = totalTemp / period;
  return averageTemp;
}
```

The temperature value was passed to the `movingAverage()` function's input variable, `temperature`. An array size of 12, `tempReading[period]`, was created to store the temperature values. The function started by subtracting the oldest reading in the array from the total temperature (12 readings). The new temperature value (`temperature`) was then stored in its place in the array (`tempReading[index]`). The new temperature value was then added to the total temperature (`totalTemp`). The index position for the array was incremented by 1. However, if the current index value was equal to the array size (12), the index value was reset to 0 since the array index was numbered from 0 - 11. The average temperature (`averageTemp`) was then calculated and returned by the function.

To monitor the temperature program during the run, the running average of the readings was printed to the serial port to be monitored on the serial plotter, which plots the data points on a real time graph. Due to the speed with which the program executed the code within a loop, not all the data points read by the Arduino were needed to monitor the status of the temperature program. A simple counter was created and incremented with each iteration of the `while()` loop within each `case`. Every 20th iteration of the loop was when the running average of the temperature reading was printed to the serial port. The code was as follows:

```
If((counter%20)==0) //Check if counter is divisible by 20
{
  Serial.println(filter);
}
```

The most important portion of the sketch was the linear temperature program loop. The temperature control was accomplished using the PID library written by Brett Beauregard [217]. As introduced before, the PID required a temperature setting (`Setpoint`) and an `Input` (running average temperature value), and an `Output` (heating duration) was returned based on the error between the input and setting, as well as the gain for each of the PID terms. The initial temperature setpoint was calculated in `case 0` (delay), while the system was still cooling from the previous modulation period. Within the `while()` loop of

`case 0`, the temperature offset was read on the analog pin and passed to the moving average function. When the duration of the delay has been met or exceeded, the program exited the `while()` loop and executed the following:

```
   startTemp = filter; //set the starting temperature for the ramp I
   rampRate = (maxTemp – startTemp)/(rampTime); //set ramp rate for ramp
(C/s)
```

This calculated the temperature programming rate (`rampRate`) from the latest temperature of the moving average. This additional step was necessary because the system may not have cooled to oven temperature during the cooling and delay periods of the ^{2}D temperature program. Thus, the temperature programming rate might have to change slightly between modulation periods, depending on the starting temperature of the temperature ramp. The system would then move to `case 1`, the linear temperature programming portion of the program. Before entering the `while()` loop, the elapsed time was calculated (updates the variable from the previous modulation period), and a timestamp was taken for the start of the PWM window.

```
   elapseTimeMS = millis() – initTime;
   windowStartTime = millis();
```

Within the `while()` loop, the temperature offset was read and the moving average value was updated and passed to the `Input` variable for the PID. The setpoint for the temperature program was then calculated based on the elapsed time, temperature programming rate, and the starting temperature. The heating duration was then calculated with the PID (stored in the variable: `Output`) based on the values of `Input` and `Setpoint` using the following code:

```
   myPID.Compute();
```

The value of `Output` was limited to a range between 0 and the window size (25). This was declared in the `setup()` function during the initialization of the PID with the following code:

```
myPID.SetOutputLimits(0, windowSize);
```

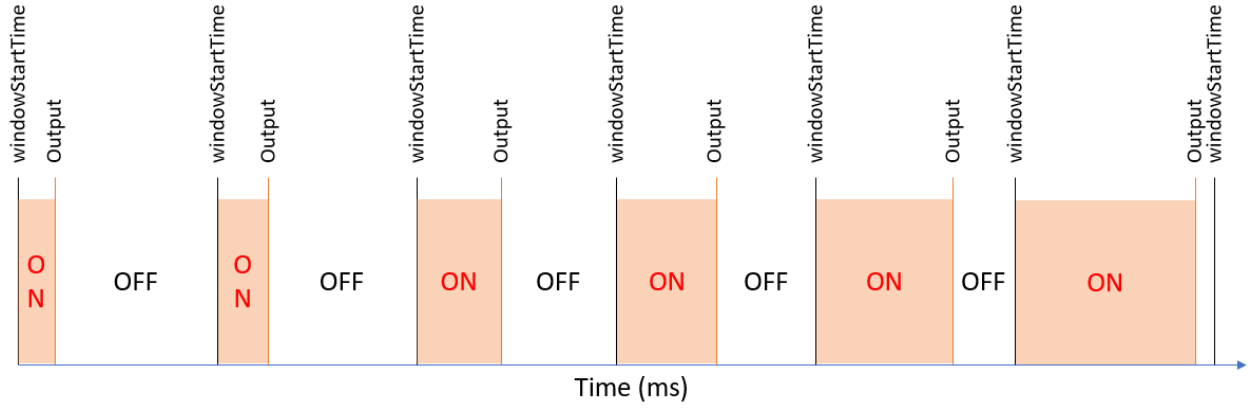

Figure 3-6: Visualization of the MOSFET PWM relative to the window timestamp, window size, and Output values of the PID.

The PWM window was updated before applying the `Output` value. The PWM window timestamp (`windowStartTime`) was checked to ensure the current time has not exceeded the window size (25 ms). If it had, the window timestamp was increased by the size of the window (25 ms) before the `Output` value was applied for heating. To determine whether to turn the switch ON or OFF, the `Output` value was compared to the elapsed time within the PWM window (`millis() - windowStartTime`). If the `Output` value was greater, the switch was turned ON for heating, or else the switch was turned OFF. The overall result of this process is shown in Figure 3-6. This process was repeated until the duration of the linear temperature ramp was reached or exceeded.

Due to the inaccuracy of the Arduino clock, which was slower than real time, this program needed to rely on an external clock or signal to reset the Arduino so that the error did not grow perpetually over the course of a GC×GC separation. This was done with this function at the end of the `while()` loop within `case 2`, the cooling portion of the temperature program:

```
channel = analogRead(channelA);
if(channel > 400)
{
   state = state - state;
   break;
}
```

During the cooling, the system was monitoring the analog pin that was connected to the discharge box. When the discharge box discharged (start of a new modulation period), the `if()` statement becomes `True`. The value of `state` was then reset to `0` so that the next iteration of the `loop()` function entered `case 0`. The `break` function was used to escape the `while()` loop, even if the elapsed time had not exceeded the cooling duration (due to the system clock being slightly slower than real time).

3.3.3 Sketch: Constant Offset

The code for the constant offset sketch was a modified version of the ²D temperature programming sketch. All of the code was copied and the code within the loop was modified. Since the program only had one goal (to maintain a constant temperature offset), the code within the `loop()` was much simpler:

```
Void loop()
{
  pidCounter = pidCounter + 1;
  while ((millis() < 10000))
  {
    zero = background();
  }
  filter = movingAverage(tempRead());
  Input = filter;
  Setpoint = offsetTemp;

  myPID.Compute();

  if ((millis() - windowStartTime) > windowSize)
  {
    windowStartTime += windowSize;
  }
  if (Output > millis() - windowStartTime)
  {
    digitalWrite(relayPin, HIGH);
  }
  else
  {
    digitalWrite(relayPin, LOW);
  }
  if ((pidCounter % 10) == 0) //Check if pidCounter is divisible by 10
  {
    Serial.println(filter);
  }
}
```

The `loop()` started with the `background()` function for the first 10,000 ms since the Arduino was first powered on or reset. This provided a thermocouple voltage reading to zero the signal. After 10,000 ms, the differential temperature was measured and the PID calculated the `Output` based on the error between the `Setpoint` (constant offset temperature) and the `Input`. The heating control was the same as discussed previously. Timing was unnecessary and did not need to be synchronized with the GC run or modulator, keeping the code simple.

3.4 Experimental

The GC×GC-FID system with the ^{2}DTPS connected to the ^{2}D column is shown in Figure 3-1. The instrument setup consisted of an Agilent 6890A GC with an Agilent 7683B autosampler and an FID (Agilent Technologies, Santa Clara, CA, USA), and the Waterloo Modulator. The column set consisted of an Rxi-5ms (29 m x 0.25 mm x 0.25 µm) ^{1}D column and an MXT-WAX (0.50 m x 0.25 mm x 0.50 µm) ^{2}D column (Restek Corporation). A 0.05 m x 0.05 mm fused silica capillary (TSP050375VS, Molex, Lisle, IL, USA) was used between the ^{1}D column and modulator, and deactivated fused silica capillaries from Restek were used between the ^{1}D column and the modulator (0.05 m x 0.05 mm), the modulator and the ^{2}D column (0.46 m x 0.25 mm), and the ^{2}D column and the FID (0.45 m x 0.25 mm). Column connections were made using SilTite® mini unions (Trajan Scientific Americas Inc.). The ^{2}DTPS consisted of an Arduino UNO R3 microcontroller (Arduino, MA, USA), a custom made switch (Science Technical Services, University of Waterloo) utilizing a metal-oxide-semiconductor field-effect transistor (MOSFET), an adjustable DC power supply (AB-5PS-D – ABRA Electronics, Montreal, QC, Canada), a thermocouple (0.003” k-type, OMEGA Engineering Inc.), and a custom-made 185 gain amplifier (Science Technical Services).

To evaluate the ^{2}DTPS, a sample of undiluted diesel from a local gas station was used. Diesel (0.2 µL) was injected at a 300:1 split, with the inlet at 250 °C. The carrier gas (H_2) was set to a constant flow of 1.5 mL/min. The GC oven temperature program started at 40 °C and increased to 210 °C at 3 °C/min,

where it was held for 10 min. The FID was set to 250 °C with 40 mL/min of H_2, 400 mL/min of air, 30 mL/min of makeup gas (N_2) + carrier gas (H_2), and an acquisition rate of 200 Hz. The modulation period for the separations were 5 s. All gases were obtained from Linde Canada (Scarborough, ON).

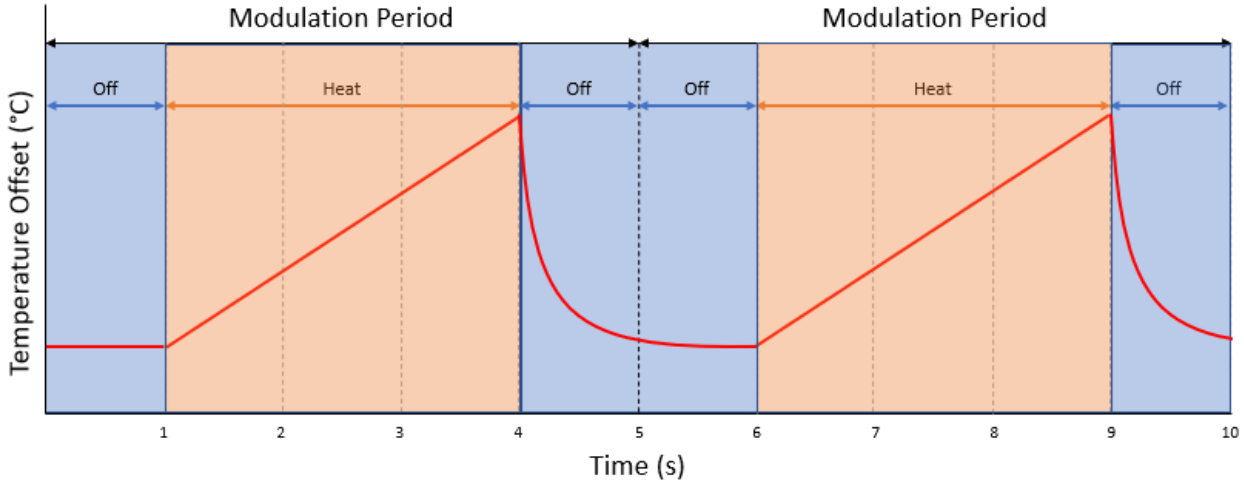

Figure 3-7: ^{2}D temperature program profile relative to the modulation period. Consisted of a 1 s delay to the heating at the start of the modulation, followed by a 3 s linear temperature ramp to the set temperature offset, and finally the heating was stopped in the final 1 s of the modulation period (5 s). Overall, it was 3 s of heating and 2 s of passive cooling.

Three ^{2}D separation temperature scenarios were tested with the ^{2}D column at oven temperature, at a constant positive temperature offset of 40 °C, and with a ^{2}D temperature program (Figure 3-7). The constant positive temperature offset and ^{2}D temperature programming were both accomplished using the ^{2}DTPS. The ^{2}D temperature program consisted of a 3 s linear temperature ramp to a positive temperature offset of 50 °C (at 16.7 °C/s) and 2 s with the heating off for the ^{2}D column to cool back to oven temperature. The cooling was split evenly (1 s) between the beginning and end of the modulation period. Each separation was run in triplicate and the results were compared for retention time reproducibility and peak resolution.

3.5 Results and Discussion

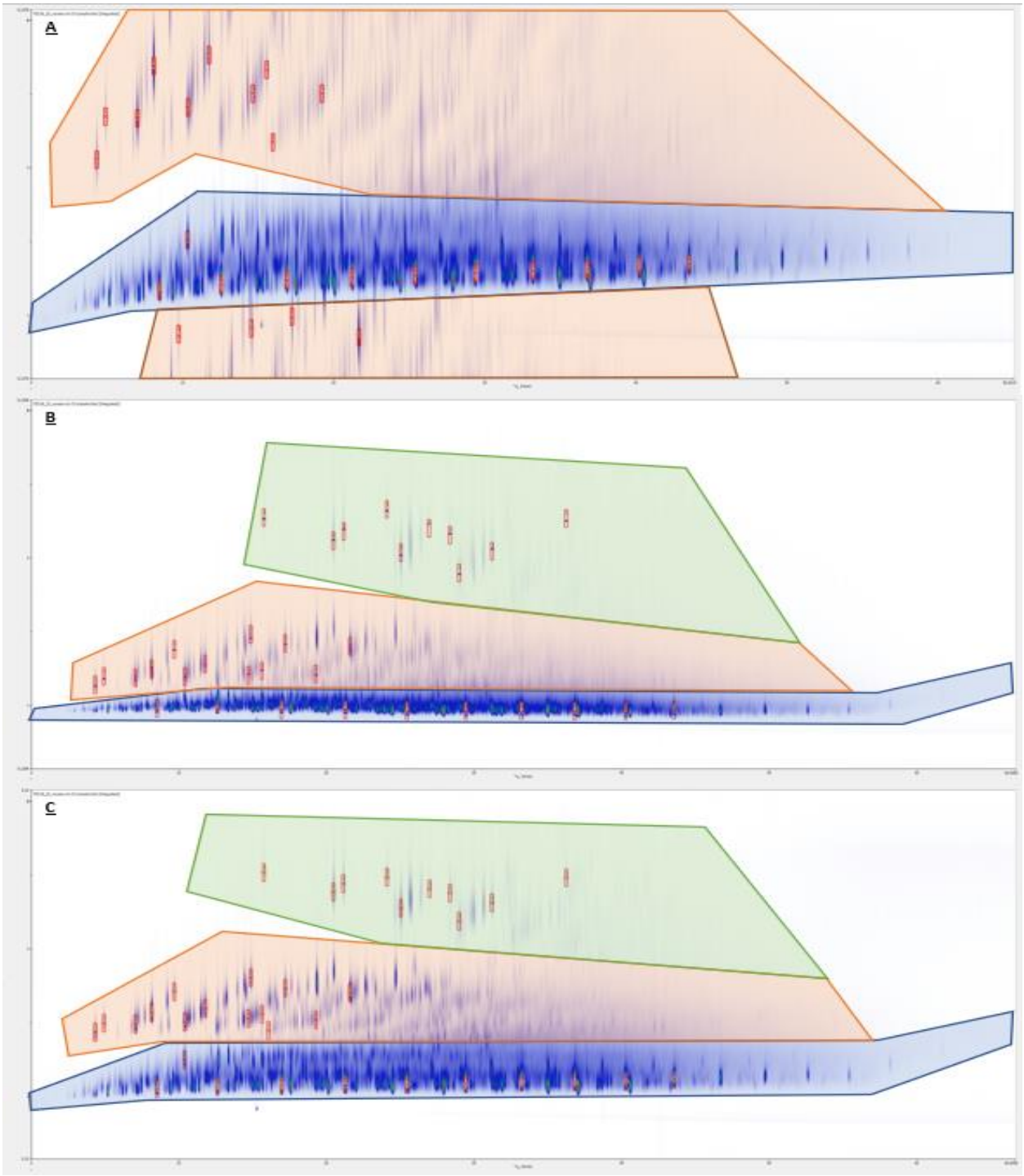

Figure 3-8: GC×GC separations of diesel using an Rxi-5ms (30 m x 0.25 mm x 0.25 mm) ^{1}D column and MXT-WAX (0.50 m x 0.25 mm x 0.50 µm) ^{2}D column. GC×GC separation without ^{2}D heating (A). Constant offset separation of 40 °C (B). Linear ^{2}D temperature programming to a 50 °C offset (C). Saturated hydrocarbons (Blue). 1-ring aromatic hydrocarbons (Orange). 2-ring aromatic hydrocarbons (green). Peaks integrated for reproducibility comparison are distinguished by the region within the red boxes for each chromatogram. ***X-axis: 0 – 66.6 min. Y-axis: 0 – 5 s****.*

The diesel separations used to evaluate the ^{2}DTPS are shown in Figure 3-8. The GC×GC separation conditions without ^{2}D heating were optimized for the ^{1}D separation. This resulted in peak wraparound for the more polar 1-ring aromatic hydrocarbons and 2-ring aromatic hydrocarbons, which coeluted with the saturated hydrocarbons. For the constant offset and ^{2}D temperature programming separations, the temperature offset was increased until wraparound peaks were eliminated.

3.5.1 System Reproducibility

System repeatability (within-day, n = 3) was compared for three ^{2}D separation conditions: without ^{2}D heating (at oven temperature), ^{2}D temperature programming, and ^{2}D constant temperature offset. For the separation without ^{2}D heating, 25 peaks were selected for the standard GC×GC separation, of which 11 were saturated hydrocarbons and 14 were 1-ring aromatic hydrocarbons. For the ^{2}D temperature programming separation, the same saturated and 1-ring aromatic hydrocarbons were selected, based on the relative positioning and intensity, and an additional ten 2-ring aromatic hydrocarbons were included, for a total of 35 peaks. For the constant offset separation, due to coelution within the band of saturated hydrocarbons and some coelution between the 1-ring aromatic and saturated hydrocarbons, only 33 of the 35 peaks from the ^{2}D temperature programming separation were used for the comparison. The peaks selected for the comparison are shown in Figure 3-8, where the red regions encapsulate the peaks integrated in the GC×GC chromatogram.

3.5.1.1 GC×GC Separation Without ^{2}D Heating

The retention time reproducibility of the GC×GC separation where the ^{2}D column was at oven temperature (Table 3-1) can be considered the benchmark of the system. This reflected the precision of the GC×GC system without the ^{2}DTPS. Two sets of RSD values were provided, labeled as “Manual” and “Automated”. The “Manual” values involved significant user intervention by checking each integrated peak for all three replicate injections to ensure proper integration of sub-peaks and that the same

Table 3-1: Reproducibility of the standard GC×GC separation of diesel without any ²D heating, utilizing the single-stage Waterloo modulator. Results are colour coded by the class of compounds (yellow: saturated hydrocarbon, green: 1-ring aromatic hydrocarbon).

	AVERAGE (MANUAL)				RSD [MANUAL | AUTOMATED]					
PEAK	^1t_r (min)	^2t_r (s)	Area	^2W_b (s)	^1t_r (%)		^2t_r (%)		Area (%)	
1	4.315	2.98	61815884	0.925	0.00	0.00	0.37	0.28	0.99	2.8
2	4.917	3.55	35027995	1.086	0.00	0.00	0.35	0.29	1.8	1.8
3	7.016	3.52	154199227	0.975	0.03	0.04	0.39	0.43	0.99	1.1
4	8.094	4.22	227617140	1.104	0.03	0.03	0.45	0.42	0.84	0.84
5	8.492	1.19	531965761	0.313	0.02	0.02	0.44	0.20	0.81	0.81
6	9.721	5.58	27850790	1.318	0.06	0.06	0.39	0.38	1.7	3.5
7	10.353	1.87	151905633	0.621	0.01	0.02	0.41	0.37	0.97	4.2
8	10.361	3.68	141735321	0.954	0.03	0.03	0.28	0.27	0.81	0.81
9	11.729	4.40	95489928	1.205	0.01	0.01	0.36	0.32	0.37	0.37
10	12.559	1.28	802820939	0.317	0.02	0.13	0.17	0.30	0.81	12
11	14.583	5.68	67612776	1.257	0.00	0.00	0.49	0.49	5.7	7.0
12	14.650	3.85	63794417	0.887	0.02	0.02	0.51	0.48	0.65	0.65
13	15.595	4.16	49930758	0.959	0.01	0.01	0.58	0.42	0.70	6.7
14	15.980	3.21	24225193	0.822	0.01	0.01	0.40	0.33	1.0	1.0
15	16.896	1.33	965853733	0.314	0.01	0.01	0.61	0.50	0.97	0.13
16	17.250	5.81	62132770	1.208	0.00	0.00	0.50	0.48	4.3	4.3
17	19.255	3.85	73015959	0.880	0.01	0.01	0.30	0.39	0.47	2.7
18	21.223	1.37	1008153288	0.307	0.02	0.02	0.74	0.61	1.8	1.7
19	21.646	5.57	221020403	1.079	0.01	0.01	0.82	0.81	0.91	1.6
20	25.392	1.40	1128336757	0.303	0.02	0.02	0.62	0.54	2.0	4.7
21	29.379	1.42	1075151800	0.307	0.02	0.03	0.78	0.70	1.6	7.8
22	33.170	1.45	1074864073	0.311	0.07	0.07	0.97	0.89	2.9	2.6
23	36.783	1.48	911973605	0.316	0.03	0.03	0.80	0.72	0.42	7.4
24	40.209	1.52	661312563	0.322	0.06	0.04	1.4	1.3	2.7	7.0
25	43.502	1.55	415265361	0.328	0.06	0.06	1.5	1.4	2.0	4.1
OVERALL AVERAGE				0.737	0.02	0.03	0.59	0.53	1.5	3.5
SATURATED HYDROCARBON				0.342	0.03	0.04	0.77	0.68	1.5	4.8
1-RING AROMATIC HYDROCARBON				1.047	0.02	0.02	0.44	0.41	1.5	2.5

sub-peaks were used for each run. This was only possible because there were no significant shifts in the ^1t_r or changes in analyte concentration where sub-peak profiles look identical between replicates. Any adjustments to the integration settings for a particular peak, to correct for improper integration of sub-peaks, would be applied to all replicates to ensure consistency. This provided the best overall RSDs for peak area but was subject to significant user bias. The "Automated" values involved minimal user intervention, with the results better reflecting the values one would obtain in routine analysis where

individual inspection of each peak would not be feasible. For these peaks, the only manual processing involved was correcting for split peaks while integration settings remained the same for all separations.

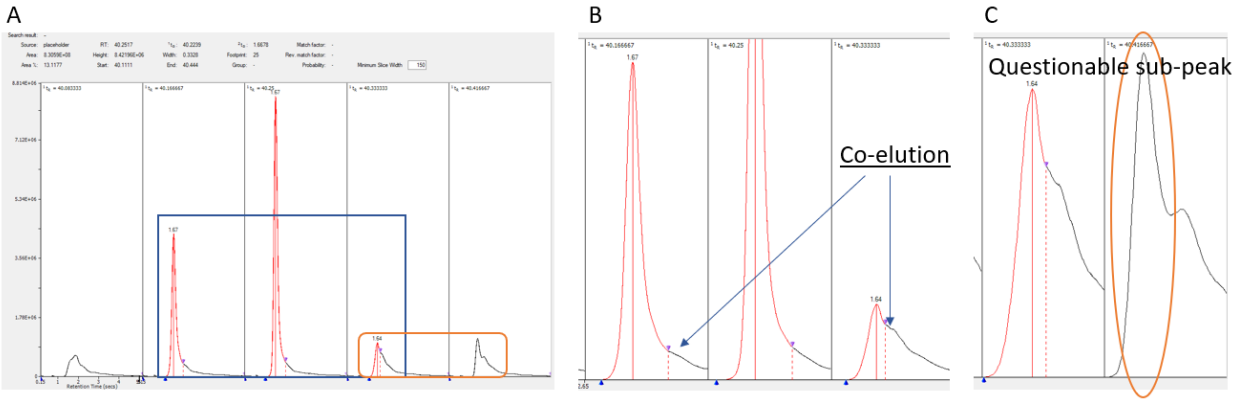

Figure 3-9: Sub-peaks of Peak 24 of the GC×GC separation (A). Zoomed in region highlighted by the blue box in (A) to show the coelution of peaks (B). Questionable sub-peaks to be grouped together for a GC×GC peak (C).

The $^{1}t_r$ reflects the GC instrument's reproducibility, although it would be slightly impacted by the modulator as all GC×GC parameters are interconnected. The average RSD for the $^{1}t_r$ following a manual check of each peak was 0.02 %, which was acceptable for an Agilent 6890 GC [214]. The average $^{1}t_r$ RSD for the saturated hydrocarbon peaks were slightly higher at 0.03 %, compared to the 1-ring aromatic hydrocarbons at 0.02 %. This was due to the coelution along the ^{1}D between the saturated hydrocarbons, which resulted in some sub-peaks that were questionable as to whether they belonged to the same compound based on their retention time and peak height (see Figure 3-9 for an example). The average $^{2}t_r$ RSD with manual checking was 0.59 %, with individual values ranging from 0.28 % to 1.5 %. This was comparable to previously published results with this modulator where the $^{2}t_r$ RSD was 0.8 % – 2 % [74]. The automated and manual values of the $^{1}t_r$ and $^{2}t_r$ RSDs were similar, however, a paired Student's t-test ($\alpha = 0.05$) showed that the differences were significant for the $^{2}t_r$ [$t(24) = 3.7$, $p = 0.001$] while it was not significant for the $^{1}t_r$ [$t(24) = 0.99$, $p = 0.33$].

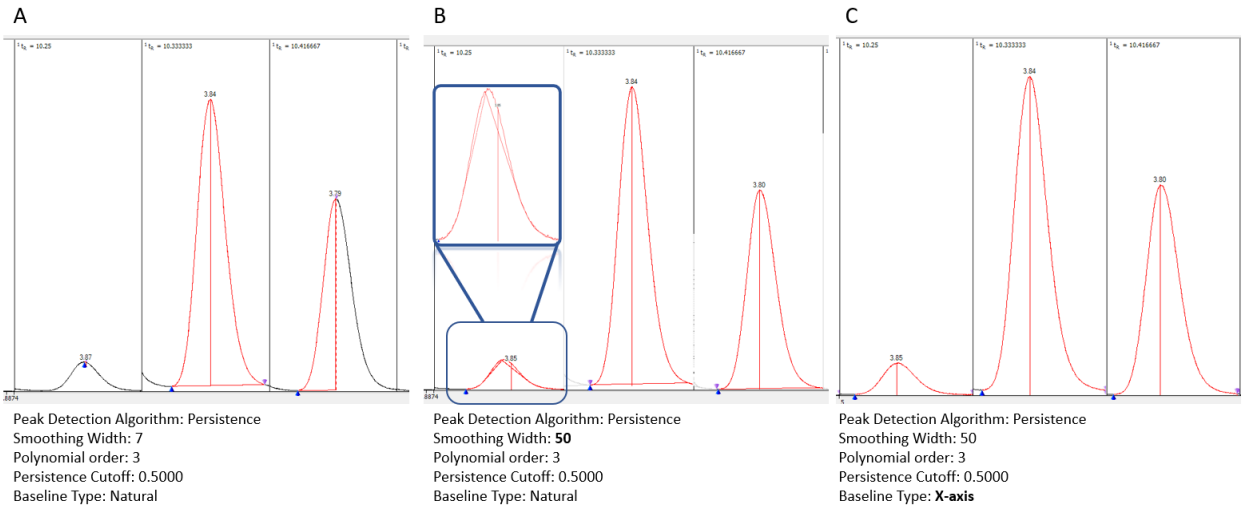

Figure 3-10: Peak detection integration parameters. Default values for persistence detection (A). Increased smoothing width to 50 (B). Changed baseline type to x-axis (C).

For peak integration, the persistence algorithm was used with a smoothing width of 50 due to the noise. At the default smoothing width (7), some peaks were only partially integrated (Figure 3-10A). With the default baseline setting of "natural", an improper baseline was drawn for some of the lower intensity peaks (Figure 3-10B). This was fixed with a baseline correction (VoidTimeBackgroundRemoval: # of minima = 20) followed by using the x-axis as the baseline (Figure 3-10C). Peak merging settings were left at their default values, except for the "sub-peak apex windows" setting where it was set to 5 % for all values. This meant that the maximum allowable shift in ^2t_r between sub-peaks was 5 % of the modulation period, which in this instance would be 0.25 s. These integration settings were used for all diesel separations (manual and automated integration) and only certain peaks (manual integration) which had integration issues were further adjusted and applied across all separations. The peak area reproducibility following manual check was 1.5 %, with most peaks being below 4 % RSD. Peaks with area RSD greater than 4 % were found to be co-eluting with other peaks. For peak 11, with a peak area RSD of 5.7 %, the resolution of the separation with the adjacent co-eluting peak was 0.7796. For the automated results, the average peak area RSD was 3.5 %, with peaks 10, 11, 13, 21, 23, and 24 being above 5 %. For peaks 11 and 13, which were 1-ring aromatic hydrocarbons that did not have issues with coelutions, the inconsistent integration of sub-peaks resulted in elevated % RSD. Figure 3-11 shows the sub-peaks for peak 13

(automated integration), where four sub-peaks were integrated in replicates 1 and 3, while only 2 sub-peaks were integrated in replicate 2. No significant peak area or retention time fluctuations were observed in the overlay of the three separations. The issues with the integration of the smaller sub-peaks were not due to the default peak filtering settings (minimum area, height, and width) since setting them to 0 did not resolve the problem. Changing the peak detection algorithm to curve-fitting did resolve the issue and is reflected in the manual results.

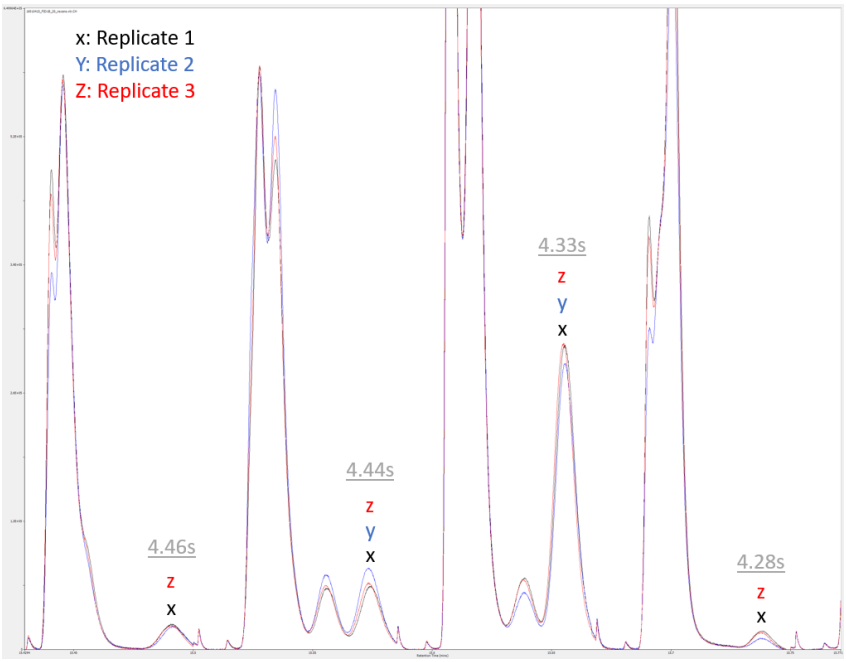

Figure 3-11: Overlay of three replicate raw chromatograms for the GC×GC separation zoomed into the region of peak 13 (four modulations). Four sub-peaks were integrated for replicates 1 and 3 (represented by "x" and "z"), while only two sub-peaks were integrated for replicate 2 represented by "y". ***X-axis: 15.4294 – 15.7710 min. Y-axis: 0 – 6.49964 × 10^5.***

3.5.1.2 GC×GC with ^{2}D Temperature Programming

With the addition of the ^{2}DTPS, both ^{2}D temperature programming (Table 3-2) as well as constant offset (Table 3-3) separations were possible. The biggest concern with the addition of this system was its effect on the retention time reproducibility in the ^{2}D. Although the ^{2}DTPS was strictly affecting the ^{2}D separation temperature, the ^1t_r could still be affected due to the coupling of the ^{1}D and ^{2}D columns. Carrier gas viscosity is dependent on the temperature, which was changing very rapidly and repeatedly during

Table 3-2: Reproducibility of a GC×GC separation of diesel with ²D temperature programming. Results are colour coded by the class of compounds (yellow: saturated hydrocarbon, green: 1-ring aromatic hydrocarbon, blue: 2-ring aromatic hydrocarbon).

	AVERAGE (MANUAL)				RSD (%) [MANUAL CHECK | AUTOMATED CHECK]					
PEAK	^1t_r (min)	^2t_r (s)	Area	^2W_b (s)	^1t_r (%)		^2t_r (%)		Area (%)	
1	4.333	1.72	58942331	0.329	0.00	0.00	0.84	0.50	0.61	0.92
2	4.917	1.85	35118211	0.353	0.00	0.00	0.31	0.32	0.68	0.73
3	7.055	1.85	152450256	0.325	0.01	0.01	0.39	0.57	0.24	0.53
4	8.152	1.99	222688729	0.352	0.01	0.01	0.75	0.29	0.62	0.72
5	8.521	0.97	485953977	0.200	0.00	0.00	0.59	0.66	0.52	0.44
6	9.673	2.26	35444659	0.411	0.06	0.00	1.1	0.65	0.32	0.96
7	10.374	1.37	158073110	0.354	0.01	0.01	0.57	0.75	0.61	0.49
8	10.398	1.89	160008940	0.325	0.00	0.00	0.58	0.67	0.60	0.80
9	11.778	2.04	131488484	0.470	0.04	0.00	0.68	0.38	0.46	0.41
10	12.607	1.00	834006031	0.205	0.00	0.00	0.34	0.61	0.56	0.48
11	14.698	1.92	71185871	0.323	0.01	0.01	0.43	0.16	0.47	0.90
12	14.870	2.47	107575733	0.435	0.01	0.01	0.19	0.36	0.41	0.35
13	15.619	1.99	52934894	0.370	0.01	0.01	0.61	0.55	0.35	0.76
14	15.750	3.89	10878344	0.820	0.00	0.00	0.63	0.53	0.35	0.71
15	16.063	1.76	29232053	0.362	0.03	0.03	0.07	0.31	0.65	0.52
16	16.953	1.02	860995395	0.208	0.01	0.01	0.59	0.97	0.55	0.64
17	17.202	2.33	101928307	0.435	0.01	0.01	0.11	0.17	0.59	0.38
18	19.290	1.91	70442597	0.327	0.01	0.01	0.72	0.83	0.70	0.69
19	20.462	3.65	79969045	0.708	0.02	0.02	0.64	0.63	0.74	0.79
20	21.135	3.75	46396751	0.731	0.06	0.02	0.03	0.16	0.59	0.78
21	21.273	1.02	991607156	0.206	0.01	0.01	0.55	0.65	2.6	2.4
22	21.587	2.29	275810362	0.376	0.03	0.03	0.74	0.85	0.73	0.70
23	24.083	3.84	16231838	0.782	0.00	0.04	0.49	0.72	3.1	11
24	25.033	3.40	106262886	0.678	0.03	0.03	0.62	0.17	0.77	2.7
25	25.442	1.03	1178539713	0.207	0.02	0.02	0.37	0.70	0.55	0.60
26	26.968	3.69	17904052	0.742	0.03	0.03	0.23	0.36	1.2	1.4
27	28.357	3.62	33072271	0.751	0.04	0.03	0.50	0.58	2.1	1.5
28	28.984	3.22	43023850	0.596	0.02	0.09	0.60	0.48	2.8	17
29	29.421	1.04	1192499114	0.210	0.08	0.08	0.67	0.58	0.62	2.5
30	31.205	3.50	55769933	0.675	0.04	0.02	0.26	0.30	2.1	2.9
31	33.208	1.05	1023343736	0.216	0.03	0.03	0.58	0.17	4.5	5.3
32	36.233	3.82	17364593	0.790	0.05	0.03	0.29	0.07	4.4	0.54
33	36.813	1.06	1097301406	0.221	0.02	0.01	0.23	0.26	2.3	3.5
34	40.257	1.07	851508382	0.227	0.05	0.06	0.58	0.38	1.7	2.0
35	43.542	1.09	471158722	0.239	0.01	0.02	0.42	0.23	0.68	7.7
OVERALL AVERAGE				0.427	0.02	0.02	0.49	0.47	1.2	2.1
SATURATED HYDROCARBON				0.215	0.02	0.03	0.49	0.51	1.3	2.6
1-RING AROMATIC HYDROCARBON				0.370	0.02	0.01	0.54	0.49	0.54	0.66
2-RING AROMATIC HYDROCARBON				0.727	0.03	0.03	0.43	0.40	1.8	3.9

the GC×GC separation. The change in flow restriction in the ²D column was not accounted for by the GC system and may have impacted the ^1t_r if the ²D temperature programming was not reproducible. The average ^1t_r and ^2t_r RSDs for the 35 peaks with ²D temperature programming were 0.02 % and 0.49 % for

the manual integration, respectively. This was comparable to the standard GC×GC system (^1t_r: 0.02 %, ^2t_r: 0.59 %). A paired Student's t-test (α = 0.05) comparing the same 25 peaks showed that the differences were not significant for the ^1t_r [t(24) = 0.79, p = 0.44] and ^2t_r [t(24) = 0.84, p = 0.41]. The ^1t_r and ^2t_r RSD of the automated results (^1t_r: 0.021 %, ^2t_r: 0.47 %) for ^{2}D temperature programming were very similar to the manual results. The paired Student's t-test (α = 0.05) showed that the differences were not significant for the ^1t_r [t(34) = 0.48, p = 0.63] and ^2t_r [t(34) = 0.53, p = 0.60].

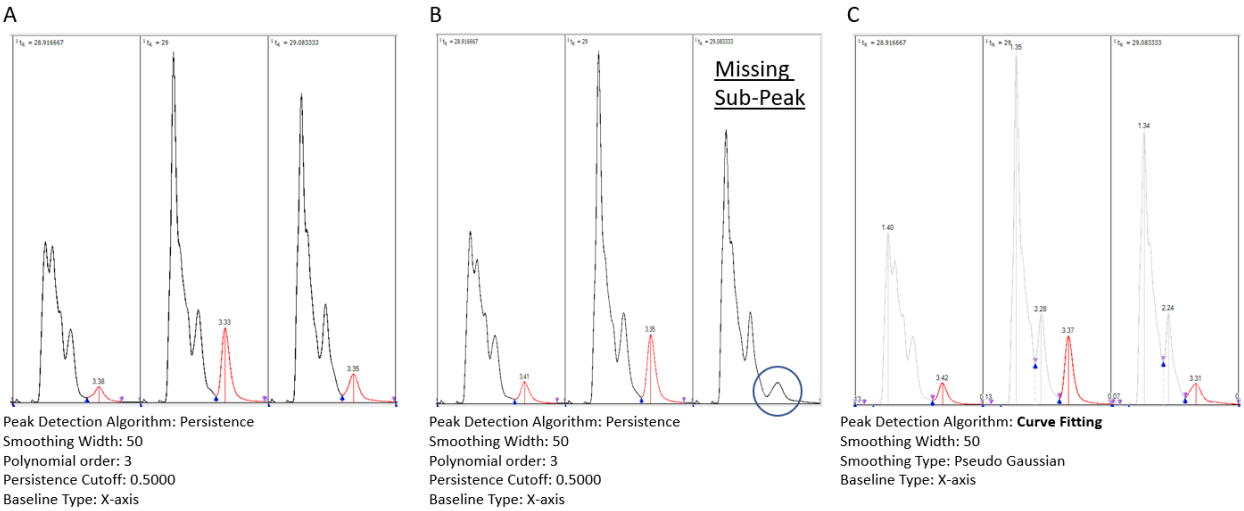

Figure 3-12: Adjusted integration settings for peaks 23, 28, 30 for the ^{2}D temperature programming separation, due to missing integration for some sub-peaks.

The integration settings used for the ^{2}D temperature programming separations were the same as discussed before. Integration of some of the GC×GC peaks (23, 28, 30) for the third replicate of the ^{2}D temperature programming separation missed some of the smaller sub-peaks (Figure 3-12). The integration algorithm was changed to curve fitting for these peaks and is reflected in the manual integration results. The average peak area reproducibility was 1.2 % for the manual results and 2.1 % for the automated results. The overall improvement in peak area reproducibility compared to the standard GC×GC separation was due to the ^{2}D temperature programming eliminating the wraparound peaks and the improvement in the S/N ratio. The paired Student's t-test (α = 0.05) showed that the differences between the peak area RSDs were borderline significant, t(24) = 2.2, p = 0.037. The automated and manual

results for the peak area RSD were compared and differences were found to not be significant, $t(34) = 1.9$, $p = 0.064$.

3.5.1.3 GC×GC with ^{2}D Constant Temperature Offset

In theory, the constant offset separation (Table 3-3) accomplished using the ^{2}DTPS should provide better reproducibility. Not only does the system not have to account for timing, thus eliminating a major source of inconsistencies, but maintaining a constant offset was much simpler than creating rapid and reproducible temperature changes (temperature programming). Although it would be ideal to use the same peaks to compare the constant offset separation (33 peaks) and temperature programming separation (35 peaks) with the ^{2}DTPS, 2 peaks were excluded due to coelutions in the former case. The average ^1t_r and ^2t_r RSD for the manual results were 0.02 % and 0.67 %, respectively. The average ^2t_r RSD was higher compared to the standard GC×GC system (0.59 %) and the ^{2}D temperature programming separation (0.49 %). A paired Student's t-test comparing the constant offset separation with the GC×GC ^{2}D separation at oven temperature [^1t_r: $t(22) = 1.0$, $p = 0.33$; ^2t_r: $t(22) = 0.21$, $p = 0.83$] and with the ^{2}D temperature programming separation [^1t_r: $t(32) = 1.7$, $p = 0.11$; ^2t_r: $t(32) = 1.3$, $p = 0.21$] showed that the differences were not significant for both the ^1t_r and ^2t_r. The highest average ^2t_r RSD in constant offset separation was likely due to the capacitive discharge of the modulator. As shown in Figure 3-5, the electromagnetic interference from the capacitive discharge was picked up by the thermocouple, resulting in an apparent drop in voltage and therefore the calculated temperature. This would be compensated by the PID, even though this was an artificial decrease in temperature, resulting in less stable constant offset. This artifact was not an issue for the ^{2}D temperature programming separation since the heating was off to cool the ^{2}D column during the discharge.

Table 3-3: Reproducibility of a GC×GC separation of diesel with a constant offset separation using the prototype ²DTPS. Results are colour coded by the class of compounds (yellow: saturated hydrocarbon, green: 1-ring aromatic hydrocarbon, blue: 2-ring aromatic hydrocarbon).

	AVERAGE (MANUAL)				RSD (%) [MANUAL CHECK | MINIMAL CHECK]					
PEAK	^1t_r (min)	^2t_r (s)	Area	^2W_b (s)	^1t_r (%)		^2t_r (%)		Area (%)	
1	4.333	1.14	57898435	0.332	0.00	0.48	0.01	1.5	0.87	0.49
2	4.917	1.25	33230821	0.354	0.00	0.00	0.69	0.58	2.1	0.41
3	7.050	1.23	150785537	0.333	0.07	0.06	0.21	0.36	1.2	1.8
4	8.146	1.35	222187912	0.421	0.07	0.06	0.13	0.48	0.83	1.6
5	8.519	0.82	483192085	0.113	0.01	0.01	0.54	0.46	0.63	3.2
6	9.667	1.63	32375858	0.471	0.00	0.06	0.01	0.49	1.9	4.4
7	10.397	1.25	174442178	0.368	0.00	0.00	0.64	0.70	2.2	3.2
8	11.770	1.43	136561179	0.478	0.03	0.02	0.37	1.1	0.41	1.1
9	12.604	0.82	1198661873	0.120	0.01	0.05	0.37	0.33	0.52	15
10	14.693	1.28	78218738	0.381	0.01	0.02	1.5	1.4	0.11	1.2
11	14.864	1.82	111634023	0.511	0.03	0.02	1.0	1.0	0.04	1.5
12	15.615	1.34	61254028	0.505	0.02	0.02	1.4	1.1	0.87	1.9
13	15.750	3.41	10531999	0.928	0.00	0.00	0.00	0.47	2.4	1.8
14	16.949	0.81	1044407245	0.132	0.02	0.01	1.2	0.77	0.84	5.6
15	17.195	1.70	115371209	0.547	0.02	0.01	0.55	0.50	0.35	2.0
16	19.288	1.29	74379094	0.456	0.01	0.00	0.19	1.9	0.36	0.72
17	20.463	3.10	80712707	0.817	0.01	0.01	0.56	2.0	1.2	1.2
18	21.167	3.24	30497802	0.888	0.00	0.01	0.89	1.6	3.6	1.5
19	21.272	0.81	1464829637	0.135	0.00	0.00	1.5	1.1	0.76	1.2
20	21.582	1.66	283861236	0.435	0.01	0.01	0.48	2.2	0.94	1.7
21	24.083	3.52	16633786	0.936	0.00	0.00	0.00	1.6	3.1	40
22	25.032	2.93	107011075	0.789	0.00	0.00	0.38	0.75	0.15	0.84
23	25.441	0.79	1372580931	0.134	0.00	0.00	0.40	0.46	0.59	1.1
24	26.962	3.26	18966565	0.923	0.04	0.04	0.96	1.0	0.53	14
25	28.361	3.20	33274803	0.901	0.01	0.01	1.6	1.3	0.37	3.1
26	28.982	2.66	43935562	0.718	0.00	0.00	0.03	0.29	0.55	1.8
27	29.422	0.79	1598644029	0.141	0.07	0.07	0.05	0.23	0.65	3.9
28	31.209	3.01	46457506	0.807	0.00	0.01	2.3	1.9	0.67	4.2
29	33.208	0.78	1233671797	0.219	0.01	0.02	0.29	0.59	0.41	17
30	36.230	3.42	8843643	0.958	0.05	0.04	1.9	2.2	0.79	20
31	36.813	0.78	1332793596	0.152	0.00	0.00	0.83	0.67	0.54	1.2
32	40.268	0.78	988777969	0.154	0.00	0.01	1.1	0.85	0.32	1.7
33	43.541	0.80	580494879	0.170	0.01	0.01	0.19	1.4	0.29	8.6
OVERALL AVERAGE				0.477	0.02	0.03	0.67	1.0	0.94	5.1
SATURATED HYDROCARBON				0.147	0.01	0.02	0.64	0.68	0.55	5.8
1-RING AROMATIC HYDROCARBON				0.430	0.02	0.06	0.55	1.0	0.94	1.7
2-RING AROMATIC HYDROCARBON				0.866	0.01	0.01	0.86	1.3	1.3	8.9

The average peak area RSD was 0.94 % for the manual results and 5.1 % for the automated results. Overall, the peak area RSD (manual integration) was comparable to the ²D temperature programming

separation (1.2 %) and the differences were not significant according to a paired Student's t-test [t(32) = 0.99, p = 0.33]. Since there were fewer coelutions (due to peak wraparound) compared to the GC×GC separation without ^{2}D heating (Manual: 1.5 %, Automated: 3.5 %), the peak area RSD (manual integration) was lower. The difference was found to be significant [t(22) = 2.5, p = 0.020].

The automated results for the constant offset separation were quite poor, particularly for peaks 24 and 30. This was because these were trace compounds in the sample with only two sub-peaks integrated. The large RSDs were due to the baseline being improperly drawn or one of the sub-peaks not being integrated. This was not an issue with the ^{2}D temperature programming separation, where even though the peak areas were similar, the peaks were narrower, improving the S/N and reducing the number of issues with automated integration. This was reflected in the automated result for the ^{2}D temperature programming separation, which had the lowest RSD for peak area.

3.5.2 Resolution and Peak Capacity Comparison

Since the GC×GC separation without ^{2}D heating resulted in significant wraparound of the 2-ring aromatics, the peaks chosen for the comparison were limited to the saturated hydrocarbons and 1-ring aromatics. Figure 3-13A highlights the region of the chromatogram used for the comparison. Figure 3-13B is a comparison of the raw GC signal of each separation, showing a single modulation. As shown in Figure 3-8B, the constant offset separation resulted in a significant loss of ^{2}D separation between the saturated hydrocarbons. Although ^{2}D temperature programming separation also resulted in some loss of separation compared to the GC×GC separation without ^{2}D heating, it was much less pronounced. To quantify the differences in separation, the resolutions between the three closely eluting peaks were compared between the three separations. Each peak was labeled 1 to 3, with their respective FWHM and ^2t_r. The ^2R_s was calculated according to Eq. (2.3), using the largest sub-peak of the GC×GC peak to estimate the ^{2}FWHM and calculate the ^2W_b using Eq. (2.5). The $R_{s,2D}$ [Eq. (2.4)] for these 3 peaks were not compared

since the ^1R_S [Eq. (2.2)] could not be determined accurately for the constant temperature offset separation. The ^1Rs between peaks 2 and 3 was overestimated due to a difference in ^1W_b (2 sub-peaks for constant offset vs. 3 sub-peaks for ^2D temperature programming and without ^2D heating). The difference in the number of sub-peaks was due to a slight shift in the ^1t_r, which modulated the 1D peak into two equal sub-peaks instead of 3 sub-peaks (2 smaller sub-peaks and 1 large sub-peak). For the GC×GC separation

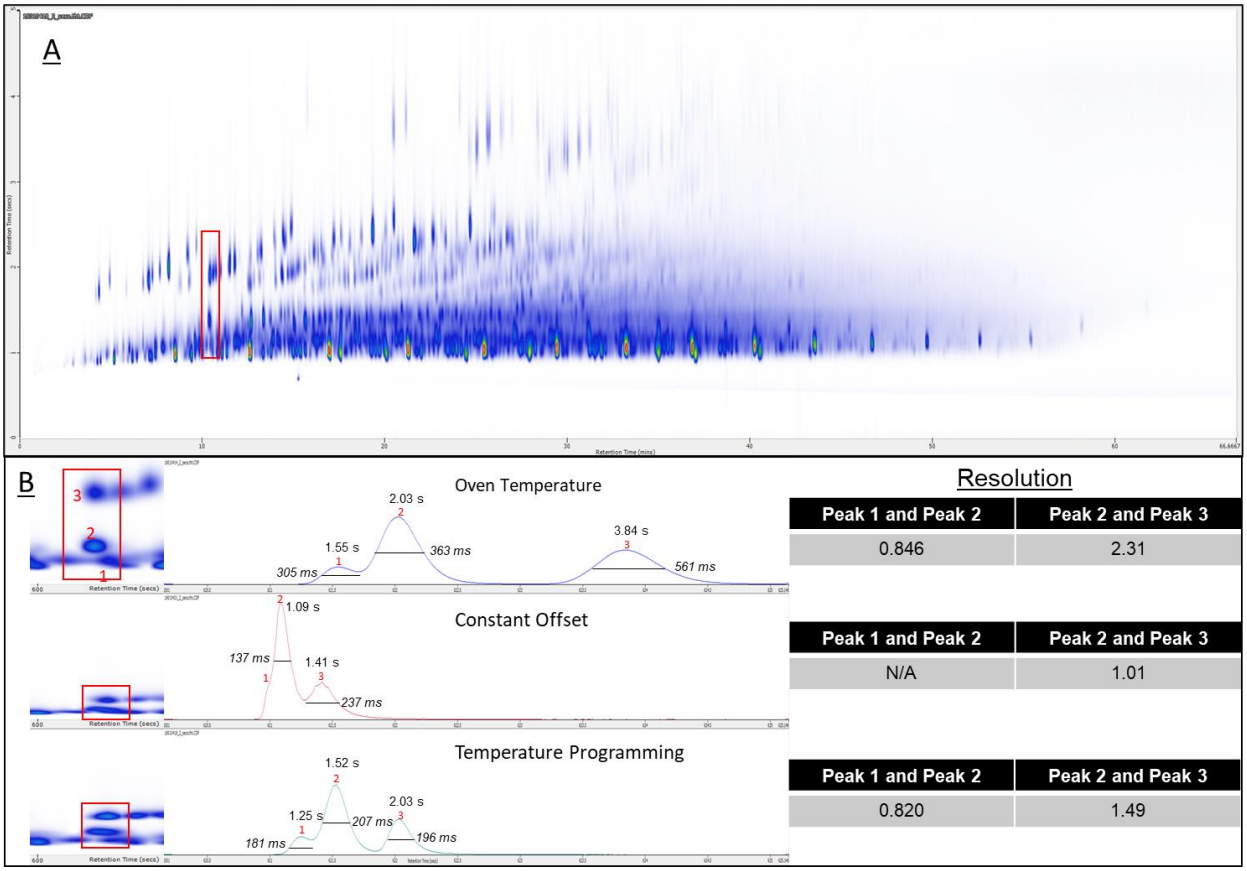

Figure 3-13: Comparison of peak resolution for 3 closely eluting peaks for the GC×GC separation without additional ^2D heating, at a constant positive temperature offset, and with ^2D temperature programming. (A) GC×GC chromatogram of the diesel separation outlining the region (in red) used for the comparison of resolution. ***X-axis: 0 – 66.6 min. Y-axis: 0 – 5 s.*** *(B) Comparison of the peak width and ^2t_r for the same modulation period for the three separations (oven temperature, constant offset, ^2D temperature programming).*

without ^2D heating, the resolution between peaks 1-2 and 2-3 was 0.737 and 2.28, respectively. For the constant offset separation, peak 1 was almost completely co-eluting with peak 2, with only a slight shoulder on the left of peak 2 to indicate the coelution. The resolution between peaks 2-3 was 1.06. For the ^2D temperature programming separation, the resolution between peaks 1-2 (0.784) was comparable

to the separation without ^{2}D heating (0.737). Although peak 1 and peak 2 were only 285 ms apart, compared to 489 ms for the GC×GC separation without ^{2}D heating, these peaks were also much narrower at 363 ms and 662 ms at the base, respectively. The resolution between peaks 2-3 was 1.52 (nearly baseline separated), which was lower than for the GC×GC separation without ^{2}D heating, but was higher than for the constant offset separation. This was achieved while eliminating wraparound peaks and maintaining resolution between the least retained compounds (peak 1and peak 2) in the ^{2}D. Data used for the calculations is found in Table B – 1 of Appendix B.

The ^{2}D peak capacity (^2n_c) was estimated using the average peak width at the base (^2W_b) for the peaks integrated in Section 3.5.1. The ^2n_c is defined as the total time of ^{2}D separation (^{2}t) divided by ^2W_b, as shown in Eq. (3.3).

$$^2n_c = \frac{^2t}{^2w_b} \tag{3.3}$$

The average ^2W_b was 0.737 s, 0.427 s, and 0.477 s for the ^{2}D separation at oven temperature, with ^{2}D temperature programming, and ^{2}D constant offset, respectively. Since wraparound peaks were eliminated for the ^{2}D temperature programming and constant offset separations, the ^{2}t for those separations was 4.307 s, which excluded the ^{2}D dead time. The ^{2}D separation at oven temperature used 5 s for ^{2}t since the entire ^{2}D separation space was used. The resulting peak capacity was 6.8, 10.1, and 9.0 for the ^{2}D separation at oven temperature, with ^{2}D temperature programming, and ^{2}D constant offset, respectively. ^{2}D temperature programming improved the ^2n_c by 48 % over the separation at oven temperature, while the ^{2}D constant offset improved ^2n_c by 32 %. It was noticed that the ^2W_b was increasing with ^2t_r for all three separations. Optimal ^{2}D temperature programming should achieve uniform ^2W_b for all peaks, which indicates that the ^{2}D temperature programming rate was not fast enough for the separation. Further improvements could be made by optimizing the ^{2}D temperature program.

3.5.3 System Practicality and Ease of Use

Although these preliminary results were very promising, the temperature measurement method lacked simplicity for ease of installation for the typical GC×GC practitioner. In addition, although the use of cement for the thermocouple improved its durability, the limitation was its reproducibility between ^{2}D column installations due to variations in cement thickness. This led to differences in response times for the temperature measurements, which affected the accuracy of the ^{2}D temperature program when rapid heating rates were used. This would not be noticed in terms of reproducibility for the same installation and does not have a direct impact on the chromatographic performance, but would be an issue with each ^{2}D column change. Furthermore, the differentially connected thermocouple did not measure the absolute GC oven or ^{2}D column temperature. This placed an upper limit on the final GC oven temperature, so that the ^{2}D temperature offset from either a ^{2}D temperature program or ^{2}D constant offset would not exceed the stationary phase's temperature limit. This was easy to forget during method development and have often led to damaged columns during the prototype's development and testing. This issue could be corrected with an additional thermocouple to measure the GC oven temperature, or ideally, by pulling the information from the GC directly.

Another concern with the system would be its practicality for a user unfamiliar with programming. Changing the temperature program or any variables of consequence, like the calibration or PID parameters involved editing the Arduino code and reuploading the compiled code to the Arduino. Thus, values cannot be changed while the Arduino was temperature programming unless one wanted to upload and consequently restart the Arduino. In addition, with the code as it was, each GC run needed the Arduino to restart in order to zero the thermocouple signal and synchronize the temperature program to the GC run. The only exception would be the constant offset separations which only required the thermocouple signal to be zeroed if necessary.

The last concern was the ^{2}DTPS's reliance on the Waterloo modulator system, specifically the discharge box. One of the problems that was noticed with the ^{2}DTPS was the inaccuracy of the built-in clock. There were two simple ways of solving this with the existing hardware: using the discharge box's discharge signal as a reference or account for the inaccuracy by calibrating the Arduino. The former was ultimately used since this did not require much effort and would not require calibration every time an Arduino was damaged/replaced during testing. In addition, the calibration may be needed even when the Arduino was undamaged due to temperature fluctuations within the laboratory. However, this resulted in the over reliance of a device that was not meant for the ^{2}DTPS, and effectively, over engineered if used for just this purpose. The next iteration of the system (section 4) addressed these core issues.

3.6 Conclusions

The prototype ^{2}DTPS demonstrated improvements in ^{2}D separation in terms of resolution and peak capacity. The addition of ^{2}D temperature programming provided greater flexibility in method optimization, with the ^{2}D column temperature being partially decoupled from the GC oven temperature. Wraparound peaks were eliminated without significant sacrifice to the resolution between weakly retained peaks. The system was characterized by good retention time reproducibility, even with rapid ^{2}D temperature programs. It also provided the highest peak capacity of the three options tested.

Although the core functions (heating, cooling, temperature control) were demonstrated with the system, the design would most likely be limited to research settings due to the fragile nature of the thermocouple connection. To improve the system, the approach should be re-examined to either pursue a new method of temperature measurement, or a more robust attachment of the thermocouple without sacrificing the precision, accuracy, and response time.

4 Final Design of the ²DTPS (Version 2.0)[iv]

The final design of the ²DTPS focused on making the system more robust and user friendly. This meant redesigning the system for an easier installation, so users would not be deterred by issues like fragile thermocouples or need to do any coding. The largest improvement or change to the design was the temperature measurement system. From examining the temperature measurement methods of other direct resistive heating designs, the thermocouple was a valid choice. However, the most well-designed system, in this author's opinion, was by Stearns et al. [177]. That system utilized a nickel-clad fused silica column for direct resistive heating, and temperature measurement was based on the column's resistance. This method of temperature measurement was the same as in an RTD, but nickel was used instead of the usual platinum. When comparing nickel and platinum, their respective temperature coefficients of resistance (TCR) are 0.0068 and 0.0039 1/K, and resistivities are 6.2 and 10.4 ($\times 10^{-8}$ Ωm) [218]. The TCR is the relative change of resistance per degree of temperature change. The resistivity is the electrical resistance of the material multiplied by its cross-sectional area and divided by its length (Ω x m^2/m). Both values are important since the GC column resistance will depend on its dimensions and resistivity, while the magnitude of the resistance change depends on the GC column resistance and TCR. The magnitude of the resistance change determines the system's sensitivity to temperature change. Between the two materials, platinum is by far the most common for RTDs, due to its TCR linearity with temperature. Since

[iv] This Chapter is based on two manuscripts submitted to Analytical Chemistry:

Chow, H. Y. J., & Górecki, T. (2023). Second dimension temperature programming system for comprehensive two-dimensional gas chromatography. part 1: precise temperature control based on column electrical resistance. *Analytical Chemistry*. In revision.

Chow, H. Y. J., & Górecki, T. (2023). Second dimension temperature programming system for comprehensive two-dimensional gas chromatography. part 2: technical improvements and compatibility with flow modulation and time-of-flight mass spectrometry. *Analytical Chemistry*. In revision.

the temperature coefficients of the two materials are comparable, nickel was a cost-effective alternative for heating and temperature measurement, creating a very efficient design, in which the GC column was used for the separation, heating, and temperature measurement.

The design by Stearns et al. [177] was adapted using Restek's Siltek-treated stainless steel GC columns (MXT) for ^{2}D temperature programming. The resistivity and TCR of stainless steel vary depending on the composition of the alloy. From the Smithells Metals Reference Book [218], its resistivity ranges from 70.4 - 108 ($\times 10^{-8}$ Ωm), depending on the composition. Some wire manufacturers have listed TCR values for their stainless steel to be 0.00085 and 0.001 (1/K) with resistivities of 69.82 and 70 ($\times 10^{-8}$ Ωm), respectively [219, 220]. This meant that the resistivity of stainless steel is roughly 10 times greater than that of nickel, but its TCR is about 7 times lower. If one were to compare two columns with identical dimensions, one made of stainless steel and the other of nickel, the power dissipated (resistive heating) by the stainless steel column would be 10 times lower. Thus, greater voltages and power would be needed to generate the same amount of heat. While Stearns et al. [177] used a 15 m nickel clad column for their fast GC application, typical ^{2}D column lengths are 0.3 m – 5 m. The lower TCR of stainless steel combined with the shorter ^{2}D column lengths would result in a smaller change in resistance per °C. For accurate temperature determination, the resistance measurement would need to be both stable and sensitive, which may be difficult to achieve when rapid temperature measurements are needed for ^{2}D temperature programming. This poses a challenge in resistively heating stainless steel columns in terms of maximum heating rate, temperature offset, and temperature measurement.

4.1 ^{2}DTPS: Utilizing a Commercial Stainless Steel Column for Temperature Measurement

The overall layout of the GC×GC system with the updated ^{2}DTPS is shown in Figure 4-1. Although the SSM is shown in the figure, SepSolve's Insight flow modulator was also tested to demonstrate the applicability of the system to flow modulation. Testing the newly designed ^{2}DTPS with the SSM provided

results that were more directly comparable to the previous setup. This was useful for spotting any issues early in the testing that could have been unrelated to the ²DTPS. No major changes were needed with the ²DTPS whether a flow modulator or a thermal modulator were used, so the overall diagram found in Figure 4-1 is an accurate representation of the ²DTPS's critical components. A complete and detailed schematic of the ²DTPS is found in Figure C – 1 and Figure C – 2 in Appendix C.

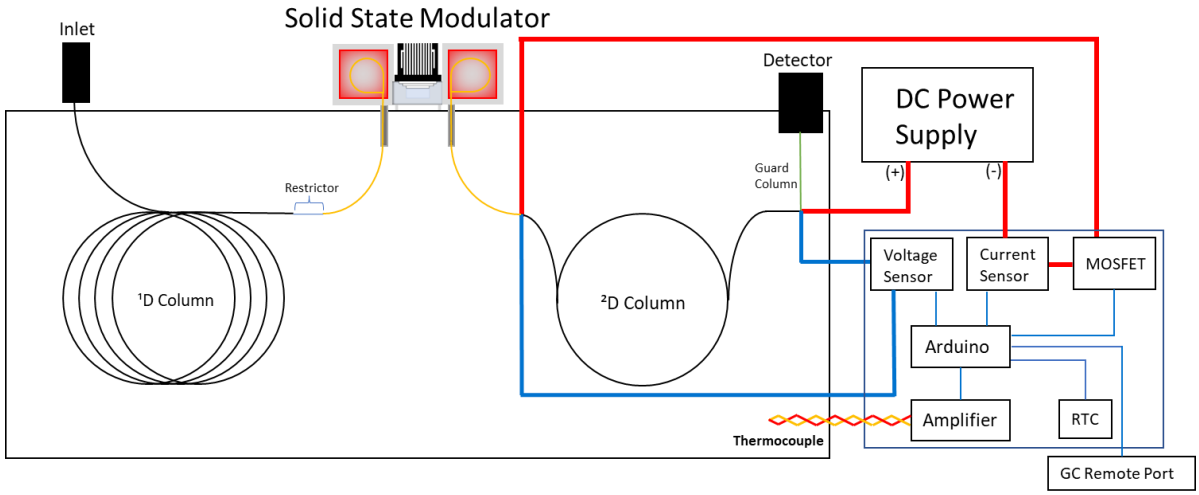

Figure 4-1: GC×GC setup used for the updated ²DTPS utilizing a resistance temperature measurement approach. Other changes/improvements include the connection with the GC remote port and the use of a real-time clock for more accurate timing in temperature programming.

4.1.1 Current and Voltage Sensors

According to Ohm's law [Eq. (4.1)], the current (I) is proportional through resistance (Ω) to the voltage (V) between two points. To determine the temperature of the ²D column, the resistance was calculated by measuring the voltage and current flowing through the column during heating. As this implies, the system was essentially blind to the column temperature if power was not passed through the column. This occurred when the column was cooling.

$$V = IR \tag{4.1}$$

Since the voltages used for heating were almost guaranteed to exceed 5 V, the voltage limit of the Arduino Uno, a voltage divider was used to reduce the voltage to be measured as shown in Figure 4-2. The average resistance of a 0.25 mm MXT column was roughly 10 Ω/m. For thermal modulators, the

typical length of a ^{2}D column is between 0.3 m and 1.5 m. With a desired current of 2 A (maximum), the voltage applied to the ^{2}D column would range from 6 V to 30 V. To reduce the measured voltage, a 100 kΩ precision-matched resistor divider (MAX5490TA05000+T, Analog Devices, Inc., MA, USA) with a resistor ratio of 5:1 was used to produce an output voltage (V_{out}) that was 1/6 of the supply voltage (V_s). This resistor ratio was sufficient for most use cases involving thermal modulators, but when a flow modulator was used, the ^{2}D column was longer, and consequently its resistance was higher. For a 3 m ^{2}D column, the resistance would be around 30 Ω. To achieve a current of 2 A, as before, 60 V would be needed for heating. For consumer power supplies, 48 VDC/2 A ones are commonly available since they meet the International Electrotechnical Commission's (IEC) Safety Extra Low Voltage (SELV) requirement of 60 VDC with an overvoltage protection setting of 120% (57.6 V) [221]. The 2 A limit is due to the National Electrical Code (NEC) Class 2 circuit specification, which allows circuits under 100 W to not require cables to be housed in a conduit or need a licensed electrician for installation [222, 223]. Using a 48 V power supply, the current through the GC column was approximately 1.6 A. This was lower than the desired 2 A and resulted in a lower maximum temperature offset and heating rate. For the flow modulator system, the resistor divider was updated with a resistor ratio of 10:1 (MAX5490VA10000+T, Analog Devices, Inc). The maximum rating for the divider was 100 V and ±1.00 mA, which was more than capable of handling the expected voltage and current at the voltage divider for heating the ^{2}D column. The values discussed are summarized in Table 4-1.

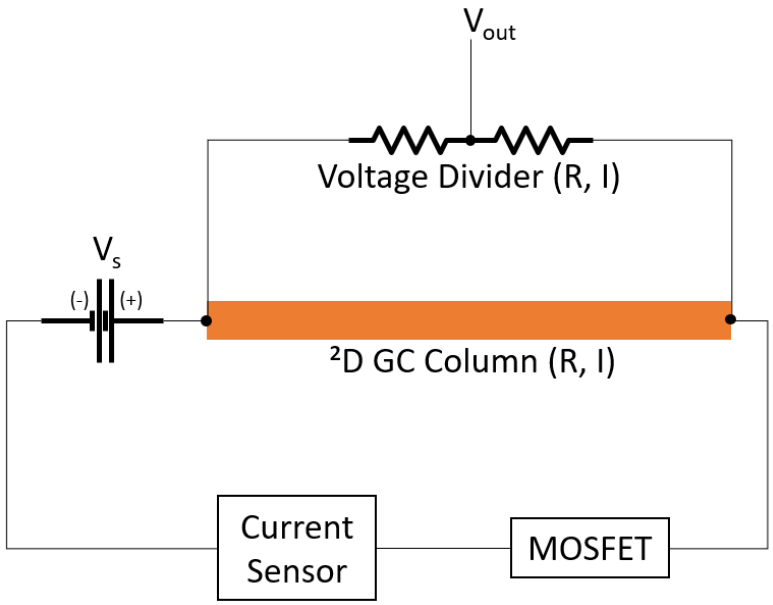

Figure 4-2: Voltage divider connected in parallel with the stainless steel ^{2}D GC column. MOSFET and current sensor connected in series with the ^{2}D GC column. Current sensor connected on the low voltage side of the circuit.

Table 4-1: Estimated voltage and current based on various column lengths and appropriate power supply voltages.

Modulator Type	Length (m)	V_s (V)	R_{column} (Ω)	I_{column} (A)	$I_{voltage\ divider}$ (mA)	V_{out} (V)
Thermal	0.3	6	3	2	0.06	1
Thermal	1.5	30	15	2	0.3	5
Flow	3	48	30	1.6	0.48	4.36

Knowing that the desired current for heating was about 1.6 – 2 A, an appropriate current sensor was selected. The INA250 (Texas Instruments Inc., TX, USA) is a current sense amplifier with an analog output, in a 16-Pin TSSOP package. It consists of an internal shunt resistor (2 mΩ) with a differential amplifier. Four different models were available depending on the gain desired, ranging from 200 mV/A to 2 V/A. The most important specifications were the gain, the maximum ratings for the input voltage (40 V), and input current (±15 A). To prevent any unexpected damage to the current sensor, it was placed on the low voltage side of the circuit, as shown in Figure 4-2. High voltage would only be experienced by the voltage divider and ^{2}D column before the current sensor. Although the INA250A3 (800 mV/A gain) was initially used when the thermal modulator was installed, this sensor was damaged during the change to the 48 V

power supply when performing the flow modulator testing. Unfortunately, this occurred during the Covid-19 pandemic, and due to supply constraints, the same current sensor was unavailable. Instead, the flow modulator experiments utilized the INA250A4 sensor (2 V/A gain), which besides the gain had identical specifications. Both versions of the chip could have been used interchangeably, as long the code was changed to account for the difference in gain. The "A3" version was chosen initially in case experiments involving currents higher than 2 A were desired in the future.

4.1.2 Determination of Temperature by Measuring Resistance

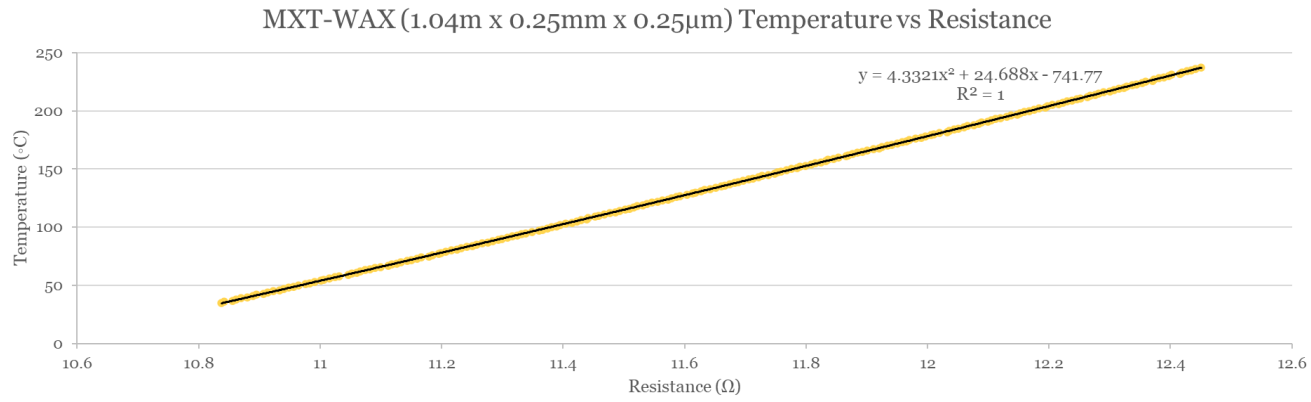

Figure 4-3: Temperature vs. resistance calibration curve for a 1.04 m x 0.25 mm x 0.25 µm MXT-WAX column. Data points in yellow; trendline in black. Resistance values at each °C of measurement were averaged over the course of the GC calibration run and a second order polynomial was fitted.

With the previous version of the [2]DTPS, the temperature was determined using a thermocouple, which required calibration by setting the GC oven to discrete temperatures. Part of the reason for this was because the GC oven temperature was not measured by the Arduino. With Version 2.0, the GC oven temperature was measured, so calibration involved recording both the GC oven temperature and the corresponding resistance measurement. For calibration, a temperature program of 35 °C (1 min) to 240 °C (1 min) was set, with a temperature programming rate of 10 °C/min for the MXT-WAX column (temperature limit: 40 °C to 250 °C/260 °C isothermal/temperature-programmed). 240 °C was a comfortable limit for the calibration of the column to prolong its longevity. This temperature limit would be adjusted accordingly to the column sets installed. The data was then exported to Excel (Microsoft

Corporation) and a second order polynomial was fitted to it, as shown in Figure 4-3. A quadratic equation was used based on the Callendar-Van Dusen equation [Eq. (4.2)], which is used for platinum RTDs that have known constants [224]. Although it would be ideal to require only one calibration with each new column installation, multiple calibrations or thermal cycles of the GC column (with electrical connections attached) were needed due to the thermal expansion and contraction of the various materials and surface oxidation of the metal components. The electrical connections would also be checked for tightness before each calibration run until the calibration had stabilized.

$$R(T) = R_0[1 + aT + bT^2] \; (for \; t \geq 0°C) \tag{4.2}$$

4.1.3 16-bit Analog-to-Digital Converter (ADC)

Both the voltage and current sensors produced analog outputs which had to be converted to digital values. The Arduino Uno has a 10-bit ADC with a full-scale range of 5 V built in. Its least significant bit (LSB) is 4.88 mV, which is the smallest change measurable by the ADC. When using the voltage divider (5:1) and the 0.800 V/A current sensor, it translates to a resolution of 29.3 mV/bit and 6.1 mA/bit, respectively. Using the MXT-Wax column (1.04 m x 0.25 mm x 0.25 µm) from Figure 4-3 as an example, the resistance of the column at 35 °C and 237 °C was measured to be 10.8379 Ω and 12.4502 Ω, respectively. With a 30 V adjustable benchtop power supply in constant voltage mode, the resistance measurement fluctuated by as much as 43.7 mΩ (at 237 °C) and the corresponding temperature (based on the calibration from Figure 4-3) would fluctuate by almost 6 °C (Table 4-2). This becomes worse when shorter columns are used, since both the column resistance and the resistance change per °C decrease.

Table 4-2: The current, resistance, and temperature values when using a 10-bit ADC, based on a constant 30 V power supply and the measured average resistance of an MXT-WAX column (1.04 m x 0.25 mm x 0.25 µm) at 35 °C and 237 °C.

Oven Temp. (°C)	Voltage (V) ± 0.5LSB	Current (A) ± 0.5LSB	Resist. (Ω)	Calc. Temp. (°C)
35	29.9854	2.7711	10.8207	32.6
35	30.0147	2.7650	10.8552	36.7
237	29.9854	2.4126	12.4284	234.2
237	30.0147	2.4065	12.4721	240.0

Therefore, a 16-bit ADC (Texas Instruments Inc.) was used to measure the voltage from the voltage divider and current sensor. Besides providing 16 bits of resolution, the ADS1115 also includes a programmable gain amplifier (PGA) for different input voltage ranges and has data conversion rates of up to 860 samples per second (SPS) [225]. Among the ready-made breakout boards (Adafruit Industries, NY, USA) with library support for Arduino, the ADS1115 had the best balance of resolution and SPS. Although the ADS1115 featured four inputs (single ended, or two differential inputs), two ADS1115 breakout boards were used for the voltage and current measurements. This was because the use of the multiplexer inside the ADS1115 to switch between single ended inputs would reduce the data rate of the ADC. With the PGA, the appropriate gain can be set based on the expected voltage input at the analog pins of the board, as shown in Table 4-3. For the 30 V power supply, the output voltage at the voltage divider should be no more than 5 V, while current sensor (0.800 V/A) should provide an output within 4.096 V. These are conservative estimates, but if a gain of 2/3 and 1 were used for the voltage divider and current sensor, respectively, the corresponding resistance and temperatures in Table 4-4 would be expected with variations of less than 0.5 °C. Real world performance did have more variation due to noise, particularly when shorter ^{2}D columns were used, and combined with PWM where measurements were only taken when the MOSFET was switched ON. However, temperature measurements fluctuated by no more than 3 °C for the short 0.5 m columns and 1 °C for the longer 3 m columns.

Table 4-3: LSB values for various gains for the ADS1115 ADC. Note: The input voltage should not exceed the supply voltage +0.3 V for the ADC, which would be 5.3 V when using the Arduino Uno's 5V pin to power the board. This does not change the resolution for the 2/3 Gain.

Gain	Voltage Range (V)	Volt/Bit (mV/bit)
2/3	±6.144	0.1875
1	±4.096	0.125
4	±2.048	0.0625
8	±1.024	0.03125
16	±0.256	0.0078125

Table 4-4: The current, resistance, and temperature values when using a 16-bit ADC, based on a constant 30 V power supply and the measured average resistance of an MXT-WAX column (1.04 m x 0.25 mm x 0.25 µm) at 35 °C and 237 °C.

Oven Temp. (°C)	Voltage (V) ± 0.5LSB	Current (A) ± 0.5LSB	Resist. (Ω)	Calc. Temp. (°C)
35	29.99944	2.768142	10.8374	34.6
35	30.00056	2.767986	10.8384	34.7
237	29.99944	2.409670	12.4496	237.0
237	30.00056	2.409513	12.4509	237.2

4.1.4 GC Oven Temperature Measurement

Since the absolute temperature of the ^{2}D column was being measured rather than the differential temperature as before, the GC oven temperature had to be measured to program the desired absolute temperature of the ^{2}D column for temperature programming purposes. The MAX31855 thermocouple amplifier breakout board was used for this purpose. Although the previously built instrumentation amplifier would also work, that system would require an additional calibration to set up. The MAX31855 has a built-in amplifier, cold-junction compensation, ADC, and digital control to directly provide the thermocouple temperature. The downside was that the temperature conversion for the k-type thermocouple was done using a linear equation [Eq. (4.3)] [226].

$$V_{OUT} = \left(41.276\ \frac{\mu V}{^\circ C}\right) \times (T_R - T_{AMB}) \tag{4.3}$$

Since the temperature – voltage relationship of the k-type thermocouple is non-linear, the error for the temperature range from -200 °C to +700 °C is ± 2 °C. If greater accuracy is desired, one can calculate the voltage using Eq. (4.3) with the thermocouple temperature and use the ITS-90 table to determine a more accurate temperature [215]. This was overly complicated to achieve greater temperature measurement accuracy, when it was the precision of the measurement that was more important. The other downside to the MAX31855 was the temperature conversion speed, being typically around 70 ms and a maximum of 100 ms. For the GC oven temperature which does not have fast temperature change, this was acceptable. However, this would not have worked for ver. 1.0 of the ^{2}DTPS (section 3) which required frequent differential temperature measurements.

4.1.5 Improving the Column Cage and Column Connection Design

The goal of the column cage was to provide an electrically insulated structure to mount the ^{2}D column to and prevent column contact with itself or the GC oven. In addition, the column cage had to be able to accomplish this for longer columns (flow modulator: 3 – 5 m). From Figure 2-2, the column cage was poorly constructed and was only capable of accommodating two loops around the cage. The newly modified column cage used springs as guides to provide at least 5 loops around the column cage without risk of unwanted shorting. The whole column cage was still covered in glass fiber sleeving (OMEGA Engineering Inc.) and was mounted in front of the GC oven fan using flexible copper straps. Although the copper straps did oxidize at the high oven temperatures, no issues were noticed regarding their durability.

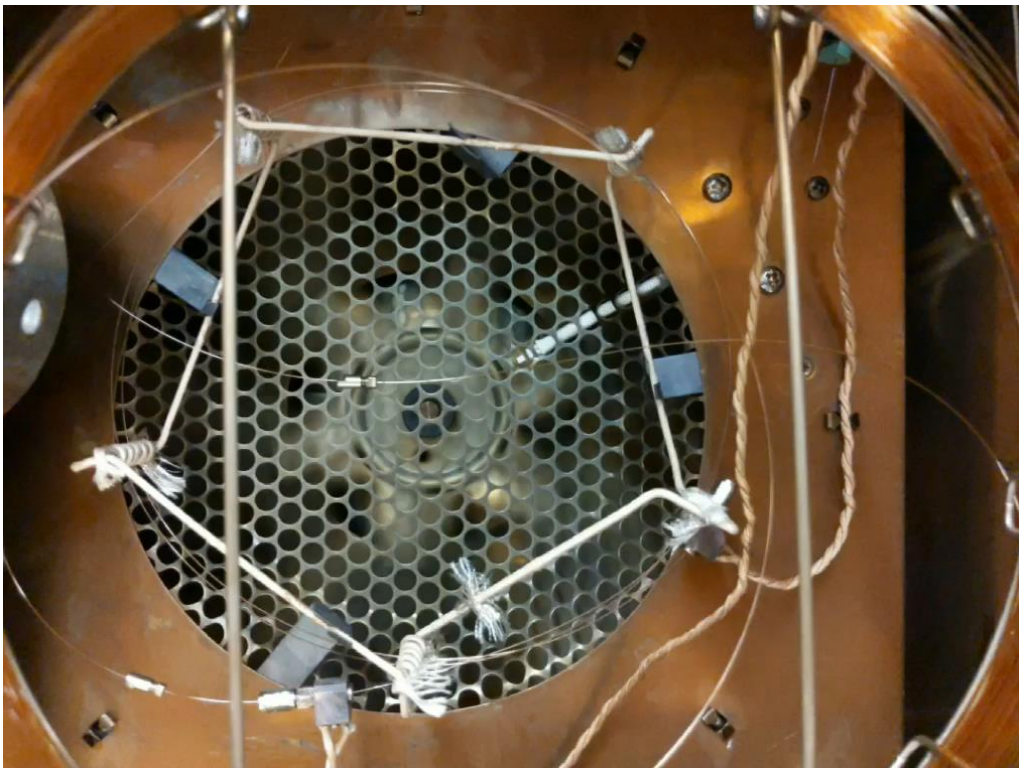

Figure 4-4: ^{2}D column mounted on the new column cage and connected using the new column clamps.

The previous wire connections to the SilTite mini-unions (Trajan Scientific and Medical) used alligator clips which were more susceptible to arcing due to poor connection as the spring aged and contact pressure weakened. This might have also affected resistance measurements, as the contact pressure

changed over time. The new wire connections, shown in Figure 4-5, used drilled copper blocks where set screws pressed the SilTite mini-union against the inner wall of the connector. Although the set screw needed tightening for the first couple of GC runs, this was similar to how new column connections at the inlet or the detector needed re-tightening after thermal cycling of the GC oven. The inner wall of the connector did require occasional cleaning with sandpaper to remove the buildup of oxidation over time when a new column was installed and the resistance was not stable.

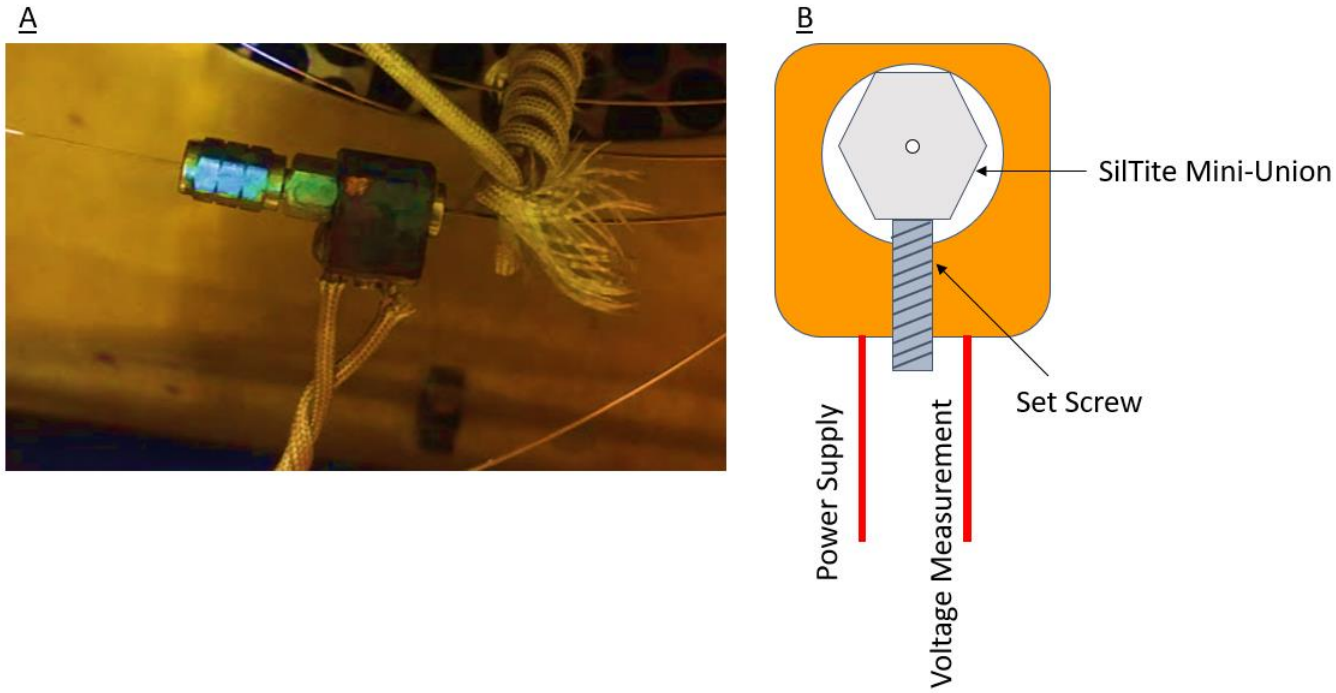

Figure 4-5: (A) New connection to the SilTite mini-unions to provide power and voltage measurement. (B) Clamp design to connect two wires to each end of the ^{2}D column through the SilTite mini-union. A set screw was used to tighten the contact between the clamp and union.

Illustrated in Figure 4-5B were two wires attached to each block which clamps onto the SilTite mini-union. One wire passed the electrical current for heating while the other wire was used for voltage measurement. The four-wire (two wires on each end) configuration provides greater accuracy in resistance measurements over a two-wire configuration. The resistance measured using the 2-wire configuration includes the resistance of the lead wires. This would be problematic because of the long leads needed to connect the ^{2}DTPS to the ^{2}D column. The four-wire configuration uses a separate pair of

wires for voltage measurement. Due to the large resistance of the voltage measurement circuit, the current passing through the voltage measurement wires was small enough for the voltage drop across the lead wires to be negligible. This allowed for accurate resistance measurements, even when low resistances were being measured.

4.1.6 Real Time Clock (RTC)

An RTC (DS3231) was added to the ^{2}DTPS to tackle the timing issue of the ceramic resonator used in the Arduino Uno. The 32 kHz (32768 Hz) clock signal of the Adafruit DS3231 breakout board was connected to digital pin (D2) on the Arduino Uno, an interrupt pin. The square wave clock signal was used to increment a counter to keep track of time. The RTC was powered by the 5 V pin on the Arduino Uno.

4.1.7 Remote Port Cable

A remote port cable was prepared using the pinout diagram from the Agilent 6890 Series Gas Chromatograph Service Manual [227]. Pins 1, 3, 6, 7, and 8, which corresponded to digital ground, start, power on, ready, and stop, respectively, were connected to the Arduino. An issue that was noticed with the remote port of the Agilent 6890A GC was a lower than expected voltage from the pins. The HIGH signal from the pins should provide 5 V; however, only ~2.5 V was measured from pin 8 (stop). For the Arduino Uno (5 V board), a voltage greater than 3 V is needed at the pin for HIGH and less than 1.5 V at the pin for LOW. Voltages between 1.5 V and 3 V are undefined and can result in the signal jumping between HIGH and LOW randomly. This would produce false stop signals, causing a pre-mature end to the ^{2}D temperature programming. To combat this issue, a logic level converter (BOB-12009, SparkFun Electronics, CO, USA) was used to shift the lower voltage up to 5 V. The LOW signal of 0 V remained unchanged in the translation.

4.1.8 Windows Forms Application

To address the issue of changing parameters for the ^{2}DTPS while the system was running, a Windows Forms application, written in C#, was used to interact and update variable values in the Arduino sketch. Serial communication was used to send data between the Windows Forms application and the Arduino. The Windows Forms application displayed the ^{2}D column temperature and either the oven temperature (during standby) or the setpoint (during temperature programming) on a live graph. Important variables including and related to the temperature program, such as the calibration, PID values, PWM window size, and column temperature limits could all be updated using the application shown in Figure 4-6. The ^{2}D temperature programs could also be saved and a sequence of different ^{2}D temperature programs could be run. This can be useful for unsupervised GC×GC optimization. The code for the application is found in C: Windows Forms Application: Form1.cs of Appendix C.

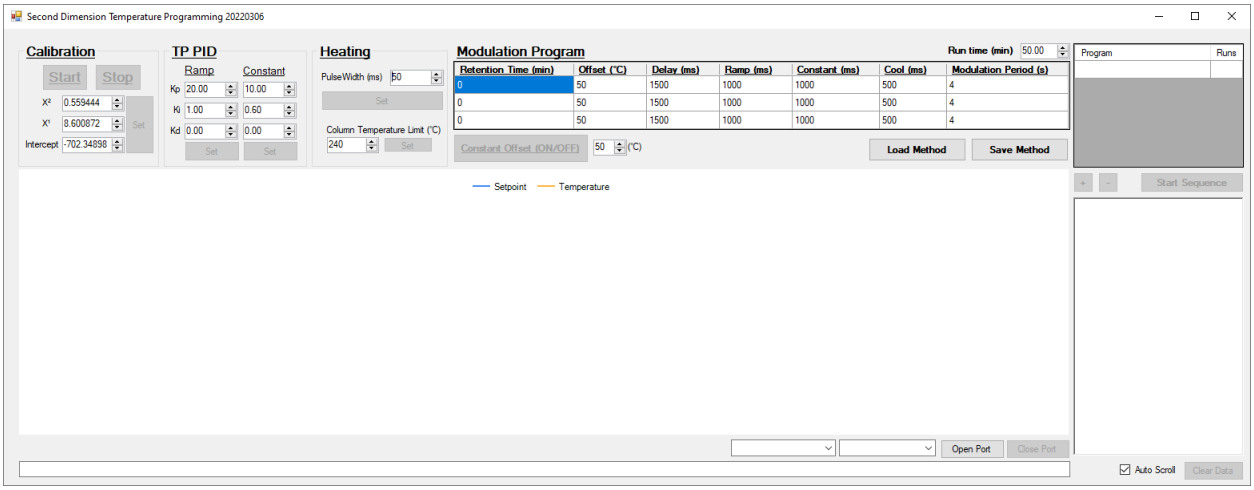

Figure 4-6: Windows Forms application for interacting with the ^{2}DTPS and displaying the temperature values. The upper section of the application window contains areas for updating values (calibration, PID, PWM, ^{2}D column temperature limit, ^{2}D temperature program, run time, sequence list). The middle section displays the data points (setpoint and ^{2}D column temperature) on a live graph (Left) and in a text box (Right). The lowest section features a read-only text box which displays the commands sent to the Arduino or any error messages.

4.1.9 Arduino Code

```
#include libraries
Declare global variables and their initial values

void setup()
{
```

```
  Initialize pin modes
  Initialize PID settings
  Set Serial communication baud rate
}

void loop()
{
  Read Serial Data, Parse Data, Execute Function

  switch(state)
  {
    case 0: Standby
    case 1: Delay the heating
    case 2: Linear temperature ramp
    case 3: Hold temperature offset
    case 4: Cool column
    case 5: Constant Temperature Offset mode
    case 6: Calibration
  }
}

Define functions
```

The overall layout of the Arduino program was the same as in section 3.3.2, but additional states were added to the `switch(state)` function. The purpose was to have a single Arduino sketch for the ^{2}DTPS, where everything can be controlled and monitored by the Windows Forms application. Changing between the different modes (standby, ^{2}D temperature programming, constant offset, calibration) with the windows application was as simple as updating the value of `state`. The complete code is found in C: ^{2}D Temperature Programming Sketch (Version 2.0) of Appendix C.

4.1.9.1 Arduino: Read Serial Data, Parse Data, Execute Function

```
recvWithStartEndMarkers();
parse_line();
execute();

void recvWithStartEndMarkers()
{
  static byte ndx = 0;
  char startMarker = '<';
  char endMarker = '>';
  char rc;
  while (Serial.available() > 0 && newData == false)
  {
    rc = Serial.read();
    if (recvInProgress == true)
    {
```

```
        if (rc != endMarker)
        {
          receivedChars[ndx] = rc;
          ndx++;
          if (ndx >= numChars)
          {
            ndx = numChars - 1;
          }
        }
        else
        {
          receivedChars[ndx] = '\0'; // terminate the string
          recvInProgress = false;
          ndx = 0;
          newData = true;
        }
      }
      else if (rc == startMarker) {
        recvInProgress = true;
      }
    }
  }
```

The code to receive serial data, parse the data, and execute the command was separated into the `recvWithStartEndMarkers()`, `parse_line()`, and `execute()` functions, respectively. "<SetPID 20 1 0>" is an example of serial data sent from the Windows Forms application to the Arduino. The `recvWithStartEndMarkers()` function reads the available serial data (1 character at a time) into the character variable, `rc`. This was important because the Arduino Serial port buffer size is 64 bytes. If a command from the Windows Forms application was larger than 64 bytes (64 characters), the command would be truncated if it was not read (into `rc`) as the data arrived. The serial data for updating the modulation program, for example, was larger than 64 bytes. When the first character arrived, it was compared to a starting marker ("<"). If the first character was the starting marker, then the subsequent characters would be transferred to the `receivedChars[numChars]` array. Each character read into `rc` was compared to the end marker (">") before being transferred to `receivedChars`. If the end marker was read, the value 0 (null character, used to terminate a string) was passed to the `receivedChars` array (Table 4-5). Note, the character "0" at index position 12 is not the same as the value 0 at index 13.

Table 4-5: Example of the values and index position for the `receivedChars` array for the command "SetPID 20 1 0".

Index	Character Value
0	S
1	E
2	T
3	P
4	I
5	D
6	
7	2
8	0
9	
10	1
11	
12	0
13	'\0'
…	Previous value(s)

Any function that works with strings will only read up to the first null terminator, so characters following the null terminator will still exist in memory but will not be read. The index value, `ndx`, was then reset to 0 to replace the values in `receivedChars` for the next command. The `newData` Boolean was then set to `True`, to indicate that new data has been received and ready to be parsed.

```
void parse_line()
{
  char *argument;
  int counter = 0;
  if (newData == true)
  {
    argument = strtok(receivedChars, " ");
    while ((argument != NULL))
    {
      if (counter < MAX_NUM_ARGS)
      {
        if (strlen(argument) < ARG_BUF_SIZE)
        {
          args[counter]= argument;
          argument = strtok(NULL, " ");
          counter++;
        }
      }
      else
      {
        break;
      }
```

```
      }
      newData = false;
    }
  }
```

The `parse_line();` function parsed the command received using the `strtok()` function. The `strtok()` function returned a pointer to a token (in this case, a string). A pointer is a reference to the address of where a value is stored in memory. The first call [`strtok(receivedChars, " ")`] of `strtok()` specified the string (`receivedChars`) and delimiter (" "), where it returned the pointer to the characters ("SetPID") before the first delimiter. The delimiter was then replaced with NULL, forming the NULL terminated string. All subsequent calls of `strtok()` specified NULL instead of the original string [`strtok(NULL, " ")`], and returned a pointer to the next token until no more tokens were available. These pointers were stored in the `*args` array (`args[counter]`). After all the pointers to the tokens were stored, the `while()` loop exited and `newData` was set to `False` so that the `recvWithStartEndMarkers()` function could read new serial data.

```
//List of functions pointers corresponding to each command
int (*commands_func[])()
{
  &SetPID,
  &SetConstPID,
  &SetHeatingPulseWidth,
  &Sequence,
  &SM,
  &StartCalibration,
  &StopCalibration,
  &SC,
  &LimitTemp,
  &ConstantOffset
};

//List of command names
const char *commands_str[] =
{
  "SetPID",
  "SetConstPID",
  "SetHeatingPulseWidth",
  "Sequence",
  "SM",
  "StartCalibration",
  "StopCalibration",
  "SC",
```

```
  "LimitTemp",
  "ConstantOffset"
};
```

Ten functions were used for the Windows Forms application to interact with the Arduino. Two lists, `commands_func` and `commands_str` stored the addresses and names of the corresponding functions, respectively.

```
int execute()
{
  for (int i = 0; i < num_commands; i++) {
    if (strcmp(args[0], commands_str[i]) == 0) {
      return (*commands_func[i])();
    }
  }
  return 0;
}
```

The `execute()` function compared the value of the first pointer (string) stored in the `args` array with the list of command names in `commands_str`. When the names matched, it returned the corresponding function at the address pointed by `commands_func[i]`. For example, if the first string in the `args` array was `SetPID`, then `&SetPID` was returned which was the address of the function, `SetPID()`, calling the function.

```
int SetPID()
{
  Serial.println("-----------------------------------");
  String KpValue = args[1];
  String KiValue = args[2];
  String KdValue = args[3];
  Kp = KpValue.toDouble();
  Ki = KiValue.toDouble();
  Kd = KdValue.toDouble();
  Serial.print("Ramp PID = "); Serial.print(Kp); Serial.print(" ");
  Serial.print(Ki); Serial.print(" "); Serial.println(Kd);
  Serial.println("-----------------------------------");
}
```

Continuing with the example, the `SetPID()` function passed the values at positions 1 to 3 in the `args` array, shown in Table 4-6, to newly initialized string variables (`KpValue`, `KiValue`, `KdValue`). The function, `.toDouble()`, converted the strings to a double and passed the value to `Kp`, `Ki`, and `Kd`, respectively. The Arduino then printed to the serial port the command and values it received, and they

were displayed by the Windows Forms application in the text box. This provided feedback for the user, ensuring the command updated the variables.

Table 4-6: Example of the values of the pointers and corresponding index position for the `args` array for the command "SetPID 20 1 0".

Index	Character Value
0	SetPID
1	20
2	1
3	0

4.1.9.2 Column Temperature: Voltage and Current Measurement

The voltage from the voltage divider and the current sensor was measured using Adafruit's ADS1115 breakout board. When the ADC was first tested, the official Adafruit library lacked certain features, such as the ability to set the data rate to the specified maximum rate of 860 SPS. The default data rate was too slow for the ²D temperature programing system, so a fork of the original Adafruit_ADSS1X15 library on GitHub was used with the ADC [228]. From reviewing the commit history to the Adafruit library, the ability to change the data rate has been added on March 18, 2021 [229]. Code related to the resistance and temperature measurement is shown below.

```
      if (timeElapsed < minPulse)
   {
       gate = HIGH;
   }
   if (gate == HIGH)
   {
       resultVolt = ((double) adsVolt.getLastConversionResults()) *
adsVolt.voltsPerBit() * 11;
       resultCurrent = ((double) adsCurrent.getLastConversionResults()) *
adsCurrent.voltsPerBit() / 2;
   }
   resultResistance = resultVolt / resultCurrent;
   temperature = tempQuad(resultResistance);
```

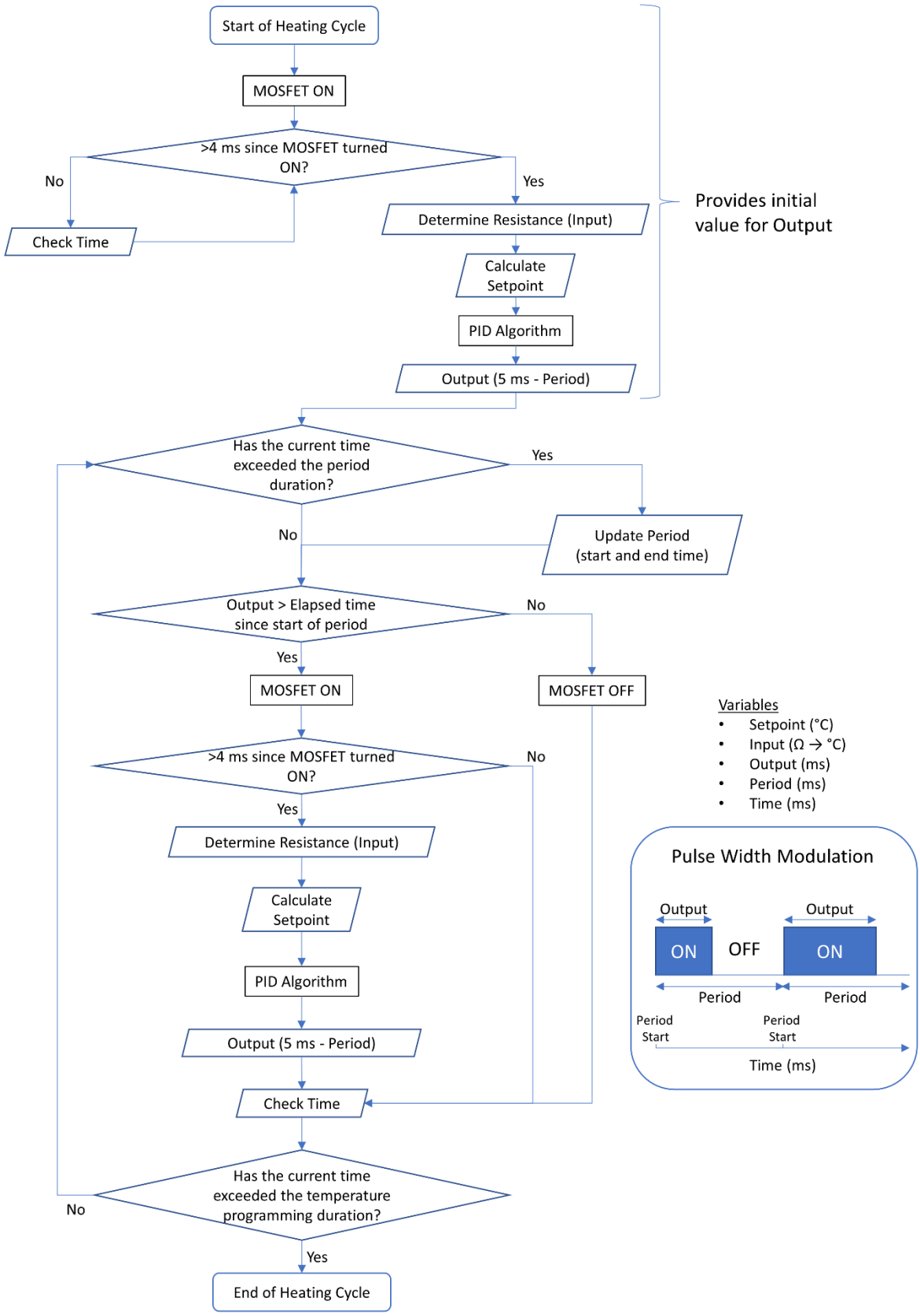

Figure 4-7: Temperature control program flow chart for the ²DTPS.

In order to measure the resistance of the column, a current needs to be delivered to the column. Rather than overcomplicating the system by supplying a constant current through the column (low current during cooling, high current during heating), the temperature was only measured when the column was heated (`gate == HIGH`). When the MOSFET switch was OFF (`gate == LOW`), the system was blind to the column temperature. This was reflected in the Windows Forms application's live graph, where the displayed column temperature during cooling was equal to the oven temperature. Due to the response time of the overall system (ADC conversion time, MOSFET switch, voltage stabilization from sudden switching), a minimum pulse duration (`minPulse`) was necessary to obtain reliable readings. The minimum pulse duration was set to 4 ms. This was determined experimentally by increasing the minimum pulse duration (1 ms at a time) until the temperature measurements produced no erratic values. Although voltage and current values were read while the MOSFET was ON, only the last recorded value from the ADCs was used to calculate the resistance and the corresponding temperature. For the PID output (pulse duration), the minimum value was set at 5 ms (`minPulse + 1`) to ensure no erratic values would be read during temperature programming. A flow chart of the temperature measurement and control is shown in Figure 4-7.

An issue with having a minimum pulse duration for temperature programming was a non-linear temperature increase at the start of the linear temperature program ramp. For example, if the adjustable benchtop power supply was set to a voltage capable of achieving a temperature ramp of 70 °C/s and a temperature ramp of 35 °C/s was set, a minimum pulse duration of 5 ms would cause the start of the linear temperature ramp to exceed the setpoint. Thus, achieving a linear temperature ramp was a balance of both the power from the PSU and the heating rate/maximum temperature offset desired.

4.1.9.3 DS3231 Real-Time Clock (RTC)

```
void isrCount()
{
  count++;
```

```
}

long msec(void)
{
  ms = count * 1000 / freq;
  return ms;
}
```

The Adafruit DS3231 Precision RTC Breakout board was used to provide a 32 kHz clock signal to the Arduino for more accurate timing. Although the Adafruit library included functions for printing the present time (year, month, day, hour, minute, second), it did not print the ms value. This was critical to the ^{2}DTPS, so the 32 kHz signal was connected to the interrupt pin (`D2`) on the Arduino. Every pulse (falling edge) would trigger the `isrCount()` function, which incremented a counter (`count++`). When the time was needed the `msec()` function was called, which would return the ms value based on the counter value. The variables `count` and `ms` were defined as unsigned long variables, which store a value between 0 - 4,294,967,295. This meant that the upper limit before the `ms` value overflowed from the calculation was approximately 131 s. To ensure this did not occur, the `count` value was reset to 0 every second during standby, at the start of every modulation period during ^{2}D temperature programming, or every 10 s for the ^{2}D constant temperature offset mode. The `msec()` function replaced the `millis()` function from the sketch for Ver. 1.0. Since `count` was reset at the start of each modulation period, fewer timestamp variables (`initTime`, `cycleTime`) were needed, simplifying the code.

4.1.9.4 Multi-^{2}D Temperature Programs

An additional feature of version 2.0 was the inclusion of multiple ^{2}D temperature programs in a single GC run. In version 1.0, the sketch used separate variables (`delayTime`, `rampTime`, `coolTime`) for each portion of the ^{2}D temperature program duration. This was inefficient when expanding to multiple temperature programs, so a two-dimensional integer array containing the start time, temperature offset, and modulation timing (delay, ramp, constant offset, and cool time) was created. The structure of the array is illustrated in Table 4-7.

Table 4-7: Array structure of multiple ^{2}D modulation programs

Program	*Start Time (modulations)*	*Temperature Offset (°C)*	*Delay (ms)*	*Ramp (ms)*	*Constant Offset (ms)*	*Cool (ms)*
Index	0	1	2	3	4	5
0	0	50	1500	1000	1000	500
1	2000	50	1500	1000	1000	500
2	3000	50	1500	1000	1000	500

```
if (currentProgram < 2)
{
   if (modulationProgram[currentProgram + 1][0] >
   modulationProgram[currentProgram][0])
   {
         if (modulationCount >= modulationProgram[currentProgram + 1][0])
         {
               currentProgram ++;
         }
   }
}
```

Switching to the next ^{2}D modulation program occurred when the start time, in number of modulations, had elapsed. If only a single ^{2}D modulation program was desired, the subsequent modulation programs could either be set with identical parameters or the start time could be set to 0. The subsequent modulation program values would only be used if their start times were greater than the current modulation program's start time. In addition, portions of the ^{2}D modulation program could also be skipped if the value was set to 0.

```
for (int i = 2; i <= state; ++i)
{
  elapsedProgram += modulationProgram[currentProgram][i];
}

timeElapsed = msec() - elapsedProgram;
```

To account for any time lost when looping and transitioning from one state to another, the `timeElapsed` was calculated by subtracting the elapsed ^{2}D temperature program time from the current time [`msec()`]. The `elapsedProgram` time was the sum of all previous durations of the modulation program. This was done because it was noticed that each state in the modulation program was taking ~1 ms longer, resulting in a drift in the ^{2}D temperature program timing. Any lost time would now be deducted from the duration of the current ^{2}D temperature program state.

4.1.9.5 Remote Start/Stop Synchronization

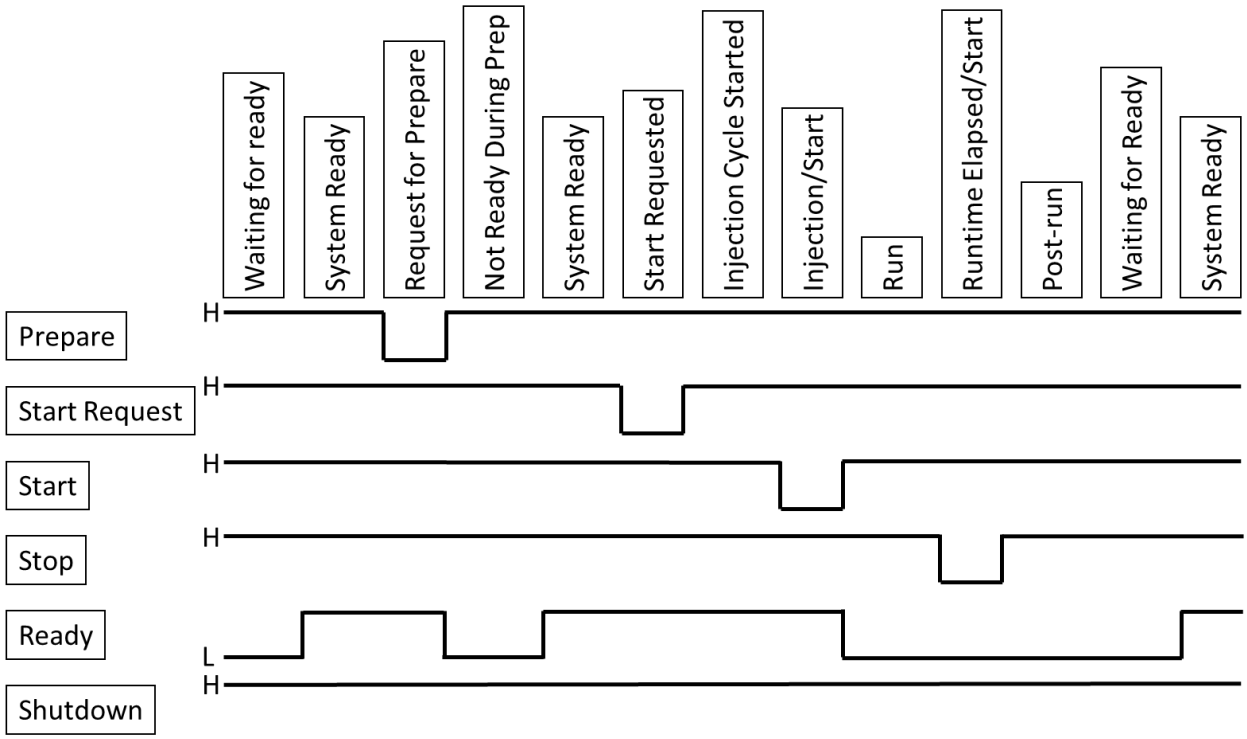

Figure 4-8: APG remote port signal start sequence from the Agilent 6890 GC service manual. Based on Ref. [227].

```
   readySignal = digitalRead(systemReady);
   // GC is ready for injection
   if (readySignal == HIGH)
   {
   Serial.println("System Ready and Waiting");
   modulationCount = 0;
   currentProgram = 0;
   modulationPeriod = 0; // reset modulation before calculation
   //assuming the modulation period will not change between programs
   for (int i = 2; i <= (temperatureProgram - 1); i++ )
   {
   //sum the different portions of the temperature program to determine the
modulation period
   modulationPeriod += modulationProgram[currentProgram][i];
   }
   if (modulationProgram[2] > 0)
   {
     state = 1;
   }
   else if (modulationProgram[3] > 0)
   {
     state = 2;
   }
   else if (modulationProgram[4] > 0)
   {
```

```
  state = 3;
}
else if (modulationProgram[5] > 0)
{
  state = 4;
}

startSignal = digitalRead(startRun);
//Wait for start signal
while (startSignal == HIGH)
{
  startSignal = digitalRead(startRun);
}
Serial.println("Start");
count = 0;
standby = false;
}
```

The signal sequence from the remote port of the Agilent 6890 series GC is shown in Figure 4-8. The ready, start, and stop signals were used to synchronize the ^{2}D temperature programming start and stop time with the GC run. During the standby `state(0)`, the ready signal (normally LOW) was monitored for the HIGH signal, indicating that the system was ready and about to make an injection. When that occurred, the counters (`modulationCount`, `currentProgram`, `modulationPeriod`) were reset and the `state` value was changed to the first state (`delay`, `ramp`, `hold`, or `cool`) the ^{2}D temperature program should enter (duration > 0). The start pin was then monitored for the `LOW` signal, indicating the start of the GC sequence.

```
void isrStop()
{
  readySignal = digitalRead(systemReady);
  if (readySignal == LOW)
  {
    if (abs(modulationCount - runTime) < 2)
    {
      Serial.println("Stop");
      state = 0;
      standby = true;
    }
  }
}

   if (modulationCount - runTime >= 0)
   {
     standby = true;
   }
```

The stop signal was attached to the last available interrupt pin (`D3`). To avoid issues with electrical noise causing a false stop to the ^{2}D temperature program, the `modulationCount` was compared to the `runTime` when the stop signal was detected. If the `modulationCount` was within 2 modulations of the end of the run, the run would be stopped by the stop signal. As an additional failsafe in the event the stop signal was not detected, the system would automatically go into standby when the `modulationCount` reached or exceeded the `runTime`.

4.1.9.6 Constant Offset Mode

When the "Constant Offset (ON/OFF)" was selected on the Windows Forms application, it toggled between the constant offset and standby states. If the constant offset mode was selected (`state = 5`), the `constantOffsetValue` was also updated. In version 1.0, a PID was used for temperature control. In version 2.0, the current ^{2}DTPS adopted a simpler thermostatic control, which adjusted the output duration by ±1 ms based on the ^{2}D column temperature offset being greater or less than the setpoint. This was done to eliminate an unnecessary set of PID values (limited memory in the Arduino), without compromising on performance. Since the system only needed to maintain a constant temperature offset, where the environment (GC oven) was almost static (slow temperature programming rate relative to the Arduino's measurement frequency), thermostatic control was adequate. Although thermostatic control was much slower to reach equilibrium (several seconds), there was an abundance of time before the start of a GC run for the system to reach the setpoint. The small adjustments of ±1 ms prevented any large fluctuations in temperature. Output values were still set to be between the `minPulse` duration and the `window` size. Since there was no need to switch between `states` in constant offset mode, the serial port was checked (`if (Serial.available() > 0)`) every 10 s for a new command. Counters were also reset at the same time to prevent overflow.

4.2 Experimental

Development and testing of the ^{2}DTPS occurred concurrently, where each major physical or software change was accompanied by a retention time reproducibility test. This was to ensure that any change would not affect the minimum requirement of producing reproducible results. The tests/changes are detailed in chronological order in sections 4.2.1 to 4.2.6.

4.2.1 ^{2}DTPS: Resistance Measurement – Temperature Determination

The test for the new ^{2}DTPS occurred after the installation of the resistance measurement – temperature determination components. The physical changes to the ^{2}DTPS were outlined in sections 4.1.1 to 4.1.5. Testing was performed on the Pegasus III TOF-MS system (LECO Corp.), which had an Agilent 6890N GC installed. This was necessary in order to use the secondary oven from the Pegasus III instrument for a direct comparison with the ^{2}DTPS. The modulator for the GC×GC setup was the SSM (J&X Technologies) with the SV modulator column (C_7 - C_{40}) installed. Although the cryogenic modulator of the Pegasus III would have yielded narrower ^{2}D peak widths compared to the SSM, a long term test would have been costly due to the high consumption of liquid nitrogen. An adjustable DC power supply (AB-5PS-D – ABRA Electronics, Montreal, QC, Canada) was used to provide constant voltage to the ^{2}D column for the ^{2}DTPS. The voltage was increased until the desired ^{2}D temperature offset was achieved within the duration of the heating. The SSM was controlled using SSCenter software ver. 1.0.19.0 (JnX Technologies). GC×GC-FID data were collected using ChromaTOF software ver. 3.32 (LECO Corp.), exported, and then processed using ChromSpace software ver. 2.1.4 (SepSolve Analytical). The ^{2}D peak widths were estimated by manually measuring the width of the largest sub-peak of the 2D peak in ChromSpace (1.5.1). The difference in ChromSpace version used was because reproducibility data was reprocessed for consistency between the different experiments (sections 4.3.1 - 4.3.5) in this chapter. All reproducibility data was processed on ChromSpace ver. 2.1.4.

The peak capacity and resolution of the GC×GC system were measured using undiluted diesel, comparing the ^{2}DTPS and secondary oven. Two different ^{2}D temperature programs were tested, one where peaks wrapped around and eluted in the dead time, and the other which had no wraparound peaks. The secondary oven's constant offset separation was optimized to make full use of the 2D separation space by having peaks elute in the dead time of the ^{2}D separation. Retention time reproducibility (within-day: n = 5, day-to-day: n = 5) was measured for both the ^{2}DTPS and secondary oven using an undiluted sample of perfume. The ^{2}D temperature programming for this separation was optimized to make full use of the 2D separation space (like the secondary oven) for this comparison. Complete details of the GC×GC-FID conditions for the diesel and perfume samples are outlined in Table C – 1 in Appendix C.

GC×GC-TOFMS was used to tentatively identify the fatty acid methyl esters (FAMEs) in the diesel sample and the major components of the Perfume sample used for retention time reproducibility. The GC×GC-TOFMS system used an Agilent 6890A, with the SSM and the Markes BenchTOF-Select (Markes International). Data acquisition and processing were completed using ChromSpace software ver. 1.5.1. The separation used the same columns as those installed in the GC×GC-FID system. The relative positioning of the peaks in the 2D space was used to match the peaks from the separation completed with the GC×GC-FID to the GC×GC-TOFMS system. Separation conditions can be found in Table C - 3 in Appendix C. A standard *n*-alkane mix (C_7 - C_{19}) was made using individual alkane standards (Sigma-Aldrich, Oakville, ON, Canada) and injected under the same conditions to determine the ^{1}D linear retention indices.

4.2.2 ^{2}DTPS: Compatibility with the TOFMS

The ^{2}DTPS's compatibility with MS was tested with the SSM and Markes BenchTOF-Select using the Agilent 6890A GC. The ^{2}DTPS was the same as in section 4.2.1. A sample of diesel (10 % v/v) diluted in CS_2 (CX0395, Sigma-Aldrich Canada Co., ON, Canada) was separated using both ^{2}D temperature programming and a constant offset using the ^{2}DTPS. This was compared to the GC×GC-TOFMS separation where the ^{2}D

column was at oven temperature and all other separation conditions were identical. This was done for both within-day (n = 5) and day-to-day runs (n = 5). The complete GC×GC-TOFMS conditions are found in Table C - 5 in Appendix C.

4.2.3 ^{2}DTPS: RTC Addition

Following the addition of the RTC, the ^{2}DTPS was tested with the GC×GC-TOFMS for both within-day and day-to-day reproducibility, using a sample of perfume (10 % v/v) diluted in reagent alcohol. The same setup as in section 4.2.2 was used. The complete GC×GC-TOFMS conditions are found in Table C - 13 of Appendix C.

4.2.4 ^{2}DTPS: Compatibility with a Flow Modulator

The compatibility of the ^{2}DTPS with a flow modulator was tested with SepSolve's Insight flow modulator. The ^{2}DTPS used had the upgrades from sections 4.1.1 - 4.1.6. Among the available commercial flow modulators, differential flow modulators including the Insight flow modulator are unique with respect to typical ^{2}D column dimensions and ^{2}D flow, both of which have a direct impact on the performance of the ^{2}DTPS. The longer ^{2}D columns typically employed by differential flow modulators pose a challenge with power requirements for heating. The operational principle of the modulator requiring high ^{2}D flow rates results in shorter modulation periods, which demand greater heating/cooling rates if the same ^{2}D temperature offsets were needed. Pairing the ^{2}DTPS with the SepSolve Insight flow modulator was likely the most challenging experiment in balancing column dimensions, flow rate, and modulation period for the ^{2}DTPS. All the variables had to be balanced on a spreadsheet prior to installation and before a GC×GC separation.

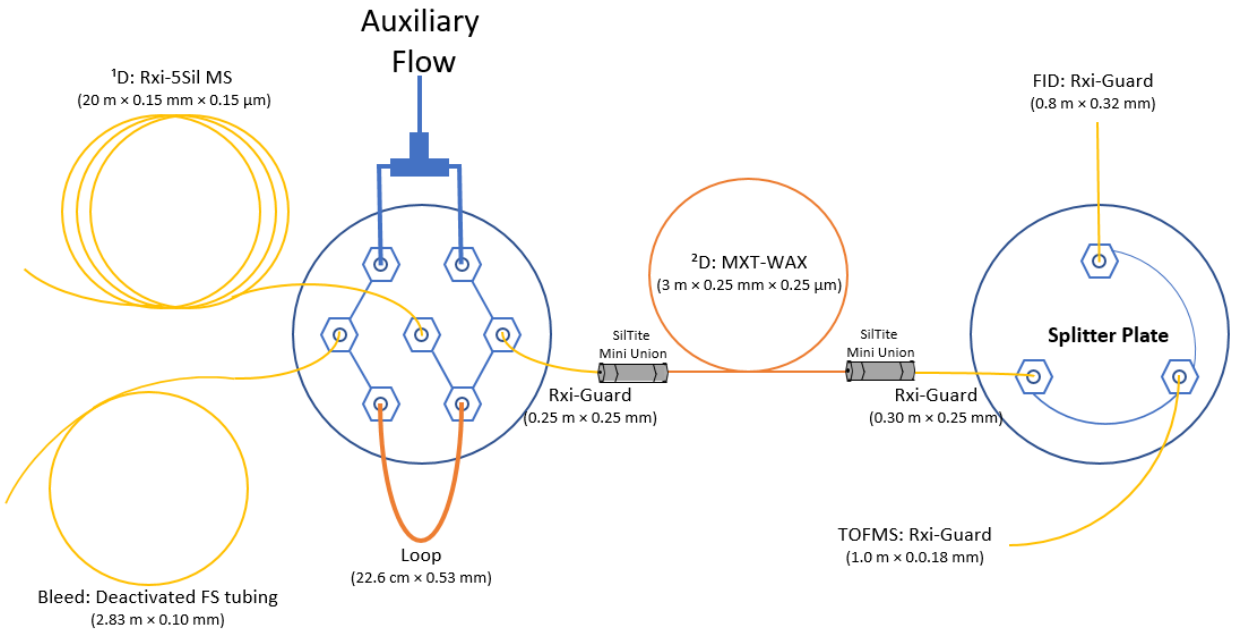

Figure 4-9: Diagram of the GC×GC column setup with the SepSolve Insight flow modulator and unpurged splitter to the FID and TOFMS.

The column dimensions (¹D, bleed column), flow rate, auxiliary pressure, and fill/flush durations were optimized with a ²D column dimension of 3 m x 0.25 mm. A ²D column of around 3 m in length was the starting point because this length left adequate headroom for ²D temperature programming with a resulting current of ~1.6 A (48 V). Longer columns would result in a lower maximum ²D temperature offset and heating rate, while a shorter column might have resulted in insufficient separation in the ²D (depending on the sample and stationary phase). The user guide for the modulator was followed to balance all other parameters, including the columns for the unpurged splitter to the FID and TOFMS. A splitter had to be used with the system due to the high ²D flow rate (18.09 mL/min) being incompatible with the TOFMS (limit = 5 mL/min). With the splitter installed and guard columns connected to the FID and TOFMS, the flows to each detector were 13.28 mL/min and 4.807 mL/min, respectively. Dead times between the splitter and the FID and TOFMS were 0.0050 min and 0.0039 min, respectively. A diagram showing the column dimensions of the whole GC×GC setup is shown in Figure 4-9. A sample of diesel (10 % v/v) diluted in CS_2 (Sigma-Aldrich Canada Co.) was separated with and without ²D

temperature programming. This was completed to determine both within-day (n = 5) and day-to-day (n = 5) reproducibility. Complete details are found in Table C - 15 of Appendix C.

4.2.5 ^{2}DTPS: Remote Port, Multiple ^{2}D Temperature Program Function, and Sequence

Completing the ^{2}DTPS as a standalone add-on device required the addition of the remote port connection (section 4.1.9.5). In addition, the multiple ^{2}D temperature program function (section 4.1.9.4) was added to the Arduino sketch and Windows Forms application. The Windows Forms application was further updated to be able to save ^{2}D temperature programming methods and run sequences. Following the physical and software update, the ^{2}DTPS reproducibility (within-day: n = 5, day-to-day: n = 5) was tested using a sample of diesel (10 % v/v) diluted in CS_2 (Sigma-Aldrich Canada Co.). The adjustable DC power supply (AB-5PS-D – ABRA Electronics) from section 4.2.1 was used after it was repaired following issues detailed in section 4.3.1.3.2. The GC×GC conditions can be found in Table C - 16 of Appendix C.

4.2.6 ^{2}DTPS: Maximum Heating Rate and Temperature Offset

The maximum heating rate and temperature offset were determined for various column dimensions (0.5 m × 0.25 mm, 1.0 m × 0.25 mm, 3.0 m × 0.25 mm, 0.5 m × 0.18 mm, 1.0 m × 0.18 mm) and power supply outputs (constant voltage; 1 – 2 A). The experiment was completed at GC oven temperatures of 35 °C, 50 °C, 100 °C, 150 °C, and 200 °C with a flow rate of 1.5 mL/min and 3.0 mL/min for the 1.0 m columns and only 3.0 mL/min for the rest of the columns. This was because it was discovered during testing that the flow rate had a negligible impact on the ^{2}D column heating. Aside from the ^{2}D column being changed for testing, the rest of the columns for the GC×GC setup remained the same as in 4.2.5. The ^{2}D temperature program set was for a 6 s modulation period, with 3 s of cooling, followed by a 2 s linear temperature program and held at the offset for 1 s. This ^{2}D temperature profile was similar to previous settings found in sections 4.2.1 - 4.2.5. The ^{2}D temperature offset applied was increased from 10 °C (5 °C/s heating rate for 2 s) until the maximum heating rate was found.

4.3 Results and Discussion

4.3.1 ^{2}DTPS: Resistance Measurement – Temperature Determination

4.3.1.1 Peak Capacity Comparison

The performance of the ^{2}DTPS was evaluated using an undiluted diesel sample to estimate the ^2n_c calculated using eq. (3.3). The average ^{2}FWHM (2.35σ) was used to calculate the average ^2W_b (4σ). For the separation without wraparound, the ^{2}t was the P_m minus the dead time in the ^{2}D. The values of 5 runs were averaged for each separation condition. To determine the average ^{2}FWHM in the ^{2}D, the selected peaks were evenly distributed across the ^{2}D, with each group of peaks denoted by the green dashed lines in Figure 4-10. This was done to reduce the bias of the average towards the narrower or broader peaks. This was particularly important for the secondary oven, where peaks broadened with increasing ^{2}D retention time (^2t_r). Due to this, the same peaks were not used in the estimation of their respective peak capacities.

The separation with the secondary oven utilized a +55 °C constant temperature offset, which resulted in wraparound peaks that eluted within the dead time of the ^{2}D, making full use of the 2D separation space (Figure 4-10A, separation A). Two different ^{2}D temperature programs were tested, one of which allowed for wraparounds to better utilize the 2D space as with the secondary oven (Figure 4-10B, separation B), and the other which completely eliminated wraparound peaks (Figure 4-10C, separation C). GC conditions were the same for each separation, with the only difference being the ^{2}D temperature program applied with each system. Enlarged chromatograms of each separation can be found in Figure C – 3, Figure C - 4, and Figure C - 5 of Appendix C.

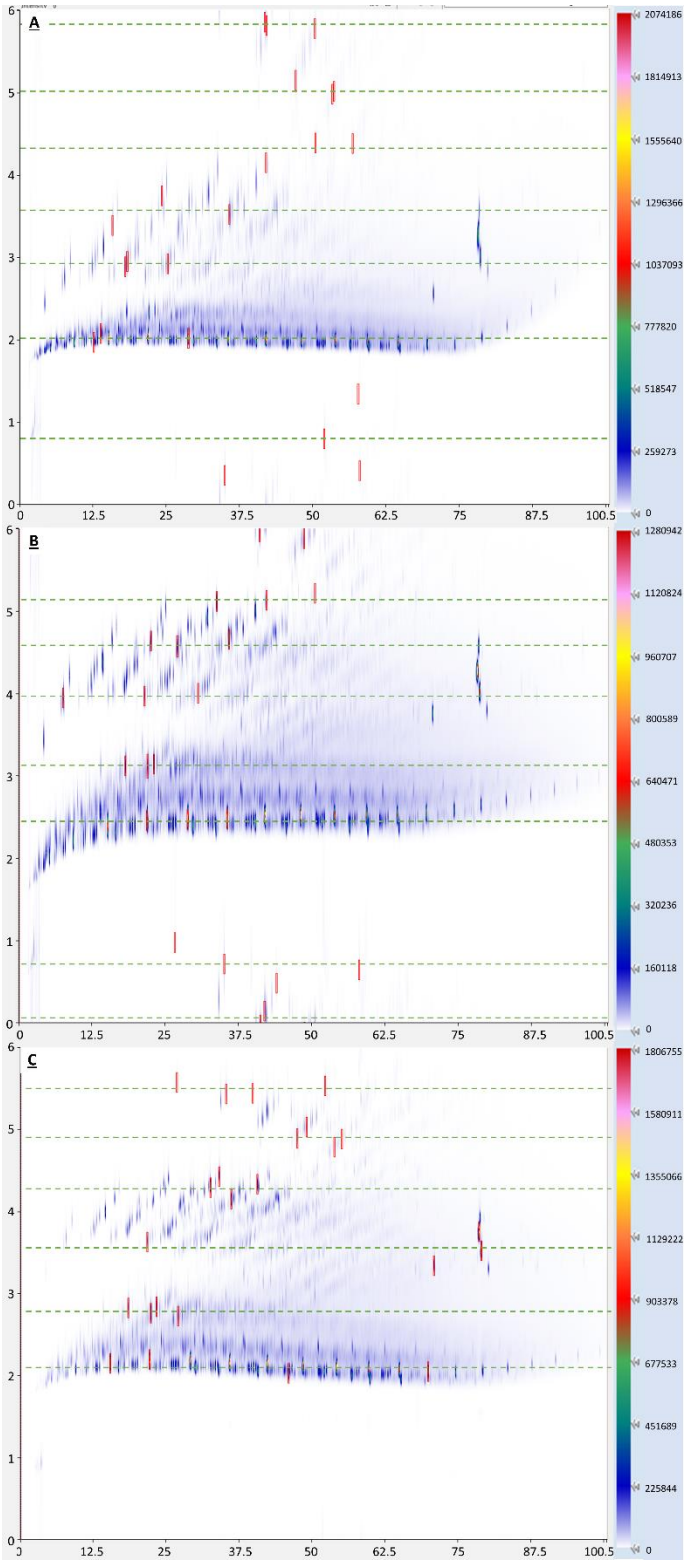

Figure 4-10: GC×GC-FID separation of diesel using an Rxi-5Sil MS W/Integra-Guard (39.219 m × 0.242 mm × 0.25 µm) ^{1}D column and an MXT-WAX (1.00 m × 0.25 mm × 0.25 µm) ^{2}D column. (A) Secondary oven with wraparound peaks. (B) ^{2}DTPS with wraparound peaks. (C) ^{2}DTPS without wraparound peaks. The dashed green lines highlight the groups of peaks (red) integrated along the ^{2}D for the calculation of peak capacity. The signal intensity is represented by the colour gradient given on the right for each chromatogram. ***X-axis: 0 – 100.5 min. Y-axis: 0 – 6 s****.*

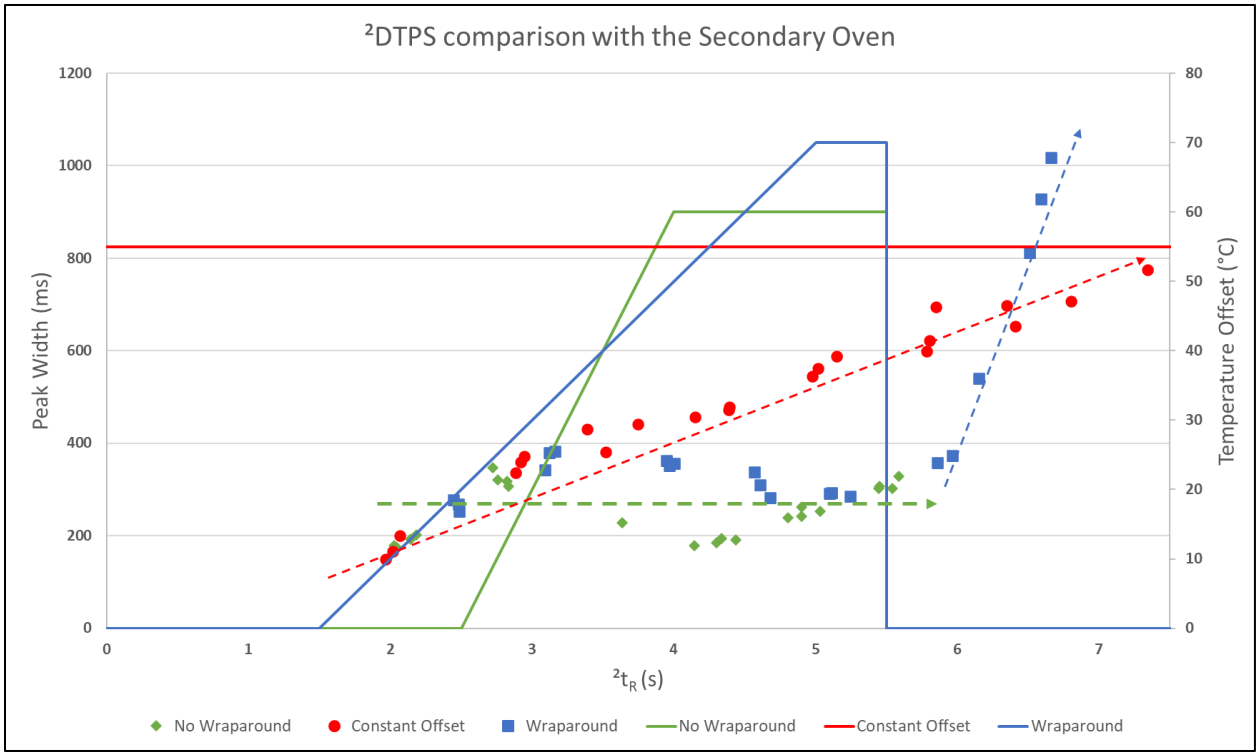

Figure 4-11: An overlay of the temperature offset applied to the ²D column with the ²W_b for each diesel separation.

Figure 4-11 shows an overlay of the ²W_b and the temperature offset applied to the ²D column. The ²FWHM for separation A ranged from 87.5 ms to 456 ms, with an average of 286 ms (²W_b = 486 ms). The ²FWHM increased linearly as a function of ²t_r, outlined by the dashed red arrow in Figure 4-11. This linear relationship can be understood from eq. (4.4), the formula for the number of theoretical plates (N), from which the peak width is proportional to the retention time. Although N is a measure of the column's separation efficiency, it is important to note that this is only an approximation as N varies with separation conditions (temperature and linear velocity) and analyte. The ²n_c for this separation was 12.4 with a ²t of 6 s.

$$N = 16(\frac{t_r}{W_b})^2 \tag{4.4}$$

The ²D temperature programming separation with wraparounds (separation B) made full use of the 2D space like separation A. The ²FWHM ranged from 148 ms to 598 ms, with an average of 247 ms (²W_b = 419 ms). The ²n_c for this separation was 14.3 with a ²t of 6 s, which was a +15 % increase over the

secondary oven separation. Most of the band broadening for the ^{2}DTPS occurred during the cooling of the system back to oven temperature at the end and beginning of each modulation period. Strongly retained peaks that were still on the ^{2}D column during cooling broadened very rapidly (outlined by the dashed blue arrow in Figure 4-11) and eluted as peaks even broader than the constant temperature offset separation. Peaks eluting within or close to the end of the ^{2}D temperature program had very similar ^{2}FWHM, which was expected with temperature programming. If the ^2n_c was calculated separately for the two parts of the ^{2}D temperature programming separation, during ^{2}D temperature programming (1.5 s to 5.5 s) and during cooling (5.5 s to 7.5 s), the peak capacities would be 12.6 and 3.0, respectively, for a total of 15.6 (+26 %). If this was done for separation A, the ^2n_c would be 10.1 and 2.9, respectively, for a total of 13.1, which was similar to the original calculation.

For separation C, a faster temperature ramp of 40 °C/s (versus 20 °C/s) was used with a longer initial delay (2.5 s vs. 1.5 s) and a longer constant offset (1.5 s vs. 0.5 s) at the final temperature. The ^{2}FWHM ranged from 102 ms to 204 ms, with an average of 142 ms (^2W_b = 242 ms). Even though the initial delay was 1 s longer and the final temperature offset was 10 °C lower than the temperature program in separation B, the early eluting peaks were still narrower. This is further investigated in section 4.3.1.4. The ^{2}D dead time was approximately 1.44 s, due to the length of the modulator column, ^{2}D column, and guard column used. Therefore, the ^2n_c for this separation was 18.8 with a ^{2}t of 4.56 s. This was a 52 % increase in ^2n_c compared to secondary oven separation and a 21 % increase in ^2n_c compared to the ^{2}D temperature programming separation with wraparound peaks, even though less separation time was available. A summary of the values can be found in Table 4-8.

Table 4-8: Comparison of ^2D peak capacity (^2n_c) between the secondary oven (with wraparound peaks) and the ^2DTPS performing ^2D temperature programming (with and without wraparound peaks). GC and modulator parameters were the same for all three separations.

	Secondary Oven (Separation A)		^2D Temperature Programming (Separation B)		^2D Temperature Programming (Separation C)
^2t (ms)	6000		6000		4560
$W_{b,avg}$ (ms)	486		419		242
^2n_c	12.4		14.3		18.8
^2t_r range	1.5 - 5.5 s	5.5 – 7.5 s	1.5 - 5.5 s	5.5 - 7.5 s	
^2t (ms)	4000	2000	4000	2000	
$W_{b,avg}$ (ms)	396	678	318	671	
^2n_c	10.1	2.9	12.6	3.0	
Total ^2n_c	13.1		15.6		

4.3.1.2 Resolution Comparison

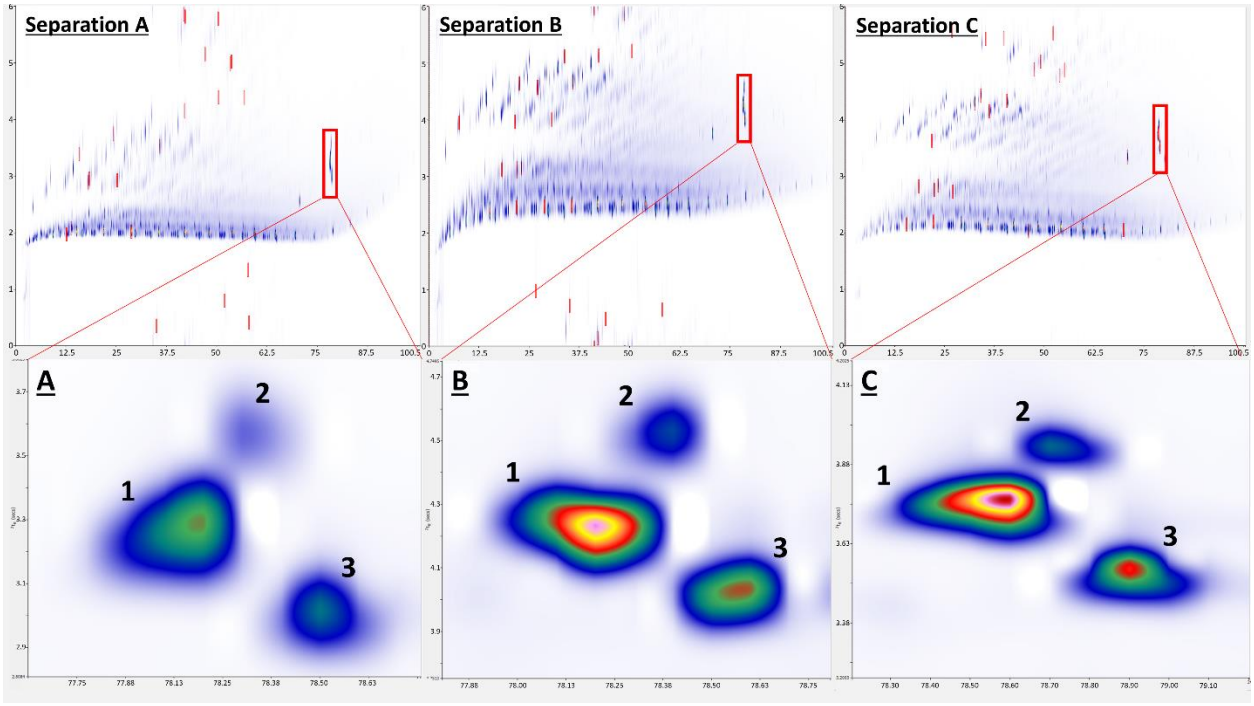

Figure 4-12: FAMEs found in the diesel were used for resolution comparison. (A) Secondary oven with wraparound peaks, (B) ^2DTPS with wraparound peaks, and (C) ^2DTPS without wraparound peaks.

Three FAMEs that eluted closely in both dimensions (Figure 4-12) were used to compare the $R_{s,2D}$ between the three separations. These FAMEs were tentatively identified as: methyl linoleate (1), methyl linolenate (2), and methyl oleate (3). The $R_{s,2D}$ between methyl linoleate (1) and methyl linolenate (2) was

0.84 for separation A, 1.05 for separation B, and 1.00 for separation C. Between methyl linolenate (2) and methyl oleate (3), the $R_{s,2D}$ was 1.66 for separation A, 2.03 for separation B, and 2.27 for separation C. Finally, between methyl linoleate (1) and methyl oleate (3), the $R_{s,2D}$ was 0.96 for separation A, 1.18 for separation B, and 1.38 for separation C. Although separation A, B, and C were not optimized to resolve these three FAMEs but rather the overall separation of the sample, the temperature-programmed separations (B and C) consistently resolved the three FAMEs better than the constant offset separation (A). It should be noted that the ^{1}D resolution was not identical between the three separations, however, the ^{2}D resolution was still consistently better for the temperature programming separations. Values for the calculation are found in Table C - 2 in Appendix C.

4.3.1.3 System Reproducibility

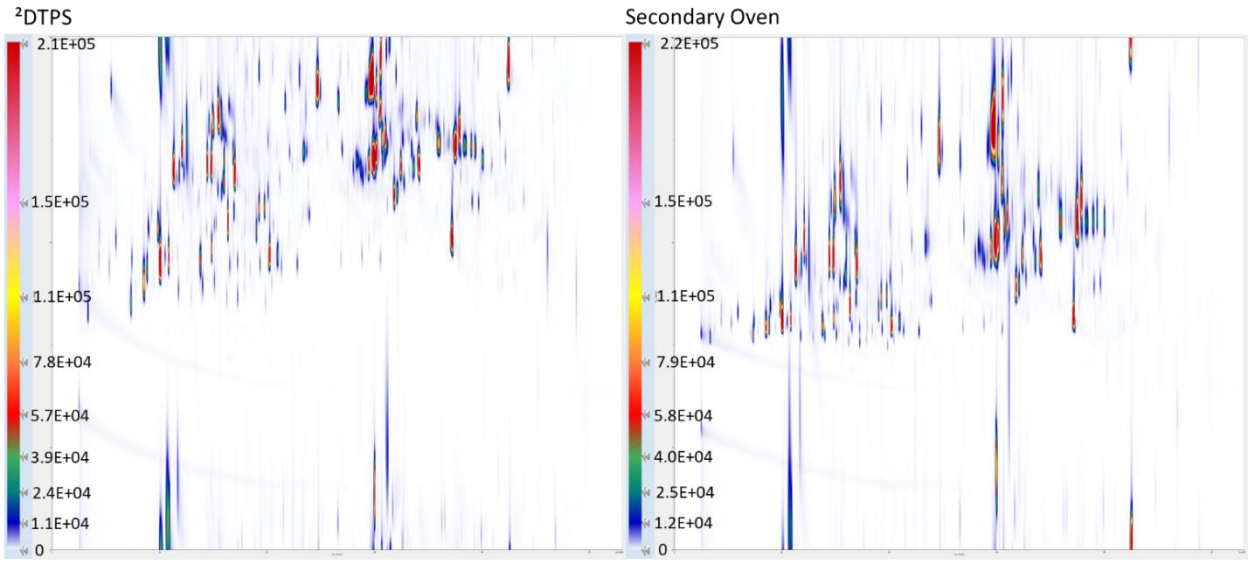

Figure 4-13: GC×GC-FID separation of a perfume sample with ^{2}D temperature programming (^{2}DTPS) or a constant temperature offset (secondary oven) in the ^{2}D. A constant temperature offset of +40 °C was used to match the elution time of the late eluting peaks in the ^{2}DTPS separation. ***X-axis: 0 – 53 min. Y-axis: 0 – 5 s****.*

To assess the reproducibility of the ^{2}DTPS, a relatively simple perfume sample (number of integrated peaks > 400) was used (Figure 4-13). The ^{1}D retention time (^1t_r), ^2t_r and peak area reproducibility were assessed. This was done for both day-to-day (n = 5) and within-day (n = 5) runs. During testing, there were some technical difficulties which resulted in fewer runs (< 5) being completed than designed on certain

days. Some of the issues experienced included a pre-mature ending to the GC run and the adjustable DC power supply not maintaining a constant voltage. The issue with the GC run ending prematurely was random and could not be diagnosed. This was experienced for both the ^{2}DTPS and the secondary oven setup. The DC power supply problem was due to the age of the PSU, where the solder on the PCB was deteriorating, affecting the resistance measurement of the PSU to provide the appropriate amount of current to achieve constant voltage. The sudden decrease in the voltage resulted in differences in the measured resistance not due to the temperature. This is discussed in section 4.3.1.3.2. Due to the unequal number of runs per day, the day-to-day reproducibility (n = 5) was calculated using a single run each day. This method of calculating the day-to-day repeatability would be used for the rest of the chapter to ensure consistency. The run selected (first run) was the same for all five days. The within-day repeatability was calculated using five back-to-back runs within a single day. GC conditions were identical for both the ^{2}D temperature programming separation and the constant temperature offset separation with the secondary oven. For the comparison, the 10 largest peaks (with a symmetry value > 90) were used. The tentative identification of the 10 peaks (Table C - 4 of Appendix C) was performed by analyzing the perfume sample on the GC×GC-TOFMS, using the National Institute of Standards and Technology (NIST) 2017 mass spectra library (NIST, Gaithersburg, Maryland, U.S.A.) and comparing the calculated linear retention indices to reported data where available. The 10 peaks from the GC×GC-FID separations were matched to the GC×GC-TOFMS separation based on the relative positions of the peaks in the 2D separation space (Figure 4-14).

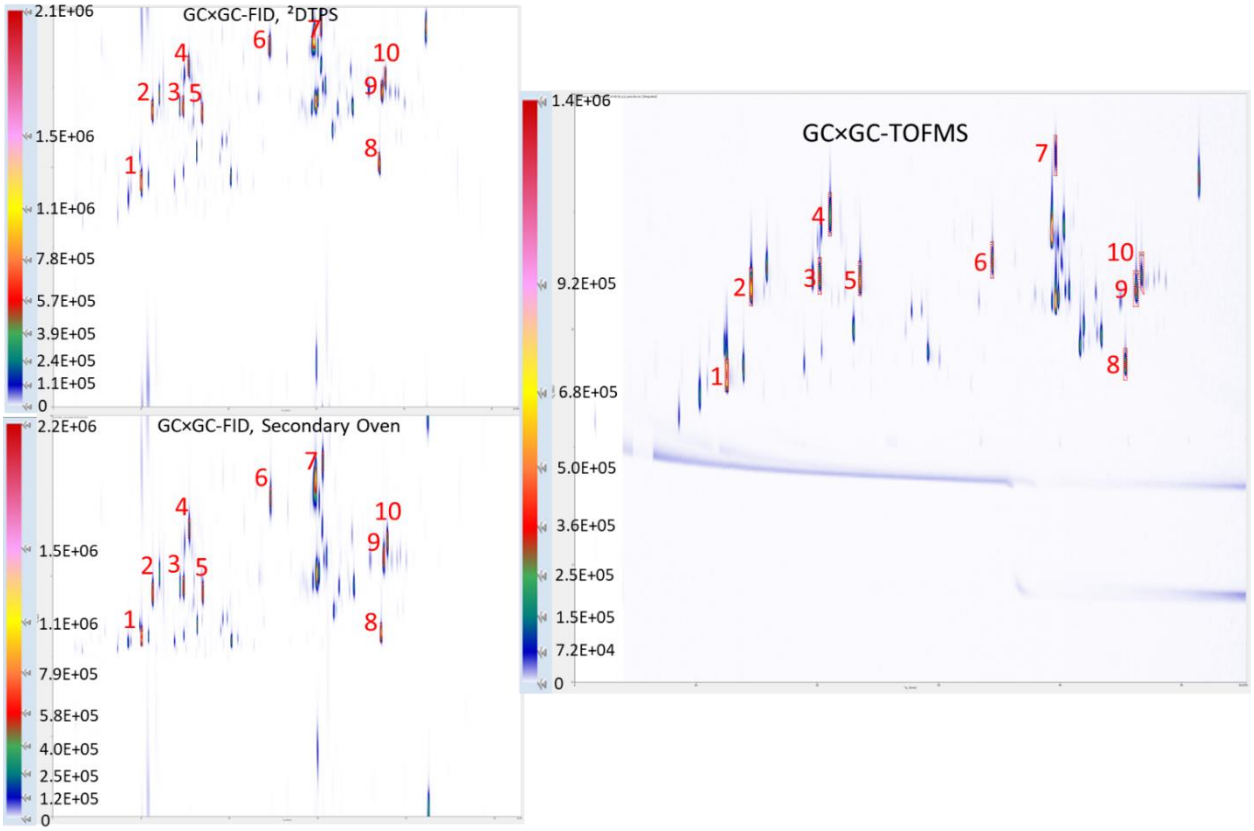

Figure 4-14: Identification of the major components in the perfume sample used to compare the reproducibility of the ²DTPS and secondary oven. The peaks from the GC×GC-FID separation were matched to the GC×GC-TOFMS separation based on the relative positioning in the 2D space and peak area %. GC×GC-FID: ***X-Axis: 0 – 53 min; Y-axis: 0 – 5 s****. GC×GC-TOFMS:* ***X-axis: 0 – 55.33 min; Y-axis: 0 – 5 s****.*

4.3.1.3.1 Reproducibility

The temperature measurement system for the ²DTPS was calibrated at the start of each day. Although such frequency of calibration was not necessary, this was done to also monitor the resistance stability (section 4.3.1.3.2) of the system after a new column installation. For the ^2t_r, the within-day RSD for the ²DTPS was 0.33 - 0.8 % and day-to-day RSD was 0.37 - 0.90 %. For the secondary oven separations, the within-day RSD for the ^2t_r was 0.10 - 0.33 % and day-to-day RSD was 0.42 - 1.19 %. This data is available in Table 4-9. Examining the ^2t_r variability over the 5 days for the secondary oven separations, a pattern common to all 10 peaks was noticed. Comparing this pattern to the barometric pressure measured at a nearby weather station (UW Weather Station) over the 5 days produced a similar pattern in variability, shown in Figure C - 6 of Appendix C. This may indicate that the GC was not compensating for the

atmospheric pressure changes properly, leading to slight changes in volumetric flow rate. However, this same effect was not noticeable with the temperature programming separations, which may indicate that the variability due to the ^{2}DTPS overshadowed the variability due to the atmospheric pressure fluctuations.

Table 4-9: ^{2}DTPS vs. Secondary Oven: within-day and day-to-day reproducibility for ^1t_r and ^2t_r for the 10 major compounds in the perfume sample.

	Within-Day: ^{2}DTPS				Within-Day: Secondary oven			
	Average		RSD (%)		Average		RSD (%)	
PEAK #	^1t_r (min)	^2t_r (s)	^1t_r	^2t_r	^1t_r (min)	^2t_r (s)	^1t_r	^2t_r
1	10.049	2.80	0.02	0.55	10.048	2.23	0.02	0.24
2	11.309	3.71	0.01	0.40	11.309	2.78	0.01	0.19
3	14.813	3.76	0.00	0.36	14.813	2.85	0.00	0.19
4	15.454	4.26	0.02	0.40	15.452	3.57	0.02	0.17
5	16.979	3.66	0.00	0.33	16.978	2.78	0.00	0.17
6	24.690	4.52	0.01	0.74	24.655	3.96	0.06	0.18
7	30.560	4.78	0.00	0.57	30.577	4.41	0.03	0.10
8	37.197	3.04	0.01	0.71	37.155	2.28	0.05	0.33
9	37.511	3.94	0.04	0.78	37.474	3.22	0.01	0.30
10	37.909	4.10	0.04	0.80	37.896	3.41	0.03	0.24
AVERAGE	-	-	0.02	0.56	-	-	0.02	0.21
	Day-to-Day: ^{2}DTPS				Day-to-Day: Secondary Oven			
	Average		RSD (%)		Average		RSD (%)	
PEAK #	^1t_r (min)	^2t_r (s)	^1t_r	^2t_r	^1t_r (min)	^2t_r (s)	^1t_r	^2t_r
1	10.027	2.83	0.27	0.89	10.042	2.25	0.12	1.19
2	11.299	3.72	0.11	0.50	11.308	2.80	0.02	0.99
3	14.804	3.77	0.09	0.43	14.812	2.87	0.01	0.92
4	15.435	4.27	0.16	0.37	15.450	3.60	0.05	1.02
5	16.968	3.68	0.09	0.41	16.977	2.80	0.01	0.92
6	24.645	4.53	0.13	0.54	24.659	3.99	0.10	0.88
7	30.539	4.78	0.12	0.52	30.567	4.44	0.07	0.40
8	37.152	3.07	0.08	0.90	37.160	2.30	0.07	1.18
9	37.473	3.96	0.08	0.71	37.479	3.24	0.01	1.09
10	37.866	4.12	0.09	0.53	37.886	3.44	0.06	1.01
AVERAGE	-	-	0.12	0.58	-	-	0.05	0.96

For the ^1t_r, the within-day RSD for the ^{2}DTPS was 0.00 - 0.04 % and day-to-day RSD was 0.08 - 0.27 %. For the secondary oven, the within-day RSD for the ^1t_r was 0.00 - 0.06 % and day-to-day RSD was 0.01 - 0.12 %. The RSD was similar for the ^{2}DTPS and secondary oven, with only the day-to-day results being slightly worse for the ^{2}DTPS. Although the two systems should have negligible impact on the ^{1}D

separation, the flow rate in the ^{1}D could be affected by the slight differences in the ^{2}D temperature offset between runs. These slight changes can influence the pressure drop along the column train, affecting the flow rate and repeatability of both the $^{1}t_r$ and $^{2}t_r$. For the ^{2}DTPS it was possible that the calibration drifted slightly from day-to-day, resulting in small differences in the measured ^{2}D column temperature, affecting the ^{2}D temperature program. Further testing with the ^{2}DTPS in the subsequent sections will provide a clearer picture of the reproducibility of the ^{2}DTPS.

Table 4-10: ^{2}DTPS vs. Secondary Oven: Within-day and day-to-day reproducibility for peak area for the 10 major compounds in the perfume sample.

WITHIN-DAY (n = 5)				
	^{2}DTPS		Secondary Oven	
PEAK #	Average	RSD (%)	Average	RSD (%)
1	49262958	1.70	49306709	1.39
2	28373075	1.39	28048575	1.12
3	18542364	1.37	18196437	1.27
4	16245203	1.28	15960820	1.25
5	19467139	1.32	19256333	1.31
6	23215236	1.02	22775114	1.27
7	20622967	0.57	20201599	1.27
8	28632773	0.93	27975040	1.16
9	38201084	0.93	37426573	1.26
10	21016126	1.27	20645066	1.04
AVERAGE		1.18		1.23
DAY-TO-DAY ^{2}DTPS				
	^{2}DTPS		Secondary Oven	
PEAK #	Average	RSD (%)	Average	RSD (%)
1	49868165	1.42	48102803	3.23
2	28447044	1.58	27719563	1.76
3	18567326	1.67	18311436	1.46
4	16251097	1.97	16089289	1.27
5	19429963	1.49	19411290	1.28
6	23250116	1.23	23080105	0.83
7	20567815	1.55	20241419	2.93
8	28556329	1.32	28376200	0.77
9	38228746	1.37	37647013	2.07
10	20994507	1.73	20917667	0.62
AVERAGE		1.53		1.62

Peak area reproducibility for the within-day runs and day-to-day runs is illustrated in Table 4-10. For the ^{2}DTPS, peak area RSD ranged from 0.9 - 1.7 % for the within-day runs and 1.2 - 2.0 % for the day-to-

day runs. The average RSD was 1.18 % for the within-day runs and 1.53 % for the day-to-day runs. For the secondary oven, peak area RSD was 1.0 - 1.4 % for within-day runs and 0.6 - 3.2 % for the day-to-day runs. The average RSD was 1.23 % for the within-day runs and 1.62 % for the day-to-day runs. GC×GC

Table 4-11: Paired Student's t-test for the within-day and day-to-day RSD results, comparing the ^{2}DTPS and secondary oven for the ^1t_r, ^2t_r, and peak area. Results that are insignificant are highlighted in green while significant results are highlighted in orange.

Within-Day (α = 0.05)					
^{1}D RT		^{2}D RT		Area	
t-stat	p-value	t-stat	p-value	t-stat	p-value
1.0	0.36	7.1	5.8×10^{-5}	0.54	0.60
Day-to-Day (α = 0.05)					
^{1}D RT		^{2}D RT		Area	
t-stat	p-value	t-stat	p-value	t-stat	p-value
5.6	3.4×10^{-4}	5.7	2.9×10^{-4}	0.30	0.77

The within-day and day-to-day RSDs for ^1t_r, ^2t_r, and peak area were compared between the ^{2}DTPS and the secondary oven using a paired Student's t-test (α = 0.05), with results presented in Table 4-11. The differences between the ^{2}DTPS and secondary oven were significant for the ^2t_r RSD for the within-day results, while the differences for the ^1t_r and ^2t_r were significant for the day-to-day results.

4.3.1.3.2 Resistance Reproducibility

The reproducibility of the measured column resistance is critical to the reproducibility of the ^{2}DTPS, since the system relies on the resistance measurement to determine temperature. To gauge the reproducibility of the measured column resistance, a new MXT-WAX column (0.52 m × 0.25 mm × 0.25 µm, not conditioned) was installed, and the GC oven temperature was ramped from 35 °C (1 min hold) to 230 °C (1 min hold) at a rate of 10 °C/min (21.5 min run). The resistance was measured by the ^{2}DTPS every 300 ms by turning on the MOSFET for 6 ms and recording the resistance after 5 ms. Waiting 5 ms before recording the resistance provided ample time for the system to stabilize, while leaving the MOSFET on for only 6 ms minimized the heating during the resistance measurement.

The resistance measurements were then averaged at each temperature (°C) and a second-order polynomial was fitted to the temperature vs. resistance data. Using a second-order polynomial, the error was < 1 °C, while for a linear equation it was < 2 °C.

Six calibrations were done on Day 1, however, calibrations 2 and 5 had some errors in the resistance measurement (Figure 4-15). Calibration 2 had a sudden decrease in measured resistance at 211 °C. It was observed that during the calibration, the output voltage of the power supply suddenly decreased causing a sudden drop (53 mΩ) in the measured resistance. Although both the current and the voltage drop across the MXT-WAX column were measured by the ^{2}DTPS to determine the resistance, adjusting the output voltage of the DC power supply did affect the resistance measured by the system. Since the resistance measurement was very sensitive to resistance changes (~4 mΩ/°C), even slight changes to the overall circuit could have had a large impact on the calculated temperature. Calibration 5 had a slight rise in resistance from 53 - 65 °C. It was unclear what may have caused this. A more stable constant voltage power supply should improve the reproducibility of the ^{2}DTPS.

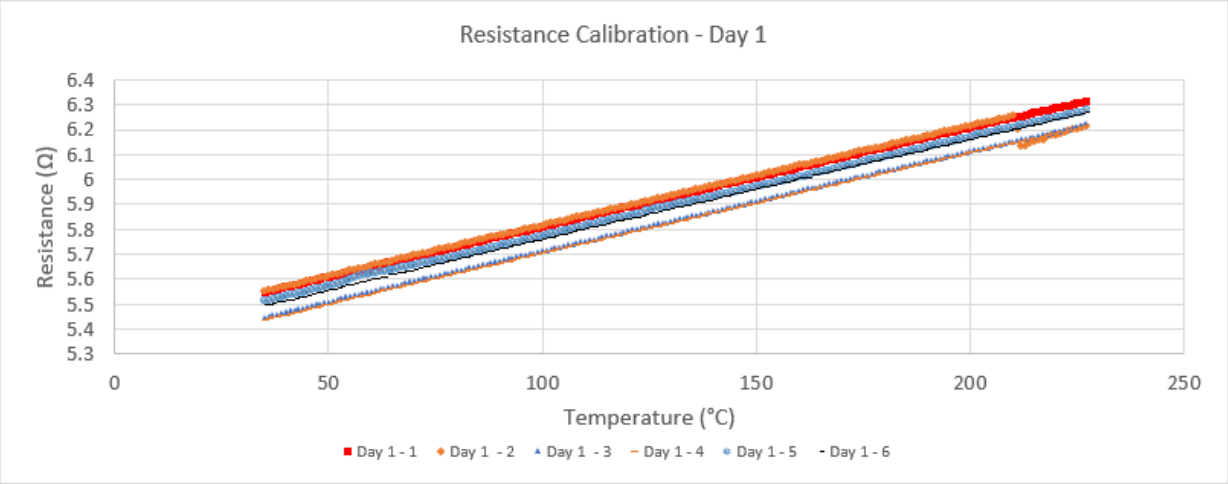

Figure 4-15: Resistance calibrations (6) of an MXT-WAX (0.52 m × 0.25 mm × 0.25 µm) on Day 1.

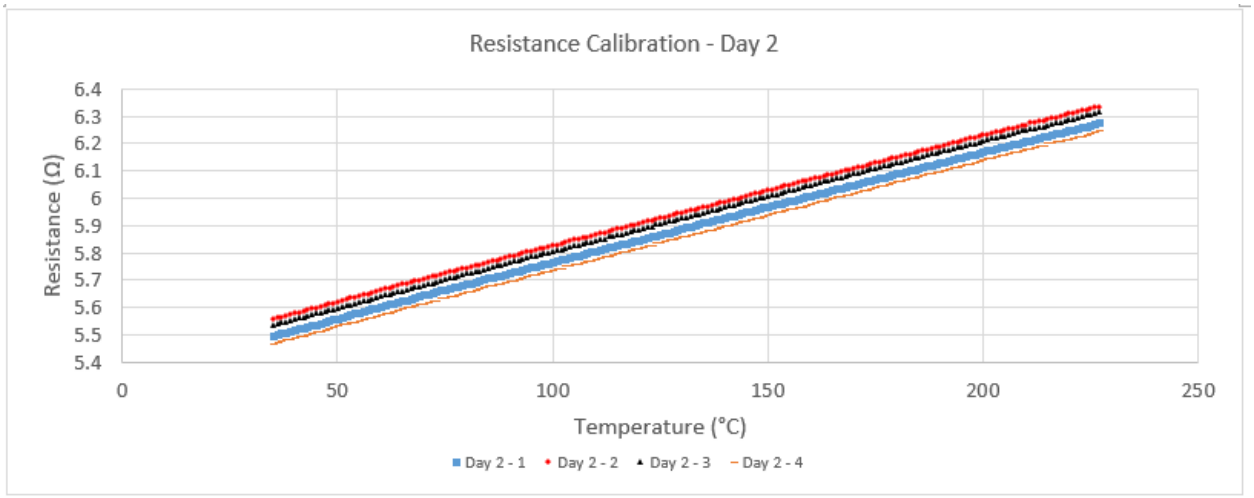

Figure 4-16: Resistance calibrations (4) of an MXT-WAX (0.52 m × 0.25 mm × 0.25 µm) on day 2.

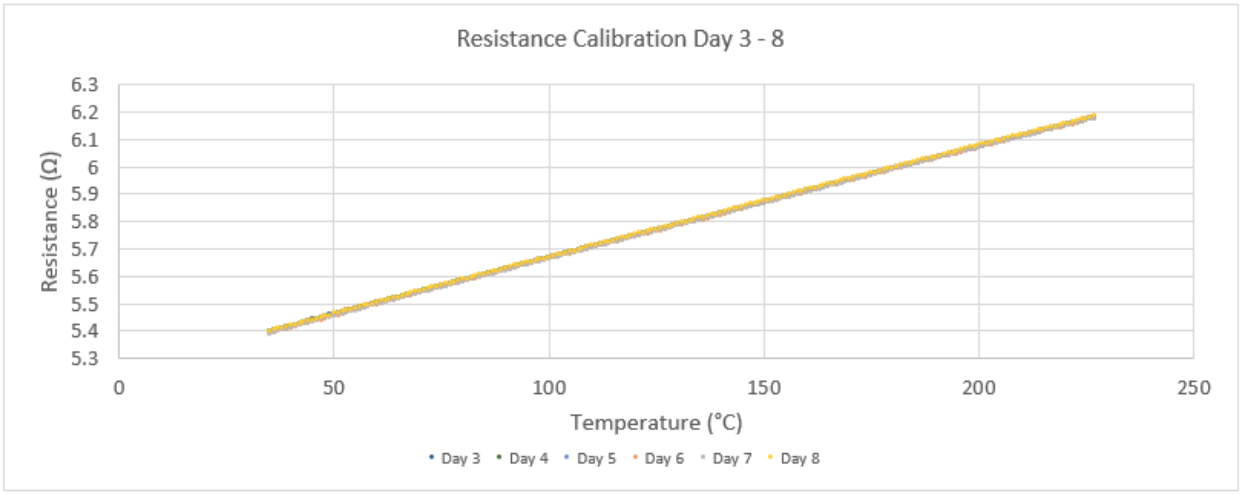

Figure 4-17: Resistance calibrations of an MXT-WAX (0.52 m × 0.25 mm × 0.25 µm) on days 3 - 8.

Four calibrations were completed on Day 2 (Figure 4-16), without issues, to match the number of successful calibrations on Day 1. Single calibrations were done from Day 3 to Day 8 (Figure 4-17). After it was confirmed on Day 4 that the column resistance had stabilized, the perfume sample was also run from Day 4 to Day 8 to collect the within-day and day-to-day repeatability data. Overall, it took a total of 10 runs over 2 days (215 min total run time), before the column resistance measurements stabilized. If the calibration from Day 3 $(6.8221(\Omega)^2 + 167.40(\Omega) - 1068)$ was used for Day 4 – 8, the error would be < 2.4 °C. This should be acceptable considering the rapid temperature programming rates used and the short

retention times in the ^{2}D. The slight differences in temperature offset between runs should have a much lower impact on the ^{2}D retention time reproducibility than if the system was used for 1D GC separations.

4.3.1.4 Investigating the ^{2}D Flow/Linear Velocity

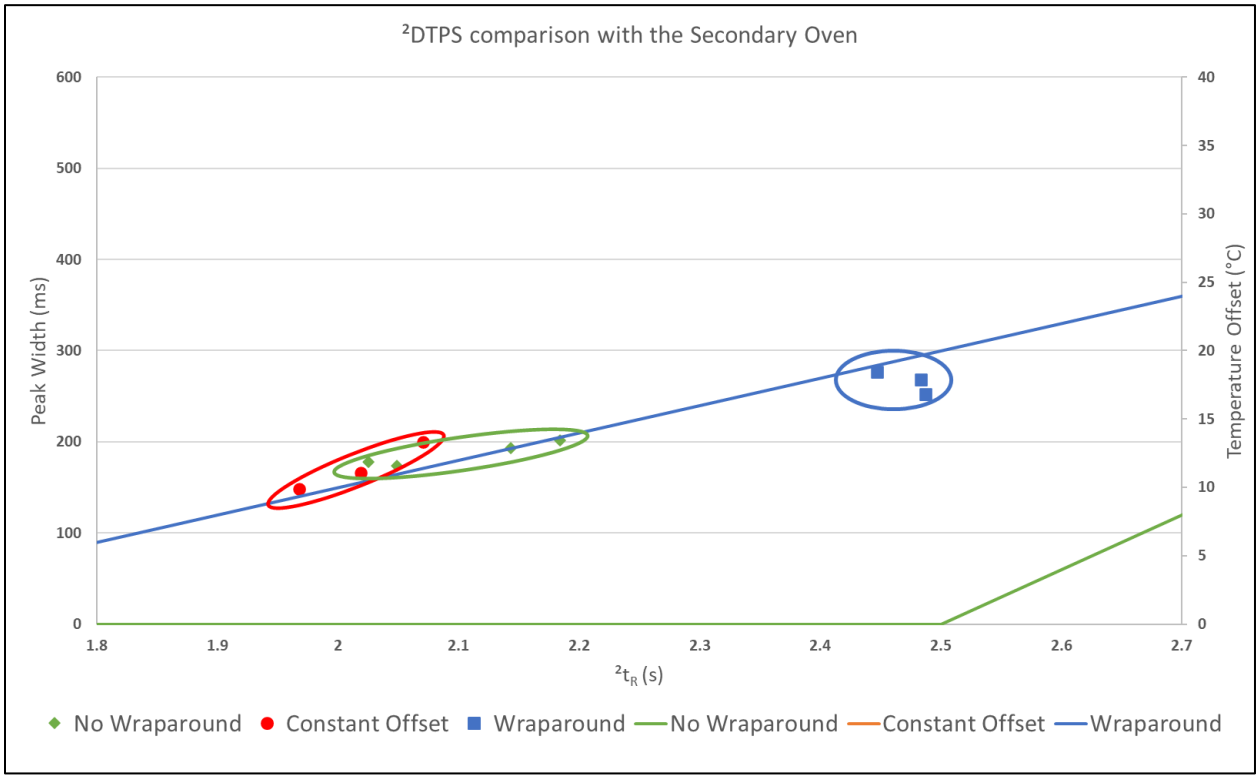

Figure 4-18: Examining the ^2W_b of the early eluting peaks relative to the ^2t_r and ^{2}D temperature offsets applied from Figure 4-11. The early eluting peaks of the temperature programming separation with wraparounds (B) eluted later and broader than the temperature programming separation without wraparounds (C), even though separation B had an earlier start to the ^{2}D heating. The constant offset temperature, not seen in the figure was +55 °C.

One aspect from section 4.3.1.1 that required further investigation was the elution time and ^2W_b of the early eluting (least retained) peaks. Shown in Figure 4-18, the red, green, and blue markers show the ^2W_b and ^2t_r of the constant offset, temperature programming without wraparound, and temperature programming with wraparound separations, respectively. The group of early eluting peaks for the constant offset and temperature programming without wraparound separations had similar ^2t_r and ^2W_b. These peaks eluted at around 2 s, which for the temperature programming separation without wraparound would have allowed the ^{2}D column to cool for ~2.5 s by the time these peaks eluted. This meant that the ^{2}D column should have been near the oven temperature during their separation. Since

the ^2W_b and ^2t_r were still comparable to the constant offset (+55 °C) separation, this would indicate that these early eluting peaks had very little retention and would therefore not be influenced much by the differences in ^{2}D temperature offset experienced. However, the early eluting peaks for the temperature programming separation with wraparounds eluted later and broader, even though the ^{2}D temperature program started earlier (1.5 s compared to 2.5 s). These early eluting peaks experienced both the rapid cooling of the ^{2}D column back to oven temperature and ~1 s of heating at 20 °C/s before eluting. If these early eluting peaks were truly not affected by the difference in temperature and all other conditions were the same, then the elution time and peak width should be similar for all three separations. Since the ^{2}D column temperature affects not only the retention of compounds but also the carrier gas viscosity, the rapid ^{2}D temperature changes may have affected the average linear velocity through the ^{2}D column. Higher temperatures result in higher gas viscosity, which might reduce the linear velocity through the ^{2}D column.

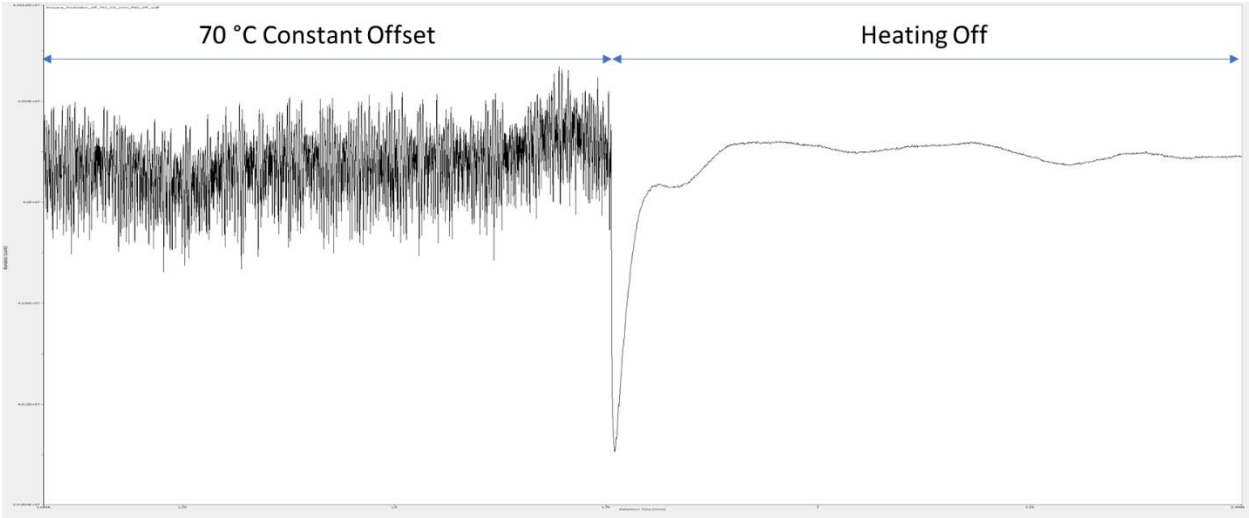

Figure 4-19: FID signal with a constant temperature offset of +70 °C by the ^{2}DTPS (LEFT) and without additional heating,^{2}DTPS OFF (RIGHT). ***X-axis: 1.0858 – 2.4998 min. Y-axis: 3.91854×10^7 – 4.38316×10^7.***

To investigate the flow and linear velocity in the ^{2}D, the carrier gas was doped with propane using a propane cylinder. The cylinder was connected directly to the inlet through a 50 cm x 50 µm fused-silica capillary. The GC inlet was set to a 1:1 split at 250 °C. The GC oven was maintained at a constant

temperature of 100 °C and a constant flow rate of 4.0 mL/min of H_2. The FID, being a mass sensitive detector, would have a signal that would change with the mass flow of propane. This allowed the FID to act as a mass flow meter to indicate the changes in linear velocity with the ^{2}D temperature offsets applied. Using the ^{2}DTPS, a 70 °C constant offset was applied and then abruptly stopped to record the FID signal with a constant offset and without additional ^{2}D heating (Figure 4-19). The rapid switching of the MOSFET generated a very noisy baseline when maintaining a 70 °C constant offset. When the power supply was switched OFF, the secondary column cooled very rapidly, and a sudden decrease in the signal was observed. This illustrated a sudden and rapid decrease in flow rate during the initial portions of cooling (most rapid temperature change) before the signal recovered and leveled out. This was unexpected since the decreasing temperature should result in a higher flow rate due to the decrease in gas viscosity. A possible explanation for this is provided later in this section. After the signal stabilized following cooling, the baseline was at around the same level as during the +70 °C constant offset. This indicated that the flow rate and linear velocity with and without a constant temperature offset were approximately the same. This would explain the similar ^2W_b and ^2t_r between the constant offset separation and the ^{2}D temperature programming separation without wraparounds. The early eluting peaks for the ^{2}D temperature programming separation should have experienced very little temperature change (~oven temperature) within the ^{2}D column since they eluted near the end of the cooling period. It was therefore likely that the longer elution time in the ^{2}D for the early eluting peaks of the ^{2}D temperature programming separation with wraparound was due to those peaks experiencing the sudden change in temperature from the start of the ^{2}D temperature program.

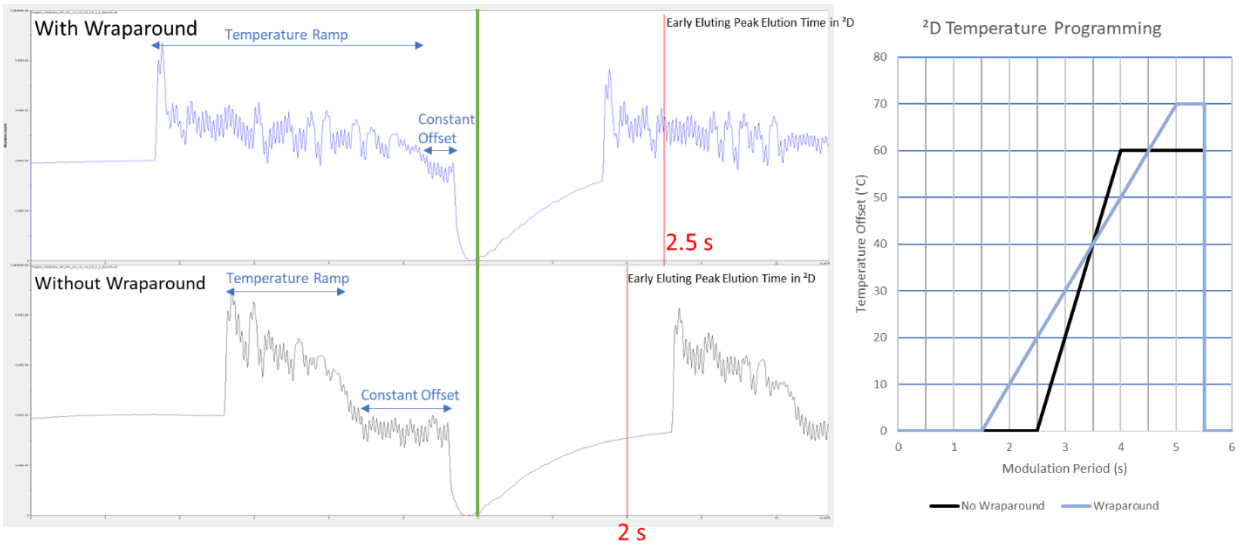

Figure 4-20: Comparing the flow/linear velocity of the carrier gas (H_2) with the two ²D temperature programs used in the peak capacity comparison. On the left are the FID signals with the ²DTPS running the two ²D temperature programs (with and without wraparound peaks)

Shown in Figure 4-20 is the FID signal with the ²DTPS performing the two ²D temperature programs used in the peak capacity comparison. The first two modulations were shown in order to establish the baseline prior to the start of ²D temperature programming. When the ²D temperature program started a sudden increase in flow was observed for both temperature programs. For the separation with wraparound peaks, a 20 °C/s temperature ramp was applied to the ²D column for 3.5 s. A sharp increase in flow was observed initially, before it quickly decreased and settled at a slightly elevated flow compared to before ²D heating was applied. The constant offset portion of the temperature program at +70 °C had similar flow to before ²D heating was applied. In comparison, the separation without wraparound peaks applied a 40 °C/s temperature ramp for 1.5 s. The faster and shorter temperature ramp resulted in a sharp increase in flow initially and remained higher compared to the 20 °C/s temperature ramp. The constant offset of +60 °C also had a similar flow to before the application of ²D heating. When the heating was turned off at 5.5 s into the modulation period, a sharp decrease in flow was observed like before. The flow was roughly the same for both ²D temperature programs during cooling. Based on the elution time of the early eluting peaks for each ²D temperature program, marked by the red line in Figure 4-20, the peaks should have eluted earlier if the ²D temperature program started before the peaks elute, due to the

sudden increase in flow. The opposite was observed, so the flow rate at the detector may not have been a complete or accurate representation of the processes occurring within the column.

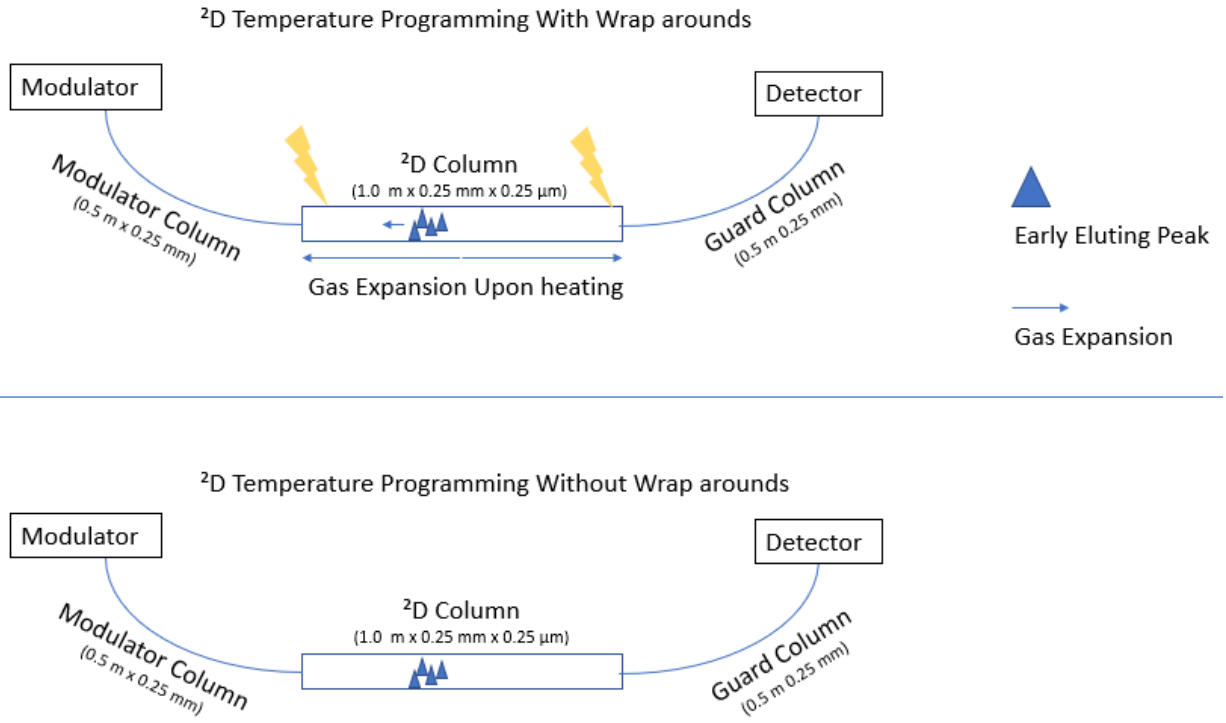

Figure 4-21: An illustration of the general ²D setup for the ²DTPS and the effects of carrier gas expansion when rapid heating is applied to the ²D column. The upper figure illustrates the early eluting peaks being pushed towards the inlet of the ²D column when ²D temperature programming starts. In the lower figure, the early eluting peaks traverse the column without experiencing any fluctuations in flow or temperature.

Split ratios of 200:1 and 20:1 were tested initially and produced the same results. It was suspected that the changes in signal may have been due to the propane being rapidly absorbed and desorbed from the stationary phase due to the heat pulses of the ²DTPS. However, since the results were the same for all three split ratios, this would be unlikely. In addition, the ²D column used (MXT-WAX polyethylene glycol stationary phase, 1.0 m × 0.25 mm × 0.25 µm) should have very little retention for propane and a thick film stationary phase (0.50 µm or 1.0 µm) was not used. On the other hand, it should be kept in mind that the carrier gas would expand and contract with changes in temperature. What was being observed at the FID may not have been a change in the total flow through the column, but a local change due to the expansion and contraction of the carrier gas within the ²D column that was being observed as rapid

changes in flow at the detector. Under isothermal conditions (constant offset or at oven temperature), the flow at the detector was roughly the same. It was only during rapid changes in temperature that changes in propane signal were observed at the FID. Since the pressure at the head of the ^{2}D column was constant, an increase in temperature should have resulted in a decrease in linear velocity due to the increase in gas viscosity. But instead, an increase in flow was observed at the FID. This was likely due to the expansion of the carrier gas within the ^{2}D column as illustrated in Figure 4-21. Since the expansion of the carrier gas occurred in both directions (towards the inlet and outlet of the ^{2}D column), the analytes could be pushed back towards the inlet of the ^{2}D column if they have not travelled far enough through it. This could explain the longer elution times when the ^{2}D temperature program started before peaks eluted. Overall, the complex nature of the system with rapidly changing conditions makes it difficult to fully determine the real time conditions within the ^{2}D column. Since the ^{2}DTPS did not cause an unacceptable negative impact on the retention time or peak area reproducibility, further investigation was not warranted. This could just be considered a unique characteristic of the system when optimizing the ^{2}D temperature profile.

4.3.2 ^{2}DTPS: Compatibility with the TOFMS

GC×GC-TOFMS separations of diesel were performed without ^{2}D heating (oven temperature), with a constant temperature offset (+27 °C), and with ^{2}D temperature programming (heating: linear temperature ramp from 2.5 s to 4.5 s to +55 °C (at 27.5 °C/s) and held at +55 °C till 5.5 s; cooling: 0 s to 2.5 s, 5.5 s to 6 s) in Figure 4-22. The 21 compounds (tentatively identified based on their mass spectra and RI) selected were evenly distributed across the ^{1}D and ^{2}D to determine the within-day and day-to-day retention time and peak area RSD (%) for the separations with ^{2}D heating (constant temperature offset and ^{2}D temperature programming). For the separation without ^{2}D heating, only 16 of the 21 compounds were found. The missing compounds were lost in the background due to wraparound and coelutions. Two different integration algorithms were used in the determination of retention time and peak area

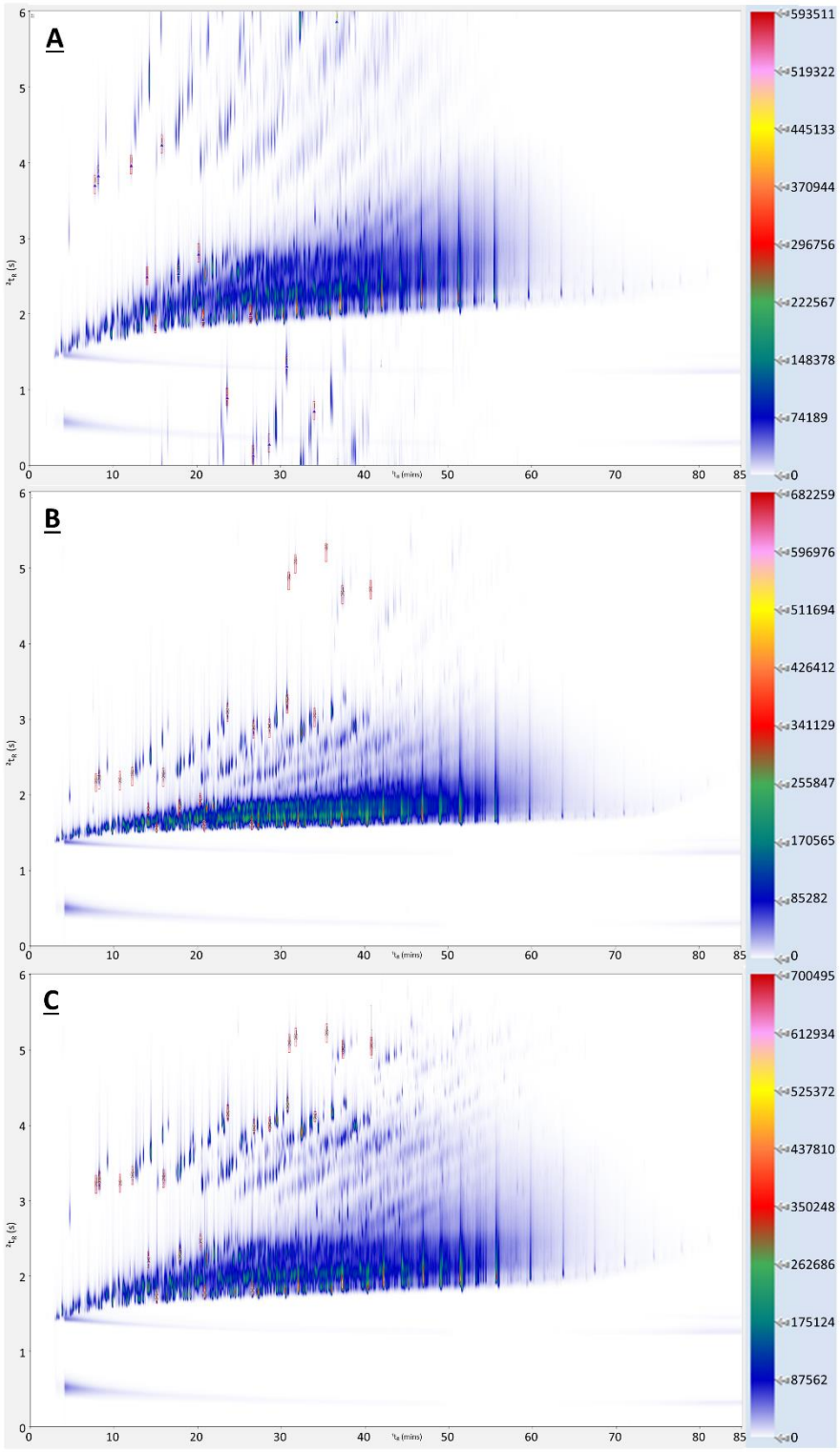

Figure 4-22: GC×GC-TOFMS separation of 10% (v/v) diesel diluted in CS_2, using the SSM and coupled with the Markes BenchTOF-Select. (A) The ²D column was at oven temperature. (B) The ²D column was at a constant positive temperature offset of 27 °C. (C) Additional heating to the ²D column was delayed for 2.5 s, followed by a linear temperature program from 2.5 s to 4.5 s to +55 °C (at 27.5 °C/s) where it was held for 1 s and cooled for the last 0.5 s of the modulation period. The constant positive temperature offset and temperature programming in the ²D were achieved using the ²DTPS. ***X-axis: 0 – 85 min. Y-axis: 0 – 6 s****.*

reproducibility: persistence and deconvolution. With deconvolution, incorrect integration of sub-peaks (only half of a sub-peak integrated) could not be corrected within the software. This led to an inflated RSD for the peak area reproducibility. Split GC×GC peaks were corrected with the exported results by manually summing the peak areas. The retention time (^1t_r, ^2t_r) of the split GC×GC peak with the largest peak area was used for RSD calculation. For the persistence algorithm, split GC×GC peaks were not observed. The smoothing width for the persistence algorithm was 15 for the separations with ^{2}D heating, and 25 for the separation without ^{2}D heating. This parameter was not available for the deconvolution algorithm. Adjusting the smoothing width eliminated the issues with half integrated sub-peaks. RSD values for both integration algorithms are provided for the within-day and day-to-day results.

For the GC×GC-TOFMS separation without ^{2}D heating, peaks from the first run of the day for each day in the 5-day test eluted earlier and broader in the ^{2}D for the first ~8.5 min of the separation. This was highlighted by the dip in the elution time in the ^{2}D for the solvent peak, shown in Figure 4-23A, but was not seen in all subsequent runs on the same day (Figure 4-23B). It was unclear what may have caused this as it was not noticed for the separations with ^{2}D heating. However, this occurred again in section 4.3.5, which used the same GC and SSM, but coupled to the FID. This was investigated in section 4.3.5.1. This issue affected the retention times of the first two peaks, ethylbenzene and *p*-xylene. Air/water checks were performed daily and there were no indications of a leak that could have caused this. Thus, only runs 2 - 5 were used to determine the retention time and peak area RSD for ethylbenzene and *p*-xylene, while the other 14 compounds used all 5 runs. Average values and RSDs for the ^1t_r, ^2t_r, and peak area of each peak for the GC×GC-TOFMS separation without ^{2}D heating, with ^{2}D temperature programming, and a constant temperature offset are found in Table C - 6 to Table C - 11 in Appendix C.

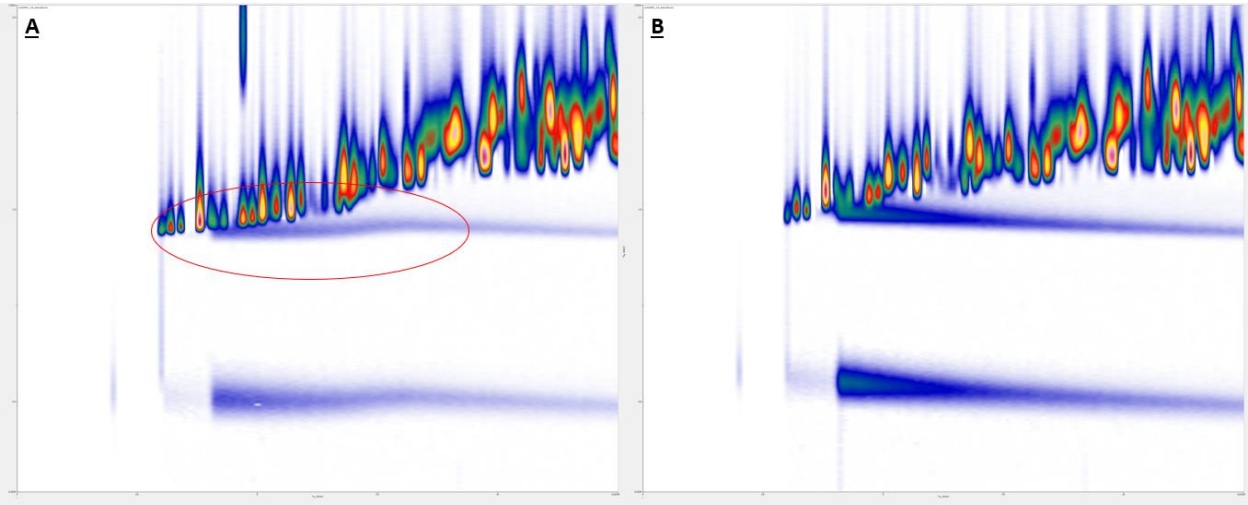

Figure 4-23: GC×GC-TOFMS separation of diesel (10 % v/v in CS_2). A) The first run of the day had a distinct increase in ^{2}D linear velocity, highlighted by the residual solvent peak circled in red. B) Second and all subsequent runs of the day did not have any flow disturbances.

4.3.2.1 Within-Day Reproducibility

Table 4-12: Within-day RSD (n=5) for the GC×GC-TOFMS separation with the ^{2}D column at oven temperature (16 peaks), with ^{2}D temperature programming (21 peaks), and with a ^{2}D constant temperature offset (21 peaks) for the ^1t_r, ^2t_r, and peak area. Deconvolution and persistence algorithms were compared, while the same baseline correction (DBC 2.0 = 0.5 s) was used for all GC×GC chromatograms. The ^{2}D temperature program was a 2.5 s delay in heating, followed by a linear temperature ramp from 2.5 s to 4.5 s to +55 °C (at 27.5 °C/s) , where it was held until 5.5 s, and cooling starting at 5.5 s. The ^{2}D constant temperature offset was +27 °C.

Within-Day (n = 5)						
^1t_r RSD (Deconvolution | Persistence, %)						
	Minimum		Maximum		Mean	
GC Oven Temperature (16 peaks)	0.00	0.00	0.11	0.16	0.02	0.03
^{2}D Temperature Program (21 peaks)	0.00	0.00	0.16	0.14	0.02	0.02
Constant Offset (21 peaks)	0.00	0.00	0.09	0.08	0.01	0.01
^2t_r RSD (%) (Deconvolution | Persistence, %)						
	Minimum		Maximum		Mean	
GC Oven Temperature (16 peaks)	0.05	0.00	0.32	0.23	0.18	0.13
^{2}D Temperature Program (21 peaks)	0.07	0.09	0.37	0.41	0.24	0.26
Constant Offset (21 peaks)	0.48	0.47	1.31	1.28	0.78	0.82
Area RSD (%) (Deconvolution | Persistence, %)						
	Minimum		Maximum		Mean	
GC Oven Temperature (16 peaks)	4.74	3.51	16.79	8.52	7.36	5.86
^{2}D Temperature Program (21 peaks)	0.65	1.30	8.37	5.36	3.40	2.47
Constant Offset (21 peaks)	1.65	1.13	18.76	6.85	6.58	3.73

Within-day reproducibility for the three separations with different ^{2}D temperature profiles is summarized in Table 4-12. A paired Student's t-test was used to compare the RSDs between the three separations. The same 16 peaks were used for the comparison involving the GC×GC-TOFMS separation at oven temperature, while all 21 peaks were used when comparing the ^{2}D temperature programming and constant offset separations. These results are summarized in Table 4-13. For the ^1t_r and ^2t_r RSDs, the values were expectedly very similar whether the deconvolution or persistence algorithm was used. The main difference was the peak area RSDs, where a lower average was found for all three separations when using the persistence algorithm. This reduced the peak area RSDs to be more comparable to the previous GC×GC setup (4.2.1), although they were still elevated. This was likely due to the difference in detectors (FID vs TOFMS) and the use of a highly volatile solvent to dilute the diesel (undiluted diesel vs. 10 % (v/v) diesel in CS_2). The addition of CS_2 could have resulted in additional sample loss due to evaporation, which should be less pronounced with the undiluted diesel that was less volatile. It was unlikely that the difference in GC models (6890N vs 6890A) would affect the reproducibility.

The paired Student's t-test showed that the difference in ^1t_r RSD was not significant. However, the differences in ^2t_r and peak area RSD were significant except for the comparison between the ^{2}D column at oven temperature and with a constant temperature offset for the peak area RSD using the deconvolution algorithm. This was due to the high variance for both separations. The average ^2t_r RSD values for all three separations were acceptable, with the constant offset separation having the largest average of 0.78 % and 0.82 % for the deconvolution and persistence algorithms, respectively. Peak area RSDs were the highest for the GC×GC-TOFMS separation with the ^{2}D column at oven temperature, being 7.36 % and 5.86 % for the deconvolution and persistence algorithms, respectively. This was likely due to wraparound peaks causing coelution and the lower S/N of the peaks. The ^{2}D column heating by the ^{2}DTPS improved the peak area reproducibility and S/N of the peaks. The constant offset had average RSDs of

6.58 % (deconvolution) and 3.73 % (persistence), while ^{2}D temperature programming had RSDs of 3.40 % (deconvolution) and 2.47 % (persistence).

Table 4-13: Paired Student's t-test for the within-day RSD results, comparing the GC×GC-TOFMS separation with the ^{2}D column at oven temperature (16 peaks), with ^{2}D temperature programming (21 peaks), and with a ^{2}D constant temperature offset (21 peaks) for the ^1t_r, ^2t_r, and peak area. The same 16 peaks were used for comparisons involving the ^{2}D column at oven temperature. Results that are insignificant are highlighted in green while significant results are highlighted in orange. The ^{2}D temperature program was a 2.5 s delay in heating, followed by a linear temperature ramp from 2.5 s to 4.5 s to +55 °C (at 27.5 °C/s), where it was held until 5.5 s, and cooling starting at 5.5 s. The ^{2}D constant temperature offset was +27 °C.

Within-Day (n = 5)				
^1t_r Paired Student's t-test (Deconvolution | Persistence)				
	t-value		p-value	
GC Oven Temp. vs. ^{2}D Temp. Prog. (df = 15)	0.036	-0.1	0.97	0.92
GC Oven Temp. vs. Constant Offset (df = 15)	0.094	1.1	0.93	0.31
^{2}D Temp. Prog. vs. Constant Offset (df = 20)	0.23	1.6	0.82	0.13
^2t_r Paired Student's t-test (Deconvolution | Persistence)				
	t-value		p-value	
GC Oven Temp. vs. ^{2}D Temp. Prog. (df = 15)	-3.3	-6.9	5.3×10^{-3}	4.9×10^{-6}
GC Oven Temp. vs. Constant Offset (df = 15)	-15.5	-14.5	1.2×10^{-10}	3.3×10^{-10}
^{2}D Temp. Prog. vs. Constant Offset (df = 20)	-9.4	-9.2	8.5×10^{-9}	1.3×10^{-8}
Area Paired Student's t-test (Deconvolution | Persistence)				
	t-value		p-value	
GC Oven Temp. vs. ^{2}D Temp. Prog. (df = 15)	4.2	7.6	7.8×10^{-4}	1.6×10^{-6}
GC Oven Temp. vs. Constant Offset (df = 15)	0.2	5.4	0.83	6.9×10^{-5}
^{2}D Temp. Prog. vs. Constant Offset (df = 20)	-3.1	-3.5	6.2×10^{-3}	2.4×10^{-3}

4.3.2.2 Day-to-Day Reproducibility

The day-to-day RSDs for the three separations and the comparison using a paired Student's t-test are summarized in Table 4-14 and Table 4-15, respectively. The day-to-day RSD for the ^1t_r and ^2t_r was comparable to the within-day results. The average ^1t_r day-to-day RSD was within 0.01 % of the within-day results. ^2t_r RSD was also similar, with an improvement for the constant offset separation from 0.78 % (deconvolution) and 0.82 % (persistence) to 0.46 % (deconvolution) and 0.44 % (persistence) for the within-day and day-to-day results, respectively. Day-to-day peak area RSD was similar to the within-day

Table 4-14: Day-to-Day RSD (n = 5) for the GC×GC-TOFMS separation with the ²D column at oven temperature (16 peaks), with ²D temperature programming (21 peaks), and with a ²D constant temperature offset (21 peaks) for the ¹t_r, ²t_r, and peak area. Deconvolution and persistence algorithms were compared, while the same baseline correction (DBC 2.0 = 0.5 s) was used for all GC×GC chromatograms. The ²D temperature program was a 2.5 s delay in heating, followed by a linear temperature ramp from 2.5 s to 4.5 s to +55 °C (at 27.5 °C/s), where it was held until 5.5 s, and cooling starting at 5.5 s. The ²D constant temperature offset was +27 °C.

Day-to-Day (n = 5)						
¹t_r RSD (Deconvolution | Persistence, %)						
	Minimum		Maximum		Mean	
GC Oven Temperature (16 peaks)	0.00	0.00	0.09	0.08	0.03	0.03
²D Temperature Program (21 peaks)	0.00	0.00	0.11	0.11	0.02	0.02
Constant Offset (21 peaks)	0.00	0.00	0.12	0.12	0.02	0.01
²t_r RSD (%) (Deconvolution | Persistence, %)						
	Minimum		Maximum		Mean	
GC Oven Temperature (16 peaks)	0.05	0.06	0.28	0.31	0.17	0.15
²D Temperature Program (21 peaks)	0.12	0.13	0.50	0.50	0.31	0.31
Constant Offset (21 peaks)	0.12	0.12	0.75	0.75	0.46	0.44
Area RSD (%) (Deconvolution | Persistence, %)						
	Minimum		Maximum		Mean	
GC Oven Temperature (16 peaks)	3.19	2.36	13.35	9.35	7.10	6.41
²D Temperature Program (21 peaks)	1.12	1.46	7.42	4.99	3.83	3.05
Constant Offset (21 peaks)	3.72	0.87	12.54	6.82	6.25	4.88

results for the deconvolution algorithm (GC Oven Temperature: 7.36 % vs. 7.10 %, ²D Temperature Programming: 3.40 % vs. 3.83 %, Constant Offset: 6.58 % vs. 6.25 %). For the persistence algorithm, it was approximately 0.55 - 1.15 % higher compared to the within-day results (GC Oven Temperature: 5.86 % vs. 6.41 %, ²D Temperature Programming: 2.47 % vs. 3.05 %, Constant Offset: 3.73 % vs. 4.88 %). The paired Student's t-test results were the same as for the within-day results. Differences in the ¹t_r RSDs were not significant, while the ²t_r and peak area RSDs were significant (except for the comparison between the ²D column at oven temperature and constant offset).

Table 4-15: Paired Student's t-test for the day-to-day RSD results, comparing the GC×GC-TOFMS separation with the ^{2}D column at oven temperature (16 peaks), with ^{2}D temperature programming (21 peaks), and with a ^{2}D constant temperature offset (21 peaks) for the ^1t_r, ^2t_r, and peak area. The same 16 peaks were used for comparisons involving the ^{2}D column at oven temperature. Results that are insignificant are highlighted in green while significant results are highlighted in orange. The ^{2}D temperature program was a 2.5 s delay in heating, followed by a linear temperature ramp from 2.5 s to 4.5 s to +55 °C (at 27.5 °C/s), where it was held until 5.5 s, and cooling starting at 5.5 s. The ^{2}D constant temperature offset was +27 °C.

Day-to-Day (n = 5)				
^1t_r Paired Student's t-test (Deconvolution | Persistence)				
	t-value		p-value	
GC Oven Temp. vs. ^{2}D Temp. Prog. (df = 15)	0.33	0.27	0.75	0.79
GC Oven Temp. vs. Constant Offset (df = 15)	0.12	1.0	0.91	0.32
^{2}D Temp. Prog. vs. Constant Offset (df = 20)	-0.41	1.8	0.69	0.09
^2t_r Paired Student's t-test (Deconvolution | Persistence)				
	t-value		p-value	
GC Oven Temp. vs. ^{2}D Temp. Prog. (df = 15)	-8.7	-10.1	3.2×10^{-7}	4.4×10^{-8}
GC Oven Temp. vs. Constant Offset (df = 15)	-4.2	-4.1	7.1×10^{-4}	9.3×10^{-4}
^{2}D Temp. Prog. vs. Constant Offset (df = 20)	-2.7	-2.5	1.4×10^{-2}	2.0×10^{-2}
Area Paired Student's t-test (Deconvolution | Persistence)				
	t-value		p-value	
GC Oven Temp. vs. ^{2}D Temp. Prog. (df = 15)	4.9	9.3	2.0×10^{-4}	1.2×10^{-7}
GC Oven Temp. vs. Constant Offset (df = 15)	1.1	5.4	0.27	7.2×10^{-5}
^{2}D Temp. Prog. vs. Constant Offset (df = 20)	-4.1	-6.6	5.3×10^{-4}	2.1×10^{-6}

4.3.2.3 Average Match Factor and Reverse Match Factor

The coupling of the TOFMS with GC×GC provided qualitative information for the identification of unknown peaks. The unknown mass spectrum was compared to a library of mass spectra, where a match factor (MF) and reverse match factor (RMF) were calculated. The MF is a comparison of the unknown spectrum to the library's spectrum, where it is scored from 0 - 1000. The more mass peaks in the unknown mass spectrum, the more peaks that would need to match with the library spectrum for a high match factor. Therefore, coelution and background noise can reduce the match factor. The RMF is the match factor where peaks in the unknown mass spectrum that are not in the library mass spectrum are ignored [230]. To evaluate the compatibility of the ^{2}DTPS with GC×GC coupled to a mass spectrometer, its effect

on the MF, RMF, and mass spectra was examined. The tentative identification was done on the GC×GC chromatograms integrated using the deconvolution algorithm.

Table 4-16: The average match factor and reverse match factor of each identification for the three separations (GC×GC-TOFMS ^{2}D: oven temperature, constant temperature offset, temperature programming) across all replicate runs. The ^{2}D temperature program was a 2.5 s delay in heating, followed by a linear temperature ramp from 2.5 s to 4.5 s to +55 °C (at 27.5 °C/s), where it was held until 5.5 s, and cooling starting at 5.5 s. The ^{2}D constant temperature offset was +27 °C.

	^{2}D: Oven Temperature		**^{2}D: Constant Offset**		**^{2}D: Temperature Programming**	
Compound	MF	RMF	MF	RMF	MF	RMF
Ethylbenzene	925	955	932	958	937	960
***p*-Xylene**	920	925	923	942	934	947
Benzene, (1-methylethyl)-	925	938	932	959	938	961
Benzene, propyl-	924	950	938	982	945	982
1H-Indene, octahydro-, cis-	850	854	865	873	882	887
Decane	759	773	882	913	898	922
***p*-Cymene**	908	918	919	948	921	945
Naphthalene, decahydro-, trans-	859	866	912	912	926	926
Naphthalene, decahydro-, cis-	851	856	892	897	908	911
Undecane	760	778	850	882	888	914
Naphthalene, 1,2,3,4-tetrahydro-	930	938	934	946	930	943
Dodecane	754	769	845	874	861	884
Naphthalene, 1,2,3,4-tetrahydro-2-methyl-	890	892	902	906	898	902
1H-Indene, 2,3-dihydro-4,7-dimethyl-	898	913	889	932	892	928
Naphthalene, 1,2,3,4-tetrahydro-6-methyl-	890	891	897	901	894	898
Naphthalene, 1-methyl-			907	907	919	922
Naphthalene, 2-methyl-			911	917	925	934
Naphthalene, 1,2,3,4-tetrahydro-1,5-dimethyl-	886	886	876	876	871	872
Biphenyl			952	952	953	953
Naphthalene, 1,7-dimethyl-			940	942	938	947
1,1'-Biphenyl, 4-methyl-			916	918	943	945
Average	871	881	905	921	914	928

The average MF and RMF values for the three separations using all replicate runs are shown in Table 4-16. A paired Student's t-test was performed to compare the within-day results, day-to-day results, and the overall results (all replicate runs), and is found in Table C - 12 of Appendix C. It was found that the

differences in the MF and RMF between the three separations were significant in all situations. Comparing the three separations, an overall improvement in the MF and RMF was observed in the following order: ^{2}D temperature programming > Constant Offset > ^{2}D: Oven temperature. This improvement was likely due to the elimination of wraparound peaks when ^{2}D heating was applied, reducing the coelutions and improving resolution, generating a cleaner mass spectrum for identification.

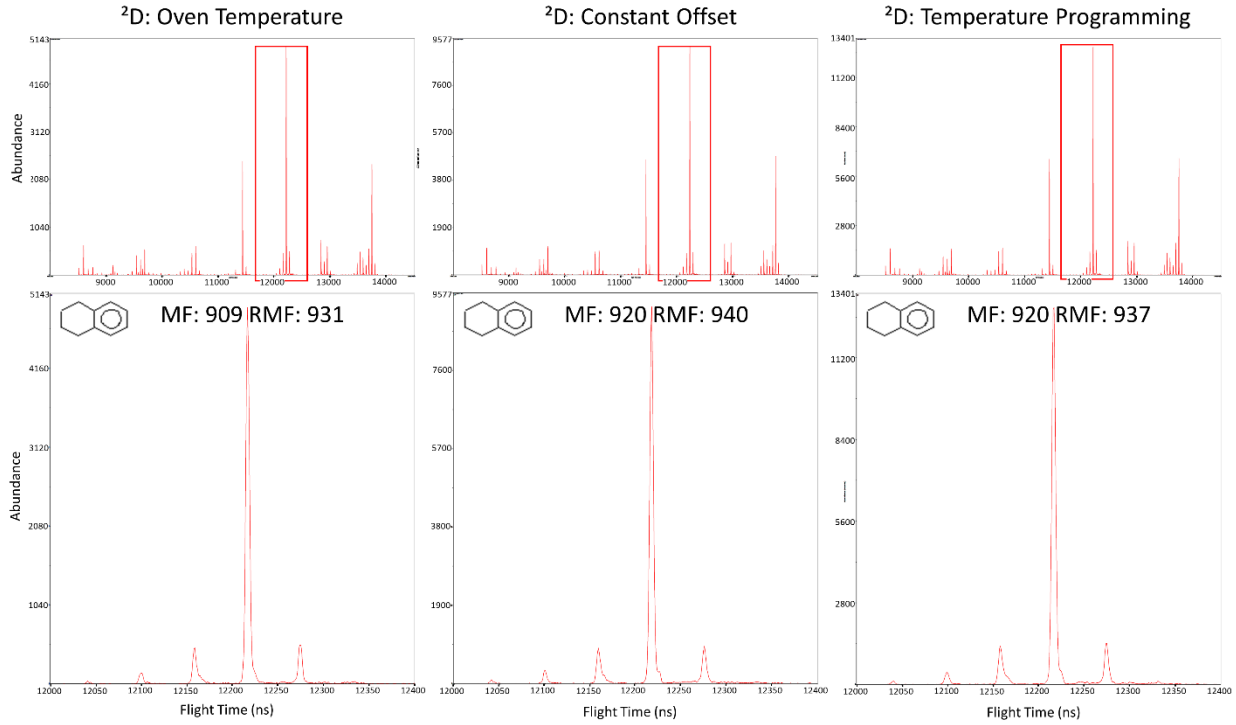

Figure 4-24: Comparing the mass spectra for 1,2,3,4-tetrahydronaphthalene for the three GC×GC-TOFMS separations (^{2}D: oven temperature, constant offset, temperature programming). The ^{2}D temperature program was a 2.5 s delay in heating, followed by a linear temperature ramp from 2.5 s to 4.5 s to +55 °C (at 27.5 °C/s), where it was held until 5.5 s, and cooling starting at 5.5 s. The ^{2}D constant temperature offset was +27 °C.

To examine if the PWM heating from the ^{2}DTPS influenced the mass spectra, the mass spectrum for 1,2,3,4-tetrahydronaphthalene was examined more closely in Figure 4-24. This peak was chosen since there was no indication of coelution in all three separations. This compound was a wraparound peak in the GC×GC-TOFMS separation, so it was more strongly retained on the ^{2}D column and would be more sensitive to temperature changes. When comparing the mass spectra, the peak shape was roughly identical between the three separations, with the main difference being the abundance (Oven

Temperature: 5143, Constant Offset: 9577, ^{2}D Temperature Programming: 13401). Overall, the ^{2}DTPS did not have a negative impact on performance of the TOFMS but demonstrated an improvement in the chromatography to generate a cleaner mass spectrum for a more confident identification.

4.3.3 ^{2}DTPS: RTC

The ^{2}DTPS was tested following the addition of the RTC and update of the code to make use of the 32 kHz clock signal. The clock frequency was calibrated following the addition of the RTC to ensure it was synchronized to the modulator timing. Using the discharge box signal as a reference, the clock frequency set in the Arduino sketch was adjusted until the ^{2}DTPS's modulation period was synchronized to the discharge box. The clock frequency used was 32761 Hz in the code. This value was outside the specifications of the DS3231, which had a maximum frequency stability of ±5 ppm (± 0.16384 Hz) with aging in the first 10 years. This deviation from the expected clock frequency of 32768 Hz could be due to inefficient coding, where some time was lost as the program switched between different segments of the temperature program and checked for new serial data to update variables. However, as long the as the clock frequency remained stable, it was sufficient for the system if the RTC was calibrated following installation onto the ^{2}DTPS.

The reproducibility testing of the updated ^{2}DTPS utilized the same GC×GC-TOFMS setup as in section 4.2.2. For the testing, the sample of perfume that was also used previously in section 4.2.1 was diluted as before to 10 % v/v due to the sensitivity of the TOFMS. The separation of the perfume sample is shown in Figure C - 7 of Appendix C, and the within-day and day-to-day RSD (%) is presented in Table 4-17. Comparing the within-day reproducibility of the $^{1}t_{r}$, $^{2}t_{r}$, and peak area to the results from section 4.3.2.1, there was an increase in the average RSD for all three values following the addition of the RTC ($^{1}t_{r}$: 0.02 % → 0.04 %, $^{2}t_{r}$: 0.26 % → 0.35 %, Area: 2.47 % → 4.44 %). An F-test to determine the equality of variances followed by the corresponding t-test was performed for each comparison. It was found that

that the differences were significant for both the ^2t_r and peak area, but the differences were insignificant for the ^1t_r. The same result was found for the day-to-day RSD, where it increased for the retention time and peak area (^1t_r: 0.04 % → 0.05 %, ^2t_r: 0.42 % → 0.52 %, Area: 6.19 % → 10.35 %) and only the difference between the ^1t_r was insignificant. All F-test and t-test results are found in Table C - 14 of Appendix C.

Table 4-17: Within-day and day-to-day RSD (%) for the GC×GC-TOFMS separation of perfume using the SSM and ^{2}DTPS after the addition of the RTC. The ^{2}D temperature program was a 2 s delay in heating, followed by a linear temperature ramp from 2 s to 3.5 s to +50 °C, where it was held until 5 s, and cooling starting at 5 s.

	Within-Day RSD (%)				Day-to-Day RSD (%)			
Peak #	^1t_r	^2t_r	Area	Area %	^1t_r	^2t_r	Area	Area %
1	0.09	0.49	1.16	4.32	0.27	0.46	9.31	1.60
2	0.00	0.55	1.95	3.70	0.00	0.45	6.72	3.51
3	0.04	0.46	2.70	6.52	0.07	0.46	6.15	4.80
4	0.00	0.34	2.03	3.88	0.00	0.42	7.24	3.18
5	0.19	0.20	3.43	1.93	0.19	0.56	7.76	2.59
6	0.05	0.36	3.49	2.39	0.05	0.44	10.07	0.86
7	0.12	0.26	2.99	2.55	0.12	0.53	7.99	2.38
8	0.04	0.38	4.39	1.74	0.03	0.58	11.31	1.59
9	0.00	0.35	5.90	2.11	0.00	0.97	10.64	1.80
10	0.00	0.39	2.83	2.40	0.00	0.38	8.06	2.17
11	0.00	0.47	5.41	1.81	0.00	0.59	11.87	1.61
12	0.03	0.17	6.09	2.21	0.03	0.45	12.43	2.09
13	0.00	0.00	5.14	2.52	0.05	0.46	13.10	3.15
14	0.01	0.42	7.99	3.35	0.01	0.48	15.73	4.92
15	0.01	0.25	7.05	2.60	0.01	0.63	13.47	3.31
16	0.01	0.56	8.46	3.98	0.01	0.52	13.77	3.19
Average	0.04	0.35	4.44	3.00	0.05	0.52	10.35	2.67

A comparison of the average peak areas of each peak across the five days showed a trend in the vial-to-vial concentrations. Furthermore, a paired Student's t-test ($\alpha = 0.05$) comparing the within-day to the day-to-day results of the area % RSD showed that the differences were insignificant, $t(15) = 1.3$, $p = 0.22$. This showed that the absolute peak area differences between days were more likely due to differences in concentration between the sample vials used on each day. It was unlikely that the addition of the RTC would have any influence on the overall system's peak area reproducibility and was more likely to have a

direct impact on the ^2t_r reproducibility. Expecting that the addition of the RTC would influence the ^2t_r reproducibility, the GC×GC separations were checked daily. The within-day runs and previous day's runs were compared to ensure the ^{2}DTPS was performing as expected with the RTC update by stacking the GC×GC chromatograms and zooming in to different regions to visually inspect the reproducibility (Figure C - 8 of Appendix C). However, since the colour gradient, which indicates the peak height, was scaled to each individual chromatogram, it was not noticed that there were peak area reproducibility issues. Although the peak area reproducibility results were unsatisfactory, further testing of the ^{2}DTPS in the subsequent sections will demonstrate that reproducibility was not an issue and that these results were an outlier. The poorer reproducibility with this GC×GC-TOFMS setup with the SSM could have been due to poor sample preparation or the autosampler syringe. In addition, the higher split ratios used with the GC×GC-TOFMS setup in 4.2.3 and 4.2.4 could have also contributed to the increased RSD.

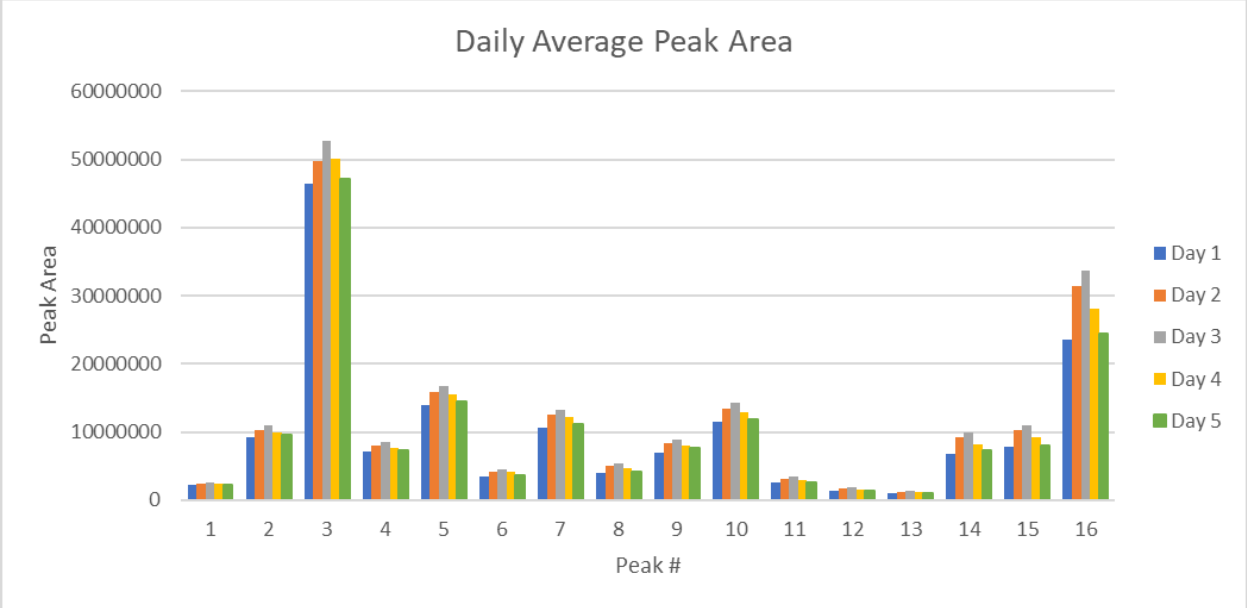

Figure 4-25: Average daily peak area over 5 days for the 16 peaks from the perfume sample used in the reproducibility test of the ^{2}DTPS with the addition of the RTC. The ^{2}D temperature program was a 2 s delay in heating, followed by a linear temperature ramp from 2 s to 3.5 s to +50 °C (at 33.3 °C/s), where it was held until 5 s, and cooling starting at 5 s.

4.3.4 ^{2}DTPS: Compatibility with a Flow Modulator

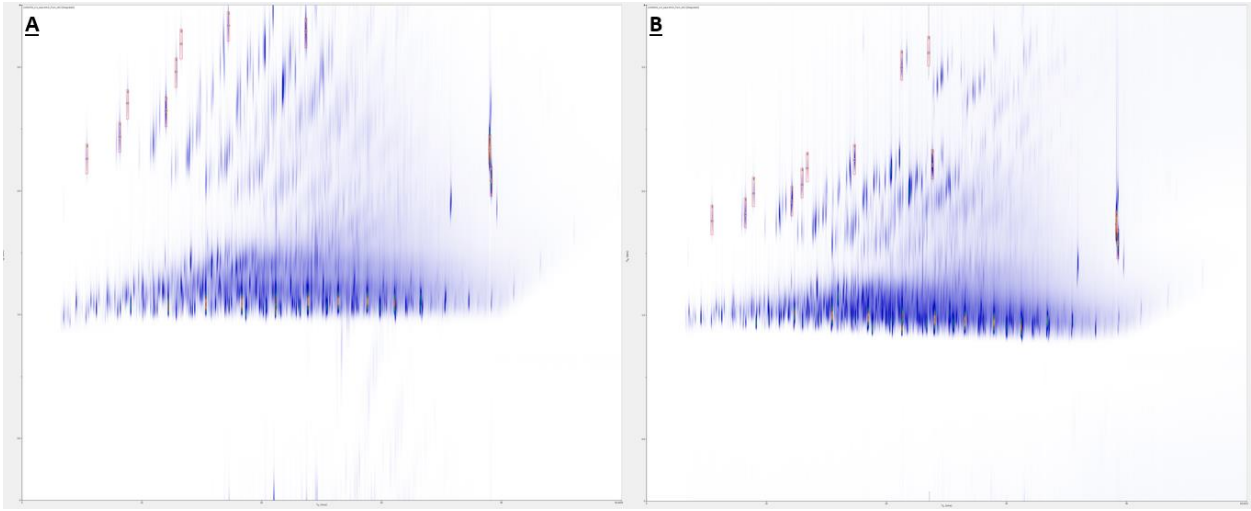

Figure 4-26: The FID chromatogram of the GC×GC separation with the SepSolve Insight flow modulator. 10 peaks were integrated for reproducibility comparison for the GC×GC separation without ^{2}D temperature programming (A), whereas 12 peaks were integrated for the reproducibility comparison for the separation with ^{2}D temperature programming (B). The ^{2}D temperature program was a 1.5 s delay in heating, followed by a linear temperature ramp from 1.5 s to 2.5 s to +50 °C (at 50 °C/s), where it was held until 3.5 s, and cooling starting at 3.5 s. ***X-axis: 0 – 50 min. Y-axis: 0 – 4 s****.*

Due to the operational principle of the differential flow modulator, the high ^{2}D flow rate (18.09 mL/min) had to be split prior to the MS due to its flow limitations. Splitting the flow to the FID and MS provides the benefit of the linear range of an FID and the qualitative aspects of identification from the MS in a single separation. Both the MS and FID data were processed to check for reproducibility of the GC×GC-FID/TOFMS system with and without ^{2}D temperature programming. The FID chromatograms are shown in Figure 4-26. Baseline correction (FID Data: Top Hat = 0.4 s, MS Data: DBC 2.0 = 0.4 s) was performed on all chromatograms and integration settings were identical for all data sets (Persistence Algorithm: smoothing width = 12, polynomial order = 3, persistence cut-off = 0.5). All FID chromatograms were cropped from 3.25 min to remove the solvent peak which obscured the diesel separation due to the difference in relative intensities. Peak merging was left as default for all data sets. 10 peaks were selected in the GC×GC separation without ^{2}D temperature programming. To simplify the processing, the 10 peaks selected were well separated in both the ^{1}D and ^{2}D to reduce issues with coelution where sub-peaks could be improperly integrated and peak merging might become inconsistent. The same 10 peaks were selected

in the GC×GC separation with ^{2}D temperature programming, with an additional two peaks (2-ring aromatics) which could not be seen in the separation without ^{2}D temperature programming. The two additional peaks were well retained on the ^{2}D column and would be more influenced by inconsistent ^{2}D temperature programming.

4.3.4.1 Reproducibility

Table 4-18: Within-day reproducibility (^1t_r, ^2t_r, area, and area %) of the GC×GC-FID/TOFMS system with the SepSolve Insight flow modulator using a diesel sample (10% v/v) diluted in CS_2 for the FID data. 10 peaks were used to estimate reproducibility with the ^{2}D column at oven temperature and 12 peaks with ^{2}D temperature programming. Peaks were tentatively identified based on the mass spectra and RI. The ^{2}D temperature program was a 1.5 s delay in heating, followed by a linear temperature ramp from 1.5 s to 2.5 s to +50 °C (at 50 °C/s) , where it was held until 3.5 s, and cooling starting at 3.5 s.

Within-Day (n = 5) RSD (%) – FID Data								
	Oven Temperature				^{2}D Temperature Programming			
Compound	^1t_r	^2t_r	Area	Area %	^1t_r	^2t_r	Area	Area %
Toluene	0.01	0.11	2.18	2.05	0.05	0.26	1.20	1.15
p-Xylene	0.08	0.14	1.92	1.94	0.03	0.18	1.10	1.12
o-Xylene	0.00	0.18	1.48	1.23	0.04	0.24	1.45	1.04
1,2,4-Trimethylbenzene	0.00	0.05	1.06	1.04	0.09	0.52	1.51	1.85
1,2,3-Trimethylbenzene	0.00	0.04	2.41	2.08	0.02	0.18	1.71	1.46
Indane	0.05	0.08	1.61	0.99	0.10	0.16	1.02	1.26
1,2,3,4-Tetrahydronaphthalene	0.07	0.04	1.25	1.39	0.01	0.19	1.77	1.54
1,2,3,4-Tetrahydro-5,6-dimethylnaphthalene	0.00	0.16	1.26	1.63	0.00	0.19	1.92	1.76
Methyl linoleate	0.03	0.14	1.79	1.36	0.02	0.41	3.34	2.06
Methyl oleate	0.03	0.14	0.79	0.99	0.02	0.19	2.88	3.05
2-Methylnaphthalene	-	-	-	-	0.01	0.09	1.94	1.73
Biphenyl	-	-	-	-	0.01	0.25	1.49	0.61
Average	0.03	0.11	1.58	1.47	0.03	0.24	1.78	1.55

Within-day RSDs (%, n = 5) for day three of the five-day reproducibility test for the GC×GC-FID/TOFMS flow modulator system are shown in Table 4-18 and Table 4-19 for the FID and MS data, respectively. A paired Student's *t*-test (Table 4-20) comparing the FID and MS data for the two ^{2}D separation conditions (oven temperature and temperature programming) showed that the difference between the two detectors were not significant for the ^1t_r, ^2t_r, and peak area. This was corroborated with the identical paired Student's t-test results when comparing the two separations using the FID and MS data. When

Table 4-19: Within-day reproducibility (^1t_r, ^2t_r, area, and area %) of the GC×GC-FID/TOFMS system with the SepSolve Insight flow modulator using a diesel sample (10% v/v) diluted in CS_2 for the MS data. 10 peaks were used to estimate reproducibility with the ^{2}D column at oven temperature and 12 peaks with ^{2}D temperature programming. Peaks were tentatively identified based on the mass spectra and RI. The ^{2}D temperature program was a 1.5 s delay in heating, followed by a linear temperature ramp from 1.5 s to 2.5 s to +50 °C (at 50 °C/s) , where it was held until 3.5 s, and cooling starting at 3.5 s.

Within-Day (n = 5) RSD (%) – MS Data								
	Oven Temperature				^{2}D Temperature Programming			
Compound	^1t_r	^2t_r	Area	Area %	^1t_r	^2t_r	Area	Area %
Toluene	0.00	0.04	1.99	0.97	0.05	0.10	1.13	0.74
p-Xylene	0.08	0.14	2.54	1.37	0.05	0.34	1.03	0.87
o-Xylene	0.00	0.23	1.62	1.11	0.04	0.11	1.73	0.93
1,2,4-Trimethylbenzene	0.00	0.12	1.41	1.25	0.10	0.56	1.50	0.35
1,2,3-Trimethylbenzene	0.00	0.06	1.04	0.34	0.04	0.48	1.02	0.43
Indane	0.00	0.15	2.86	1.92	0.11	0.28	1.13	0.64
1,2,3,4-Tetrahydronaphthalene	0.04	0.08	1.68	0.75	0.00	0.16	2.10	1.15
1,2,3,4-Tetrahydro-5,6-dimethylnaphthalene	0.00	0.13	1.16	0.35	0.00	0.32	1.65	0.75
Methyl linoleate	0.02	0.02	1.11	1.32	0.02	0.85	3.91	2.98
Methyl oleate	0.03	0.04	1.13	1.72	0.02	0.63	2.07	1.95
2-Methylnaphthalene	-	-	-	-	0.01	0.13	1.18	0.75
Biphenyl	-	-	-	-	0.04	0.32	2.11	2.04
Average	0.02	0.10	1.66	1.11	0.04	0.36	1.71	1.13

comparing the GC×GC separations (10 peaks), ^{2}D temperature programming did result in an increase in the average ^2t_r RSD, from 0.11 % to 0.25 % for the FID data and from 0.10 % to 0.38 % for the MS data. This was shown to be significant according to the paired Student's t-test. Although this increase was significant, a 0.38 % RSD for ^2t_r reproducibility was still acceptable and would not affect the integration when processing chromatograms based on retention time windows.

Expanding beyond just the third day for the within-day data, the findings in the comparison between the two separations were less conclusive. Shown in Table 4-21 were the average within-day RSD for both separations and detectors and the paired Student's t-test results. The differences in ^2t_r RSD between the two separations were significant for each day for the FID data, while for the MS data, they were not significant for four of the five days. For the peak area reproducibility, the differences were significant for

three of the five days for the FID, and significant for four of the five days for the MS data. Overall, although the differences were significant in some cases, the RSDs were acceptable for both separations.

Table 4-20: Paired Student's t-test comparison of the within-day (n = 5) ^{2}D separations at oven temperature and ^{2}D temperature programming for the GC×GC-FID/TOFMS flow modulator setup. The FID data was compared to the MS data for each GC×GC separation. The two GC×GC separations were compared for both the FID and MS data. This was completed for the ^1t_r, ^2t_r, and peak area. The ^{2}D temperature program was a 1.5 s delay in heating, followed by a linear temperature ramp from 1.5 s to 2.5 s to +50 °C (at 50 °C/s) , where it was held until 3.5 s, and cooling starting at 3.5 s.

Within-Day – Paired Student's t-test (α = 0.05)							
		^1t_r		^2t_r		Area	
		t-stat	*p*-value	*t*-stat	*p*-value	*t*-stat	*p*-value
FID vs. MS	Oven Temp. (*df* = 9)	1.7	0.12	0.23	0.82	0.34	0.74
	^{2}D Temp. Prog. (*df* = 11)	1.6	0.13	2.1	0.058	0.45	0.66
Oven Temperature vs. ^{2}D Temperature Programming	FID (*df* = 9)	0.72	0.49	3.4	8.4×10^{-3}	0.65	0.53
	MS (*df* = 9)	1.5	0.16	3.1	1.2×10^{-2}	0.17	0.87

Table 4-21: Comparison of the within-day ^{2}D separation at oven temperature and with ^{2}D temperature programming for the GC×GC-FID/TOFMS flow modulator setup. Within-day (n = 5) average values for the 10 peaks were compared between each separation/detector for each day. Paired Student's t-test was performed to compare the within day results. The ^{2}D temperature program was a 1.5 s delay in heating, followed by a linear temperature ramp from 1.5 s to 2.5 s to +50 °C (at 50 °C/s) , where it was held until 3.5 s, and cooling starting at 3.5 s.

Average Within-Day RSD (%, n = 5)										
	Day 1		Day 2		Day 3		Day 4		Day 5	
	Oven	^{2}DTPS	Oven	^{2}DTPS	Oven	^{2}DTPS	Oven	^{2}DTPS	Oven	^{2}DTPS
^2t_r - FID	0.11	0.22	0.12	0.28	0.11	0.25	0.13	0.27	0.14	0.32
^2t_r - MS	0.13	0.24	0.25	0.26	0.10	0.38	0.27	0.24	0.19	0.15
Area - FID	1.58	3.54	1.83	3.27	1.58	1.79	1.25	3.03	2.47	2.65
Area - MS	2.04	4.24	2.21	4.22	1.66	1.73	2.20	3.01	2.41	3.19
Oven Temperature vs. ^{2}D Temperature Programming: Within-Day (α = 0.05, df = 9)										
	Day 1		Day 2		Day 3		Day 4		Day 5	
	t-stat	p-value	t-stat	p-value	t-stat	p-value	t-stat	p-value	t-stat	p-value
^2t_r - FID	3.62	6.0×10^{-3}	5.95	2.2×10^{-4}	3.36	8.0×10^{-3}	3.07	1.3×10^{-2}	3.34	9.0×10^{-3}
^2t_r - MS	2.23	0.053	0.17	0.87	3.14	1.2×10^{-2}	0.49	0.64	1.32	0.22
Area - FID	6.98	6.4×10^{-5}	5	7.4×10^{-4}	0.65	0.53	6.44	1.2×10^{-4}	0.6	0.56
Area - MS	5.4	4.6×10^{-4}	4.7	1.1×10^{-3}	0.2	0.87	5.2	5.9×10^{-4}	2.3	4.4×10^{-2}

Table 4-22: Day-to-Day reproducibility using a diesel sample (10% v/v) diluted in CS_2 for the GC×GC-FID/TOFMS system with the SepSolve Insight flow modulator. 10 peaks were used to estimate reproducibility without ^{2}D temperature programming and 12 peaks with ^{2}D temperature programming. Peaks were tentatively identified based on the mass spectra and RI from both separation conditions. The ^{2}D temperature program was a 1.5 s delay in heating, followed by a linear temperature ramp from 1.5 s to 2.5 s to +50 °C (at 50 °C/s), where it was held until 3.5 s, and cooling starting at 3.5 s.

Day-to-Day (n = 5) RSD (%) – FID Data								
	Oven Temperature				^{2}D Temperature Programming			
Compound	^1t_r	^2t_r	Area	Area %	^1t_r	^2t_r	Area	Area %
Toluene	0.15	0.25	2.29	1.68	0.04	0.34	2.82	1.30
p-Xylene	0.11	0.31	1.72	1.13	0.04	0.37	3.67	2.03
o-Xylene	0.02	0.19	1.63	0.96	0.04	0.37	3.50	1.78
1,2,4-Trimethylbenzene	0.00	0.16	1.79	1.13	0.10	0.79	4.23	2.83
1,2,3-Trimethylbenzene	0.01	0.20	2.50	2.48	0.02	0.48	1.67	1.15
Indane	0.05	0.15	0.81	0.73	0.01	0.28	3.08	2.09
1,2,3,4-Tetrahydronaphthalene	0.04	0.16	3.92	3.24	0.01	0.29	3.10	1.30
1,2,3,4-Tetrahydro-5,6-dimethylnaphthalene	0.00	0.32	2.64	1.95	0.00	0.25	4.70	2.82
Methyl linoleate	0.02	0.32	0.70	1.32	0.02	0.47	3.17	2.42
Methyl oleate	0.04	0.17	0.98	1.01	0.02	0.40	3.09	2.99
2-Methylnaphthalene	-	-	-	-	0.02	0.47	3.11	1.14
Biphenyl	-	-	-	-	0.01	0.26	2.41	0.82
Average	0.04	0.22	1.90	1.56	0.03	0.40	3.21	1.89
Day-to-Day (n = 5) RSD (%) – MS Data								
	Oven Temperature				^{2}D Temperature Programming			
Compound	^1t_r	^2t_r	Area	Area %	^1t_r	^2t_r	Area	Area %
Toluene	0.22	0.41	2.51	1.66	0.04	0.32	3.16	0.93
p-Xylene	0.10	0.38	2.04	0.74	0.04	0.29	3.03	0.68
o-Xylene	0.03	0.18	2.27	0.95	0.04	0.34	3.61	0.59
1,2,4-Trimethylbenzene	0.13	0.31	1.70	0.62	0.10	0.91	3.98	0.96
1,2,3-Trimethylbenzene	0.10	0.20	2.44	2.87	0.02	0.41	4.19	1.20
Indane	0.04	0.19	3.01	1.50	0.00	0.31	3.35	1.17
1,2,3,4-Tetrahydronaphthalene	0.05	0.20	1.22	0.75	0.01	0.29	3.96	1.29
1,2,3,4-Tetrahydro-5,6-dimethylnaphthalene	0.00	0.30	2.41	0.98	0.05	0.27	3.63	1.06
Methyl linoleate	0.02	0.30	1.04	1.18	0.02	0.73	3.28	3.92
Methyl oleate	0.03	0.12	1.26	1.71	0.00	0.44	2.11	3.89
2-Methylnaphthalene	-	-	-	-	0.03	0.37	3.07	0.41
Biphenyl	-	-	-	-	0.05	0.38	3.07	1.37
Average	0.07	0.26	1.99	1.30	0.03	0.42	3.37	1.46

Table 4-23: Paired Student's t-test comparison of the day-to-day (n = 5) ^{2}D separation at oven temperature and with ^{2}D temperature programming for the GC×GC-FID/TOFMS flow modulator setup. The FID data were compared to the MS data for each GC×GC separation. The two GC×GC separations were compared for both the FID and MS data. This was completed for the ^1t_r, ^2t_r, and peak area. The ^{2}D temperature program was a 1.5 s delay in heating, followed by a linear temperature ramp from 1.5 s to 2.5 s to +50 °C (at 50 °C/s), where it was held until 3.5 s, and cooling starting at 3.5 s.

Day-to-Day – Paired Student's t-test (α = 0.05)							
		^1t_r		^2t_r		Area	
		t-stat	*p*-value	*t*-stat	*p*-value	*t*-stat	*p*-value
FID vs. MS	Oven Temp. (df = 9)	1.8	0.11	1.6	0.14	0.2	0.81
	^{2}D Temp. Prog. (df = 11)	0.77	0.46	0.83	0.43	0.57	0.58
Oven Temperature vs. ^{2}D Temperature Programming	FID (df = 9)	0.75	0.47	3.1	1.2×10^{-2}	3.4	7.5×10^{-3}
	MS (df = 9)	2.0	0.072	2.4	4.0×10^{-2}	5.8	2.7×10^{-4}

Day-to-day reproducibility values of the ^{2}D separations at oven temperature and with ^{2}D temperature programming for the FID and MS data are shown in Table 4-22. The addition of ^{2}D temperature programming increased the ^2t_r RSD from 0.22 % to 0.40 % for the FID and 0.26 % to 0.42 % for the MS. The peak area RSDs also increased from 1.90 % to 3.21 % for the FID and 1.99 % to 3.37 % for the MS data. The paired Student's t-test comparison between the two separations showed that these differences were significant (Table 4-23). Compared to the within-day results, the day-to-day RSDs were higher for the ^1t_r, ^2t_r, and peak area, which was expected.

Table 4-24: Paired Student's t-test comparison between of the ^{2}D separation at oven temperature and with ^{2}D temperature programming for the GC×GC-FID/TOFMS flow modulator setup for the area % of 10 peaks. The comparison was made for both within-day results and day-to-day results for the FID and MS. The ^{2}D temperature program was a 1.5 s delay in heating, followed by a linear temperature ramp from 1.5 s to 2.5 s to +50 °C (at 50 °C/s) , where it was held until 3.5 s, and cooling starting at 3.5 s.

Area % (α = 0.05, *df* = 9)							
Within-Day - FID		Day-to-Day - FID		Within-Day - MS		Day-to-Day - MS	
t-stat	p-value	t-stat	p-value	t-stat	p-value	t-stat	p-value
0.56	0.59	1.23	0.25	0.12	0.91	0.66	0.53

The RSDs for the area % were also included in Table 4-19 and Table 4-22. The area % is the percent area of the peak compared to the total integrated area (total area of the 10 or 12 peaks). Since the relative

response factors of the FID for the hydrocarbons chosen were similar for most compounds, the area % value may be a better representation of the peak area reproducibility [231, 232]. The area % should remain constant, even with run-to-run differences in injection volume or concentration changes due to evaporation. This was reflected in the average area % RSD being consistently lower than the average peak area RSDs. A paired Student's t-test comparison of the area % reproducibility between the two separations showed that the differences were not significant for the within-day and day-to-day results, for both the FID and MS data (Table 4-24).

4.3.5 ^{2}DTPS: Remote Port, Multiple ^{2}D Temperature Program, Sequence

Reproducibility of the ^{2}DTPS (Ver. 2.0) was tested using a GC×GC-FID system with the SSM. A diesel sample diluted in CS_2 (10 % v/v) was used. Although the sample did not need to be diluted with the linear range of the FID (>10^7), it was done to provide additional results for a comparison with the results from section 4.3.2 - 4.3.4 which used diluted samples [233]. With the new physical and software updates, reproducibility testing was much easier. The ^{2}D temperature programming method was saved, and a sequence was run daily as with the SSM and Agilent GC. Six runs were done each day in case the retention time/peak width issue detailed in section 4.3.2 occurred. This was indeed observed again for the separation without ^{2}D heating, where the ^{2}DTPS's PSU was switched OFF. This was further investigated in section 4.3.5.1 following the reproducibility testing. The first run was disregarded and only the subsequent 5 runs were used for the reproducibility. Five days of runs were completed for the testing. Using the same GC×GC method, the reproducibility test was repeated with the ^{2}DTPS power supply switched off to provide this GC×GC setup's reproducibility data for comparison. 10 peaks were integrated for the GC×GC separation without ^{2}D temperature programming, while additional 4 peaks (2-ring aromatics) were included for a total of 14 peaks for the separation with the ^{2}DTPS (Table 4-25). Reproducibility was compared using a paired Student's t-test for the 10 peaks.

Table 4-25: Within-day and day-to-day reproducibility using a diesel sample (10% v/v) diluted in CS_2 for the GC×GC-SSM-FID and GC×GC-SSM-²DTPS-FID systems. 10 peaks were used to estimate the reproducibility without ²D temperature programming (GC×GC-SSM-FID) and 14 peaks with ²D temperature programming (GC×GC-SSM-²DTPS-FID). The ²D temperature program was a 3 s delay in heating, followed by a linear temperature ramp from 3 s to 5 s to +60 °C (at 30 °C/s) , where it was held until 5.5 s, and cooling starting at 5.5 s.

	Within-Day (n = 5)						**Day-to-Day (n = 5)**					
	GC×GC-SSM			²DTPS			GC×GC-SSM			²DTPS		
Peak #	^1t_r	^2t_r (s)	Area	^1t_r	^2t_r (s)	Area	^1t_r	^2t_r (s)	Area	^1t_r	^2t_r (s)	Area
1	0.06	0.19	3.33	0.00	0.27	1.89	0.08	0.31	2.90	0.27	0.72	2.86
2	0.06	0.19	4.34	0.00	0.26	2.49	0.05	0.31	2.73	0.00	0.29	1.66
3	0.01	0.13	3.84	0.14	0.30	2.65	0.02	0.27	3.07	0.14	0.45	1.54
4	0.01	0.24	3.93	0.08	0.35	2.69	0.01	0.24	3.56	0.08	0.44	1.44
5	0.01	0.10	3.64	0.00	0.18	2.91	0.01	0.23	3.47	0.00	0.23	1.38
6	0.00	0.19	3.72	0.00	0.38	2.76	0.01	0.25	3.01	0.01	0.47	1.54
7	0.01	0.14	3.17	0.00	0.19	2.63	0.01	0.25	3.24	0.08	0.29	1.67
8	0.01	0.17	3.32	0.00	0.21	2.83	0.17	0.20	2.94	0.00	0.42	2.13
9	0.01	0.13	3.14	0.03	0.38	2.39	0.02	0.28	2.97	0.02	0.52	2.05
10	0.03	0.11	2.78	0.00	0.35	2.64	0.03	0.38	1.53	0.00	0.38	2.93
11	-	-	-	0.00	0.15	2.91	-	-	-	0.01	0.52	1.66
12	-	-	-	0.00	0.21	2.61	-	-	-	0.00	0.55	1.82
13	-	-	-	0.03	0.45	2.48	-	-	-	0.04	0.28	1.70
14	-	-	-	0.00	0.39	2.64	-	-	-	0.00	0.50	1.46
Average	0.02	0.16	3.52	0.02	0.29	2.61	0.04	0.27	2.94	0.05	0.43	1.85

Similar to previous results, the use of the ²DTPS for ²D temperature programming resulted in an increase in the average ^2t_r RSD (%) for both the within-day and day-to-day results. In both cases (within-day: 0.29 %, day-to-day: 0.43 %), the ^2t_r RSD (%) was still acceptable and should not affect the identification of peaks for systems relying on retention time for identification. Unlike before, average peak area RSD (%) decreased with the use of ²D temperature programming for both the within-day (3.52 % → 2.61 %) and day-to-day (2.94 % → 1.85 %) results. The paired Student's t-test comparison between the ²D temperature programming and with the ²D at oven temperature showed that the differences were significant for both the ^2t_r and peak area reproducibility, while they were insignificant for the ^1t_r reproducibility. These results were within expectations. The lower RSDs for the day-to-day peak area reproducibility for both separations compared to the within-day values were unexpected. For both

separations, day 3 had the highest within-day peak area RSD out of the 5 days. The within-day peak area reproducibility for the separation without ^{2}D temperature programming from day 1 to day 5 was 1.96 %, 1.34 %, 3.52 %, 2.93 %, and 2.45 %, respectively. For the separation with ^{2}D temperature programming, it was 2.11 %, 1.96 %, 2.61 %, 0.92 %, and 0.83 %, respectively. A paired Student's t-test comparing the within-day (day 3) results to the day-to-day results was performed for both separations (Table 4-27). It was found that the differences in ^2t_r and peak area RSD were significant. Bartlett's test and Levene test were also performed on both sets of data to test for equal variances between each day. The Levene test was completed in case the data had a non-normal distribution. It was found that the variances were equal across the 5 days for both separations according to both tests.

Table 4-26: Paired Student's t-test (α = 0.05) comparison between the GC×GC separation with the ^{2}D at oven temperature and with ^{2}D temperature programming for the ^1t_r, ^2t_r, and peak area of 10 peaks. *The comparison was done for both the within-day and day-to-day results. The ^{2}D temperature program was a 3 s delay in heating, followed by a linear temperature ramp from 3 s to 5 s to +60 °C (at 30 °C/s) , where it was held until 5.5 s, and cooling starting at 5.5 s.*

	Within-Day (df = 9, α = 0.05)		**Day-to-Day (df = 9, α = 0.05)**	
	t-stat	*p*-value	*t*-stat	*p*-value
^1t_r	0.31	0.76	0.62	0.55
^2t_r	5.22	5.5×10^{-4}	3.33	8.8×10^{-3}
Area	5.84	2.5×10^{-4}	3.07	1.3×10^{-2}

Table 4-27: Paired Student's t-test (α = 0.05) comparison of the within-day results to the day-to-day results for each separation (GC×GC-SSM-FID and GC×GC-SSM-^{2}DTPS-FID). *The ^{2}D temperature program was a 3 s delay in heating, followed by a linear temperature ramp from 3 s to 5 s to +60 °C (at 30 °C/s) , where it was held until 5.5 s, and cooling starting at 5.5 s.*

	GC×GC-SSM (df = 9, α = 0.05)		**GC×GC-SSM-2DTPS (df = 13, α = 0.05)**	
	t-stat	*p*-value	*t*-stat	*p*-value
^1t_r	1.23	0.24	1.31	0.22
^2t_r	3.36	5.1×10^{-3}	4.77	1.0×10^{-3}
Area	4.23	9.8×10^{-4}	3.54	6.3×10^{-3}

4.3.5.1 Investigating the Retention Time Shift and Peak Broadening in 1st Run

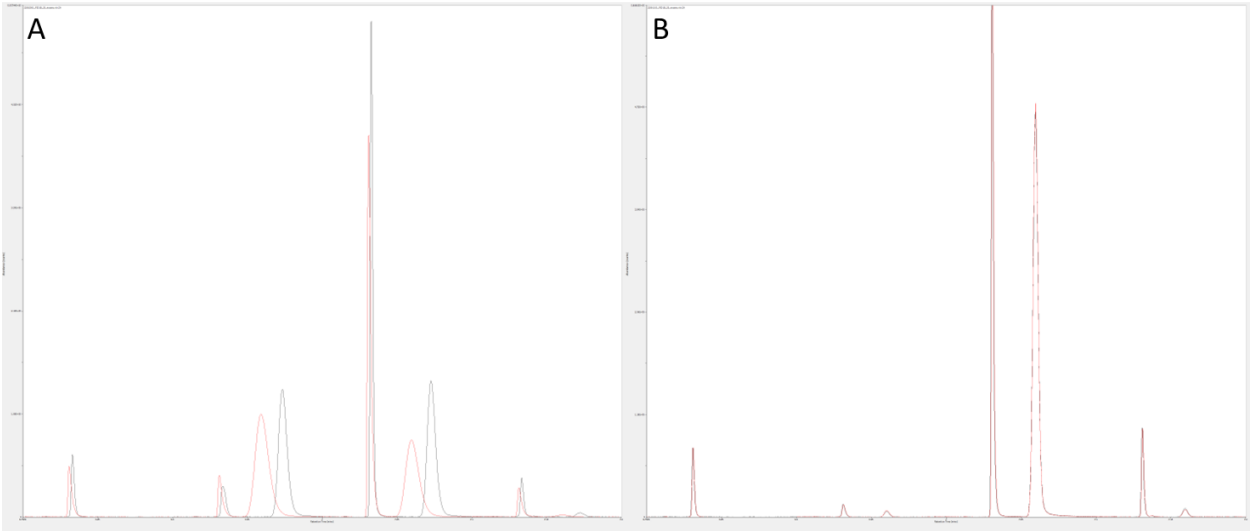

Figure 4-27: Comparing 1D signal [6.8 minutes to 7.2 minutes] of the first (red) and second (black) back-to-back runs on day three of the GC×GC separations without ^{2}D temperature programming (A) and with ^{2}D temperature programming (B). (A) Peaks were eluting earlier and broader in the ^{2}D for the first run compared to the second run. (B) No retention time shifts and changes in peak width was observed for the ^{2}D temperature programming separations. The ^{2}D temperature program was a 3 s delay in heating, followed by a linear temperature ramp from 3 s to 5 s to +60 °C (at 30 °C/s) , where it was held until 5.5 s, and cooling starting at 5.5 s.

As shown in Figure 4-27, there was reduced retention on the ^{2}D column for the first run of the GC×GC separation without ^{2}D temperature programming for each day of the 5-day reproducibility testing. This was not observed for the ^{2}D temperature programming separations. This phenomenon was also experienced in 4.3.2 for the separation without additional ^{2}D heating. The components in common for both setups were the GC (6890A), SSM, and columns. This was not observed in the other GC×GC-FID setup, which utilized the 6890N from the LECO Pegasus III with the SSM and secondary oven. Since this problem only occurred for the first run when the ^{2}D column did not experience any additional heating, it was suspected that contamination was collecting at the ^{2}D column overnight (flow at 0.5 mL/min, oven at 35 °C). With ^{2}D heating (temperature programming or constant offset), the contamination collected at the ^{2}D column would elute during the dead time of the ^{1}D column, preventing the issue observed.

To test this hypothesis, three back-to-back separations were performed each day for four days. The first two days were GC×GC separations without ^{2}D temperature programming, completed as in previous

sections for reproducibility testing. This was done to confirm that the issue with the first run was reproducible and still existed with the setup. The day before the first day of testing, 10 % (v/v) diesel (diluted in CS_2) was separated to replicate the initial conditions of the GC×GC setup for the first day of runs. The retention time shift and peak broadening were observed on the first run for both days. The second and third run exhibited no signs of retention time shift or peak broadening. This confirmed that the issue persisted with the setup.

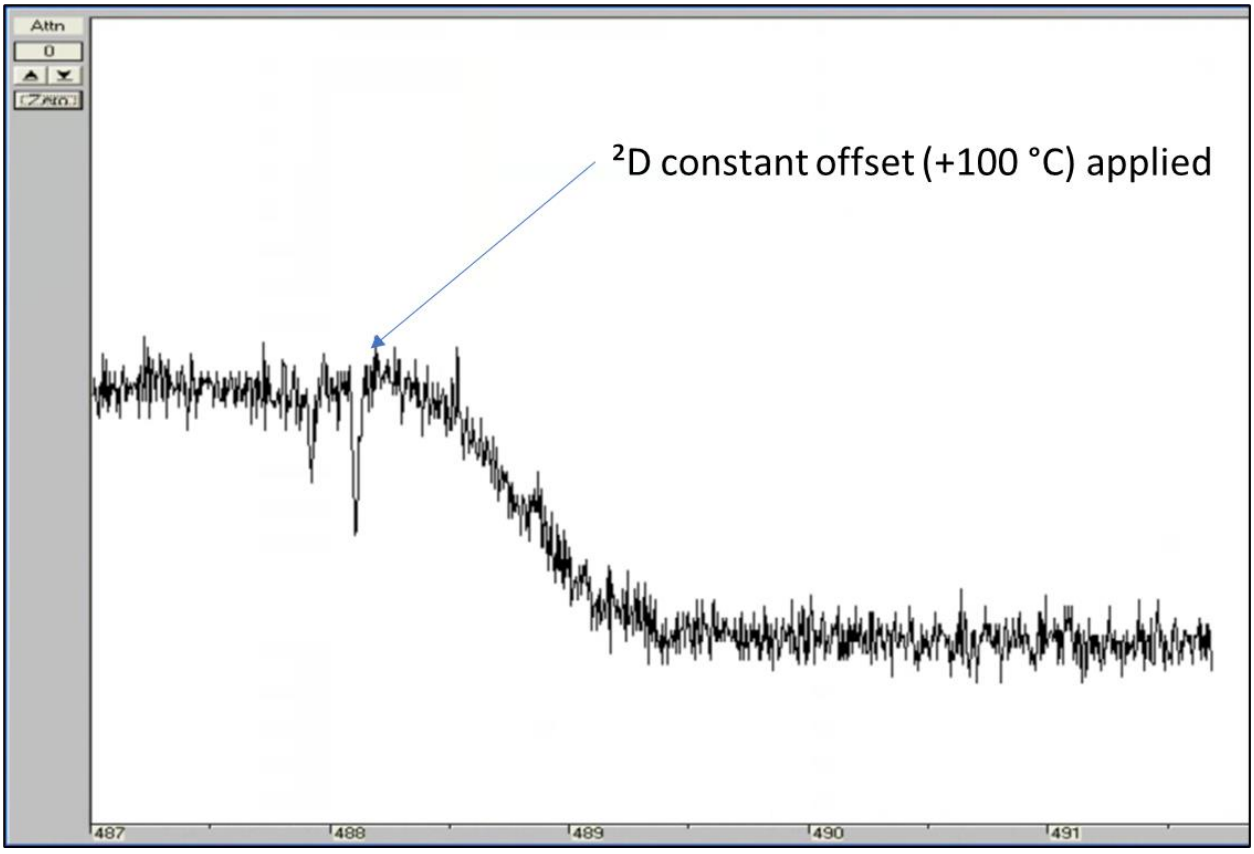

Figure 4-28: FID background signal as the ²DTPS applied a +100 °C offset to the ²D column, heating it to 135 °C. A noticeable drop in the background signal was observed before it leveled off.

On day 3, the ²DTPS was set to a 100 °C constant positive temperature offset before the first run and the baseline was monitored (Figure 4-28). The SSM was also set to its initial state (Entry/Exit: 135 °C, Trap: 9 °C) in preparation for the GC×GC separations. Shortly after the ²D constant offset was applied, a noticeable decrease in the background signal was observed. After the background signal leveled off and settled, the ²D constant offset was stopped, allowing the ²D column to cool back to oven temperature.

The three back-to-back separations were performed and no noticeable shifts in retention or peak broadening was observed. To confirm that the contamination was only collecting at the ^{2}D column and not the modulator column [Rxi-1ms (0.69 m x 0.25 mm x 1.0 µm) + deactivated fused-silica (0.48 m x 0.25 mm)] which had a thick stationary phase, the ^{2}D constant offset was applied without the SSM being heated to its initial state on day four. Once the background signal leveled off, the ^{2}D column was allowed to cool back to oven temperature. The SSM was then set to its initial state (Entry and Exit Hot Zones: +100 °C) and the GC×GC separations proceeded. This order of events was important to determine if any contaminants that may have collected at SSM would re-contaminate the ^{2}D column. Again, no noticeable shifts in retention or peak broadening were observed for the three back-to-back runs. This confirmed that the contamination was not collecting in the modulator column (Rxi-1ms), but only in the ^{2}D column (MXT-WAX). This could be due to the nature of the stationary phases, non-polar versus polar or dimethyl polysiloxane versus Carbowax^{TM} polyethylene glycol, and the contaminants. The reduced retention and broadening of the peaks from the contamination of the ^{2}D column was likely caused by a reduced focusing effect from the retention gap [deactivated fused-silica (0.48 m x 0.25 mm)] between the trapping zone of the SSM and the ^{2}D column. As the GC oven temperature increased, the contamination gradually eluted from the ^{2}D column, restoring performance. This occurred at around ~8.5 min or ~51.5 °C. To prevent this issue with future GC×GC separations, the first separation of the day could be discarded, the oven could be set to 50 °C overnight to prevent the buildup of contamination, or a complete inlet maintenance, including the cleaning of the carrier gas lines and split exhaust lines could be done to fix this problem.

4.3.6 Recommended Power Supply Output

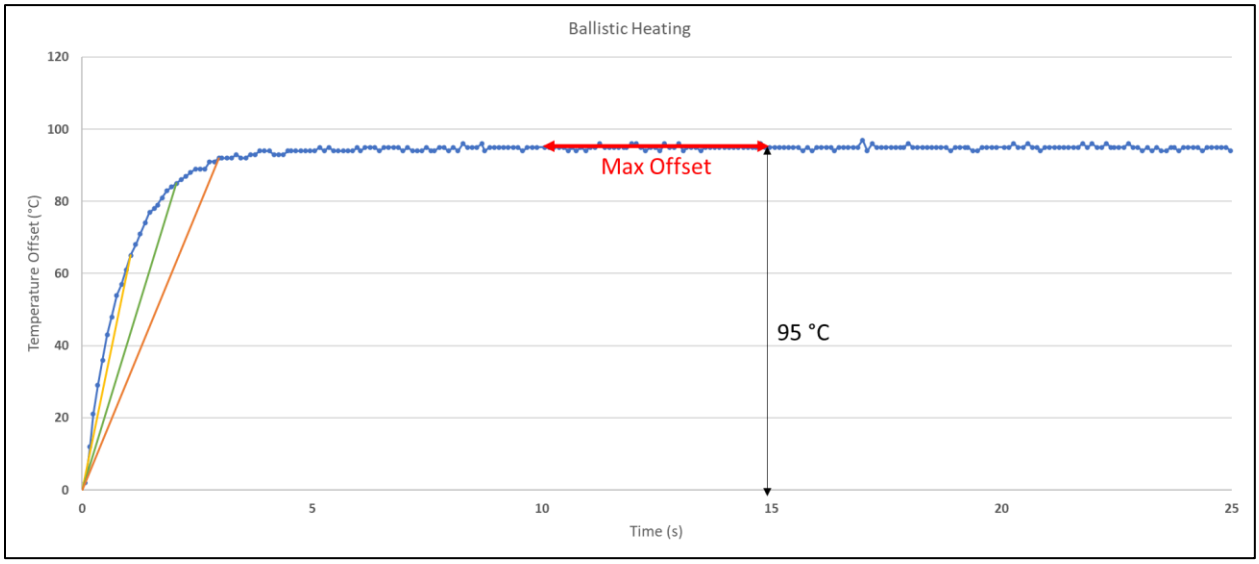

Figure 4-29: Ballistic heating with the ²DTPS. Data was from a 0.5 m x 0.18 mm x 0.20 µm column at an oven temperature of 35 °C and PSU voltage of 9.5 V. The yellow, green, and orange lines illustrate the theoretical maximum heating rate for 1 s, 2 s, and 3 s durations, respectively. The maximum temperature offset was determined from the average temperature offset over a 5 s duration after the system reached a steady state.

To determine the recommended power supply specifications based on the constant temperature offset or heating rate and the ²D column dimensions, the relationship between the power supply output (voltage, current) and its maximum temperature offset and heating rate needed to be established. The ²DTPS' maximum temperature offset was determined by setting a constant temperature offset greater than the system's maximum temperature offset. This forced the PWM to be at 100 % duty cycle when trying to get the temperature to reach setpoint. Shown in Figure 4-29, the ballistic heating conditions from section 2 were recreated by setting the ²DTPS to a constant offset above the maximum offset. A setpoint of +120 °C was applied while the system's maximum offset was 95 °C. Once the system had reached a steady state, the ²D column temperature data was collected for a period of 5 s (~50 data points) and averaged to determine the maximum ²D temperature offset. Using this data, the theoretical maximum heating rate for any heating duration can be determined, represented by the yellow, green, and orange lines in Figure 4-29 for the 1 s, 2 s, and 3 s heating durations, respectively. However, this would not reflect the ²DTPS' maximum heating rate since that was affected by the PID heating control.

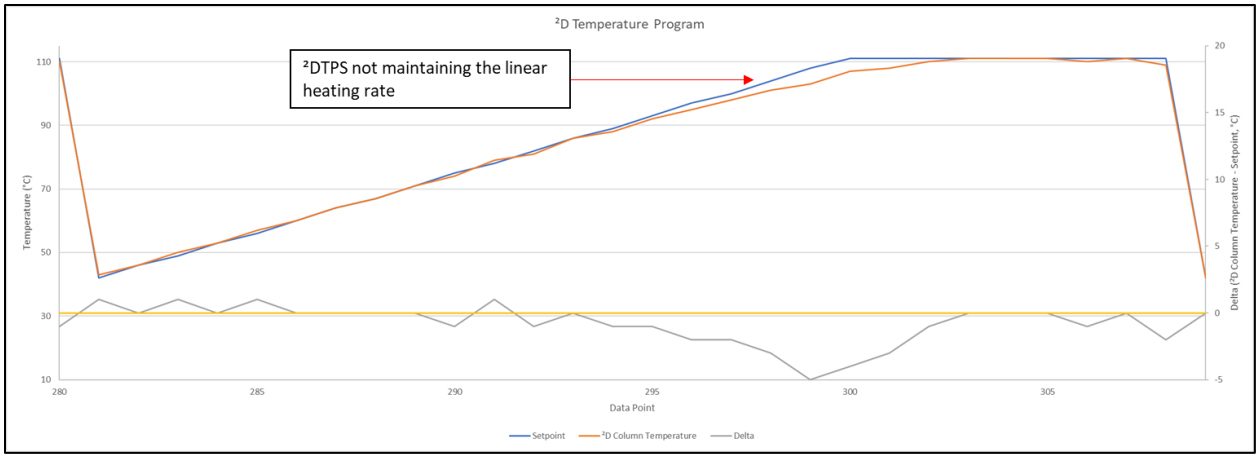

Figure 4-30: ²DTPS being unable to maintain the set heating rate due to insufficient power from the PSU. Data was from the 1 m x 0.18 mm x 0.2 µm column being heated to an offset of 76 °C over 2 s for a heating rate of 38 °C/s and held at the final offset for 1 s. The GC oven was at 35 °C and the column flow was 3 mL/min. Data shows a single modulation from the 2-minute test. The ²D column temperature (orange) and setpoint (blue) is given on the left y-axis. The delta (ΔT = ²D column temperature – setpoint, grey) is given on the right y-axis. A yellow horizontal line is provided to indicate the delta = 0 position, to highlight when the ²D column temperature overshoots and undershoots the setpoint during ²D temperature programming.

To determine the maximum heating rate of the ²DTPS, the average absolute difference between the setpoint and ²D column temperature ($|\Delta T|_{avg}$) was calculated for 2 minutes of testing (20 modulations, 6 s modulation period, 3 s of heating/3 s of cooling, 10 Hz data rate, ~600 data points). The ²D temperature program consisted of 3 s of cooling, followed by a 2 s linear temperature ramp, and held at the final temperature for 1 s. This provided a quantitative value to measure the ²DTPS' variability and accuracy during both the linear ramp and constant offset hold. Using the MXT-WAX (1 m x 0.25 mm x 0.25 µm) column for preliminary testing, the maximum heating rate was estimated from the live graph on the Windows Forms application at an oven temperature of 35 °C and at PSU voltages of 12 V, 14 V, 16 V, 18 V and 20 V. Figure 4-30 is an example of the ²D temperature program failing to maintain the heating rate. Near the end of the linear temperature program, the ²DTPS was undershooting the setpoint due to a lack of power from the PSU. This was an indication that the system had gone beyond its maximum heating rate. The $|\Delta T|_{avg}$ was found to be greater than 0.75 °C for ²D temperature programs that were beyond the ²DTPS' maximum heating rate. Using this value as the limit, the fastest heating rate that could achieve a $|\Delta T|_{avg}$ that was less than or equal to 0.75 °C was the ²DTPS' maximum heating rate for the given conditions (oven temperature, power, column dimensions). The data from the 2 s linear

temperature ramp testing is found in Table C - 17 from Appendix C. A total of 2084 data points were collected for the 2 s linear temperature ramp testing, of which 185 data points corresponded to the maximum heating rate based on the column dimensions, oven temperature, and power applied. The additional data points provided valuable information on the ²DTPS' PID characteristics and allowed for further improvement in the PID code.

4.3.6.1 Maximum Heating Rate and Maximum Offset

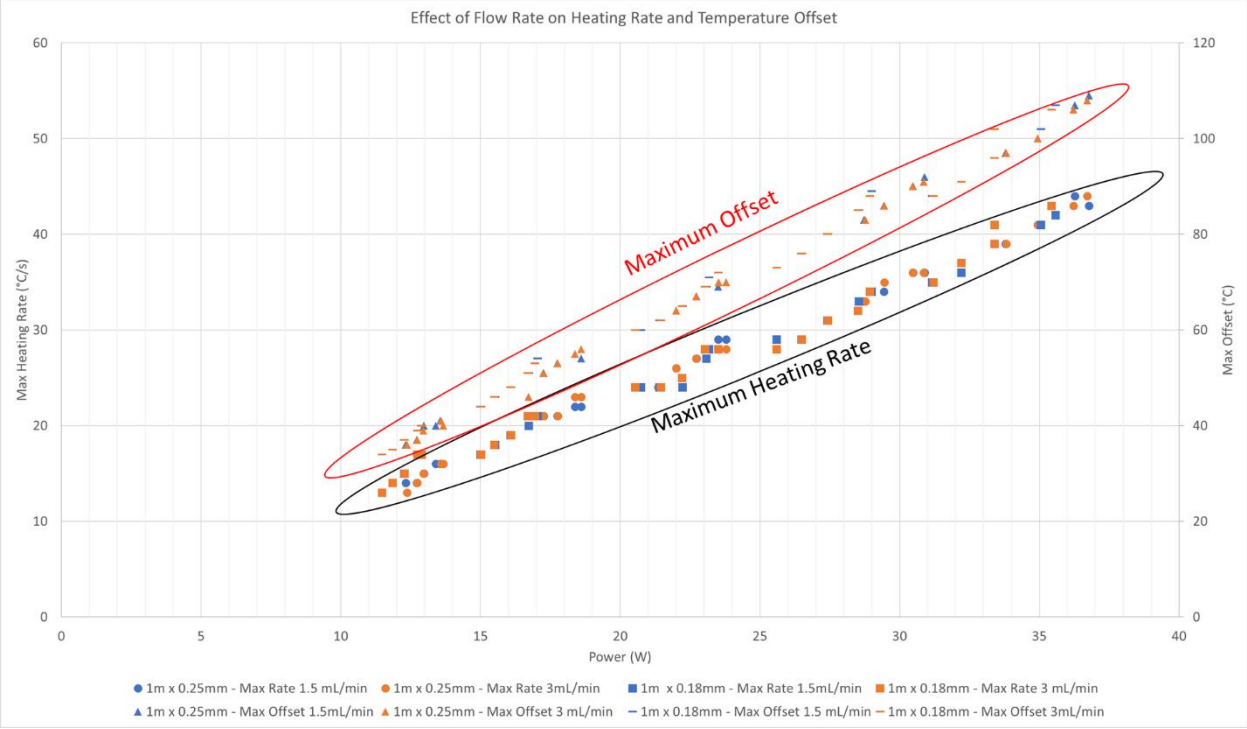

Figure 4-31: The effect of flow rate on the maximum heating rate and temperature offset for the ²DTPS. 1.5 mL/min (blue) and 3 mL/min (orange) were compared for a 1 m x 0.25 mm (heating rate – circle; offset - triangle) and 1 m x 0.18 mm column (heating rate – square; offset - dash).

Carrier gas (He) flows of 1.5 mL/min and 3 mL/min were tested for the 1 m x 0.25 mm and 1 m x 0.18 mm columns. However, as shown in Figure 4-31, the difference in flow had little impact on the maximum heating rate and temperature offset. Circled in black was the maximum heating rate (primary y-axis) for both columns with the 1.5 mL/min results in blue and 3 mL/min results in orange. For most cases, the maximum heating rate was identical with any difference being no more than 1 °C/s. This was the same for the maximum temperature offset (secondary y-axis), circled in red, where only a single data

point had a difference of 2 °C between the two flows while the majority were identical. Thus, data for the 0.5 m x 0.18 mm, 0.5 m x 0.25 mm, and 3 m x 0.25 mm columns were only collected at a flow rate of 3 mL/min.

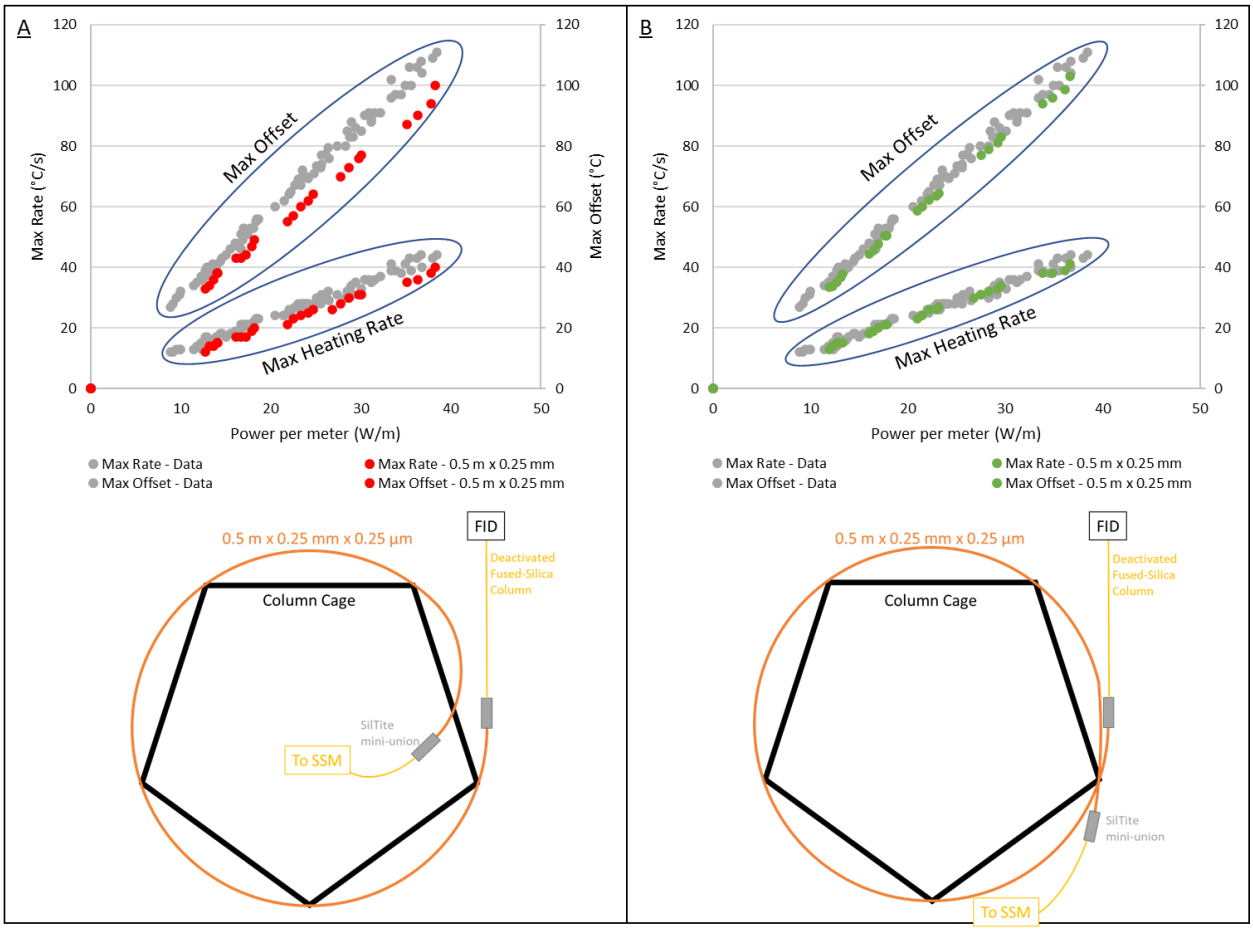

Figure 4-32: Comparison of the maximum heating rate and offset for two different column installations (0.5 m x 0.25 mm x 0.25 µm column dimensions). (A) The head of the 0.5 m x 0.25 mm x 0.25 µm column did not follow the outer circle of the column cage, resulting in a lower heating rate and temperature offset. (B) Both ends of the 0.5 m x 0.25 mm x 0.25 µm column were held close to one of the column cage supports, ensuring the ²D column followed the outer circle of the column cage like the other column installations.

The testing for the 0.5 m x 0.25 mm x 0.25 µm MXT-WAX column was repeated as it was noticed that the data was an outlier compared to the other columns. Shown in Figure 4-32 is the maximum heating rate and temperature offset data for all columns with the power normalized to the column length. The data for the 0.5 m x 0.25 mm column was differentiated from the other columns in red and green. In Figure 4-32A, the data for the first trial of the 0.5 m x 0.25 mm column is shown. Both the maximum

heating rate and temperature offset for the 0.5 m x 0.25 mm column were lower compared to the other data. The main difference was that the head of the ^{2}D column was positioned in front of the oven fan rather than being fixed to the column cage. The lower maximum heating rate and offset may have been due to a change in the convection pattern over the column that resulted in greater heat dissipation. When the column was retested after collecting the data for all other columns, the column was installed on the column cage like the other columns, as shown in Figure 4-32B. The resulting maximum heating rate and offset were better aligned with the other data. The results from Figure 4-32A may indicate that better cooling performance was possible by reducing the diameter of the column cage to ensure the entire column was within the GC oven fan opening. However, this would also lower the maximum heating rate and temperature offset.

To calculate the standard deviation of the maximum offset and heating rate, the ideal methodology would have been to reinstall the column and repeat the ^{2}D temperature program. Repeating the column installation to generate replicate sets of data for a single column dimension was prohibitive not only due to substantial increase in the number of data points, but also in the time consumed for installation and calibration. However, it would provide the variability due to the slight differences in column positioning within the GC oven, which would affect the heat dissipation due to a change in convection patterns. Although repeating the ^{2}D temperature program would be faster and could provide the variability due to the ^{2}DTPS' PID heating control, the very large number of data points in the experiment still made this prohibitive. All of this would only be feasible if the scope of the experiment was reduced to testing only a single column dimension, but the data generated would not provide enough information to recommend PSU outputs for the many possible conditions (column dimension, oven temperature, flow rate). To estimate the variability of the measurements, the standard deviation of the resistance measurements during the calibration of the column (explained in section 4.1.2) at oven temperatures of 35 °C, 50 °C, 100 °C, 150 °C, and 200 °C were calculated. The resistance was then converted to °C using the second

order polynomial from the calibration. From the 27 calibrations and 5 oven temperatures (total = 135), the average standard deviation was 0.66 °C, with the minimum and maximum being 0.26 °C and 1.47 °C, respectively. This would have made the error bars too small relative to the scale of graphs and obscure the data points, so they were not included. This was an underestimation of the error due to the multitude of factors that affect the temperature offset.

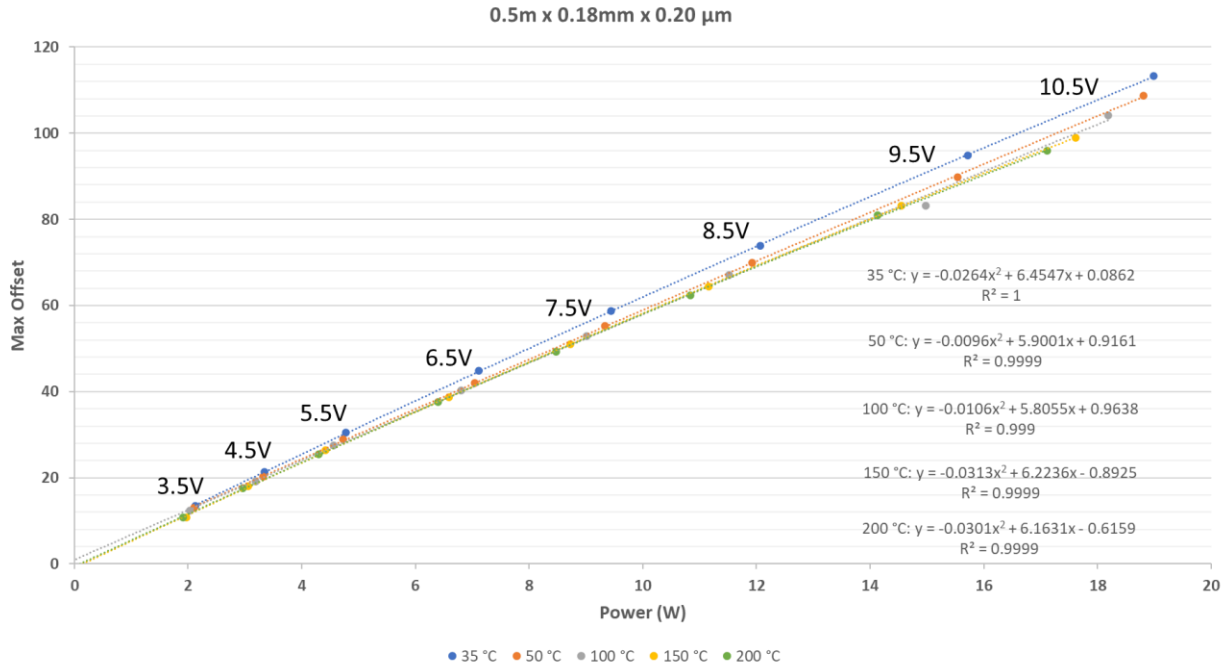

Figure 4-33: Correlation between the oven temperature and the maximum temperature offset for the

During testing, it was noticed that there was a correlation between the maximum offset and the oven temperature. Shown in Figure 4-33 is the maximum temperature offset achieved at oven temperatures of 35 °C, 50 °C, 100 °C, 150 °C, and 200 °C, for PSU voltages of 3.5 V, 4.5 V, 5.5 V, 6.5 V, 7.5 V, 8.5 V, 9.5 V, and 10.5 V. The small differences in power delivered to the ^{2}D column were due to the increase in column resistance with increasing temperature, resulting in a decrease in current and power. At the higher PSU voltages, there was a noticeable difference in the maximum temperature offset between the 35 °C measurements and 50 °C measurements. At 35 °C, the vent at the rear of the Agilent 6890A GC was open, which may have affected the air convection conditions within the GC oven. This could have reduced the

heat dissipation of the column, resulting in a higher maximum offset. Residual (observed value – calculated value) plots of the data fitted to a linear and second-order polynomial are found in Figure C - 9 of Appendix C. The residual plot for the linear model (Figure C - 9A) showed a non-linear relationship. Fitting the data to a second-order polynomial resulted in a residual plot (Figure C - 9B) with a more random distribution that was closer to zero.

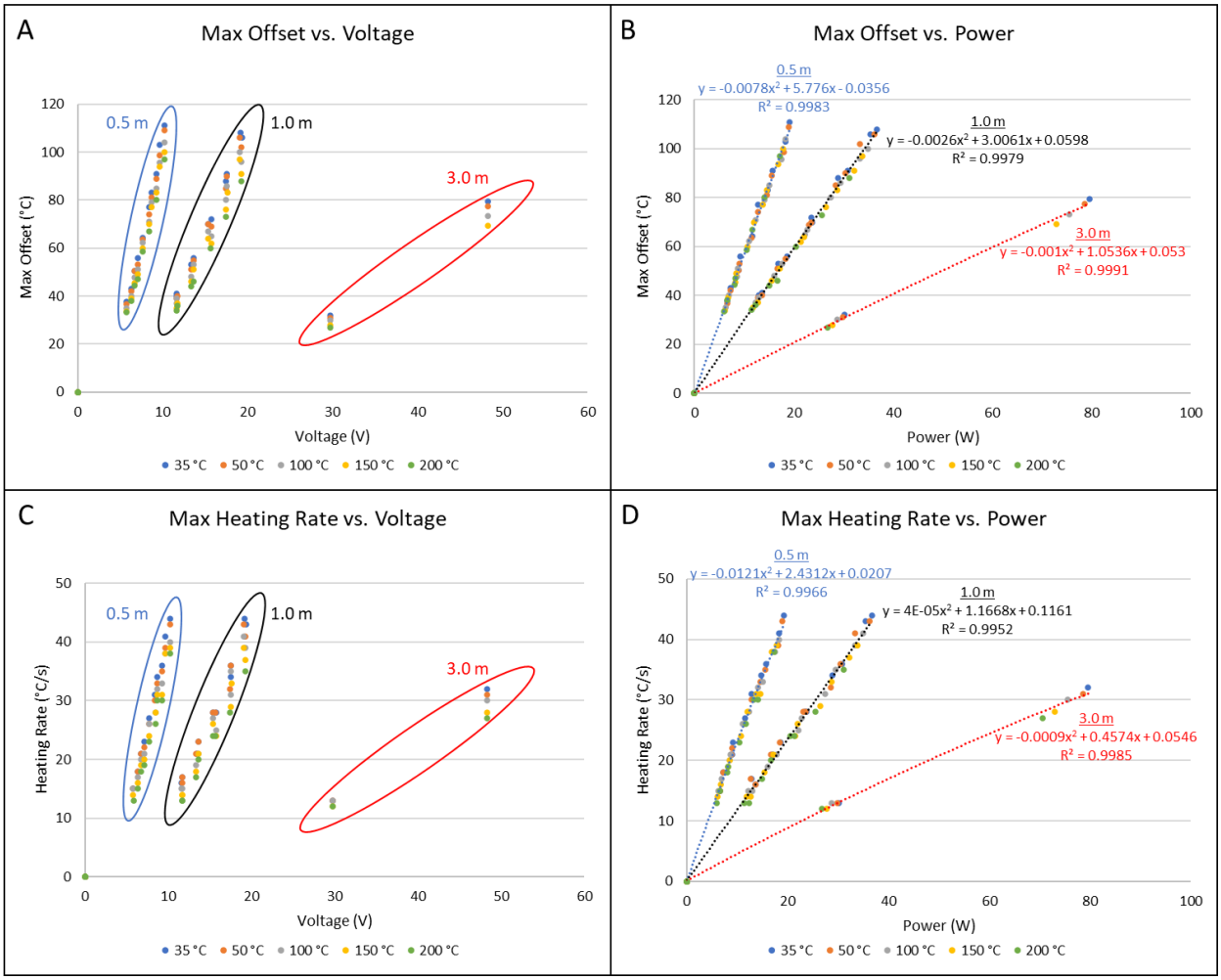

Figure 4-34: Relationship between the maximum temperature offset and heating rate with the voltage and power used to heat the ²D column. The maximum offset and heating rate increased with voltage and power, with the results grouped according to the column length. Columns (I.D. = 0.25 mm and 0.18 mm) of 0.5 m, 1.0 m, and 3.0 m were tested at a flow rate of 3 mL/min and oven temperatures of 35 °C, 50 °C, 100 °C, 150 °C, and 200 °C.

The maximum heating rate and offset for each column and oven temperature were plotted versus the voltage and power applied in Figure 4-34. The heating rate and temperature offset were dependent on the energy (power × time) inputted into the system (²D column) and energy lost due to conduction

(column unions), convection (oven air bath), and radiation. Power (Eq. (2.1)) is dependent on the voltage, current, and resistance, which are all interdependent variables [Eq. (4.1)]. Since the voltage (current × resistance) was approximately constant, the current (decreased) and resistance (increased) of the ^{2}D column changed with oven temperature (increase). As shown in Figure 4-34A/C, this resulted in the vertical groups of peaks for each column as the oven temperature increased, resulting in a decrease in power (current^2 × resistance) delivered to the ^{2}D column. In Figure 4-34B/D, the maximum temperature offset and heating rate were correlated with the power according to the column length (thermal mass). Although the 0.18 mm column had a lower thermal mass than the 0.25 mm column of the same length, the difference in maximum temperature offset and heating rate was negligible.

The maximum heating rate and offset were plotted with the current, power per meter, and power per ohm in Figure 4-35. Since power is proportional to the current^2, the relationship between the max offset (Figure 4-35A) and heating rate (Figure 4-35B) to the current applied was evidently non-linear. Since the current was proportional to the column resistance, which was proportional to its dimensions and oven temperature, the data could be fitted to a single second order polynomial, unlike Figure 4-34. This was also the case for Figure 4-35C/D and Figure 4-35D/E, where the power applied was normalized to the column length and resistance, respectively. The corresponding residual plots to Figure 4-35 can be found in Figure C - 10 of Appendix C, where the distribution of the residuals around zero was found to be random. Normalizing the power by the resistance of the column results in the current^2, which was effectively a power transformation ($x = x^2$) of Figure 4-35A /B. This resulted in a similar distribution of the residuals between Figure C - 10A/B and Figure C - 10E/F. Since the power transformation transforms the non-linear relationship closer to linearity, the residual plot for the data (max heating rate vs. power per Ω and max offset vs. power per Ω) fitted to a linear model is found in Figure C - 10G/H. The distribution of the residuals was similar between the linear and non-linear model; however, the residuals for the maximum heating

rate and offset at $A^2 = 0$ were 0.65 °C/s and 1.21 °C for the linear model, compared to 0.01 °C/s and - 0.18 °C for the non-linear model.

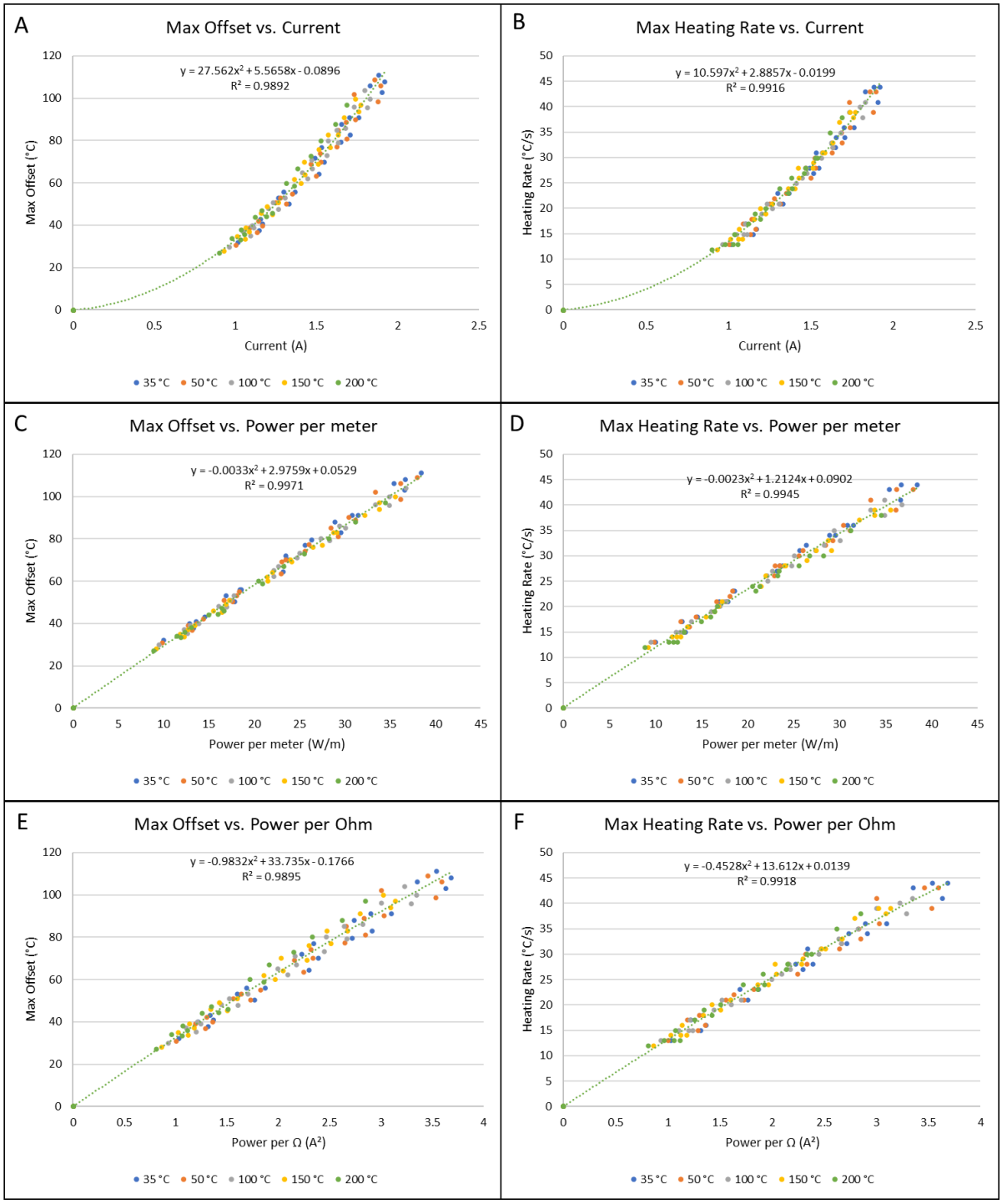

Figure 4-35: Relationship between the maximum temperature offset and heating rate with the current, power/meter, and power/Ω used to heat the ²D column. Columns (I.D. = 0.25 mm and 0.18 mm) of 0.5 m, 1.0 m, and 3.0 m were tested at a flow rate of 3 mL/min and oven temperatures of 35 °C, 50 °C, 100 °C, 150 °C, and 200 °C. A second order polynomial was fitted to all data.

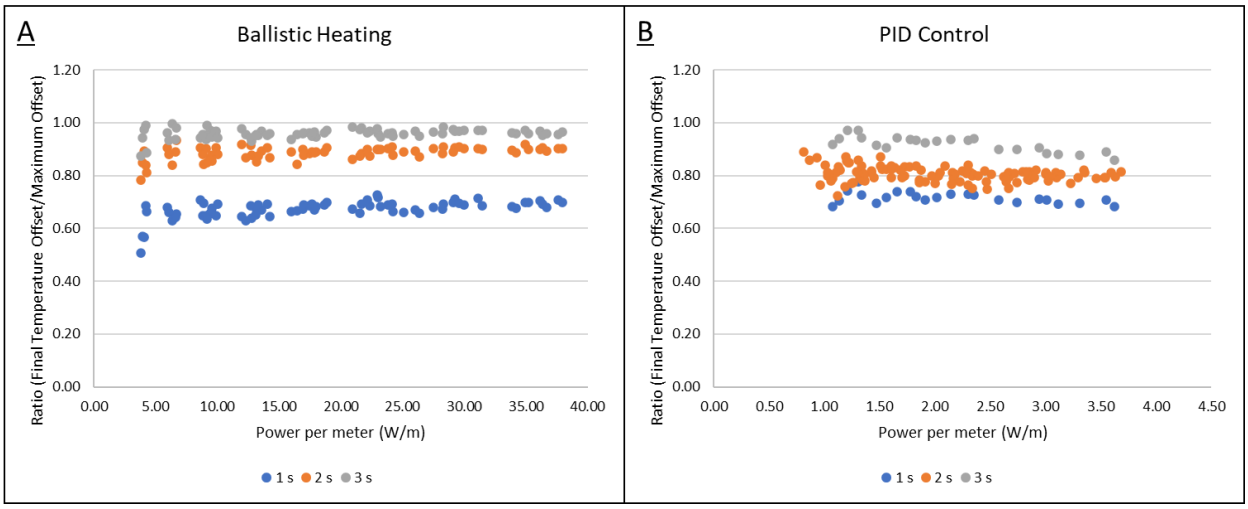

Figure 4-36: Ratio of the final temperature offset achieved for a particular heating duration (1 s, 2 s, 3 s) and the maximum temperature offset for various columns (0.5 m x 0.18 mm, 0.5 m x 0.25 mm, 3.015 m x 0.25 mm). (A) Ratio calculated from the temperature offset achieved at 1 s, 2 s, and 3 s for ballistic heating, as shown in Figure 4-29. (B) Ratio calculated from the largest temperature offset of the ²D temperature program that passed the criteria of $|\Delta T|_{avg} \leq 0.75$ °C, for linear temperature program durations of 1 s, 2 s, and 3 s with a final temperature offset held for 2 s, 1 s, and 0 s, respectively. The ²D temperature programs were all for a 6 s modulation (3 s of cooling, 3 s heating). The 2 s linear temperature program data was for all columns (0.5 m x 0.25 mm, 1.0 m x 0.25 mm, 3.0 m x 0.25 mm, 0.5 m x 0.18 mm, 1.0 m x 0.18 mm) tested. The 1 s and 3 s data were collected for the 0.5 m x 0.25 mm column.

The maximum heating rate was dependent on the final temperature offset and the duration. From Figure 4-29, although the final temperature offset increased with the heating duration, the linear heating rate decreased. Since data was only collected for a 2 s linear temperature ramp, the recommended PSU power would not be applicable for shorter or longer linear temperature ramps of the same heating rate. To estimate the maximum heating rate for a 1 s and 3 s linear temperature ramp the relationship between the final temperature offset reached and the heating duration was examined using the ballistic heating data collected for the 0.5 m x 0.18 mm, 0.5 m x 0.25 mm, and 3.015 m x 0.25 mm. This data is found in Table C - 18 of Appendix C. The final temperature offset was normalized to the maximum temperature offset to compare the data between the various columns and heating durations. The normalized temperature, shown in Figure 4-36 as the ratio (final temperature offset/maximum offset), was plotted with the power normalized to the column length. In Figure 4-36A, the data from ballistic heating was plotted, showing a consistent ratio for each heating duration. The mean and standard deviation of the ratios for the 1 s, 2 s, and 3 s heating durations were as follows: (M = 0.67, S.D. = 0.03), (M = 0.88,

S.D. = 0.03), (M = 0.96, S.D. = 0.02). This was then applied to the maximum heating rate data (2 s duration) collected for all columns in Figure 4-36B, where the mean and standard deviation of the ratio was 0.81 and 0.03, respectively. Understandably, the value based on PID control resulted in a lower ratio (lower final temperature offset). This was because any overshoot of the setpoint by the ^{2}DTPS would result in a decrease in the duty cycle, which for a rapidly increasing setpoint can then result in the system undershooting the next setpoint. To catch up to the setpoint would require more than the minimum power needed to theoretically achieve the heating rate. Most importantly, the ratio calculated from the maximum heating rate data also showed a consistent ratio like the ballistic heating data. Using the 0.5 m x 0.25 mm column, the maximum heating rate ($|\Delta T|avg \leqslant 0.75$ °C) and corresponding ratios for a 1 s and 3 s linear temperature program were determined. This data is found in Table C - 19 of Appendix C. Both ^{2}D temperature programs were still for a 6 s modulation period consisting of 3 s of cooling and 3 s of heating. For the 1 s linear temperature ramp, the final temperature offset was held for 2 s, while the 3 s linear temperature ramp did not have a final temperature offset hold. The mean and standard deviation of the ratios for the 1 s and 3 s heating durations were as follows: (M = 0.72, S.D. = 0.02), (M = 0.92, S.D. = 0.03). Due to the 2 s final temperature offset hold for the 1 s linear temperature program, it resulted in an overestimation of the ratio, where its average ratio was greater than the ratio from the ballistic heating data. The criterion of the $|\Delta T|avg \leqslant 0.75$ °C would need to be lowered to account for the longer hold, or an alternate metric would be needed to better reflect the 1 s maximum heating rate.

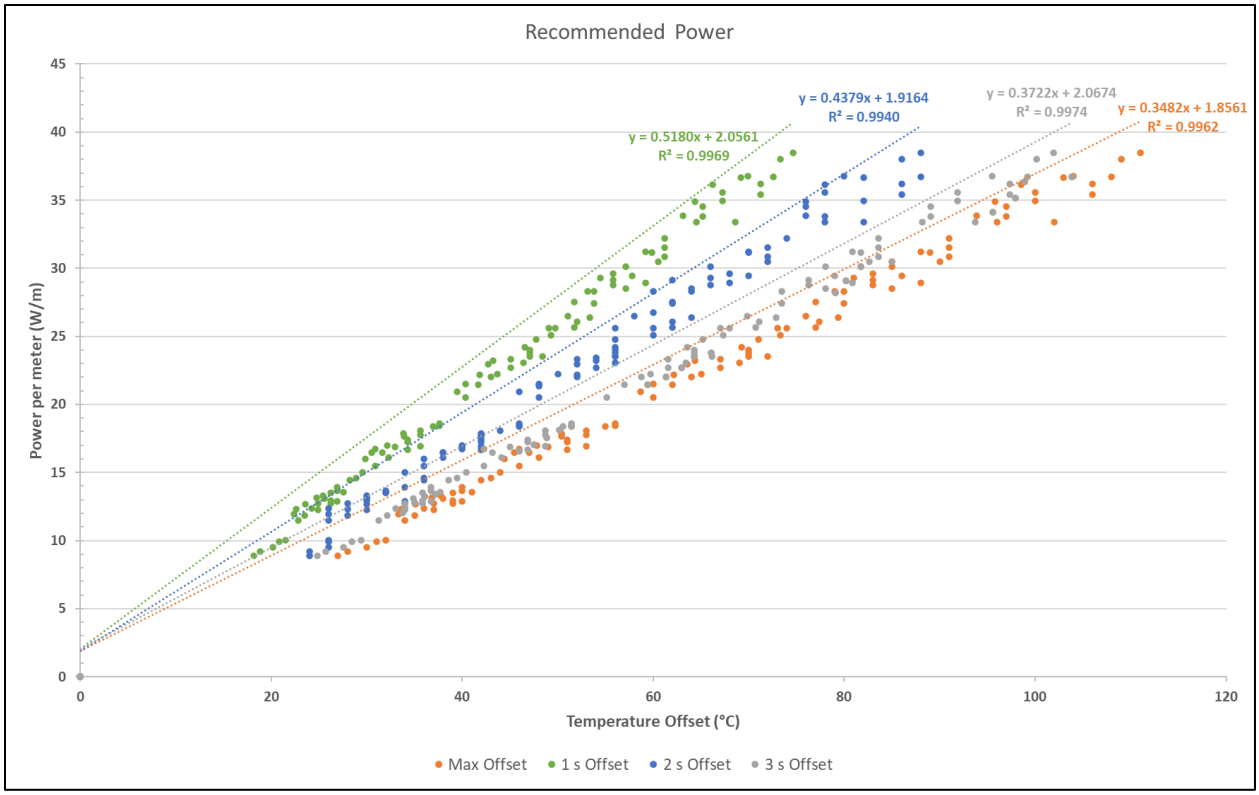

Figure 4-37: Recommended minimum power needed, normalized to the column length, based on the temperature offset intended.

The final temperature offsets of the maximum heating rates for a 1 s, 2 s, and 3 s linear temperature ramp as well as the maximum temperature offset were plotted with the power normalized to the column length in Figure 4-37. A line was fitted to each set of data and a translation of +2.2 W/m was applied so that each line would fall above each corresponding set of data points. This was to ensure that the recommended power would be sufficient to achieve the linear temperature ramp. To estimate the temperature offset for the 1 s linear ramp, the average ratio (0.67) from the ballistic heating data was multiplied by the maximum temperature offset data collected for all columns during the maximum heating rate (2 s linear ramp) testing. For the 3 s linear ramp, the average ratio (0.92) collected from the 0.5 m x 0.25 mm column was used to estimate the temperature offset for all other columns. Although the recommended minimum power can be calculated from the equations in Figure 4-37, the optimizations to the PID code (section 4.3.6.2) expanded the usable range of heating rates, allowing for lower heating rates and smoother ^{2}D temperature programming. This helps simplify the recommended power supply

specifications to voltages that provide 1.9 A of current for high heating rate and temperature offset applications, and 1.5 A for lower heating rate and temperature offsets. The lower limit for the heating rate and offset and the need for a 1.5 A output from the power supply were due to the minimum output duration of 6 ms (12 % duty cycle, 50 ms period). As shown from the $|\Delta T|_{avg}$ data in Figure 4-38 in the next section (4.3.6.2), the lower limit for the ratio was roughly 0.2. Using a power supply voltage that provides 1.5 A for the column would provide a maximum offset of around 70 °C (Figure 4-35A), which means the lower offset limit would be about 14 °C. In terms of ^{2}D temperature programming, this would be below what is reasonably expected and lower than what has been used in sections 4.3.1 to 4.3.5.

4.3.6.2 Changes to the PID Code

During the maximum heating rate testing (2 s duration), it was noticed that the $|\Delta T|_{avg}$ would occasionally be greater than expected, even when the ^{2}D temperature program was not near its maximum heating rate. A closer inspection of the ^{2}D temperature program and its ΔT values revealed sudden drops in the ^{2}D column temperature during both the linear temperature ramp and constant offset hold at the end of the ^{2}D temperature program. These drops in temperature were due to the ^{2}D column temperature overshooting the setpoint and then over-correcting. Since the setpoint for a ^{2}D temperature program increases at a rapid rate, aggressive PID values were needed to keep up with the moving setpoint. However, these aggressive PID values would also result in the duty cycle instantly decreasing to 12 % (6 ms ON, 44 ms OFF), the minimum value, at even the slightest (1 °C) overshoot. This was not an issue in previous sections (4.3.1 - 4.3.5) where the PID values were constant, but rather the adjustable PSU voltage was optimized to the ^{2}D temperature program set. This flexibility would not be available for users intending to use a power supply with a fixed power output. To address this issue, the PID code for the ^{2}DTPS was changed, and its effects were monitored through the $|\Delta T|_{avg}$ values during the maximum heating rate tests. It is important to note that these changes did not affect the determination of the maximum heating rate as the ^{2}D temperature programming data was monitored to ensure that $|\Delta T|_{avg}$

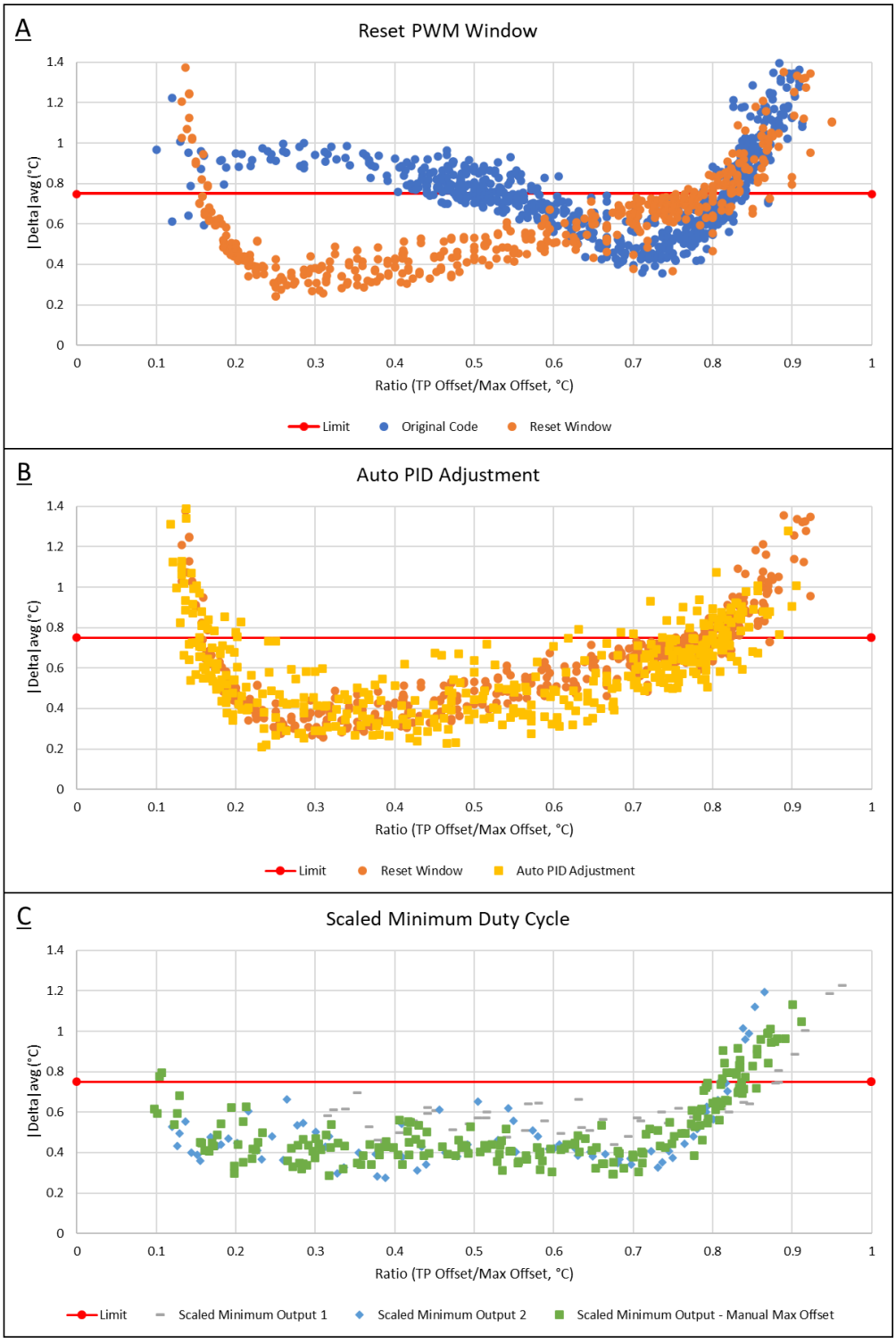

Figure 4-38: Improving the PSU output tolerance by broadening the ²DTPS' acceptable temperature programming range and eliminating user optimization of PID values through improvements to the PID code. Data was from the following ²D temperature program: 3 s cooling, 2 s linear temperature ramp, 1 s constant offset hold (at the final temperature offset). The ratio was the final temperature offset of the temperature ramp normalized to the maximum temperature offset. The limit was an $|\Delta T|_{avg} \leq 0.75$ °C. (A) Comparing the original code (used in 4.3.1 - 4.3.5) to the addition of a PWM window reset when the system undershoots the setpoint. (B) Added an auto PID value adjustment based on the ratio of the temperature program offset and the estimated maximum offset. (C) Scaling the minimum duty cycle of the ²DTPS with the ratio.

values greater than 0.75 °C were due to the ²DTPS not maintaining the heating rate as shown in Figure 4-30. Three major changes were made to reduce or simplify user input regarding the PID control and improve the ²DTPS' handling of overshooting the setpoint.

```
if (Setpoint - temperature >= 1)
{
  windowStartTime = timeElapsed;
}
```

The first change to the code was the inclusion of a reset for the PWM window start time. Figure 3-6 illustrated the PWM heating control with the window start times fixed at regular intervals according to the window size. When the system overshot the setpoint and caused the duty cycle to decrease and consequently turn OFF the heating, the system had to wait until the start of the next window before a new measurement would take place. For a rapidly increasing setpoint when temperature programming, this would be very detrimental and result in an apparent dip in the ²D temperature. To address this issue, if the setpoint exceeded the last known ²D column temperature by 1 °C or more, the window start time would reset to allow the system to take a new temperature measurement and recalculate the PID output. For the constant offset hold, the setpoint had to exceed the ²D column temperature by 2 °C or more to trigger the window reset to prevent overshooting the setpoint. The result of this change is illustrated in Figure 4-38A, comparing the original code to the addition of the window reset code. The addition of the window reset code expanded the lower range of ratios for a PSU output. The original code was used for the 1 m x 0.25 mm and the 0.5 m x 0.25 mm (first trial). The original code with the addition of the window reset code was used for the 1 m x 0.18 mm column for PSU voltages of 12 V to 18 V.

```
   int adjustPID()
   {
     maxOffset = -
0.9832*resultCurrent*resultCurrent*resultCurrent*resultCurrent+33.735*resultC
urrent*resultCurrent-0.1766;
     //maxOffset = 65.83721;
     ratio = (modulationProgram[currentProgram][1]) / maxOffset;
     if (ratio < 0.25 )
     {
       Kp = 5; //Ramp Proportional Gain
```

```
       Ki = 0.2; //Ramp Integral Gain (reacts to difference)
       Kd = 0.0; //Ramp Differential Gain (reduces over reaction)
       constKp = 5; //Constant Offset Proportional Gain
       constKi = 0.2; //Constant Offset Integral Gain (reacts to difference)
       constKd = 0.0; //Constant Offset Differential Gain (reduces over
reaction)
       Serial.print("Ramp PID = "); Serial.print(Kp); Serial.print(" ");
Serial.print(Ki); Serial.print(" "); Serial.println(Kd);//
       Serial.print("Constant Offset PID = "); Serial.print(constKp);
Serial.print(" "); Serial.print(constKi); Serial.print(" ");
Serial.println(constKd);
     }
     else if (ratio < 0.4)
     {
       Kp = 5; //Ramp Proportional Gain
       Ki = 0.3; //Ramp Integral Gain (reacts to difference)
       Kd = 0.0; //Ramp Differential Gain (reduces over reaction)
       constKp = 5; //Constant Offset Proportional Gain
       constKi = 0.3; //Constant Offset Integral Gain (reacts to difference)
       constKd = 0.0; //Constant Offset Differential Gain (reduces over
reaction)
       Serial.print("Ramp PID = "); Serial.print(Kp); Serial.print(" ");
Serial.print(Ki); Serial.print(" "); Serial.println(Kd);//
       Serial.print("Constant Offset PID = "); Serial.print(constKp);
Serial.print(" "); Serial.print(constKi); Serial.print(" ");
Serial.println(constKd);
     }
     else if (ratio < 0.6)
     {
       Kp = 6; //Ramp Proportional Gain
       Ki = 0.6; //Ramp Integral Gain (reacts to difference)
       Kd = 0.0; //Ramp Differential Gain (reduces over reaction)
       constKp = 6; //Constant Offset Proportional Gain
       constKi = 0.6; //Constant Offset Integral Gain (reacts to difference)
       constKd = 0.0; //Constant Offset Differential Gain (reduces over
reaction)
       Serial.print("Ramp PID = "); Serial.print(Kp); Serial.print(" ");
Serial.print(Ki); Serial.print(" "); Serial.println(Kd);//
       Serial.print("Constant Offset PID = "); Serial.print(constKp);
Serial.print(" "); Serial.print(constKi); Serial.print(" ");
Serial.println(constKd);
     }
     else
     {
       Kp = 11; //Ramp Proportional Gain
       Ki = 0.8; //Ramp Integral Gain (reacts to difference)
       Kd = 0.0; //Ramp Differential Gain (reduces over reaction)
       constKp = 11; //Constant Offset Proportional Gain
       constKi = 0.7; //Constant Offset Integral Gain (reacts to difference)
       constKd = 0.01; //Constant Offset Differential Gain (reduces over
reaction)
       Serial.print("Ramp PID = "); Serial.print(Kp); Serial.print(" ");
Serial.print(Ki); Serial.print(" "); Serial.println(Kd);//
       Serial.print("Constant Offset PID = "); Serial.print(constKp);
Serial.print(" "); Serial.print(constKi); Serial.print(" ");
Serial.println(constKd);
     }
```

```
}
```

Although PID values can be set by the user in the Windows Forms application, this may not be appropriate for a general user. Thus, multiple sets of pre-optimized PID values were added into the `adjustPID()` function, where a suitable set of PID values was used based on the ratio between the final temperature offset and the estimated maximum temperature offset. Shown in Figure 4-38B is the comparison of the $|\Delta T|_{avg}$ values of the window reset code and the window reset code with the addition of the automated PID value adjustment. With the auto adjustment of the PID values, there was more variability in the $|\Delta T|_{avg}$ values across the range of ratios. This was due to inaccurate estimations of the maximum temperature offset, resulting in the wrong set of PID values to be used. Although it did not cause the $|\Delta T|_{avg}$ to fail the 0.75 °C criterion, the results were less predictable. In hindsight, this was a premature implementation of the idea, as not all columns were tested at this point and the maximum temperature offset estimation was based on data from the 1.0 m x 0.25 mm, 0.5 m x 0.25 mm (first trial), and the 1.0 m x 0.18 mm column (12 – 18 V). A more appropriate test of the pre-optimized PID values would have been to manually input the maximum offset for the ^{2}DTPS.

```
Output = kp * error + ki * iError + kd * dError;
  if (Output > window)
  {
    Output = window;
  }
  else if (Output < (ratio  * lastOutput)) //Smooth out the Output
  {
    Output = ratio * lastOutput;
  }
  if (state == 2) //higher minimum for temperature ramp
  {
    if (Output < (window * relativeOffset)) //Scaled Minimum Output floor
    {
      Output = window * relativeOffset;
    }
  }
  if (state == 3) //relaxed minimum for constant offset
  {
    if (Output < (window * ratio * 0.8)) //Scaled Minimum Output floor
    {
      Output = window * ratio * 0.8;
    }
  }
  if (Output < minOutput)
```

```
{
  Output = minOutput;
}
```

To further improve the ^{2}DTPS' handling of overshooting the setpoint, the minimum Output of the PID calculation was modified to scale with the relative offset between the ^{2}D temperature offset and maximum heating offset. The closer the ^{2}D temperature offset was to the maximum offset, the higher the minimum Output should be. The first implementation of the scaled minimum Output, shown as Scaled Minimum Output 1 in Figure 4-38C, scaled minimum Output to the window size (50 ms) multiplied by the relative offset (temperature offset/maximum offset). This was applied to the 3.0 m x 0.25 mm column (30.8 V) testing. Although this worked well for the linear temperature ramp, this was found to be too aggressive for the constant offset hold, where the ^{2}DTPS tended to overshoot the fixed setpoint. Scaled Minimum Output 2 in Figure 4-38C scaled the minimum output during the constant offset hold to 80 % of the relative offset. This was applied to the 3.0 m x 0.25 mm column (48 V) testing. The result was an overall improvement to the ^{2}D temperature programming, but the variability due to the auto PID adjustment was still affecting the results. As a result, the maximum offset was manually inputted into the ^{2}DTPS to better assess the overall changes to ^{2}D temperature programming. This data is shown as Scaled Minimum Output – Manual Max Offset in Figure 4-38C, which was from the 2nd trial of the 0.5 m x 0.25 mm testing (6 V to 10 V). With all the changes to the PID code, the result was a slightly lower $|\Delta T|_{avg}$ in comparison to the original code and a significantly broader range of usable heating rates and temperature offsets for a single power output.

4.4 Summary and Conclusions

Table 4-28: Summary of the reproducibility of the GC×GC system without the ²DTPS where the ²D was at oven temperature or at a constant positive temperature offset with the secondary oven. The RSD (%) from 4.3.2 used the values from the persistence algorithm. Paired Student's t-test results when compared to the ²DTPS are highlighted in green and orange to designate differences that were insignificant and significant, respectively.

GC×GC						
			^1t_r (RSD %)			
			Oven Temperature		Secondary Oven	
Section	System	Sample	Within-Day	Day-to-Day	Within-Day	Day-to-Day
4.3.1	GC×GC-SSM-FID	Perfume	-	-	0.02	0.05
4.3.2	GC×GC-SSM-TOFMS	Diesel (10 %)	0.03	0.03	-	-
4.3.3	GC×GC-SSM-TOFMS	Perfume (10 %)	-	-	-	-
4.3.4	GC×GC-FM-TOFMS/**FID**	Diesel (10 %)	0.03	0.04	-	-
4.3.4	GC×GC-FM-**TOFMS**/FID	Diesel (10 %)	0.02	0.07	-	-
4.3.5	GC×GC-SSM-FID	Diesel (10 %)	0.02	0.04	-	-
			^2t_r (RSD %)			
			Oven Temperature		Secondary Oven	
Section	System	Sample	Within-Day	Day-to-Day	Within-Day	Day-to-Day
4.3.1	GC×GC-SSM-FID	Perfume	-	-	0.21	0.96
4.3.2	GC×GC-SSM-TOFMS	Diesel (10 %)	0.13	0.15	-	-
4.3.3	GC×GC-SSM-TOFMS	Perfume (10 %)	-	-	-	-
4.3.4	GC×GC-FM-TOFMS/**FID**	Diesel (10 %)	0.11	0.22	-	-
4.3.4	GC×GC-FM-**TOFMS**/FID	Diesel (10 %)	0.10	0.26	-	-
4.3.5	GC×GC-SSM-FID	Diesel (10 %)	0.16	0.27	-	-
			Area (RSD %)			
			Oven Temperature		Secondary Oven	
Section	System	Sample	Within-Day	Day-to-Day	Within-Day	Day-to-Day
4.3.1	GC×GC-SSM-FID	Perfume	-	-	1.23	1.62
4.3.2	GC×GC-SSM-TOFMS	Diesel (10 %)	5.86	6.41	-	-
4.3.3	GC×GC-SSM-TOFMS	Perfume (10 %)	-	-	-	-
4.3.4	GC×GC-FM-TOFMS/**FID**	Diesel (10 %)	1.58	1.90	-	-
4.3.4	GC×GC-FM-**TOFMS**/FID	Diesel (10 %)	1.66	1.99	-	-
4.3.5	GC×GC-SSM-FID	Diesel (10 %)	3.52	2.94	-	-

Table 4-29: Summary of the reproducibility of the GC×GC system using the ²DTPS for both ²D temperature programming and ²D constant positive temperature offset. The RSD (%) from 4.3.2 used the values from the persistence algorithm. Section 4.3.3 had higher than expected peak area RSD (%) due to vial-to-vial variation in concentration. Paired Student's t-test results when compared to the GC×GC system without the ²DTPS running are highlighted in green and orange to designate differences that were insignificant and significant, respectively.

GC×GC + ²DTPS						
			^1t_r (RSD %)			
			²D Temp. Prog.		Constant Offset	
Section	System	Sample	Within-Day	Day-to-Day	Within-Day	Day-to-Day
4.3.1	GC×GC-SSM-FID	Perfume	0.02	0.12	-	-
4.3.2	GC×GC-SSM-TOFMS	Diesel (10 %)	0.02	0.02	0.01	0.01
4.3.3	GC×GC-SSM-TOFMS	Perfume (10 %)	0.04	0.05	-	-
4.3.4	GC×GC-FM-TOFMS/**FID**	Diesel (10 %)	0.03	0.03	-	-
4.3.4	GC×GC-FM-**TOFMS**/FID	Diesel (10 %)	0.04	0.03	-	-
4.3.5	GC×GC-SSM-FID	Diesel (10 %)	0.02	0.05	-	-
			^2t_r (RSD %)			
			²D Temp. Prog.		Constant Offset	
Section	System	Sample	Within-Day	Day-to-Day	Within-Day	Day-to-Day
4.3.1	GC×GC-SSM-FID	Perfume	0.56	0.58	-	-
4.3.2	GC×GC-SSM-TOFMS	Diesel (10 %)	0.26	0.31	0.82	0.44
4.3.3	GC×GC-SSM-TOFMS	Perfume (10 %)	0.35	0.52	-	-
4.3.4	GC×GC-FM-TOFMS/**FID**	Diesel (10 %)	0.24	0.40	-	-
4.3.4	GC×GC-FM-**TOFMS**/FID	Diesel (10 %)	0.36	0.42	-	-
4.3.5	GC×GC-SSM-FID	Diesel (10 %)	0.29	0.43	-	-
			Area (RSD %)			
			²D Temp. Prog.		Constant Offset	
Section	System	Sample	Within-Day	Day-to-Day	Within-Day	Day-to-Day
4.3.1	GC×GC-SSM-FID	Perfume	1.18	1.53	-	-
4.3.2	GC×GC-SSM-TOFMS	Diesel (10 %)	2.47	3.05	3.73	4.88
4.3.3	GC×GC-SSM-TOFMS	Perfume (10 %)	4.44	10.35	-	-
4.3.4	GC×GC-FM-TOFMS/**FID**	Diesel (10 %)	1.78	3.21	-	-
4.3.4	GC×GC-FM-**TOFMS**/FID	Diesel (10 %)	1.71	3.37	-	-
4.3.5	GC×GC-SSM-FID	Diesel (10 %)	2.61	1.85	-	-

A summary of the reproducibility results from 4.3.1 to 4.3.5 for the GC×GC systems, without the ²DTPS and with the ²DTPS, is found in Table 4-28 and Table 4-29, respectively. Through five separate experiments, the ^1t_r reproducibility looked unaffected by the addition of the ²DTPS. The exception was the first experiment (4.3.1), where there was likely an issue with the GC ambient pressure sensor which was

supposed to compensate for the changes in atmospheric pressure day-to-day. For the ^2t_r, the increase in RSD (%) with the use of the ^{2}DTPS was significant in all experiments for both the within-day and day-to-day reproducibility. The average within-day RSD across the five experiments for the ^2t_r with ^{2}D temperature programming was 0.34 %, while the day-to-day RSD was 0.44 %. This was compared to an average (excluding section 4.3.1) within-day RSD of 0.13 % and day-to-day RSD of 0.23 % for the GC×GC separation without the ^{2}DTPS. The effect of the ^{2}DTPS on peak area reproducibility was less conclusive since many factors affect the absolute peak area. Although best efforts were made to ensure homogeneity between samples used within an experiment, slight differences between vials, sample evaporation, autosampler injection volume, split ratio, and software integration all play a role in the variability of peak area. With ^{2}D temperature programming, the average within-day reproducibility (excluding section 4.3.3) was 1.95 %, while day-to-day reproducibility was 2.60 %. Without the ^{2}DTPS, the average within-day reproducibility was 2.77 % while day-to-day reproducibility was 2.97 %.

The recommended power supply specification testing generated a substantial amount of data on the maximum offset and heating rate of the ^{2}DTPS, based on the power supply output and column dimensions. Using this data, the ^{2}DTPS can now estimate the maximum offset to within 10 °C based on the measured current (A) flowing through the column. Although the error was still larger than desired, the improvements to the PID temperature control code relaxed the requirements of the power supply output. This allowed for just two power supply output recommendations based on column dimensions: a power supply voltage that provides 1.9 A for the fastest heating rates and highest maximum offsets, and 1.5 A for more moderate to low heating rates and maximum offsets.

In conclusion, the ^{2}DTPS was tested with various modulators (thermal and flow) and detectors (ambient and vacuum), each with their own operational principles. The result was a comprehensive examination of the ^{2}DTPS under various ^{2}D column dimensions, flow rates and modulation periods to characterize its reproducibility, as well as its performance and drawbacks. The overall reproducibility of

the GC×GC system with the addition of the ^{2}DTPS was acceptable for routine analysis. The peak capacity and S/N were improved with ^{2}D temperature programming, which benefits the analysis of complex samples and identification of trace components.

5 Characterization of Renewable Hydrocarbon Samples

Many products, chemicals, and fuels are derived from petroleum, but efforts are being made to transition towards more sustainable, renewable, and environmentally friendly solutions [234, 235, 236, 237, 238, 239, 240]. These approaches replace the traditional feedstock, petroleum, with biomass, a renewable organic material from plants and animals. Biomass can be used in the production of fuels like biodiesel [236, 241] or jet fuel [242], bio-lubricants [235, 243], polyurethanes [238], personal care formulations [239], surfactants [240], and chemicals [244]. Research on new production processes and feedstocks is ongoing, to develop competitive bio-based products that are economical with characteristics comparable to or improved compared to their petroleum based counterparts. Approached by an Ontario based company, we were asked to help characterize products from various stages of their proprietary refining process [245, 246, 247]. A general overview of their production process is shown in Figure 5-1.

Figure 5-1: Ontario based company's production pathway of hydrocarbon products from plant oil and animal fats.

Fat splitting is a hydrolysis reaction involving one mole of triacylglycerol reacting with three moles of water to produce three moles of fatty acids (FAs) and one mole of glycerol. Industrial fat splitting methods include the Twitchell process and the Colgate-Emery process [248, 249]. The Twitchell process is the hydrolysis of fats in water, sulfuric acid, and a Twitchell reagent (alkylarylsulfonate or petroleum sulfonates), where the mixture is boiled for 12 – 20 hours in an open tank [248, 250]. The advantage of this technique is the low apparatus cost since high temperatures and pressures are not needed. The Colgate-Emery process, which largely replaced the Twitchell process, hydrolyzes the fats with water under high temperature (500 °F) and pressure (725 psi) in an industrial sized column without the need for catalysts [249]. For large scale production of fatty acids, this method is more economical compared to the

Twitchell method. The Ontario based company reacted a base, either sodium or potassium hydroxide, with the fats to yield glycerol and the salts of the fatty acids in a saponification reaction [245]. The fatty acid salts were then neutralized with mineral acid to yield free fatty acids (FFAs). Although this was done at the research stage, the Colgate-Emery process would be used in the industrial pilot-scale stage [245].

Following the fat splitting step was the decarboxylation of the free fatty acids (FFAs) through Kolbe electrolysis [245]. Kolbe electrolysis has not been used in industrial applications, in part due to its high energy consumption [246, 251]. Energy consumption can be improved, however, through careful selection of the feedstock to control the fatty acid composition of the reaction mixture [246]. A higher weight percentage of saturated fatty acids is needed to reduce the energy consumption. In the Kolbe electrolysis reaction, 2 moles of fatty acid salts are decarboxylated yielding radicals of the aliphatic chain which dimerize, with 2 moles of carbon dioxide as by-products. Unsymmetrical dimers would be produced from plant oil and animal feedstocks as triacylglycerols with three identical fatty acids are rare [252].

The final step in their production process was hydrofinishing, for the isomerization of alkanes and hydrogenation of double bonds using a bifunctional catalyst containing platinum and an alumina-silica solid acid catalyst [245]. Their patent also details an olefin metathesis reaction for the production of linear alpha olefins that can be used for the production of polymers, detergents, or fine chemicals [246]. A recent patent application was specifically for squalane and squalane derivatives using the same overall process [247]. The hydrocarbons produced in this stage would be separated for the various applications they were intended for.

5.1 Experimental

5.1.1 Characterization of Renewable Hydrocarbon Products – Samples L and H

Renewable hydrocarbon products, designated as L and H, were produced with the intention for use in personal care products. Samples were first characterized by GC×GC-TOFMS, using the Agilent 6890A GC

coupled with the Markes BenchTOF-Select and the SSM. Both undiluted and diluted samples were analyzed by GC×GC-TOFMS. Samples were diluted by adding 500 µL of the sample into a 5 mL volumetric flask and filling to the mark with *n*-hexane (Sigma-Aldrich). A standard *n*-alkane mix (C_7 to C_{24}) was prepared using individual alkane standards (Sigma-Aldrich) and injected under the same conditions to determine the ^{1}D linear retention indices. Following characterization of the different compound classes in each sample, the samples were then quantified by GC×GC-FID using the same column set. ^{2}D temperature programming was performed to optimize the ^{2}D separation and enhance the S/N of trace compounds. Three replicates were completed for each sample where the concentration of the compounds was estimated using toluene (Sigma-Aldrich) as the external standard. Calibration solutions were made by diluting toluene in hexane, with details found in Table D - 3.The GC×GC-TOFMS and GC×GC-FID conditions can be found in Table D - 1 of Appendix D.

5.1.2 Effect of the Refining Process on Sample L

Two batches of sample L from before and after their decoloring process, as well as a sample from before their hydrogenation step (pre-hydrogenated sample) were analyzed by GC×GC-FID/TOFMS. A reverse column set featuring an MXT-WAX column (20.8 m × 0.25 mm × 0.50 µm + 23.624 m × 0.25 mm × 0.25 µm) in the ^{1}D and an MXT-1 column (0.625 m × 0.25 mm × 0.25 µm) in the ^{2}D was used for the separations. Due to insufficient length from a single MXT-WAX column, two MXT-WAX columns with the same inner diameter (0.25 mm) but different stationary phase thicknesses (0.25 µm and 0.50 µm) were connected using a SilTite mini-union for the ^{1}D column. The same hardware from section 5.1.1 was used, with the addition of a purged splitter (Agilent G3180B) for dual detection. The purged splitter was connected to the back inlet of the GC to apply a constant pressure of 2 psi. The same standard *n*-alkane mix (C_7 to C_{24}) from section 5.1.1 was used to determine the ^{1}D linear retention indices of the compounds. The GC×GC-FID/TOFMS conditions can be found in Table D - 5, while the flow rates between the splitter and detectors are presented in Table D - 6 of Appendix D.

5.1.3 Characterization of Kolbe Electrolysis By-Products

Wax by-products from the Kolbe electrolysis process were characterized using the same GC×GC-FID/TOFMS setup from 5.1.2. The solid wax samples were weighed into 10 mL volumetric flasks and diluted to mark with CS_2. Final sample concentrations are found in Table D - 7 of Appendix D. A backflush of 10x the void volume was applied at the end of the run to remove the heavier hydrocarbons (C_{30}, C_{32}, C_{34}, C_{36}) and FAs (> C16:0). These compounds were analyzed by GC-MS (Agilent 6890 GC/5973 MSD) using a Zebron-5HT Inferno column and running a linear temperature program to 400 °C. Details of the GC-QMS method are found in Table D - 8 of Appendix D. The following standards were used to confirm the elution region on the GC×GC chromatogram for each class of compounds: 1-undecene (TCI America, OR, USA), 1-dodecene (Dr. Gauthier, Department of Chemistry, UW), 1-tridecene (TCI America), 1-tetradecene (TCI America), cyclododecane (TCI America), 1-hexadecanol (Dr. Chong, Department of Chemistry, UW), 2-hexadecanol (Sigma-Aldrich), palmitic acid (Sigma-Aldrich) and metyl hexadecanoate. Some chemicals were obtained from other groups in the Department of Chemistry at the University of Waterloo. These were old chemicals whose source was unknown. Methyl hexadecanoate (C16:0 FAME) was produced from palmitic acid according to the method by Ichihara and Fukubayashi [253]. Two *n*-alkane mixes (C_7 - C_{24} and C_7 - C_{24}, C_{28}, C_{32}, C_{36}, C_{40}; Sigma-Aldrich) were used to determine the linear ^{1}D RI of the GC×GC-FID/TOFMS and GC-MS separations, respectively. Details of the GC×GC-FID/TOFMS method and the pressure program used for the backflush are found in Table D - 9 and Table D - 10 of Appendix D.

5.2 Results and Discussion

5.2.1 Renewable Hydrocarbon Products

Samples L and H were first characterized by GC×GC-TOFMS to determine the different classes of compounds present. Significant tailing was observed for the higher concentration compounds (primarily

linear and branched alkanes) when using the BenchTOF. The tailing was due to the closed design of the ion source which was previously reported [254]. A comparison of the GC×GC chromatograms for the undiluted samples (TOFMS and FID) and 10 times diluted samples (TOFMS) are shown in Figure D - 1 of Appendix D. Although a 10 times dilution in hexane reduced the tailing of both samples L and H, substantial tailing was still observed. GC×GC conditions for both the GC×GC-TOFMS and GC×GC-FID setup were similar, with the differences being the injection amount (TOFMS: 0.2 µL with 400:1 split; FID: 1.0 µL with 100:1 split), flow rate (TOFMS: 2.0 mL/min; FID: 4.0 mL/min), and column outlet conditions (TOFMS: vacuum; FID: ambient). Tailing was not observed with the FID signal, demonstrating that the tailing peaks were not due to the chromatographic system but were detector specific.

The stencil feature in the ChromeSpace software was used to draw around the regions where each class of compounds eluteed within the GC×GC chromatogram (Figure 5-2). These stencils were drawn using the parametric filtering feature within ChromSpace as a guide to highlight the different classes of compounds. Parametric filtering displays data points which match the ion abundance rules set [255, 256, 257]. These rules were expressions which evaluate the mass spectrum and retention times (^1t_r, ^2t_r) for peak classification based on the expected fragmentation patterns for a compound class and their expected retention times based on the column set. Parametric filter expressions were used for linear (*n*) and branched (*i*) alkanes, mononaphthenes/alkenes, dinaphthenes, monoaromatics, and naphthalenes. The expressions used can be found in Table D - 2 of Appendix D. The expression for trinaphthenes, from Lissitsyna et al. [257], did not work for the samples as the perhydrophenalene peak (tentatively identified based on RI, mass spectrum and elution region) was not highlighted. A stencil for trinaphthenes was drawn between the monoaromatics and dinaphthenes, where it was expected to elute, following the same pattern as the other compound classes. 2-methylnaphthalene was also found in both samples, but a stencil was not drawn around the region since it was eluting with the monoaromatics due to wraparound. Since there can be mismatches or compounds not categorized when using this approach [255, 256], the

resulting chromatograms following parametric filtering were verified based on their mass spectra and ^{1}D linear retention indices.

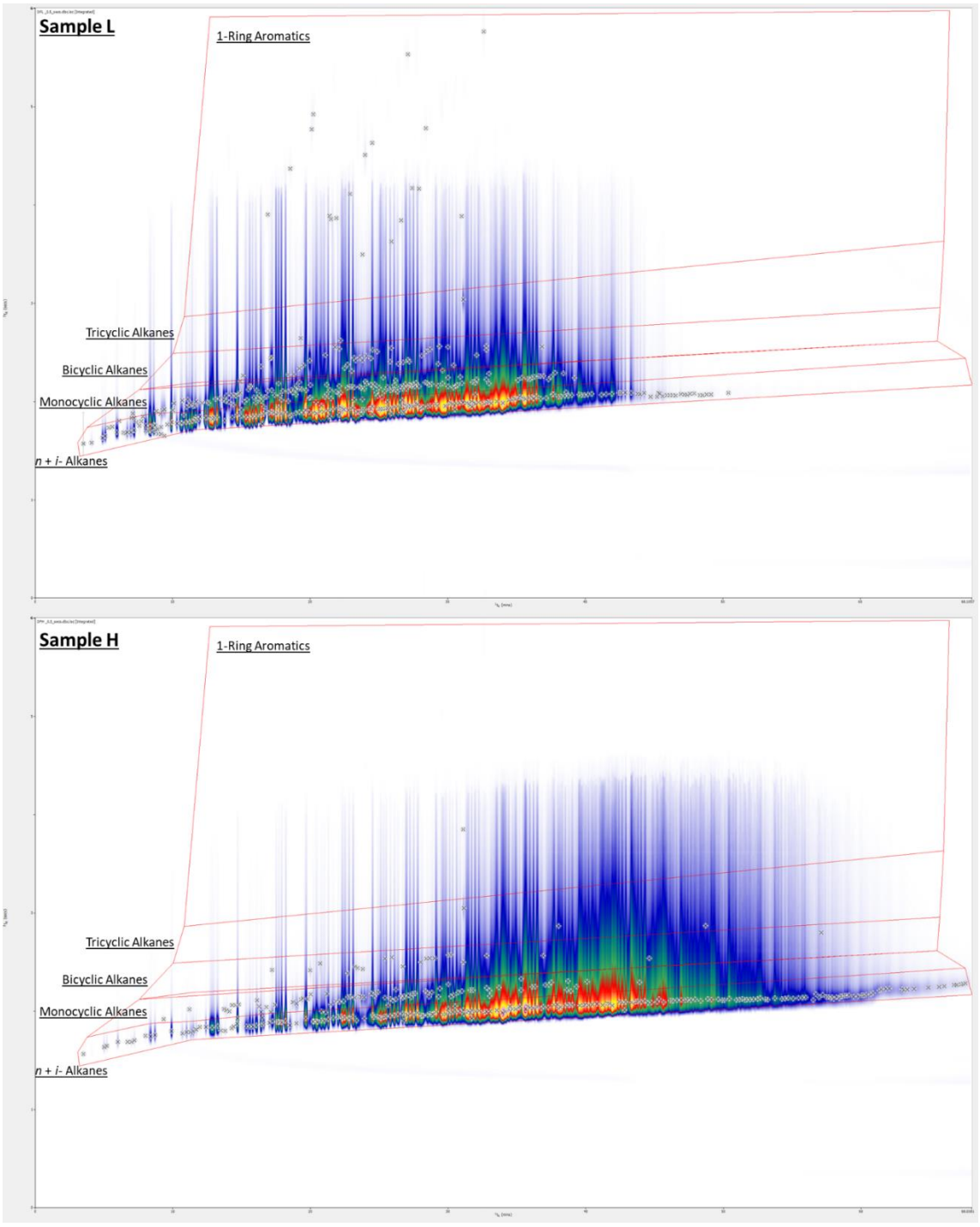

Figure 5-2: GC×GC-TOFMS separations of undiluted samples of L and H. Stencils were drawn around each class of compounds (n+i-alkanes, mononaphthenes and alkenes, dinaphthenes, trinapthenes, monoaromatics) that could be differentiated by parametric filtering. The stencil for diaromatics was not drawn due to a full wraparound where compounds from this class were eluting with the monoaromatics. ***X-axis: 0 – 68.1 min. Y-axis: 0 – 6 s****.*

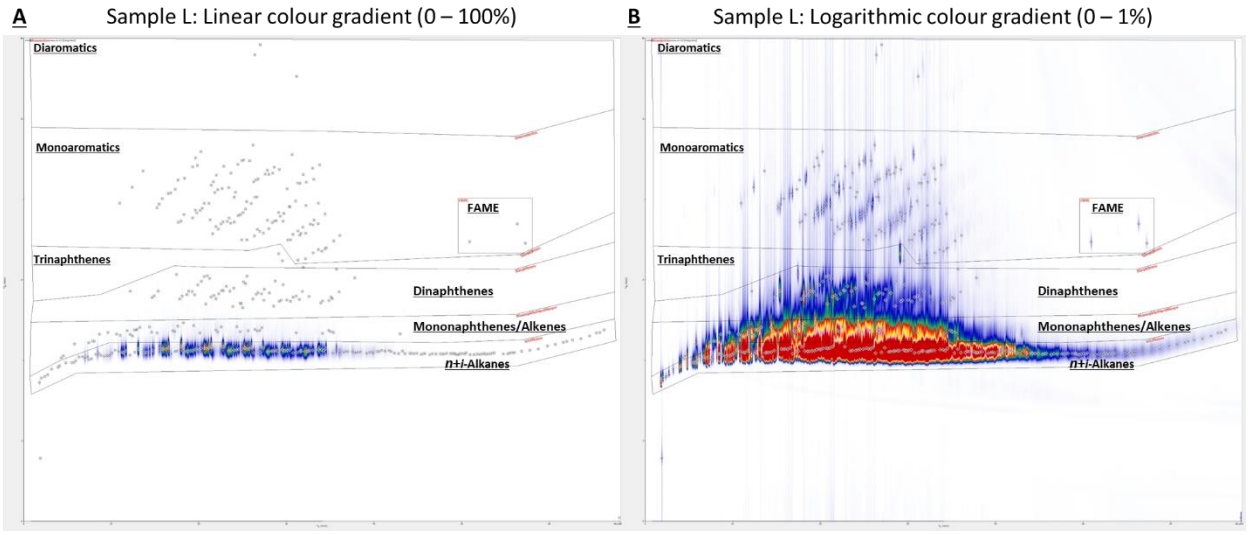

Figure 5-3: GC×GC-FID separation of sample L. (A) Shows a linear colour gradient from an intensity of 0 to the tallest peak. (B) Shows a logarithmic colour gradient from 0 to 1 % of the tallest peak. ***X-axis: 0 – 68.1 min. Y-axis: 0 – 6 s****.*

After the compound classes were identified, the samples were analyzed by GC×GC-FID for group-type semi-quantitation. ^{2}D temperature programming was applied to improve the S/N of the trace aromatics in the sample and eliminate wraparound peaks to identify the diaromatics in the sample. The same column set and GC temperature program were used to maintain the overall elution pattern of the different compound classes from the GC×GC-TOFMS separation. The flow rate was increased from 2 mL/min to 4 mL/min to increase the ^{2}D linear velocity and reduce the ^{2}D dead time to provide more ^{2}D space for separation. Figure 5-3 shows the GC×GC-FID separation of sample L with both a linear (A) and logarithmic (B) colour gradient. Although the data was the same, using a logarithmic gradient and setting the maximum intensity of the colour gradient to 1 % of the tallest peak highlighted the trace compounds in the sample, which was difficult to visualize due to the large difference in concentrations between the different compound classes. This helped with drawing stencils around the trace compounds. Dual detection (GC×GC-FID/TOFMS) could have been implemented using a purged splitter following the ^{2}D column when using the SSM or an unpurged splitter when using the Insight flow modulator. This would have reduced the analysis time and simplified the group type identification in the FID chromatogram. However, utilizing a purged splitter following the ^{2}D column would increase the ^{2}D column outlet pressure

and reduce the ^{2}D linear velocity. This would increase the ^{2}D dead time and make optimizing the ^{2}D temperature program more difficult. Utilizing the flow modulator with an unpurged splitter, like in section 4.2.4, would be more restrictive in method optimization (^{2}D column dimensions, modulation period, ^{1}D and ^{2}D flow rate) and would reduce the flexibility (lower maximum heating rate and offset, reduced duration for heating and cooling) of the ^{2}D temperature program. Taking into consideration all the above factors, this setup was not pursued at the early stages of the collaboration for only two samples.

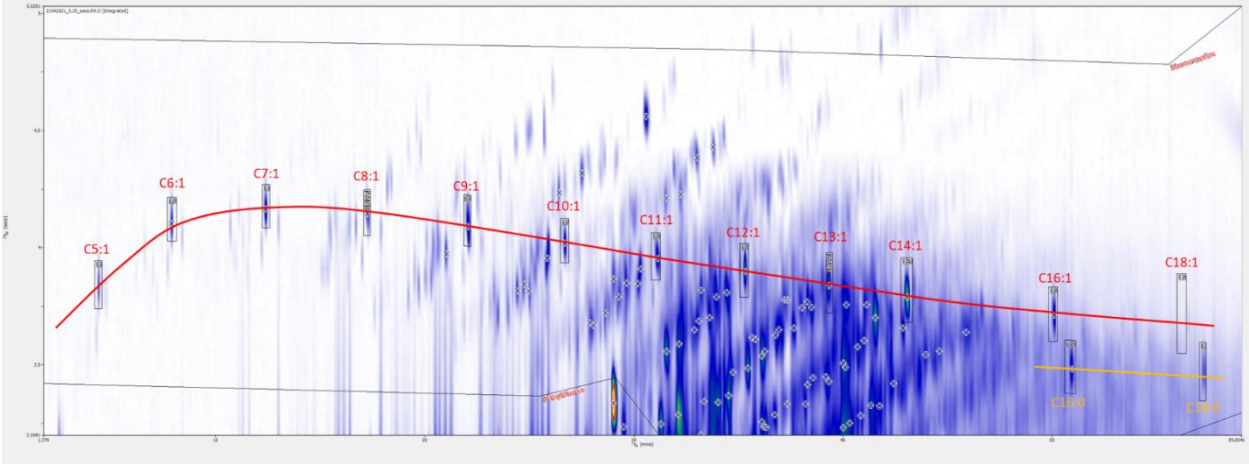

Figure 5-4: Suspected FAME peaks based on RI and elution pattern from the GC×GC-FID separation of sample H. ***X-axis: 1.779 - 59.05 min. Y-axis: 3.1991 – 5.0291 s****.*

In Figure 5-3B, three additional peaks that did not follow the elution pattern of the other compound classes were found. These peaks were not noticed or integrated in the GC×GC-TOFMS chromatogram due to the low ion abundance. The default deconvolution settings applied a minimum ion count of 2000, which helps reduce noise, while the ion count was <600 for the base peak of the mass spectra. The top match for two of the three peaks were hexadecanoic acid methyl ester (FAME C16:0) and octadecanoic acid methyl ester (FAME C18:0), which was corroborated by their ^{1}D linear RI. The third peak was unfortunately coeluting with bleed and could not be tentatively identified or deconvoluted, but an extracted ion chromatogram of 74 m/z, a characteristic ion for FAMEs, showed a very faint peak. Based on the linear ^{1}D RI (2095), the unidentified peak may have been methyl oleate (FAME C18:1). Sample H also appeared to contain three FAME peaks, where two of the FAMEs were C16:0 and C18:0. The linear ^{1}D RI (1898) of the

third FAME peak would indicate that it may have been methyl palmitoleate (C16:1). In addition to the four prominent FAME peaks from the two samples, well separated from the monoaromatic peaks, a set of peaks suspected to be homologous to the C16:1 and C18:1 FAMEs was also observed. These peaks were eluting among the monoaromatic peaks in the chromatogram, as shown in Figure 5-4. Their linear ^{1}D RI ranged from 885 to 1695 with a retention index difference of approximately 100 units between each peak. The FAMEs found in the GC×GC-FID chromatogram of sample H were not detected in the GC×GC-TOFMS chromatogram. The average peak areas from the GC×GC-FID chromatogram for the FAMEs in sample H were roughly half of what was present in sample L, and the largest FAME peak (C16:0) in the GC×GC-TOFMS chromatogram of sample L only had a S/N of 6. The presence of FAMEs in these samples was unsurprising when considering the starting material and their production process. It was possible these FAMEs were excess reactants from the Kolbe electrolysis step, which were processed along with the aliphatic hydrocarbons in the final hydrofinishing process to yield FAMEs with an aliphatic tail of various lengths.

The FID response factors (RFs) for *n+i*-alkanes, cycloalkanes, alkenes, benzenes (alkyl-substituted), and naphthalenes (alkyl-substituted) are very similar, with the exception of benzene and toluene [231, 232, 258]. To estimate the concentrations for each class of compounds in the sample, toluene (not found in the sample) was used as an external standard. The relative response factor (RRF) calculated from the RFs reported by Rome and McIntyre for toluene (RF = 0.490) and decane (RF = 0.462) was 1.06 [259]. This was similar to the relative sensitivity value of toluene (1.07), published by Dietz, which was used to normalize the peak area for weight percent determination [231]. All other hydrocarbons (n+i-alkanes, cyclopentanes, cyclohexanes, monoaromatics (except benzene and toluene), and alkenes) had reported relative sensitivity values close to 1.0 [231]. Therefore, a correction factor of 1.07 was applied to the peak areas of the toluene calibration curve. Since the carbon atom from the carboxyl group (-COO) of the FAMEs does not contribute to the FID response, this reduces its response factor and an RRF needs to be

applied to correct for the decreased signal [260]. For FA or FAME quantitation, RRFs were typically calculated using a FAME as a reference and could not be related back to toluene for quantitation [261, 262]. Therefore, the theoretical RRF (with toluene as the reference) was calculated from the theoretical RFs of the corresponding FAMEs and toluene. The theoretical RFs were calculated based on combustion enthalpies, which were estimated from their molecular formulas [263]. For methyl hexadecanoate (C16:0) and methyl heptadecanoate (C17:0), their theoretical RRFs were 1.04 and 1.03, respectively. These RRFs were similar to the other hydrocarbon classes and were therefore not applied when taking into consideration the trace amounts found in the samples. The toluene calibration curves are found in Figure D - 2 to Figure D - 4, while the calibration data is found in Table D - 3 of Appendix D.

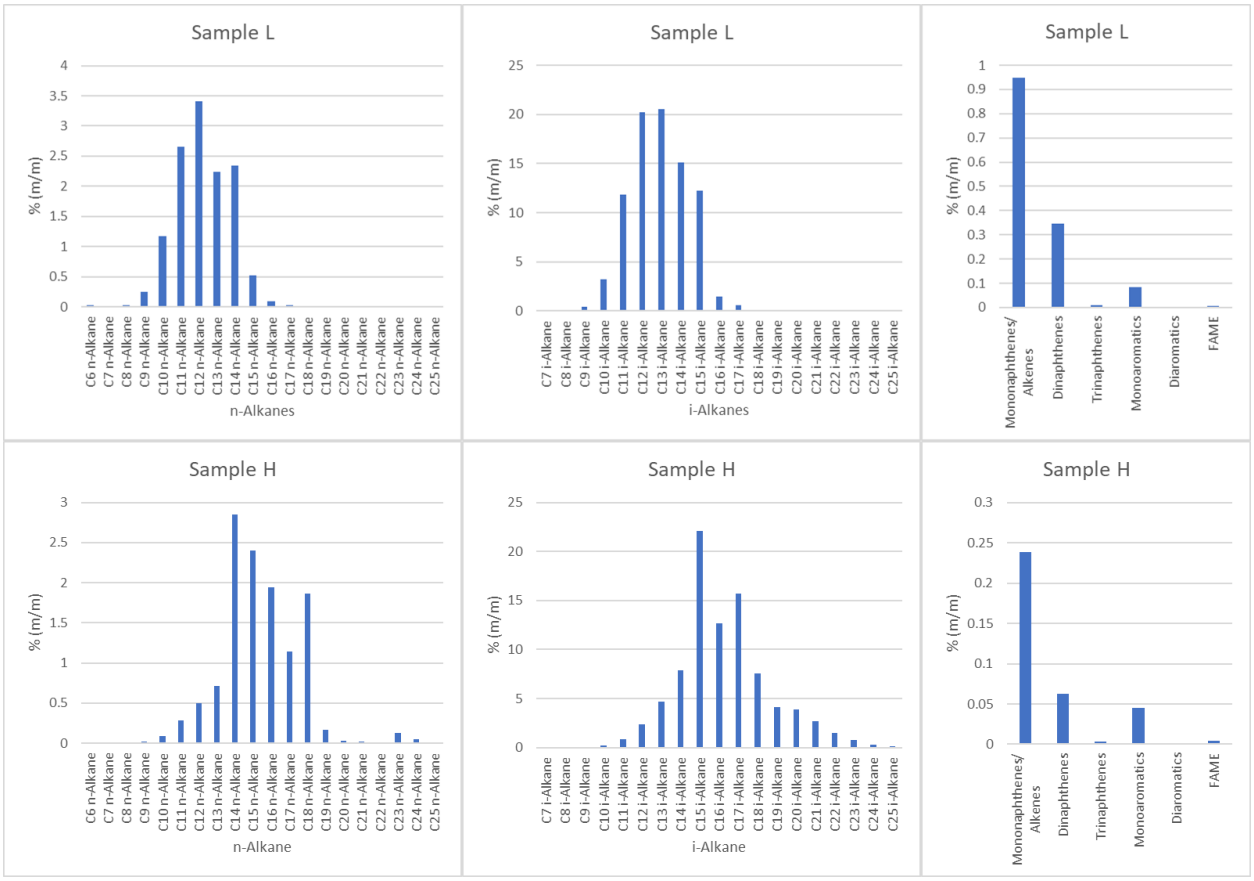

Figure 5-5: The n-Alkane, i-Alkane, mononaphthene/alkene, dinaphthene, trinaphthene, monoaromatic, diaromatic, and FAME distribution of samples L and H.

Samples L and H contained the same classes of compounds, with *n+i*-alkanes making up approximately 99% of the samples. Sample L contained a greater amount of naphthenes/alkenes, aromatics and FAMEs compared to sample H. The primary difference between samples L and H was the distribution of the *n+i*-alkanes, with sample L containing primarily alkanes in the range of C_9 to C_{17}, while sample H contained alkanes from C_{10} to C_{24}. The hydrocarbon group type distributions of samples L and H are found in Table D - 4 of Appendix D. The composition of the samples was similar to mineral oil, which is used in food additives, cosmetics, and pharmaceuticals [264]. For the quantitation of mineral oils in cosmetics, hydrocarbons are typically quantified into two groups: mineral oil saturated hydrocarbons (MOSH) and mineral oil aromatic hydrocarbons (MOAH) [264, 265]. Of particular concern are polycyclic aromatic hydrocarbons (PAHs) with three to seven rings that may be potentially carcinogenic [264, 265]. These compounds would need to be removed in the refining process in accordance with the European cosmetics regulation EC/1223/2009. Although aromatic hydrocarbons (one and two rings) were found in both samples, the only PAHs found were alkylated naphthalenes, which made up 0.001 % and 0.002 % of samples L and H, respectively. For medicinal grade white mineral oil used in both food and cosmetics, the MOAH quantity is typically less than 0.1 % [266]. For samples L and H, total aromatic content was found to be 0.08 % and 0.05 %, respectively. The FAME content in samples L and H was 0.01 % and 0.005 %, respectively. Although FAMEs are used in the cosmetics industry, it was unlikely they were intended to be in the final product [267]. Further purification in the production process would likely be needed for commercial applications.

5.2.2 Effect of the Refining Production Process

The two physical changes made to the previous GC×GC setup (section 5.1.1) was the use of a reverse column set and a purged splitter for dual detection (FID/TOFMS). Using a purged splitter produced both qualitative and quantitative data in a single separation, reducing the number of injections and processing time when trying to match the separations of two very different systems (GC×GC-FID and GC×GC-TOFMS).

The motivation for a reverse column set was the improved compound class separation for group type analysis, particularly for the separation between the *n+i*-alkanes and mononaphthenes. However, the addition of the purged splitter increased the ^{2}D column outlet pressure and was more difficult to optimize than previous setups.

5.2.2.1 Method Optimization

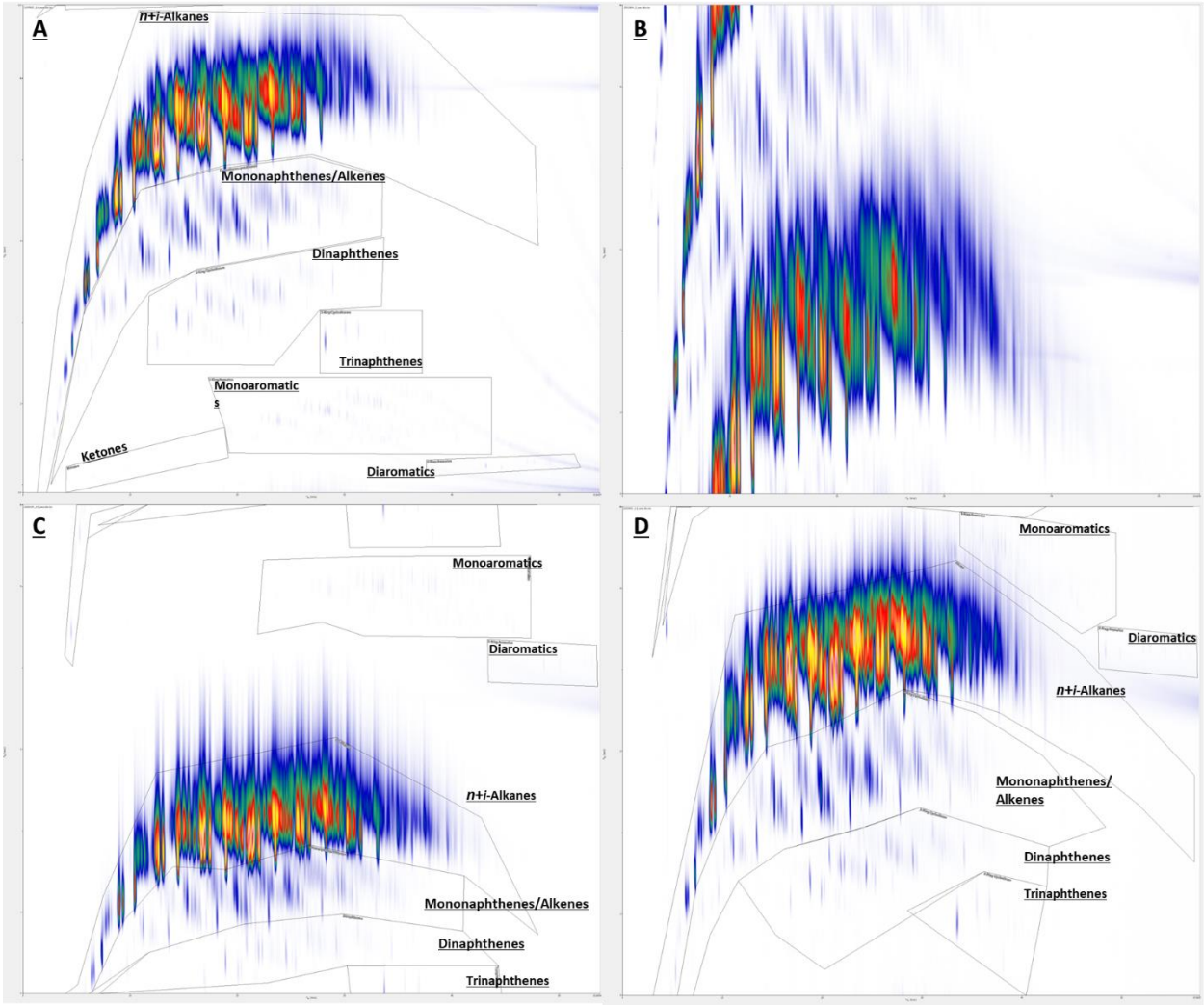

Figure 5-6: Method optimization using a pre-hydrogenated sample for the GC×GC-FID/TOFMS system with a reverse column set and purged splitter. (A) Optimized GC×GC-TOFMS separation for the pre-hydrogenated sample. ***X-axis: 0 – 53.8 min. Y-axis: 0.9 – 6.9 s****. (B) GC×GC-FID/TOFMS separation following the addition of a purged splitter with a constant auxiliary pressure set of 4 psi.* ***X-axis: 0 – 53.8 min. Y-axis: 0 – 6 s****. (C) Reduced column flow to 1.2 mL/min and constant auxiliary pressure to 2 psi.* ***X-axis: 0 – 53.8 min. Y-axis: 0 – 6 s****. (D) 3 second ^{2}D temperature program applied: 1.5 s delay followed by a 1.5 s linear ramp to a 30 °C offset (at 20 °C/s).* ***X-axis: 0 – 57.8 min. Y-axis: 0 – 6 s****.*

Shown in Figure 5-6 is the method optimization process of the GC×GC-FID/TOFMS system using a pre-hydrogenated sample which had a higher amount of aromatics compared to the previous samples. This ensured that all compound classes that were expected in these two batches of samples would be well separated. Figure 5-6A presents the optimized GC×GC-TOFMS separation of the pre-hydrogenated sample. The GC column flow was 2.0 mL/min (He) and the GC temperature program was 35 °C to 98 °C at 3 °C/min followed by a 2.5 °C/min ramp to 180 °C for a 53.8 min run. After the installation of the purged splitter for dual detection, the resulting separation of the pre-hydrogenated sample without any changes to the GC×GC method is shown in Figure 5-6B. The column dimensions between the splitter and the two detectors, as well as the auxiliary pressure applied (4 psi), were based on the example splitter configuration for an atmospheric detector (FID) and MS detector from the SepSolve manual [268]. Changing the ^{2}D column outlet pressure from vacuum to 4 psi resulted in a significant decrease in linear velocity in both the ^{1}D (40 cm/s to 32 cm/s) and ^{2}D (209 cm/s to 55 cm/s). Multiple wraparounds were observed where the most abundant *n+i*-alkanes peaks broadened to roughly 3 s, which was half the modulation period. The column flow was then reduced to 1.2 mL/min and the auxiliary pressure was lowered to 2 psi in Figure 5-6C. The ^{1}D linear velocity decreased to 24 cm/s, which increased the ^{1}D retention time and elution temperature of the compounds. The ^{2}D linear velocity also decreased to 37 cm/s, however, less wraparound was observed due to the higher elution temperature which resulted in less retention in the ^{2}D. In Figure 5-6D, a three second ^{2}D temperature program was applied for the six second modulation period. The ^{2}D temperature program was a 1.5 s delay followed by a 1.5 s linear temperature ramp to a 30 °C offset (at 20 °C/s). This was an effective ^{2}D temperature program after several preliminary experiments. The final GC oven temperature was also increased to 190 °C, but this would have no effect on the separation except extending the run time to 57.8 min. Overall separation and regions where each class of compounds eluted were similar to the GC×GC-TOFMS separation in Figure 5-6A. However, based on the elution time of the aromatic compounds which should have the least

retention on the PDMS (non-polar) stationary phase, all other compound classes (alkanes, naphthenes, alkenes) were wraparound peaks. Compared to Figure 5-6C, the overall GC×GC separation space was better utilized with the addition of ^{2}D temperature programming. This was the optimized method used for this set of samples.

5.2.2.2 Comparison of Samples Before and After Decoloring

Table 5-1: Group-type quantitation for two batches of renewable hydrocarbon samples before and after a proprietary decoloring process.

	Batch-1 Pre-Decoloring		**Batch-1 Decolored**		**Diff.**
	Area	Area %	Area	Area %	Area %
***n+i*-Alkanes**	18,603,770,808	98.20	19,101,161,333	98.27	0.07
Mononaphthenes Alkenes	283,413,319	1.50	276,777,672	1.42	-0.07
Dinaphthenes	55,435,476	0.29	57,102,087	0.29	0.001
Trinaphthenes	2,145,726	0.01	1,987,194	0.01	-0.001
Monoaromatics	6,816	0.00004	-	0.00	0.00
Diaromatics	-	0.00	-	0.00	0.00
Sum	18,944,772,144	100.00	19,437,028,285	100.00	
	Batch-2 Pre-Decoloring		**Batch-2 Decolored**		
	Area	Area %	Area	Area %	
***n+i*-Alkanes**	19,031,499,880	98.21	19,078,005,898	98.27	0.07
Mononaphthenes /Alkenes	287,826,657	1.49	276,374,018	1.42	-0.06
Dinaphthenes	57,755,769	0.30	56,967,821	0.29	-0.05
Trinaphthenes	2,003,553	0.01	2,043,239	0.01	0.00
Monoaromatics	-	0.00	-	0.00	0.00
Diaromatics	-	0.00	-	0.00	0.00
Sum	19,379,085,860	100.00	19,413,390,976	100.00	

	Sample L: Pre-Hydrogenated	
	Area	Area %
***n+i*-Alkanes**	19,077,839,098	98.27
Mononaphthenes /Alkenes	279,021,667	1.44
Dinaphthenes	54,487,306	0.28
Trinaphthenes	1,995,743	0.01
Monoaromatics	728,383	0.004
Diaromatics	377,977	0.002
Sum	19,379,085,860	100.00

After stencils were drawn around each class of compounds using the same procedure as 5.2.1, the FID data was integrated to compare the area % of each class of compounds. Since quantitation was not requested, the area % was sufficient for the purpose of understanding any compositional changes during the decoloring process. Stencils for the *n+i*-alkane region were not further separated into their carbon numbers as these were the same products (sample L) with the same distribution of alkanes. Comparing the pre-decoloring and decolored samples from both batches, the decoloring process resulted in very little change in the overall hydrocarbon composition of the sample. The area % of mononaphthenes/alkenes decreased by 0.06 - 0.07 %, while the area % of alkanes increased by 0.07 %. Other groups of hydrocarbons had little to no change in area %. The purpose of the decolorization process was the removal of pigments [269], which are not amenable to analysis by GC. Other color-inducing molecules which were amenable to GC were the aromatic compounds [270]. The trace amounts of monoaromatics found in batch 1 were removed after the decoloring step. The pre-hydrogenated sample analyzed contained 0.004 % and 0.002 % of monoaromatics and diaromatics, respectively. Based on the samples received and analyzed from the company previously (not discussed), the hydrogenation treatment occurred before the decolorization step. Although this pre-hydrogenated sample did not belong to either batches of sample L, the difference in aromatic content between the pre-hydrogenated and the pre-decoloring samples would indicate that the hydrogenation process removed most of the aromatics in the sample.

5.2.3 Characterization of Kolbe Electrolysis By-Products

The GC×GC-FID/TOFMS method used in 5.1.2 was further optimized using the pre-hydrogenated sample in Figure 5-7. The ^{2}D temperature program in Figure 5-7A was updated to match the modulation period (6 s) to use a 2.5 s linear temperature ramp to +30 °C (at 12 °C/s), where it was held for 0.5 s before cooling back to oven temperature over 3 s. The overall separation was similar to Figure 5-6D, but with narrower peak widths for the *n+i*-alkanes. This ^{2}D temperature program was used for the rest of the experiments. Figure 5-7B addressed the increase in ^{2}D retention time for the compounds eluting from

21 min in the separation when the GC temperature programming rate changed from 3 °C/min to 2.5 °C/min. Although this was effective for the GC×GC-TOFMS separation (Figure 5-6A), it was not necessary for this setup with the purged splitter. A single temperature ramp was used instead, where the new GC temperature program was 35 °C to 190 °C at 3 °C/min. Following the initial analysis of the wax by-products by GC×GC-FID/TOFMS, it was found that the sample contained trace hydrocarbons in the range of 9 to 14 carbons, but was predominantly made up of heavier hydrocarbons (>C_{15}) and a variety of oxygenated species. Due to the abundance of heavier hydrocarbons and oxygenated species that have greater retention on the ^{1}D column, the starting temperature of the temperature program was increased to 100 °C, while the final temperature was raised to 230 °C, where it was held for 18 min. The temperature programming rate remained unchanged.

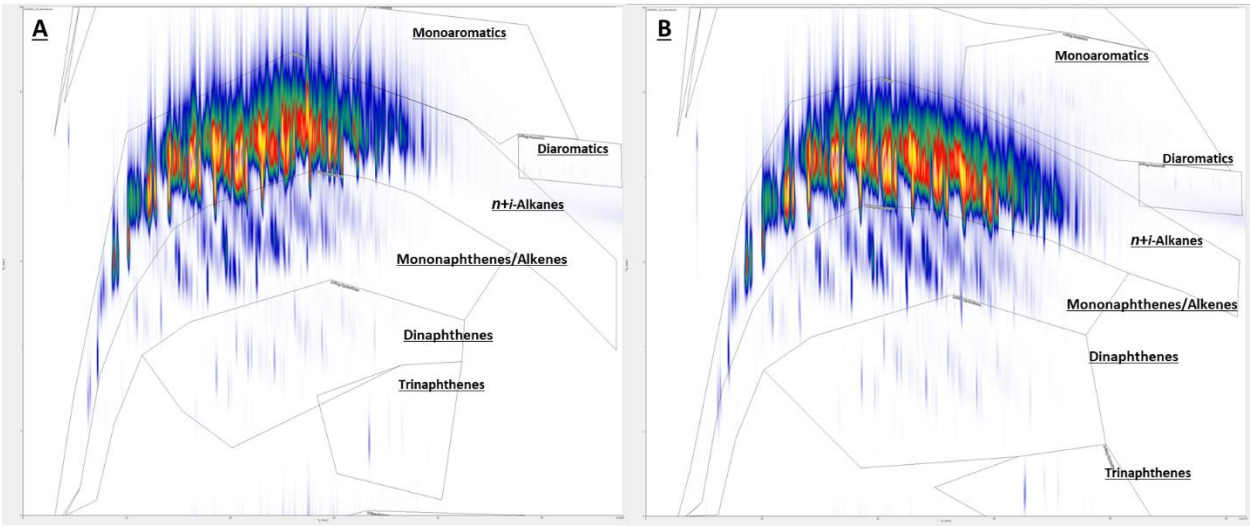

Figure 5-7: Further optimization of the GC×GC-FID/TOFMS method using the pre-hydrogenated sample. (A) Six second ^{2}D temperature program applied: 2.5 s linear temperature ramp to a 30 °C offset (at 12 °C/s), where it was held at +30 °C for 0.5 s and cooled in the final 3 s of the modulation period. ***X-axis: 0 – 57.8 min. Y-axis: 0 – 6 s****. (B) GC temperature program changed from two ramps to a single ramp: 35 °C to 190 °C at a rate of 3 °C/min.* ***X-axis: 0 – 51.67 min. Y-axis: 0 – 6 s****.*

Wax by-products from the Kolbe electrolysis process were characterized by GC×GC-FID/TOFMS and GC-QMS. Initial work during the method optimization exhibited carry over peaks (high boiling point alkanes) from prior injections. Subsequent analysis by GC-QMS on the high temperature ZB-5HT Inferno column (temperature limit: 430 °C) showed that these samples were primarily a mixture of these high

boiling point alkanes (C_{30}, C_{32}, C_{34}, C_{36}). Since these compounds could not be eluted within a reasonable run time with the temperature limitation of the MXT-WAX column (260 °C), a backflush was necessary at the end of the analysis. Thus, characterization of the wax samples was completed by GC×GC-FID/TOFMS, and any highly boiling compounds lost in the backflush would be characterized by GC-QMS. Identification of the compounds relied on the mass spectra from both the Markes BenchTOF and Agilent 5973, the ^{1}D linear RI on both the polar stationary phase (GC×GC: MXT-WAX) and non-polar stationary phase (GC: 5%-phenyl-95%-dimethylpolysiloxane), and the elution pattern in the GC×GC chromatogram. Findings from the GC-QMS analysis were summarized but not discussed in detail as they were not relevant to this thesis. Seven wax samples were received and analyzed, but the focus of the discussion will be on the tentative identification of sample T2 that contained the greatest diversity of compound classes. As a result of the project ending prematurely due to the company's financial circumstances, further work beyond the characterization of the samples was not performed.

5.2.3.1 Tentative Identification of Compounds

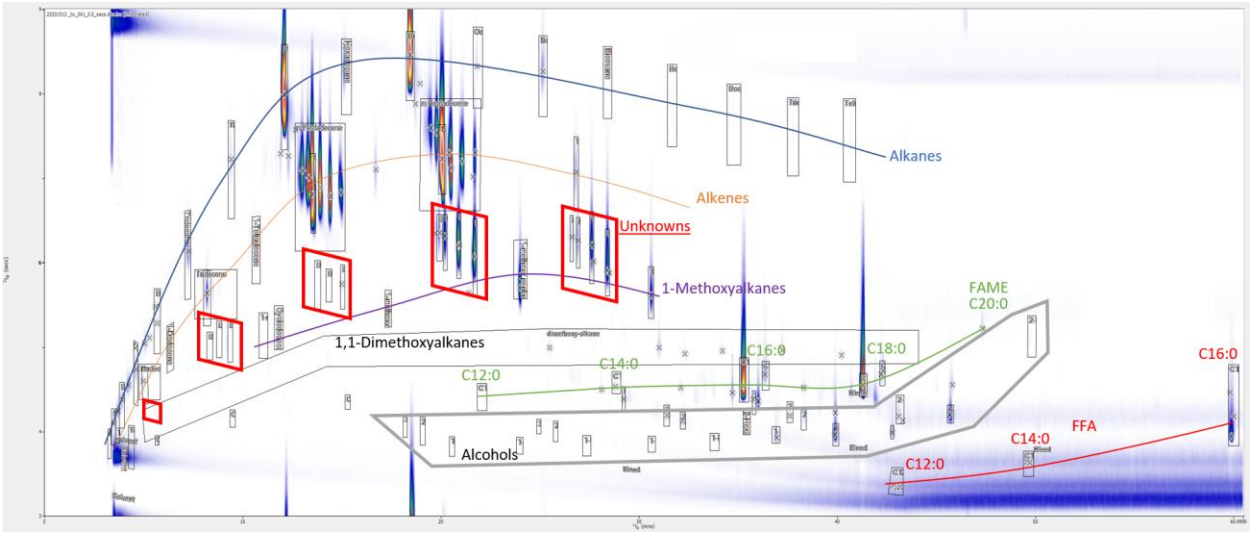

Figure 5-8: GC×GC-FID/TOFMS separation of wax sample T2 with various compound classes labeled.

The GC×GC-FID/TOFMS chromatogram for sample T2 is shown in Figure 5-8. Standards for 1-alkenes (C_{11}, C_{12}, C_{13}, C_{14}), cycloalkane (C_{12}), 1-alcohol (C_{16}), 2-alcohol (C_{16}), FA (C_{16}), and FAME (C_{16}) were used to

verify the elution region for the respective compound classes. A summary of the compounds identified in the wax samples from the GC×GC-FID/TOFMS and GC-MS separations is found in Figure D - 10 of Appendix D.

5.2.3.1.1 Alkene Identification

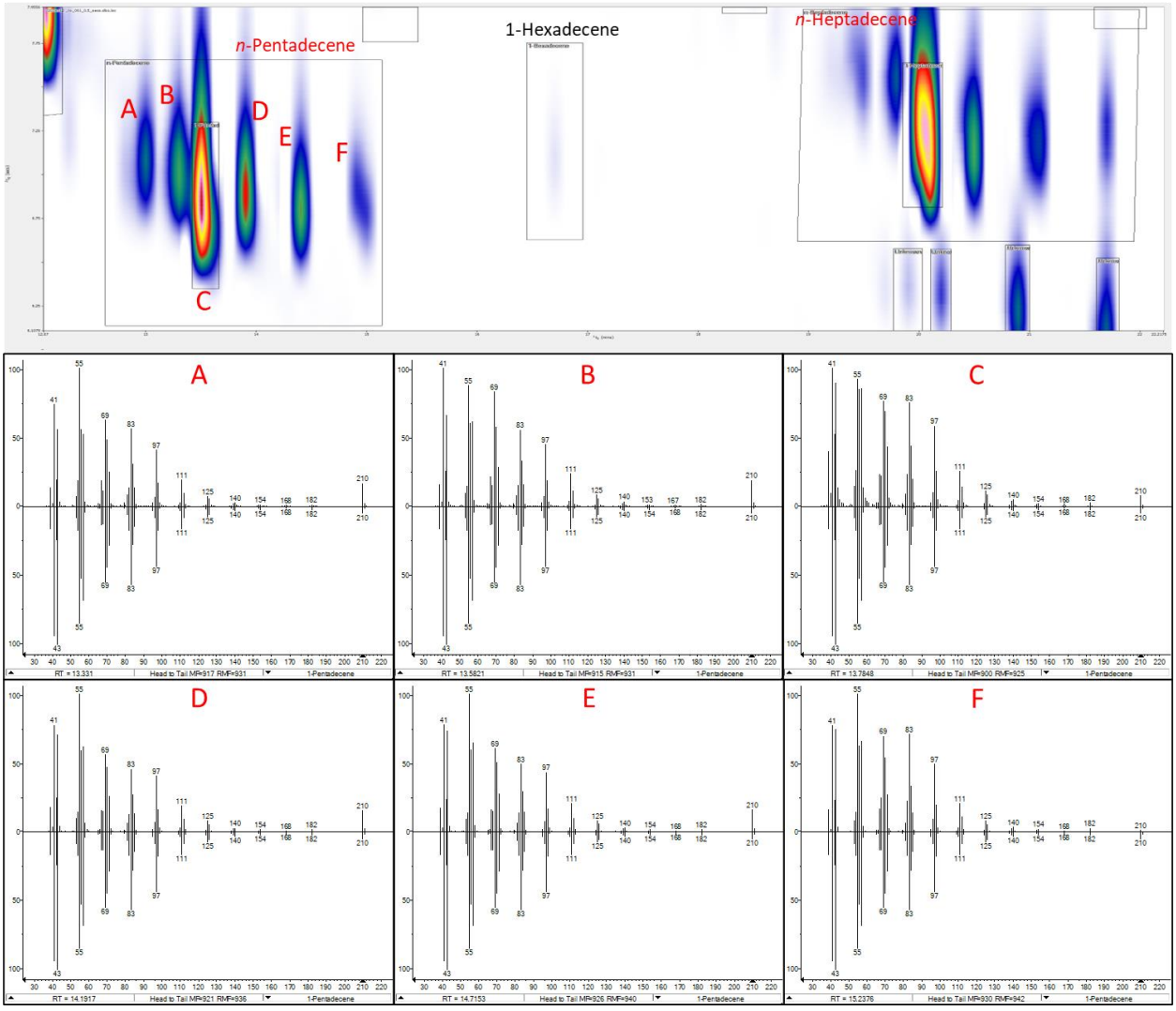

Figure 5-9: Upper: Two groups of peaks from the wax sample, T2, were tentatively identified as n-pentadecene and n-heptadecene. Lower: Head-to-tail plots showing the spectral match of the unknown to the top hit (1-pentadecene) from the NIST 17 MS library (EI) search. The mass spectra for the six n-pentadecene peaks are labeled as A to F. The RI (wax column) ranged from 1526 to 1589.

Shown in Figure 5-9 is a group of *n*-pentadecene and *n*-heptadecene peaks. The mass spectra for the six *n*-pentadecene peaks were very similar, with the top hit being 1-pentadecene for all peaks. Although the mass spectra were similar, the base peak for spectra A, D, E, and F was 55 m/z, while B and C had a

base peak of 41 m/z. Taking into account these slight differences in the mass spectra and the relative peak areas between the six peaks, these peaks were matched to peaks found in the GC-MS separation. The most abundant *n*-pentadecene peak was tentatively identified as 1-pentadecene, with a RI of 1543 (library: 1544) on the MXT-WAX column and 1491 (library: 1493) on the Zebron-5HT. The same procedure was followed for the other groups of alkene peaks found in sample T2 (*n*-heptadecene) and other wax samples.

5.2.3.1.2 1-methoxyalkanes and 1,1-dimethoxyalkanes

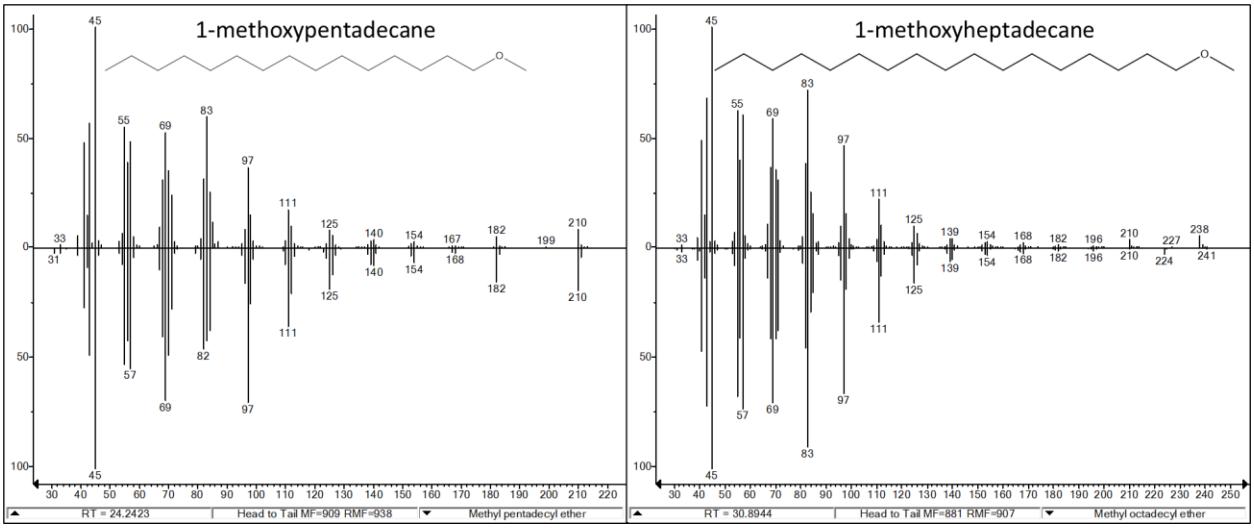

Figure 5-10: Head-to-tail plots showing the spectral match of the unknown to the top hit from the NIST 17 MS library (EI) search. Mass spectra for peaks tentatively identified as 1-methoxypentadecane and 1-methoxyheptadecane found in wax sample T2.

The mass spectra for two peaks tentatively identified as 1-methoxypentadecane and 1-methoxyheptadecane, found in sample T2, are shown in Figure 5-10. Characteristic fragments for 1-methoxyalkanes include the base peak at 45 m/z [-CH_2-OMe], an $M^+ - 32$ fragment from the loss of MeOH, and the groups of peaks separated by 14 m/z from the loss of CH_2 [271]. The RI of 1-methoxypentadecane was 1858 on the MXT-WAX and 1725 on the Zebron-5HT. Although its RI was not available in the NIST (2017) library, it was available for 1-methoxydodecane (VF-5MS: 1424), 1-methoxytetradecane (5 % phenyl: 1632), and 1-methoxyoctadecane (5 % phenyl: 2034). The RI difference (ΔRI) between the successive 1-methoxy-*n*-alkanes was approximately 100 units. Based on the RI of 1-methoxyalkanes available in the library, the expected RI on the Zebron-5HT column should be between 1724 to 1734,

which was in line with the experimental RI of 1725. The 1-methoxyheptadecane peak was identified based on the characteristic fragments in its mass spectra ($M^+ - 32$ fragment of 238 m/z, base peak of 45 m/z), elution region on the GC×GC chromatogram, and its RI on both stationary phases. Its mass spectrum was not available in the NIST library. The RI was 2060 and 1925 on the MXT-WAX and Zebron-5HT columns respectively, which agrees with the expected ΔRI of 200 units on both columns.

Table 5-2: Retention index data for 1,1-dimethoxyalkanes found in the wax samples. Only 1,1-dimethoxypentadecane was found in the GC-MS separation.

		Experimental		NIST Library	
Compounds	$M^+ - 31$	MXT-Wax (RI)	Zebron-5HT (RI)	Wax (RI)	5% Phenyl (RI)
1,1-Dimethoxyhexane	115	1164	-	1156	980
1,1-Dimethoxyheptane	129	1264	-	1265	1080
1,1-Dimethoxyoctane	143	1363	-	1366	-
1,1-Dimethoxynonane	157	1463	-	1465	-
1,1-Dimethoxydecane	171	1565	-	1567	-
1,1-Dimethoxyundecane	185	1667	-	1668	-
1,1-Dimethoxydodecane	199	1769	-	1769	-
1,1-Dimethoxytridecane	213	1870	-	-	-
1,1-Dimethoxytetradecane	227	1970	-	-	-
1,1-Dimethoxypentadecane	241	2072	2071	-	-
1,1-Dimethoxyhexadecane	255	2174	-	-	-
1,1-Dimethoxyheptadecane	269	2272	-	-	-
1,1-Dimethoxyoctadecane	283	2370	-	-	-

1,1-Dimethoxyalkanes have a base peak at 75 m/z (MeO-CH-Ome) and an an $M^+ - 31$ fragment from the loss of -Ome. For wax sample T2, 1,1-dimethoxyalkanes with an alkyl carbon length of C_6 to C_{18} were detected in the GC×GC separation. Only 1,1-dimethoxypentadecane was found in the GC-MS separation due to the trace amount found in the sample for other 1,1-dimethoxyalkanes. The higher sensitivity of the GC×GC separation was due to the greater resolution from the comprehensive 2D separation, the focusing effect of the SSM, and further improvement in S/N and peak capacity from the ^{2}DTPS. RI data are summarized in Table 5-2.

5.2.3.1.3 Fas, FAMEs, FAEEs

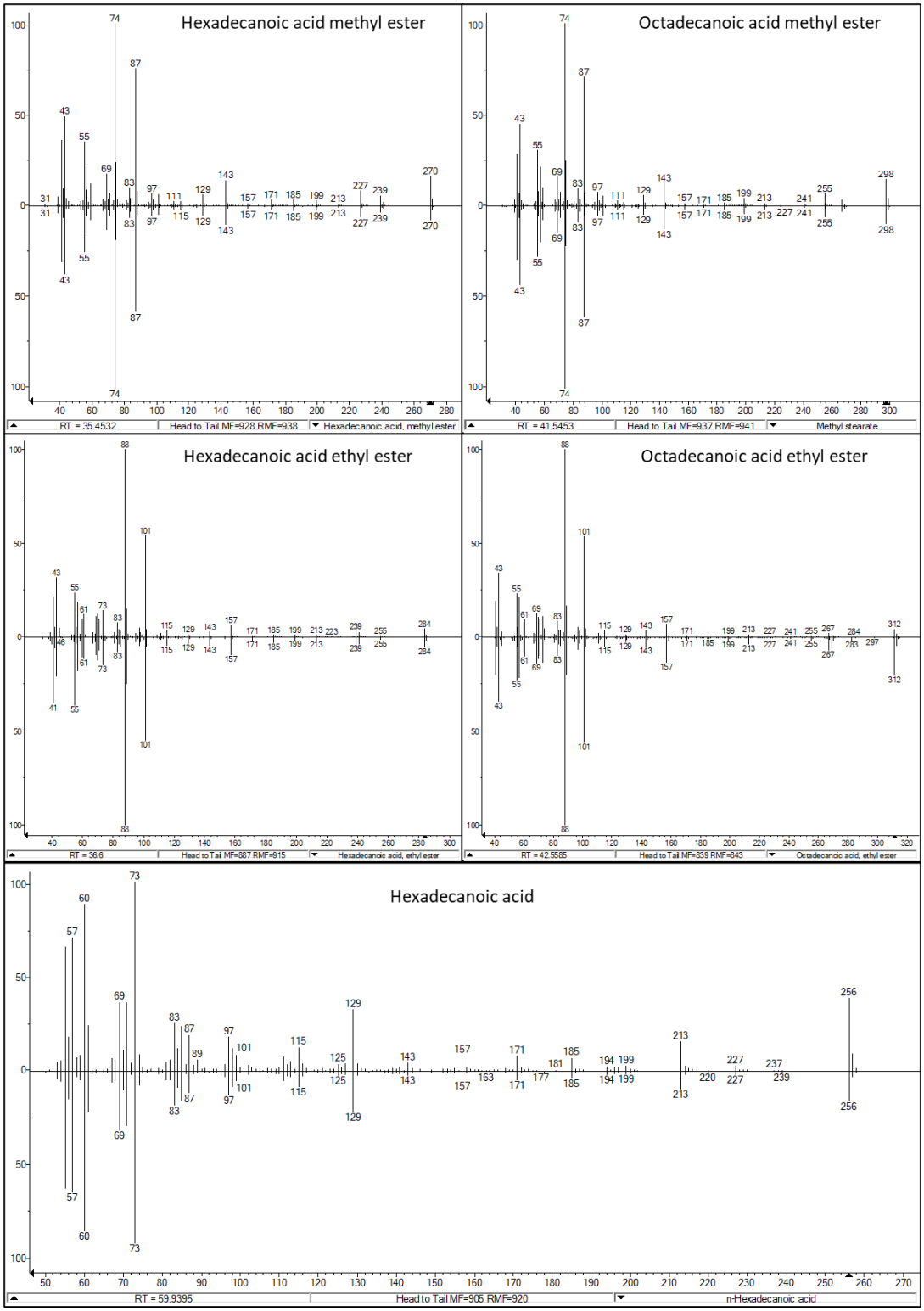

Figure 5-11: Head-to-tail plots showing the spectral match of the unknown to the top hit from the NIST 17 MS library (EI) search. Mass spectra for C16:0 (FA, FAME, FAEE) and C18:0 (FAME and FAEE) found in wax sample T2.

Shown in Figure 5-11 are the mass spectra of a FA, FAMEs, and FAEEs found in wax sample T2. FAMEs have characteristic fragment ions at 74 m/z [$CH_3OCOHCH_2$, McLafferty] and 87 m/z [$CH_3OCOC_2H_4]^+$, while the relative abundance of the molecular ion increases with the alkyl chain length [272]. Two prominent peaks for C16:0 and C18:0 FAMEs were found in sample T2, while other FAMEs (C8:0, C12:0, C14:0, C15:0, C17:0) were only found in trace amounts. The fatty acid ethyl esters (FAEEs) of C16:0 and C18:0 were also found in the sample, eluting near the FAMEs. The characteristic fragments of FAEEs were 88 m/z and 101 m/z, an increase of 14 m/z from the characteristic fragments of FAMEs due to the additional methylene group (CH_2). Hexadecanoic acid was also found, while octadecanoic acid was lost in the backflush but detected in the GC-MS separation. C16:0 FAME was confirmed using the standard produced from palmitic acid.

5.2.3.1.4 Linear Alcohols

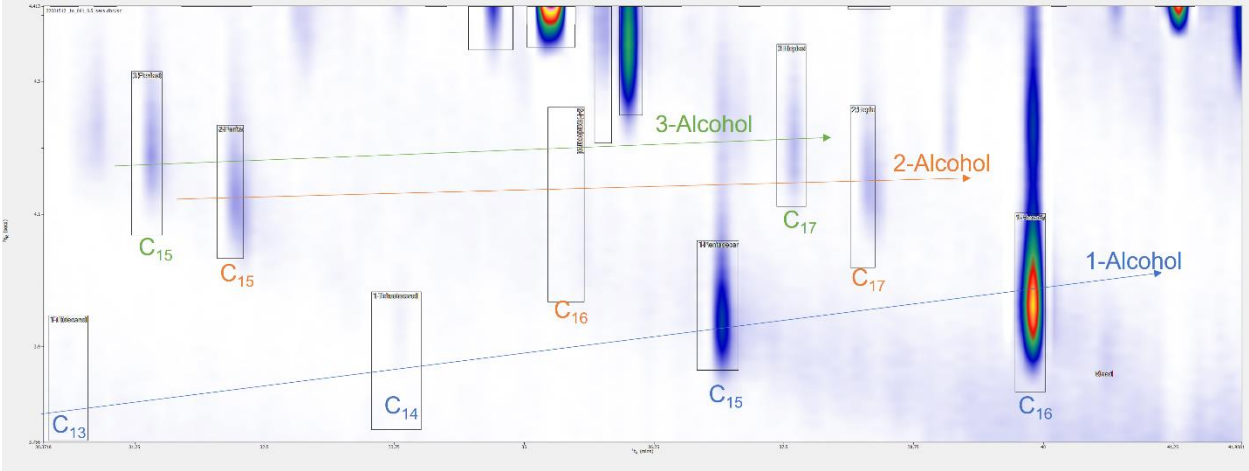

Figure 5-12: GC×GC separation of wax sample T2, zoomed into the region where the linear alcohols eluted. The position of the alcohol group on the linear hydrocarbon chain is denoted by the first number: 1-alcohol (-OH at C_1), 2-alcohol (-OH at C_2), and 3-alcohols (-OH at C_3) eluted. The ^1t_r and ^2t_r of 1-hexadecanol and 2-hexadecanol were verified using standards.

Figure 5-12 shows the region of the GC×GC separation where the linear alcohols eluted. The number (1-alcohol, 2-alcohol, 3-alcohol) denotes the position of the alcohol (-OH) group on the molecule rather than primary, secondary, or tertiary alcohols. 1-hexadecanol and 2-hexadecanol were used to confirm the elution region of the alcohols in the GC×GC chromatogram and confirmed the identification of 1-

hexadecanol in sample T2. The RI for 1-hexadecanol was 2360 and 1878 on the MXT-WAX and Zebron-5HT columns, respectively. The RI for 2-hexadecanol was 2210 and 1803 on the MXT-WAX and Zebron-5HT columns, respectively. A ΔRI of approximately 100 units was used as a guide for labeling the other 1-alcohols and 2-alcohols in the sample. 3-pentadecanol (Wax: 2085) and 3-heptadecanol (Wax: 2284) were identified based on the mass spectra, but their Ris were not available in the library. However, the RI for 3-tetradecanol of 1984±4 for the wax stationary phase was available in the NIST library, which matched the ΔRI expected for the 3-alcohols found.

5.2.3.1.5 Unknown Compounds

Five groups of related but unknown compounds were highlighted in red in Figure 5-8. These peaks eluted below the *n*-alkene peaks in the GC×GC separation with each group of compounds differing by 28 m/z (C_4H_4). Each group contained five unknowns where their mass spectra contained groups of peaks around 41 m/z, 55 m/z, 69 m/z, 83 m/z, 97 m/z, and 111 m/z from the loss of CH_2, indicating an alkyl chain in their structure. The base peak for each compound in the group of unknowns in order of ^1t_r was 115 m/z, 101 m/z, 87 m/z, 73 m/z, and 59 m/z, which were $[CH_3OCO(CH_2)_n]^+$ fragments typical for FAMEs. Although it was likely that these unknown compounds were oxygenated species, they eluted at a greater ^2t_r compared to the other oxygenated compounds (increasing ^2t_r: FA, alcohols, FAMEs, 1,1-dimethoxyalkanes, 1-methoxyalkanes) in the sample, indicating that they were relatively non-polar. The top matches from the NIST library were either relatively poor (MF and RMF <800), the RI (Wax and 5 % phenyl) did not match, or the compound structure (polarity) did not fit the elution pattern of the GC×GC chromatogram. The top 10 matches for each unknown included at least one oxygen atom in the structure. Compounds included alcohols, esters, and ethers. The top matches for the unknowns with a base peak of 59 m/z and 73 m/z were both 3° alcohols with the alcohol group on the second carbon (59 m/z) or the third carbon (73 m/z). Although this may be possible, it would need to be verified with a standard. Mass spectra of the soft (14 eV) and hard (70 eV) ionization for the two groups of unknowns found in wax sample T2 are found in

Figure D - 5 to Figure D - 9 of Appendix D. Due to the early end to the collaboration, further efforts in elucidating the structure of the unknowns were not continued.

5.3 Conclusions

The combination of GC×GC-TOFMS and GC×GC-FID with ^{2}D temperature programming was effective for group type identification and quantitation of renewable hydrocarbon samples. Having separate systems made method optimization simpler, without any compromises needed for dual detection or flow modulation. The ion source design resulted in significant tailing, which made identification of trace compounds more difficult when they were coeluting with the more abundant paraffins. Utilizing the same ^{1}D/^{2}D columns and GC temperature program allowed the structure of the chromatograms to be comparable for the identification of compounds from the FID signal. Utilizing ^{2}D temperature programming was necessary to improve the S/N for the quantitation of trace compounds in the samples.

The GC×GC-FID/TOFMS-^{2}DTPS system improved the workflow for group type identification and quantitation. The use of a purged splitter generated positive backpressure which made method optimization more difficult but allowed for backflushing the system when dealing with high boiling point compounds. The application of ^{2}D temperature programming was necessary to improve the peak capacity and maximize the 2D separation space, particularly when separating a diverse set of compound classes. Comparison of the pre-decoloring and decolored samples showed a small increase in alkanes and an almost equivalent decrease in mononaphthenes. The overall hydrofinishing process (hydrogenation and decolorization) was effective in removing all aromatics generated to produce products suitable for personal care. The by-product samples from the Kolbe electrolysis process contained a diverse range of oxygenated species and hydrocarbons. These samples demonstrated the separation capabilities of the GC×GC-FID/TOFMS-^{2}DTPS over the conventional GC-MS separation. The use of a polar (MXT-WAX) and semi-polar (5 % phenyl) stationary phase to determine the linear ^{1}D RI in combination with mass spectral

identification and structured GC×GC chromatograms provided greater confidence in the tentative identification of compounds in the wax samples.

6 Summary and Future Work

6.1 Summary

GC×GC has grown considerably since its introduction back in 1991 [7]. Research started with a focus on modulator development, which led to the commercialization of various modulator designs. As modulator development matured, research shifted towards chemometrics and applications. Combining the technological advancements in hardware and software made GC×GC the most powerful analytical technique for the separation of complex samples of VOCs and SVOCs. However, further improvements in peak capacity can be unlocked with existing GC×GC systems by addressing the general elution problem in the ^{2}D. This thesis illustrated the development process of a ^{2}D temperature programming system.

The proof-of-concept design demonstrated the potential of ^{2}D temperature programming using a ballistic heating system. Two aspects of the design that carried forward to the final design were the heating and cooling methods. Direct resistive heating of a commercial stainless steel column provided sufficient heating rates for ^{2}D temperature programming. The thermal mass of the stainless steel column was small enough to be cooled within the timespan of the modulation period using only the forced convection within the GC oven. The use of commercial stainless steel columns provided users the access to a large selection of stationary phases and column dimensions. Through the results of the ballistic heating experiments, it was understood that heating needed to be delayed at the start of the modulation period to allow less retained compounds to separate prior to ^{2}D temperature programming. Although the system lacked any precise temperature control, ballistic heating was still successful in improving the ^{2}D separation compared to a constant temperature offset.

The next step in the development was to achieve true ^{2}D temperature programming. This was accomplished with an Arduino microcontroller and a differential thermocouple system. As the first true ^{2}D temperature programming system, its reproducibility and separation performance (resolution and

peak capacity) were measured. A paired Student's t-test comparing the RSDs between the separations with and without ^{2}D temperature programming showed that the differences were not significant for the ^1t_r and ^2t_r. ^{2}D temperature programming improved the resolution and peak capacity compared to the constant offset separation and separation without any additional ^{2}D heating.

The last update to the system focused on robustness and ease of use. The temperature measurement method was completely redesigned, where the overall ^{2}D column temperature was based on the electrical resistance of the column. This eliminated the fragile thermocouple connection to the ^{2}D column in previous designs, while the electrical connections to the ^{2}D columns were redesigned for better contact and four-wire resistance measurement. This was necessary to measure the small resistance changes involved. The inaccuracy of the built-in Arduino clock was addressed using an RTC, and a remote port connection was added so that the ^{2}DTPS could be a completely standalone system. This was demonstrated with both thermal and flow modulators, as well as an FID and a TOFMS, accounting for a majority of GC×GC setups used. Reproducibility was tested with each GC×GC setup and with any hardware changes to the ^{2}DTPS to provide sufficient data to demonstrate its robustness under a variety of conditions. To provide recommended power supply specifications, the relationship between the power supply output (power) and the heating rate, temperature offset, and column dimensions (length and inner diameter) were determined. During the data collection process, the temperature control algorithm was simultaneously optimized to further improve the system. The overall reproducibility of the ^{2}DTPS was acceptable while providing added flexibility in optimizing the ^{2}D separation. Both the peak capacity and the S/N ratio were improved with ^{2}D temperature programming.

To demonstrate the ^{2}DTPS in a real-world application, renewable hydrocarbon samples from a local Ontario company were analyzed to aid in the research and development process. ^{2}D temperature programming was applied to GC×GC-TOFMS and GC×GC-FID separations for group type analysis of two renewable hydrocarbon products. The S/N ratio of trace aromatics in the sample increased with ^{2}D

temperature programming to aid in their quantitation. The ^{2}DTPS was also used with a GC×GC-FID/TOFMS system that utilized a purged splitter for dual detection. The added flexibility of ^{2}D temperature programming eased the method optimization process while the purged splitter provided the option of backflushing for high boiling point compounds. The reverse column set was better suited for group type identification of samples from various steps in the production process. The combined information from the structured GC×GC separation, linear ^{1}D RI (polar and semi-polar stationary phases), and mass spectral identification provided greater confidence in tentative compound identification despite the lack of standards for positive identification. The use of ^{2}D temperature programming was important in increasing the peak capacity for the separation of wax samples which contained a diverse range of oxygenated species and hydrocarbons.

6.2 Future Work

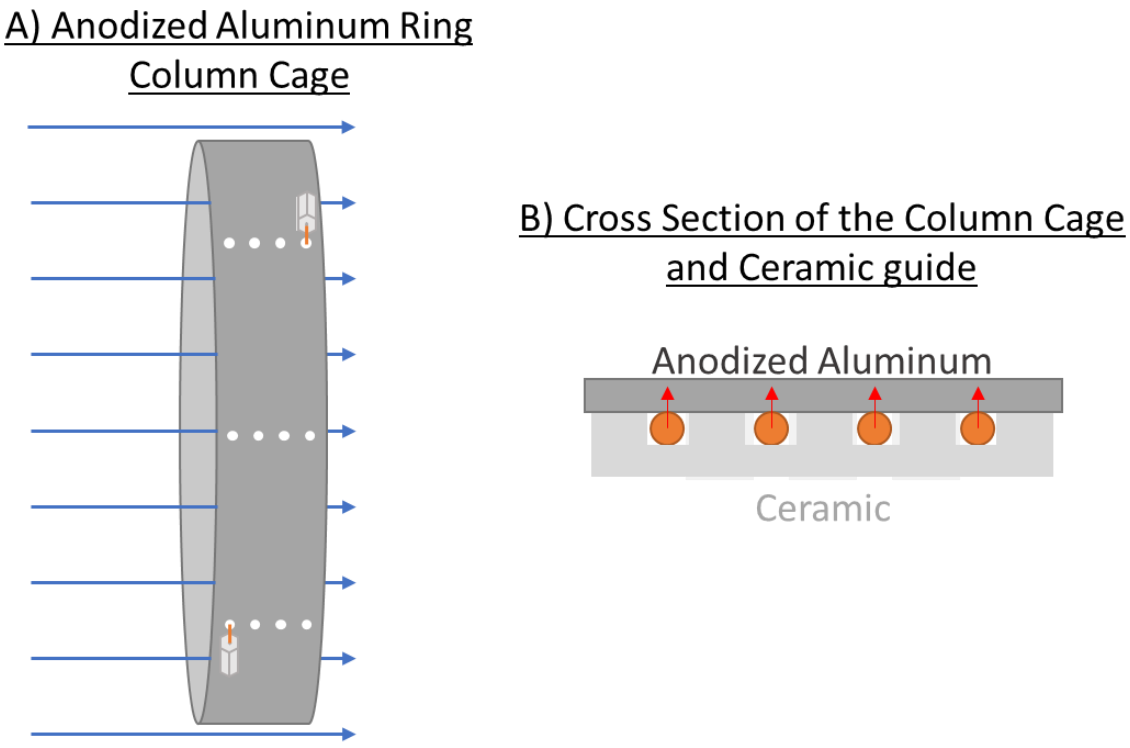

Figure 6-1: Proposed column cage design to improve cooling. A) The column cage is constructed from an anodized aluminum ring where ceramic guides are attached to segregate the ^{2}D column loops on the inside of the column cage. Holes are drilled through the aluminum ring for the ends of the ^{2}D column to pass through. B) Cross sectional view of the ^{2}D column being in contact with the anodized aluminum column cage and held in place by the ceramic guides.

Improvements to the ^{2}D column cooling can be made to reduce the cooling duration and provide more time for heating within a modulation period. The current column cage uses springs as guides for each loop of the column. This design minimizes the amount of contact between the column cage and the ^{2}D column to maximize the air flow over the ^{2}D column for cooling. Cooling duration can be reduced by redesigning the column cage to improve the overall heat transfer. The proposed design, shown in Figure 6-1, uses an anodized aluminum ring as the column cage to conduct heat away from the ^{2}D column. The surface of the column cage needs to be anodized to provide an electrically non-conductive layer. Ceramic guides would be milled and attached to the inside of the column cage to keep the ^{2}D column loops separated. Contact pressure between the ^{2}D column and the column cage would rely on the torsional force of the stainless steel ^{2}D column tubing trying to unwind. The thermal conductivity of aluminum at 20 °C is significantly greater at 204.0 $Wm^{-1}K^{-1}$, as compared to air which is 0.026 $Wm^{-1}K^{-1}$. With this design, cooling would be a mix of conductive heat transfer from the ^{2}D column to the aluminum ring and convective heat transfer from the ^{2}D column to the air. Holes can be drilled into the column cage for the ^{2}D column to be threaded through and attachment of the SilTite mini-unions. The downside of improving the passive cooling of the ^{2}D column would be an increased difficulty in heating the column. Power supply output (W) would need to be increased to achieve the same heating rate and temperature offset, which may become an issue for differential flow modulators which utilize longer ^{2}D columns. The experiment performed in section 4.3.6 can be repeated with the new column cage for comparison of heating and cooling rates.

Restek's MXT columns are not the only commercially available metal columns. Agilent also produces steel columns (ProSteel and UltiMetal) of various dimensions which have not been tested with the ^{2}DTPS. Testing the ^{2}DTPS with metal columns by other manufacturers is important in determining its compatibility with existing products. The Restek's MXT and Agilent's ProSteel columns have both been tested as capillary traps in the Waterloo modulator (1.2.1.3.1). A notable physical difference between the columns, discovered when making the traps, was their rigidity. The Agilent ProSteel columns were much

softer, which may be an indication of a different alloy composition. This could affect column's resistivity, TCR and heat capacity, which would affect the sensitivity of the temperature measurement (°C/Ω), the heating rate, maximum offset and cooling rate.

The Agilent 6890 GC was used throu"hout'the testing of the ^{2}DTPS. testing the system with other GC models would be important to examine the differences in cooling and the remote port connection. The ^{2}DTPS relied on the convection within the GC oven for cooling the ^{2}D column. The column was mounted directly in front of the GC fan to maximize the cooling performance. This may not always be an option depending on the GC model and the available mounting possibilities. This would need to be tested and modified as needed to maximize the cooling of the ^{2}D column. The wiring of the remote port for each manufacturer would need to be checked with a separate remote cable built for each manufacturer so that the wire connections match with what is expected on the ^{2}DTPS. The order of the remote signal sequence, and the logic between High and Low states may also differ between manufacturers. A simple addition to the code to adjust the logic based on the manufacturer can be done. A drop-down menu in the Windows Forms application can be used to select the GC model and switch the start/stop signal logic on the Arduino.

References

[1] A. T. James and J. P. Martin, *National Institute for Medical Research,* vol. 50, pp. 679 - 690, 1952.

[2] K. D. Bartle and P. Myers, *Trends in Analytical Chemistry,* vol. 21, pp. 547 - 557, 2002.

[3] L. S. Ettre, *Journal of High Resolution Chromatography & Chromatography Communications,* vol. 10, pp. 221 - 230, 1987.

[4] C. G. Horvath and S. R. Lipsky, *Analytical Chemistry,* vol. 14, pp. 1893 - 1893, 1967.

[5] J. M. Davis and J. C. Giddings, *Analytical Chemistry,* vol. 55, pp. 418 - 424, 1983.

[6] J. C. Giddings, *Journal of Chromatography A,* vol. 703, pp. 3 - 15, 1995.

[7] Z. Liu and J. B. Phillips, *Journal of Chromatographic Science,* vol. 29, pp. 227 - 231, 1991.

[8] M. C. Simmons and L. R. Snyder, *Analytical Chemistry,* vol. 30, pp. 32 - 35, 1958.

[9] P. Q. Tranchida, D. Sciarrone, P. Dugo and L. Mondello, *Analytica Chimica Acta,* vol. 716, pp. 66 - 75, 2012.

[10] T. Górecki, J. Harynuk and O. Panic, *Journal of Separation Science,* vol. 27, pp. 359 - 379, 2004.

[11] B. A. Weggler, L. M. Dubois, N. Gawlitta, T. Gröger, J. Moncur, L. Mondello, S. Reichenbach, P. Tranchida, Z. Zhao, R. Zimmermann, M. Zoccali and J.-F. Focant, *Journal of Chromatography A,* vol. 1635, p. 461721, 2021.

[12] M. J. Wilde, B. Zhao, R. L. Cordell, W. Ibrahim, A. Singapuri, N. J. Greening, C. E. Brightling, S. Siddiqui, P. S. Monks and R. C. Free, *Analytical Chemistry,* vol. 92, pp. 13953 - 13960, 2020.

[13] M. Edwards, A. Mostafa and T. Górecki, *Analytical and Bioanalytical Chemistry,* vol. 401, pp. 2335 - 2349, 2011.

[14] P. Q. Tranchida, G. Purcaro, P. Dugo and L. Mondello, *Trends in Analytical Chemistry,* vol. 30, pp. 1437 - 1461, 2011.

[15] B. R. Kowalski, *Journal of Chemical Information and Computer Sciences,* vol. 15, pp. 201 - 203, 1975.

[16] S. Wold, *Chemometrics and Intelligent Laboratory Systems,* vol. 30, pp. 109 - 115, 1995.

[17] P.-H. Stefanuto, A. Smolinska and J.-F. Focant, *Trends in Analytical Chemistry,* vol. 139, p. 116251, 2021.

[18] A. Muto, C. T. Müller, L. Bruno, L. McGregor, A. Ferrante, A. A. C. Chiapetta, M. B. Bitoni, H. J. Rogers and N. D. Spadafora, *Scientific Reports,* vol. 10, p. 18333, 2020.

[19] T. S. Bos, W. C. Knol, S. R. Molenaar, L. E. Niezen, P. J. Schoenmakers, G. W. Somsen and B. W. Pirok, *Journal of Separation Science,* vol. 43, pp. 1678 - 1727, 2020.

[20] H. D. Bean, J. E. Hill and J.-M. D. Dimandja, *Journal of Chromatography A,* vol. 1394, pp. 111 - 117, 2015.

[21] W. B. Dunn, D. Broadhurst, P. Begley, E. Zelena, S. Francis-McIntrye, N. Anderson, M. Brown, J. D. Knowles, A. Halsall, J. N. Haselden, A. W. Nicholls, I. D. Wilson, D. B. Kell, R. Goodacre

and The Human Serum Metabolome (HUSERMET) Consortium, *Nature Protocols,* vol. 6, pp. 1060 - 1083, 2011.

[22] P. E. Sudol, K. M. Pierce, S. E. Prebihalo, K. J. Skogerboe, B. W. Wright and R. E. Synovec, *Analytica Chimica Acta,* vol. 1132, pp. 157 - 186, 2020.

[23] B. J. Pollo, C. A. Teixeira, J. R. Belinato, M. F. Furlan, I. C. d. M. Cunha, C. R. Vaz, G. V. Volpato and F. Augusto, *Trends in Analytical Chemistry,* vol. 134, p. 116111, 2021.

[24] S. E. Prebihalo, K. L. Berrier, C. E. Freye, H. D. Bahaghighat, N. R. Moore, D. K. Pinkerton and R. E. Synovec, *Analytical Chemistry,* vol. 90, pp. 505 - 532, 2018.

[25] A. M. Muscalu and T. Górecki, *Trends in Analytical Chemistry,* vol. 106, pp. 225 - 245, 2018.

[26] P. Q. Tranchida, G. Purcaro, M. Maimone and L. Mondello, *Journal of Separation Science,* vol. 39, pp. 149-161, 2016.

[27] B. Gruber, B. Weggler, R. Jaramillo, K. Murrell, P. Piotrowski and F. Dorman, *Trends in Analytical Chemistry,* vol. 105, pp. 292 - 301, 2018.

[28] E. A. Higgins Keppler, C. L. Jenkins, T. J. Davis and H. D. Bean, *Trends in Analytical Chemistry,* vol. 109, pp. 275 - 286, 2018.

[29] B. J. Pollo, G. L. Alexandrino, F. Augusto and L. W. Hantao, *Trends in Analytical Chemistry,* vol. 105, pp. 202 - 217, 2018.

[30] S. Fernando, A. Renaguli, M. S. Milligan, J. J. Pagano, P. K. Hopke, T. M. Holsen and B. S. Crimmins, *Environmental Science & Technology,* vol. 52, pp. 2909 - 2917, 2018.

[31] P. E. Sudol, M. Galletta, P. Q. Tranchida, M. Zoccali, L. Mondello and R. E. Synovec, *Journal of Chromatography A,* vol. 1662, p. 462735, 2022.

[32] L. N. Kates, P. I. Richards and C. D. Sandau, *Forensic Science International,* vol. 310, p. 110256, 2020.

[33] E. Barberis, E. Amede, S. Khoso, L. Castello, P. P. Sainaghi, M. Bellan, P. E. Balbo, G. Patti, D. Brustia, M. Giordano, R. Rolla, A. Chiocchetti, G. Romani, M. Manfredi and R. Vaschetto, *Metabolites,* vol. 11, pp. 847 - 857, 2021.

[34] C. I. Mack, B. Egert, E. Liberto, C. H. Weinert, A. Bub, I. Hoffmann, C. Bicchi, S. E. Kulling and C. Cordero, *Molecular Nutrition Food Research,* vol. 63, p. 1801060, 2019.

[35] LECO Corporation, "LECO's GCxGC Comprehensive Two-Dimensional Gas Chromatography," [Online]. Available: https://www.leco.com/component/edocman/?task=document.viewdoc&id=53&Itemid=.

[36] Z. Liu and J. B. Phillips, *Journal of Microcolumn Separations,* vol. 1, no. 5, pp. 249 - 256, 1989.

[37] Z. Liu and J. B. Phillips, *Journal of Microcolumn Separations,* vol. 1, pp. 159 - 162, 1989.

[38] Z. Liu and J. B. Phillips, *Journal of Microcolumn Separations,* vol. 2, pp. 33 - 40, 1990.

[39] Z. Liu and J. B. Phillips, *Journal of Microcolumn Separations,* vol. 6, pp. 229 - 235, 1994.

[40] J. B. Phillips and J. Beens, *Journal of Chromatography A,* vol. 856, pp. 331 - 347, 1999.

[41] J. B. Phillips, D. Luu and J. B. Pawliszyn, *Analytical Chemistry,* vol. 57, pp. 2779 - 2787, 1985.

[42] J. B. Phillips and Z. Liu, *Journal of Chromatographic Science,* vol. 29, pp. 227 - 231, 1991.

[43] J. B. Phillips, R. B. Gaines, J. Blomberg, F. W. van der Wielen, J.-M. Dimandja, V. Green, J. Granger, D. Patterson, L. Racovalis, H.-J. de Geus, J. de Boer, P. Haglund, J. Lipsky, V. Sinha and E. B. Ledford, Jr., *Journal of High Resolution Chromatography,* vol. 22, no. 1, pp. 3 - 10, 1999.

[44] C. J. Venkatramani and J. B. Phillips, *Journal of Microcolumn Separation,* vol. 5, pp. 511 - 516, 1993.

[45] V. Mucédola, L. C. Vieira, D. Pierone, A. L. Gobbi, R. J. Poppi and L. W. Hantao, *Talanta,* vol. 164, pp. 470 - 476, 2017.

[46] J. B. Phillips and E. B. Ledford, *Field Analytical Chemistry and Technology,* vol. 1, no. 1, pp. 23 - 29, 1996.

[47] R. B. Gaines and G. S. Frysinger, *Journal of Chromatography A,* vol. 1045, pp. 263 - 264, 2004.

[48] J. Beens, H. Boelens and R. Tijssen, *Journal of High Resolution Chromatography,* vol. 21, pp. 47 - 54, 1998.

[49] P. J. Marriott and R. M. Kinghorn, *Analytical Chemistry,* vol. 69, pp. 2582 - 2588, 1997.

[50] R. M. Kinghorn and P. J. Marriott, *Journal of High Resolution Chromatography,* vol. 21, pp. 32 - 38, 1998.

[51] R. M. Kinghorn, P. J. Marriott and P. J. Dawes, *Journal of Microcolumn Separations,* vol. 10, pp. 611-616, 1998.

[52] R. M. Kinghorn and P. J. Marriott, *Journal of High Resolution Chromatography,* vol. 21, pp. 620-622, 1998.

[53] P. J. Marriott and R. M. Kinghorn, *Analytical Sciences,* vol. 14, pp. 651 - 659, 1998.

[54] P. J. Marriott, R. M. Kinghorn, R. Ong, P. Morrison, P. Haglund and M. Harju, *Journal of High Resolution Chromatography,* vol. 23, pp. 253 - 258, 2000.

[55] P. Haglund, M. Harju, C. Danielsson and P. Marriott, *Journal of Chromatography A,* vol. 962, pp. 127 - 134, 2002.

[56] R. M. Kinghorn, P. J. Marriott and P. A. Dawes, *Journal of High Resolution Chromatography,* vol. 23, pp. 245 - 252, 2000.

[57] E. B. Ledford Jr., in *23rd International Symposium on Capillary Chromatography*, Riva del Garda, Italy, 5-10 June 2000.

[58] P. Stevens, 10 September 2009. [Online]. Available: https://www.leco.com/images/e-seminar_archive/videos/MiscGeneral/GCxGC%20Theory-Practice-Automation%20Sept%2010%202009%20e-Seminar-GEN.pdf.

[59] E. B. Ledford Jr., C. A. Billesbach and J. R. Termaat, "Transverse Thermal Modulation". United States Patent US20010037727A1, 08 November 2001.

[60] E. M. Kristenson, P. Korytár, C. Danielsson, M. Kallio, M. Brandt, J. Mäkelä, R. J. Vreuls, J. Beens and U. A. Brinkman, *Journal of Chromatography A,* vol. 1019, pp. 65 - 77, 2003.

[61] G. Semard, M. Adahchour and J.-F. Focant, "Chapter 2 Basic Instrumentation for GCxGC," in *Comprehensive Two Dimensional Gas Chromatography*, Amsterdam, Elsevier, 2009, pp. 15-48.

[62] P. Stevens and J. Binkley, "Evaluation of a Liquid Cryogen-Fee Thermal Modulation for GCxGC," [Online]. Available: https://www.leco.com/images/e-seminar_archive/posters/MiscGeneral/Liquid_Cryogen-Free_Thermal_Modulator_GCxGC-TOFMS_PS_Pcon09_LPSS-010.pdf. [Accessed 26 04 2018].

[63] J. Beens, M. Adahchour, R. J. Vreuls, K. van Altena and U. A. Brinkman, *Journal of Chromatography A,* vol. 919, pp. 127 - 132, 2001.

[64] M. Adahchour, J. Beens and U. A. Brinkman, *Analyst,* vol. 128, pp. 213 - 216, 2003.

[65] Thermo Fisher Scientific, "Thermo Scientific Trace GC Ultra Multi-channel gas chromatograph," [Online]. Available: http://tools.thermofisher.com/content/sfs/brochures/Thermo-Scientific-TRACE-GC-Ultra.pdf. [Accessed 11 April 2022].

[66] E. B. Ledford Jr., C. A. Billesbach and J. R. Termaat, in *Pittcon 2002*, New Orleans, LA, USA, 17-22 March 2002.

[67] E. B. Ledford Jr., J. R. TerMaat and C. A. Billesbach, "Technical Note KT030606-1: What is Loop Modulation?," [Online]. Available: https://web.archive.org/web/20041024130207/http://www.zoex.com:80/technote_kt030606-1.html. [Accessed 25 04 2018].

[68] "Zoex Corporation, Products," Zoex Corporation, [Online]. Available: http://zoex.com/products/. [Accessed 26 04 2018].

[69] "Introducing the NEW ZX-2 Closed Cycle Refrigeration Thermal Modulated GC x GC System," [Online]. Available: http://zoex.com/wp-content/uploads/2012/07/ZX2-Product-Specs.pdf. [Accessed 26 04 2018].

[70] "ZX-1 Thermal Modulation GC x GC System," [Online]. Available: http://zoex.com/wp-content/uploads/2012/07/ZX1-Product-Specs.pdf. [Accessed 26 04 2018].

[71] M. Pursch, P. Eckerle, J. Biel, R. Streck, H. Cortes, K. Sun and B. Winniford, *Journal of Chromatography A,* vol. 1019, pp. 43 - 51, 2003.

[72] J. Harynuk and T. Górecki, *Journal of Chromatography A,* vol. 1019, pp. 53 - 63, 2003.

[73] A. Mostafa and T. Górecki, *Analytical Chemistry,* vol. 88, pp. 5414 - 5423, 2016.

[74] A. M. Muscalu, M. Edwards, T. Górecki and E. J. Reiner, *Journal of Chromatography A,* vol. 1391, pp. 93 - 101, 2015.

[75] O. Panić, T. Górecki, C. McNeish, A. H. Goldstein, B. J. Williams, D. R. Worton, S. V. Hering and N. M. Kreisberg, *Journal of Chromatography A,* vol. 1218, pp. 3070 - 3079, 2011.

[76] D. R. Worton, N. M. Kreisberg, G. Isaacman, A. P. Teng, C. McNeish, T. Górecki, S. V. Hering and A. H. Goldstein, *Aerosol Science and Technology,* vol. 46, pp. 380 - 393, 2012.

[77] M. R. Jacobs, M. Edwards, T. Górecki, P. N. Nesterenko and R. A. Shellie, *Journal of Chromatography A,* vol. 1463, pp. 162 - 168, 2016.

[78] A. H. Goldstein, D. R. Worton, B. J. Williams, S. V. Hering, N. M. Kreisberg, O. Panić and T. Górecki, *Journal of Chromatography A,* vol. 1186, pp. 340 - 347, 2008.

[79] S.-J. Kim, S. M. Reidy, B. P. Block, K. D. Wise, E. T. Zellers and K. Kurabayashi, *Lab Chip,* vol. 10, pp. 1647 - 1654, 2010.

[80] S.-J. Kim, G. Serrano, K. D. Wise, K. Kurabayashi and E. T. Zellers, *Analytical Chemistry,* vol. 83, pp. 5556 - 5562, 2011.

[81] G. Serrano, D. Paul, S.-J. Kim, K. Kurabayashi and E. T. Zellers, *Analytical Chemistry,* vol. 84, pp. 6973 - 6980, 2012.

[82] S.-J. Kim and K. Kurabayashi, *Sensors and Actuators B,* vol. 181, pp. 518 - 522, 2013.

[83] W. R. Collin, N. Nuñovero, D. Paul, K. Kurabayashi and E. T. Zellers, *Journal of Chromatography A,* vol. 1444, pp. 114 - 122, 2016.

[84] J&X Technologies, "J&X Technologies," [Online]. Available: http://www.jnxtec.com/.

[85] J. Luong, X. Guan, S. Xu, R. Gras and R. A. Shellie, *Analytical Chemistry,* vol. 88, pp. 8428 - 8432, 2016.

[86] J&X Technologies, "SSM1800 Solid State Modulator for Comprehensive Two Dimensional Gas Chromatography (GCxGC) Second Edition," January 2018. [Online]. Available: http://prod87c5f.hkpic1.websiteonline.cn/upload/SSM1800_InstallationandOperation_v2_2018.pdf.

[87] J. Harynuk and T. Górecki, *Journal of Separation Science,* vol. 27, pp. 431 - 441, 2004.

[88] N. Oldridge, O. Panic and T. Górecki, *Journal of Separation Science,* vol. 31, pp. 3375 - 3384, 2008.

[89] T. Veriotti and R. Sacks, *Analytical Chemistry,* vol. 73, pp. 3045 - 3050, 2001.

[90] J. V. Seeley, *Journal of Chromatography A,* vol. 1255, pp. 24 - 37, 2012.

[91] C. A. Bruckner, B. J. Prazen and R. E. Synovec, *Analytical Chemistry,* vol. 70, pp. 2796 - 2804, 1998.

[92] A. E. Sinha, K. J. Johnson, B. J. Prazen, S. V. Lucas, C. G. Fraga and R. E. Synovec, *Journal of Chromatography A,* vol. 983, pp. 195 - 204, 2003.

[93] C. E. Freye, L. Mu and R. E. Synovec, *Journal of Chromatography A,* vol. 1424, pp. 127 - 133, 2015.

[94] J. V. Seeley, F. Kramp and C. J. Hicks, *Analytical Chemistry,* vol. 72, pp. 4346 - 4352, 2000.

[95] J. V. Seeley, N. J. Micyus, S. V. Bandurski, S. K. Seeley and J. D. McCurry, *Analytical Chemistry,* vol. 79, pp. 1840 - 1847, 2007.

[96] K. M. Sharif, S. T. Chin, C. Kulsing and P. J. Marriott, *Trends in Analytical Chemistry,* vol. 82, pp. 35 - 54, 2016.

[97] D. R. Deans, *Journal of Chromatography,* vol. 18, pp. 477 - 481, 1965.

[98] D. R. Deans, *Chromatographia,* vol. 1, pp. 18 - 22, 1968.

[99] A. Ghosh, C. T. Bates, S. K. Seeley and J. V. Selley, *Journal of Chromatography A,* vol. 1291, pp. 146 - 154, 2013.

[100] J. V. Seeley, N. E. Schimmel and S. K. Seeley, *Journal of Chromatography A,* vol. 1536, pp. 6 - 15, 2018.

[101] LECO Corporation, "FLUX™ GCxGC The operation, use, and concepts behind a diverting flow technique," 16 12 2019. [Online]. Available: https://knowledge.leco.com/component/edocman/flux-modulator-white-paper-209-281-004/viewdocument?Itemid=1821. [Accessed 09 08 2021].

[102] P. A. Bueno and J. V. Seeley, *Journal of Chromatography A,* vol. 1027, pp. 3 - 10, 2004.

[103] J. V. Seeley, N. J. Micyus, J. D. McCurry and S. K. Seeley, *American Laboratory,* vol. 38, pp. 24 - 26, 2006.

[104] M. Poliak, M. Kochman and A. Amirav, *Journal of Chromatography A,* vol. 1186, pp. 189 - 195, 2008.

[105] M. Ston, R. Cabala, V. M. Bierhanzl, J. Krajicek and Z. Bosakova, *Journal of Chromatographic Science,* vol. 54, pp. 1481 - 1488, 2016.

[106] J. F. Griffith, W. L. Winniford, K. Sun, R. Edam and J. C. Luong, *Journal of Chromatography A,* vol. 1226, pp. 116 - 123, 2012.

[107] C. Duhamel, P. Cardinael, V. Peulon-Agasse, R. Firor, L. Pascaud, G. Semard-Jousset, P. Giusti and V. Livadaris, *Journal of Chromatography A,* vol. 1387, pp. 95 - 103, 2015.

[108] J. Krupcik, R. Gorovenko, I. Spanik, P. Sandra and M. Giardina, *Journal of Chromatography A,* vol. 1466, pp. 113 - 128, 2016.

[109] A. E. Sinha, B. J. Prazen, C. G. Fraga and R. E. Synovec, *Journal of Chromatography A,* vol. 2003, pp. 79 - 87, 2003.

[110] P. Q. Tranchida, F. A. Franchina, P. Dugo and L. Mondello, *Journal of Chromatography A,* vol. 1359, pp. 271 - 276, 2014.

[111] P. Q. Tranchida, G. Purcaro, A. Visco, L. Conte, P. Dugo, P. Dawes and L. Mondello, *Journal of Chromatography A,* vol. 1218, pp. 3140 - 3145, 2011.

[112] F. A. Franchina, M. Maimone, P. Q. Tranchida and L. Mondello, *Journal of Chromatography A,* vol. 1441, pp. 134 - 139, 2016.

[113] H. Cai and S. D. Stearns, *Analytical Chemistry,* vol. 76, pp. 6064 - 6076, 2004.

[114] H. D. Bahaghighat, C. E. Freye, D. V. Gough, P. E. Sudol and R. E. Synovec, *Journal of Chromatography A,* vol. 1573, pp. 115 - 124, 2018.

[115] T. J. Trinklein, D. V. Gough, C. G. Warren, G. S. Ochoa and R. E. Synovec, *Journal of Chromatography A,* vol. 1609, p. 460488, 2020.

[116] C. E. Freye, H. D. Bahaghighat and R. E. Synovec, *Talanta,* vol. 177, pp. 142 - 149, 2018.

[117] S. Schöneich, D. V. Gough, T. J. Trinklein and R. E. Synovec, *Journal of Chromatography A,* vol. 1620, p. 460982, 2020.

[118] S. Schöneich, T. J. Trinklein, C. G. Warren and R. E. Synovec, *Analytica Chimica Acta,* vol. 1134, pp. 115 - 124, 2020.

[119] X. Guan, J. Luong, Z. Yu and H. Jiang, *Analytical Chemistry,* vol. 92, pp. 6251 - 6256, 2020.

[120] J&X Technologies, "Quasi-stop airflow modulator," J&X Technologies, [Online]. Available: http://www.jnxtec.com/Productdetails?product_id=5&brd=1. [Accessed 16 December 2021].

[121] R. Mehta, "Activated Research Company Offers Stop-Flow Modulation Solution for GCxGC," activated research company, 20 November 2020. [Online]. Available: https://www.activatedresearch.com/wp-content/uploads/2021/05/20201120_Press_Release_ARC_Offers_Stop_Flow_Modulation_Solution_for_GCxGC.pdf. [Accessed 16 December 2021].

[122] A. Mostafa, M. Edwards and T. Górecki, *Journal of Chromatography A,* vol. 1255, pp. 38 - 55, 2012.

[123] F. C.-Y. Wang, *Journal of Chromatography A,* vol. 1489, pp. 126 - 133, 2017.

[124] P.-H. Stefanuto, K. A. Perrault, L. M. Dubois, B. L'Homme, C. Allen, C. Loughnane, N. Ochiai and J.-F. Focant, *Journal of Chromatography A,* vol. 1507, pp. 45 - 52, 2017.

[125] J. Harynuk, T. Górecki and J. d. Zeeuw, *Journal of Chromatography A,* vol. 1071, pp. 21 - 27, 2005.

[126] M. S. Klee, J. Cochran, M. Merrick and L. M. Blumberg, *Journal of Chromatography A,* vol. 1383, pp. 151 - 159, 2015.

[127] P. Harvey and R. A. Shellie, *Journal of Chromatography A,* vol. 1218, pp. 3153 - 3158, 2011.

[128] R. E. Murphy, M. R. Schure and J. P. Foley, *Analytical Chemistry,* vol. 70, pp. 1585 - 1594, 1998.

[129] W. Khummueng, J. Harynuk and P. J. Marriott, *Analytical Chemistry,* vol. 78, pp. 4578 - 4587, 2006.

[130] P. J. Marriott and C. von Mühlen, *Scientia Chromatographica,* vol. 8, pp. 7 - 23, 2016.

[131] H. D. Bahaghighat, C. E. Freye, D. V. Gough and R. E. Synovec, *Journal of Chromatography A,* vol. 1583, pp. 117 - 123, 2019.

[132] E. Engel, J. Ratel, P. Blinet, S. T. Chin, G. Rose and P. J. Marriott, *Journal of Chromatography A,* vol. 1311, pp. 140 - 148, 2013.

[133] C. Zhang, I. C. Ingram, L. W. Hantao and J. L. Anderson, *Journal of Chromatography A,* vol. 1386, pp. 89 - 97, 2015.

[134] C. E. Freye, B. D. Fitz, M. C. Billingsley and R. E. Synovec, *Talanta,* vol. 153, pp. 203 - 210, 2016.

[135] R. C. Blase, E. L. Patrick, J. N. Mitchell and M. Libardoni, *Analytical Chemistry Research,* vol. 3, pp. 54 - 62, 2015.

[136] S. Samanipour, P. Dimitriou-Christidis, J. Gros, A. Grange and J. S. Arey, *Journal of Chromatography A,* vol. 1375, pp. 123 - 139, 2015.

[137] D. Xia, L. Gao, S. Zhu and M. Zheng, *Analytical and Bioanalytical Chemistry,* vol. 406, pp. 7561-7570, 2014.

[138] P. Dimitriou-Christidis, A. Bonvin, S. Samanipour, J. Hollender, R. Rutler, J. Westphale, J. Gros and S. J. Arey, *Environmental Science & Technology,* vol. 49, pp. 7614 - 7625, 2015.

[139] P. J. Marriott, "Detector Technologies and Applications in Comprehensive Two-Dimensional Gas Chromatography," in *Comprehensive Chromatography in Combination with Mass Spectrometry*, Hoboken, John Wiley & Sons, Inc., 2011, pp. 243 - 280.

[140] S.-T. Chin, Z.-Y. Wu, P. D. Morrison and P. J. Marriott, *Analytical Methods,* vol. 2, pp. 243 - 253, 2010.

[141] D. Ryan and P. Marriott, *Journal of Separation Science,* vol. 29, pp. 2375 - 2382, 2006.

[142] S. A. Kevin, I. Sawicki, D. D. Carlton, Jr., H. Fan, H. M. McNair, J. P. Nimmo, P. Kroll, J. Smuts, P. Walsh and D. Harrison, *Analytical Chemistry,* vol. 86, pp. 8329 - 8335, 2014.

[143] T. Groger, B. Gruber, D. Harrison, M. Saraji-Bozorgzad, M. Mthembu, A. Sutherland and R. Zimmermann, *Analytical Chemistry,* vol. 88, pp. 3031 - 3039, 2016.

[144] P. Q. Tranchida, F. A. Franchina, P. Dugo and L. Mondello, *Mass Spectrometry Reviews,* vol. 35, pp. 524 - 534, 2016.

[145] M. Ubukata, K. J. Jobst, E. J. Reiner, S. E. Reichenbach, Q. Tao, J. Hang, Z. Wu, A. John Dane and R. B. Cody, *Journal of Chromatography A,* vol. 1395, pp. 152 - 159, 2015.

[146] S. Naeher, S. K. Lengger and K. Grice, *Journal of Chromatography A,* vol. 1435, pp. 125 - 135, 2016.

[147] K. M. Blum, P. L. Andersson, G. Renman, L. Ahrens, M. Gros, K. Wiberg and P. Haglund, *Science of the Total Environment,* vol. 575, pp. 265 - 275, 2017.

[148] S. Carlin, U. Vrhovsek, P. Franceschi, C. Lotti, L. Bontempo, F. Camin, D. Toubiana, F. Zottele, G. Toller, A. Fait and F. Mattivi, *Food Chemistry,* vol. 208, pp. 68 - 80, 2016.

[149] P.-H. Stefanuto, K. A. Perrault, S. Stadler, R. Pesesse, H. N. LeBlanc, S. L. Forbes and J.-F. Focant, *Analytical and Bioanalytical Chemistry,* vol. 407, pp. 4767 - 4778, 2015.

[150] G. Cao, H. Cai, X. Cong, X. Liu, X. Ma, Y. Lou, K. Qin and B. Cai, *Analyst,* vol. 137, pp. 3828 - 3835, 2012.

[151] A. M. Sulej-Suchomska, Z. Polkowska, T. Chmiel, T. M. Dymerski, Z. J. Kokot and J. Namiesnik, *Analytical Methods,* vol. 8, pp. 4509 - 4520, 2016.

[152] C. Martins, T. Brandão, A. Almeida and S. M. Rocha, *Journal of Separation Science,* vol. 38, pp. 2140 - 2148, 2015.

[153] C. J. Millow, S. A. Mackintosh, R. L. Lewison, N. G. Dodder and E. Hoh, *PLoS ONE,* vol. 10, p. e0127205, 2015.

[154] G. S. Frysinger and R. B. Gaines, *Journal of High Resolution Chromatography,* vol. 22, pp. 251 - 255, 1999.

[155] M. Adahchour, M. Brandt, H.-U. Baier, R. J. Vreuls, A. M. Batenburg and U. A. T. Brinkman, *Journal of Chromatography A,* vol. 1067, pp. 245 - 254, 2005.

[156] S. Hashimoto, Y. Takazawa, A. Fushimi, K. Tanabe, Y. Shibata, T. Ieda, N. Ochiai, H. Kanda, T. Ohura, Q. Tao and S. E. Reichenbach, *Journal of Chromatography A,* vol. 1218, pp. 3799 - 3810, 2011.

[157] A. Fushimi, S. Hashimoto, T. Ieda, N. Ochiai, Y. Takazawa, Y. Fujitani and K. Tanabe, *Journal of Chromatography A,* vol. 1252, pp. 164 - 170, 2012.

[158] P. Q. Tranchida, F. A. Franchina, M. Zoccali, S. Panto, D. Sciarrone, P. Dugo and L. Mondello, *Journal of Chromatography A,* vol. 1278, pp. 153 - 159, 2013.

[159] F. A. Franchina, M. E. Machado, P. Q. Tranchida, C. A. Zini, E. B. Caramao and L. Mondello, *Journal of Chromatography A,* vol. 1387, pp. 86 - 94, 2015.

[160] H. J. Tobias, Y. Zhang, R. J. Auchus and J. T. Brenna, *Analytical Chemistry,* vol. 83, pp. 7158 - 7165, 2011.

[161] H. J. Tobias, G. L. Sacks, Y. Zhang and J. T. Brenna, *Analytical Chemistry,* vol. 80, pp. 8613 - 8621, 2008.

[162] SepSolve Analytical Ltd., "Technical note: Tandem Ionisation - Revolutionary soft ionization to enhance confidence in identification," May 2021. [Online]. Available: https://www.sepsolve.com/uploads/brochure/2021-05-04-13-57-57-33-SepSolve%20White%20Paper%20043%20(Tandem%20Ionisation%20technical%20note).pdf. [Accessed 23 February 2022].

[163] LECO Corporation, "MULTI-MODE SOURCE (MMS)," 2021. [Online]. Available: https://knowledge.leco.com/brochures/multi-mode-source-mms-209-295/viewdocument/1904. [Accessed 23 February 2022].

[164] L. R. Snyder, Principles of Adsorption Chromatography; The Separation of Nonionic Organic Compounds, New York: M. Dekker, 1968.

[165] L. R. Snyder and D. L. Saunders, *Journal of Chromatographic Science,* vol. 7, pp. 195 - 208, 1969.

[166] J. C. Giddings, *Journal of Chemical Education,* vol. 39, pp. 569 - 573, 1962.

[167] A. Wang, H. Dennis Tolley and M. L. Lee, *Journal of Chromatography A,* vol. 1261, pp. 46 - 57, 2012.

[168] M. R. Jacobs, E. F. Hilder and R. A. Shellie, *Analytica Chimica Acta,* vol. 803, pp. 2 - 14, 2013.

[169] E. U. Ehrmann, H. P. Dharmasena, K. Carney and E. B. Overton, *Journal of Chromatographic Science,* vol. 34, pp. 533 - 539, 1996.

[170] J. Dallüge, R. Ou-Aissa, J. J. Vreuls and U. A. Brinkman, *Journal of High Resolution Chromatography,* vol. 22, pp. 459 - 464, 1999.

[171] A. B. Fialkov, M. Morag and A. Amirav, *Jounal of Chromatography A,* vol. 1218, pp. 9375 - 9383, 2011.

[172] Agilent Technologies, Inc., "Agilent Low Thermal Mass (LTM) Series II System for Gas Chromatography," 27 April 2020. [Online]. Available: https://www.agilent.com/cs/library/datasheets/public/5990-7688EN.pdf. [Accessed 22 December 2020].

[173] R. L. Firor, "Using a Dual LTM Series II System with Flow Modulated Comprehensive GCxGC," 20 June 2011. [Online]. Available: https://www.agilent.com/cs/library/applications/5990-8391EN.pdf. [Accessed 22 December 2020].

[174] Valco Instruments Company Inc., "Fast GC Column/Fan Modules," Valco Instruments Company Inc., [Online]. Available: https://www.vici.com/gc/column-fan-modules.php. [Accessed 22 December 2020].

[175] M. E. Hail and R. A. Yost, *Analytical Chemistry,* vol. 61, pp. 2410 - 2416, 1989.

[176] V. Jain and J. B. Phillips, *Journal of Chromatographic Science,* vol. 33, pp. 55 - 59, 1995.

[177] S. D. Stearns, H. Cai, J. A. Koehn, M. Brisbin, C. Cowles, C. Bishop, S. Puente and D. Ashworth, *Journal of Chromatography A,* vol. 1217, pp. 4629 - 4638, 2010.

[178] F. Xu, W. Guan, G. Yao and Y. Guan, *Journal of Chromatography A,* vol. 1186, pp. 183 - 188, 2008.

[179] OMEGA Engineering, "RTD," 28 August 2018. [Online]. Available: https://www.omega.ca/en/resources/rtd. [Accessed 28 October 2021].

[180] American Society for Testing and Materials, MANUAL ON THE USE OF THERMOCOUPLES IN TEMPERATURE MEASUREMENT, STP 470B, Baltimore: American Society for Testing and Materials, 1981.

[181] OMEGA Engineering, "Working principles of thermocouples," 05 March 2019. [Online]. Available: https://www.omega.ca/en/resources/how-thermocouples-work. [Accessed 28 October 2021].

[182] G. Recktenwald, "Conversion of thermocouple voltage to temperature," *Portland State University,* vol. 23, 2010.

[183] OMEGA Engineering, "Thermocouple Response Time," 17 April 2019. [Online]. Available: https://www.omega.ca/en/resources/thermocouples-response-time. [Accessed 28 October 2021].

[184] OMEGA Engineering, "RTD vs Thermocouples," 17 April 2019. [Online]. Available: https://www.omega.ca/en/resources/rtd-vs-thermocouple. [Accessed 28 October 2021].

[185] P. Boeker and J. Leppert, *Analytical Chemistry,* vol. 87, pp. 9033 - 9041, 2015.

[186] OMEGA Engineering, "Infrared Thermometer," 29 August 2018. [Online]. Available: https://www.omega.ca/en/resources/infrared-thermometer. [Accessed 28 October 2021].

[187] OMEGA Engineering, " What is a Thermistor and how does it work?," 28 August 2018. [Online]. Available: https://www.omega.ca/en/resources/thermistor. [Accessed 28 October 2021].

[188] B. Chowdhury and F. Karasek, *Journal of Chromatographic Science,* vol. 8, pp. 199 - 202, 1970.

[189] AGC Instruments Ltd., "Hot Wire Filaments & Thermistors," June 2010. [Online]. Available: https://agc-instruments.com/wp-content/uploads/2010/06/Hot_Wire_Filaments_Thermistors_Brochure_4.pdf. [Accessed 23 February 2022].

[190] Arduino, "What is Arduino?," Arduino, 05 February 2018. [Online]. Available: https://www.arduino.cc/en/Guide/Introduction. [Accessed 27 September 2021].

[191] Arduino, "Arduino Nano 33 BLE Sense," Arduino, 22 September 2021. [Online]. Available: https://store-usa.arduino.cc/products/arduino-nano-33-ble-sense?selectedStore=us. [Accessed 27 September 2021].

[192] Wiring, "Wiring," Wiring, [Online]. Available: http://wiring.org.co/about.html. [Accessed 27 September 2021].

[193] Raspberry Pi, "Raspberry Pi Pico Datasheet," 30 September 2021. [Online]. Available: https://datasheets.raspberrypi.com/pico/pico-datasheet.pdf. [Accessed 28 October 2021].

[194] Raspberry Pi, "Raspberry Pi Pico," 21 January 2021. [Online]. Available: https://www.raspberrypi.com/products/raspberry-pi-pico/. [Accessed 01 November 2021].

[195] Arduino, "Arduino Nano Every," 27 August 2021. [Online]. Available: https://store-usa.arduino.cc/products/arduino-nano-every. [Accessed 01 November 2021].

[196] M. K. Das, S. C. Bishwal, A. Das, D. Dabral, A. Varshney, V. K. Badireddy and R. Nanda, *Analytical Chemistry,* vol. 86, pp. 1229 - 1237, 2014.

[197] G. S. Groenewold, K. M. Johnson, S. C. Fox, C. Rae, C. A. Zarzana, B. R. Kersten, S. M. Rowe, T. L. Westover, G. L. Gresham, R. M. Emerson and A. N. Hoover, *Energy Fuels,* vol. 31, pp. 1620 - 1630, 2017.

[198] B. Kalinová, J. Kindl, P. Jiroš, P. Žáček, S. Vašíčková, M. Buděšínský and I. Valterová, *Journal of Natural Products,* vol. 72, pp. 8 - 13, 2009.

[199] V. V. Lobodin, W. K. Robbins, J. Lu and R. P. Rodgers, *Energy Fuels,* vol. 29, pp. 6177 - 6186, 2015.

[200] T. L. Tasker, W. D. Burgos, P. Piotrowski, L. Castillo-Meza, T. A. Blewett, K. B. Ganow, A. Stallworth, P. L. M. Delompré, G. G. Goss, L. B. Fowler, J. P. Vanden Heuvel, F. Dorman and N. R. Warner, *Environmental Science & Technology,* vol. 52, pp. 7081 - 7091, 2018.

[201] A. M. Booth, P. A. Sutton, A. Anthony Lewis, A. C. Lewis, A. Scarlett, W. Chau and S. J. Rowland, *Environmental Science & Technology,* vol. 2007, pp. 457 - 464, 2007.

[202] J. H. Winnike, X. Wei, K. J. Knagge, S. D. Colman, S. D. Gregory and X. Zhang, *Journal of Proteome Research,* vol. 14, pp. 1810 - 1817, 2015.

[203] J. Manheim, K. Wehde, W. T. J. Zhang, P. Vozka, M. Romanczyk, G. Kilaz and H. I. Kenttämaa, *Journal of the Americal Society for Mass Spectrometry,* vol. 30, pp. 2670 - 2677, 2019.

[204] H. Parastar, J. R. Radović, M. Jalali-Heravi, S. Diez, J. M. Bayona and R. Tauler, *Analytical Chemistry,* vol. 83, pp. 9289 - 9297, 2011.

[205] R. K. Nelson, K. M. Gosselin, D. J. Hollander, S. A. Murawski, A. Gracia, C. M. Reddy and J. R. Radović, *Energy Fuels,* vol. 33, pp. 3925 - 3933, 2019.

[206] M. J. Gómez, S. Herrera, D. Solé, E. García-Calvo and A. R. Fernández-Alba, *Analytical Chemistry,* vol. 83, pp. 2638 - 3647, 2011.

[207] M. Z. Özel, J. F. Hamilton and A. C. Lewis, *Environmental Science & Technology,* vol. 45, pp. 1497 - 1505, 2011.

[208] S. Risticevic and J. Pawliszyn, *Analytical Chemistry,* vol. 85, pp. 8987 - 8995, 213.

[209] C. Manzano, E. Hoh and S. L. Massey Simonich, *Environmental Science & Technology,* vol. 46, pp. 7677 - 7684, 2012.

[210] D. Nabi and J. S. Arey, *Environmental Science & Technology,* vol. 51, pp. 3001 - 3011, 2017.

[211] H. C. Reinardy, A. G. Scarlett, T. B. Henry, C. E. West, L. Mark Hewitt, R. A. Frank and S. J. Rowland, *Environmental Science & Technology,* vol. 47, pp. 6614 - 6620, 2013.

[212] R. D. Deese, R. E. Morris, A. E. Metz, K. M. Myers, K. Johnson and T. N. Loegel, *Energy Fuels,* vol. 33, pp. 6659 - 6669, 2019.

[213] J. V. Seeley, S. K. Seeley, E. K. Libby and J. D. McCurry, *Journal of Chromatographic Science,* vol. 45, pp. 650 - 656, 2007.

[214] Agilent Technologies, "Retention Time Reproducibility of the Agilent 6890 Plus GC," August 1999. [Online]. Available: https://www.agilent.com/cs/library/technicaloverviews/public/59686420.pdf.

[215] National Institute of Standards and Technology, "ITS-90 Table for type K thermocouple," 29 12 1999. [Online]. Available: https://srdata.nist.gov/its90/download/type_k.tab. [Accessed 18 05 2022].

[216] K. J. Åström and R. M. Murray, "PID Control," in *Feedback Systems*, Princeton, Princeton University Press, 2008, pp. 293 - 313.

[217] B. Beauregard, "Arduino-PID-Library," 20 June 2017. [Online]. Available: https://github.com/br3ttb/Arduino-PID-Library/.

[218] W. F. Gale and T. C. Totemeier, Smithells Metals Reference Book, Kidlington: Elsevier Butterworth-Heinemann, 2004.

[219] Calibornia Fine Wire Co., "STAINLESS STEEL 304 MATERIAL #:100192," California Fine Wire Co., 23 June 2020. [Online]. Available: https://calfinewire.com/datasheets/100192-stainlesssteel304/. [Accessed 18 November 2021].

[220] Scott Precision Wire, "Stainless Steel 304L," Scott Precision Wire, 23 April 2021. [Online]. Available: https://www.scottprecisionwire.com/technical-data/alloy-data-sheets/stainless-steel-304l/. [Accessed 18 November 2021].

[221] D. Norton, "What does SELV mean for power supplies?," 14 May 2013. [Online]. Available: https://www.edn.com/what-does-selv-mean-for-power-supplies/. [Accessed 17 August 2022].

[222] Alpha Technologies Services, "NEC CLASS 2 FAQs," [Online]. Available: https://www.alpha.ca/index.php/nec-class-2-faqs. [Accessed 17 August 2022].

[223] Rockwell Automation, "Designing NEC Class 2 Circuits," July 2012. [Online]. Available: https://literature.rockwellautomation.com/idc/groups/literature/documents/wp/1692-wp001_-en-p.pdf. [Accessed 17 August 2022].

[224] M. S. Van Dusen, *Journal of the American Chemical Soceity,* vol. 47, pp. 326 - 332, 1925.

[225] Texas Instruments, "ADS111x Ultra-Small, Low-Power, I2C-Compatible, 860-SPS, 16-Bit ADCs With Internal Reference, Oscillator, and Programmable Comparator datasheet (Rev. D)," Texas Instruments, January 2018. [Online]. Available: file:///C:/Users/John%20Chow/Downloads/ads1115.pdf. [Accessed 29 December 2021].

[226] Maxim Integrated Products, "MAX31855," February 2012. [Online]. Available: https://cdn-shop.adafruit.com/datasheets/MAX31855.pdf. [Accessed 17 August 2022].

[227] Agilent Technologies Inc., "6890 Series Gas Chromatograph Service Manual," Agilent Technologies, Inc., Wilmington, 2001.

[228] Dennis, "soligen2010/Adafruit_ADS1X15," [Online]. Available: https://github.com/soligen2010/Adafruit_ADS1X15. [Accessed 11 September 2018].

[229] Adafruit Industries, "adafruit/Adafruit_ADS1X15," Adafruit Industries, [Online]. Available: https://github.com/adafruit/Adafruit_ADS1X15. [Accessed 29 December 2021].

[230] The NIST Mass Spectrometry Data Center, "NIST Standard Reference Database 1A," June 2008. [Online]. Available: https://chemdata.nist.gov/mass-spc/ms-search/docs/Ver20Man.pdf. [Accessed 01 June 2022].

[231] W. A. Dietz, *Journal of Chromatographic Science,* vol. 5, pp. 68 - 71, 1967.

[232] H. Y. Tong and F. W. Karasek, *Analytical Chemistry,* vol. 56, pp. 2124 - 2128, 1984.

[233] Agilent Technologies, "Agilent 6890N Network Gas Chromatograph," 24 January 2007. [Online]. Available: https://www.agilent.com/cs/library/specifications/Public/5989-3290EN.pdf. [Accessed 27 June 2022].

[234] S. Bom, J. Jorge, H. Ribeiro and J. Marto, *Journal of Cleaner Production,* vol. 225, pp. 270 - 290, 2019.

[235] C. K. Ho, K. B. McAuley and B. A. Peppley, *Renewable and Sustainable Energy Reviews,* vol. 113, p. 109261, 2019.

[236] S. K. Hoekman, A. Broch, C. Robbins, E. Ceniceros and M. Natarajan, *Renewable and Sustainable Energy Reviews,* vol. 16, pp. 143 - 169, 2012.

[237] J. Zakzeski, P. C. A. Bruijnincx, A. L. Jongerius and B. M. Weckhuysen, *Chemical Reviews,* vol. 110, pp. 3552 - 3599, 2010.

[238] T. A. P. Hai, M. Tessman, N. Neelakantan, A. A. Samoylov, Y. Ito and B. S. Rajput, *Biomacromolecules,* vol. 22, pp. 1770 - 1794, 2021.

[239] F. Mellou, A. Varvaresou and S. Papageorgiou, *International Journal of Cosmetic Science,* vol. 41, pp. 517 - 525, 2019.

[240] S. Le Guenic, L. Chaveriat, V. Lequart, N. Joly and P. Martin, *Journal of Surfactants and Detergents,* vol. 22, pp. 5 - 21, 2019.

[241] M. Moon, W.-K. Park, S. Y. Lee, K.-R. Hwang, S. Lee, M.-S. Kim, B. Kim, Y.-K. Oh and J.-S. Lee, *Renewable and Sustainable Energy Reviews,* vol. 160, p. 112269, 2022.

[242] M. Moreira, A. C. Gurgel and J. E. A. Seabra, *Environmental Science & Technology,* vol. 48, pp. 14756 - 14763, 2014.

[243] T. M. Panchal, A. Patel, D. Chauhan, M. Thomas and J. V. Patel, *Renewable and Sustainable Energy Reviews,* vol. 70, pp. 65 - 70, 2017.

[244] M. J. Biddy, C. Scarlata and C. Kinchin, "Chemicals from Biomass: A Market Assessment of Bioproducts with Near-Term Potential," March 2016. [Online]. Available: https://www.nrel.gov/docs/fy16osti/65509.pdf. [Accessed 27 September 2022].

[245] D. Malevich, J. Dambacher, F. Lockwood, L. Zhang, W. Mabee and C. Joshi, *TechConnect Briefs,* vol. 2, pp. 187 - 192, 2016.

[246] D. Malevich and G. T. T. Gibson, "Production of Hydrocarbons from plant oil and animal fat". USA Patent 9611554, 15 September 2015.

[247] C. Joshi, S. Lee and D. Malevich, "Process for producing synthetic squalane and squalane derivatives". USA Patent WO-2020220134-A1, 11 May 2020.

[248] O. J. Ackelsberg, *Journal of the American Oil Chemists Society,* vol. 35, pp. 635 - 640, 1958.

[249] H. L. Barnebey and A. C. Brown, *Journal of the American Oil Chemists Society,* vol. 25, pp. 95 - 99, 1948.

[250] E. Twitchell, "Process of decomposing fats or oils into fatty acids and glycerin". USA Patent 601603, 29 March 1898.

[251] A. Ziogas, H. Pennemann and G. Kolb, *Electrocatalysis,* vol. 11, pp. 432 - 442, 2020.

[252] A. H. Lichtenstein, "Fats and Oils," in *Encyclopedia of Human Nutrition (Third Edition)*, Waltham, Academic Press, 2013, pp. 201 - 208.

[253] K. Ichihara and Y. Fukubayashi, *Journal of Lipid Research,* vol. 51, pp. 635 - 640, 2010.

[254] H. A. Boswell, M. Edwards and T. Górecki, *Separations,* vol. 7, p. 70, 2020.

[255] W. Welthagen, J. Schnelle-Kreis and R. Zimmermann, *Journal of Chromatography A,* vol. 1019, pp. 233 - 249, 2003.

[256] L. Vogt, T. Gröger and R. Zimmermann, *Journal of Chromatography A,* vol. 1150, pp. 2 - 12, 2007.

[257] K. Lissitsyna, S. Huertas, L. Quintero and L. Polo, *Fuel,* vol. 116, pp. 716 - 722, 2014.

[258] M. Morval, I. Pályka and I. Molnár-Perl, *Journal of Chromatographic Science,* vol. 30, pp. 448 - 452, 1992.

[259] K. Rome and A. McIntyre, *Chromatography Today,* vol. May/June, pp. 52 - 56, 2012.

[260] C. L. Faiola, M. H. Erickson, V. L. Fricaud, B. T. Jobson and T. M. VanReken, *Atmospheric Measurement Techniques,* vol. 5, pp. 1911 - 1923, 2012.

[261] F. Ulberth, R. G. Gabernig and F. Schrammel, *Journal of American Oil Chemists' Society,* vol. 76, pp. 263 - 266, 1999.

[262] R. G. Ackman and J. C. Sipos, *Journal of the American Oil Chemists' Society,* vol. 41, pp. 377 - 378, 1964.

[263] J.-Y. Saint Laumer, E. Cicchetti, P. Merie, J. Egger and A. Chaintreau, *Analytical Chemistry,* vol. 82, pp. 6457 - 6462, 2010.

[264] R. Pirow, A. Blume, N. Hellwig, M. Herzler, B. Huhse, C. Hutzler, K. Pfaff, H.-J. Thierse, T. Tralau, B. Vieth and A. Luch, *Critical Reviews in Toxicology,* vol. 49, pp. 742 - 789, 2019.

[265] S. Weber, T. Schmidt, P. Schumacher, T. Kuballa, G. Mildau, S. G. Walch, A. Hartwig and D. W. Lachenmeier, *Journal of Chemistry,* vol. 2019, pp. 1 - 10, 2019.

[266] L. Jouanneau, "Manufacture of Mineral OIl and Wax Composition and Specifications," in *Mocrinis II Workshop*, Brussels, 2017.

[267] G. R. Kelm and R. R. Wickett, "The role of Fatty Acids in Cosmetic Technology," in *Fatty Acids - Chemistry, Synthesis, and Applications*, London, Academic Press, 2017, pp. 385 - 404.

[268] Agilent Technologies, "Agilent G3180B Two-Way Splitter Kit With Makeup Gas Installation and Operation Guide," April 2006. [Online]. Available: https://usermanual.wiki/Agilent-Technologies/AgilentTechnologiesG3180BUsersManual413162.971967402.pdf. [Accessed 27 October 2022].

[269] G. W. O'Neil, G. Knothe, J. R. Williams, N. P. Burlow and C. M. Reddy, *Fuel,* vol. 179, pp. 229 - 234, 2016.

[270] J. E. Lee, Z.-H. Li, E. D. Christensen and T. L. Alleman, *Energy & Fuels,* vol. 36, pp. 7592 - 7598, 2022.

[271] A. Muylert, Y. Kuwahara, T. Hongpattarakere and Y. Asano, *Scientific Reports,* vol. 8, p. 11730, 2018.

[272] C. K. Fagerquist, R. A. Neese and M. K. Hellerstein, *Journal of the American Society for Mass Spectrometry,* vol. 10, pp. 430 - 439, 1999.

Appendix

Appendix A Chapter 2 Supplementary Data and Figures

Table A – 1: Heating times measured using a 0.003" K-type thermocouple directly soldered to an MXT column of various dimensions, measured at different oven temperatures and for different temperature offsets.

Heating Times									
Col. Len. (m)	Col. I.D. (mm)	Oven Temp. (°C)	Temp. Offset (°C)	Current (A)	Trial 1 (s)	Trial 2 (s)	Trial 3 (s)	Avg. (s)	S.D.
1.00	0.25	50	40	1.50	1.6	1.5	1.5	1.5	0.1
1.00	0.25	50	30	1.21	1.5	1.5	1.4	1.5	0.1
1.00	0.25	50	20	1.00	1.5	1.5	1.5	1.5	0.0
1.00	0.25	100	40	1.45	1.5	1.5	1.5	1.5	0.0
1.00	0.25	100	30	1.21	1.5	1.5	1.5	1.5	0.0
1.00	0.25	100	20	0.95	1.4	1.4	1.4	1.4	0.0
1.00	0.25	150	40	1.46	1.5	1.5	1.5	1.5	0.0
1.00	0.25	200	40	1.46	1.6	1.5	1.6	1.6	0.1
0.75	0.25	50	40	1.39	1.5	1.6	1.5	1.5	0.1
0.75	0.25	50	30	1.23	1.4	1.4	1.4	1.4	0.0
0.75	0.25	50	20	0.93	1.4	1.3	1.2	1.3	0.1
0.75	0.25	100	40	1.32	1.4	1.5	1.4	1.4	0.1
0.75	0.25	100	30	1.21	1.2	1.4	1.3	1.3	0.1
0.75	0.25	100	20	0.93	1.2	1.2	1.2	1.2	0.0
0.75	0.25	150	40	1.42	1.5	1.5	1.4	1.5	0.1
0.75	0.25	150	30	1.25	1.4	1.4	1.4	1.4	0.0
0.75	0.25	150	20	0.96	1.3	1.3	1.4	1.3	0.1
0.75	0.25	200	40	1.36	1.4	1.4	1.2	1.3	0.1
0.75	0.25	200	30	1.21	1.2	1.2	1.2	1.2	0.0
0.75	0.25	200	20	0.97	1.2	1.2	1.3	1.2	0.1
0.50	0.25	50	40	1.48	2	2.4	2.2	2.2	0.2
0.50	0.25	50	30	1.27	2.5	2.2	2.4	2.4	0.2
0.50	0.25	50	20	1.07	2.4	2	2.1	2.2	0.2
0.50	0.25	100	40	1.48	2	2.4	2	2.1	0.2
0.50	0.25	100	30	1.24	2.1	1.8	2.1	2.0	0.2
0.50	0.25	100	20	1.01	1.7	2	2	1.9	0.2
0.50	0.25	150	40	1.45	2	1.8	2	1.9	0.1
0.50	0.25	150	30	1.22	1.7	2	1.9	1.9	0.2
0.50	0.25	150	20	1.02	1.6	1.5	1.6	1.6	0.1
0.50	0.25	200	40	1.37	2	2	2.2	2.1	0.1
0.50	0.25	200	30	1.21	1.8	1.9	1.7	1.8	0.1
0.50	0.25	200	20	1.02	2	2.3	1.8	2.0	0.3

0.50	0.18	50	40	1.12	1.5	1.4	1.6	1.5	0.1
0.50	0.18	50	30	0.98	1.4	1.6	1.5	1.5	0.1
0.50	0.18	50	20	0.79	1.2	1.2	1.2	1.2	0.0
0.50	0.18	100	40	1.13	1.5	1.6	2	1.7	0.3
0.50	0.18	100	30	0.98	1.6	1.4	1.6	1.5	0.1
0.50	0.18	100	20	0.79	1.4	1.3	1.2	1.3	0.1
0.50	0.18	150	40	1.13	1.4	1.6	1.5	1.5	0.1
0.50	0.18	150	30	0.98	1.4	1.4	1.6	1.5	0.1
0.50	0.18	150	20	0.78	1.5	1.4	1.3	1.4	0.1
0.50	0.18	200	40	1.12	1.5	1.4	1.5	1.5	0.1
0.50	0.18	200	30	0.98	1.5	1.6	1.4	1.5	0.1
0.50	0.18	200	20	0.78	1.4	1.4	1.3	1.4	0.1
0.50	0.18	250	40	1.06	1.6	1.5	1.8	1.6	0.2
0.50	0.18	250	30	0.92	1.4	1.5	1.4	1.4	0.1
0.50	0.18	250	20	0.75	1.2	1.2	1.2	1.2	0.0

Table A – 2: Cooling times measured using a 0.003" K-type thermocouple directly soldered to an MXT column of various dimensions, measured at different oven temperatures and for different temperature offsets.

Cooling Times									
Col. Len. (m)	Col. I.D. (mm)	Oven Temp. (°C)	Temp. Offset (°C)	Current (A)	Trial 1 (s)	Trial 2 (s)	Trial 3 (s)	Avg. (s)	S.D.
1.00	0.25	50	40	1.46	1.8	1.9	1.9	1.9	0.1
1.00	0.25	50	30	1.26	1.8	1.8	1.8	1.8	0.0
1.00	0.25	50	20	1.03	1.6	1.7	1.6	1.6	0.1
1.00	0.25	100	40	1.44	1.8	1.8	1.7	1.8	0.1
1.00	0.25	100	30	1.18	1.7	1.7	1.7	1.7	0.0
1.00	0.25	100	20	0.99	1.5	1.6	1.5	1.5	0.1
1.00	0.25	150	40	1.46	1.6	1.7	1.7	1.7	0.1
1.00	0.25	150	30	1.27	1.5	1.6	1.6	1.6	0.1
1.00	0.25	150	20	1.02	1.4	1.5	1.4	1.4	0.1
1.00	0.25	200	40	1.46	1.6	1.6	1.6	1.6	0.0
1.00	0.25	200	30	1.27	1.5	1.5	1.5	1.5	0.0
1.00	0.25	200	20	1.06	1.4	1.4	1.4	1.4	0.0
0.75	0.25	50	40	1.39	1.9	1.8	1.8	1.8	0.1
0.75	0.25	50	30	1.25	1.6	1.5	1.6	1.6	0.1
0.75	0.25	50	20	0.99	1.3	1.2	1.2	1.2	0.1
0.75	0.25	100	40	1.39	1.5	1.6	1.6	1.6	0.1
0.75	0.25	100	30	1.26	1.4	1.4	1.4	1.4	0.0
0.75	0.25	100	20	0.99	1.2	1.2	1.1	1.2	0.1
0.75	0.25	150	40	1.41	1.4	1.4	1.5	1.4	0.1
0.75	0.25	150	30	1.22	1.3	1.2	1.4	1.3	0.1
0.75	0.25	150	20	0.99	1.1	1.2	1.1	1.1	0.1

0.75	0.25	200	40	1.37	1.4	1.4	1.4	1.4	0.0
0.75	0.25	200	30	1.27	1.3	1.2	1.2	1.2	0.1
0.75	0.25	200	20	1.02	1.1	1.1	1.2	1.1	0.1
0.50	0.25	50	40	1.45	2.2	2.2	2.1	2.2	0.1
0.50	0.25	50	30	1.26	2	2	2.2	2.1	0.1
0.50	0.25	50	20	1.01	2	2	2.1	2.0	0.1
0.50	0.25	100	40	1.44	2.2	2	2	2.1	0.1
0.50	0.25	100	30	1.24	2.1	2	1.9	2.0	0.1
0.50	0.25	100	20	1.02	1.8	1.7	1.9	1.8	0.1
0.50	0.25	150	40	1.42	2.2	2.1	2.1	2.1	0.1
0.50	0.25	150	30	1.25	1.9	2	2	2.0	0.1
0.50	0.25	150	20	1.02	1.9	1.8	1.8	1.8	0.1
0.50	0.25	200	40	1.42	2	2	2.1	2.0	0.1
0.50	0.25	200	30	1.25	1.8	1.9	1.9	1.9	0.1
0.50	0.25	200	20	1.01	1.7	1.8	1.8	1.8	0.1
0.50	0.18	50	40	1.12	1.5	1.8	1.6	1.6	0.2
0.50	0.18	50	30	0.98	1.6	1.4	1.4	1.5	0.1
0.50	0.18	50	20	0.79	1.2	1	1.3	1.2	0.2
0.50	0.18	100	40	1.13	1.6	1.7	2	1.8	0.2
0.50	0.18	100	30	0.98	1.4	1.5	1.5	1.5	0.1
0.50	0.18	100	20	0.79	1.3	1.1	1.2	1.2	0.1
0.50	0.18	150	40	1.13	1.6	1.6	1.5	1.6	0.1
0.50	0.18	150	30	0.98	1.6	1.5	1.6	1.6	0.1
0.50	0.18	150	20	0.78	1.4	1.3	1.3	1.3	0.1
0.50	0.18	200	40	1.12	1.5	1.4	1.5	1.5	0.1
0.50	0.18	200	30	0.98	1.5	1.5	1.6	1.5	0.1
0.50	0.18	200	20	0.78	1.4	1.2	1.2	1.3	0.1
0.50	0.18	250	40	1.06	1.7	1.6	1.7	1.7	0.1
0.50	0.18	250	30	0.92	1.4	1.6	1.4	1.5	0.1
0.50	0.18	250	20	0.75	1.2	1.2	1.3	1.2	0.1

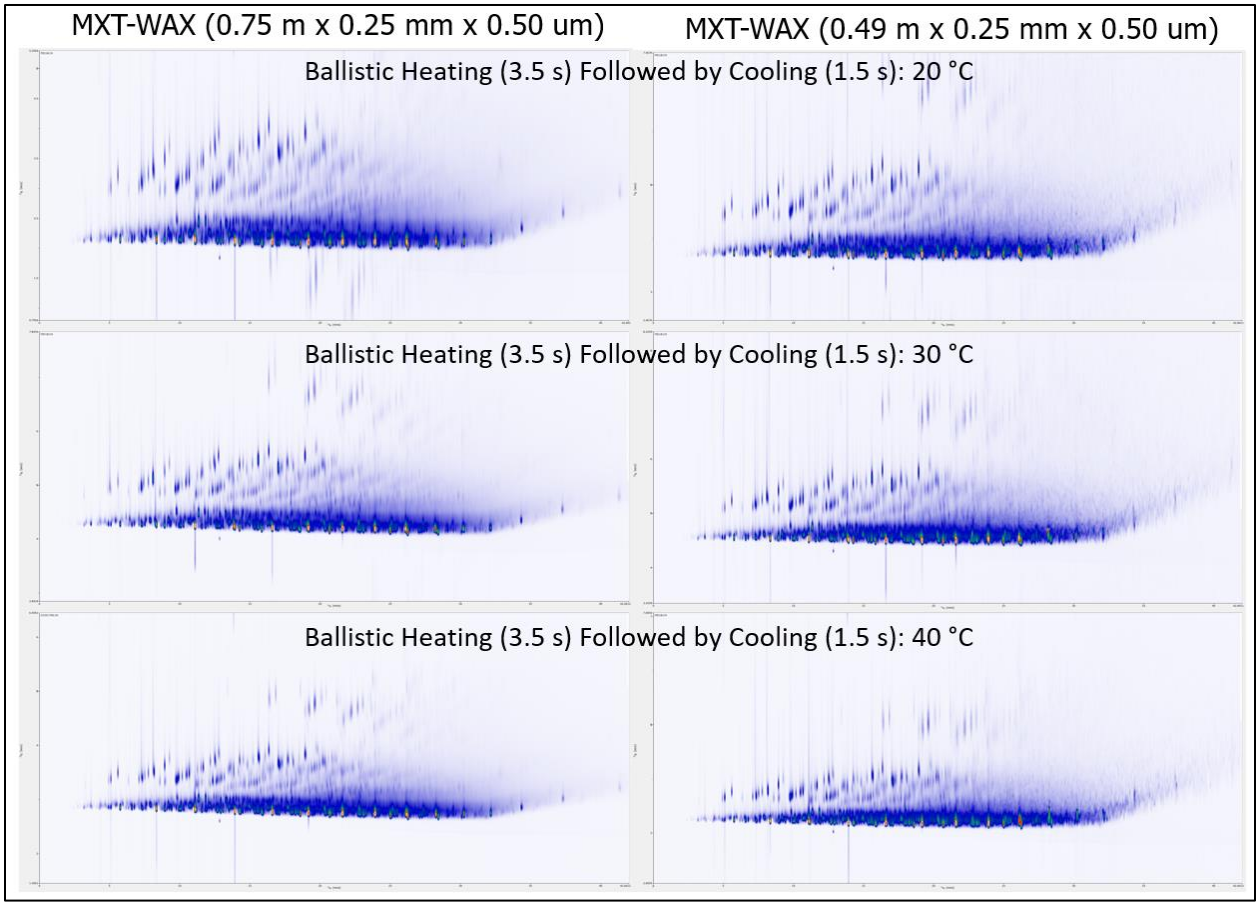

Figure A – 1: Comparison of a 0.75 m and 0.49 m MXT-WAX (0.25 mm x 0.50 µm) ^{2}D column using ballistic heating in configuration 1. ***X-axis: 0 – 42 min. 5 s modulation period****.*

Table A – 3: Retention times and % RSDs for 10 peaks after five consecutive injections of diesel with second dimension ballistic heating.

Peak	Retention Time	Trial 1	Trial 2	Trial 3	Trial 4	Trial 5	Mean	SD	RSD (%)
1	^1t_r (min)	11.933	11.933	11.933	11.933	11.933	11.933	0.000	0.00
	^2t_r (s)	1.25	1.27	1.27	1.26	1.27	1.26	0.01	0.62
2	^1t_r (min)	20.400	20.400	20.400	20.400	20.400	20.400	0.000	0.00
	^2t_r (s)	1.31	1.31	1.31	1.30	1.32	1.31	0.01	0.36
3	^1t_r (min)	28.533	28.533	28.533	28.533	28.533	28.533	0.000	0.00
	^2t_r (s)	1.31	1.34	1.33	1.33	1.32	1.33	0.01	0.97
4	^1t_r (min)	39.467	39.467	39.467	39.400	39.467	39.453	0.030	0.08
	^2t_r (s)	1.42	1.36	1.38	1.35	1.36	1.38	0.03	2.0
5	^1t_r (min)	48.933	48.933	48.933	48.933	48.933	48.933	0.000	0.00
	^2t_r (s)	1.46	1.45	1.42	1.482	1.44	1.45	0.02	1.6
6	^1t_r (min)	7.933	7.933	7.933	7.933	7.933	7.933	0.000	0.00
	^2t_r (s)	1.69	1.68	1.70	1.68	1.70	1.69	0.01	0.41
7	^1t_r (min)	14.333	14.333	14.333	14.333	14.333	14.333	0.000	0.00
	^2t_r (s)	2.21	2.21	2.21	2.21	2.21	2.21	0.00	0.16
8	^1t_r (min)	18.733	18.733	18.733	18.733	18.733	18.733	0.000	0.00
	^2t_r (s)	2.22	2.20	2.21	2.20	2.21	2.21	0.01	0.36
9	^1t_r (min)	21.000	21.000	21.000	21.000	21.000	21.000	0.000	0.00
	^2t_r (s)	2.13	2.13	2.15	2.13	2.13	2.13	0.01	0.39
10	^1t_r (min)	24.000	24.000	24.000	24.000	24.000	24.000	0.000	0.00
	^2t_r (s)	2.29	2.28	2.28	2.29	2.27	2.28	0.01	0.50

Table A – 4: Retention times and % RSDs for 10 peaks after five consecutive injections of diesel for a standard GC×GC separation.

Peak	Retention Time	Trial 1	Trial 2	Trial 3	Trial 4	Trial 5	Mean	SD	RSD (%)
1	^1t_r (min)	11.933	11.933	11.933	11.933	11.933	11.933	0.000	0.00
	^2t_r (s)	1.50	1.50	1.49	1.49	1.50	1.50	0.01	0.49
2	^1t_r (min)	20.400	20.400	20.400	20.400	20.400	20.400	0.000	0.00
	^2t_r (s)	1.60	1.61	1.61	1.59	1.61	1.61	0.01	0.46
3	^1t_r (min)	28.533	28.533	28.533	28.533	28.533	28.533	0.000	0.00
	^2t_r (s)	1.67	1.69	1.68	1.68	1.68	1.68	0.01	0.49
4	^1t_r (min)	39.400	39.400	39.400	39.400	39.400	39.400	0.000	0.00
	^2t_r (s)	1.77	1.80	1.81	1.82	1.78	1.80	0.02	1.2
5	^1t_r (min)	48.867	48.867	48.867	48.867	48.867	48.867	0.000	0.00
	^2t_r (s)	1.92	1.94	1.97	1.97	1.98	1.96	0.02	1.2
6	^1t_r (min)	7.867	7.800	7.800	7.867	7.867	7.840	0.037	0.47
	^2t_r (s)	2.11	2.13	2.14	2.10	2.10	2.12	0.02	0.80
7	^1t_r (min)	14.267	14.267	14.267	14.267	14.267	14.267	0.000	0.00
	^2t_r (s)	3.07	3.08	3.08	3.07	3.08	3.08	0.00	0.14
8	^1t_r (min)	18.667	18.667	18.667	18.667	18.667	18.667	0.000	0.00
	^2t_r (s)	3.11	3.10	3.14	3.10	3.11	3.11	0.01	0.43
9	^1t_r (min)	20.933	20.933	20.933	20.933	20.933	20.933	0.000	0.00
	^2t_r (s)	2.95	2.98	2.94	2.96	2.94	2.96	0.02	0.66
10	^1t_r (min)	23.933	23.933	23.933	23.933	23.933	23.933	0.000	0.00
	^2t_r (s)	3.26	3.31	3.27	3.29	3.28	3.28	0.02	0.64

Table A – 5: $R_{s,2D}$ comparison of 5 peak pairs for GC×GC separation without ^{2}D heating, with ^{2}D ballistic heating (30 °C), and with a ^{2}D constant offset (20 °C).

Standard GC×GC								
Peak	^1t_r (min)	^1W_b (min)	^2t_r (s)	^{2}FWHM (s)	^2W_b (s)	^1R_s	^2R_s	$R_{s,2D}$
1	10.309	0.199	1.55	0.194	0.329	0.14	1.84	1.85
2	10.333	0.133	2.31	0.292	0.495			
3	12.034	0.267	1.59	0.148	0.252	1.08	0.99	1.47
4	12.285	0.200	1.94	0.272	0.462			
5	22.145	0.266	1.94	0.247	0.419	0.30	2.57	2.58
6	22.046	0.399	3.30	0.378	0.642			
7	25.156	0.267	3.21	0.357	0.606	0.22	1.58	1.60
8	25.200	0.133	4.14	0.334	0.568			
9	26.377	0.333	3.34	0.427	0.726	0.14	1.52	1.53
10	26.419	0.266	4.44	0.423	0.719			
Avg.	-	0.246	-	0.307	0.522	0.38	1.70	1.81
Ballistic Heating (30 °C)								
Peak	^1t_r (min)	^1W_b (min)	^2t_r (s)	^{2}FWHM (s)	^2W_b (s)	^1R_s	^2R_s	$R_{s,2D}$
1	10.330	0.265	3.80	0.151	0.256	0.12	1.65	1.65
2	10.358	0.201	4.33	0.229	0.389			
3	12.032	0.200	3.82	0.122	0.207	1.27	0.83	1.51
4	12.285	0.200	4.06	0.218	0.371			
5	22.147	0.267	4.01	0.215	0.365	0.38	2.20	2.23
6	22.021	0.399	4.77	0.195	0.331			
7	25.159	0.267	4.75	0.196	0.333	0.20	1.29	1.31
8	25.200	0.133	5.13	0.153	0.261			
9	26.382	0.267	4.81	0.258	0.438	0.18	1.19	1.20
10	26.424	0.200	5.24	0.163	0.277			
Avg.	-	0.240	-	0.190	0.323	0.43	1.43	1.58
Constant Offset (20 °C)								
Peak	^1t_r (min)	^1W_b (min)	^2t_r (s)	^{2}FWHM (s)	^2W_b (s)	^1R_s	^2R_s	$R_{s,2D}$
1	10.320	0.199	1.25	0.112	0.191	0.01	1.27	1.27
2	10.317	0.267	1.53	0.149	0.253			
3	12.051	0.266	1.25	0.095	0.162	1.00	0.76	1.26
4	12.316	0.265	1.40	0.143	0.242			
5	22.215	0.266	1.35	0.160	0.273	0.32	1.71	1.74
6	22.108	0.400	1.85	0.188	0.319			
7	25.179	0.200	1.82	0.176	0.299	0.21	1.20	1.22
8	25.221	0.200	2.20	0.194	0.329			
9	26.432	0.200	1.86	0.211	0.358	0.05	1.24	1.24
10	26.444	0.266	2.28	0.188	0.320			
Avg.	-	0.253	-	0.162	0.274	0.32	1.24	1.34
Constant Offset (30 °C)								
Peak	^1t_r (min)	^1W_b (min)	^2t_r (s)	^{2}FWHM (s)	^2W_b (s)	^1R_s	^2R_s	$R_{s,2D}$
1	10.309	0.200	3.65	0.092	0.156	0.23	0.93	0.96
2	10.356	0.200	3.82	0.126	0.214			
3	12.045	0.266	3.64	0.081	0.137	0.86	0.62	1.06

4	12.273	0.266	3.75	0.117	0.199			
5	22.190	0.267	3.67	0.107	0.182	0.68	1.57	1.71
6	22.009	0.267	3.97	0.124	0.210			
7	25.170	0.200	3.95	0.128	0.217	0.02	1.07	1.07
8	25.173	0.200	4.17	0.117	0.199			
9	26.394	0.267	3.96	0.152	0.259	0.16	1.08	1.10
10	26.431	0.200	4.24	0.144	0.245			
Avg.	-	0.233	-	0.119	0.202	0.39	1.06	1.18

Appendix B Chapter 3 Supplementary Data and Code

Table B – 1: R_s comparison of 2 peak pairs for GC×GC separation without ^{2}D heating, with ^{2}D temperature programming (50 °C), and with a ^{2}D constant offset (40 °C) using the prototype ^{2}DTPS.

^{2}D Temperature Programming									
	Peak	^1t_r (min)	^1W_b (min)	^2t_r (s)	FWHM (s)	^2W_b (s)	^1R_s	^2R_s	$R_{s,2D}$
Pair 1	1	10.463	0.250	1.23	0.220	0.374	0.31	0.78	0.84
	2	10.374	0.333	1.52	0.208	0.353			
Pair 2	2	10.374	0.333	1.52	0.208	0.353	0.074	1.52	1.52
	3	10.398	0.334	2.03	0.189	0.321			
Constant Offset									
		^1t_r (min)	^1W_b (min)	^2t_r (s)	FWHM (s)	^2W_b (s)	^1R_s	^2R_s	$R_{s,2D}$
Pair 2	2	10.378	0.250	1.08	0.136	0.231	1.91	1.06	2.18
	3	10.934	0.333	1.39	0.206	0.349			
GC×GC without additional ^{2}D heating									
		^1t_r (min)	^1W_b (min)	^2t_r (s)	FWHM (s)	^2W_b (s)	^1R_s	^2R_s	$R_{s,2D}$
Pair 1	1	10.394	0.250	1.53	0.412	0.700	0.14	0.74	0.75
	2	10.353	0.333	2.02	0.368	0.625			
Pair 2	2	10.353	0.333	2.02	0.368	0.625	0.095	2.28	2.28
	3	10.385	0.332	3.87	0.559	0.950			

B: ^{2}D Temperature Programming Sketch – Prototype (Version 1.0)

```
#include <PID_v1.h>

//Arduino Pins
#define channelA A0 // discharge box channel I (White)
#define 279nitial A1 // discharge box channel II (Green)
#define relayPin 6  // DC power switch (High = on, Low = off)(Blue)
#define thermocouple A4 //Amplified Thermocouple Signal

//Temperature Ramp Parameters
int state = 0; //start on state 0 (delay)
279nitial channelDischarge = false; //false = discharge reset sequence
279nitial ramp = true; //true = linear ; false = Exponential
float maxTemp = 20; //in degrees C
float delayTime = 1; //in s
float rampTime = 2; //in s
float coolTime = 1.5; //in s
float rampRate;
float startTemp;

//Zero signal at start of run
const int numReadings = 25; //running average of 25 points
int readings[numReadings];      // the readings from the analog input
int readIndex = 0;              // the index of the current reading
```

```
int total = 0;                  // the running total
float average = 0;                // the average
float zero;

//Temperature Moving Average
const int period = 12; //running average of 12 points
int tempReading[period];      // the readings from the analog input
int index = 0;              // the index of the current reading
int totalTemp = 0;                  // the running total
float averageTemp = 0;                // the average
float filter;


unsigned long cycleTime;
int counter = 0; //to reduce the number of readings sent through Serial

//PID parameters
double Kp=1.5; //Initial Proportional Gain
double Ki=0.9; //Initial Integral Gain (reacts to difference)
double Kd=0.3; //Initial Differential Gain (reduces over reaction)
double Input, Output, Setpoint;
unsigned long windowSize = 25;
unsigned long initTime;
unsigned long windowStartTime;

int channel; //variable to store channel discharge value

//Object Instantiation
PID myPID(&Input, &Output, &Setpoint, Kp, Ki, Kd, DIRECT);

void setup()
{
 Serial.begin(115200); //Start a serial session
 pinMode(channelA, INPUT);
 pinMode(280nitial, INPUT);
 pinMode(thermocouple, INPUT); //280nitialize thermocouple as an input
 pinMode(relayPin, OUTPUT); //initialize the relayPin as an output
 digitalWrite(relayPin, LOW); //keep power supply off

 //initialize all readings to 0
   for (int thisReading = 0; thisReading < numReadings; thisReading++)
   {
    readings[thisReading] = 0;
   }
   for (int thisReading = 0; thisReading < period; thisReading++)
   {
    tempReading[thisReading] = 0;
   }


 //PID Setup
   myPID.SetOutputLimits(0, windowSize);
   myPID.SetTunings(Kp, Ki, Kd);
   myPID.SetMode(AUTOMATIC);
}

void loop()
```

```
   {
     while(!channelDischarge)
     {
       zero = background();
       channel = analogRead(channelA);
       if(channel > 500)
       {
         channelDischarge = true;
       }
     }
     double elapseTimeMS;
     double elapseTime;
      switch (state)
      {
         case 0: //delay
            initTime = millis();
            cycleTime = delayTime*1000;

            //reset counter
            counter = 0;

            //Determine time left in current phase
            elapseTimeMS = millis() - initTime;
            while(elapseTimeMS < cycleTime)
            {
              counter = counter + 1;
              digitalWrite(relayPin, LOW);
              //Determine time left in current phase
              elapseTimeMS = millis() - initTime;

              filter = movingAverage(tempRead());
               if((counter%20)==0) //Check if counter is divisible by 20
               {
                    Serial.println(filter);
               }
            }

            startTemp = filter; //set the starting temperature for the ramp
(C)
            rampRate = (maxTemp - startTemp)/(rampTime); //set ramp rate for
ramp (C/s)

            state = state + 1;
            break;
         case 1: //ramp Time
            initTime = millis();
            cycleTime = rampTime*1000;

            //reset PID counter
            counter = 0;

            //time elapsed since the start of temperature ramp
            elapseTimeMS = millis() - initTime;

            windowStartTime = millis();
            while(elapseTimeMS < cycleTime)
            {
```

```
      counter = counter + 1;

      filter = movingAverage(tempRead());

      Input = filter;
      elapseTime = elapseTimeMS/1000; //in seconds
      Setpoint = (elapseTime * rampRate)+startTemp;
      myPID.Compute();

      if((millis() - windowStartTime) > windowSize)
      {
        windowStartTime += windowSize;
      }
      if(Output > millis() - windowStartTime)
      {
        digitalWrite(relayPin, HIGH);
      }
      else
      {
        digitalWrite(relayPin, LOW);
      }

      if((counter%20)==0) //Check if counter is divisible by 20
      {
         Serial.println(filter);
      }

      //Elapsed time since start of temperature ramp
      elapseTimeMS = millis() - initTime;
   }
   state = state + 1;
   break;
case 2: //cool
   initTime = millis();
   cycleTime = coolTime*1000;

   //reset PID counter
   counter = 0;

   //Determine time left in current phase
   elapseTimeMS = millis() - initTime;
   while(elapseTimeMS < cycleTime)
   {
       counter = counter + 1;
       digitalWrite(relayPin, LOW);
       //Determine time left in current phase
       elapseTimeMS = millis() - initTime;

       filter = movingAverage(tempRead());

      if((counter%20)==0) //Check if counter is divisible by 20
      {
           Serial.println(filter);
      }
      //Start monitoring for the channel discharge
        channel = analogRead(channelA);
        if(channel > 400)
```

```
                {
                   state = state - state;
                   break;
                }
             }
             state = state - state;
             break;
       }
   }

   //Read Differential Temperature from Thermocouple
   float tempRead(void)
   {
      float voltage = analogRead(thermocouple) * 5 / 1023.000 * 1000; //needs
to be in mV
      float temperature = (voltage - zero) / 5.765795526;
      return temperature;
   }

   //Zero the background signal at the beginning of the run
   float background(void)
   {
     // subtract the last reading:
     total = total - readings[readIndex];
     // read from the sensor:
     readings[readIndex] = analogRead(thermocouple) * 5 / 1023.000 * 1000;
//needs to be in mV
     // add the reading to the total:
     total = total + readings[readIndex];
     // advance to the next position in the array:
     readIndex = readIndex + 1;

     // if we're at the end of the array…
     if (readIndex >= numReadings)
     {
       // …wraparound to the beginning:
       readIndex = 0;
     }

     // calculate the average:
     average = total / numReadings;
     return average;
   }

   float movingAverage(float temperature)
   {
     // subtract the last reading:
     totalTemp = totalTemp - tempReading[index];
     // read from the sensor:
     tempReading[index] = temperature;
     // add the reading to the total:
     totalTemp = totalTemp+ tempReading[index];
     // advance to the next position in the array:
     index = index + 1;

     // if we're at the end of the array…
     if (index >= period)
```

```
  {
    // …wrap around to the beginning:
    index = 0;
  }

  // calculate the average:
  averageTemp = totalTemp / period;
  return averageTemp;
}
```

Appendix C Chapter 4 Supplementary Data, Figures, and Code

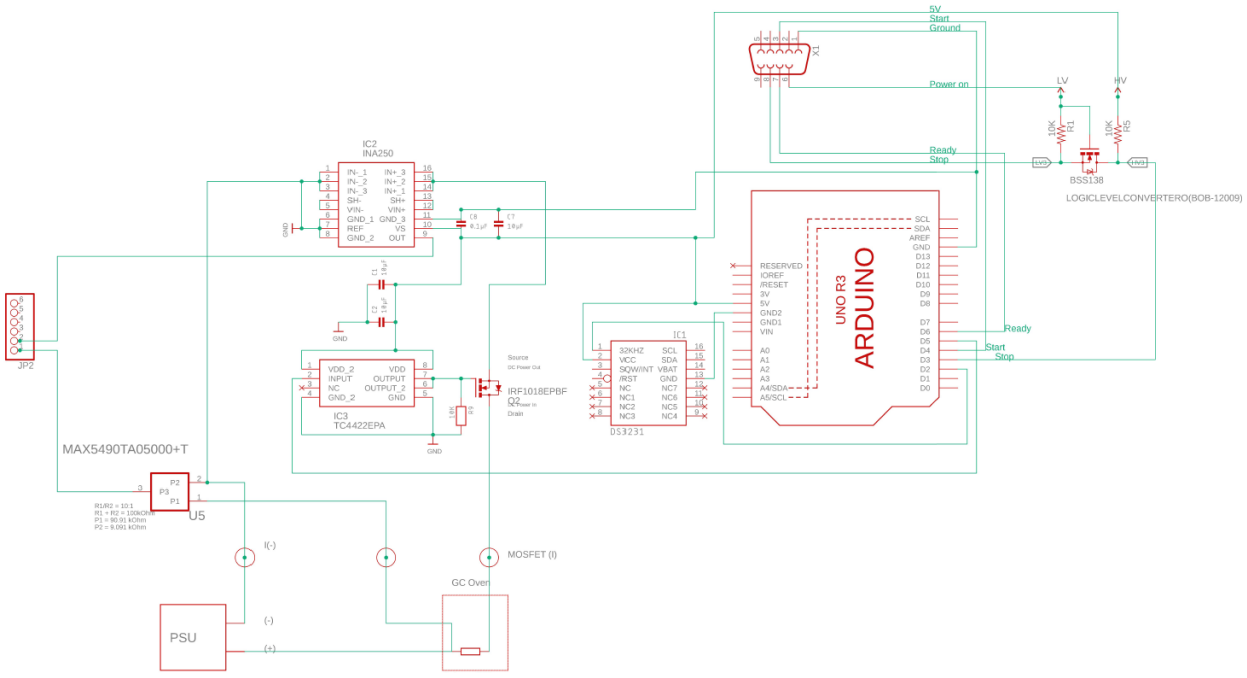

Figure C – 1: Schematic of the components soldered to a SparkFun Arduino ProtoShield – Bare PCB. This board was mounted at the very top (Protoboard 1) of a 3-layer stack (Top to Bottom: Protoboard 1, Protoboard 2, Arduino Uno R3).

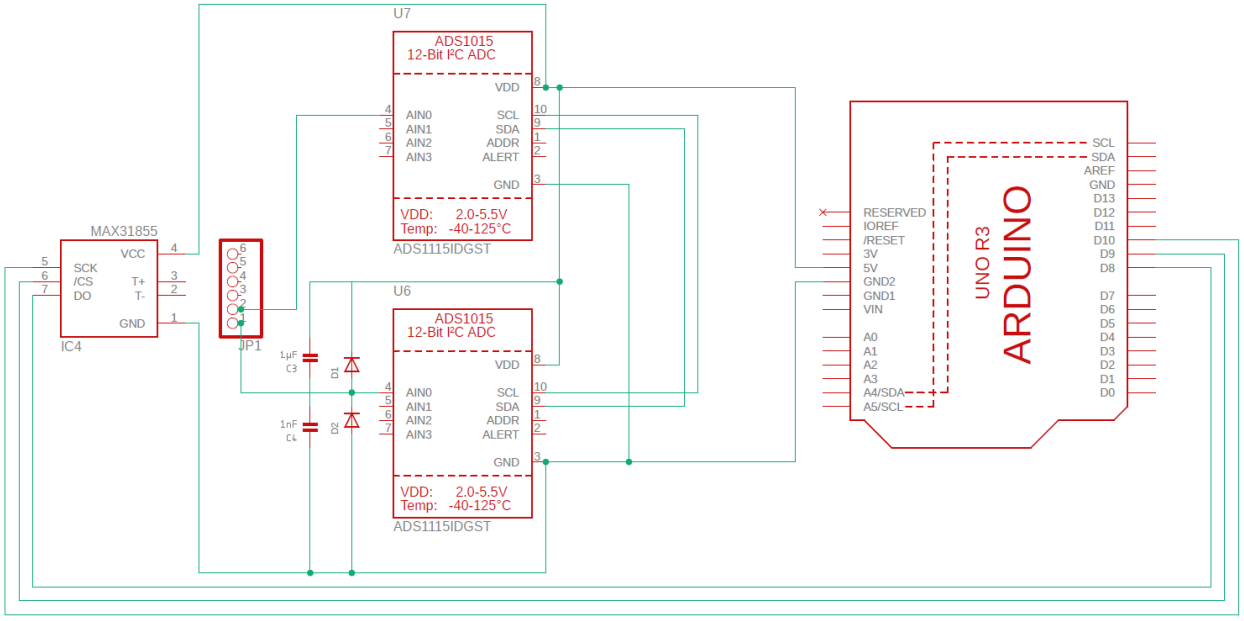

Figure C – 2: Schematic of the components soldered to a SparkFun Arduino ProtoShield – Bare PCB. This board was mounted in the middle (Protoboard 2) of a 3-layer stack (Top to Bottom: Protoboard 1, Protoboard 2, Arduino Uno R3).

Table C – 1: GC×GC-FID conditions for testing the ²DTPS with the new resistance-temperature measurement system.

Overall System Performance of the ²DTPS with Resistance-Temperature Measurement						
Test	Peak Capacity			Retention Time Reproducibility		
Sample	Diesel			Perfume		
Inlet	1.0 µL, 250 °C, 40:1 split			1.0 µL, 200 °C, 15:1 split		
¹D Column	*Rxi-5Sil MS W/Integra-Guard* (39.219 m × 0.242 mm × 0.25 µm)					
²D Column	*MXT-WAX* (1.00 m × 0.25 mm × 0.25 µm)			*MXT-WAX* (0.52 m × 0.25 mm × 0.25 µm)		
²D Column to FID	*Guard* (0.44 m × 0.25 mm)					
Carrier Gas	H_2 99.999%, 4.0 mL/min			H_2 99.999%, 2.5 mL/min		
Oven	°C/min	Next °C	Hold (min)	°C/min	Next °C	Hold (min)
		35	2		50	2
	2	230	1	5	140	5
				5	160	5
				5	230	5
Detector (FID)	Temperature: 250 °C, H_2: 40 mL/min, Air: 400 mL/min, N_2 + Carrier: 30 mL/min, Data: 100 Hz					
Modulator	SV 1.07 m × 0.25 mm			SV 1.07 m × 0.25 mm		
	P_m: 6 s			P_m: 5 s		
	Entry Hot Zone	+0 °C (320 °C cap)		Entry Hot Zone	+0 °C (320 °C cap)	
	Exit Hot Zone	+30 °C (320 °C cap)		Exit Hot Zone	+30 °C (320 °C cap)	
	Cold Zone	-51 °C (oven < 150 °C)		Cold Zone	-51 °C (oven < 150 °C)	
		9 °C (oven > 150 °C)			9 °C (oven > 150 °C)	
²DTPS	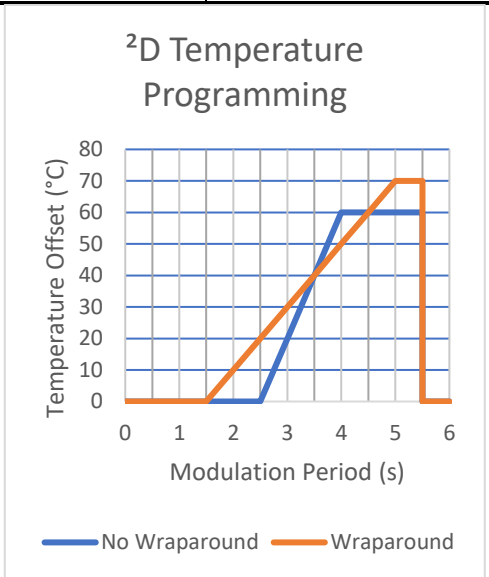			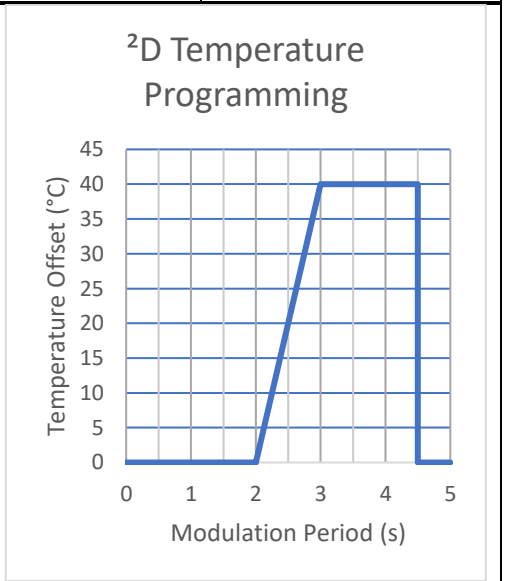		
Secondary Oven	+55 °C			+40 °C		

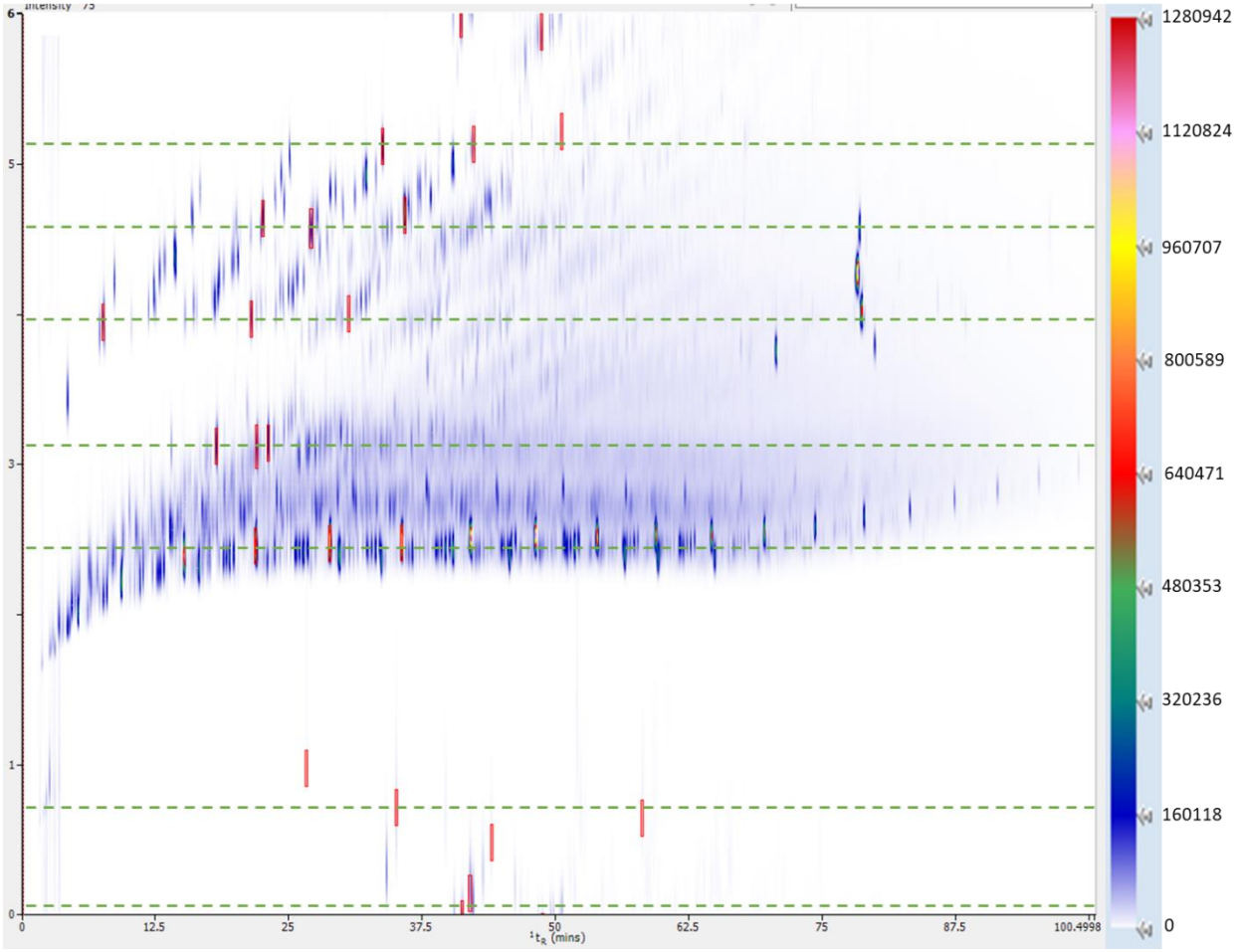

Figure C – 3: GC×GC-FID separation of diesel with ^{2}D temperature programming using an Rxi-5Sil MS W/Integra-Guard (39.219 m × 0.242 mm × 0.25 µm) ^{1}D column and an MXT-WAX (1.00 m × 0.25 mm × 0.25 µm) ^{2}D column. ^{2}D temperature programming: 1.5 s delay, 70 °C linear temperature increase over 3.5 s at 20 °C/s, hold at 70 °C for 0.5 s, cool for 0.5 s. Optimized for complete usage of 2D space (has wraparound peaks).

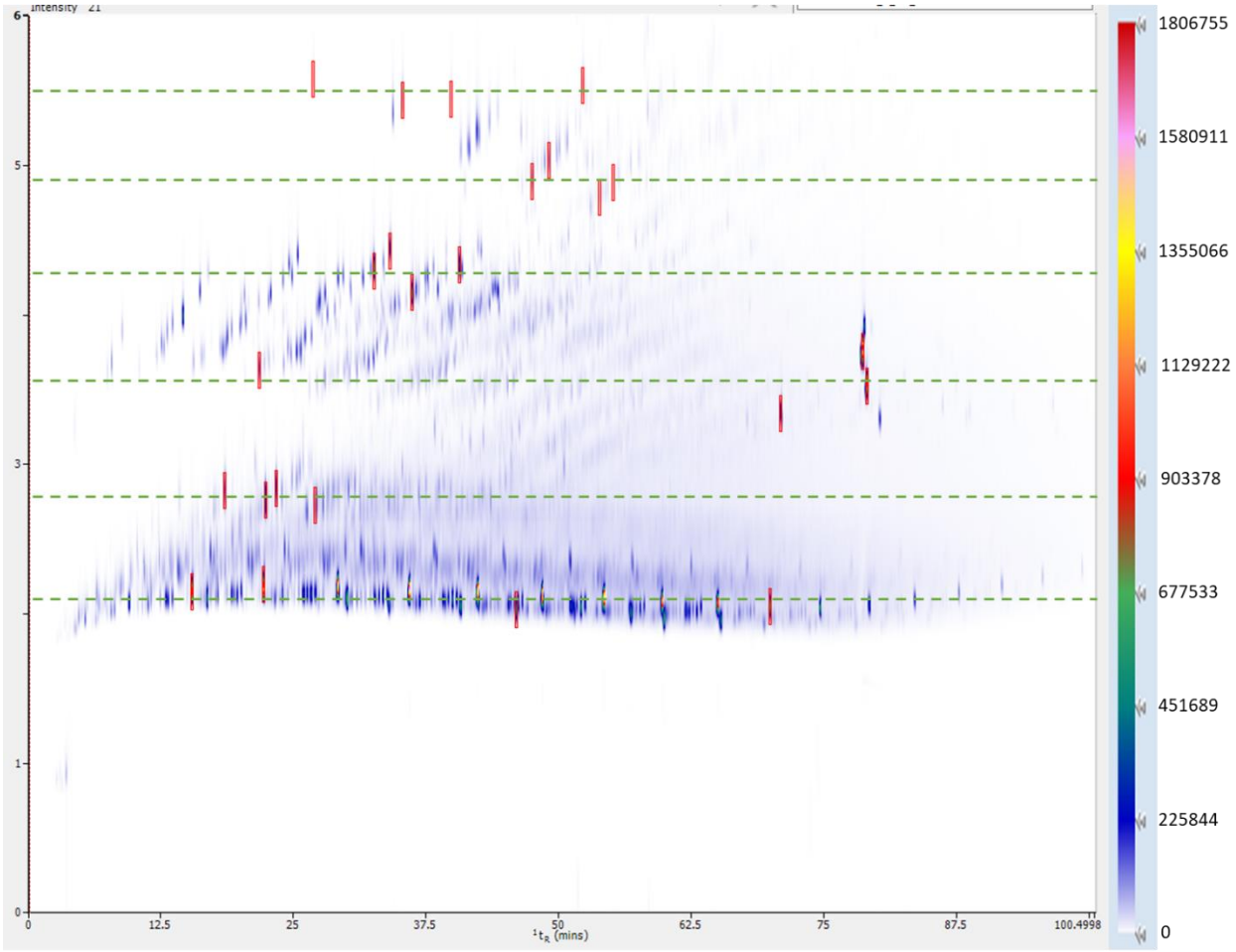

Figure C - 4: GC×GC-FID separation of diesel with ²D temperature programming using an Rxi-5Sil MS W/Integra-Guard (39.219 m × 0.242 mm × 0.25 µm) ¹D column and an MXT-WAX (1.00 m × 0.25 mm × 0.25 µm) ²D column. ²D temperature programming: 2.5 s delay, 70 °C linear temperature increase over 1.5 s (at 20 °C/s) , hold at 60 °C for 1.5 s, cool for 0.5 s. Optimized ²D peak width (no wraparound peaks).

Figure C - 5: GC×GC-FID separation of diesel with secondary oven using an Rxi-5Sil MS W/Integra-Guard (39.219 m × 0.242 mm × 0.25 µm) ^{1}D column and an MXT-WAX (1.00 m × 0.25 mm × 0.25 µm) ^{2}D column. Constant temperature offset of +55 °C. Optimized ^{2}D peak width (no wraparound peaks).

Table C - 2: Resolution comparison between the secondary oven and ²DTPS (with and without wraparound) for FAMEs in the diesel sample.

Secondary Oven			
	^1R_s	^2R_s	$R_{s,2D}$
methyl linoleate (1) vs. methyl linolenate (2)	0.35	0.76	0.84
methyl linolenate (2) vs. methyl oleate (3)	0.37	1.61	1.66
methyl linoleate (1) vs. methyl oleate (3)	0.52	0.81	0.96
²DTPS With Wraparound			
	^1R_s	^2R_s	$R_{s,2D}$
methyl linoleate (1) vs. methyl linolenate (2)	0.31	1.00	1.05
methyl linolenate (2) vs. methyl oleate (3)	0.42	1.99	2.03
methyl linoleate (1) vs. methyl oleate (3)	0.62	1.00	1.18
²DTPS Without Wraparound			
	^1R_s	^2R_s	$R_{s,2D}$
methyl linoleate (1) vs. methyl linolenate (2)	0.40	0.92	1.00
methyl linolenate (2) vs. methyl oleate (3)	0.33	2.24	2.27
methyl linoleate (1) vs. methyl oleate (3)	0.54	1.27	1.38

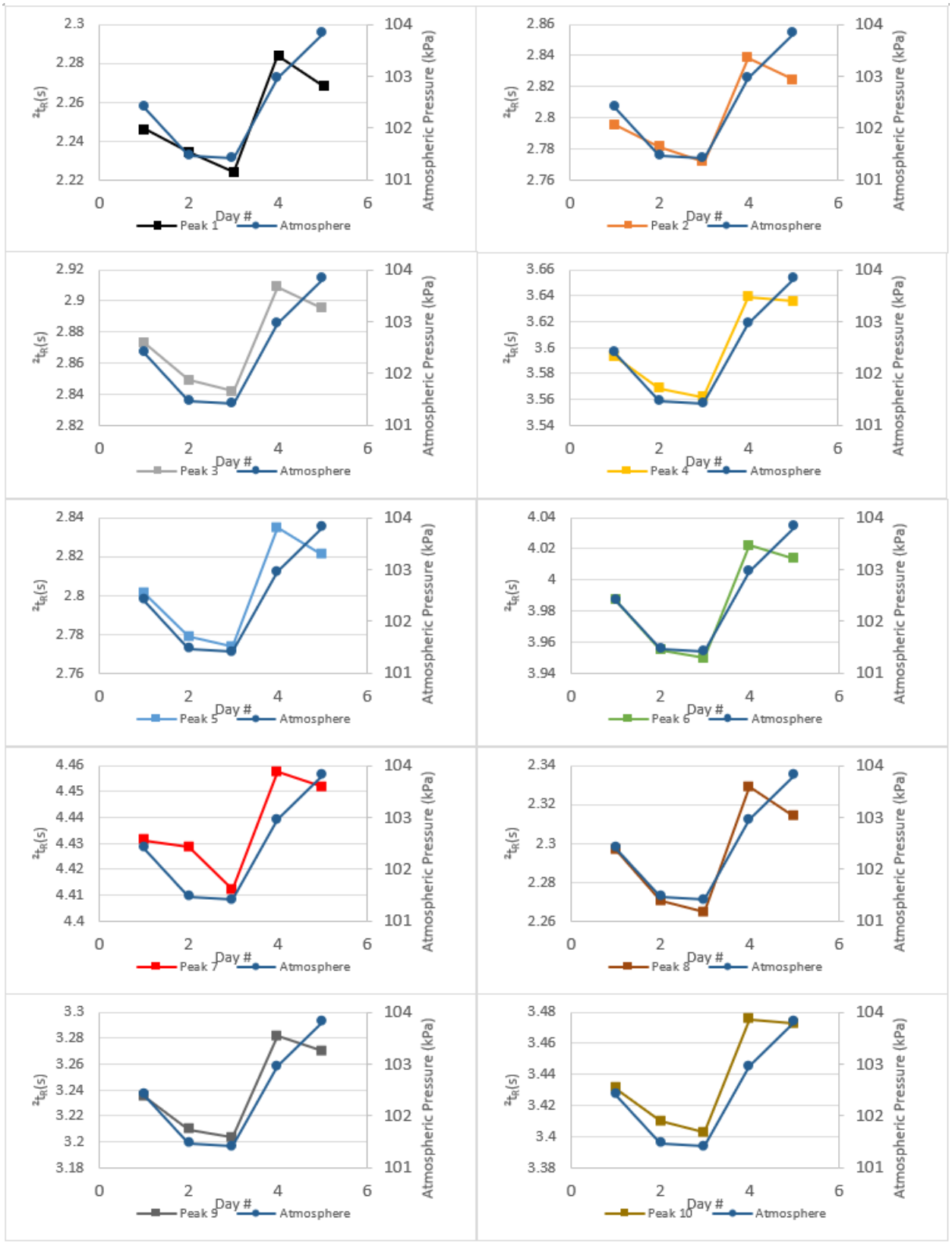

Figure C - 6: Comparing the ^2t_r to the atmospheric pressure for 10 peaks used to test system reproducibility (secondary oven) over 5 days.

Table C - 3: GC×GC-TOFMS conditions for the identification of compounds in the perfume and diesel samples.

Overall System Performance of the ²DTPS with Resistance-Temperature Measurement – (Tentative Identification)			
Sample	Diesel and Perfume		
Inlet	1.0 µL, 250 °C, 300:1 split		
¹D Column	*Rxi-5Sil MS W/Integra-Guard* (39.219 m × 0.242 mm × 0.25 µm)		
²D Column	*MXT-WAX* (0.5 m × 0.25 mm × 0.25 µm)		
Transfer Line	*Guard (*0.51 m x 0.25 mm*)*		
Carrier Gas	He 99.999%, 1.0 mL/min		
Oven	°C/min	Next °C	Hold (min)
		50	2
	3	210	
Detector (TOFMS)	Filament (V)	1.7	
	Filament Delay (s)	240	
	Mass Range (m/z)	50 - 600	
	Data Rate (Hz)	50	
	Transfer Line (°C)	240	
	Ion source (°C)	250	
Modulator	Column	SV 1.07 m × 0.25 mm	
	Modulation Period	6 s	
	Entry Hot Zone	+0 °C (320 °C cap)	
	Exit Hot Zone	+30 °C (320 °C cap)	
	Cold Zone	-51 °C (oven < 150 °C)	
		9 °C (oven > 150 °C)	

Table C - 4: Tentative identification of the 10 major compounds present in the perfume sample and n-alkanes used for the linear retention index calculations. (-) denotes that the information was not found. Peaks 4 and 5 were unidentified due to a low match factor (<700).

Peak #	Retention Time	Tentative Identification	Match Factor	Reverse Match Factor	Retention Index Calculated	Retention Index Reported
1	12.5571	Limonene	897	928	1027	1030
2	14.5959	1-Octen-2-ol, 2,6-dimethyl-	784	791	1072	1073
3	20.2259	Ethyl Linalool	784	857	1195	1170
4	21.1077	Unidentified	-	-	1214	-
5	23.5804	Unidentified	-	-	1269	-
6	34.4569	Lilial	867	884	1527	1532
7	40.3627	Triethyl Citrate	868	883	1683	1659
8	45.419	Isopropyl Myristate	835	851	1828	1824
9	46.3264	Galaxolide	858	872	1855	1850
10	46.7579	Versalide	789	837	1865	-
Octane	4.5325					
Nonane	7.3898					
Decane	11.3386					
Undecane	15.8386					
Dodecane	20.4725					
Tridecane	24.9758					
Tetradecane	29.2699					
Pentadecane	33.3921					
Hexadecane	37.2666					
Heptadecane	40.9797					
Octadecane	44.475					
Nonadecane	47.8445					

Table C - 5: GC×GC-TOFMS conditions for testing the ²DTPS with a TOFMS.

Compatibility of ²DTPS with MS			
Test	Retention Time Reproducibility		
Sample	10% Diesel (v/v %)		
Inlet	0.2 µL, 250 °C, 300:1 split		
¹D Column	Rxi-5Sil MS W/Integra-Guard (30 m × 0.25 mm × 0.25 µm)		
²D Column	*MXT-WAX* (1.00 m × 0.25 mm × 0.25 µm)		
Transfer Line	*Guard (*0.476 m x 0.25 mm*)*		
Carrier Gas	He 99.999%, 3.5 mL/min		
Oven	°C/min	Next °C	Hold (min)
		35	2.5
	2.5	230	4.5
Detector (TOFMS)	Filament (V)	1.6	
	Filament Delay (s)	180	
	Mass Range (m/z)	50 - 600	
	Data Rate (Hz)	100	
	Transfer Line (°C)	250	
	Ion source (°C)	300	
Modulator	Column	Guard (0.48 m x 0.25 mm) + Rxi-1ms (0.69 m x 0.25 mm x 1.0 µm)	
	Modulation Period	6 s	
	Entry Hot Zone	+30 °C (320 °C cap)	
	Exit Hot Zone	+120 °C (320 °C cap)	
	Cold Zone	-51 °C (oven < 150 °C)	
		9 °C (oven > 150 °C)	
²DTPS	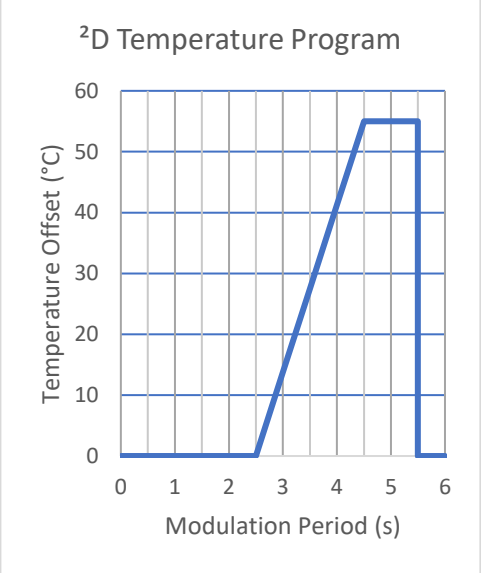	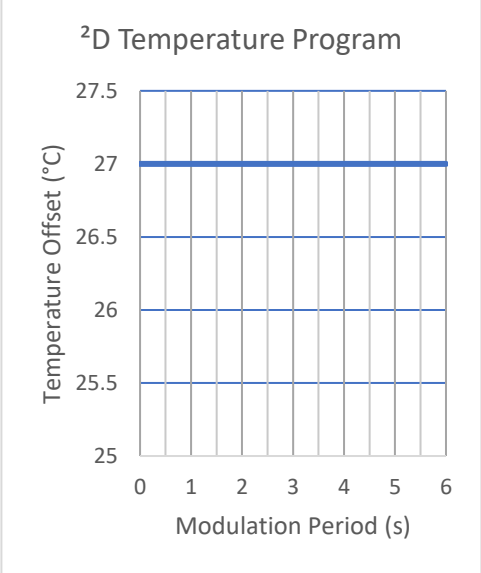	

Table C - 6: Within-day (n=5) and day-to-day (n=5) RSD for the ^1t_r and ^2t_r of the GC×GC-TOFMS separation with the ^{2}D column at oven temperature (16 peaks). Deconvolution and persistence algorithms were compared, while the same baseline correction (DBC 2.0 = 0.5s) was used for all GC×GC chromatograms.

WITHIN-DAY (DECONVOLUTION | PERSISTENCE) GC×GC-TOFMS (^{2}D COLUMN: GC OVEN TEMPERATURE)								
	Average				RSD (%)			
COMPOUND	^1t_r (min)		^2t_r (s)		^1t_r		^2t_r	
ethylbenzene	7.800	7.800	4.04	4.04	0.00	0.00	0.32	0.12
***p*-xylene**	8.200	8.189	4.17	4.17	0.00	0.16	0.05	0.17
benzene, (1-methylethyl)-	10.620	10.625	4.10	4.08	0.11	0.05	0.27	0.08
benzene, propyl-	12.130	12.130	4.31	4.31	0.05	0.04	0.27	0.20
1*H*-indene, octahydro-, *cis*-	14.031	14.030	2.51	2.51	0.02	0.02	0.14	0.21
decane	15.022	15.000	1.88	1.89	0.00	0.00	0.14	0.00
***p*-cymene**	15.785	15.785	4.27	4.27	0.05	0.05	0.25	0.16
naphthalene, decahydro-, *trans*-	17.764	17.765	2.57	2.57	0.01	0.00	0.12	0.11
naphthalene, decahydro-, *cis*-	20.200	20.200	2.82	2.82	0.00	0.00	0.23	0.00
undecane	20.731	20.708	1.96	1.97	0.00	0.01	0.12	0.21
naphthalene, 1,2,3,4-tetrahydro-	23.600	23.600	6.93	6.93	0.00	0.00	0.17	0.16
dodecane	26.431	26.429	2.01	2.02	0.00	0.00	0.16	0.23
naphthalene, 1,2,3,4-tetrahydro-2-methyl-	26.708	26.710	6.16	6.16	0.02	0.00	0.20	0.08
1*H*-indene, 2,3-dihydro-4,7-dimethyl-	28.600	28.609	6.30	6.31	0.00	0.07	0.19	0.15
naphthalene, 1,2,3,4-tetrahydro-6-methyl-	30.722	30.720	7.34	7.34	0.02	0.01	0.06	0.10
naphthalene, 1,2,3,4-tetrahydro-1,5-dimethyl-	34.000	34.002	6.71	6.72	0.00	0.01	0.13	0.10
AVERAGE					0.02	0.03	0.18	0.13
DAY-TO-DAY (DECONVOLUTION | PERSISTENCE) GC×GC-TOFMS (^{2}D COLUMN: GC OVEN TEMPERATURE)								
	Average				RSD (%)			
COMPOUND	^1t_r (min)		^2t_r (s)		^1t_r		^2t_r	
ethylbenzene	7.800	7.800	4.04	4.04	0.00	0.00	0.15	0.11
***p*-xylene**	8.197	8.185	4.17	4.17	0.06	0.07	0.18	0.09
benzene, (1-methylethyl)-	10.612	10.623	4.09	4.09	0.09	0.07	0.22	0.12
benzene, propyl-	12.128	12.128	4.31	4.31	0.06	0.07	0.17	0.14
1*H*-indene, octahydro-, *cis*-	14.026	14.029	2.51	2.51	0.06	0.03	0.21	0.20
decane	15.022	15.000	1.88	1.89	0.02	0.00	0.26	0.22
***p*-cymene**	15.789	15.790	4.27	4.26	0.06	0.07	0.20	0.18
naphthalene, decahydro-, *trans*-	17.763	17.763	2.57	2.57	0.01	0.02	0.18	0.23
naphthalene, decahydro-, *cis*-	20.200	20.200	2.82	2.82	0.00	0.00	0.21	0.23
undecane	20.728	20.708	1.95	1.96	0.03	0.01	0.28	0.31
naphthalene, 1,2,3,4-tetrahydro-	23.600	23.600	6.93	6.93	0.00	0.00	0.06	0.08
dodecane	26.431	26.428	2.01	2.02	0.00	0.00	0.24	0.24
naphthalene, 1,2,3,4-tetrahydro-2-methyl-	26.704	26.706	6.16	6.15	0.02	0.02	0.08	0.06
1*H*-indene, 2,3-dihydro-4,7-dimethyl-	28.600	28.601	6.31	6.32	0.00	0.08	0.09	0.09

naphthalene, 1,2,3,4-tetrahydro-6-methyl-	30.718	30.718	7.34	7.34	0.01	0.01	0.05	0.06
naphthalene, 1,2,3,4-tetrahydro-1,5-dimethyl-	34.000	34.000	6.72	6.72	0.00	0.00	0.07	0.06
AVERAGE					0.03	0.03	0.17	0.15

Table C - 7: Within-day (n=5) and day-to-day (n=5) standard deviation and RSD for the peak area of the GC×GC-TOFMS separation with the ²D column at oven temperature (16 peaks). Deconvolution and persistence algorithms were compared, while the same baseline correction (DBC 2.0 = 0.5s) was used for all GC×GC chromatograms.

WITHIN-DAY (DECONVOLUTION | PERSISTENCE) GC×GC-TOFMS (²D COLUMN: GC OVEN TEMPERATURE)						
COMPOUND	Average Peak Area		Std. Dev.		RSD (%)	
ethylbenzene	1292321	1320556	61290	80330	4.74	6.08
***p*-xylene**	4567870	4815651	267733	233617	5.86	4.85
benzene, (1-methylethyl)-	543520	595304	42134	34203	7.75	5.75
benzene, propyl-	1586505	1622081	87982	87539	5.55	5.40
1*H*-indene, octahydro-, *cis*-	3109572	3210699	182647	191987	5.87	5.98
decane	15849557	16090551	1010930	801053	6.38	4.98
***p*-cymene**	1913574	1923972	149907	147894	7.83	7.69
naphthalene, decahydro-, *trans*-	11067629	11398360	722522	657095	6.53	5.76
naphthalene, decahydro-, *cis*-	2160551	2233417	109044	138119	5.05	6.18
undecane	25180820	23054027	1470030	808184	5.84	3.51
naphthalene, 1,2,3,4-tetrahydro-	4894584	4925828	316539	309084	6.47	6.27
dodecane	31825369	25813366	3029396	1081178	9.52	4.19
naphthalene, 1,2,3,4-tetrahydro-2-methyl-	5009679	5208306	375475	325951	7.49	6.26
1*H*-indene, 2,3-dihydro-4,7-dimethyl-	2755225	2799808	204057	173184	7.41	6.19
naphthalene, 1,2,3,4-tetrahydro-6-methyl-	6488324	6963242	1089283	434195	16.79	6.24
naphthalene, 1,2,3,4-tetrahydro-1,5-dimethyl-	1198338	1309471	103730	111558	8.66	8.52
AVERAGE					7.36	5.86

WITHIN-DAY (DECONVOLUTION | PERSISTENCE) GC×GC-TOFMS (²D COLUMN: GC OVEN TEMPERATURE)						
COMPOUND	Average Peak Area		Std. Dev.		RSD (%)	
ethylbenzene	1260964	1282884	71150	74362	5.64	5.80
***p*-xylene**	4523089	4657520	279017	231788	6.17	4.98
benzene, (1-methylethyl)-	505307	578459	43569	34948	8.62	6.04
benzene, propyl-	1568866	1600584	113900	99473	7.26	6.21
1*H*-indene, octahydro-, *cis*-	2991176	3207406	119279	192119	3.99	5.99
decane	15675449	16045264	777039	731584	4.96	4.56
***p*-cymene**	1834315	1875817	96644	117213	5.27	6.25
naphthalene, decahydro-, *trans*-	11104409	11466824	884685	742699	7.97	6.48
naphthalene, decahydro-, *cis*-	2174821	2257245	151058	169518	6.95	7.51
undecane	24964565	23114537	796396	545682	3.19	2.36
naphthalene, 1,2,3,4-tetrahydro-	4900113	4919388	320468	344112	6.54	7.00
dodecane	33298910	26962273	2256254	1741237	6.78	6.46
naphthalene, 1,2,3,4-tetrahydro-2-methyl-	5033822	5234752	427387	396369	8.49	7.57
1*H*-indene, 2,3-dihydro-4,7-dimethyl-	2781948	2837761	241802	233608	8.69	8.23
naphthalene, 1,2,3,4-tetrahydro-6-methyl-	7034796	7043613	687433	548052	9.77	7.78
naphthalene, 1,2,3,4-tetrahydro-1,5-dimethyl-	1221198	1321660	162987	123616	13.35	9.35
AVERAGE					7.10	6.41

Table C - 8: Within-day (n=5) and day-to-day (n=5) RSD for the ^1t_r and ^2t_r of the GC×GC-TOFMS separation with ^2D temperature programming (21 peaks). Deconvolution and persistence algorithms were compared, while the same baseline correction (DBC 2.0 = 0.5s) was used for all GC×GC chromatograms.

WITHIN-DAY (DECONVOLUTION | PERSISTENCE) GC×GC-TOFMS (^{2}D COLUMN: TEMPERATURE PROGRAM)								
	Average				RSD (%)			
COMPOUND	^1t_r (min)		^2t_r (s)		^1t_r		^2t_r	
ethylbenzene	7.835	7.835	3.19	3.19	0.16	0.14	0.22	0.28
***p*-xylene**	8.226	8.227	3.25	3.25	0.04	0.03	0.30	0.28
benzene, (1-methylethyl)-	10.700	10.700	3.21	3.21	0.00	0.00	0.33	0.31
benzene, propyl-	12.200	12.200	3.32	3.31	0.00	0.00	0.23	0.21
1*H*-indene, octahydro-, *cis*-	14.100	14.100	2.20	2.20	0.00	0.00	0.27	0.41
decane	15.078	15.087	1.71	1.71	0.00	0.13	0.27	0.27
***p* -cymene**	15.900	15.900	3.29	3.28	0.00	0.00	0.28	0.31
naphthalene, decahydro-, *trans*-	17.850	17.849	2.24	2.24	0.01	0.02	0.29	0.32
naphthalene, decahydro-, *cis*-	20.300	20.300	2.45	2.44	0.00	0.00	0.21	0.29
undecane	20.826	20.805	1.75	1.76	0.01	0.00	0.28	0.31
naphthalene, 1,2,3,4-tetrahydro-	23.596	23.596	4.13	4.14	0.02	0.03	0.12	0.16
dodecane	26.527	26.526	1.79	1.79	0.01	0.01	0.29	0.35
naphthalene, 1,2,3,4-tetrahydro-2-methyl-	26.707	26.711	3.95	3.95	0.02	0.01	0.20	0.22
1*H*-indene, 2,3-dihydro-4,7-dimethyl-	28.600	28.604	3.99	3.99	0.00	0.08	0.32	0.20
naphthalene, 1,2,3,4-tetrahydro-6-methyl-	30.721	30.721	4.24	4.24	0.01	0.01	0.29	0.26
naphthalene, 1-methyl-	30.943	30.942	5.08	5.08	0.01	0.01	0.18	0.15
naphthalene, 2-methyl-	31.700	31.702	5.17	5.17	0.00	0.01	0.19	0.19
naphthalene, 1,2,3,4-tetrahydro-1,5-dimethyl-	34.012	34.012	4.10	4.10	0.00	0.00	0.37	0.38
biphenyl	35.404	35.406	5.23	5.23	0.02	0.02	0.19	0.21
naphthalene, 1,7-dimethyl-	37.334	37.334	5.01	5.01	0.01	0.01	0.18	0.16
1,1'-biphenyl, 4-methyl-	40.725	40.726	5.06	5.06	0.01	0.01	0.07	0.09
AVERAGE					0.02	0.02	0.24	0.26
DAY-TO-DAY (DECONVOLUTION | PERSISTENCE) GC×GC-TOFMS (^{2}D COLUMN: TEMPERATURE PROGRAM)								
	Average				RSD (%)			
COMPOUND	^1t_r (min)		^2t_r (s)		^1t_r		^2t_r	
ethylbenzene	7.836	7.836	3.20	3.20	0.11	0.11	0.37	0.36
***p*-xylene**	8.226	8.227	3.26	3.26	0.04	0.04	0.27	0.28
benzene, (1-methylethyl)-	10.700	10.700	3.22	3.22	0.00	0.00	0.33	0.26
benzene, propyl-	12.200	12.200	3.32	3.32	0.00	0.00	0.36	0.35
1*H*-indene, octahydro-, *cis*-	14.100	14.100	2.21	2.21	0.00	0.00	0.36	0.35
decane	15.084	15.086	1.71	1.71	0.10	0.10	0.50	0.50
***p* -cymene**	15.900	15.900	3.29	3.30	0.00	0.00	0.35	0.38
naphthalene, decahydro-, *trans*-	17.845	17.848	2.25	2.25	0.03	0.02	0.50	0.46

naphthalene, decahydro-, *cis*-	20.300	20.300	2.45	2.45	0.00	0.00	0.28	0.35
undecane	20.825	20.803	1.76	1.76	0.00	0.02	0.39	0.42
naphthalene, 1,2,3,4-tetrahydro-	23.593	23.5921	4.144	4.145	0.02	0.02	0.22	0.24
dodecane	26.527	26.526	1.80	1.80	0.00	0.01	0.37	0.32
naphthalene, 1,2,3,4-tetrahydro-2-methyl-	26.704	26.710	3.96	3.96	0.02	0.01	0.21	0.22
1*H*-indene, 2,3-dihydro-4,7-dimethyl-	28.599	28.593	3.99	4.00	0.01	0.05	0.12	0.13
naphthalene, 1,2,3,4-tetrahydro-6-methyl-	30.719	30.720	4.24	4.24	0.01	0.01	0.21	0.19
naphthalene, 1-methyl-	30.939	30.939	5.09	5.09	0.02	0.02	0.26	0.26
naphthalene, 2-methyl-	31.701	31.702	5.19	5.19	0.01	0.01	0.34	0.33
naphthalene, 1,2,3,4-tetrahydro-1,5-dimethyl-	34.008	34.010	4.11	4.11	0.01	0.01	0.23	0.18
biphenyl	35.402	35.404	5.24	5.24	0.01	0.01	0.33	0.35
naphthalene, 1,7-dimethyl-	37.331	37.331	5.02	5.02	0.01	0.01	0.25	0.25
1,1'-biphenyl, 4-methyl-	40.722	40.723	5.06	5.07	0.01	0.01	0.29	0.30
AVERAGE					0.02	0.02	0.31	0.31

Table C - 9: Within-day (n=5) and day-to-day (n=5) standard deviation and RSD for the peak area of the GC×GC-TOFMS separation with the ²D temperature programming (21 peaks). Deconvolution and persistence algorithms were compared, while the same baseline correction (DBC 2.0 = 0.5s) was used for all GC×GC chromatograms.

WITHIN-DAY (DECONVOLUTION | PERSISTENCE) GC×GC-TOFMS (²D COLUMN: TEMPERATURE PROGRAM)						
COMPOUND	Average Peak Area		Std. Dev.		RSD (%)	
ethylbenzene	1346753	1365288	43874	20267	3.26	1.48
***p*-xylene**	5240005	5333514	226948	85111	4.33	1.60
benzene, (1-methylethyl)-	666212	682032	13283	10262	1.99	1.50
benzene, propyl-	1794284	1970249	80172	105205	4.47	5.34
1*H*-indene, octahydro-, *cis*-	2465060	2532390	50604	75149	2.05	2.97
decane	13907989	14715034	894585	307668	6.43	2.09
***p*-cymene**	1901031	1883551	57098	35655	3.00	1.89
naphthalene, decahydro-, *trans*-	11401600	10536139	954648	202624	8.37	1.92
naphthalene, decahydro-, *cis*-	2107299	2185988	67971	52919	3.23	2.42
undecane	21210938	18066876	459287	234841	2.17	1.30
naphthalene, 1,2,3,4-tetrahydro-	5803604	5757103	107761	99880	1.86	1.73
dodecane	28077656	23212248	1546985	1243832	5.51	5.36
naphthalene, 1,2,3,4-tetrahydro-2-methyl-	5864163	5869888	38378	113405	0.65	1.93
1*H*-indene, 2,3-dihydro-4,7-dimethyl-	3284823	3355833	86617	77998	2.64	2.32
naphthalene, 1,2,3,4-tetrahydro-6-methyl-	8061645	7949595	156732	161735	1.94	2.03
naphthalene, 1-methyl-	1504285	1482169	31488	30279	2.09	2.04
naphthalene, 2-methyl-	880219	952526	18760	21917	2.13	2.30
naphthalene, 1,2,3,4-tetrahydro-1,5-dimethyl-	1837931	1810791	57687	58143	3.14	3.21
biphenyl	861905	881991	52309	23361	6.07	2.65
naphthalene, 1,7-dimethyl-	2709656	2652678	76407	71094	2.82	2.68
1,1'-biphenyl, 4-methyl-	1376907	1394502	44547	44001	3.24	3.16
AVERAGE					3.40	2.47
DAY-TO-DAY (DECONVOLUTION | PERSISTENCE) GC×GC-TOFMS (²D COLUMN: TEMPERATURE PROGRAM)						
COMPOUND	Average Peak Area		Std. Dev.		RSD (%)	
ethylbenzene	1364736	1389218	19071	27602	1.40	1.99
***p*-xylene**	5278400	5347379	59026	151021	1.12	2.82
benzene, (1-methylethyl)-	681183	703648	16481	21433	2.42	3.05
benzene, propyl-	1930188	2031326	91012	86901	4.72	4.28
1*H*-indene, octahydro-, *cis*-	2522284	2579407	40215	37705	1.59	1.46
decane	14110156	15031016	1047535	470304	7.42	3.13
***p*-cymene**	1953606	1945204	49584	47295	2.54	2.43
naphthalene, decahydro-, *trans*-	11495388	10821552	547452	240902	4.76	2.23
naphthalene, decahydro-, *cis*-	2219308	2236004	95622	39064	4.31	1.75
undecane	21768290	18573890	757750	401795	3.48	2.16
naphthalene, 1,2,3,4-tetrahydro-	6035104	5996238	157177	169588	2.60	2.83

dodecane	29214283	24182953	2029718	615795	6.95	2.55
naphthalene, 1,2,3,4-tetrahydro-2-methyl-	6043443	6061255	124361	132921	2.06	2.19
1*H*-indene, 2,3-dihydro-4,7-dimethyl-	3460435	3519677	118198	116110	3.42	3.30
naphthalene, 1,2,3,4-tetrahydro-6-methyl-	8411904	8292851	234045	226650	2.78	2.73
naphthalene, 1-methyl-	1596419	1574618	70426	64875	4.41	4.12
naphthalene, 2-methyl-	952464	1006383	46959	39062	4.93	3.88
naphthalene, 1,2,3,4-tetrahydro-1,5-dimethyl-	1975317	1925632	85349	72443	4.32	3.76
biphenyl	911527	934225	55537	39202	6.09	4.20
naphthalene, 1,7-dimethyl-	2884232	2825598	121939	117633	4.23	4.16
1,1'-biphenyl, 4-methyl-	1476662	1498871	72914	74827	4.94	4.99
AVERAGE					3.83	3.05

Table C - 10: Within-day (n=5) and day-to-day (n=5) RSD for the ^1t_r and ^2t_r of the GC×GC-TOFMS separation with a constant positive temperature offset in the ^2D (21 peaks). Deconvolution and persistence algorithms were compared, while the same baseline correction (DBC 2.0 = 0.5s) was used for all GC×GC chromatograms.

WITHIN-DAY (DECONVOLUTION | PERSISTENCE) GC×GC-TOFMS (^2D COLUMN: CONSTANT OFFSET)								
	Average				RSD (%)			
COMPOUND	^1t_r (min)		^2t_r (s)		^1t_r		^2t_r	
ethylbenzene	7.841	7.840	2.18	2.18	0.09	0.08	0.94	0.98
***p*-xylene**	8.227	8.228	2.22	2.22	0.02	0.02	0.88	0.89
benzene, (1-methylethyl)-	10.700	10.700	2.20	2.20	0.00	0.00	0.67	0.68
benzene, propyl-	12.200	12.200	2.28	2.28	0.00	0.00	0.83	0.91
1*H*-indene, octahydro-, *cis*-	14.100	14.100	1.80	1.80	0.00	0.00	0.65	0.73
decane	15.078	15.100	1.56	1.56	0.00	0.00	0.50	0.47
***p*-cymene**	15.900	15.900	2.25	2.25	0.00	0.00	0.77	0.86
naphthalene, decahydro-, *trans*-	17.829	17.848	1.83	1.83	0.08	0.01	0.51	0.53
naphthalene, decahydro-, *cis*-	20.300	20.300	1.91	1.91	0.00	0.00	0.68	0.64
undecane	20.825	20.833	1.59	1.59	0.00	0.01	0.52	0.52
naphthalene, 1,2,3,4-tetrahydro-	23.592	23.592	3.10	3.10	0.02	0.02	0.80	0.89
dodecane	26.527	26.534	1.60	1.61	0.00	0.02	0.48	0.60
naphthalene, 1,2,3,4-tetrahydro-2-methyl-	26.702	26.702	2.89	2.88	0.02	0.02	0.73	0.76
1*H*-indene, 2,3-dihydro-4,7-dimethyl-	28.600	28.604	2.93	2.92	0.00	0.03	0.89	1.05
naphthalene, 1,2,3,4-tetrahydro-6-methyl-	30.714	30.714	3.24	3.24	0.01	0.01	0.65	0.59
naphthalene, 1-methyl-	30.932	30.933	4.87	4.87	0.02	0.02	0.86	0.84
naphthalene, 2-methyl-	31.700	31.700	5.09	5.09	0.00	0.00	1.03	1.02
naphthalene, 1,2,3,4-tetrahydro-1,5-dimethyl-	34.002	34.004	3.04	3.04	0.01	0.02	0.73	0.80
biphenyl	35.400	35.400	5.24	5.24	0.00	0.00	1.07	1.21
naphthalene, 1,7-dimethyl-	37.325	37.325	4.68	4.68	0.01	0.01	0.99	0.93
1,1'-biphenyl, 4-methyl-	40.700	40.716	4.73	4.71	0.00	0.01	1.31	1.28
AVERAGE					0.01	0.01	0.78	0.82
DAY-TO-DAY (DECONVOLUTION | PERSISTENCE) GC×GC-TOFMS (^2D COLUMN: CONSTANT OFFSET)								
	Average				RSD (%)			
COMPOUND	^1t_r (min)		^2t_r (s)		^1t_r		^2t_r	
ethylbenzene	7.851	7.851	2.17	2.17	0.12	0.12	0.47	0.44
***p*-xylene**	8.231	8.231	2.21	2.21	0.04	0.04	0.47	0.45
benzene, (1-methylethyl)-	10.700	10.700	2.19	2.19	0.00	0.00	0.46	0.40
benzene, propyl-	12.200	12.200	2.27	2.27	0.00	0.00	0.49	0.46
1*H*-indene, octahydro-, *cis*-	14.100	14.100	1.79	1.79	0.00	0.00	0.28	0.28
decane	15.086	15.100	1.56	1.56	0.08	0.00	0.17	0.24
***p*-cymene**	15.900	15.900	2.24	2.24	0.00	0.00	0.42	0.41
naphthalene, decahydro-, *trans*-	17.844	17.851	1.82	1.82	0.06	0.01	0.27	0.23

naphthalene, decahydro-, *cis*-	20.306	20.300	1.90	1.91	0.04	0.00	0.63	0.34
undecane	20.825	20.836	1.58	1.59	0.00	0.01	0.13	0.15
naphthalene, 1,2,3,4-tetrahydro-	23.598	23.597	3.08	3.08	0.02	0.02	0.66	0.65
dodecane	26.526	26.5383	1.601	1.606	0.00	0.01	0.12	0.12
naphthalene, 1,2,3,4-tetrahydro-2-methyl-	26.702	26.705	2.87	2.87	0.00	0.01	0.50	0.46
1*H*-indene, 2,3-dihydro-4,7-dimethyl-	28.600	28.602	2.90	2.90	0.00	0.01	0.60	0.57
naphthalene, 1,2,3,4-tetrahydro-6-methyl-	30.717	30.717	3.21	3.21	0.01	0.01	0.64	0.66
naphthalene, 1-methyl-	30.937	30.937	4.83	4.83	0.01	0.01	0.75	0.75
naphthalene, 2-methyl-	31.700	31.700	5.05	5.05	0.00	0.00	0.70	0.67
naphthalene, 1,2,3,4-tetrahydro-1,5-dimethyl-	34.008	34.010	3.02	3.02	0.01	0.01	0.42	0.41
biphenyl	35.400	35.400	5.19	5.19	0.00	0.00	0.70	0.68
naphthalene, 1,7-dimethyl-	37.329	37.329	4.66	4.66	0.01	0.01	0.48	0.55
1,1'-biphenyl, 4-methyl-	40.713	40.719	4.74	4.73	0.02	0.00	0.35	0.42
AVERAGE					0.02	0.01	0.46	0.44

Table C - 11: Within-day (n=5) and day-to-day (n=5) standard deviation and RSD for the peak area of the GC×GC-TOFMS separation with a constant positive temperature offset in the ²D (21 peaks). Deconvolution and persistence algorithms were compared, while the same baseline correction (DBC 2.0 = 0.5s) was used for all GC×GC chromatograms.

WITHIN-DAY (DECONVOLUTION | PERSISTENCE) GC×GC-TOFMS (²D COLUMN: CONSTANT OFFSET)						
COMPOUND	Average Peak Area		Std. Dev.		RSD (%)	
ethylbenzene	1161854	1174903	58818	46269	5.06	3.94
***p*-xylene**	4399283	4470725	145453	132971	3.31	2.97
benzene, (1-methylethyl)-	613991	620681	30396	28282	4.95	4.56
benzene, propyl-	1601899	1666021	82548	114152	5.15	6.85
1*H*-indene, octahydro-, *cis*-	2551789	2792547	152541	56347	5.98	2.02
decane	12605224	10978913	763896	162807	6.06	1.48
***p*-cymene**	1780253	1760080	66180	97454	3.72	5.54
naphthalene, decahydro-, *trans*-	11547675	10176918	1244113	129851	10.77	1.28
naphthalene, decahydro-, *cis*-	2340355	2510819	422730	28468	18.06	1.13
undecane	19744525	15169799	3703707	347463	18.76	2.29
naphthalene, 1,2,3,4-tetrahydro-	4906341	4884395	141792	136260	2.89	2.79
dodecane	23326942	23138029	3528122	830609	15.12	3.59
naphthalene, 1,2,3,4-tetrahydro-2-methyl-	5026820	4831524	162682	271777	3.24	5.63
1*H*-indene, 2,3-dihydro-4,7-dimethyl-	2851270	2969510	46957	130635	1.65	4.40
naphthalene, 1,2,3,4-tetrahydro-6-methyl-	7061601	6975193	178748	227087	2.53	3.26
naphthalene, 1-methyl-	898876	895248	59617	38349	6.63	4.28
naphthalene, 2-methyl-	594353	617630	22217	40020	3.74	6.48
naphthalene, 1,2,3,4-tetrahydro-1,5-dimethyl-	1604305	1646953	73194	63914	4.56	3.88
biphenyl	490841	497547	28594	19245	5.83	3.87
naphthalene, 1,7-dimethyl-	1800945	1901389	79950	85573	4.44	4.50
1,1'-biphenyl, 4-methyl-	666392	891491	38379	32658	5.76	3.66
AVERAGE					6.58	3.73
DAY-TO-DAY (DECONVOLUTION | PERSISTENCE) GC×GC-TOFMS (²D COLUMN: TEMPERATURE PROGRAM)						
COMPOUND	Average Peak Area		Std. Dev.		RSD (%)	
ethylbenzene	1256610	1272231	61035	59617	4.86	4.69
***p*-xylene**	4755837	4804467	205278	206359	4.32	4.30
benzene, (1-methylethyl)-	668348	682813	34838	36737	5.21	5.38
benzene, propyl-	1748145	1796681	101300	92141	5.79	5.13
1*H*-indene, octahydro-, *cis*-	2790939	2972469	174983	119758	6.27	4.03
decane	12995828	11431752	735389	315190	5.66	2.76
***p*-cymene**	1915265	1895174	93633	97799	4.89	5.16
naphthalene, decahydro-, *trans*-	11427926	10707355	425082	362311	3.72	3.38
naphthalene, decahydro-, *cis*-	2819180	2725298	353645	148023	12.54	5.43
undecane	23464208	15890689	2486800	473302	10.60	2.98
naphthalene, 1,2,3,4-tetrahydro-	5247550	5234963	249543	256472	4.76	4.90

dodecane	23758035	23144911	1309571	201935	5.51	0.87
naphthalene, 1,2,3,4-tetrahydro-2-methyl-	5377839	5372432	253796	340040	4.72	6.33
1*H*-indene, 2,3-dihydro-4,7-dimethyl-	3092077	3213437	163256	171821	5.28	5.35
naphthalene, 1,2,3,4-tetrahydro-6-methyl-	7632817	7545043	414233	390220	5.43	5.17
naphthalene, 1-methyl-	966024	976636	52833	53164	5.47	5.44
naphthalene, 2-methyl-	643490	678946	34175	40491	5.31	5.96
naphthalene, 1,2,3,4-tetrahydro-1,5-dimethyl-	1800668	1805777	136687	120123	7.59	6.65
biphenyl	526782	539999	27889	31624	5.29	5.86
naphthalene, 1,7-dimethyl-	1977873	2069701	126930	123342	6.42	5.96
1,1'-biphenyl, 4-methyl-	792278	930611	91765	63484	11.58	6.82
AVERAGE					6.25	4.88

Table C - 12: Paired Student's t-test for the overall, within-day , and day-to-day RSD results, comparing the GC×GC-TOFMS separation with the ^{2}D column at oven temperature (16 peaks), with ^{2}D temperature programming (21 peaks), and with a ^{2}D constant offset (21 peaks) for the MF and RMF. The same 16 peaks were used for comparisons involving the ^{2}D column at oven temperature. Results that are insignificant are highlighted in green while significant results are highlighted in orange

Overall: Paired Student's t-test (α = 0.05)				
	MF		RMF	
	t-stat	p-value	t-stat	p-value
GC Oven Temp. vs. ^{2}D Temp. Prog. (df = 15)	3.0	8.1×10^{-3}	3.4	3.6×10^{-3}
GC Oven Temp. vs. Constant Offset (df = 15)	2.9	1.2×10^{-2}	3.5	3.0×10^{-3}
^{2}D Temp. Prog. vs. Constant Offset (df = 20)	3.7	1.4×10^{-3}	3.0	6.4×10^{-3}
Within-Day : Paired Student's t-test (α = 0.05)				
	MF		RMF	
	t-stat	p-value	t-stat	p-value
GC Oven Temp. vs. ^{2}D Temp. Prog. (df = 15)	3.0	8.6×10^{-3}	3.3	4.9×10^{-3}
GC Oven Temp. vs. Constant Offset (df = 15)	2.8	1.3×10^{-2}	3.4	3.8×10^{-3}
^{2}D Temp. Prog. vs. Constant Offset (df = 20)	2.5	2.1×10^{-2}	2.3	3.1×10^{-2}
Day-to-Day: Paired Student's t-test (α = 0.05)				
	MF		RMF	
	t-stat	p-value	t-stat	p-value
GC Oven Temp. vs. ^{2}D Temp. Prog. (df = 15)	3.1	7.7×10^{-3}	3.5	3.3×10^{-3}
GC Oven Temp. vs. Constant Offset (df = 15)	2.9	1.2×10^{-2}	3.5	2.9×10^{-3}
^{2}D Temp. Prog. vs. Constant Offset (df = 20)	3.8	1.1×10^{-3}	3.2	4.8×10^{-3}

Table C - 13: GC×GC-TOFMS conditions for testing the ²DTPS with the addition of a RTC

²DTPS – RTC Addition			
Test	Retention Time Reproducibility		
Sample	10% Perfume (v/v %)		
Inlet	0.2 µL, 250 °C, 450:1 split		
¹D Column	Rxi-5Sil MS W/Integra-Guard (30 m × 0.25 mm × 0.25 µm)		
²D Column	*MXT-WAX* (1.00 m × 0.25 mm × 0.25 µm)		
Transfer Line	Guard (0.476 m x 0.25 mm)		
Carrier Gas	He 99.999%, 2.0 mL/min		
Oven	°C/min	Next °C	Hold (min)
		50	2
	5	80	3
	5	150	5
	5	230	0
Detector (TOFMS)	Filament (V)	1.6	
	Filament Delay (s)	210	
	Mass Range (m/z)	35 - 600	
	Data Rate (Hz)	50	
	Transfer Line (°C)	250	
	Ion source (°C)	250	
Modulator	Column	Guard (0.48 m x 0.25 mm) + Rxi-1ms (0.69 m x 0.25 mm x 1.0 µm)	
	Modulation Period	6 s	
	Entry Hot Zone	+30 °C (320 °C cap)	
	Exit Hot Zone	+120 °C (320 °C cap)	
	Cold Zone	-51 °C	
		9 °C (oven > 150 °C)	
²DTPS	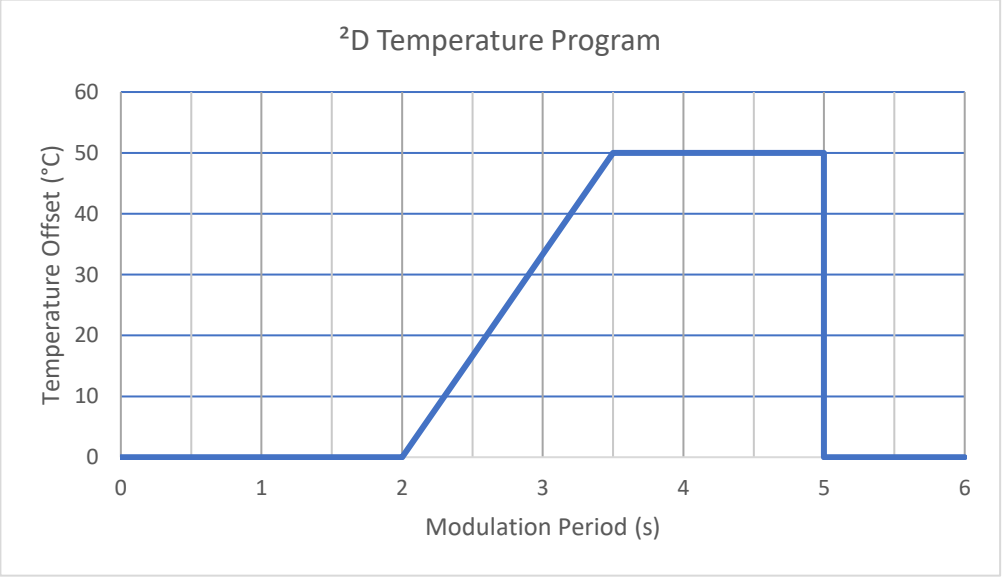		

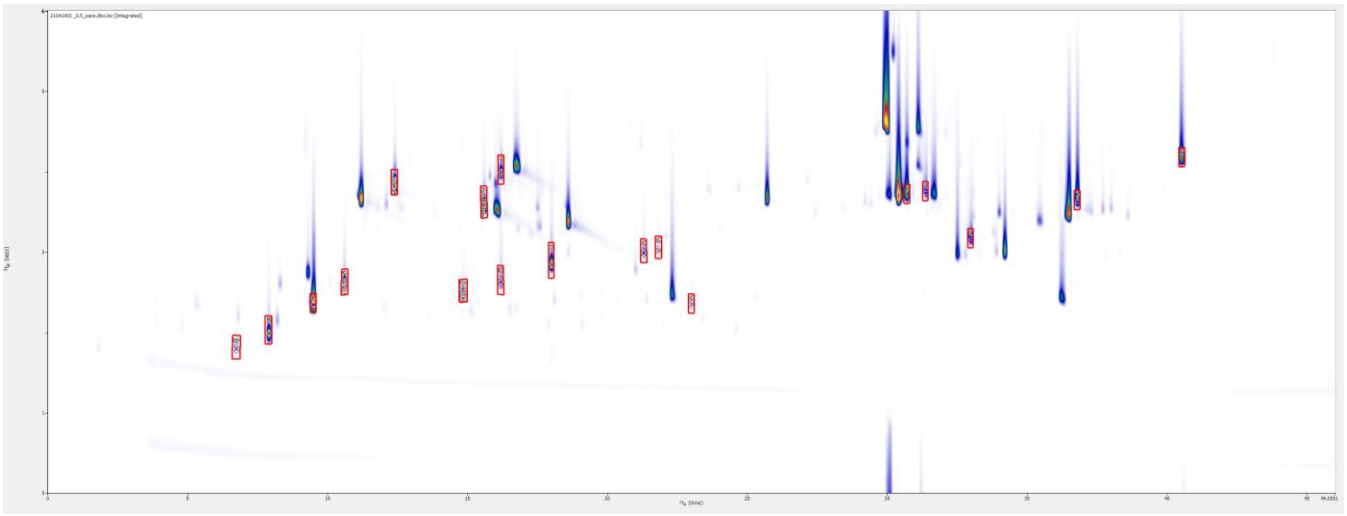

Figure C - 7: GC×GC-TOFMS separation of a commercial perfume sample (10% v/v) diluted in reagent alcohol using the SSM and ^{2}DTPS with the addition of a RTC. 16 peaks were integrated for the within-day (n = 5) and day-to-day (n = 5) reproducibility. ***X-axis: 0 – 46 min. Y-axis: 0 – 6 s****.*

Table C - 14: Comparison of the within-day and day-to-day results before and after the addition of the RTC. An F-test was performed to determine the equality of the variances. This was followed by the corresponding t-test. Results that are insignificant are highlighted in green while significant results are highlighted in orange.

	Within-Day				**Day-to-Day**			
	F-Test		t-test		F-Test		t-test	
	F-stat	p-value	t-stat	p-value	F-stat	p-value	t-stat	p-value
$^{1}t_r$	1.76	0.12	0.82	0.42	1.23	0.32	0.31	0.76
$^{2}t_r$	3.31	6.8×10^{-3}	2.36	3.0×10^{-2}	1.32	0.2747	2.50	2.0×10^{-2}
Area	4.13	1.9×10^{-3}	3.24	3.9×10^{-3}	1.43	0.2246	4.78	3.1×10^{-5}

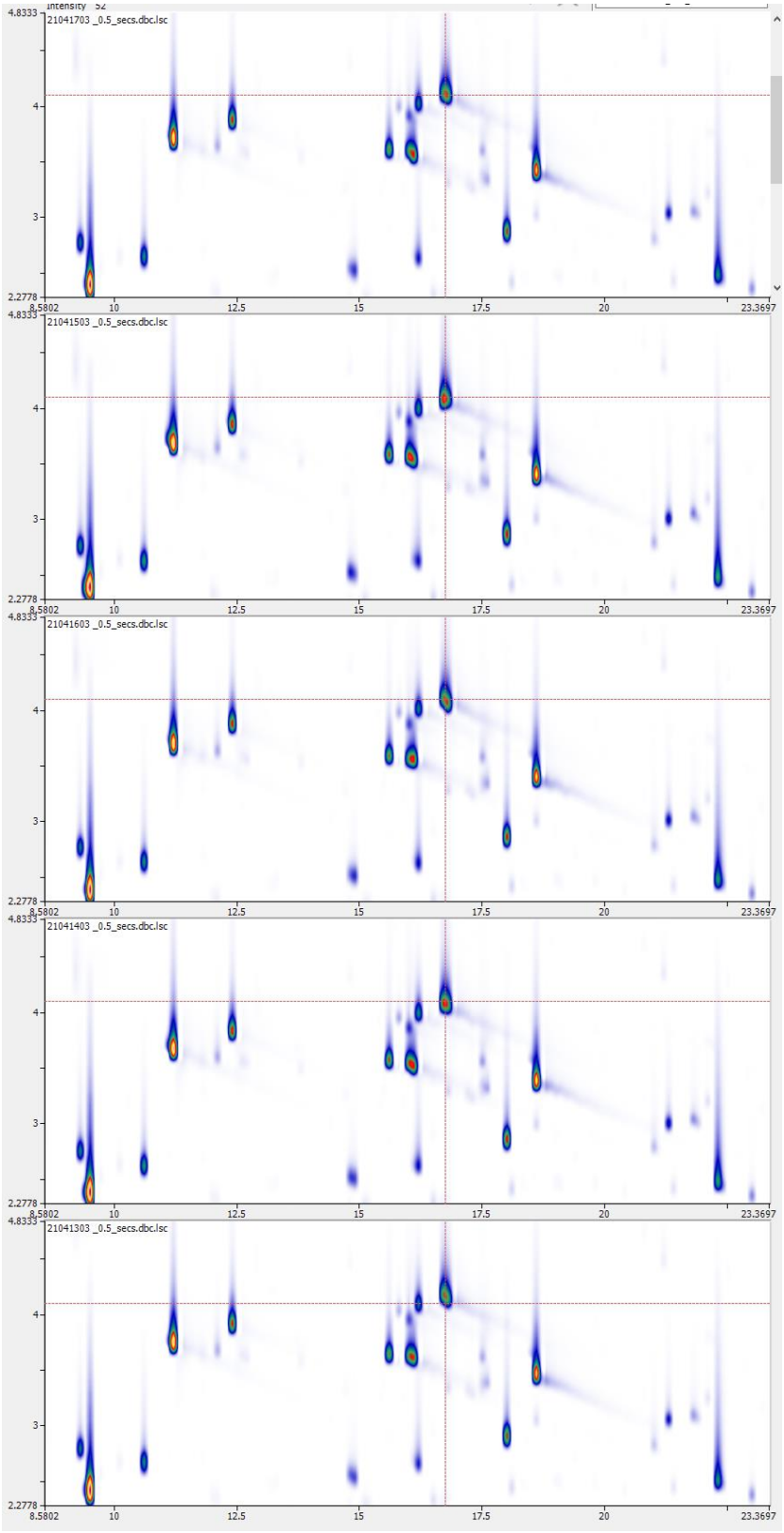

Figure C - 8: Visual check of the third run of each day in the five-day reproducibility test of the GC×GC-TOFMS separation of perfume by zooming into a region (^1t_r: 8.58 – 23.37 min, ^2t_r: 2.278 – 4.833 s).

Table C - 15: GC×GC-FID/TOFMS conditions for testing the ²DTPS with the SepSolve Insight Flow Modulator

²DTPS – Flow Modulator Compatibility			
Test	Retention Time Reproducibility		
Sample	10% Diesel (v/v %)		
Inlet	0.2 µL, 250 °C, 100:1 split		
¹D Column	Rxi-5Sil MS (20 m × 0.15 mm × 0.15 µm)		
Bleed Column	Deactivated Fused Silica tubing (2.83 m × 0.10 mm)		
Modulator plate to ²D column	Guard (0.25 m x 0.25 mm)		
²D Column	MXT-WAX (3.00 m × 0.25 mm × 0.25 µm)		
²D column to Splitter plate	Guard (0.30 m x 0.25 mm)		
Splitter to FID	Guard (0.8 m x 0.32 mm)		
Splitter to TOF	Guard (1.0 m x 0.18 mm)		
¹D Flow	He 99.999%, 0.60 mL/min		
²D Flow	He 99.999%, 18.09 mL/min		
Oven	°C/min	Next °C	Hold (min)
		35	1
	5	230	10
Detector (FID)	Temperature: 250 °C, H_2: 40 mL/min, Air: 400 mL/min, N_2 + Carrier: 30 mL/min, Data: 100 Hz		
Detector (TOFMS)	Filament (V)	1.6	
	Filament Delay (s)	198	
	Mass Range (m/z)	45 - 600	
	Data Rate (Hz)	100	
	Transfer Line (°C)	250	
	Ion source (°C)	250	
Modulator	Flush Time (ms)	250	
	Fill Time (ms)	3.75	
	Modulation Period (s)	4	
²DTPS	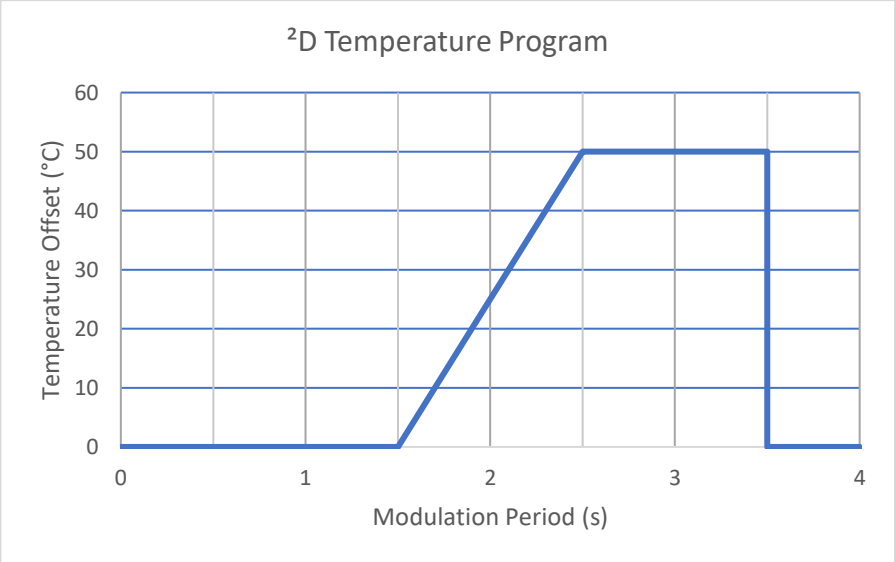		

Table C - 16: GC×GC-FID/TOFMS conditions for testing the ²DTPS with the addition of a remote port and multiple ²D temperature programming function

<table>
<tr><th colspan="5">²DTPS – Remote Port Addition/Multiple ²D Temperature Program/Sequence</th></tr>
<tr><td>Test</td><td colspan="4">Retention Time Reproducibility</td></tr>
<tr><td>Sample</td><td colspan="4">10% Diesel (v/v %)</td></tr>
<tr><td>Inlet</td><td colspan="4">1.0 µL, 250 °C, 100:1 split</td></tr>
<tr><td>¹D Column</td><td colspan="4">Rxi-5Sil MS W/Integra-Guard (30 m × 0.25 mm × 0.25 µm)</td></tr>
<tr><td>¹D to Modulator Column</td><td colspan="4">Deactivated fused silica capillary (0.05 m x 0.05 mm)</td></tr>
<tr><td>²D Column</td><td colspan="4">*MXT-WAX* (1.00 m × 0.25 mm × 0.25 µm)</td></tr>
<tr><td>²D to FID</td><td colspan="4">Guard (0.15 m x 0.25 mm)</td></tr>
<tr><td>Flow</td><td colspan="4">He 99.999%, 3.0 mL/min</td></tr>
<tr><td rowspan="3">Oven</td><td>°C/min</td><td colspan="2">Next °C</td><td>Hold (min)</td></tr>
<tr><td></td><td colspan="2">35</td><td>3</td></tr>
<tr><td>3</td><td colspan="2">230</td><td>20</td></tr>
<tr><td>Detector (FID)</td><td colspan="4">Temperature: 300 °C, H_2: 40 mL/min, Air: 400 mL/min, N_2 + Carrier: 30 mL/min, Data: 100 Hz</td></tr>
<tr><td rowspan="5">Modulator</td><td>Column</td><td colspan="3">Guard (0.48 m x 0.25 mm) + Rxi-1ms (0.69 m x 0.25 mm x 1.0 µm)</td></tr>
<tr><td>Modulation Period</td><td colspan="3">6 s</td></tr>
<tr><td>Entry Hot Zone</td><td colspan="3">+100 °C (300 °C cap)</td></tr>
<tr><td>Exit Hot Zone</td><td colspan="3">+100 °C (300 °C cap)</td></tr>
<tr><td rowspan="2">Cold Zone</td><td colspan="3">-51 °C (oven < 150 °C)</td></tr>
<tr><td colspan="3">9 °C (oven > 150 °C)</td></tr>
<tr><td>²DTPS</td><td colspan="4"> 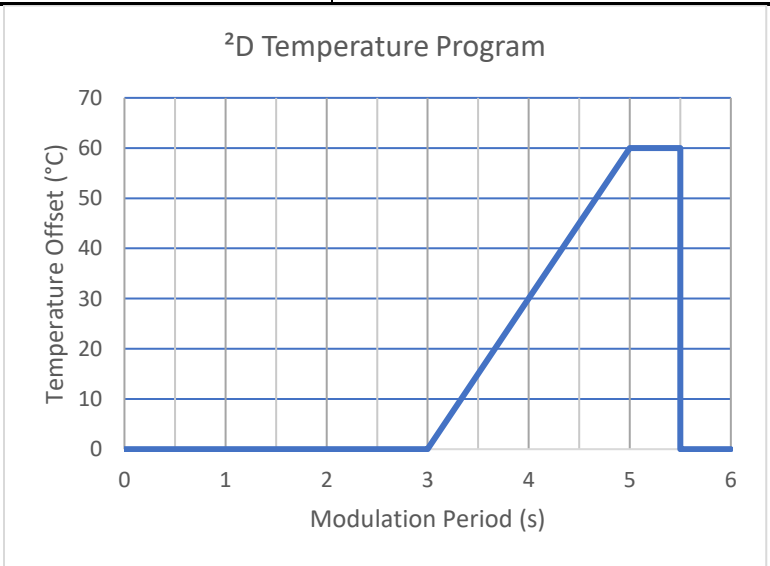
</td></tr>
</table>

Table C - 17: Heating rate (2 s duration) and maximum temperature offset results for various column dimensions [length (L.), inner diameter (I.D.)], flow rate (F), oven temperatures, and power supply output [voltage (V), current (I)] measured at the ²DTPS. The resistance (Ω), power (W), and power normalized to the length (W/m) were calculated from the measured values. The standard deviation (S.D.) was the S.D. of the Ω measurement (converted to °C) during the column calibration (temperature versus resistance) at the oven temperature. Highlighted in red was the maximum heating rate for each set of conditions. Data for each column was collected in the order shown. The first set of data for the 0.5 m x 0.25 mm column had lower than expected heating rates and maximum offsets. The testing was repeated at the end. Some data points for the maximum temperature offset or heating rate may not be available (#NA) due to the temperature limits of the stationary phase.

L. (m)	I.D. (mm)	F (mL/min)	Oven (°C)	V	I	Ω	W	W/m	Max Offset (°C)	Rate (°C/s)	$\lvert\Delta T\rvert_{avg.}$ (°C)	S.D. (°C)
1	0.25	1.5	35	11.600	1.168	9.932	13.549	13.549	41	5	0.921	0.772
1	0.25	1.5	35	11.600	1.168	9.932	13.549	13.549	41	10	0.895	0.772
1	0.25	1.5	35	11.600	1.168	9.932	13.549	13.549	41	11	0.760	0.772
1	0.25	1.5	35	11.600	1.168	9.932	13.549	13.549	41	12	0.672	0.772
1	0.25	1.5	35	11.600	1.168	9.932	13.549	13.549	41	13	0.541	0.772
1	0.25	1.5	35	11.600	1.168	9.932	13.549	13.549	41	14	0.529	0.772
1	0.25	1.5	35	11.600	1.168	9.932	13.549	13.549	41	15	0.455	0.772
1	0.25	1.5	35	11.600	1.168	9.932	13.549	13.549	41	16	0.596	0.772
1	0.25	1.5	35	11.600	1.168	9.932	13.549	13.549	41	17	0.808	0.772
1	0.25	1.5	35	11.600	1.168	9.932	13.549	13.549	41	18	1.085	0.772
1	0.25	1.5	50	11.600	1.155	10.043	13.398	13.398	40	15	0.518	1.019
1	0.25	1.5	50	11.600	1.155	10.043	13.398	13.398	40	16	0.589	1.019
1	0.25	1.5	50	11.600	1.155	10.043	13.398	13.398	40	17	0.872	1.019
1	0.25	1.5	50	11.600	1.155	10.043	13.398	13.398	40	18	1.129	1.019
1	0.25	1.5	100	11.620	1.116	10.412	12.968	12.968	40	12	0.650	0.643
1	0.25	1.5	100	11.620	1.116	10.412	12.968	12.968	40	13	0.557	0.643
1	0.25	1.5	100	11.620	1.116	10.412	12.968	12.968	40	14	0.564	0.643
1	0.25	1.5	100	11.620	1.116	10.412	12.968	12.968	40	15	0.714	0.643
1	0.25	1.5	100	11.620	1.116	10.412	12.968	12.968	40	16	0.886	0.643
1	0.25	1.5	100	11.620	1.116	10.412	12.968	12.968	40	17	1.289	0.643
1	0.25	1.5	150	11.700	1.087	10.764	12.718	12.718	37	12	0.641	0.713
1	0.25	1.5	150	11.700	1.087	10.764	12.718	12.718	37	13	0.616	0.713
1	0.25	1.5	150	11.700	1.087	10.764	12.718	12.718	37	14	0.667	0.713
1	0.25	1.5	150	11.700	1.087	10.764	12.718	12.718	37	15	0.794	0.713
1	0.25	1.5	150	11.700	1.087	10.764	12.718	12.718	37	16	1.105	0.713
1	0.25	1.5	150	11.700	1.087	10.764	12.718	12.718	37	17	1.532	0.713
1	0.25	1.5	200	11.680	1.055	11.071	12.322	12.322	36	12	0.715	1.054
1	0.25	1.5	200	11.680	1.055	11.071	12.322	12.322	36	13	0.631	1.054
1	0.25	1.5	200	11.680	1.055	11.071	12.322	12.322	36	14	0.744	1.054
1	0.25	1.5	200	11.680	1.055	11.071	12.322	12.322	36	15	0.908	1.054
1	0.25	1.5	200	11.680	1.055	11.071	12.322	12.322	36	16	1.178	1.054
1	0.25	1.5	200	11.680	1.055	11.071	12.322	12.322	36	17	1.757	1.054
1	0.25	1.5	35	13.600	1.368	9.942	18.605	18.605	54	5	0.800	0.716
1	0.25	1.5	35	13.600	1.368	9.942	18.605	18.605	54	10	0.892	0.716
1	0.25	1.5	35	13.600	1.368	9.942	18.605	18.605	54	15	0.692	0.716
1	0.25	1.5	35	13.600	1.368	9.942	18.605	18.605	54	17	0.636	0.716
1	0.25	1.5	35	13.600	1.368	9.942	18.605	18.605	54	18	0.522	0.716
1	0.25	1.5	35	13.600	1.368	9.942	18.605	18.605	54	19	0.478	0.716
1	0.25	1.5	35	13.600	1.368	9.942	18.605	18.605	54	20	0.511	0.716
1	0.25	1.5	35	13.600	1.368	9.942	18.605	18.605	54	21	0.502	0.716
1	0.25	1.5	35	13.600	1.368	9.942	18.605	18.605	54	22	0.656	0.716
1	0.25	1.5	35	13.600	1.368	9.942	18.605	18.605	54	23	0.819	0.716
1	0.25	1.5	35	13.600	1.368	9.942	18.605	18.605	54	24	1.078	0.716
1	0.25	1.5	35	13.600	1.368	9.942	18.605	18.605	54	25	1.445	0.716
1	0.25	1.5	35	13.600	1.368	9.942	18.605	18.605	54	26	2.041	0.716
1	0.25	1.5	50	13.600	1.352	10.059	18.387	18.387	55	20	0.429	0.968

1	0.25	1.5	50	13.600	1.352	10.059	18.387	18.387	55	21	0.502	0.968
1	0.25	1.5	50	13.600	1.352	10.059	18.387	18.387	55	22	0.613	0.968
1	0.25	1.5	50	13.600	1.352	10.059	18.387	18.387	55	23	0.774	0.968
1	0.25	1.5	50	13.600	1.352	10.059	18.387	18.387	55	24	0.997	0.968
1	0.25	1.5	50	13.600	1.352	10.059	18.387	18.387	55	25	1.365	0.968
1	0.25	1.5	50	13.600	1.352	10.059	18.387	18.387	55	26	1.748	0.968
1	0.25	1.5	100	13.600	1.305	10.421	17.748	17.748	53	21	0.667	0.764
1	0.25	1.5	100	13.600	1.305	10.421	17.748	17.748	53	22	0.899	0.764
1	0.25	1.5	100	13.600	1.305	10.421	17.748	17.748	53	23	1.123	0.764
1	0.25	1.5	100	13.600	1.305	10.421	17.748	17.748	53	24	1.484	0.764
1	0.25	1.5	100	13.600	1.305	10.421	17.748	17.748	53	25	1.929	0.764
1	0.25	1.5	150	13.630	1.266	10.766	17.256	17.256	51	19	0.487	0.557
1	0.25	1.5	150	13.630	1.266	10.766	17.256	17.256	51	20	0.570	0.557
1	0.25	1.5	150	13.630	1.266	10.766	17.256	17.256	51	21	0.711	0.557
1	0.25	1.5	150	13.630	1.266	10.766	17.256	17.256	51	22	0.958	0.557
1	0.25	1.5	150	13.630	1.266	10.766	17.256	17.256	51	23	1.252	0.557
1	0.25	1.5	200	13.620	1.228	11.091	16.725	16.725	46	19	0.617	0.564
1	0.25	1.5	200	13.620	1.228	11.091	16.725	16.725	46	20	0.708	0.564
1	0.25	1.5	200	13.620	1.228	11.091	16.725	16.725	46	21	1.085	0.564
1	0.25	1.5	200	13.620	1.228	11.091	16.725	16.725	46	22	1.429	0.564
1	0.25	1.5	35	15.380	1.547	9.942	23.793	23.793	70	5	0.792	0.661
1	0.25	1.5	35	15.380	1.547	9.942	23.793	23.793	70	10	0.880	0.661
1	0.25	1.5	35	15.380	1.547	9.942	23.793	23.793	70	15	0.802	0.661
1	0.25	1.5	35	15.380	1.547	9.942	23.793	23.793	70	16	0.816	0.661
1	0.25	1.5	35	15.380	1.547	9.942	23.793	23.793	70	17	0.787	0.661
1	0.25	1.5	35	15.380	1.547	9.942	23.793	23.793	70	18	0.753	0.661
1	0.25	1.5	35	15.380	1.547	9.942	23.793	23.793	70	19	0.714	0.661
1	0.25	1.5	35	15.380	1.547	9.942	23.793	23.793	70	20	0.702	0.661
1	0.25	1.5	35	15.380	1.547	9.942	23.793	23.793	70	25	0.380	0.661
1	0.25	1.5	35	15.380	1.547	9.942	23.793	23.793	70	26	0.440	0.661
1	0.25	1.5	35	15.380	1.547	9.942	23.793	23.793	70	27	0.500	0.661
1	0.25	1.5	35	15.380	1.547	9.942	23.793	23.793	70	28	0.590	0.661
1	0.25	1.5	35	15.380	1.547	9.942	23.793	23.793	70	29	0.733	0.661
1	0.25	1.5	35	15.380	1.547	9.942	23.793	23.793	70	30	0.891	0.661
1	0.25	1.5	35	15.380	1.547	9.942	23.793	23.793	70	31	1.321	0.661
1	0.25	1.5	50	15.380	1.528	10.065	23.501	23.501	69	16	0.769	1.380
1	0.25	1.5	50	15.380	1.528	10.065	23.501	23.501	69	17	0.800	1.380
1	0.25	1.5	50	15.380	1.528	10.065	23.501	23.501	69	18	0.761	1.380
1	0.25	1.5	50	15.380	1.528	10.065	23.501	23.501	69	19	0.730	1.380
1	0.25	1.5	50	15.380	1.528	10.065	23.501	23.501	69	20	0.693	1.380
1	0.25	1.5	50	15.380	1.528	10.065	23.501	23.501	69	27	0.528	1.380
1	0.25	1.5	50	15.380	1.528	10.065	23.501	23.501	69	28	0.618	1.380
1	0.25	1.5	50	15.380	1.528	10.065	23.501	23.501	69	29	0.739	1.380
1	0.25	1.5	50	15.380	1.528	10.065	23.501	23.501	69	30	0.950	1.380
1	0.25	1.5	100	15.390	1.477	10.420	22.731	22.731	67	17	0.790	0.642
1	0.25	1.5	100	15.390	1.477	10.420	22.731	22.731	67	18	0.757	0.642
1	0.25	1.5	100	15.390	1.477	10.420	22.731	22.731	67	19	0.635	0.642
1	0.25	1.5	100	15.390	1.477	10.420	22.731	22.731	67	20	0.608	0.642
1	0.25	1.5	100	15.390	1.477	10.420	22.731	22.731	67	27	0.663	0.642
1	0.25	1.5	100	15.390	1.477	10.420	22.731	22.731	67	28	0.787	0.642
1	0.25	1.5	100	15.390	1.477	10.420	22.731	22.731	67	29	1.049	0.642
1	0.25	1.5	100	15.390	1.477	10.420	22.731	22.731	67	30	1.346	0.642
1	0.25	1.5	150	15.390	1.430	10.762	22.008	22.008	64	17	0.785	1.069
1	0.25	1.5	150	15.390	1.430	10.762	22.008	22.008	64	18	0.739	1.069
1	0.25	1.5	150	15.390	1.430	10.762	22.008	22.008	64	19	0.659	1.069
1	0.25	1.5	150	15.390	1.430	10.762	22.008	22.008	64	25	0.602	1.069

1	0.25	1.5	150	15.390	1.430	10.762	22.008	22.008	64	26	0.733	1.069
1	0.25	1.5	150	15.390	1.430	10.762	22.008	22.008	64	27	0.973	1.069
1	0.25	1.5	150	15.390	1.430	10.762	22.008	22.008	64	28	1.220	1.069
1	0.25	1.5	200	15.400	1.387	11.103	21.360	21.360	#N/A	16	0.811	0.750
1	0.25	1.5	200	15.400	1.387	11.103	21.360	21.360	#N/A	17	0.769	0.750
1	0.25	1.5	200	15.400	1.387	11.103	21.360	21.360	#N/A	18	0.685	0.750
1	0.25	1.5	200	15.400	1.387	11.103	21.360	21.360	#N/A	19	0.629	0.750
1	0.25	1.5	200	15.400	1.387	11.103	21.360	21.360	#N/A	24	0.650	0.750
1	0.25	1.5	200	15.400	1.387	11.103	21.360	21.360	#N/A	25	0.774	0.750
1	0.25	1.5	200	15.400	1.387	11.103	21.360	21.360	#N/A	26	0.959	0.750
1	0.25	1.5	200	15.400	1.387	11.103	21.360	21.360	#N/A	27	1.248	0.750
1	0.25	1.5	35	17.530	1.762	9.949	30.888	30.888	92	17	0.833	0.735
1	0.25	1.5	35	17.530	1.762	9.949	30.888	30.888	92	18	0.817	0.735
1	0.25	1.5	35	17.530	1.762	9.949	30.888	30.888	92	19	0.866	0.735
1	0.25	1.5	35	17.530	1.762	9.949	30.888	30.888	92	20	0.841	0.735
1	0.25	1.5	35	17.530	1.762	9.949	30.888	30.888	92	21	0.784	0.735
1	0.25	1.5	35	17.530	1.762	9.949	30.888	30.888	92	22	0.733	0.735
1	0.25	1.5	35	17.530	1.762	9.949	30.888	30.888	92	23	0.707	0.735
1	0.25	1.5	35	17.530	1.762	9.949	30.888	30.888	92	35	0.542	0.735
1	0.25	1.5	35	17.530	1.762	9.949	30.888	30.888	92	36	0.617	0.735
1	0.25	1.5	35	17.530	1.762	9.949	30.888	30.888	92	37	0.871	0.735
1	0.25	1.5	35	17.530	1.762	9.949	30.888	30.888	92	38	1.183	0.735
1	0.25	1.5	35	17.530	1.762	9.949	30.888	30.888	92	39	1.137	0.735
1	0.25	1.5	50	17.510	1.741	10.057	30.485	30.485	90	20	0.852	0.776
1	0.25	1.5	50	17.510	1.741	10.057	30.485	30.485	90	21	0.783	0.776
1	0.25	1.5	50	17.510	1.741	10.057	30.485	30.485	90	22	0.721	0.776
1	0.25	1.5	50	17.510	1.741	10.057	30.485	30.485	90	23	0.689	0.776
1	0.25	1.5	50	17.510	1.741	10.057	30.485	30.485	90	35	0.567	0.776
1	0.25	1.5	50	17.510	1.741	10.057	30.485	30.485	90	36	0.642	0.776
1	0.25	1.5	50	17.510	1.741	10.057	30.485	30.485	90	37	0.768	0.776
1	0.25	1.5	50	17.510	1.741	10.057	30.485	30.485	90	38	1.012	0.776
1	0.25	1.5	100	17.520	1.680	10.429	29.434	29.434	86	20	0.831	0.759
1	0.25	1.5	100	17.520	1.680	10.429	29.434	29.434	86	21	0.707	0.759
1	0.25	1.5	100	17.520	1.680	10.429	29.434	29.434	86	22	0.738	0.759
1	0.25	1.5	100	17.520	1.680	10.429	29.434	29.434	86	23	0.687	0.759
1	0.25	1.5	100	17.520	1.680	10.429	29.434	29.434	86	33	0.532	0.759
1	0.25	1.5	100	17.520	1.680	10.429	29.434	29.434	86	34	0.660	0.759
1	0.25	1.5	100	17.520	1.680	10.429	29.434	29.434	86	35	0.847	0.759
1	0.25	1.5	100	17.520	1.680	10.429	29.434	29.434	86	36	0.988	0.759
1	0.25	1.5	150	17.590	1.633	10.772	28.724	28.724	83	19	0.835	0.893
1	0.25	1.5	150	17.590	1.633	10.772	28.724	28.724	83	20	0.811	0.893
1	0.25	1.5	150	17.590	1.633	10.772	28.724	28.724	83	21	0.753	0.893
1	0.25	1.5	150	17.590	1.633	10.772	28.724	28.724	83	22	0.668	0.893
1	0.25	1.5	150	17.590	1.633	10.772	28.724	28.724	83	33	0.688	0.893
1	0.25	1.5	150	17.590	1.633	10.772	28.724	28.724	83	34	0.862	0.893
1	0.25	1.5	150	17.590	1.633	10.772	28.724	28.724	83	35	1.007	0.893
1	0.25	1.5	200	17.590	1.586	11.091	27.898	27.898	#N/A	20	0.848	0.721
1	0.25	1.5	200	17.590	1.586	11.091	27.898	27.898	#N/A	21	0.818	0.721
1	0.25	1.5	200	17.590	1.586	11.091	27.898	27.898	#N/A	22	0.684	0.721
1	0.25	1.5	200	17.590	1.586	11.091	27.898	27.898	#N/A	33	0.538	0.721
1	0.25	1.5	200	17.590	1.586	11.091	27.898	27.898	#N/A	34	0.458	0.721
1	0.25	1.5	200	17.590	1.586	11.091	27.898	27.898	#N/A	35	0.545	0.721
1	0.25	1.5	35	19.140	1.921	9.964	36.768	36.768	109	22	0.763	0.725
1	0.25	1.5	35	19.140	1.921	9.964	36.768	36.768	109	23	0.775	0.725
1	0.25	1.5	35	19.140	1.921	9.964	36.768	36.768	109	24	0.756	0.725
1	0.25	1.5	35	19.140	1.921	9.964	36.768	36.768	109	25	0.709	0.725

1	0.25	1.5	35	19.140	1.921	9.964	36.768	36.768	109	26	0.745	0.725
1	0.25	1.5	35	19.140	1.921	9.964	36.768	36.768	109	41	0.427	0.725
1	0.25	1.5	35	19.140	1.921	9.964	36.768	36.768	109	42	0.537	0.725
1	0.25	1.5	35	19.140	1.921	9.964	36.768	36.768	109	43	0.706	0.725
1	0.25	1.5	35	19.140	1.921	9.964	36.768	36.768	109	44	0.834	0.725
1	0.25	1.5	35	19.140	1.921	9.964	36.768	36.768	109	45	1.215	0.725
1	0.25	1.5	50	19.110	1.898	10.068	36.271	36.271	107	22	0.841	0.571
1	0.25	1.5	50	19.110	1.898	10.068	36.271	36.271	107	23	0.785	0.571
1	0.25	1.5	50	19.110	1.898	10.068	36.271	36.271	107	24	0.747	0.571
1	0.25	1.5	50	19.110	1.898	10.068	36.271	36.271	107	25	0.769	0.571
1	0.25	1.5	50	19.110	1.898	10.068	36.271	36.271	107	26	0.753	0.571
1	0.25	1.5	50	19.110	1.898	10.068	36.271	36.271	107	27	0.712	0.571
1	0.25	1.5	50	19.110	1.898	10.068	36.271	36.271	107	42	0.421	0.571
1	0.25	1.5	50	19.110	1.898	10.068	36.271	36.271	107	43	0.694	0.571
1	0.25	1.5	50	19.110	1.898	10.068	36.271	36.271	107	44	0.736	0.571
1	0.25	1.5	50	19.110	1.898	10.068	36.271	36.271	107	45	1.030	0.571
1	0.25	1.5	100	19.100	1.829	10.443	34.934	34.934	100	22	0.795	0.461
1	0.25	1.5	100	19.100	1.829	10.443	34.934	34.934	100	23	0.843	0.461
1	0.25	1.5	100	19.100	1.829	10.443	34.934	34.934	100	24	0.741	0.461
1	0.25	1.5	100	19.100	1.829	10.443	34.934	34.934	100	25	0.737	0.461
1	0.25	1.5	100	19.100	1.829	10.443	34.934	34.934	100	26	0.730	0.461
1	0.25	1.5	100	19.100	1.829	10.443	34.934	34.934	100	27	0.731	0.461
1	0.25	1.5	100	19.100	1.829	10.443	34.934	34.934	100	40	0.546	0.461
1	0.25	1.5	100	19.100	1.829	10.443	34.934	34.934	100	41	0.639	0.461
1	0.25	1.5	100	19.100	1.829	10.443	34.934	34.934	100	42	0.858	0.461
1	0.25	1.5	100	19.100	1.829	10.443	34.934	34.934	100	43	1.048	0.461
1	0.25	1.5	150	19.080	1.771	10.774	33.791	33.791	97	22	0.788	0.684
1	0.25	1.5	150	19.080	1.771	10.774	33.791	33.791	97	23	0.757	0.684
1	0.25	1.5	150	19.080	1.771	10.774	33.791	33.791	97	24	0.744	0.684
1	0.25	1.5	150	19.080	1.771	10.774	33.791	33.791	97	25	0.726	0.684
1	0.25	1.5	150	19.080	1.771	10.774	33.791	33.791	97	26	0.660	0.684
1	0.25	1.5	150	19.080	1.771	10.774	33.791	33.791	97	27	0.627	0.684
1	0.25	1.5	150	19.080	1.771	10.774	33.791	33.791	97	39	0.676	0.684
1	0.25	1.5	150	19.080	1.771	10.774	33.791	33.791	97	40	0.886	0.684
1	0.25	1.5	150	19.080	1.771	10.774	33.791	33.791	97	41	0.909	0.684
1	0.25	1.5	200	19.080	1.720	11.093	32.818	32.818	#N/A	21	0.900	0.623
1	0.25	1.5	200	19.080	1.720	11.093	32.818	32.818	#N/A	22	0.780	0.623
1	0.25	1.5	200	19.080	1.720	11.093	32.818	32.818	#N/A	23	0.747	0.623
1	0.25	1.5	200	19.080	1.720	11.093	32.818	32.818	#N/A	24	0.745	0.623
1	0.25	1.5	200	19.080	1.720	11.093	32.818	32.818	#N/A	25	0.745	0.623
1	0.25	3	35	11.620	1.169	9.940	13.584	13.584	41	10	0.887	0.772
1	0.25	3	35	11.620	1.169	9.940	13.584	13.584	41	11	0.760	0.772
1	0.25	3	35	11.620	1.169	9.940	13.584	13.584	41	12	0.712	0.772
1	0.25	3	35	11.620	1.169	9.940	13.584	13.584	41	13	0.547	0.772
1	0.25	3	35	11.620	1.169	9.940	13.584	13.584	41	14	0.515	0.772
1	0.25	3	35	11.620	1.169	9.940	13.584	13.584	41	15	0.489	0.772
1	0.25	3	35	11.620	1.169	9.940	13.584	13.584	41	16	0.599	0.772
1	0.25	3	35	11.620	1.169	9.940	13.584	13.584	41	17	0.751	0.772
1	0.25	3	35	11.620	1.169	9.940	13.584	13.584	41	18	1.077	0.772
1	0.25	3	50	11.610	1.155	10.052	13.410	13.410	40	15	0.527	1.019
1	0.25	3	50	11.720	1.166	10.051	13.666	13.666	40	16	0.611	1.019
1	0.25	3	50	11.620	1.156	10.052	13.433	13.433	40	17	0.822	1.019
1	0.25	3	50	11.620	1.156	10.052	13.433	13.433	40	18	1.132	1.019
1	0.25	3	100	11.620	1.115	10.422	12.956	12.956	39	12	0.668	0.643
1	0.25	3	100	11.620	1.115	10.422	12.956	12.956	39	13	0.581	0.643
1	0.25	3	100	11.620	1.115	10.422	12.956	12.956	39	14	0.610	0.643

1	0.25	3	100	11.620	1.115	10.422	12.956	12.956	39	15	0.669	0.643
1	0.25	3	100	11.620	1.115	10.422	12.956	12.956	39	16	0.886	0.643
1	0.25	3	100	11.620	1.115	10.422	12.956	12.956	39	17	1.253	0.643
1	0.25	3	150	11.700	1.088	10.754	12.730	12.730	37	12	0.603	0.713
1	0.25	3	150	11.700	1.088	10.754	12.730	12.730	37	13	0.687	0.713
1	0.25	3	150	11.700	1.088	10.754	12.730	12.730	37	14	0.694	0.713
1	0.25	3	150	11.700	1.088	10.754	12.730	12.730	37	15	0.860	0.713
1	0.25	3	150	11.700	1.088	10.754	12.730	12.730	37	16	1.185	0.713
1	0.25	3	150	11.700	1.088	10.754	12.730	12.730	37	17	1.680	0.713
1	0.25	3	200	11.710	1.057	11.079	12.377	12.377	36	12	0.655	1.054
1	0.25	3	200	11.710	1.057	11.079	12.377	12.377	36	13	0.625	1.054
1	0.25	3	200	11.710	1.057	11.079	12.377	12.377	36	14	0.756	1.054
1	0.25	3	200	11.710	1.057	11.079	12.377	12.377	36	15	0.979	1.054
1	0.25	3	200	11.710	1.057	11.079	12.377	12.377	36	16	1.454	1.054
1	0.25	3	200	11.710	1.057	11.079	12.377	12.377	36	17	2.116	1.054
1	0.25	3	35	13.600	1.368	9.942	18.605	18.605	56	20	0.436	0.716
1	0.25	3	35	13.600	1.368	9.942	18.605	18.605	56	21	0.455	0.716
1	0.25	3	35	13.600	1.368	9.942	18.605	18.605	56	22	0.628	0.716
1	0.25	3	35	13.600	1.368	9.942	18.605	18.605	56	23	0.740	0.716
1	0.25	3	35	13.600	1.368	9.942	18.605	18.605	56	24	0.945	0.716
1	0.25	3	35	13.600	1.368	9.942	18.605	18.605	56	25	1.279	0.716
1	0.25	3	50	13.600	1.352	10.059	18.387	18.387	55	21	0.517	0.968
1	0.25	3	50	13.600	1.352	10.059	18.387	18.387	55	22	0.608	0.968
1	0.25	3	50	13.600	1.352	10.059	18.387	18.387	55	23	0.717	0.968
1	0.25	3	50	13.600	1.352	10.059	18.387	18.387	55	24	0.920	0.968
1	0.25	3	50	13.600	1.352	10.059	18.387	18.387	55	25	1.288	0.968
1	0.25	3	100	13.600	1.306	10.413	17.762	17.762	53	19	0.483	0.764
1	0.25	3	100	13.600	1.306	10.413	17.762	17.762	53	20	0.559	0.764
1	0.25	3	100	13.600	1.306	10.413	17.762	17.762	53	21	0.675	0.764
1	0.25	3	100	13.600	1.306	10.413	17.762	17.762	53	22	0.831	0.764
1	0.25	3	100	13.600	1.306	10.413	17.762	17.762	53	23	1.040	0.764
1	0.25	3	100	13.600	1.306	10.413	17.762	17.762	53	24	1.480	0.764
1	0.25	3	150	13.620	1.266	10.758	17.243	17.243	51	19	0.494	0.557
1	0.25	3	150	13.620	1.266	10.758	17.243	17.243	51	20	0.599	0.557
1	0.25	3	150	13.620	1.266	10.758	17.243	17.243	51	21	0.740	0.557
1	0.25	3	150	13.620	1.266	10.758	17.243	17.243	51	22	1.041	0.557
1	0.25	3	150	13.620	1.266	10.758	17.243	17.243	51	23	1.348	0.557
1	0.25	3	150	13.620	1.266	10.758	17.243	17.243	51	24	1.702	0.557
1	0.25	3	200	13.620	1.228	11.091	16.725	16.725	46	19	0.649	0.564
1	0.25	3	200	13.620	1.228	11.091	16.725	16.725	46	20	0.718	0.564
1	0.25	3	200	13.620	1.228	11.091	16.725	16.725	46	21	1.104	0.564
1	0.25	3	200	13.620	1.228	11.091	16.725	16.725	46	22	1.436	0.564
1	0.25	3	35	15.380	1.547	9.942	23.793	23.793	70	15	0.802	0.661
1	0.25	3	35	15.380	1.547	9.942	23.793	23.793	70	16	0.815	0.661
1	0.25	3	35	15.380	1.547	9.942	23.793	23.793	70	17	0.789	0.661
1	0.25	3	35	15.380	1.547	9.942	23.793	23.793	70	18	0.720	0.661
1	0.25	3	35	15.380	1.547	9.942	23.793	23.793	70	27	0.501	0.661
1	0.25	3	35	15.380	1.547	9.942	23.793	23.793	70	28	0.601	0.661
1	0.25	3	35	15.380	1.547	9.942	23.793	23.793	70	29	0.775	0.661
1	0.25	3	35	15.380	1.547	9.942	23.793	23.793	70	30	0.890	0.661
1	0.25	3	35	15.380	1.547	9.942	23.793	23.793	70	31	1.307	0.661
1	0.25	3	50	15.380	1.529	10.059	23.516	23.516	70	17	0.799	1.380
1	0.25	3	50	15.380	1.529	10.059	23.516	23.516	70	18	0.764	1.380
1	0.25	3	50	15.380	1.529	10.059	23.516	23.516	70	19	0.726	1.380
1	0.25	3	50	15.380	1.529	10.059	23.516	23.516	70	20	0.683	1.380
1	0.25	3	50	15.380	1.529	10.059	23.516	23.516	70	28	0.601	1.380

1	0.25	3	50	15.380	1.529	10.059	23.516	23.516	70	29	0.786	1.380
1	0.25	3	50	15.380	1.529	10.059	23.516	23.516	70	30	0.968	1.380
1	0.25	3	50	15.380	1.529	10.059	23.516	23.516	70	31	1.145	1.380
1	0.25	3	100	15.390	1.476	10.427	22.716	22.716	67	17	0.783	0.642
1	0.25	3	100	15.390	1.476	10.427	22.716	22.716	67	18	0.711	0.642
1	0.25	3	100	15.390	1.476	10.427	22.716	22.716	67	19	0.658	0.642
1	0.25	3	100	15.390	1.476	10.427	22.716	22.716	67	20	0.608	0.642
1	0.25	3	100	15.390	1.476	10.427	22.716	22.716	67	26	0.524	0.642
1	0.25	3	100	15.390	1.476	10.427	22.716	22.716	67	27	0.666	0.642
1	0.25	3	100	15.390	1.476	10.427	22.716	22.716	67	28	0.794	0.642
1	0.25	3	100	15.390	1.476	10.427	22.716	22.716	67	29	1.016	0.642
1	0.25	3	150	15.390	1.430	10.762	22.008	22.008	64	17	0.771	1.069
1	0.25	3	150	15.390	1.430	10.762	22.008	22.008	64	18	0.721	1.069
1	0.25	3	150	15.390	1.430	10.762	22.008	22.008	64	19	0.650	1.069
1	0.25	3	150	15.390	1.430	10.762	22.008	22.008	64	25	0.605	1.069
1	0.25	3	150	15.390	1.430	10.762	22.008	22.008	64	26	0.739	1.069
1	0.25	3	150	15.390	1.430	10.762	22.008	22.008	64	27	0.970	1.069
1	0.25	3	150	15.390	1.430	10.762	22.008	22.008	64	28	1.248	1.069
1	0.25	3	200	15.390	1.388	11.088	21.361	21.361	#N/A	16	0.815	0.750
1	0.25	3	200	15.390	1.388	11.088	21.361	21.361	#N/A	17	0.747	0.750
1	0.25	3	200	15.390	1.388	11.088	21.361	21.361	#N/A	18	0.684	0.750
1	0.25	3	200	15.390	1.388	11.088	21.361	21.361	#N/A	24	0.603	0.750
1	0.25	3	200	15.390	1.388	11.088	21.361	21.361	#N/A	25	0.765	0.750
1	0.25	3	200	15.390	1.388	11.088	21.361	21.361	#N/A	26	0.980	0.750
1	0.25	3	35	17.520	1.761	9.949	30.853	30.853	91	20	0.801	0.735
1	0.25	3	35	17.520	1.761	9.949	30.853	30.853	91	21	0.822	0.735
1	0.25	3	35	17.520	1.761	9.949	30.853	30.853	91	22	0.722	0.735
1	0.25	3	35	17.520	1.761	9.949	30.853	30.853	91	23	0.735	0.735
1	0.25	3	35	17.520	1.761	9.949	30.853	30.853	91	35	0.597	0.735
1	0.25	3	35	17.520	1.761	9.949	30.853	30.853	91	36	0.599	0.735
1	0.25	3	35	17.520	1.761	9.949	30.853	30.853	91	37	0.751	0.735
1	0.25	3	35	17.520	1.761	9.949	30.853	30.853	91	38	0.933	0.735
1	0.25	3	50	17.510	1.740	10.063	30.467	30.467	90	20	0.855	0.776
1	0.25	3	50	17.510	1.740	10.063	30.467	30.467	90	21	0.705	0.776
1	0.25	3	50	17.510	1.740	10.063	30.467	30.467	90	22	0.742	0.776
1	0.25	3	50	17.510	1.740	10.063	30.467	30.467	90	23	0.686	0.776
1	0.25	3	50	17.510	1.740	10.063	30.467	30.467	90	35	0.675	0.776
1	0.25	3	50	17.510	1.740	10.063	30.467	30.467	90	36	0.715	0.776
1	0.25	3	50	17.510	1.740	10.063	30.467	30.467	90	37	0.870	0.776
1	0.25	3	50	17.510	1.740	10.063	30.467	30.467	90	38	1.021	0.776
1	0.25	3	100	17.520	1.681	10.422	29.451	29.451	86	19	0.819	0.759
1	0.25	3	100	17.520	1.681	10.422	29.451	29.451	86	20	0.801	0.759
1	0.25	3	100	17.520	1.681	10.422	29.451	29.451	86	21	0.788	0.759
1	0.25	3	100	17.520	1.681	10.422	29.451	29.451	86	22	0.747	0.759
1	0.25	3	100	17.520	1.681	10.422	29.451	29.451	86	23	0.705	0.759
1	0.25	3	100	17.520	1.681	10.422	29.451	29.451	86	33	0.456	0.759
1	0.25	3	100	17.520	1.681	10.422	29.451	29.451	86	34	0.555	0.759
1	0.25	3	100	17.520	1.681	10.422	29.451	29.451	86	35	0.627	0.759
1	0.25	3	100	17.520	1.681	10.422	29.451	29.451	86	36	0.782	0.759
1	0.25	3	100	17.520	1.681	10.422	29.451	29.451	86	37	0.899	0.759
1	0.25	3	150	17.600	1.635	10.765	28.776	28.776	83	20	0.830	0.893
1	0.25	3	150	17.600	1.635	10.765	28.776	28.776	83	21	0.774	0.893
1	0.25	3	150	17.600	1.635	10.765	28.776	28.776	83	22	0.713	0.893
1	0.25	3	150	17.600	1.635	10.765	28.776	28.776	83	33	0.679	0.893
1	0.25	3	150	17.600	1.635	10.765	28.776	28.776	83	34	0.817	0.893
1	0.25	3	150	17.600	1.635	10.765	28.776	28.776	83	35	1.009	0.893

1	0.25	3	200	17.480	1.576	11.091	27.548	27.548	#N/A	21	0.843	0.721
1	0.25	3	200	17.480	1.576	11.091	27.548	27.548	#N/A	22	0.705	0.721
1	0.25	3	200	17.480	1.576	11.091	27.548	27.548	#N/A	23	0.647	0.721
1	0.25	3	200	17.480	1.576	11.091	27.548	27.548	#N/A	33	0.542	0.721
1	0.25	3	200	17.480	1.576	11.091	27.548	27.548	#N/A	34	0.536	0.721
1	0.25	3	200	17.480	1.576	11.091	27.548	27.548	#N/A	35	0.544	0.721
1	0.25	3	35	19.120	1.920	9.958	36.710	36.710	108	23	0.774	0.725
1	0.25	3	35	19.120	1.920	9.958	36.710	36.710	108	24	0.745	0.725
1	0.25	3	35	19.120	1.920	9.958	36.710	36.710	108	25	0.704	0.725
1	0.25	3	35	19.120	1.920	9.958	36.710	36.710	108	26	0.731	0.725
1	0.25	3	35	19.120	1.920	9.958	36.710	36.710	108	42	0.577	0.725
1	0.25	3	35	19.120	1.920	9.958	36.710	36.710	108	43	0.553	0.725
1	0.25	3	35	19.120	1.920	9.958	36.710	36.710	108	44	0.735	0.725
1	0.25	3	35	19.120	1.920	9.958	36.710	36.710	108	45	0.977	0.725
1	0.25	3	50	19.100	1.896	10.074	36.214	36.214	106	22	0.795	0.571
1	0.25	3	50	19.100	1.896	10.074	36.214	36.214	106	23	0.823	0.571
1	0.25	3	50	19.100	1.896	10.074	36.214	36.214	106	24	0.825	0.571
1	0.25	3	50	19.100	1.896	10.074	36.214	36.214	106	25	0.795	0.571
1	0.25	3	50	19.100	1.896	10.074	36.214	36.214	106	26	0.733	0.571
1	0.25	3	50	19.100	1.896	10.074	36.214	36.214	106	42	0.477	0.571
1	0.25	3	50	19.100	1.896	10.074	36.214	36.214	106	43	0.729	0.571
1	0.25	3	50	19.100	1.896	10.074	36.214	36.214	106	44	0.813	0.571
1	0.25	3	50	19.100	1.896	10.074	36.214	36.214	106	45	1.030	0.571
1	0.25	3	100	19.090	1.830	10.432	34.935	34.935	100	22	0.769	0.461
1	0.25	3	100	19.090	1.830	10.432	34.935	34.935	100	23	0.833	0.461
1	0.25	3	100	19.090	1.830	10.432	34.935	34.935	100	24	0.772	0.461
1	0.25	3	100	19.090	1.830	10.432	34.935	34.935	100	25	0.770	0.461
1	0.25	3	100	19.090	1.830	10.432	34.935	34.935	100	26	0.755	0.461
1	0.25	3	100	19.090	1.830	10.432	34.935	34.935	100	27	0.741	0.461
1	0.25	3	100	19.090	1.830	10.432	34.935	34.935	100	40	0.583	0.461
1	0.25	3	100	19.090	1.830	10.432	34.935	34.935	100	41	0.560	0.461
1	0.25	3	100	19.090	1.830	10.432	34.935	34.935	100	42	0.952	0.461
1	0.25	3	100	19.090	1.830	10.432	34.935	34.935	100	43	1.157	0.461
1	0.25	3	150	19.080	1.772	10.767	33.810	33.810	97	22	0.782	0.684
1	0.25	3	150	19.080	1.772	10.767	33.810	33.810	97	23	0.845	0.684
1	0.25	3	150	19.080	1.772	10.767	33.810	33.810	97	24	0.745	0.684
1	0.25	3	150	19.080	1.772	10.767	33.810	33.810	97	25	0.734	0.684
1	0.25	3	150	19.080	1.772	10.767	33.810	33.810	97	38	0.565	0.684
1	0.25	3	150	19.080	1.772	10.767	33.810	33.810	97	39	0.685	0.684
1	0.25	3	150	19.080	1.772	10.767	33.810	33.810	97	40	0.815	0.684
1	0.25	3	150	19.080	1.772	10.767	33.810	33.810	97	41	0.947	0.684
1	0.25	3	200	19.070	1.720	11.087	32.800	32.800	#N/A	21	0.873	0.623
1	0.25	3	200	19.070	1.720	11.087	32.800	32.800	#N/A	22	0.741	0.623
1	0.25	3	200	19.070	1.720	11.087	32.800	32.800	#N/A	23	0.753	0.623
1	0.25	3	200	19.080	1.720	11.093	32.818	32.818	#N/A	24	0.811	0.623
1	0.25	3	200	19.080	1.720	11.093	32.818	32.818	#N/A	25	0.750	0.623
1	0.25	3	200	19.080	1.720	11.093	32.818	32.818	#N/A	26	0.647	0.623
0.5	0.25	3	35	5.885	1.192	4.938	7.013	14.026	38	5	0.956	0.773
0.5	0.25	3	35	5.885	1.192	4.938	7.013	14.026	38	6	0.948	0.773
0.5	0.25	3	35	5.885	1.192	4.938	7.013	14.026	38	7	0.905	0.773
0.5	0.25	3	35	5.885	1.192	4.938	7.013	14.026	38	8	0.890	0.773
0.5	0.25	3	35	5.885	1.192	4.938	7.013	14.026	38	9	0.910	0.773
0.5	0.25	3	35	5.885	1.192	4.938	7.013	14.026	38	10	0.854	0.773
0.5	0.25	3	35	5.885	1.192	4.938	7.013	14.026	38	11	0.767	0.773
0.5	0.25	3	35	5.885	1.192	4.938	7.013	14.026	38	12	0.659	0.773
0.5	0.25	3	35	5.885	1.192	4.938	7.013	14.026	38	13	0.533	0.773

0.5	0.25	3	35	5.885	1.192	4.938	7.013	14.026	38	14	0.557	0.773
0.5	0.25	3	35	5.885	1.192	4.938	7.013	14.026	38	15	0.648	0.773
0.5	0.25	3	35	5.885	1.192	4.938	7.013	14.026	38	16	0.769	0.773
0.5	0.25	3	35	5.885	1.192	4.938	7.013	14.026	38	17	1.027	0.773
0.5	0.25	3	35	5.885	1.192	4.938	7.013	14.026	38	18	1.409	0.773
0.5	0.25	3	50	5.950	1.190	5.000	7.080	14.160	38	10	0.863	0.962
0.5	0.25	3	50	5.950	1.190	5.000	7.080	14.160	38	11	0.782	0.962
0.5	0.25	3	50	5.950	1.190	5.000	7.080	14.160	38	12	0.639	0.962
0.5	0.25	3	50	5.950	1.190	5.000	7.080	14.160	38	13	0.513	0.962
0.5	0.25	3	50	5.950	1.190	5.000	7.080	14.160	38	14	0.535	0.962
0.5	0.25	3	50	5.950	1.190	5.000	7.080	14.160	38	15	0.657	0.962
0.5	0.25	3	50	5.950	1.190	5.000	7.080	14.160	38	16	0.799	0.962
0.5	0.25	3	50	5.950	1.190	5.000	7.080	14.160	38	17	1.185	0.962
0.5	0.25	3	100	5.952	1.146	5.195	6.818	13.637	36	10	0.839	1.002
0.5	0.25	3	100	5.952	1.146	5.195	6.818	13.637	36	11	0.716	1.002
0.5	0.25	3	100	5.952	1.146	5.195	6.818	13.637	36	12	0.636	1.002
0.5	0.25	3	100	5.952	1.146	5.195	6.818	13.637	36	13	0.611	1.002
0.5	0.25	3	100	5.952	1.146	5.195	6.818	13.637	36	14	0.675	1.002
0.5	0.25	3	100	5.952	1.146	5.195	6.818	13.637	36	15	0.860	1.002
0.5	0.25	3	100	5.952	1.146	5.195	6.818	13.637	36	16	1.142	1.002
0.5	0.25	3	100	5.952	1.146	5.195	6.818	13.637	36	17	1.613	1.002
0.5	0.25	3	150	5.953	1.106	5.382	6.584	13.168	34	9	0.910	1.173
0.5	0.25	3	150	5.953	1.106	5.382	6.584	13.168	34	10	0.830	1.173
0.5	0.25	3	150	5.953	1.106	5.382	6.584	13.168	34	11	0.734	1.173
0.5	0.25	3	150	5.953	1.106	5.382	6.584	13.168	34	12	0.640	1.173
0.5	0.25	3	150	5.953	1.106	5.382	6.584	13.168	34	13	0.648	1.173
0.5	0.25	3	150	5.953	1.106	5.382	6.584	13.168	34	14	0.743	1.173
0.5	0.25	3	150	5.953	1.106	5.382	6.584	13.168	34	15	1.093	1.173
0.5	0.25	3	150	5.953	1.106	5.382	6.584	13.168	34	16	1.520	1.173
0.5	0.25	3	200	5.956	1.072	5.557	6.383	12.766	33	9	0.933	0.520
0.5	0.25	3	200	5.956	1.072	5.557	6.383	12.766	33	10	0.838	0.520
0.5	0.25	3	200	5.956	1.072	5.557	6.383	12.766	33	11	0.743	0.520
0.5	0.25	3	200	5.956	1.072	5.557	6.383	12.766	33	12	0.680	0.520
0.5	0.25	3	200	5.956	1.072	5.557	6.383	12.766	33	13	0.765	0.520
0.5	0.25	3	200	5.956	1.072	5.557	6.383	12.766	33	14	0.948	0.520
0.5	0.25	3	200	5.956	1.072	5.557	6.383	12.766	33	15	1.313	0.520
0.5	0.25	3	200	5.956	1.072	5.557	6.383	12.766	33	16	1.816	0.520
0.5	0.25	3	35	6.700	1.356	4.941	9.085	18.170	49	5	0.885	0.779
0.5	0.25	3	35	6.700	1.356	4.941	9.085	18.170	49	6	0.950	0.779
0.5	0.25	3	35	6.700	1.356	4.941	9.085	18.170	49	7	0.896	0.779
0.5	0.25	3	35	6.700	1.356	4.941	9.085	18.170	49	8	0.925	0.779
0.5	0.25	3	35	6.700	1.356	4.941	9.085	18.170	49	9	0.919	0.779
0.5	0.25	3	35	6.700	1.356	4.941	9.085	18.170	49	10	0.891	0.779
0.5	0.25	3	35	6.700	1.356	4.941	9.085	18.170	49	11	0.861	0.779
0.5	0.25	3	35	6.700	1.356	4.941	9.085	18.170	49	12	0.854	0.779
0.5	0.25	3	35	6.700	1.356	4.941	9.085	18.170	49	13	0.830	0.779
0.5	0.25	3	35	6.700	1.356	4.941	9.085	18.170	49	14	0.791	0.779
0.5	0.25	3	35	6.700	1.356	4.941	9.085	18.170	49	15	0.655	0.779
0.5	0.25	3	35	6.700	1.356	4.941	9.085	18.170	49	16	0.605	0.779
0.5	0.25	3	35	6.700	1.356	4.941	9.085	18.170	49	17	0.497	0.779
0.5	0.25	3	35	6.700	1.356	4.941	9.085	18.170	49	18	0.424	0.779
0.5	0.25	3	35	6.700	1.356	4.941	9.085	18.170	49	19	0.555	0.779
0.5	0.25	3	35	6.700	1.356	4.941	9.085	18.170	49	20	0.696	0.779
0.5	0.25	3	35	6.700	1.356	4.941	9.085	18.170	49	21	1.121	0.779
0.5	0.25	3	35	6.700	1.356	4.941	9.085	18.170	49	22	1.318	0.779
0.5	0.25	3	50	6.698	1.339	5.002	8.970	17.940	47	10	0.924	0.682

0.5	0.25	3	50	6.698	1.339	5.002	8.970	17.940	47	11	0.868	0.682
0.5	0.25	3	50	6.698	1.339	5.002	8.970	17.940	47	12	0.864	0.682
0.5	0.25	3	50	6.698	1.339	5.002	8.970	17.940	47	13	0.705	0.682
0.5	0.25	3	50	6.698	1.339	5.002	8.970	17.940	47	14	0.681	0.682
0.5	0.25	3	50	6.698	1.339	5.002	8.970	17.940	47	15	0.620	0.682
0.5	0.25	3	50	6.698	1.339	5.002	8.970	17.940	47	16	0.526	0.682
0.5	0.25	3	50	6.698	1.339	5.002	8.970	17.940	47	17	0.454	0.682
0.5	0.25	3	50	6.698	1.339	5.002	8.970	17.940	47	18	0.562	0.682
0.5	0.25	3	50	6.698	1.339	5.002	8.970	17.940	47	19	0.693	0.682
0.5	0.25	3	50	6.698	1.339	5.002	8.970	17.940	47	20	0.845	0.682
0.5	0.25	3	50	6.698	1.339	5.002	8.970	17.940	47	21	1.176	0.682
0.5	0.25	3	100	6.700	1.289	5.198	8.636	17.272	44	10	0.937	0.622
0.5	0.25	3	100	6.700	1.289	5.198	8.636	17.272	44	11	0.888	0.622
0.5	0.25	3	100	6.700	1.289	5.198	8.636	17.272	44	12	0.845	0.622
0.5	0.25	3	100	6.700	1.289	5.198	8.636	17.272	44	13	0.704	0.622
0.5	0.25	3	100	6.700	1.289	5.198	8.636	17.272	44	14	0.604	0.622
0.5	0.25	3	100	6.700	1.289	5.198	8.636	17.272	44	15	0.479	0.622
0.5	0.25	3	100	6.700	1.289	5.198	8.636	17.272	44	16	0.525	0.622
0.5	0.25	3	100	6.700	1.289	5.198	8.636	17.272	44	17	0.607	0.622
0.5	0.25	3	100	6.700	1.289	5.198	8.636	17.272	44	18	0.756	0.622
0.5	0.25	3	100	6.700	1.289	5.198	8.636	17.272	44	19	0.903	0.622
0.5	0.25	3	100	6.700	1.289	5.198	8.636	17.272	44	20	1.280	0.622
0.5	0.25	3	150	6.700	1.245	5.382	8.341	16.681	43	10	0.944	1.224
0.5	0.25	3	150	6.700	1.245	5.382	8.341	16.681	43	11	0.877	1.224
0.5	0.25	3	150	6.700	1.245	5.382	8.341	16.681	43	12	0.849	1.224
0.5	0.25	3	150	6.700	1.245	5.382	8.341	16.681	43	13	0.706	1.224
0.5	0.25	3	150	6.700	1.245	5.382	8.341	16.681	43	14	0.643	1.224
0.5	0.25	3	150	6.700	1.245	5.382	8.341	16.681	43	15	0.569	1.224
0.5	0.25	3	150	6.700	1.245	5.382	8.341	16.681	43	16	0.572	1.224
0.5	0.25	3	150	6.700	1.245	5.382	8.341	16.681	43	17	0.725	1.224
0.5	0.25	3	150	6.700	1.245	5.382	8.341	16.681	43	18	0.840	1.224
0.5	0.25	3	150	6.700	1.245	5.382	8.341	16.681	43	19	1.096	1.224
0.5	0.25	3	150	6.700	1.245	5.382	8.341	16.681	43	20	1.530	1.224
0.5	0.25	3	200	6.700	1.205	5.558	8.076	16.152	43	10	0.966	1.302
0.5	0.25	3	200	6.700	1.205	5.558	8.076	16.152	43	11	0.890	1.302
0.5	0.25	3	200	6.700	1.205	5.558	8.076	16.152	43	12	0.818	1.302
0.5	0.25	3	200	6.700	1.205	5.558	8.076	16.152	43	13	0.738	1.302
0.5	0.25	3	200	6.700	1.205	5.558	8.076	16.152	43	14	0.660	1.302
0.5	0.25	3	200	6.700	1.205	5.558	8.076	16.152	43	15	0.614	1.302
0.5	0.25	3	200	6.700	1.205	5.558	8.076	16.152	43	16	0.671	1.302
0.5	0.25	3	200	6.700	1.205	5.558	8.076	16.152	43	17	0.732	1.302
0.5	0.25	3	200	6.700	1.205	5.558	8.076	16.152	43	18	1.014	1.302
0.5	0.25	3	200	6.700	1.205	5.558	8.076	16.152	43	19	1.400	1.302
0.5	0.25	3	200	6.700	1.205	5.558	8.076	16.152	43	20	1.996	1.302
0.5	0.25	3	35	7.821	1.582	4.943	12.373	24.747	64	5	0.876	0.770
0.5	0.25	3	35	7.821	1.582	4.943	12.373	24.747	64	6	0.883	0.770
0.5	0.25	3	35	7.821	1.582	4.943	12.373	24.747	64	7	0.891	0.770
0.5	0.25	3	35	7.821	1.582	4.943	12.373	24.747	64	8	0.916	0.770
0.5	0.25	3	35	7.821	1.582	4.943	12.373	24.747	64	9	0.889	0.770
0.5	0.25	3	35	7.821	1.582	4.943	12.373	24.747	64	10	0.913	0.770
0.5	0.25	3	35	7.821	1.582	4.943	12.373	24.747	64	11	0.892	0.770
0.5	0.25	3	35	7.821	1.582	4.943	12.373	24.747	64	12	0.886	0.770
0.5	0.25	3	35	7.821	1.582	4.943	12.373	24.747	64	13	0.881	0.770
0.5	0.25	3	35	7.821	1.582	4.943	12.373	24.747	64	14	0.882	0.770
0.5	0.25	3	35	7.821	1.582	4.943	12.373	24.747	64	15	0.801	0.770
0.5	0.25	3	35	7.821	1.582	4.943	12.373	24.747	64	16	0.806	0.770

0.5	0.25	3	35	7.821	1.582	4.943	12.373	24.747	64	17	0.768	0.770
0.5	0.25	3	35	7.821	1.582	4.943	12.373	24.747	64	18	0.720	0.770
0.5	0.25	3	35	7.821	1.582	4.943	12.373	24.747	64	19	0.640	0.770
0.5	0.25	3	35	7.821	1.582	4.943	12.373	24.747	64	20	0.646	0.770
0.5	0.25	3	35	7.821	1.582	4.943	12.373	24.747	64	21	0.485	0.770
0.5	0.25	3	35	7.821	1.582	4.943	12.373	24.747	64	22	0.418	0.770
0.5	0.25	3	35	7.821	1.582	4.943	12.373	24.747	64	23	0.446	0.770
0.5	0.25	3	35	7.821	1.582	4.943	12.373	24.747	64	24	0.455	0.770
0.5	0.25	3	35	7.821	1.582	4.943	12.373	24.747	64	25	0.555	0.770
0.5	0.25	3	35	7.821	1.582	4.943	12.373	24.747	64	26	0.670	0.770
0.5	0.25	3	35	7.821	1.582	4.943	12.373	24.747	64	27	0.833	0.770
0.5	0.25	3	35	7.821	1.582	4.943	12.373	24.747	64	28	1.114	0.770
0.5	0.25	3	35	7.821	1.582	4.943	12.373	24.747	64	29	1.439	0.770
0.5	0.25	3	35	7.821	1.582	4.943	12.373	24.747	64	30	1.888	0.770
0.5	0.25	3	50	7.771	1.553	5.003	12.069	24.139	62	15	0.853	0.324
0.5	0.25	3	50	7.771	1.553	5.003	12.069	24.139	62	16	0.808	0.324
0.5	0.25	3	50	7.771	1.553	5.003	12.069	24.139	62	17	0.750	0.324
0.5	0.25	3	50	7.771	1.553	5.003	12.069	24.139	62	18	0.704	0.324
0.5	0.25	3	50	7.771	1.553	5.003	12.069	24.139	62	19	0.678	0.324
0.5	0.25	3	50	7.771	1.553	5.003	12.069	24.139	62	20	0.582	0.324
0.5	0.25	3	50	7.771	1.553	5.003	12.069	24.139	62	21	0.428	0.324
0.5	0.25	3	50	7.771	1.553	5.003	12.069	24.139	62	22	0.426	0.324
0.5	0.25	3	50	7.771	1.553	5.003	12.069	24.139	62	23	0.431	0.324
0.5	0.25	3	50	7.771	1.553	5.003	12.069	24.139	62	24	0.488	0.324
0.5	0.25	3	50	7.771	1.553	5.003	12.069	24.139	62	25	0.600	0.324
0.5	0.25	3	50	7.771	1.553	5.003	12.069	24.139	62	26	0.786	0.324
0.5	0.25	3	50	7.771	1.553	5.003	12.069	24.139	62	27	1.011	0.324
0.5	0.25	3	50	7.771	1.553	5.003	12.069	24.139	62	28	1.236	0.324
0.5	0.25	3	50	7.771	1.553	5.003	12.069	24.139	62	29	1.746	0.324
0.5	0.25	3	100	7.789	1.498	5.199	11.668	23.335	60	13	0.868	0.936
0.5	0.25	3	100	7.789	1.498	5.199	11.668	23.335	60	14	0.890	0.936
0.5	0.25	3	100	7.789	1.498	5.199	11.668	23.335	60	15	0.809	0.936
0.5	0.25	3	100	7.789	1.498	5.199	11.668	23.335	60	16	0.773	0.936
0.5	0.25	3	100	7.789	1.498	5.199	11.668	23.335	60	17	0.682	0.936
0.5	0.25	3	100	7.789	1.498	5.199	11.668	23.335	60	18	0.659	0.936
0.5	0.25	3	100	7.789	1.498	5.199	11.668	23.335	60	19	0.633	0.936
0.5	0.25	3	100	7.789	1.498	5.199	11.668	23.335	60	20	0.534	0.936
0.5	0.25	3	100	7.789	1.498	5.199	11.668	23.335	60	21	0.397	0.936
0.5	0.25	3	100	7.789	1.498	5.199	11.668	23.335	60	22	0.484	0.936
0.5	0.25	3	100	7.789	1.498	5.199	11.668	23.335	60	23	0.577	0.936
0.5	0.25	3	100	7.789	1.498	5.199	11.668	23.335	60	24	0.711	0.936
0.5	0.25	3	100	7.789	1.498	5.199	11.668	23.335	60	25	0.872	0.936
0.5	0.25	3	100	7.789	1.498	5.199	11.668	23.335	60	26	1.158	0.936
0.5	0.25	3	100	7.789	1.498	5.199	11.668	23.335	60	27	1.443	0.936
0.5	0.25	3	100	7.789	1.498	5.199	11.668	23.335	60	28	1.913	0.936
0.5	0.25	3	150	7.789	1.447	5.384	11.269	22.539	57	14	0.877	1.053
0.5	0.25	3	150	7.789	1.447	5.384	11.269	22.539	57	15	0.763	1.053
0.5	0.25	3	150	7.789	1.447	5.384	11.269	22.539	57	16	0.759	1.053
0.5	0.25	3	150	7.789	1.447	5.384	11.269	22.539	57	17	0.691	1.053
0.5	0.25	3	150	7.789	1.447	5.384	11.269	22.539	57	18	0.667	1.053
0.5	0.25	3	150	7.789	1.447	5.384	11.269	22.539	57	19	0.579	1.053
0.5	0.25	3	150	7.789	1.447	5.384	11.269	22.539	57	20	0.561	1.053
0.5	0.25	3	150	7.789	1.447	5.384	11.269	22.539	57	21	0.486	1.053
0.5	0.25	3	150	7.789	1.447	5.384	11.269	22.539	57	22	0.630	1.053
0.5	0.25	3	150	7.789	1.447	5.384	11.269	22.539	57	23	0.704	1.053
0.5	0.25	3	150	7.789	1.447	5.384	11.269	22.539	57	24	0.875	1.053

0.5	0.25	3	150	7.789	1.447	5.384	11.269	22.539	57	25	1.173	1.053
0.5	0.25	3	150	7.789	1.447	5.384	11.269	22.539	57	26	1.471	1.053
0.5	0.25	3	200	7.791	1.402	5.559	10.920	21.841	55	13	0.900	1.471
0.5	0.25	3	200	7.791	1.402	5.559	10.920	21.841	55	14	0.867	1.471
0.5	0.25	3	200	7.791	1.402	5.559	10.920	21.841	55	15	0.817	1.471
0.5	0.25	3	200	7.791	1.402	5.559	10.920	21.841	55	16	0.747	1.471
0.5	0.25	3	200	7.791	1.402	5.559	10.920	21.841	55	17	0.709	1.471
0.5	0.25	3	200	7.791	1.402	5.559	10.920	21.841	55	18	0.624	1.471
0.5	0.25	3	200	7.791	1.402	5.559	10.920	21.841	55	19	0.616	1.471
0.5	0.25	3	200	7.791	1.402	5.559	10.920	21.841	55	20	0.607	1.471
0.5	0.25	3	200	7.791	1.402	5.559	10.920	21.841	55	21	0.643	1.471
0.5	0.25	3	200	7.791	1.402	5.559	10.920	21.841	55	22	0.771	1.471
0.5	0.25	3	200	7.791	1.402	5.559	10.920	21.841	55	23	1.179	1.471
0.5	0.25	3	200	7.791	1.402	5.559	10.920	21.841	55	24	1.242	1.471
0.5	0.25	3	200	7.791	1.402	5.559	10.920	21.841	55	25	1.554	1.471
0.5	0.25	3	35	8.626	1.744	4.945	15.047	30.095	77	5	1.010	0.778
0.5	0.25	3	35	8.626	1.744	4.945	15.047	30.095	77	6	0.963	0.778
0.5	0.25	3	35	8.626	1.744	4.945	15.047	30.095	77	7	0.919	0.778
0.5	0.25	3	35	8.626	1.744	4.945	15.047	30.095	77	8	0.950	0.778
0.5	0.25	3	35	8.626	1.744	4.945	15.047	30.095	77	9	0.977	0.778
0.5	0.25	3	35	8.626	1.744	4.945	15.047	30.095	77	10	0.965	0.778
0.5	0.25	3	35	8.626	1.744	4.945	15.047	30.095	77	11	1.002	0.778
0.5	0.25	3	35	8.626	1.744	4.945	15.047	30.095	77	12	0.958	0.778
0.5	0.25	3	35	8.626	1.744	4.945	15.047	30.095	77	13	0.931	0.778
0.5	0.25	3	35	8.626	1.744	4.945	15.047	30.095	77	14	0.941	0.778
0.5	0.25	3	35	8.626	1.744	4.945	15.047	30.095	77	15	0.842	0.778
0.5	0.25	3	35	8.626	1.744	4.945	15.047	30.095	77	16	0.907	0.778
0.5	0.25	3	35	8.626	1.744	4.945	15.047	30.095	77	17	0.923	0.778
0.5	0.25	3	35	8.626	1.744	4.945	15.047	30.095	77	18	0.872	0.778
0.5	0.25	3	35	8.626	1.744	4.945	15.047	30.095	77	19	0.920	0.778
0.5	0.25	3	35	8.626	1.744	4.945	15.047	30.095	77	20	0.868	0.778
0.5	0.25	3	35	8.626	1.744	4.945	15.047	30.095	77	21	0.742	0.778
0.5	0.25	3	35	8.626	1.744	4.945	15.047	30.095	77	22	0.702	0.778
0.5	0.25	3	35	8.626	1.744	4.945	15.047	30.095	77	23	0.656	0.778
0.5	0.25	3	35	8.626	1.744	4.945	15.047	30.095	77	24	0.572	0.778
0.5	0.25	3	35	8.626	1.744	4.945	15.047	30.095	77	25	0.528	0.778
0.5	0.25	3	35	8.626	1.744	4.945	15.047	30.095	77	26	0.459	0.778
0.5	0.25	3	35	8.626	1.744	4.945	15.047	30.095	77	27	0.473	0.778
0.5	0.25	3	35	8.626	1.744	4.945	15.047	30.095	77	28	0.394	0.778
0.5	0.25	3	35	8.626	1.744	4.945	15.047	30.095	77	29	0.417	0.778
0.5	0.25	3	35	8.626	1.744	4.945	15.047	30.095	77	30	0.418	0.778
0.5	0.25	3	35	8.626	1.744	4.945	15.047	30.095	77	31	0.636	0.778
0.5	0.25	3	35	8.626	1.744	4.945	15.047	30.095	77	32	0.830	0.778
0.5	0.25	3	35	8.626	1.744	4.945	15.047	30.095	77	33	0.986	0.778
0.5	0.25	3	35	8.626	1.744	4.945	15.047	30.095	77	34	1.118	0.778
0.5	0.25	3	35	8.626	1.744	4.945	15.047	30.095	77	35	1.468	0.778
0.5	0.25	3	35	8.626	1.744	4.945	15.047	30.095	77	36	2.025	0.778
0.5	0.25	3	50	8.636	1.725	5.006	14.901	29.802	76	18	0.913	1.204
0.5	0.25	3	50	8.636	1.725	5.006	14.901	29.802	76	19	0.865	1.204
0.5	0.25	3	50	8.636	1.725	5.006	14.901	29.802	76	20	0.869	1.204
0.5	0.25	3	50	8.636	1.725	5.006	14.901	29.802	76	21	0.868	1.204
0.5	0.25	3	50	8.636	1.725	5.006	14.901	29.802	76	22	0.638	1.204
0.5	0.25	3	50	8.636	1.725	5.006	14.901	29.802	76	23	0.592	1.204
0.5	0.25	3	50	8.636	1.725	5.006	14.901	29.802	76	24	0.537	1.204
0.5	0.25	3	50	8.636	1.725	5.006	14.901	29.802	76	25	0.486	1.204
0.5	0.25	3	50	8.636	1.725	5.006	14.901	29.802	76	26	0.410	1.204

0.5	0.25	3	50	8.636	1.725	5.006	14.901	29.802	76	27	0.443	1.204
0.5	0.25	3	50	8.636	1.725	5.006	14.901	29.802	76	28	0.356	1.204
0.5	0.25	3	50	8.636	1.725	5.006	14.901	29.802	76	29	0.452	1.204
0.5	0.25	3	50	8.636	1.725	5.006	14.901	29.802	76	30	0.526	1.204
0.5	0.25	3	50	8.636	1.725	5.006	14.901	29.802	76	31	0.704	1.204
0.5	0.25	3	50	8.636	1.725	5.006	14.901	29.802	76	32	0.875	1.204
0.5	0.25	3	50	8.636	1.725	5.006	14.901	29.802	76	33	1.154	1.204
0.5	0.25	3	50	8.636	1.725	5.006	14.901	29.802	76	34	1.534	1.204
0.5	0.25	3	100	8.637	1.661	5.200	14.344	28.688	73	19	0.804	0.926
0.5	0.25	3	100	8.637	1.661	5.200	14.344	28.688	73	20	0.848	0.926
0.5	0.25	3	100	8.637	1.661	5.200	14.344	28.688	73	21	0.667	0.926
0.5	0.25	3	100	8.637	1.661	5.200	14.344	28.688	73	22	0.667	0.926
0.5	0.25	3	100	8.637	1.661	5.200	14.344	28.688	73	23	0.503	0.926
0.5	0.25	3	100	8.637	1.661	5.200	14.344	28.688	73	24	0.504	0.926
0.5	0.25	3	100	8.637	1.661	5.200	14.344	28.688	73	25	0.461	0.926
0.5	0.25	3	100	8.637	1.661	5.200	14.344	28.688	73	26	0.486	0.926
0.5	0.25	3	100	8.637	1.661	5.200	14.344	28.688	73	27	0.476	0.926
0.5	0.25	3	100	8.637	1.661	5.200	14.344	28.688	73	28	0.542	0.926
0.5	0.25	3	100	8.637	1.661	5.200	14.344	28.688	73	29	0.675	0.926
0.5	0.25	3	100	8.637	1.661	5.200	14.344	28.688	73	30	0.738	0.926
0.5	0.25	3	100	8.637	1.661	5.200	14.344	28.688	73	31	0.975	0.926
0.5	0.25	3	100	8.637	1.661	5.200	14.344	28.688	73	32	1.353	0.926
0.5	0.25	3	100	8.637	1.661	5.200	14.344	28.688	73	33	1.671	0.926
0.5	0.25	3	150	8.640	1.604	5.385	13.862	27.723	70	18	0.826	0.453
0.5	0.25	3	150	8.640	1.604	5.385	13.862	27.723	70	19	0.798	0.453
0.5	0.25	3	150	8.640	1.604	5.385	13.862	27.723	70	20	0.775	0.453
0.5	0.25	3	150	8.640	1.604	5.385	13.862	27.723	70	21	0.660	0.453
0.5	0.25	3	150	8.640	1.604	5.385	13.862	27.723	70	22	0.596	0.453
0.5	0.25	3	150	8.640	1.604	5.385	13.862	27.723	70	23	0.502	0.453
0.5	0.25	3	150	8.640	1.604	5.385	13.862	27.723	70	24	0.496	0.453
0.5	0.25	3	150	8.640	1.604	5.385	13.862	27.723	70	25	0.484	0.453
0.5	0.25	3	150	8.640	1.604	5.385	13.862	27.723	70	26	0.538	0.453
0.5	0.25	3	150	8.640	1.604	5.385	13.862	27.723	70	27	0.633	0.453
0.5	0.25	3	150	8.640	1.604	5.385	13.862	27.723	70	28	0.725	0.453
0.5	0.25	3	150	8.640	1.604	5.385	13.862	27.723	70	29	0.844	0.453
0.5	0.25	3	150	8.640	1.604	5.385	13.862	27.723	70	30	1.034	0.453
0.5	0.25	3	150	8.640	1.604	5.385	13.862	27.723	70	31	1.418	0.453
0.5	0.25	3	150	8.640	1.604	5.385	13.862	27.723	70	32	1.923	0.453
0.5	0.25	3	200	8.638	1.554	5.560	13.420	26.840	#N/A	18	0.825	1.144
0.5	0.25	3	200	8.638	1.554	5.560	13.420	26.840	#N/A	19	0.821	1.144
0.5	0.25	3	200	8.638	1.554	5.560	13.420	26.840	#N/A	20	0.661	1.144
0.5	0.25	3	200	8.638	1.554	5.560	13.420	26.840	#N/A	21	0.599	1.144
0.5	0.25	3	200	8.638	1.554	5.560	13.420	26.840	#N/A	22	0.540	1.144
0.5	0.25	3	200	8.638	1.554	5.560	13.420	26.840	#N/A	23	0.471	1.144
0.5	0.25	3	200	8.638	1.554	5.560	13.420	26.840	#N/A	24	0.513	1.144
0.5	0.25	3	200	8.638	1.554	5.560	13.420	26.840	#N/A	25	0.584	1.144
0.5	0.25	3	200	8.638	1.554	5.560	13.420	26.840	#N/A	26	0.597	1.144
0.5	0.25	3	200	8.638	1.554	5.560	13.420	26.840	#N/A	27	0.811	1.144
0.5	0.25	3	200	8.638	1.554	5.560	13.420	26.840	#N/A	28	0.902	1.144
0.5	0.25	3	200	8.638	1.554	5.560	13.420	26.840	#N/A	29	1.185	1.144
0.5	0.25	3	200	8.638	1.554	5.560	13.420	26.840	#N/A	30	1.458	1.144
0.5	0.25	3	35	9.727	1.967	4.946	19.129	38.258	100	5	1.678	0.742
0.5	0.25	3	35	9.727	1.967	4.946	19.129	38.258	100	6	1.227	0.742
0.5	0.25	3	35	9.727	1.967	4.946	19.129	38.258	100	7	0.955	0.742
0.5	0.25	3	35	9.727	1.967	4.946	19.129	38.258	100	8	0.940	0.742
0.5	0.25	3	35	9.727	1.967	4.946	19.129	38.258	100	9	0.916	0.742

0.5	0.25	3	35	9.727	1.967	4.946	19.129	38.258	100	10	0.953	0.742
0.5	0.25	3	35	9.727	1.967	4.946	19.129	38.258	100	11	0.921	0.742
0.5	0.25	3	35	9.727	1.967	4.946	19.129	38.258	100	12	0.963	0.742
0.5	0.25	3	35	9.727	1.967	4.946	19.129	38.258	100	13	1.000	0.742
0.5	0.25	3	35	9.727	1.967	4.946	19.129	38.258	100	14	0.987	0.742
0.5	0.25	3	35	9.727	1.967	4.946	19.129	38.258	100	15	0.946	0.742
0.5	0.25	3	35	9.727	1.967	4.946	19.129	38.258	100	16	0.985	0.742
0.5	0.25	3	35	9.727	1.967	4.946	19.129	38.258	100	17	0.988	0.742
0.5	0.25	3	35	9.727	1.967	4.946	19.129	38.258	100	18	0.951	0.742
0.5	0.25	3	35	9.727	1.967	4.946	19.129	38.258	100	19	0.942	0.742
0.5	0.25	3	35	9.727	1.967	4.946	19.129	38.258	100	20	0.925	0.742
0.5	0.25	3	35	9.727	1.967	4.946	19.129	38.258	100	21	0.803	0.742
0.5	0.25	3	35	9.727	1.967	4.946	19.129	38.258	100	22	0.793	0.742
0.5	0.25	3	35	9.727	1.967	4.946	19.129	38.258	100	23	0.761	0.742
0.5	0.25	3	35	9.727	1.967	4.946	19.129	38.258	100	24	0.796	0.742
0.5	0.25	3	35	9.727	1.967	4.946	19.129	38.258	100	25	0.786	0.742
0.5	0.25	3	35	9.727	1.967	4.946	19.129	38.258	100	26	0.709	0.742
0.5	0.25	3	35	9.727	1.967	4.946	19.129	38.258	100	27	0.675	0.742
0.5	0.25	3	35	9.727	1.967	4.946	19.129	38.258	100	28	0.647	0.742
0.5	0.25	3	35	9.727	1.967	4.946	19.129	38.258	100	29	0.624	0.742
0.5	0.25	3	35	9.727	1.967	4.946	19.129	38.258	100	30	0.560	0.742
0.5	0.25	3	35	9.727	1.967	4.946	19.129	38.258	100	31	0.537	0.742
0.5	0.25	3	35	9.727	1.967	4.946	19.129	38.258	100	32	0.434	0.742
0.5	0.25	3	35	9.727	1.967	4.946	19.129	38.258	100	33	0.426	0.742
0.5	0.25	3	35	9.727	1.967	4.946	19.129	38.258	100	34	0.421	0.742
0.5	0.25	3	35	9.727	1.967	4.946	19.129	38.258	100	35	0.476	0.742
0.5	0.25	3	35	9.727	1.967	4.946	19.129	38.258	100	36	0.426	0.742
0.5	0.25	3	35	9.727	1.967	4.946	19.129	38.258	100	37	0.498	0.742
0.5	0.25	3	35	9.727	1.967	4.946	19.129	38.258	100	38	0.615	0.742
0.5	0.25	3	35	9.727	1.967	4.946	19.129	38.258	100	39	0.619	0.742
0.5	0.25	3	35	9.727	1.967	4.946	19.129	38.258	100	40	0.715	0.742
0.5	0.25	3	35	9.727	1.967	4.946	19.129	38.258	100	41	0.874	0.742
0.5	0.25	3	35	9.727	1.967	4.946	19.129	38.258	100	42	1.182	0.742
0.5	0.25	3	35	9.727	1.967	4.946	19.129	38.258	100	43	1.448	0.742
0.5	0.25	3	35	9.727	1.967	4.946	19.129	38.258	100	44	1.752	0.742
0.5	0.25	3	35	9.728	1.966	4.948	19.123	38.246	100	5	0.970	0.742
0.5	0.25	3	35	9.728	1.966	4.948	19.123	38.246	100	6	0.615	0.742
0.5	0.25	3	35	9.728	1.966	4.948	19.123	38.246	100	7	0.645	0.742
0.5	0.25	3	35	9.728	1.966	4.948	19.123	38.246	100	8	0.596	0.742
0.5	0.25	3	50	9.727	1.943	5.007	18.898	37.796	94	23	0.851	1.163
0.5	0.25	3	50	9.727	1.943	5.007	18.898	37.796	94	24	0.817	1.163
0.5	0.25	3	50	9.727	1.943	5.007	18.898	37.796	94	25	0.758	1.163
0.5	0.25	3	50	9.727	1.943	5.007	18.898	37.796	94	26	0.729	1.163
0.5	0.25	3	50	9.727	1.943	5.007	18.898	37.796	94	27	0.671	1.163
0.5	0.25	3	50	9.727	1.943	5.007	18.898	37.796	94	28	0.570	1.163
0.5	0.25	3	50	9.727	1.943	5.007	18.898	37.796	94	29	0.593	1.163
0.5	0.25	3	50	9.727	1.943	5.007	18.898	37.796	94	30	0.550	1.163
0.5	0.25	3	50	9.727	1.943	5.007	18.898	37.796	94	31	0.482	1.163
0.5	0.25	3	50	9.727	1.943	5.007	18.898	37.796	94	32	0.399	1.163
0.5	0.25	3	50	9.727	1.943	5.007	18.898	37.796	94	33	0.459	1.163
0.5	0.25	3	50	9.727	1.943	5.007	18.898	37.796	94	34	0.506	1.163
0.5	0.25	3	50	9.727	1.943	5.007	18.898	37.796	94	35	0.477	1.163
0.5	0.25	3	50	9.727	1.943	5.007	18.898	37.796	94	36	0.610	1.163
0.5	0.25	3	50	9.727	1.943	5.007	18.898	37.796	94	37	0.695	1.163
0.5	0.25	3	50	9.727	1.943	5.007	18.898	37.796	94	38	0.701	1.163
0.5	0.25	3	50	9.727	1.943	5.007	18.898	37.796	94	39	0.760	1.163

0.5	0.25	3	50	9.727	1.943	5.007	18.898	37.796	94	40	0.876	1.163
0.5	0.25	3	50	9.727	1.943	5.007	18.898	37.796	94	41	1.121	1.163
0.5	0.25	3	50	9.727	1.943	5.007	18.898	37.796	94	42	1.416	1.163
0.5	0.25	3	50	9.727	1.943	5.007	18.898	37.796	94	43	1.845	1.163
0.5	0.25	3	100	9.723	1.869	5.203	18.172	36.344	90	23	0.787	1.027
0.5	0.25	3	100	9.723	1.869	5.203	18.172	36.344	90	24	0.779	1.027
0.5	0.25	3	100	9.723	1.869	5.203	18.172	36.344	90	25	0.753	1.027
0.5	0.25	3	100	9.723	1.869	5.203	18.172	36.344	90	26	0.693	1.027
0.5	0.25	3	100	9.723	1.869	5.203	18.172	36.344	90	27	0.658	1.027
0.5	0.25	3	100	9.723	1.869	5.203	18.172	36.344	90	28	0.564	1.027
0.5	0.25	3	100	9.723	1.869	5.203	18.172	36.344	90	29	0.537	1.027
0.5	0.25	3	100	9.723	1.869	5.203	18.172	36.344	90	30	0.435	1.027
0.5	0.25	3	100	9.723	1.869	5.203	18.172	36.344	90	31	0.444	1.027
0.5	0.25	3	100	9.723	1.869	5.203	18.172	36.344	90	32	0.360	1.027
0.5	0.25	3	100	9.723	1.869	5.203	18.172	36.344	90	33	0.477	1.027
0.5	0.25	3	100	9.723	1.869	5.203	18.172	36.344	90	34	0.555	1.027
0.5	0.25	3	100	9.723	1.869	5.203	18.172	36.344	90	35	0.606	1.027
0.5	0.25	3	100	9.723	1.869	5.203	18.172	36.344	90	36	0.620	1.027
0.5	0.25	3	100	9.723	1.869	5.203	18.172	36.344	90	37	0.795	1.027
0.5	0.25	3	100	9.723	1.869	5.203	18.172	36.344	90	38	0.924	1.027
0.5	0.25	3	100	9.723	1.869	5.203	18.172	36.344	90	39	1.182	1.027
0.5	0.25	3	100	9.723	1.869	5.203	18.172	36.344	90	40	1.429	1.027
0.5	0.25	3	150	9.731	1.806	5.387	17.578	35.157	87	20	0.869	0.840
0.5	0.25	3	150	9.731	1.806	5.387	17.578	35.157	87	21	0.826	0.840
0.5	0.25	3	150	9.731	1.806	5.387	17.578	35.157	87	22	0.852	0.840
0.5	0.25	3	150	9.731	1.806	5.387	17.578	35.157	87	23	0.726	0.840
0.5	0.25	3	150	9.731	1.806	5.387	17.578	35.157	87	24	0.705	0.840
0.5	0.25	3	150	9.731	1.806	5.387	17.578	35.157	87	25	0.707	0.840
0.5	0.25	3	150	9.731	1.806	5.387	17.578	35.157	87	26	0.606	0.840
0.5	0.25	3	150	9.731	1.806	5.387	17.578	35.157	87	27	0.622	0.840
0.5	0.25	3	150	9.731	1.806	5.387	17.578	35.157	87	28	0.539	0.840
0.5	0.25	3	150	9.731	1.806	5.387	17.578	35.157	87	29	0.497	0.840
0.5	0.25	3	150	9.731	1.806	5.387	17.578	35.157	87	30	0.458	0.840
0.5	0.25	3	150	9.731	1.806	5.387	17.578	35.157	87	31	0.455	0.840
0.5	0.25	3	150	9.731	1.806	5.387	17.578	35.157	87	32	0.439	0.840
0.5	0.25	3	150	9.731	1.806	5.387	17.578	35.157	87	33	0.522	0.840
0.5	0.25	3	150	9.731	1.806	5.387	17.578	35.157	87	34	0.578	0.840
0.5	0.25	3	150	9.731	1.806	5.387	17.578	35.157	87	35	0.639	0.840
0.5	0.25	3	150	9.731	1.806	5.387	17.578	35.157	87	36	0.854	0.840
0.5	0.25	3	150	9.731	1.806	5.387	17.578	35.157	87	37	1.007	0.840
0.5	0.25	3	150	9.731	1.806	5.387	17.578	35.157	87	38	1.659	0.840
0.5	0.25	3	150	9.731	1.806	5.387	17.578	35.157	87	39	2.009	0.840
0.5	0.25	3	200	9.737	1.750	5.562	17.043	34.085	#N/A	20	0.802	1.448
0.5	0.25	3	200	9.737	1.750	5.562	17.043	34.085	#N/A	21	0.729	1.448
0.5	0.25	3	200	9.737	1.750	5.562	17.043	34.085	#N/A	22	0.788	1.448
0.5	0.25	3	200	9.737	1.750	5.562	17.043	34.085	#N/A	23	0.723	1.448
0.5	0.25	3	200	9.737	1.750	5.562	17.043	34.085	#N/A	24	0.741	1.448
0.5	0.25	3	200	9.737	1.750	5.562	17.043	34.085	#N/A	25	0.671	1.448
0.5	0.25	3	200	9.737	1.750	5.562	17.043	34.085	#N/A	26	0.587	1.448
0.5	0.25	3	200	9.737	1.750	5.562	17.043	34.085	#N/A	27	0.569	1.448
0.5	0.25	3	200	9.737	1.750	5.562	17.043	34.085	#N/A	28	0.513	1.448
0.5	0.25	3	200	9.737	1.750	5.562	17.043	34.085	#N/A	29	0.529	1.448
0.5	0.25	3	200	9.737	1.750	5.562	17.043	34.085	#N/A	30	0.504	1.448
1	0.18	1.5	35	11.660	1.105	10.555	12.881	12.881	40	5	0.244	0.511
1	0.18	1.5	35	11.660	1.105	10.555	12.881	12.881	40	8	0.384	0.511
1	0.18	1.5	35	11.660	1.105	10.555	12.881	12.881	40	11	0.414	0.511

1	0.18	1.5	35	11.660	1.105	10.555	12.881	12.881	40	14	0.449	0.511
1	0.18	1.5	35	11.660	1.105	10.555	12.881	12.881	40	16	0.466	0.511
1	0.18	1.5	35	11.660	1.105	10.555	12.881	12.881	40	17	0.655	0.511
1	0.18	1.5	35	11.660	1.105	10.555	12.881	12.881	40	18	0.800	0.511
1	0.18	1.5	35	11.660	1.105	10.555	12.881	12.881	40	19	1.111	0.511
1	0.18	1.5	50	11.666	1.092	10.687	12.735	12.735	39	5	0.339	0.666
1	0.18	1.5	50	11.666	1.092	10.687	12.735	12.735	39	6	0.385	0.666
1	0.18	1.5	50	11.666	1.092	10.687	12.735	12.735	39	7	0.414	0.666
1	0.18	1.5	50	11.666	1.092	10.687	12.735	12.735	39	8	0.438	0.666
1	0.18	1.5	50	11.666	1.092	10.687	12.735	12.735	39	9	0.514	0.666
1	0.18	1.5	50	11.666	1.092	10.687	12.735	12.735	39	10	0.499	0.666
1	0.18	1.5	50	11.666	1.092	10.687	12.735	12.735	39	11	0.542	0.666
1	0.18	1.5	50	11.666	1.092	10.687	12.735	12.735	39	12	0.507	0.666
1	0.18	1.5	50	11.666	1.092	10.687	12.735	12.735	39	13	0.463	0.666
1	0.18	1.5	50	11.666	1.092	10.687	12.735	12.735	39	14	0.483	0.666
1	0.18	1.5	50	11.666	1.092	10.687	12.735	12.735	39	15	0.719	0.666
1	0.18	1.5	50	11.666	1.092	10.687	12.735	12.735	39	16	0.667	0.666
1	0.18	1.5	50	11.666	1.092	10.687	12.735	12.735	39	17	0.731	0.666
1	0.18	1.5	50	11.666	1.092	10.687	12.735	12.735	39	18	0.957	0.666
1	0.18	1.5	100	11.672	1.050	11.112	12.261	12.261	37	5	0.359	0.772
1	0.18	1.5	100	11.672	1.050	11.112	12.261	12.261	37	6	0.452	0.772
1	0.18	1.5	100	11.672	1.050	11.112	12.261	12.261	37	7	0.427	0.772
1	0.18	1.5	100	11.672	1.050	11.112	12.261	12.261	37	8	0.529	0.772
1	0.18	1.5	100	11.672	1.050	11.112	12.261	12.261	37	9	0.536	0.772
1	0.18	1.5	100	11.672	1.050	11.112	12.261	12.261	37	10	0.612	0.772
1	0.18	1.5	100	11.672	1.050	11.112	12.261	12.261	37	11	0.576	0.772
1	0.18	1.5	100	11.672	1.050	11.112	12.261	12.261	37	12	0.609	0.772
1	0.18	1.5	100	11.672	1.050	11.112	12.261	12.261	37	13	0.632	0.772
1	0.18	1.5	100	11.672	1.050	11.112	12.261	12.261	37	14	0.709	0.772
1	0.18	1.5	100	11.672	1.050	11.112	12.261	12.261	37	15	0.702	0.772
1	0.18	1.5	100	11.672	1.050	11.112	12.261	12.261	37	16	0.909	0.772
1	0.18	1.5	100	11.672	1.050	11.112	12.261	12.261	37	17	1.436	0.772
1	0.18	1.5	150	11.679	1.015	11.512	11.849	11.849	35	5	0.349	0.415
1	0.18	1.5	150	11.679	1.015	11.512	11.849	11.849	35	6	0.411	0.415
1	0.18	1.5	150	11.679	1.015	11.512	11.849	11.849	35	7	0.420	0.415
1	0.18	1.5	150	11.679	1.015	11.512	11.849	11.849	35	8	0.436	0.415
1	0.18	1.5	150	11.679	1.015	11.512	11.849	11.849	35	9	0.492	0.415
1	0.18	1.5	150	11.679	1.015	11.512	11.849	11.849	35	10	0.523	0.415
1	0.18	1.5	150	11.679	1.015	11.512	11.849	11.849	35	11	0.612	0.415
1	0.18	1.5	150	11.679	1.015	11.512	11.849	11.849	35	12	0.670	0.415
1	0.18	1.5	150	11.679	1.015	11.512	11.849	11.849	35	13	0.698	0.415
1	0.18	1.5	150	11.679	1.015	11.512	11.849	11.849	35	14	0.633	0.415
1	0.18	1.5	150	11.679	1.015	11.512	11.849	11.849	35	15	0.811	0.415
1	0.18	1.5	150	11.679	1.015	11.512	11.849	11.849	35	16	1.123	0.415
1	0.18	1.5	200	11.678	0.982	11.895	11.465	11.465	34	5	0.377	0.843
1	0.18	1.5	200	11.678	0.982	11.895	11.465	11.465	34	6	0.431	0.843
1	0.18	1.5	200	11.678	0.982	11.895	11.465	11.465	34	7	0.457	0.843
1	0.18	1.5	200	11.678	0.982	11.895	11.465	11.465	34	8	0.532	0.843
1	0.18	1.5	200	11.678	0.982	11.895	11.465	11.465	34	9	0.546	0.843
1	0.18	1.5	200	11.678	0.982	11.895	11.465	11.465	34	10	0.607	0.843
1	0.18	1.5	200	11.678	0.982	11.895	11.465	11.465	34	11	0.714	0.843
1	0.18	1.5	200	11.678	0.982	11.895	11.465	11.465	34	12	0.722	0.843
1	0.18	1.5	200	11.678	0.982	11.895	11.465	11.465	34	13	0.734	0.843
1	0.18	1.5	200	11.678	0.982	11.895	11.465	11.465	34	14	0.768	0.843
1	0.18	1.5	200	11.678	0.982	11.895	11.465	11.465	34	15	1.052	0.843
1	0.18	1.5	35	13.411	1.270	10.562	17.029	17.029	54	5	0.505	0.568

1	0.18	1.5	35	13.411	1.270	10.562	17.029	17.029	54	6	0.393	0.568
1	0.18	1.5	35	13.411	1.270	10.562	17.029	17.029	54	7	0.324	0.568
1	0.18	1.5	35	13.411	1.270	10.562	17.029	17.029	54	8	0.269	0.568
1	0.18	1.5	35	13.411	1.270	10.562	17.029	17.029	54	9	0.283	0.568
1	0.18	1.5	35	13.411	1.270	10.562	17.029	17.029	54	10	0.312	0.568
1	0.18	1.5	35	13.411	1.270	10.562	17.029	17.029	54	11	0.311	0.568
1	0.18	1.5	35	13.411	1.270	10.562	17.029	17.029	54	12	0.332	0.568
1	0.18	1.5	35	13.411	1.270	10.562	17.029	17.029	54	13	0.365	0.568
1	0.18	1.5	35	13.411	1.270	10.562	17.029	17.029	54	14	0.397	0.568
1	0.18	1.5	35	13.411	1.270	10.562	17.029	17.029	54	15	0.453	0.568
1	0.18	1.5	35	13.411	1.270	10.562	17.029	17.029	54	16	0.512	0.568
1	0.18	1.5	35	13.411	1.270	10.562	17.029	17.029	54	17	0.500	0.568
1	0.18	1.5	35	13.411	1.270	10.562	17.029	17.029	54	18	0.579	0.568
1	0.18	1.5	35	13.411	1.270	10.562	17.029	17.029	54	19	0.594	0.568
1	0.18	1.5	35	13.411	1.270	10.562	17.029	17.029	54	20	0.623	0.568
1	0.18	1.5	35	13.411	1.270	10.562	17.029	17.029	54	21	0.706	0.568
1	0.18	1.5	35	13.411	1.270	10.562	17.029	17.029	54	22	0.791	0.568
1	0.18	1.5	35	13.411	1.270	10.562	17.029	17.029	54	23	0.921	0.568
1	0.18	1.5	35	13.411	1.270	10.562	17.029	17.029	54	24	1.354	0.568
1	0.18	1.5	50	13.367	1.250	10.691	16.712	16.712	51	5	0.491	0.518
1	0.18	1.5	50	13.367	1.250	10.691	16.712	16.712	51	6	0.385	0.518
1	0.18	1.5	50	13.367	1.250	10.691	16.712	16.712	51	7	0.317	0.518
1	0.18	1.5	50	13.367	1.250	10.691	16.712	16.712	51	8	0.325	0.518
1	0.18	1.5	50	13.367	1.250	10.691	16.712	16.712	51	9	0.298	0.518
1	0.18	1.5	50	13.367	1.250	10.691	16.712	16.712	51	10	0.345	0.518
1	0.18	1.5	50	13.367	1.250	10.691	16.712	16.712	51	11	0.361	0.518
1	0.18	1.5	50	13.367	1.250	10.691	16.712	16.712	51	12	0.349	0.518
1	0.18	1.5	50	13.367	1.250	10.691	16.712	16.712	51	13	0.422	0.518
1	0.18	1.5	50	13.367	1.250	10.691	16.712	16.712	51	14	0.458	0.518
1	0.18	1.5	50	13.367	1.250	10.691	16.712	16.712	51	15	0.481	0.518
1	0.18	1.5	50	13.367	1.250	10.691	16.712	16.712	51	16	0.516	0.518
1	0.18	1.5	50	13.367	1.250	10.691	16.712	16.712	51	17	0.515	0.518
1	0.18	1.5	50	13.367	1.250	10.691	16.712	16.712	51	18	0.575	0.518
1	0.18	1.5	50	13.367	1.250	10.691	16.712	16.712	51	19	0.616	0.518
1	0.18	1.5	50	13.367	1.250	10.691	16.712	16.712	51	20	0.595	0.518
1	0.18	1.5	50	13.367	1.250	10.691	16.712	16.712	51	21	0.756	0.518
1	0.18	1.5	50	13.367	1.250	10.691	16.712	16.712	51	22	0.921	0.518
1	0.18	1.5	50	13.367	1.250	10.691	16.712	16.712	51	23	1.139	0.518
1	0.18	1.5	50	13.367	1.250	10.691	16.712	16.712	51	24	1.582	0.518
1	0.18	1.5	100	13.368	1.203	11.114	16.078	16.078	48	5	0.437	0.565
1	0.18	1.5	100	13.368	1.203	11.114	16.078	16.078	48	6	0.426	0.565
1	0.18	1.5	100	13.368	1.203	11.114	16.078	16.078	48	7	0.355	0.565
1	0.18	1.5	100	13.368	1.203	11.114	16.078	16.078	48	8	0.342	0.565
1	0.18	1.5	100	13.368	1.203	11.114	16.078	16.078	48	9	0.375	0.565
1	0.18	1.5	100	13.368	1.203	11.114	16.078	16.078	48	10	0.382	0.565
1	0.18	1.5	100	13.368	1.203	11.114	16.078	16.078	48	11	0.375	0.565
1	0.18	1.5	100	13.368	1.203	11.114	16.078	16.078	48	12	0.436	0.565
1	0.18	1.5	100	13.368	1.203	11.114	16.078	16.078	48	13	0.426	0.565
1	0.18	1.5	100	13.368	1.203	11.114	16.078	16.078	48	14	0.480	0.565
1	0.18	1.5	100	13.368	1.203	11.114	16.078	16.078	48	15	0.508	0.565
1	0.18	1.5	100	13.368	1.203	11.114	16.078	16.078	48	16	0.595	0.565
1	0.18	1.5	100	13.368	1.203	11.114	16.078	16.078	48	17	0.561	0.565
1	0.18	1.5	100	13.368	1.203	11.114	16.078	16.078	48	18	0.612	0.565
1	0.18	1.5	100	13.368	1.203	11.114	16.078	16.078	48	19	0.689	0.565
1	0.18	1.5	100	13.368	1.203	11.114	16.078	16.078	48	20	0.763	0.565
1	0.18	1.5	100	13.368	1.203	11.114	16.078	16.078	48	21	1.039	0.565

1	0.18	1.5	100	13.368	1.203	11.114	16.078	16.078	48	22	1.277	0.565
1	0.18	1.5	150	13.365	1.161	11.515	15.512	15.512	46	5	0.447	0.677
1	0.18	1.5	150	13.365	1.161	11.515	15.512	15.512	46	7	0.379	0.677
1	0.18	1.5	150	13.365	1.161	11.515	15.512	15.512	46	9	0.418	0.677
1	0.18	1.5	150	13.365	1.161	11.515	15.512	15.512	46	11	0.438	0.677
1	0.18	1.5	150	13.365	1.161	11.515	15.512	15.512	46	13	0.525	0.677
1	0.18	1.5	150	13.365	1.161	11.515	15.512	15.512	46	15	0.604	0.677
1	0.18	1.5	150	13.365	1.161	11.515	15.512	15.512	46	16	0.615	0.677
1	0.18	1.5	150	13.365	1.161	11.515	15.512	15.512	46	17	0.718	0.677
1	0.18	1.5	150	13.365	1.161	11.515	15.512	15.512	46	18	0.689	0.677
1	0.18	1.5	150	13.365	1.161	11.515	15.512	15.512	46	19	0.761	0.677
1	0.18	1.5	150	13.365	1.161	11.515	15.512	15.512	46	20	0.982	0.677
1	0.18	1.5	150	13.365	1.161	11.515	15.512	15.512	46	21	1.321	0.677
1	0.18	1.5	200	13.358	1.123	11.896	14.999	14.999	44	5	0.518	0.784
1	0.18	1.5	200	13.358	1.123	11.896	14.999	14.999	44	7	0.377	0.784
1	0.18	1.5	200	13.358	1.123	11.896	14.999	14.999	44	9	0.450	0.784
1	0.18	1.5	200	13.358	1.123	11.896	14.999	14.999	44	11	0.530	0.784
1	0.18	1.5	200	13.358	1.123	11.896	14.999	14.999	44	13	0.600	0.784
1	0.18	1.5	200	13.358	1.123	11.896	14.999	14.999	44	15	0.673	0.784
1	0.18	1.5	200	13.358	1.123	11.896	14.999	14.999	44	16	0.692	0.784
1	0.18	1.5	200	13.358	1.123	11.896	14.999	14.999	44	17	0.709	0.784
1	0.18	1.5	200	13.358	1.123	11.896	14.999	14.999	44	18	0.861	0.784
1	0.18	1.5	200	13.358	1.123	11.896	14.999	14.999	44	19	1.000	0.784
1	0.18	1.5	200	13.358	1.123	11.896	14.999	14.999	44	20	1.430	0.784
1	0.18	1.5	35	15.645	1.481	10.562	23.174	23.174	71	5	1.127	0.532
1	0.18	1.5	35	15.645	1.481	10.562	23.174	23.174	71	6	0.663	0.532
1	0.18	1.5	35	15.645	1.481	10.562	23.174	23.174	71	7	0.440	0.532
1	0.18	1.5	35	15.645	1.481	10.562	23.174	23.174	71	9	0.319	0.532
1	0.18	1.5	35	15.645	1.481	10.562	23.174	23.174	71	11	0.256	0.532
1	0.18	1.5	35	15.645	1.481	10.562	23.174	23.174	71	13	0.319	0.532
1	0.18	1.5	35	15.645	1.481	10.562	23.174	23.174	71	15	0.331	0.532
1	0.18	1.5	35	15.645	1.481	10.562	23.174	23.174	71	17	0.397	0.532
1	0.18	1.5	35	15.645	1.481	10.562	23.174	23.174	71	19	0.483	0.532
1	0.18	1.5	35	15.645	1.481	10.562	23.174	23.174	71	21	0.518	0.532
1	0.18	1.5	35	15.645	1.481	10.562	23.174	23.174	71	23	0.625	0.532
1	0.18	1.5	35	15.645	1.481	10.562	23.174	23.174	71	25	0.734	0.532
1	0.18	1.5	35	15.645	1.481	10.562	23.174	23.174	71	26	0.659	0.532
1	0.18	1.5	35	15.645	1.481	10.562	23.174	23.174	71	27	0.703	0.532
1	0.18	1.5	35	15.645	1.481	10.562	23.174	23.174	71	28	0.749	0.532
1	0.18	1.5	35	15.645	1.481	10.562	23.174	23.174	71	29	0.815	0.532
1	0.18	1.5	35	15.645	1.481	10.562	23.174	23.174	71	30	0.871	0.532
1	0.18	1.5	35	15.645	1.481	10.562	23.174	23.174	71	31	1.054	0.532
1	0.18	1.5	35	15.645	1.481	10.562	23.174	23.174	71	33	1.763	0.532
1	0.18	1.5	50	15.707	1.469	10.694	23.071	23.071	69	5	1.022	0.442
1	0.18	1.5	50	15.707	1.469	10.694	23.071	23.071	69	6	0.618	0.442
1	0.18	1.5	50	15.707	1.469	10.694	23.071	23.071	69	7	0.418	0.442
1	0.18	1.5	50	15.707	1.469	10.694	23.071	23.071	69	25	0.667	0.442
1	0.18	1.5	50	15.707	1.469	10.694	23.071	23.071	69	26	0.736	0.442
1	0.18	1.5	50	15.707	1.469	10.694	23.071	23.071	69	27	0.736	0.442
1	0.18	1.5	50	15.707	1.469	10.694	23.071	23.071	69	28	0.793	0.442
1	0.18	1.5	50	15.707	1.469	10.694	23.071	23.071	69	29	0.876	0.442
1	0.18	1.5	100	15.713	1.414	11.113	22.217	22.217	65	5	0.706	0.748
1	0.18	1.5	100	15.713	1.414	11.113	22.217	22.217	65	6	0.511	0.748
1	0.18	1.5	100	15.713	1.414	11.113	22.217	22.217	65	7	0.392	0.748
1	0.18	1.5	100	15.713	1.414	11.113	22.217	22.217	65	24	0.645	0.748
1	0.18	1.5	100	15.713	1.414	11.113	22.217	22.217	65	25	0.776	0.748

1	0.18	1.5	100	15.713	1.414	11.113	22.217	22.217	65	26	0.766	0.748
1	0.18	1.5	100	15.713	1.414	11.113	22.217	22.217	65	27	0.835	0.748
1	0.18	1.5	100	15.713	1.414	11.113	22.217	22.217	65	28	1.037	0.748
1	0.18	1.5	150	15.697	1.363	11.515	21.397	21.397	62	5	0.662	0.655
1	0.18	1.5	150	15.697	1.363	11.515	21.397	21.397	62	6	0.448	0.655
1	0.18	1.5	150	15.697	1.363	11.515	21.397	21.397	62	7	0.388	0.655
1	0.18	1.5	150	15.697	1.363	11.515	21.397	21.397	62	23	0.676	0.655
1	0.18	1.5	150	15.697	1.363	11.515	21.397	21.397	62	24	0.731	0.655
1	0.18	1.5	150	15.697	1.363	11.515	21.397	21.397	62	25	0.795	0.655
1	0.18	1.5	150	15.697	1.363	11.515	21.397	21.397	62	26	0.922	0.655
1	0.18	1.5	200	15.709	1.320	11.900	20.737	20.737	60	5	0.627	0.669
1	0.18	1.5	200	15.709	1.320	11.900	20.737	20.737	60	6	0.501	0.669
1	0.18	1.5	200	15.709	1.320	11.900	20.737	20.737	60	7	0.393	0.669
1	0.18	1.5	200	15.709	1.320	11.900	20.737	20.737	60	22	0.664	0.669
1	0.18	1.5	200	15.709	1.320	11.900	20.737	20.737	60	23	0.701	0.669
1	0.18	1.5	200	15.709	1.320	11.900	20.737	20.737	60	24	0.715	0.669
1	0.18	1.5	200	15.709	1.320	11.900	20.737	20.737	60	25	0.954	0.669
1	0.18	1.5	200	15.709	1.320	11.900	20.737	20.737	60	26	1.163	0.669
1	0.18	1.5	35	17.500	1.657	10.562	28.995	28.995	89	5	2.748	0.543
1	0.18	1.5	35	17.500	1.657	10.562	28.995	28.995	89	6	1.513	0.543
1	0.18	1.5	35	17.500	1.657	10.562	28.995	28.995	89	7	0.823	0.543
1	0.18	1.5	35	17.500	1.657	10.562	28.995	28.995	89	8	0.631	0.543
1	0.18	1.5	35	17.500	1.657	10.562	28.995	28.995	89	9	0.447	0.543
1	0.18	1.5	35	17.500	1.657	10.562	28.995	28.995	89	11	0.310	0.543
1	0.18	1.5	35	17.500	1.657	10.562	28.995	28.995	89	14	0.346	0.543
1	0.18	1.5	35	17.500	1.657	10.562	28.995	28.995	89	17	0.338	0.543
1	0.18	1.5	35	17.500	1.657	10.562	28.995	28.995	89	20	0.438	0.543
1	0.18	1.5	35	17.500	1.657	10.562	28.995	28.995	89	23	0.511	0.543
1	0.18	1.5	35	17.500	1.657	10.562	28.995	28.995	89	26	0.590	0.543
1	0.18	1.5	35	17.500	1.657	10.562	28.995	28.995	89	29	0.641	0.543
1	0.18	1.5	35	17.500	1.657	10.562	28.995	28.995	89	30	0.658	0.543
1	0.18	1.5	35	17.500	1.657	10.562	28.995	28.995	89	31	0.641	0.543
1	0.18	1.5	35	17.500	1.657	10.562	28.995	28.995	89	32	0.698	0.543
1	0.18	1.5	35	17.500	1.657	10.562	28.995	28.995	89	33	0.738	0.543
1	0.18	1.5	35	17.500	1.657	10.562	28.995	28.995	89	34	0.750	0.543
1	0.18	1.5	35	17.500	1.657	10.562	28.995	28.995	89	35	0.754	0.543
1	0.18	1.5	35	17.500	1.657	10.562	28.995	28.995	89	36	0.845	0.543
1	0.18	1.5	35	17.500	1.657	10.562	28.995	28.995	89	37	1.091	0.543
1	0.18	1.5	35	17.500	1.657	10.562	28.995	28.995	89	38	1.182	0.543
1	0.18	1.5	50	17.467	1.633	10.694	28.530	28.530	85	5	2.240	0.663
1	0.18	1.5	50	17.467	1.633	10.694	28.530	28.530	85	6	1.247	0.663
1	0.18	1.5	50	17.467	1.633	10.694	28.530	28.530	85	7	0.795	0.663
1	0.18	1.5	50	17.467	1.633	10.694	28.530	28.530	85	8	0.543	0.663
1	0.18	1.5	50	17.467	1.633	10.694	28.530	28.530	85	9	0.432	0.663
1	0.18	1.5	50	17.467	1.633	10.694	28.530	28.530	85	31	0.652	0.663
1	0.18	1.5	50	17.467	1.633	10.694	28.530	28.530	85	32	0.690	0.663
1	0.18	1.5	50	17.467	1.633	10.694	28.530	28.530	85	33	0.722	0.663
1	0.18	1.5	50	17.467	1.633	10.694	28.530	28.530	85	34	0.755	0.663
1	0.18	1.5	50	17.467	1.633	10.694	28.530	28.530	85	35	0.879	0.663
1	0.18	1.5	100	17.456	1.571	11.115	27.416	27.416	80	6	0.900	0.477
1	0.18	1.5	100	17.456	1.571	11.115	27.416	27.416	80	7	0.622	0.477
1	0.18	1.5	100	17.456	1.571	11.115	27.416	27.416	80	8	0.478	0.477
1	0.18	1.5	100	17.456	1.571	11.115	27.416	27.416	80	9	0.381	0.477
1	0.18	1.5	100	17.456	1.571	11.115	27.416	27.416	80	28	0.701	0.477
1	0.18	1.5	100	17.456	1.571	11.115	27.416	27.416	80	29	0.672	0.477
1	0.18	1.5	100	17.456	1.571	11.115	27.416	27.416	80	30	0.705	0.477

1	0.18	1.5	100	17.456	1.571	11.115	27.416	27.416	80	31	0.697	0.477
1	0.18	1.5	100	17.456	1.571	11.115	27.416	27.416	80	32	0.840	0.477
1	0.18	1.5	100	17.456	1.571	11.115	27.416	27.416	80	33	0.861	0.477
1	0.18	1.5	150	17.460	1.516	11.517	26.472	26.472	76	5	1.207	0.513
1	0.18	1.5	150	17.460	1.516	11.517	26.472	26.472	76	6	0.740	0.513
1	0.18	1.5	150	17.460	1.516	11.517	26.472	26.472	76	7	0.520	0.513
1	0.18	1.5	150	17.460	1.516	11.517	26.472	26.472	76	8	0.442	0.513
1	0.18	1.5	150	17.460	1.516	11.517	26.472	26.472	76	26	0.677	0.513
1	0.18	1.5	150	17.460	1.516	11.517	26.472	26.472	76	27	0.718	0.513
1	0.18	1.5	150	17.460	1.516	11.517	26.472	26.472	76	28	0.715	0.513
1	0.18	1.5	150	17.460	1.516	11.517	26.472	26.472	76	29	0.725	0.513
1	0.18	1.5	150	17.460	1.516	11.517	26.472	26.472	76	30	0.789	0.513
1	0.18	1.5	150	17.460	1.516	11.517	26.472	26.472	76	31	0.795	0.513
1	0.18	1.5	200	17.451	1.467	11.900	25.593	25.593	73	5	0.759	0.605
1	0.18	1.5	200	17.451	1.467	11.900	25.593	25.593	73	6	0.520	0.605
1	0.18	1.5	200	17.451	1.467	11.900	25.593	25.593	73	7	0.445	0.605
1	0.18	1.5	200	17.451	1.467	11.900	25.593	25.593	73	10	0.511	0.605
1	0.18	1.5	200	17.451	1.467	11.900	25.593	25.593	73	11	0.336	0.605
1	0.18	1.5	200	17.451	1.467	11.900	25.593	25.593	73	15	0.305	0.605
1	0.18	1.5	200	17.451	1.467	11.900	25.593	25.593	73	20	0.394	0.605
1	0.18	1.5	200	17.451	1.467	11.900	25.593	25.593	73	28	0.651	0.605
1	0.18	1.5	200	17.451	1.467	11.900	25.593	25.593	73	29	0.735	0.605
1	0.18	1.5	200	17.451	1.467	11.900	25.593	25.593	73	30	0.854	0.605
1	0.18	1.5	35	19.387	1.835	10.565	35.575	35.575	107	5	4.222	0.573
1	0.18	1.5	35	19.387	1.835	10.565	35.575	35.575	107	7	1.529	0.573
1	0.18	1.5	35	19.387	1.835	10.565	35.575	35.575	107	9	0.663	0.573
1	0.18	1.5	35	19.387	1.835	10.565	35.575	35.575	107	11	0.330	0.573
1	0.18	1.5	35	19.387	1.835	10.565	35.575	35.575	107	13	0.295	0.573
1	0.18	1.5	35	19.387	1.835	10.565	35.575	35.575	107	15	0.314	0.573
1	0.18	1.5	35	19.387	1.835	10.565	35.575	35.575	107	17	0.330	0.573
1	0.18	1.5	35	19.387	1.835	10.565	35.575	35.575	107	19	0.281	0.573
1	0.18	1.5	35	19.387	1.835	10.565	35.575	35.575	107	21	0.268	0.573
1	0.18	1.5	35	19.387	1.835	10.565	35.575	35.575	107	23	0.343	0.573
1	0.18	1.5	35	19.387	1.835	10.565	35.575	35.575	107	25	0.344	0.573
1	0.18	1.5	35	19.387	1.835	10.565	35.575	35.575	107	27	0.416	0.573
1	0.18	1.5	35	19.387	1.835	10.565	35.575	35.575	107	29	0.413	0.573
1	0.18	1.5	35	19.387	1.835	10.565	35.575	35.575	107	31	0.362	0.573
1	0.18	1.5	35	19.387	1.835	10.565	35.575	35.575	107	33	0.403	0.573
1	0.18	1.5	35	19.387	1.835	10.565	35.575	35.575	107	35	0.487	0.573
1	0.18	1.5	35	19.387	1.835	10.565	35.575	35.575	107	37	0.539	0.573
1	0.18	1.5	35	19.387	1.835	10.565	35.575	35.575	107	39	0.664	0.573
1	0.18	1.5	35	19.387	1.835	10.565	35.575	35.575	107	41	0.641	0.573
1	0.18	1.5	35	19.387	1.835	10.565	35.575	35.575	108	42	0.681	0.573
1	0.18	1.5	35	19.387	1.835	10.565	35.575	35.575	107	43	0.829	0.573
1	0.18	1.5	35	19.387	1.835	10.565	35.575	35.575	107	45	1.123	0.573
1	0.18	1.5	50	19.361	1.810	10.696	35.046	35.046	102	7	1.387	1.049
1	0.18	1.5	50	19.361	1.810	10.696	35.046	35.046	102	8	0.880	1.049
1	0.18	1.5	50	19.361	1.810	10.696	35.046	35.046	102	9	0.619	1.049
1	0.18	1.5	50	19.361	1.810	10.696	35.046	35.046	102	10	0.369	1.049
1	0.18	1.5	50	19.361	1.810	10.696	35.046	35.046	102	11	0.403	1.049
1	0.18	1.5	50	19.361	1.810	10.696	35.046	35.046	102	12	0.302	1.049
1	0.18	1.5	50	19.361	1.810	10.696	35.046	35.046	102	36	0.610	1.049
1	0.18	1.5	50	19.361	1.810	10.696	35.046	35.046	102	37	0.676	1.049
1	0.18	1.5	50	19.361	1.810	10.696	35.046	35.046	102	38	0.685	1.049
1	0.18	1.5	50	19.361	1.810	10.696	35.046	35.046	102	39	0.656	1.049
1	0.18	1.5	50	19.361	1.810	10.696	35.046	35.046	102	40	0.671	1.049

1	0.18	1.5	50	19.361	1.810	10.696	35.046	35.046	102	41	0.722	1.049
1	0.18	1.5	50	19.361	1.810	10.696	35.046	35.046	102	42	0.826	1.049
1	0.18	1.5	100	19.264	1.733	11.116	33.385	33.385	96	7	0.917	0.684
1	0.18	1.5	100	19.264	1.733	11.116	33.385	33.385	96	8	0.628	0.684
1	0.18	1.5	100	19.264	1.733	11.116	33.385	33.385	96	9	0.472	0.684
1	0.18	1.5	100	19.264	1.733	11.116	33.385	33.385	96	37	0.638	0.684
1	0.18	1.5	100	19.264	1.733	11.116	33.385	33.385	96	38	0.723	0.684
1	0.18	1.5	100	19.264	1.733	11.116	33.385	33.385	96	39	0.750	0.684
1	0.18	1.5	100	19.264	1.733	11.116	33.385	33.385	96	40	0.863	0.684
1	0.18	1.5	150	19.258	1.672	11.516	32.204	32.204	91	6	1.127	0.696
1	0.18	1.5	150	19.258	1.672	11.516	32.204	32.204	91	7	0.706	0.696
1	0.18	1.5	150	19.258	1.672	11.516	32.204	32.204	91	8	0.493	0.696
1	0.18	1.5	150	19.258	1.672	11.516	32.204	32.204	91	35	0.658	0.696
1	0.18	1.5	150	19.258	1.672	11.516	32.204	32.204	91	36	0.629	0.696
1	0.18	1.5	150	19.258	1.672	11.516	32.204	32.204	91	37	0.776	0.696
1	0.18	1.5	150	19.258	1.672	11.516	32.204	32.204	91	38	0.841	0.696
1	0.18	1.5	200	19.259	1.618	11.901	31.166	31.166	88	5	1.923	0.805
1	0.18	1.5	200	19.259	1.618	11.901	31.166	31.166	88	6	0.886	0.805
1	0.18	1.5	200	19.259	1.618	11.901	31.166	31.166	88	7	0.548	0.805
1	0.18	1.5	200	19.259	1.618	11.901	31.166	31.166	88	33	0.665	0.805
1	0.18	1.5	200	19.259	1.618	11.901	31.166	31.166	88	34	0.631	0.805
1	0.18	1.5	200	19.259	1.618	11.901	31.166	31.166	88	35	0.679	0.805
1	0.18	1.5	200	19.259	1.618	11.901	31.166	31.166	88	36	0.840	0.805
1	0.18	3	35	11.667	1.105	10.557	12.894	12.894	40	5	0.244	0.511
1	0.18	3	35	11.667	1.105	10.557	12.894	12.894	40	6	0.380	0.511
1	0.18	3	35	11.667	1.105	10.557	12.894	12.894	40	7	0.370	0.511
1	0.18	3	35	11.667	1.105	10.557	12.894	12.894	40	8	0.389	0.511
1	0.18	3	35	11.667	1.105	10.557	12.894	12.894	40	9	0.434	0.511
1	0.18	3	35	11.667	1.105	10.557	12.894	12.894	40	10	0.469	0.511
1	0.18	3	35	11.667	1.105	10.557	12.894	12.894	40	11	0.476	0.511
1	0.18	3	35	11.667	1.105	10.557	12.894	12.894	40	12	0.507	0.511
1	0.18	3	35	11.667	1.105	10.557	12.894	12.894	40	13	0.431	0.511
1	0.18	3	35	11.667	1.105	10.557	12.894	12.894	40	14	0.376	0.511
1	0.18	3	35	11.667	1.105	10.557	12.894	12.894	40	15	0.368	0.511
1	0.18	3	35	11.667	1.105	10.557	12.894	12.894	40	16	0.554	0.511
1	0.18	3	35	11.667	1.105	10.557	12.894	12.894	40	17	0.678	0.511
1	0.18	3	35	11.667	1.105	10.557	12.894	12.894	40	18	0.836	0.511
1	0.18	3	35	11.667	1.105	10.557	12.894	12.894	40	19	1.107	0.511
1	0.18	3	50	11.667	1.092	10.686	12.738	12.738	39	5	0.276	0.666
1	0.18	3	50	11.667	1.092	10.686	12.738	12.738	39	6	0.394	0.666
1	0.18	3	50	11.667	1.092	10.686	12.738	12.738	39	7	0.393	0.666
1	0.18	3	50	11.667	1.092	10.686	12.738	12.738	39	8	0.470	0.666
1	0.18	3	50	11.667	1.092	10.686	12.738	12.738	39	9	0.466	0.666
1	0.18	3	50	11.667	1.092	10.686	12.738	12.738	39	10	0.491	0.666
1	0.18	3	50	11.667	1.092	10.686	12.738	12.738	39	11	0.556	0.666
1	0.18	3	50	11.667	1.092	10.686	12.738	12.738	39	12	0.547	0.666
1	0.18	3	50	11.667	1.092	10.686	12.738	12.738	39	13	0.523	0.666
1	0.18	3	50	11.667	1.092	10.686	12.738	12.738	39	14	0.517	0.666
1	0.18	3	50	11.667	1.092	10.686	12.738	12.738	39	15	0.666	0.666
1	0.18	3	50	11.667	1.092	10.686	12.738	12.738	39	16	0.687	0.666
1	0.18	3	50	11.667	1.092	10.686	12.738	12.738	39	17	0.729	0.666
1	0.18	3	50	11.667	1.092	10.686	12.738	12.738	39	18	1.348	0.666
1	0.18	3	100	11.674	1.051	11.108	12.267	12.267	37	5	0.342	0.772
1	0.18	3	100	11.674	1.051	11.108	12.267	12.267	37	6	0.486	0.772
1	0.18	3	100	11.674	1.051	11.108	12.267	12.267	37	7	0.485	0.772
1	0.18	3	100	11.674	1.051	11.108	12.267	12.267	37	8	0.504	0.772

1	0.18	3	100	11.674	1.051	11.108	12.267	12.267	37	9	0.523	0.772
1	0.18	3	100	11.674	1.051	11.108	12.267	12.267	37	10	0.588	0.772
1	0.18	3	100	11.674	1.051	11.108	12.267	12.267	37	11	0.673	0.772
1	0.18	3	100	11.674	1.051	11.108	12.267	12.267	37	12	0.601	0.772
1	0.18	3	100	11.674	1.051	11.108	12.267	12.267	37	13	0.606	0.772
1	0.18	3	100	11.674	1.051	11.108	12.267	12.267	37	14	0.661	0.772
1	0.18	3	100	11.674	1.051	11.108	12.267	12.267	37	15	0.669	0.772
1	0.18	3	100	11.674	1.051	11.108	12.267	12.267	37	16	0.830	0.772
1	0.18	3	100	11.674	1.051	11.108	12.267	12.267	37	17	1.480	0.772
1	0.18	3	150	11.679	1.014	11.514	11.846	11.846	35	5	0.373	0.415
1	0.18	3	150	11.679	1.014	11.514	11.846	11.846	35	6	0.395	0.415
1	0.18	3	150	11.679	1.014	11.514	11.846	11.846	35	7	0.428	0.415
1	0.18	3	150	11.679	1.014	11.514	11.846	11.846	35	8	0.444	0.415
1	0.18	3	150	11.679	1.014	11.514	11.846	11.846	35	9	0.535	0.415
1	0.18	3	150	11.679	1.014	11.514	11.846	11.846	35	10	0.555	0.415
1	0.18	3	150	11.679	1.014	11.514	11.846	11.846	35	11	0.581	0.415
1	0.18	3	150	11.679	1.014	11.514	11.846	11.846	35	12	0.657	0.415
1	0.18	3	150	11.679	1.014	11.514	11.846	11.846	35	13	0.691	0.415
1	0.18	3	150	11.679	1.014	11.514	11.846	11.846	35	14	0.646	0.415
1	0.18	3	150	11.679	1.014	11.514	11.846	11.846	35	15	0.831	0.415
1	0.18	3	200	11.678	0.982	11.898	11.463	11.463	34	5	0.438	0.843
1	0.18	3	200	11.678	0.982	11.898	11.463	11.463	34	6	0.469	0.843
1	0.18	3	200	11.678	0.982	11.898	11.463	11.463	34	7	0.511	0.843
1	0.18	3	200	11.678	0.982	11.898	11.463	11.463	34	8	0.525	0.843
1	0.18	3	200	11.678	0.982	11.898	11.463	11.463	34	9	0.555	0.843
1	0.18	3	200	11.678	0.982	11.898	11.463	11.463	34	10	0.629	0.843
1	0.18	3	200	11.678	0.982	11.898	11.463	11.463	34	11	0.660	0.843
1	0.18	3	200	11.678	0.982	11.898	11.463	11.463	34	12	0.675	0.843
1	0.18	3	200	11.678	0.982	11.898	11.463	11.463	34	13	0.694	0.843
1	0.18	3	200	11.678	0.982	11.898	11.463	11.463	34	14	0.788	0.843
1	0.18	3	200	11.678	0.982	11.898	11.463	11.463	34	15	0.984	0.843
1	0.18	3	35	13.377	1.267	10.560	16.947	16.947	53	5	0.465	0.568
1	0.18	3	35	13.377	1.267	10.560	16.947	16.947	53	6	0.347	0.568
1	0.18	3	35	13.377	1.267	10.560	16.947	16.947	53	7	0.297	0.568
1	0.18	3	35	13.377	1.267	10.560	16.947	16.947	53	8	0.309	0.568
1	0.18	3	35	13.377	1.267	10.560	16.947	16.947	53	9	0.302	0.568
1	0.18	3	35	13.377	1.267	10.560	16.947	16.947	53	10	0.315	0.568
1	0.18	3	35	13.377	1.267	10.560	16.947	16.947	53	11	0.304	0.568
1	0.18	3	35	13.377	1.267	10.560	16.947	16.947	53	12	0.364	0.568
1	0.18	3	35	13.377	1.267	10.560	16.947	16.947	53	13	0.412	0.568
1	0.18	3	35	13.377	1.267	10.560	16.947	16.947	53	14	0.431	0.568
1	0.18	3	35	13.377	1.267	10.560	16.947	16.947	53	15	0.449	0.568
1	0.18	3	35	13.377	1.267	10.560	16.947	16.947	53	16	0.509	0.568
1	0.18	3	35	13.377	1.267	10.560	16.947	16.947	53	17	0.548	0.568
1	0.18	3	35	13.377	1.267	10.560	16.947	16.947	53	18	0.546	0.568
1	0.18	3	35	13.377	1.267	10.560	16.947	16.947	53	19	0.589	0.568
1	0.18	3	35	13.377	1.267	10.560	16.947	16.947	53	20	0.635	0.568
1	0.18	3	35	13.377	1.267	10.560	16.947	16.947	53	21	0.684	0.568
1	0.18	3	35	13.377	1.267	10.560	16.947	16.947	53	22	0.847	0.568
1	0.18	3	35	13.377	1.267	10.560	16.947	16.947	53	23	0.968	0.568
1	0.18	3	35	13.377	1.267	10.560	16.947	16.947	53	24	1.338	0.568
1	0.18	3	50	13.357	1.249	10.693	16.686	16.686	51	5	0.469	0.518
1	0.18	3	50	13.357	1.249	10.693	16.686	16.686	51	6	0.351	0.518
1	0.18	3	50	13.357	1.249	10.693	16.686	16.686	51	7	0.312	0.518
1	0.18	3	50	13.357	1.249	10.693	16.686	16.686	51	8	0.313	0.518
1	0.18	3	50	13.357	1.249	10.693	16.686	16.686	51	9	0.335	0.518

1	0.18	3	50	13.357	1.249	10.693	16.686	16.686	51	10	0.356	0.518
1	0.18	3	50	13.357	1.249	10.693	16.686	16.686	51	11	0.351	0.518
1	0.18	3	50	13.357	1.249	10.693	16.686	16.686	51	12	0.336	0.518
1	0.18	3	50	13.357	1.249	10.693	16.686	16.686	51	13	0.420	0.518
1	0.18	3	50	13.357	1.249	10.693	16.686	16.686	51	14	0.454	0.518
1	0.18	3	50	13.357	1.249	10.693	16.686	16.686	51	15	0.460	0.518
1	0.18	3	50	13.357	1.249	10.693	16.686	16.686	51	16	0.473	0.518
1	0.18	3	50	13.357	1.249	10.693	16.686	16.686	51	17	0.529	0.518
1	0.18	3	50	13.357	1.249	10.693	16.686	16.686	51	18	0.644	0.518
1	0.18	3	50	13.357	1.249	10.693	16.686	16.686	51	19	0.629	0.518
1	0.18	3	50	13.357	1.249	10.693	16.686	16.686	51	20	0.681	0.518
1	0.18	3	50	13.357	1.249	10.693	16.686	16.686	51	21	0.690	0.518
1	0.18	3	50	13.357	1.249	10.693	16.686	16.686	51	22	0.836	0.518
1	0.18	3	50	13.357	1.249	10.693	16.686	16.686	51	23	1.257	0.518
1	0.18	3	50	13.357	1.249	10.693	16.686	16.686	51	24	1.611	0.518
1	0.18	3	100	13.369	1.203	11.114	16.082	16.082	48	5	0.420	0.565
1	0.18	3	100	13.369	1.203	11.114	16.082	16.082	48	6	0.387	0.565
1	0.18	3	100	13.369	1.203	11.114	16.082	16.082	48	7	0.309	0.565
1	0.18	3	100	13.369	1.203	11.114	16.082	16.082	48	8	0.341	0.565
1	0.18	3	100	13.369	1.203	11.114	16.082	16.082	48	9	0.367	0.565
1	0.18	3	100	13.369	1.203	11.114	16.082	16.082	48	10	0.416	0.565
1	0.18	3	100	13.369	1.203	11.114	16.082	16.082	48	11	0.385	0.565
1	0.18	3	100	13.369	1.203	11.114	16.082	16.082	48	12	0.423	0.565
1	0.18	3	100	13.369	1.203	11.114	16.082	16.082	48	13	0.482	0.565
1	0.18	3	100	13.369	1.203	11.114	16.082	16.082	48	14	0.482	0.565
1	0.18	3	100	13.369	1.203	11.114	16.082	16.082	48	15	0.534	0.565
1	0.18	3	100	13.369	1.203	11.114	16.082	16.082	48	16	0.582	0.565
1	0.18	3	100	13.369	1.203	11.114	16.082	16.082	48	17	0.674	0.565
1	0.18	3	100	13.369	1.203	11.114	16.082	16.082	48	18	0.664	0.565
1	0.18	3	100	13.369	1.203	11.114	16.082	16.082	48	19	0.632	0.565
1	0.18	3	100	13.369	1.203	11.114	16.082	16.082	48	20	0.770	0.565
1	0.18	3	100	13.369	1.203	11.114	16.082	16.082	48	21	1.038	0.565
1	0.18	3	100	13.369	1.203	11.114	16.082	16.082	48	22	1.327	0.565
1	0.18	3	150	13.357	1.160	11.516	15.493	15.493	46	5	0.425	0.677
1	0.18	3	150	13.357	1.160	11.516	15.493	15.493	46	7	0.374	0.677
1	0.18	3	150	13.357	1.160	11.516	15.493	15.493	46	9	0.404	0.677
1	0.18	3	150	13.357	1.160	11.516	15.493	15.493	46	11	0.461	0.677
1	0.18	3	150	13.357	1.160	11.516	15.493	15.493	46	13	0.534	0.677
1	0.18	3	150	13.357	1.160	11.516	15.493	15.493	46	15	0.641	0.677
1	0.18	3	150	13.357	1.160	11.516	15.493	15.493	46	16	0.652	0.677
1	0.18	3	150	13.357	1.160	11.516	15.493	15.493	46	17	0.661	0.677
1	0.18	3	150	13.357	1.160	11.516	15.493	15.493	46	18	0.743	0.677
1	0.18	3	150	13.357	1.160	11.516	15.493	15.493	46	19	0.802	0.677
1	0.18	3	150	13.357	1.160	11.516	15.493	15.493	46	20	1.025	0.677
1	0.18	3	150	13.357	1.160	11.516	15.493	15.493	46	21	1.445	0.677
1	0.18	3	200	13.364	1.123	11.900	15.009	15.009	44	5	0.513	0.784
1	0.18	3	200	13.364	1.123	11.900	15.009	15.009	44	7	0.415	0.784
1	0.18	3	200	13.364	1.123	11.900	15.009	15.009	44	9	0.429	0.784
1	0.18	3	200	13.364	1.123	11.900	15.009	15.009	44	11	0.487	0.784
1	0.18	3	200	13.364	1.123	11.900	15.009	15.009	44	13	0.555	0.784
1	0.18	3	200	13.364	1.123	11.900	15.009	15.009	44	15	0.697	0.784
1	0.18	3	200	13.364	1.123	11.900	15.009	15.009	44	16	0.635	0.784
1	0.18	3	200	13.364	1.123	11.900	15.009	15.009	44	17	0.708	0.784
1	0.18	3	200	13.364	1.123	11.900	15.009	15.009	44	18	0.842	0.784
1	0.18	3	200	13.364	1.123	11.900	15.009	15.009	44	19	1.075	0.784
1	0.18	3	200	13.364	1.123	11.900	15.009	15.009	44	20	1.409	0.784

1	0.18	3	35	15.759	1.492	10.563	23.511	23.511	72	5	1.073	0.532
1	0.18	3	35	15.759	1.492	10.563	23.511	23.511	72	6	0.685	0.532
1	0.18	3	35	15.759	1.492	10.563	23.511	23.511	72	7	0.505	0.532
1	0.18	3	35	15.759	1.492	10.563	23.511	23.511	72	9	0.285	0.532
1	0.18	3	35	15.759	1.492	10.563	23.511	23.511	72	11	0.272	0.532
1	0.18	3	35	15.759	1.492	10.563	23.511	23.511	72	13	0.286	0.532
1	0.18	3	35	15.759	1.492	10.563	23.511	23.511	72	15	0.370	0.532
1	0.18	3	35	15.759	1.492	10.563	23.511	23.511	72	17	0.434	0.532
1	0.18	3	35	15.759	1.492	10.563	23.511	23.511	72	19	0.472	0.532
1	0.18	3	35	15.759	1.492	10.563	23.511	23.511	72	21	0.500	0.532
1	0.18	3	35	15.759	1.492	10.563	23.511	23.511	72	23	0.631	0.532
1	0.18	3	35	15.759	1.492	10.563	23.511	23.511	72	25	0.695	0.532
1	0.18	3	35	15.759	1.492	10.563	23.511	23.511	72	26	0.730	0.532
1	0.18	3	35	15.759	1.492	10.563	23.511	23.511	72	27	0.690	0.532
1	0.18	3	35	15.759	1.492	10.563	23.511	23.511	72	28	0.722	0.532
1	0.18	3	35	15.759	1.492	10.563	23.511	23.511	72	29	0.836	0.532
1	0.18	3	35	15.759	1.492	10.563	23.511	23.511	72	30	0.904	0.532
1	0.18	3	35	15.759	1.492	10.563	23.511	23.511	72	31	1.039	0.532
1	0.18	3	50	15.695	1.468	10.692	23.037	23.037	69	5	1.028	0.442
1	0.18	3	50	15.695	1.468	10.692	23.037	23.037	69	6	0.595	0.442
1	0.18	3	50	15.695	1.468	10.692	23.037	23.037	69	7	0.465	0.442
1	0.18	3	50	15.695	1.468	10.692	23.037	23.037	69	26	0.691	0.442
1	0.18	3	50	15.695	1.468	10.692	23.037	23.037	69	27	0.664	0.442
1	0.18	3	50	15.695	1.468	10.692	23.037	23.037	69	28	0.708	0.442
1	0.18	3	50	15.695	1.468	10.692	23.037	23.037	69	29	0.886	0.442
1	0.18	3	50	15.695	1.468	10.692	23.037	23.037	69	30	1.009	0.442
1	0.18	3	100	15.713	1.413	11.117	22.210	22.210	65	5	0.705	0.748
1	0.18	3	100	15.713	1.413	11.117	22.210	22.210	65	6	0.486	0.748
1	0.18	3	100	15.713	1.413	11.117	22.210	22.210	65	7	0.342	0.748
1	0.18	3	100	15.713	1.413	11.117	22.210	22.210	65	23	0.711	0.748
1	0.18	3	100	15.713	1.413	11.117	22.210	22.210	65	24	0.686	0.748
1	0.18	3	100	15.713	1.413	11.117	22.210	22.210	65	25	0.719	0.748
1	0.18	3	100	15.713	1.413	11.117	22.210	22.210	65	26	0.782	0.748
1	0.18	3	100	15.713	1.413	11.117	22.210	22.210	65	28	0.878	0.748
1	0.18	3	150	15.718	1.365	11.516	21.454	21.454	62	5	0.650	0.655
1	0.18	3	150	15.718	1.365	11.516	21.454	21.454	62	6	0.480	0.655
1	0.18	3	150	15.718	1.365	11.516	21.454	21.454	62	7	0.377	0.655
1	0.18	3	150	15.718	1.365	11.516	21.454	21.454	62	23	0.693	0.655
1	0.18	3	150	15.718	1.365	11.516	21.454	21.454	62	24	0.699	0.655
1	0.18	3	150	15.718	1.365	11.516	21.454	21.454	62	25	0.809	0.655
1	0.18	3	150	15.718	1.365	11.516	21.454	21.454	62	26	0.954	0.655
1	0.18	3	200	15.687	1.318	11.899	20.681	20.681	60	5	0.618	0.669
1	0.18	3	200	15.687	1.318	11.899	20.681	20.681	60	6	0.503	0.669
1	0.18	3	200	15.687	1.318	11.899	20.681	20.681	60	7	0.385	0.669
1	0.18	3	200	15.687	1.318	11.899	20.681	20.681	60	21	0.602	0.669
1	0.18	3	200	15.687	1.318	11.899	20.681	20.681	60	22	0.708	0.669
1	0.18	3	200	15.628	1.313	11.899	20.526	20.526	60	23	0.625	0.669
1	0.18	3	200	15.628	1.313	11.899	20.526	20.526	60	24	0.736	0.669
1	0.18	3	200	15.628	1.313	11.899	20.526	20.526	60	25	0.806	0.669
1	0.18	3	35	17.484	1.655	10.564	28.936	28.936	88	5	2.645	0.543
1	0.18	3	35	17.484	1.655	10.564	28.936	28.936	88	6	1.377	0.543
1	0.18	3	35	17.484	1.655	10.564	28.936	28.936	88	7	0.950	0.543
1	0.18	3	35	17.484	1.655	10.564	28.936	28.936	88	8	0.604	0.543
1	0.18	3	35	17.484	1.655	10.564	28.936	28.936	88	9	0.445	0.543
1	0.18	3	35	17.484	1.655	10.564	28.936	28.936	88	12	0.302	0.543
1	0.18	3	35	17.484	1.655	10.564	28.936	28.936	88	15	0.314	0.543

1	0.18	3	35	17.484	1.655	10.564	28.936	28.936	88	18	0.357	0.543
1	0.18	3	35	17.484	1.655	10.564	28.936	28.936	88	21	0.440	0.543
1	0.18	3	35	17.484	1.655	10.564	28.936	28.936	88	24	0.565	0.543
1	0.18	3	35	17.484	1.655	10.564	28.936	28.936	88	27	0.608	0.543
1	0.18	3	35	17.484	1.655	10.564	28.936	28.936	88	30	0.643	0.543
1	0.18	3	35	17.484	1.655	10.564	28.936	28.936	88	33	0.736	0.543
1	0.18	3	35	17.484	1.655	10.564	28.936	28.936	88	34	0.720	0.543
1	0.18	3	35	17.484	1.655	10.564	28.936	28.936	88	35	0.845	0.543
1	0.18	3	35	17.484	1.655	10.564	28.936	28.936	88	36	0.911	0.543
1	0.18	3	35	17.484	1.655	10.564	28.936	28.936	88	37	1.064	0.543
1	0.18	3	35	17.484	1.655	10.564	28.936	28.936	88	38	1.213	0.543
1	0.18	3	50	17.458	1.632	10.694	28.499	28.499	85	5	2.217	0.663
1	0.18	3	50	17.458	1.632	10.694	28.499	28.499	85	6	1.248	0.663
1	0.18	3	50	17.458	1.632	10.694	28.499	28.499	85	7	0.786	0.663
1	0.18	3	50	17.458	1.632	10.694	28.499	28.499	85	8	0.584	0.663
1	0.18	3	50	17.458	1.632	10.694	28.499	28.499	85	9	0.417	0.663
1	0.18	3	50	17.458	1.632	10.694	28.499	28.499	85	31	0.722	0.663
1	0.18	3	50	17.458	1.632	10.694	28.499	28.499	85	32	0.750	0.663
1	0.18	3	50	17.458	1.632	10.694	28.499	28.499	85	33	0.763	0.663
1	0.18	3	50	17.458	1.632	10.694	28.499	28.499	85	34	0.771	0.663
1	0.18	3	50	17.458	1.632	10.694	28.499	28.499	85	35	0.766	0.663
1	0.18	3	100	17.461	1.571	11.117	27.427	27.427	80	6	0.913	0.477
1	0.18	3	100	17.461	1.571	11.117	27.427	27.427	80	7	0.595	0.477
1	0.18	3	100	17.461	1.571	11.117	27.427	27.427	80	8	0.483	0.477
1	0.18	3	100	17.461	1.571	11.117	27.427	27.427	80	9	0.368	0.477
1	0.18	3	100	17.461	1.571	11.117	27.427	27.427	80	28	0.660	0.477
1	0.18	3	100	17.461	1.571	11.117	27.427	27.427	80	29	0.691	0.477
1	0.18	3	100	17.461	1.571	11.117	27.427	27.427	80	30	0.692	0.477
1	0.18	3	100	17.461	1.571	11.117	27.427	27.427	80	31	0.742	0.477
1	0.18	3	100	17.461	1.571	11.117	27.427	27.427	80	32	0.790	0.477
1	0.18	3	100	17.461	1.571	11.117	27.427	27.427	80	33	0.952	0.477
1	0.18	3	150	17.466	1.517	11.517	26.488	26.488	76	5	1.030	0.513
1	0.18	3	150	17.466	1.517	11.517	26.488	26.488	76	6	0.742	0.513
1	0.18	3	150	17.466	1.517	11.517	26.488	26.488	76	7	0.485	0.513
1	0.18	3	150	17.466	1.517	11.517	26.488	26.488	76	28	0.733	0.513
1	0.18	3	150	17.466	1.517	11.517	26.488	26.488	76	29	0.737	0.513
1	0.18	3	150	17.466	1.517	11.517	26.488	26.488	76	30	0.768	0.513
1	0.18	3	150	17.466	1.517	11.517	26.488	26.488	76	31	0.857	0.513
1	0.18	3	200	17.452	1.467	11.900	25.595	25.595	73	5	0.765	0.605
1	0.18	3	200	17.452	1.467	11.900	25.595	25.595	73	6	0.506	0.605
1	0.18	3	200	17.452	1.467	11.900	25.595	25.595	73	28	0.686	0.605
1	0.18	3	200	17.452	1.467	11.900	25.595	25.595	73	29	0.761	0.605
1	0.18	3	200	17.452	1.467	11.900	25.595	25.595	73	30	0.841	0.605
1	0.18	3	35	19.345	1.831	10.565	35.423	35.423	106	7	1.817	0.573
1	0.18	3	35	19.345	1.831	10.565	35.423	35.423	106	8	1.007	0.573
1	0.18	3	35	19.345	1.831	10.565	35.423	35.423	106	9	0.700	0.573
1	0.18	3	35	19.345	1.831	10.565	35.423	35.423	106	10	0.463	0.573
1	0.18	3	35	19.345	1.831	10.565	35.423	35.423	106	11	0.395	0.573
1	0.18	3	35	19.345	1.831	10.565	35.423	35.423	106	15	0.280	0.573
1	0.18	3	35	19.345	1.831	10.565	35.423	35.423	106	20	0.314	0.573
1	0.18	3	35	19.345	1.831	10.565	35.423	35.423	106	25	0.477	0.573
1	0.18	3	35	19.345	1.831	10.565	35.423	35.423	106	30	0.488	0.573
1	0.18	3	35	19.345	1.831	10.565	35.423	35.423	106	35	0.664	0.573
1	0.18	3	35	19.345	1.831	10.565	35.423	35.423	106	40	0.686	0.573
1	0.18	3	35	19.345	1.831	10.565	35.423	35.423	106	41	0.639	0.573
1	0.18	3	35	19.345	1.831	10.565	35.423	35.423	106	42	0.733	0.573

1	0.18	3	35	19.345	1.831	10.565	35.423	35.423	106	43	0.746	0.573
1	0.18	3	35	19.345	1.831	10.565	35.423	35.423	106	44	0.918	0.573
1	0.18	3	50	19.362	1.810	10.696	35.051	35.051	102	7	1.341	1.049
1	0.18	3	50	19.362	1.810	10.696	35.051	35.051	102	8	0.809	1.049
1	0.18	3	50	19.362	1.810	10.696	35.051	35.051	102	9	0.622	1.049
1	0.18	3	50	19.362	1.810	10.696	35.051	35.051	102	10	0.342	1.049
1	0.18	3	50	19.362	1.810	10.696	35.051	35.051	102	39	0.679	1.049
1	0.18	3	50	19.362	1.810	10.696	35.051	35.051	102	40	0.690	1.049
1	0.18	3	50	19.362	1.810	10.696	35.051	35.051	102	41	0.723	1.049
1	0.18	3	50	19.362	1.810	10.696	35.051	35.051	102	42	0.828	1.049
1	0.18	3	100	19.266	1.733	11.117	33.389	33.389	96	7	0.871	0.684
1	0.18	3	100	19.266	1.733	11.117	33.389	33.389	96	8	0.560	0.684
1	0.18	3	100	19.266	1.733	11.117	33.389	33.389	96	9	0.431	0.684
1	0.18	3	100	19.266	1.733	11.117	33.389	33.389	96	37	0.686	0.684
1	0.18	3	100	19.266	1.733	11.117	33.389	33.389	96	38	0.638	0.684
1	0.18	3	100	19.266	1.733	11.117	33.389	33.389	96	39	0.733	0.684
1	0.18	3	100	19.266	1.733	11.117	33.389	33.389	96	40	0.859	0.684
1	0.18	3	150	19.258	1.672	11.517	32.203	32.203	91	6	1.100	0.696
1	0.18	3	150	19.258	1.672	11.517	32.203	32.203	91	7	0.654	0.696
1	0.18	3	150	19.258	1.672	11.517	32.203	32.203	91	8	0.514	0.696
1	0.18	3	150	19.258	1.672	11.517	32.203	32.203	91	35	0.676	0.696
1	0.18	3	150	19.258	1.672	11.517	32.203	32.203	91	36	0.591	0.696
1	0.18	3	150	19.258	1.672	11.517	32.203	32.203	91	37	0.690	0.696
1	0.18	3	150	19.258	1.672	11.517	32.203	32.203	91	38	0.782	0.696
1	0.18	3	200	19.271	1.619	11.901	31.206	31.206	88	6	0.933	0.805
1	0.18	3	200	19.271	1.619	11.901	31.206	31.206	88	7	0.605	0.805
1	0.18	3	200	19.271	1.619	11.901	31.206	31.206	88	8	0.435	0.805
1	0.18	3	200	19.271	1.619	11.901	31.206	31.206	88	33	0.732	0.805
1	0.18	3	200	19.271	1.619	11.901	31.206	31.206	88	34	0.649	0.805
1	0.18	3	200	19.271	1.619	11.901	31.206	31.206	88	35	0.737	0.805
1	0.18	3	200	19.271	1.619	11.901	31.206	31.206	88	36	0.764	0.805
0.5	0.18	3	35	6.312	1.155	5.463	7.293	14.587	43	5	0.209	0.376
0.5	0.18	3	35	6.312	1.155	5.463	7.293	14.587	43	6	0.277	0.376
0.5	0.18	3	35	6.312	1.155	5.463	7.293	14.587	43	7	0.311	0.376
0.5	0.18	3	35	6.312	1.155	5.463	7.293	14.587	43	8	0.269	0.376
0.5	0.18	3	35	6.312	1.155	5.463	7.293	14.587	43	9	0.253	0.376
0.5	0.18	3	35	6.312	1.155	5.463	7.293	14.587	43	10	0.228	0.376
0.5	0.18	3	35	6.312	1.155	5.463	7.293	14.587	43	11	0.348	0.376
0.5	0.18	3	35	6.312	1.155	5.463	7.293	14.587	43	12	0.382	0.376
0.5	0.18	3	35	6.312	1.155	5.463	7.293	14.587	43	13	0.355	0.376
0.5	0.18	3	35	6.312	1.155	5.463	7.293	14.587	43	14	0.429	0.376
0.5	0.18	3	35	6.312	1.155	5.463	7.293	14.587	43	15	0.555	0.376
0.5	0.18	3	35	6.312	1.155	5.463	7.293	14.587	43	16	0.502	0.376
0.5	0.18	3	35	6.312	1.155	5.463	7.293	14.587	43	17	0.546	0.376
0.5	0.18	3	35	6.312	1.155	5.463	7.293	14.587	43	18	0.595	0.376
0.5	0.18	3	35	6.312	1.155	5.463	7.293	14.587	43	19	0.764	0.376
0.5	0.18	3	50	6.313	1.142	5.527	7.210	14.420	42	5	0.221	0.442
0.5	0.18	3	50	6.313	1.142	5.527	7.210	14.420	42	6	0.253	0.442
0.5	0.18	3	50	6.313	1.142	5.527	7.210	14.420	42	7	0.290	0.442
0.5	0.18	3	50	6.313	1.142	5.527	7.210	14.420	42	8	0.271	0.442
0.5	0.18	3	50	6.313	1.142	5.527	7.210	14.420	42	9	0.240	0.442
0.5	0.18	3	50	6.313	1.142	5.527	7.210	14.420	42	10	0.233	0.442
0.5	0.18	3	50	6.313	1.142	5.527	7.210	14.420	42	11	0.402	0.442
0.5	0.18	3	50	6.313	1.142	5.527	7.210	14.420	42	12	0.367	0.442
0.5	0.18	3	50	6.313	1.142	5.527	7.210	14.420	42	13	0.414	0.442
0.5	0.18	3	50	6.313	1.142	5.527	7.210	14.420	42	14	0.560	0.442

0.5	0.18	3	50	6.313	1.142	5.527	7.210	14.420	42	15	0.570	0.442
0.5	0.18	3	50	6.313	1.142	5.527	7.210	14.420	42	16	0.571	0.442
0.5	0.18	3	50	6.313	1.142	5.527	7.210	14.420	42	17	0.584	0.442
0.5	0.18	3	50	6.313	1.142	5.527	7.210	14.420	42	18	0.674	0.442
0.5	0.18	3	50	6.313	1.142	5.527	7.210	14.420	42	19	1.009	0.442
0.5	0.18	3	100	6.313	1.101	5.732	6.953	13.906	40	5	0.267	0.571
0.5	0.18	3	100	6.313	1.101	5.732	6.953	13.906	40	6	0.289	0.571
0.5	0.18	3	100	6.313	1.101	5.732	6.953	13.906	40	7	0.269	0.571
0.5	0.18	3	100	6.313	1.101	5.732	6.953	13.906	40	8	0.322	0.571
0.5	0.18	3	100	6.313	1.101	5.732	6.953	13.906	40	9	0.332	0.571
0.5	0.18	3	100	6.313	1.101	5.732	6.953	13.906	40	10	0.443	0.571
0.5	0.18	3	100	6.313	1.101	5.732	6.953	13.906	40	11	0.480	0.571
0.5	0.18	3	100	6.313	1.101	5.732	6.953	13.906	40	12	0.493	0.571
0.5	0.18	3	100	6.313	1.101	5.732	6.953	13.906	40	13	0.534	0.571
0.5	0.18	3	100	6.313	1.101	5.732	6.953	13.906	40	14	0.648	0.571
0.5	0.18	3	100	6.313	1.101	5.732	6.953	13.906	40	15	0.655	0.571
0.5	0.18	3	100	6.313	1.101	5.732	6.953	13.906	40	16	0.661	0.571
0.5	0.18	3	100	6.313	1.101	5.732	6.953	13.906	40	17	0.680	0.571
0.5	0.18	3	100	6.313	1.101	5.732	6.953	13.906	40	18	0.905	0.571
0.5	0.18	3	150	6.321	1.067	5.924	6.744	13.489	39	5	0.310	0.423
0.5	0.18	3	150	6.321	1.067	5.924	6.744	13.489	39	6	0.291	0.423
0.5	0.18	3	150	6.321	1.067	5.924	6.744	13.489	39	7	0.363	0.423
0.5	0.18	3	150	6.321	1.067	5.924	6.744	13.489	39	8	0.349	0.423
0.5	0.18	3	150	6.321	1.067	5.924	6.744	13.489	39	9	0.351	0.423
0.5	0.18	3	150	6.321	1.067	5.924	6.744	13.489	39	10	0.489	0.423
0.5	0.18	3	150	6.321	1.067	5.924	6.744	13.489	39	11	0.507	0.423
0.5	0.18	3	150	6.321	1.067	5.924	6.744	13.489	39	12	0.580	0.423
0.5	0.18	3	150	6.321	1.067	5.924	6.744	13.489	39	13	0.723	0.423
0.5	0.18	3	150	6.321	1.067	5.924	6.744	13.489	39	14	0.668	0.423
0.5	0.18	3	150	6.321	1.067	5.924	6.744	13.489	39	15	0.634	0.423
0.5	0.18	3	150	6.321	1.067	5.924	6.744	13.489	39	16	0.718	0.423
0.5	0.18	3	150	6.321	1.067	5.924	6.744	13.489	39	17	0.879	0.423
0.5	0.18	3	200	6.325	1.037	6.102	6.556	13.113	38	5	0.290	0.511
0.5	0.18	3	200	6.325	1.037	6.102	6.556	13.113	38	6	0.309	0.511
0.5	0.18	3	200	6.325	1.037	6.102	6.556	13.113	38	7	0.347	0.511
0.5	0.18	3	200	6.325	1.037	6.102	6.556	13.113	38	8	0.379	0.511
0.5	0.18	3	200	6.325	1.037	6.102	6.556	13.113	38	9	0.544	0.511
0.5	0.18	3	200	6.325	1.037	6.102	6.556	13.113	38	10	0.614	0.511
0.5	0.18	3	200	6.325	1.037	6.102	6.556	13.113	38	11	0.631	0.511
0.5	0.18	3	200	6.325	1.037	6.102	6.556	13.113	38	12	0.791	0.511
0.5	0.18	3	200	6.325	1.037	6.102	6.556	13.113	38	13	0.778	0.511
0.5	0.18	3	200	6.325	1.037	6.102	6.556	13.113	38	14	0.752	0.511
0.5	0.18	3	200	6.325	1.037	6.102	6.556	13.113	38	15	0.810	0.511
0.5	0.18	3	200	6.325	1.037	6.102	6.556	13.113	38	16	0.979	0.511
0.5	0.18	3	200	6.325	1.037	6.102	6.556	13.113	38	17	1.278	0.511
0.5	0.18	3	35	7.098	1.300	5.460	9.229	18.458	56	5	0.505	0.378
0.5	0.18	3	35	7.098	1.300	5.460	9.229	18.458	56	6	0.392	0.378
0.5	0.18	3	35	7.098	1.300	5.460	9.229	18.458	56	7	0.357	0.378
0.5	0.18	3	35	7.098	1.300	5.460	9.229	18.458	56	8	0.378	0.378
0.5	0.18	3	35	7.098	1.300	5.460	9.229	18.458	56	9	0.360	0.378
0.5	0.18	3	35	7.098	1.300	5.460	9.229	18.458	56	10	0.315	0.378
0.5	0.18	3	35	7.098	1.300	5.460	9.229	18.458	56	11	0.263	0.378
0.5	0.18	3	35	7.098	1.300	5.460	9.229	18.458	56	12	0.291	0.378
0.5	0.18	3	35	7.098	1.300	5.460	9.229	18.458	56	13	0.400	0.378
0.5	0.18	3	35	7.098	1.300	5.460	9.229	18.458	56	14	0.373	0.378
0.5	0.18	3	35	7.098	1.300	5.460	9.229	18.458	56	15	0.319	0.378

0.5	0.18	3	35	7.098	1.300	5.460	9.229	18.458	56	16	0.274	0.378
0.5	0.18	3	35	7.098	1.300	5.460	9.229	18.458	56	17	0.312	0.378
0.5	0.18	3	35	7.098	1.300	5.460	9.229	18.458	56	18	0.477	0.378
0.5	0.18	3	35	7.098	1.300	5.460	9.229	18.458	56	19	0.525	0.378
0.5	0.18	3	35	7.098	1.300	5.460	9.229	18.458	56	20	0.488	0.378
0.5	0.18	3	35	7.098	1.300	5.460	9.229	18.458	56	21	0.497	0.378
0.5	0.18	3	35	7.098	1.300	5.460	9.229	18.458	56	22	0.541	0.378
0.5	0.18	3	35	7.098	1.300	5.460	9.229	18.458	56	23	0.712	0.378
0.5	0.18	3	35	7.098	1.300	5.460	9.229	18.458	56	24	0.980	0.378
0.5	0.18	3	50	7.065	1.280	5.521	9.041	18.082	53	5	0.378	0.443
0.5	0.18	3	50	7.065	1.280	5.521	9.041	18.082	53	6	0.431	0.443
0.5	0.18	3	50	7.065	1.280	5.521	9.041	18.082	53	7	0.422	0.443
0.5	0.18	3	50	7.065	1.280	5.521	9.041	18.082	53	8	0.413	0.443
0.5	0.18	3	50	7.065	1.280	5.521	9.041	18.082	53	9	0.374	0.443
0.5	0.18	3	50	7.065	1.280	5.521	9.041	18.082	53	10	0.326	0.443
0.5	0.18	3	50	7.065	1.280	5.521	9.041	18.082	53	11	0.326	0.443
0.5	0.18	3	50	7.065	1.280	5.521	9.041	18.082	53	12	0.306	0.443
0.5	0.18	3	50	7.065	1.280	5.521	9.041	18.082	53	13	0.393	0.443
0.5	0.18	3	50	7.065	1.280	5.521	9.041	18.082	53	14	0.395	0.443
0.5	0.18	3	50	7.065	1.280	5.521	9.041	18.082	53	15	0.372	0.443
0.5	0.18	3	50	7.065	1.280	5.521	9.041	18.082	53	16	0.336	0.443
0.5	0.18	3	50	7.065	1.280	5.521	9.041	18.082	53	17	0.339	0.443
0.5	0.18	3	50	7.065	1.280	5.521	9.041	18.082	53	18	0.504	0.443
0.5	0.18	3	50	7.065	1.280	5.521	9.041	18.082	53	19	0.505	0.443
0.5	0.18	3	50	7.065	1.280	5.521	9.041	18.082	53	20	0.502	0.443
0.5	0.18	3	50	7.065	1.280	5.521	9.041	18.082	53	21	0.504	0.443
0.5	0.18	3	50	7.065	1.280	5.521	9.041	18.082	53	22	0.635	0.443
0.5	0.18	3	50	7.065	1.280	5.521	9.041	18.082	53	23	0.864	0.443
0.5	0.18	3	100	7.062	1.234	5.724	8.712	17.424	51	5	0.478	0.529
0.5	0.18	3	100	7.062	1.234	5.724	8.712	17.424	51	6	0.381	0.529
0.5	0.18	3	100	7.062	1.234	5.724	8.712	17.424	51	7	0.425	0.529
0.5	0.18	3	100	7.062	1.234	5.724	8.712	17.424	51	8	0.414	0.529
0.5	0.18	3	100	7.062	1.234	5.724	8.712	17.424	51	9	0.393	0.529
0.5	0.18	3	100	7.062	1.234	5.724	8.712	17.424	51	10	0.367	0.529
0.5	0.18	3	100	7.062	1.234	5.724	8.712	17.424	51	11	0.338	0.529
0.5	0.18	3	100	7.062	1.234	5.724	8.712	17.424	51	12	0.436	0.529
0.5	0.18	3	100	7.062	1.234	5.724	8.712	17.424	51	13	0.449	0.529
0.5	0.18	3	100	7.062	1.234	5.724	8.712	17.424	51	14	0.377	0.529
0.5	0.18	3	100	7.062	1.234	5.724	8.712	17.424	51	15	0.361	0.529
0.5	0.18	3	100	7.062	1.234	5.724	8.712	17.424	51	16	0.389	0.529
0.5	0.18	3	100	7.062	1.234	5.724	8.712	17.424	51	17	0.531	0.529
0.5	0.18	3	100	7.062	1.234	5.724	8.712	17.424	51	18	0.504	0.529
0.5	0.18	3	100	7.062	1.234	5.724	8.712	17.424	51	19	0.549	0.529
0.5	0.18	3	100	7.062	1.234	5.724	8.712	17.424	51	20	0.626	0.529
0.5	0.18	3	100	7.062	1.234	5.724	8.712	17.424	51	21	0.657	0.529
0.5	0.18	3	100	7.062	1.234	5.724	8.712	17.424	51	22	0.879	0.529
0.5	0.18	3	150	7.065	1.195	5.913	8.441	16.882	49	5	0.421	0.599
0.5	0.18	3	150	7.065	1.195	5.913	8.441	16.882	49	6	0.487	0.599
0.5	0.18	3	150	7.065	1.195	5.913	8.441	16.882	49	7	0.453	0.599
0.5	0.18	3	150	7.065	1.195	5.913	8.441	16.882	49	8	0.397	0.599
0.5	0.18	3	150	7.065	1.195	5.913	8.441	16.882	49	9	0.444	0.599
0.5	0.18	3	150	7.065	1.195	5.913	8.441	16.882	49	10	0.413	0.599
0.5	0.18	3	150	7.065	1.195	5.913	8.441	16.882	49	11	0.417	0.599
0.5	0.18	3	150	7.065	1.195	5.913	8.441	16.882	49	12	0.478	0.599
0.5	0.18	3	150	7.065	1.195	5.913	8.441	16.882	49	13	0.501	0.599
0.5	0.18	3	150	7.065	1.195	5.913	8.441	16.882	49	14	0.417	0.599

0.5	0.18	3	150	7.065	1.195	5.913	8.441	16.882	49	15	0.444	0.599
0.5	0.18	3	150	7.065	1.195	5.913	8.441	16.882	49	16	0.576	0.599
0.5	0.18	3	150	7.065	1.195	5.913	8.441	16.882	49	17	0.561	0.599
0.5	0.18	3	150	7.065	1.195	5.913	8.441	16.882	49	18	0.570	0.599
0.5	0.18	3	150	7.065	1.195	5.913	8.441	16.882	49	19	0.584	0.599
0.5	0.18	3	150	7.065	1.195	5.913	8.441	16.882	49	20	0.727	0.599
0.5	0.18	3	150	7.065	1.195	5.913	8.441	16.882	49	21	1.005	0.599
0.5	0.18	3	200	7.076	1.162	6.087	8.225	16.451	47	5	0.507	0.519
0.5	0.18	3	200	7.076	1.162	6.087	8.225	16.451	47	6	0.469	0.519
0.5	0.18	3	200	7.076	1.162	6.087	8.225	16.451	47	7	0.456	0.519
0.5	0.18	3	200	7.076	1.162	6.087	8.225	16.451	47	8	0.445	0.519
0.5	0.18	3	200	7.076	1.162	6.087	8.225	16.451	47	9	0.442	0.519
0.5	0.18	3	200	7.076	1.162	6.087	8.225	16.451	47	10	0.439	0.519
0.5	0.18	3	200	7.076	1.162	6.087	8.225	16.451	47	11	0.489	0.519
0.5	0.18	3	200	7.076	1.162	6.087	8.225	16.451	47	12	0.462	0.519
0.5	0.18	3	200	7.076	1.162	6.087	8.225	16.451	47	13	0.501	0.519
0.5	0.18	3	200	7.076	1.162	6.087	8.225	16.451	47	14	0.458	0.519
0.5	0.18	3	200	7.076	1.162	6.087	8.225	16.451	47	15	0.637	0.519
0.5	0.18	3	200	7.076	1.162	6.087	8.225	16.451	47	16	0.662	0.519
0.5	0.18	3	200	7.076	1.162	6.087	8.225	16.451	47	17	0.609	0.519
0.5	0.18	3	200	7.076	1.162	6.087	8.225	16.451	47	18	0.657	0.519
0.5	0.18	3	200	7.076	1.162	6.087	8.225	16.451	47	19	0.720	0.519
0.5	0.18	3	200	7.076	1.162	6.087	8.225	16.451	47	20	0.889	0.519
0.5	0.18	3	35	8.375	1.531	5.469	12.824	25.649	77	5	0.823	0.344
0.5	0.18	3	35	8.375	1.531	5.469	12.824	25.649	77	6	0.658	0.344
0.5	0.18	3	35	8.375	1.531	5.469	12.824	25.649	77	7	0.542	0.344
0.5	0.18	3	35	8.375	1.531	5.469	12.824	25.649	77	8	0.462	0.344
0.5	0.18	3	35	8.375	1.531	5.469	12.824	25.649	77	9	0.473	0.344
0.5	0.18	3	35	8.375	1.531	5.469	12.824	25.649	77	10	0.428	0.344
0.5	0.18	3	35	8.375	1.531	5.469	12.824	25.649	77	11	0.409	0.344
0.5	0.18	3	35	8.375	1.531	5.469	12.824	25.649	77	12	0.412	0.344
0.5	0.18	3	35	8.375	1.531	5.469	12.824	25.649	77	13	0.345	0.344
0.5	0.18	3	35	8.375	1.531	5.469	12.824	25.649	77	14	0.333	0.344
0.5	0.18	3	35	8.375	1.531	5.469	12.824	25.649	77	15	0.333	0.344
0.5	0.18	3	35	8.375	1.531	5.469	12.824	25.649	77	16	0.320	0.344
0.5	0.18	3	35	8.375	1.531	5.469	12.824	25.649	77	17	0.285	0.344
0.5	0.18	3	35	8.375	1.531	5.469	12.824	25.649	77	18	0.299	0.344
0.5	0.18	3	35	8.375	1.531	5.469	12.824	25.649	77	19	0.345	0.344
0.5	0.18	3	35	8.375	1.531	5.469	12.824	25.649	77	20	0.355	0.344
0.5	0.18	3	35	8.375	1.531	5.469	12.824	25.649	77	21	0.357	0.344
0.5	0.18	3	35	8.375	1.531	5.469	12.824	25.649	77	22	0.336	0.344
0.5	0.18	3	35	8.375	1.531	5.469	12.824	25.649	77	23	0.323	0.344
0.5	0.18	3	35	8.375	1.531	5.469	12.824	25.649	77	24	0.319	0.344
0.5	0.18	3	35	8.375	1.531	5.469	12.824	25.649	77	25	0.351	0.344
0.5	0.18	3	35	8.375	1.531	5.469	12.824	25.649	77	26	0.433	0.344
0.5	0.18	3	35	8.375	1.531	5.469	12.824	25.649	77	27	0.515	0.344
0.5	0.18	3	35	8.375	1.531	5.469	12.824	25.649	77	28	0.553	0.344
0.5	0.18	3	35	8.375	1.531	5.469	12.824	25.649	77	29	0.589	0.344
0.5	0.18	3	35	8.375	1.531	5.469	12.824	25.649	77	30	0.572	0.344
0.5	0.18	3	35	8.375	1.531	5.469	12.824	25.649	77	31	0.718	0.344
0.5	0.18	3	35	8.375	1.531	5.469	12.824	25.649	77	32	0.845	0.344
0.5	0.18	3	50	8.410	1.523	5.522	12.809	25.618	74	5	0.664	0.604
0.5	0.18	3	50	8.410	1.523	5.522	12.809	25.618	74	6	0.594	0.604
0.5	0.18	3	50	8.410	1.523	5.522	12.809	25.618	74	7	0.519	0.604
0.5	0.18	3	50	8.410	1.523	5.522	12.809	25.618	74	25	0.393	0.604
0.5	0.18	3	50	8.410	1.523	5.522	12.809	25.618	74	26	0.594	0.604

0.5	0.18	3	50	8.410	1.523	5.522	12.809	25.618	74	27	0.611	0.604
0.5	0.18	3	50	8.410	1.523	5.522	12.809	25.618	74	28	0.531	0.604
0.5	0.18	3	50	8.410	1.523	5.522	12.809	25.618	74	29	0.678	0.604
0.5	0.18	3	50	8.410	1.523	5.522	12.809	25.618	74	30	0.688	0.604
0.5	0.18	3	50	8.410	1.523	5.522	12.809	25.618	74	31	0.877	0.604
0.5	0.18	3	100	8.422	1.471	5.724	12.392	24.784	71	5	0.641	0.585
0.5	0.18	3	100	8.422	1.471	5.724	12.392	24.784	71	6	0.551	0.585
0.5	0.18	3	100	8.422	1.471	5.724	12.392	24.784	71	7	0.537	0.585
0.5	0.18	3	100	8.422	1.471	5.724	12.392	24.784	71	25	0.536	0.585
0.5	0.18	3	100	8.422	1.471	5.724	12.392	24.784	71	26	0.571	0.585
0.5	0.18	3	100	8.422	1.471	5.724	12.392	24.784	71	27	0.644	0.585
0.5	0.18	3	100	8.422	1.471	5.724	12.392	24.784	71	28	0.630	0.585
0.5	0.18	3	100	8.422	1.471	5.724	12.392	24.784	71	29	0.781	0.585
0.5	0.18	3	100	8.422	1.471	5.724	12.392	24.784	71	30	0.803	0.585
0.5	0.18	3	150	8.421	1.425	5.911	11.997	23.994	70	5	0.540	0.503
0.5	0.18	3	150	8.421	1.425	5.911	11.997	23.994	70	6	0.535	0.503
0.5	0.18	3	150	8.421	1.425	5.911	11.997	23.994	70	25	0.647	0.503
0.5	0.18	3	150	8.421	1.425	5.911	11.997	23.994	70	26	0.610	0.503
0.5	0.18	3	150	8.421	1.425	5.911	11.997	23.994	70	27	0.636	0.503
0.5	0.18	3	150	8.421	1.425	5.911	11.997	23.994	70	28	0.742	0.503
0.5	0.18	3	150	8.421	1.425	5.911	11.997	23.994	70	29	0.923	0.503
0.5	0.18	3	200	8.423	1.384	6.087	11.656	23.312	67	5	0.566	0.643
0.5	0.18	3	200	8.423	1.384	6.087	11.656	23.312	67	6	0.507	0.643
0.5	0.18	3	200	8.423	1.384	6.087	11.656	23.312	67	24	0.668	0.643
0.5	0.18	3	200	8.423	1.384	6.087	11.656	23.312	67	25	0.723	0.643
0.5	0.18	3	200	8.423	1.384	6.087	11.656	23.312	67	26	0.743	0.643
0.5	0.18	3	200	8.423	1.384	6.087	11.656	23.312	67	27	0.808	0.643
0.5	0.18	3	200	8.423	1.384	6.087	11.656	23.312	67	28	0.903	0.643
0.5	0.18	3	35	9.254	1.703	5.436	15.757	31.513	91	5	2.110	0.317
0.5	0.18	3	35	9.254	1.703	5.436	15.757	31.513	91	6	1.060	0.317
0.5	0.18	3	35	9.254	1.703	5.436	15.757	31.513	91	7	0.751	0.317
0.5	0.18	3	35	9.254	1.703	5.436	15.757	31.513	91	8	0.526	0.317
0.5	0.18	3	35	9.254	1.703	5.436	15.757	31.513	91	9	0.541	0.317
0.5	0.18	3	35	9.254	1.703	5.436	15.757	31.513	91	10	0.566	0.317
0.5	0.18	3	35	9.254	1.703	5.436	15.757	31.513	91	11	0.580	0.317
0.5	0.18	3	35	9.254	1.703	5.436	15.757	31.513	91	15	0.446	0.317
0.5	0.18	3	35	9.254	1.703	5.436	15.757	31.513	91	20	0.373	0.317
0.5	0.18	3	35	9.254	1.703	5.436	15.757	31.513	91	25	0.401	0.317
0.5	0.18	3	35	9.254	1.703	5.436	15.757	31.513	91	30	0.398	0.317
0.5	0.18	3	35	9.254	1.703	5.436	15.757	31.513	91	35	0.632	0.317
0.5	0.18	3	35	9.254	1.703	5.436	15.757	31.513	91	36	0.679	0.317
0.5	0.18	3	35	9.254	1.703	5.436	15.757	31.513	91	37	0.789	0.317
0.5	0.18	3	35	9.254	1.703	5.436	15.757	31.513	91	38	0.861	0.317
0.5	0.18	3	50	9.258	1.684	5.498	15.589	31.177	89	5	1.863	0.297
0.5	0.18	3	50	9.258	1.684	5.498	15.589	31.177	89	6	1.019	0.297
0.5	0.18	3	50	9.258	1.684	5.498	15.589	31.177	89	7	0.705	0.297
0.5	0.18	3	50	9.258	1.684	5.498	15.589	31.177	89	8	0.508	0.297
0.5	0.18	3	50	9.258	1.684	5.498	15.589	31.177	89	9	0.605	0.297
0.5	0.18	3	50	9.258	1.684	5.498	15.589	31.177	89	15	0.468	0.297
0.5	0.18	3	50	9.258	1.684	5.498	15.589	31.177	89	20	0.348	0.297
0.5	0.18	3	50	9.258	1.684	5.498	15.589	31.177	89	25	0.366	0.297
0.5	0.18	3	50	9.258	1.684	5.498	15.589	31.177	89	30	0.409	0.297
0.5	0.18	3	50	9.258	1.684	5.498	15.589	31.177	89	33	0.610	0.297
0.5	0.18	3	50	9.258	1.684	5.498	15.589	31.177	89	34	0.637	0.297
0.5	0.18	3	50	9.258	1.684	5.498	15.589	31.177	89	35	0.712	0.297
0.5	0.18	3	50	9.258	1.684	5.498	15.589	31.177	89	36	0.804	0.297

0.5	0.18	3	50	9.258	1.684	5.498	15.589	31.177	90	37	0.885	0.297
0.5	0.18	3	100	9.260	1.625	5.698	15.051	30.101	85	5	1.312	0.439
0.5	0.18	3	100	9.260	1.625	5.698	15.051	30.101	85	6	0.717	0.439
0.5	0.18	3	100	9.260	1.625	5.698	15.051	30.101	85	7	0.643	0.439
0.5	0.18	3	100	9.260	1.625	5.698	15.051	30.101	85	8	0.566	0.439
0.5	0.18	3	100	9.260	1.625	5.698	15.051	30.101	85	15	0.501	0.439
0.5	0.18	3	100	9.260	1.625	5.698	15.051	30.101	85	20	0.393	0.439
0.5	0.18	3	100	9.260	1.625	5.698	15.051	30.101	85	25	0.475	0.439
0.5	0.18	3	100	9.260	1.625	5.698	15.051	30.101	85	30	0.711	0.439
0.5	0.18	3	100	9.260	1.625	5.698	15.051	30.101	85	31	0.692	0.439
0.5	0.18	3	100	9.260	1.625	5.698	15.051	30.101	85	32	0.739	0.439
0.5	0.18	3	100	9.260	1.625	5.698	15.051	30.101	85	33	0.691	0.439
0.5	0.18	3	100	9.260	1.625	5.698	15.051	30.101	85	34	0.763	0.439
0.5	0.18	3	100	9.260	1.625	5.698	15.051	30.101	85	35	0.898	0.439
0.5	0.18	3	150	9.260	1.573	5.885	14.570	29.141	83	5	1.123	0.782
0.5	0.18	3	150	9.260	1.573	5.885	14.570	29.141	83	6	0.726	0.782
0.5	0.18	3	150	9.260	1.573	5.885	14.570	29.141	83	7	0.564	0.782
0.5	0.18	3	150	9.260	1.573	5.885	14.570	29.141	83	10	0.734	0.782
0.5	0.18	3	150	9.260	1.573	5.885	14.570	29.141	83	15	0.481	0.782
0.5	0.18	3	150	9.260	1.573	5.885	14.570	29.141	83	20	0.529	0.782
0.5	0.18	3	150	9.260	1.573	5.885	14.570	29.141	83	25	0.485	0.782
0.5	0.18	3	150	9.260	1.573	5.885	14.570	29.141	83	30	0.718	0.782
0.5	0.18	3	150	9.260	1.573	5.885	14.570	29.141	83	31	0.745	0.782
0.5	0.18	3	150	9.260	1.573	5.885	14.570	29.141	83	32	0.800	0.782
0.5	0.18	3	150	9.260	1.573	5.885	14.570	29.141	83	33	0.813	0.782
0.5	0.18	3	200	9.263	1.528	6.063	14.152	28.303	80	5	0.997	0.486
0.5	0.18	3	200	9.263	1.528	6.063	14.152	28.303	80	6	0.725	0.486
0.5	0.18	3	200	9.263	1.528	6.063	14.152	28.303	80	7	0.594	0.486
0.5	0.18	3	200	9.263	1.528	6.063	14.152	28.303	80	10	0.732	0.486
0.5	0.18	3	200	9.263	1.528	6.063	14.152	28.303	80	15	0.517	0.486
0.5	0.18	3	200	9.263	1.528	6.063	14.152	28.303	80	20	0.580	0.486
0.5	0.18	3	200	9.263	1.528	6.063	14.152	28.303	80	25	0.486	0.486
0.5	0.18	3	200	9.263	1.528	6.063	14.152	28.303	80	29	0.619	0.486
0.5	0.18	3	200	9.263	1.528	6.063	14.152	28.303	80	30	0.659	0.486
0.5	0.18	3	200	9.263	1.528	6.063	14.152	28.303	80	31	0.749	0.486
0.5	0.18	3	200	9.263	1.528	6.063	14.152	28.303	80	32	0.893	0.486
0.5	0.18	3	35	10.224	1.881	5.434	19.236	38.472	111	5	4.643	0.352
0.5	0.18	3	35	10.224	1.881	5.434	19.236	38.472	111	6	4.666	0.352
0.5	0.18	3	35	10.224	1.881	5.434	19.236	38.472	111	7	1.847	0.352
0.5	0.18	3	35	10.224	1.881	5.434	19.236	38.472	111	8	1.068	0.352
0.5	0.18	3	35	10.224	1.881	5.434	19.236	38.472	111	9	0.812	0.352
0.5	0.18	3	35	10.224	1.881	5.434	19.236	38.472	111	10	0.686	0.352
0.5	0.18	3	35	10.224	1.881	5.434	19.236	38.472	111	11	0.679	0.352
0.5	0.18	3	35	10.224	1.881	5.434	19.236	38.472	111	15	0.593	0.352
0.5	0.18	3	35	10.224	1.881	5.434	19.236	38.472	111	20	0.426	0.352
0.5	0.18	3	35	10.224	1.881	5.434	19.236	38.472	111	25	0.673	0.352
0.5	0.18	3	35	10.224	1.881	5.434	19.236	38.472	111	30	0.495	0.352
0.5	0.18	3	35	10.224	1.881	5.434	19.236	38.472	111	35	0.457	0.352
0.5	0.18	3	35	10.224	1.881	5.434	19.236	38.472	111	40	0.656	0.352
0.5	0.18	3	35	10.224	1.881	5.434	19.236	38.472	111	41	0.529	0.352
0.5	0.18	3	35	10.224	1.881	5.434	19.236	38.472	111	42	0.534	0.352
0.5	0.18	3	35	10.224	1.881	5.434	19.236	38.472	111	43	0.630	0.352
0.5	0.18	3	35	10.224	1.881	5.434	19.236	38.472	111	44	0.738	0.352
0.5	0.18	3	35	10.224	1.881	5.434	19.236	38.472	111	45	0.874	0.352
0.5	0.18	3	50	10.221	1.860	5.495	19.013	38.025	109	8	0.993	0.422
0.5	0.18	3	50	10.221	1.860	5.495	19.013	38.025	109	9	0.837	0.422

0.5	0.18	3	50	10.221	1.860	5.495	19.013	38.025	109	10	0.713	0.422
0.5	0.18	3	50	10.221	1.860	5.495	19.013	38.025	109	11	0.753	0.422
0.5	0.18	3	50	10.221	1.860	5.495	19.013	38.025	109	15	0.546	0.422
0.5	0.18	3	50	10.221	1.860	5.495	19.013	38.025	109	20	0.468	0.422
0.5	0.18	3	50	10.221	1.860	5.495	19.013	38.025	109	25	0.662	0.422
0.5	0.18	3	50	10.221	1.860	5.495	19.013	38.025	109	30	0.516	0.422
0.5	0.18	3	50	10.221	1.860	5.495	19.013	38.025	109	35	0.436	0.422
0.5	0.18	3	50	10.221	1.860	5.495	19.013	38.025	109	40	0.531	0.422
0.5	0.18	3	50	10.221	1.860	5.495	19.013	38.025	109	41	0.549	0.422
0.5	0.18	3	50	10.221	1.860	5.495	19.013	38.025	109	42	0.697	0.422
0.5	0.18	3	50	10.221	1.860	5.495	19.013	38.025	109	43	0.716	0.422
0.5	0.18	3	50	10.221	1.860	5.495	19.013	38.025	109	44	0.826	0.422
0.5	0.18	3	100	10.230	1.797	5.694	18.380	36.761	104	8	0.970	0.590
0.5	0.18	3	100	10.230	1.797	5.694	18.380	36.761	104	9	0.783	0.590
0.5	0.18	3	100	10.230	1.797	5.694	18.380	36.761	104	10	0.694	0.590
0.5	0.18	3	100	10.230	1.797	5.694	18.380	36.761	104	15	0.584	0.590
0.5	0.18	3	100	10.230	1.797	5.694	18.380	36.761	104	20	0.547	0.590
0.5	0.18	3	100	10.230	1.797	5.694	18.380	36.761	104	25	0.672	0.590
0.5	0.18	3	100	10.230	1.797	5.694	18.380	36.761	104	30	0.556	0.590
0.5	0.18	3	100	10.230	1.797	5.694	18.380	36.761	104	35	0.499	0.590
0.5	0.18	3	100	10.230	1.797	5.694	18.380	36.761	104	39	0.641	0.590
0.5	0.18	3	100	10.230	1.797	5.694	18.380	36.761	104	40	0.673	0.590
0.5	0.18	3	100	10.230	1.797	5.694	18.380	36.761	104	41	0.820	0.590
0.5	0.18	3	100	10.230	1.797	5.694	18.380	36.761	104	42	0.841	0.590
0.5	0.18	3	150	10.229	1.739	5.882	17.790	35.579	100	8	0.817	0.378
0.5	0.18	3	150	10.229	1.739	5.882	17.790	35.579	100	9	0.671	0.378
0.5	0.18	3	150	10.229	1.739	5.882	17.790	35.579	100	10	0.776	0.378
0.5	0.18	3	150	10.229	1.739	5.882	17.790	35.579	100	15	0.584	0.378
0.5	0.18	3	150	10.229	1.739	5.882	17.790	35.579	100	20	0.514	0.378
0.5	0.18	3	150	10.229	1.739	5.882	17.790	35.579	100	25	0.637	0.378
0.5	0.18	3	150	10.229	1.739	5.882	17.790	35.579	100	30	0.707	0.378
0.5	0.18	3	150	10.229	1.739	5.882	17.790	35.579	100	35	0.769	0.378
0.5	0.18	3	150	10.229	1.739	5.882	17.790	35.579	100	37	0.618	0.378
0.5	0.18	3	150	10.229	1.739	5.882	17.790	35.579	100	38	0.837	0.378
0.5	0.18	3	150	10.229	1.739	5.882	17.790	35.579	100	39	0.882	0.378
0.5	0.18	3	150	10.229	1.739	5.882	17.790	35.579	100	40	0.849	0.378
0.5	0.18	3	150	10.229	1.739	5.882	17.790	35.579	101	41	0.849	0.378
0.5	0.18	3	200	10.227	1.688	6.057	17.267	34.534	97	8	0.793	0.841
0.5	0.18	3	200	10.227	1.688	6.057	17.267	34.534	97	9	0.855	0.841
0.5	0.18	3	200	10.227	1.688	6.057	17.267	34.534	97	10	0.829	0.841
0.5	0.18	3	200	10.227	1.688	6.057	17.267	34.534	97	15	0.597	0.841
0.5	0.18	3	200	10.227	1.688	6.057	17.267	34.534	97	20	0.620	0.841
0.5	0.18	3	200	10.227	1.688	6.057	17.267	34.534	97	25	0.719	0.841
0.5	0.18	3	200	10.227	1.688	6.057	17.267	34.534	97	30	0.747	0.841
0.5	0.18	3	200	10.227	1.688	6.057	17.267	34.534	97	35	0.930	0.841
0.5	0.18	3	200	10.227	1.688	6.057	17.267	34.534	97	36	0.835	0.841
0.5	0.18	3	200	10.227	1.688	6.057	17.267	34.534	97	37	0.901	0.841
0.5	0.18	3	200	10.227	1.688	6.057	17.267	34.534	97	38	0.938	0.841
0.5	0.18	3	200	10.227	1.688	6.057	17.267	34.534	97	39	1.075	0.841
3.015	0.25	3	35	29.735	1.016	29.265	30.213	10.021	32	5	0.581	0.360
3.015	0.25	3	35	29.735	1.016	29.265	30.213	10.021	32	6	0.461	0.360
3.015	0.25	3	35	29.735	1.016	29.265	30.213	10.021	32	7	0.625	0.360
3.015	0.25	3	35	29.735	1.016	29.265	30.213	10.021	32	8	0.571	0.360
3.015	0.25	3	35	29.735	1.016	29.265	30.213	10.021	32	9	0.641	0.360
3.015	0.25	3	35	29.735	1.016	29.265	30.213	10.021	32	10	0.662	0.360
3.015	0.25	3	35	29.735	1.016	29.265	30.213	10.021	32	11	0.481	0.360

3.015	0.25	3	35	29.735	1.016	29.265	30.213	10.021	32	12	0.621	0.360
3.015	0.25	3	35	29.735	1.016	29.265	30.213	10.021	32	13	0.601	0.360
3.015	0.25	3	35	29.735	1.016	29.265	30.213	10.021	32	14	0.805	0.360
3.015	0.25	3	50	29.746	1.004	29.633	29.860	9.904	31	5	0.610	0.573
3.015	0.25	3	50	29.746	1.004	29.633	29.860	9.904	31	6	0.451	0.573
3.015	0.25	3	50	29.746	1.004	29.633	29.860	9.904	31	7	0.607	0.573
3.015	0.25	3	50	29.746	1.004	29.633	29.860	9.904	31	8	0.599	0.573
3.015	0.25	3	50	29.746	1.004	29.633	29.860	9.904	31	9	0.646	0.573
3.015	0.25	3	50	29.746	1.004	29.633	29.860	9.904	31	10	0.508	0.573
3.015	0.25	3	50	29.746	1.004	29.633	29.860	9.904	31	11	0.556	0.573
3.015	0.25	3	50	29.746	1.004	29.633	29.860	9.904	31	12	0.522	0.573
3.015	0.25	3	50	29.746	1.004	29.633	29.860	9.904	31	13	0.648	0.573
3.015	0.25	3	50	29.746	1.004	29.633	29.860	9.904	31	14	0.888	0.573
3.015	0.25	3	100	29.753	0.966	30.815	28.729	9.529	30	5	0.614	0.855
3.015	0.25	3	100	29.753	0.966	30.815	28.729	9.529	30	6	0.500	0.855
3.015	0.25	3	100	29.753	0.966	30.815	28.729	9.529	30	7	0.515	0.855
3.015	0.25	3	100	29.753	0.966	30.815	28.729	9.529	30	8	0.477	0.855
3.015	0.25	3	100	29.753	0.966	30.815	28.729	9.529	30	9	0.495	0.855
3.015	0.25	3	100	29.753	0.966	30.815	28.729	9.529	30	10	0.439	0.855
3.015	0.25	3	100	29.753	0.966	30.815	28.729	9.529	30	11	0.548	0.855
3.015	0.25	3	100	29.753	0.966	30.815	28.729	9.529	30	12	0.616	0.855
3.015	0.25	3	100	29.753	0.966	30.815	28.729	9.529	30	13	0.745	0.855
3.015	0.25	3	100	29.753	0.966	30.815	28.729	9.529	30	14	1.188	0.855
3.015	0.25	3	150	29.752	0.931	31.940	27.713	9.192	28	5	0.695	0.639
3.015	0.25	3	150	29.752	0.931	31.940	27.713	9.192	28	6	0.558	0.639
3.015	0.25	3	150	29.752	0.931	31.940	27.713	9.192	28	7	0.543	0.639
3.015	0.25	3	150	29.752	0.931	31.940	27.713	9.192	28	8	0.511	0.639
3.015	0.25	3	150	29.752	0.931	31.940	27.713	9.192	28	9	0.523	0.639
3.015	0.25	3	150	29.752	0.931	31.940	27.713	9.192	28	10	0.572	0.639
3.015	0.25	3	150	29.752	0.931	31.940	27.713	9.192	28	11	0.576	0.639
3.015	0.25	3	150	29.752	0.931	31.940	27.713	9.192	28	12	0.642	0.639
3.015	0.25	3	150	29.752	0.931	31.940	27.713	9.192	28	13	1.004	0.639
3.015	0.25	3	200	29.756	0.901	33.015	26.818	8.895	27	5	0.529	0.448
3.015	0.25	3	200	29.756	0.901	33.015	26.818	8.895	27	6	0.593	0.448
3.015	0.25	3	200	29.756	0.901	33.015	26.818	8.895	27	7	0.572	0.448
3.015	0.25	3	200	29.756	0.901	33.015	26.818	8.895	27	8	0.556	0.448
3.015	0.25	3	200	29.756	0.901	33.015	26.818	8.895	27	9	0.563	0.448
3.015	0.25	3	200	29.756	0.901	33.015	26.818	8.895	27	10	0.601	0.448
3.015	0.25	3	200	29.756	0.901	33.015	26.818	8.895	27	11	0.631	0.448
3.015	0.25	3	200	29.756	0.901	33.015	26.818	8.895	27	12	0.746	0.448
3.015	0.25	3	200	29.756	0.901	33.015	26.818	8.895	27	13	1.225	0.448
3.015	0.25	3	35	48.277	1.648	29.287	79.577	26.394	79	5	0.431	0.271
3.015	0.25	3	35	48.277	1.648	29.287	79.577	26.394	79	6	0.389	0.271
3.015	0.25	3	35	48.277	1.648	29.287	79.577	26.394	79	7	0.434	0.271
3.015	0.25	3	35	48.277	1.648	29.287	79.577	26.394	79	9	0.411	0.271
3.015	0.25	3	35	48.277	1.648	29.287	79.577	26.394	79	11	0.534	0.271
3.015	0.25	3	35	48.277	1.648	29.287	79.577	26.394	79	13	0.299	0.271
3.015	0.25	3	35	48.277	1.648	29.287	79.577	26.394	79	15	0.284	0.271
3.015	0.25	3	35	48.277	1.648	29.287	79.577	26.394	79	17	0.311	0.271
3.015	0.25	3	35	48.277	1.648	29.287	79.577	26.394	79	19	0.382	0.271
3.015	0.25	3	35	48.277	1.648	29.287	79.577	26.394	79	21	0.463	0.271
3.015	0.25	3	35	48.277	1.648	29.287	79.577	26.394	79	23	0.481	0.271
3.015	0.25	3	35	48.277	1.648	29.287	79.577	26.394	79	25	0.386	0.271
3.015	0.25	3	35	48.277	1.648	29.287	79.577	26.394	79	27	0.348	0.271
3.015	0.25	3	35	48.277	1.648	29.287	79.577	26.394	79	29	0.327	0.271
3.015	0.25	3	35	48.277	1.648	29.287	79.577	26.394	79	31	0.520	0.271

3.015	0.25	3	35	48.277	1.648	29.287	79.577	26.394	79	32	0.660	0.271
3.015	0.25	3	35	48.277	1.648	29.287	79.577	26.394	79	33	0.917	0.271
3.015	0.25	3	50	48.279	1.628	29.658	78.590	26.066	77	5	0.494	0.413
3.015	0.25	3	50	48.279	1.628	29.658	78.590	26.066	77	6	0.359	0.413
3.015	0.25	3	50	48.279	1.628	29.658	78.590	26.066	77	7	0.440	0.413
3.015	0.25	3	50	48.279	1.628	29.658	78.590	26.066	77	9	0.366	0.413
3.015	0.25	3	50	48.279	1.628	29.658	78.590	26.066	77	11	0.546	0.413
3.015	0.25	3	50	48.279	1.628	29.658	78.590	26.066	77	13	0.326	0.413
3.015	0.25	3	50	48.279	1.628	29.658	78.590	26.066	77	15	0.274	0.413
3.015	0.25	3	50	48.279	1.628	29.658	78.590	26.066	77	17	0.340	0.413
3.015	0.25	3	50	48.279	1.628	29.658	78.590	26.066	77	19	0.416	0.413
3.015	0.25	3	50	48.279	1.628	29.658	78.590	26.066	77	21	0.619	0.413
3.015	0.25	3	50	48.279	1.628	29.658	78.590	26.066	77	23	0.419	0.413
3.015	0.25	3	50	48.279	1.628	29.658	78.590	26.066	77	25	0.404	0.413
3.015	0.25	3	50	48.279	1.628	29.658	78.590	26.066	77	27	0.339	0.413
3.015	0.25	3	50	48.279	1.628	29.658	78.590	26.066	77	29	0.373	0.413
3.015	0.25	3	50	48.279	1.628	29.658	78.590	26.066	77	30	0.480	0.413
3.015	0.25	3	50	48.279	1.628	29.658	78.590	26.066	77	31	0.566	0.413
3.015	0.25	3	50	48.279	1.628	29.658	78.590	26.066	77	32	0.795	0.413
3.015	0.25	3	50	48.279	1.628	29.658	78.590	26.066	77	33	1.120	0.413
3.015	0.25	3	100	48.278	1.566	30.837	75.582	25.069	73	5	0.553	0.550
3.015	0.25	3	100	48.278	1.566	30.837	75.582	25.069	73	7	0.468	0.550
3.015	0.25	3	100	48.278	1.566	30.837	75.582	25.069	73	9	0.479	0.550
3.015	0.25	3	100	48.278	1.566	30.837	75.582	25.069	73	11	0.501	0.550
3.015	0.25	3	100	48.278	1.566	30.837	75.582	25.069	73	13	0.400	0.550
3.015	0.25	3	100	48.278	1.566	30.837	75.582	25.069	73	15	0.379	0.550
3.015	0.25	3	100	48.278	1.566	30.837	75.582	25.069	73	17	0.401	0.550
3.015	0.25	3	100	48.278	1.566	30.837	75.582	25.069	73	19	0.440	0.550
3.015	0.25	3	100	48.278	1.566	30.837	75.582	25.069	73	21	0.511	0.550
3.015	0.25	3	100	48.278	1.566	30.837	75.582	25.069	73	23	0.418	0.550
3.015	0.25	3	100	48.278	1.566	30.837	75.582	25.069	73	25	0.367	0.550
3.015	0.25	3	100	48.278	1.566	30.837	75.582	25.069	73	27	0.352	0.550
3.015	0.25	3	100	48.278	1.566	30.837	75.582	25.069	73	28	0.442	0.550
3.015	0.25	3	100	48.278	1.566	30.837	75.582	25.069	73	29	0.602	0.550
3.015	0.25	3	100	48.278	1.566	30.837	75.582	25.069	73	30	0.702	0.550
3.015	0.25	3	100	48.278	1.566	30.837	75.582	25.069	73	31	0.987	0.550
3.015	0.25	3	150	48.289	1.511	31.961	72.957	24.198	69	5	0.401	0.414
3.015	0.25	3	150	48.289	1.511	31.961	72.957	24.198	69	7	0.446	0.414
3.015	0.25	3	150	48.289	1.511	31.961	72.957	24.198	69	9	0.362	0.414
3.015	0.25	3	150	48.289	1.511	31.961	72.957	24.198	69	11	0.478	0.414
3.015	0.25	3	150	48.289	1.511	31.961	72.957	24.198	69	13	0.393	0.414
3.015	0.25	3	150	48.289	1.511	31.961	72.957	24.198	69	15	0.427	0.414
3.015	0.25	3	150	48.289	1.511	31.961	72.957	24.198	69	17	0.441	0.414
3.015	0.25	3	150	48.289	1.511	31.961	72.957	24.198	69	19	0.556	0.414
3.015	0.25	3	150	48.289	1.511	31.961	72.957	24.198	69	21	0.440	0.414
3.015	0.25	3	150	48.289	1.511	31.961	72.957	24.198	69	23	0.394	0.414
3.015	0.25	3	150	48.289	1.511	31.961	72.957	24.198	69	25	0.407	0.414
3.015	0.25	3	150	48.289	1.511	31.961	72.957	24.198	69	27	0.518	0.414
3.015	0.25	3	150	48.289	1.511	31.961	72.957	24.198	69	28	0.750	0.414
3.015	0.25	3	150	48.289	1.511	31.961	72.957	24.198	69	29	1.014	0.414
3.015	0.25	3	200	48.293	1.462	33.039	70.590	23.413	#N/A	5	0.449	0.541
3.015	0.25	3	200	48.293	1.462	33.039	70.590	23.413	#N/A	7	0.497	0.541
3.015	0.25	3	200	48.293	1.462	33.039	70.590	23.413	#N/A	9	0.657	0.541
3.015	0.25	3	200	48.293	1.462	33.039	70.590	23.413	#N/A	11	0.461	0.541
3.015	0.25	3	200	48.293	1.462	33.039	70.590	23.413	#N/A	13	0.425	0.541
3.015	0.25	3	200	48.293	1.462	33.039	70.590	23.413	#N/A	15	0.409	0.541

3.015	0.25	3	200	48.293	1.462	33.039	70.590	23.413	#N/A	17	0.472	0.541
3.015	0.25	3	200	48.293	1.462	33.039	70.590	23.413	#N/A	19	0.524	0.541
3.015	0.25	3	200	48.293	1.462	33.039	70.590	23.413	#N/A	21	0.466	0.541
3.015	0.25	3	200	48.293	1.462	33.039	70.590	23.413	#N/A	23	0.396	0.541
3.015	0.25	3	200	48.293	1.462	33.039	70.590	23.413	#N/A	25	0.468	0.541
3.015	0.25	3	200	48.293	1.462	33.039	70.590	23.413	#N/A	26	0.592	0.541
3.015	0.25	3	200	48.293	1.462	33.039	70.590	23.413	#N/A	27	0.731	0.541
3.015	0.25	3	200	48.293	1.462	33.039	70.590	23.413	#N/A	28	1.065	0.541
0.5	0.25	3	35	5.784	1.149	5.036	6.644	13.288	38	5	0.358	0.421
0.5	0.25	3	35	5.784	1.149	5.036	6.644	13.288	38	7	0.342	0.421
0.5	0.25	3	35	5.784	1.149	5.036	6.644	13.288	38	9	0.384	0.421
0.5	0.25	3	35	5.784	1.149	5.036	6.644	13.288	38	11	0.317	0.421
0.5	0.25	3	35	5.784	1.149	5.036	6.644	13.288	38	13	0.322	0.421
0.5	0.25	3	35	5.784	1.149	5.036	6.644	13.288	38	15	0.569	0.421
0.5	0.25	3	35	5.784	1.149	5.036	6.644	13.288	39	16	0.796	0.421
0.5	0.25	3	35	5.784	1.149	5.036	6.644	13.288	38	17	1.131	0.421
0.5	0.25	3	50	5.786	1.135	5.096	6.569	13.138	37	5	0.330	0.612
0.5	0.25	3	50	5.786	1.135	5.096	6.569	13.138	37	7	0.388	0.612
0.5	0.25	3	50	5.786	1.135	5.096	6.569	13.138	37	9	0.431	0.612
0.5	0.25	3	50	5.786	1.135	5.096	6.569	13.138	37	11	0.306	0.612
0.5	0.25	3	50	5.786	1.135	5.096	6.569	13.138	37	13	0.304	0.612
0.5	0.25	3	50	5.786	1.135	5.096	6.569	13.138	37	15	0.661	0.612
0.5	0.25	3	50	5.786	1.135	5.096	6.569	13.138	37	16	0.843	0.612
0.5	0.25	3	100	5.790	1.095	5.286	6.343	12.686	35	5	0.346	0.590
0.5	0.25	3	100	5.790	1.095	5.286	6.343	12.686	35	7	0.424	0.590
0.5	0.25	3	100	5.790	1.095	5.286	6.343	12.686	35	9	0.436	0.590
0.5	0.25	3	100	5.790	1.095	5.286	6.343	12.686	35	11	0.441	0.590
0.5	0.25	3	100	5.790	1.095	5.286	6.343	12.686	35	13	0.424	0.590
0.5	0.25	3	100	5.790	1.095	5.286	6.343	12.686	35	15	0.720	0.590
0.5	0.25	3	100	5.790	1.095	5.286	6.343	12.686	35	16	1.046	0.590
0.5	0.25	3	150	5.796	1.061	5.462	6.151	12.302	34	5	0.406	0.352
0.5	0.25	3	150	5.796	1.061	5.462	6.151	12.302	34	7	0.507	0.352
0.5	0.25	3	150	5.796	1.061	5.462	6.151	12.302	34	9	0.458	0.352
0.5	0.25	3	150	5.796	1.061	5.462	6.151	12.302	34	11	0.426	0.352
0.5	0.25	3	150	5.796	1.061	5.462	6.151	12.302	34	13	0.541	0.352
0.5	0.25	3	150	5.796	1.061	5.462	6.151	12.302	34	14	0.698	0.352
0.5	0.25	3	150	5.796	1.061	5.462	6.151	12.302	34	15	0.964	0.352
0.5	0.25	3	200	5.798	1.031	5.623	5.978	11.957	33	5	0.469	0.958
0.5	0.25	3	200	5.798	1.031	5.623	5.978	11.957	33	7	0.549	0.958
0.5	0.25	3	200	5.798	1.031	5.623	5.978	11.957	33	9	0.515	0.958
0.5	0.25	3	200	5.798	1.031	5.623	5.978	11.957	33	11	0.536	0.958
0.5	0.25	3	200	5.798	1.031	5.623	5.978	11.957	33	12	0.518	0.958
0.5	0.25	3	200	5.798	1.031	5.623	5.978	11.957	33	13	0.577	0.958
0.5	0.25	3	200	5.798	1.031	5.623	5.978	11.957	33	14	0.772	0.958
0.5	0.25	3	35	6.713	1.331	5.044	8.934	17.868	50	5	0.296	0.358
0.5	0.25	3	35	6.713	1.331	5.044	8.934	17.868	50	9	0.341	0.358
0.5	0.25	3	35	6.713	1.331	5.044	8.934	17.868	50	14	0.357	0.358
0.5	0.25	3	35	6.713	1.331	5.044	8.934	17.868	50	17	0.292	0.358
0.5	0.25	3	35	6.713	1.331	5.044	8.934	17.868	50	21	0.720	0.358
0.5	0.25	3	35	6.713	1.331	5.044	8.934	17.868	50	22	0.945	0.358
0.5	0.25	3	50	6.710	1.315	5.103	8.821	17.642	50	5	0.334	0.748
0.5	0.25	3	50	6.710	1.315	5.103	8.821	17.642	50	8	0.286	0.748
0.5	0.25	3	50	6.710	1.315	5.103	8.821	17.642	50	11	0.386	0.748
0.5	0.25	3	50	6.710	1.315	5.103	8.821	17.642	50	14	0.347	0.748
0.5	0.25	3	50	6.710	1.315	5.103	8.821	17.642	50	17	0.293	0.748
0.5	0.25	3	50	6.710	1.315	5.103	8.821	17.642	50	20	0.545	0.748

0.5	0.25	3	50	6.710	1.315	5.103	8.821	17.642	50	21	0.705	0.748
0.5	0.25	3	50	6.710	1.315	5.103	8.821	17.642	50	22	1.011	0.748
0.5	0.25	3	100	6.707	1.268	5.290	8.504	17.007	48	5	0.353	0.331
0.5	0.25	3	100	6.707	1.268	5.290	8.504	17.007	48	8	0.320	0.331
0.5	0.25	3	100	6.707	1.268	5.290	8.504	17.007	48	11	0.428	0.331
0.5	0.25	3	100	6.707	1.268	5.290	8.504	17.007	48	14	0.359	0.331
0.5	0.25	3	100	6.707	1.268	5.290	8.504	17.007	48	17	0.347	0.331
0.5	0.25	3	100	6.707	1.268	5.290	8.504	17.007	48	20	0.693	0.331
0.5	0.25	3	100	6.707	1.268	5.290	8.504	17.007	48	21	0.950	0.331
0.5	0.25	3	150	6.707	1.228	5.462	8.235	16.471	45	5	0.370	0.656
0.5	0.25	3	150	6.707	1.228	5.462	8.235	16.471	45	8	0.350	0.656
0.5	0.25	3	150	6.707	1.228	5.462	8.235	16.471	45	11	0.424	0.656
0.5	0.25	3	150	6.707	1.228	5.462	8.235	16.471	45	14	0.440	0.656
0.5	0.25	3	150	6.707	1.228	5.462	8.235	16.471	45	17	0.444	0.656
0.5	0.25	3	150	6.707	1.228	5.462	8.235	16.471	45	19	0.731	0.656
0.5	0.25	3	150	6.707	1.228	5.462	8.235	16.471	45	20	0.964	0.656
0.5	0.25	3	200	6.710	1.193	5.624	8.005	16.011	44	5	0.416	0.732
0.5	0.25	3	200	6.710	1.193	5.624	8.005	16.011	44	8	0.384	0.732
0.5	0.25	3	200	6.710	1.193	5.624	8.005	16.011	44	11	0.527	0.732
0.5	0.25	3	200	6.710	1.193	5.624	8.005	16.011	44	14	0.485	0.732
0.5	0.25	3	200	6.710	1.193	5.624	8.005	16.011	44	17	0.495	0.732
0.5	0.25	3	200	6.710	1.193	5.624	8.005	16.011	44	18	0.646	0.732
0.5	0.25	3	200	6.710	1.193	5.624	8.005	16.011	44	19	0.885	0.732
0.5	0.25	3	35	7.657	1.516	5.050	11.609	23.218	64	5	0.449	0.398
0.5	0.25	3	35	7.657	1.516	5.050	11.609	23.218	64	9	0.349	0.398
0.5	0.25	3	35	7.657	1.516	5.050	11.609	23.218	64	13	0.389	0.398
0.5	0.25	3	35	7.657	1.516	5.050	11.609	23.218	64	17	0.355	0.398
0.5	0.25	3	35	7.657	1.516	5.050	11.609	23.218	64	21	0.325	0.398
0.5	0.25	3	35	7.657	1.516	5.050	11.609	23.218	64	25	0.384	0.398
0.5	0.25	3	35	7.657	1.516	5.050	11.609	23.218	64	26	0.561	0.398
0.5	0.25	3	35	7.657	1.516	5.050	11.609	23.218	64	27	0.713	0.398
0.5	0.25	3	35	7.657	1.516	5.050	11.609	23.218	64	28	0.993	0.398
0.5	0.25	3	50	7.659	1.499	5.110	11.480	22.960	64	5	0.449	0.486
0.5	0.25	3	50	7.659	1.499	5.110	11.480	22.960	64	9	0.318	0.486
0.5	0.25	3	50	7.659	1.499	5.110	11.480	22.960	64	13	0.342	0.486
0.5	0.25	3	50	7.659	1.499	5.110	11.480	22.960	64	17	0.313	0.486
0.5	0.25	3	50	7.659	1.499	5.110	11.480	22.960	64	21	0.345	0.486
0.5	0.25	3	50	7.659	1.499	5.110	11.480	22.960	64	25	0.461	0.486
0.5	0.25	3	50	7.659	1.499	5.110	11.480	22.960	64	26	0.655	0.486
0.5	0.25	3	50	7.659	1.499	5.110	11.480	22.960	64	27	0.828	0.486
0.5	0.25	3	100	7.662	1.447	5.296	11.086	22.171	62	5	0.409	0.695
0.5	0.25	3	100	7.662	1.447	5.296	11.086	22.171	62	9	0.337	0.695
0.5	0.25	3	100	7.662	1.447	5.296	11.086	22.171	62	13	0.389	0.695
0.5	0.25	3	100	7.662	1.447	5.296	11.086	22.171	62	17	0.406	0.695
0.5	0.25	3	100	7.662	1.447	5.296	11.086	22.171	62	21	0.351	0.695
0.5	0.25	3	100	7.662	1.447	5.296	11.086	22.171	62	25	0.653	0.695
0.5	0.25	3	100	7.662	1.447	5.296	11.086	22.171	62	26	0.748	0.695
0.5	0.25	3	100	7.662	1.447	5.296	11.086	22.171	62	27	0.988	0.695
0.5	0.25	3	150	7.670	1.403	5.466	10.763	21.527	60	5	0.407	0.527
0.5	0.25	3	150	7.670	1.403	5.466	10.763	21.527	60	9	0.373	0.527
0.5	0.25	3	150	7.670	1.403	5.466	10.763	21.527	60	13	0.443	0.527
0.5	0.25	3	150	7.670	1.403	5.466	10.763	21.527	60	17	0.365	0.527
0.5	0.25	3	150	7.670	1.403	5.466	10.763	21.527	60	21	0.387	0.527
0.5	0.25	3	150	7.670	1.403	5.466	10.763	21.527	60	24	0.646	0.527
0.5	0.25	3	150	7.670	1.403	5.466	10.763	21.527	60	25	0.831	0.527
0.5	0.25	3	200	7.676	1.364	5.625	10.473	20.946	59	5	0.446	0.594

0.5	0.25	3	200	7.676	1.364	5.625	10.473	20.946	59	9	0.414	0.594
0.5	0.25	3	200	7.676	1.364	5.625	10.473	20.946	59	13	0.396	0.594
0.5	0.25	3	200	7.676	1.364	5.625	10.473	20.946	59	17	0.426	0.594
0.5	0.25	3	200	7.676	1.364	5.625	10.473	20.946	59	21	0.491	0.594
0.5	0.25	3	200	7.676	1.364	5.625	10.473	20.946	59	23	0.608	0.594
0.5	0.25	3	200	7.676	1.364	5.625	10.473	20.946	59	24	0.795	0.594
0.5	0.25	3	35	8.673	1.706	5.082	14.800	29.599	83	5	0.528	0.405
0.5	0.25	3	35	8.673	1.706	5.082	14.800	29.599	83	7	0.478	0.405
0.5	0.25	3	35	8.673	1.706	5.082	14.800	29.599	83	9	0.605	0.405
0.5	0.25	3	35	8.673	1.706	5.082	14.800	29.599	83	11	0.662	0.405
0.5	0.25	3	35	8.673	1.706	5.082	14.800	29.599	83	13	0.429	0.405
0.5	0.25	3	35	8.673	1.706	5.082	14.800	29.599	83	15	0.385	0.405
0.5	0.25	3	35	8.673	1.706	5.082	14.800	29.599	83	17	0.543	0.405
0.5	0.25	3	35	8.673	1.706	5.082	14.800	29.599	83	19	0.611	0.405
0.5	0.25	3	35	8.673	1.706	5.082	14.800	29.599	83	21	0.651	0.405
0.5	0.25	3	35	8.673	1.706	5.082	14.800	29.599	83	23	0.404	0.405
0.5	0.25	3	35	8.673	1.706	5.082	14.800	29.599	83	25	0.423	0.405
0.5	0.25	3	35	8.673	1.706	5.082	14.800	29.599	83	27	0.383	0.405
0.5	0.25	3	35	8.673	1.706	5.082	14.800	29.599	83	29	0.370	0.405
0.5	0.25	3	35	8.673	1.706	5.082	14.800	29.599	83	31	0.407	0.405
0.5	0.25	3	35	8.673	1.706	5.082	14.800	29.599	83	33	0.625	0.405
0.5	0.25	3	35	8.673	1.706	5.082	14.800	29.599	83	34	0.744	0.405
0.5	0.25	3	35	8.673	1.706	5.082	14.800	29.599	83	35	0.960	0.405
0.5	0.25	3	35	8.673	1.706	5.082	14.800	29.599	83	36	1.194	0.405
0.5	0.25	3	50	8.668	1.688	5.134	14.636	29.271	81	5	0.538	0.554
0.5	0.25	3	50	8.668	1.688	5.134	14.636	29.271	81	7	0.431	0.554
0.5	0.25	3	50	8.668	1.688	5.134	14.636	29.271	81	9	0.419	0.554
0.5	0.25	3	50	8.668	1.688	5.134	14.636	29.271	81	11	0.421	0.554
0.5	0.25	3	50	8.668	1.688	5.134	14.636	29.271	81	13	0.426	0.554
0.5	0.25	3	50	8.668	1.688	5.134	14.636	29.271	81	15	0.441	0.554
0.5	0.25	3	50	8.668	1.688	5.134	14.636	29.271	81	17	0.552	0.554
0.5	0.25	3	50	8.668	1.688	5.134	14.636	29.271	81	19	0.391	0.554
0.5	0.25	3	50	8.668	1.688	5.134	14.636	29.271	81	21	0.421	0.554
0.5	0.25	3	50	8.668	1.688	5.134	14.636	29.271	81	23	0.384	0.554
0.5	0.25	3	50	8.668	1.688	5.134	14.636	29.271	81	25	0.421	0.554
0.5	0.25	3	50	8.668	1.688	5.134	14.636	29.271	81	27	0.344	0.554
0.5	0.25	3	50	8.668	1.688	5.134	14.636	29.271	81	29	0.396	0.554
0.5	0.25	3	50	8.668	1.688	5.134	14.636	29.271	81	31	0.496	0.554
0.5	0.25	3	50	8.668	1.688	5.134	14.636	29.271	81	32	0.617	0.554
0.5	0.25	3	50	8.668	1.688	5.134	14.636	29.271	81	33	0.649	0.554
0.5	0.25	3	50	8.668	1.688	5.134	14.636	29.271	81	34	0.856	0.554
0.5	0.25	3	100	8.671	1.634	5.308	14.165	28.330	79	5	0.592	0.458
0.5	0.25	3	100	8.671	1.634	5.308	14.165	28.330	79	7	0.488	0.458
0.5	0.25	3	100	8.671	1.634	5.308	14.165	28.330	79	9	0.452	0.458
0.5	0.25	3	100	8.671	1.634	5.308	14.165	28.330	79	11	0.436	0.458
0.5	0.25	3	100	8.671	1.634	5.308	14.165	28.330	79	13	0.448	0.458
0.5	0.25	3	100	8.671	1.634	5.308	14.165	28.330	79	15	0.427	0.458
0.5	0.25	3	100	8.671	1.634	5.308	14.165	28.330	79	17	0.536	0.458
0.5	0.25	3	100	8.671	1.634	5.308	14.165	28.330	79	19	0.462	0.458
0.5	0.25	3	100	8.671	1.634	5.308	14.165	28.330	79	21	0.391	0.458
0.5	0.25	3	100	8.671	1.634	5.308	14.165	28.330	79	23	0.390	0.458
0.5	0.25	3	100	8.671	1.634	5.308	14.165	28.330	79	25	0.403	0.458
0.5	0.25	3	100	8.671	1.634	5.308	14.165	28.330	79	27	0.395	0.458
0.5	0.25	3	100	8.671	1.634	5.308	14.165	28.330	79	29	0.432	0.458
0.5	0.25	3	100	8.671	1.634	5.308	14.165	28.330	79	31	0.537	0.458
0.5	0.25	3	100	8.671	1.634	5.308	14.165	28.330	79	32	0.631	0.458

0.5	0.25	3	100	8.671	1.634	5.308	14.165	28.330	79	33	0.822	0.458
0.5	0.25	3	100	8.671	1.634	5.308	14.165	28.330	79	34	0.960	0.458
0.5	0.25	3	150	8.677	1.585	5.474	13.756	27.512	77	5	0.681	0.452
0.5	0.25	3	150	8.677	1.585	5.474	13.756	27.512	77	7	0.543	0.452
0.5	0.25	3	150	8.677	1.585	5.474	13.756	27.512	77	9	0.499	0.452
0.5	0.25	3	150	8.677	1.585	5.474	13.756	27.512	77	11	0.464	0.452
0.5	0.25	3	150	8.677	1.585	5.474	13.756	27.512	77	13	0.432	0.452
0.5	0.25	3	150	8.677	1.585	5.474	13.756	27.512	77	15	0.456	0.452
0.5	0.25	3	150	8.677	1.585	5.474	13.756	27.512	77	17	0.502	0.452
0.5	0.25	3	150	8.677	1.585	5.474	13.756	27.512	77	19	0.396	0.452
0.5	0.25	3	150	8.677	1.585	5.474	13.756	27.512	77	21	0.408	0.452
0.5	0.25	3	150	8.677	1.585	5.474	13.756	27.512	77	23	0.418	0.452
0.5	0.25	3	150	8.677	1.585	5.474	13.756	27.512	77	25	0.410	0.452
0.5	0.25	3	150	8.677	1.585	5.474	13.756	27.512	77	27	0.379	0.452
0.5	0.25	3	150	8.677	1.585	5.474	13.756	27.512	77	29	0.481	0.452
0.5	0.25	3	150	8.677	1.585	5.474	13.756	27.512	77	30	0.527	0.452
0.5	0.25	3	150	8.677	1.585	5.474	13.756	27.512	77	31	0.613	0.452
0.5	0.25	3	150	8.677	1.585	5.474	13.756	27.512	77	32	0.786	0.452
0.5	0.25	3	150	8.677	1.585	5.474	13.756	27.512	77	33	0.914	0.452
0.5	0.25	3	200	8.674	1.542	5.625	13.374	26.748	#N/A	5	0.678	0.466
0.5	0.25	3	200	8.674	1.542	5.625	13.374	26.748	#N/A	7	0.505	0.466
0.5	0.25	3	200	8.674	1.542	5.625	13.374	26.748	#N/A	9	0.540	0.466
0.5	0.25	3	200	8.674	1.542	5.625	13.374	26.748	#N/A	11	0.468	0.466
0.5	0.25	3	200	8.674	1.542	5.625	13.374	26.748	#N/A	13	0.513	0.466
0.5	0.25	3	200	8.674	1.542	5.625	13.374	26.748	#N/A	15	0.495	0.466
0.5	0.25	3	200	8.674	1.542	5.625	13.374	26.748	#N/A	17	0.624	0.466
0.5	0.25	3	200	8.674	1.542	5.625	13.374	26.748	#N/A	19	0.484	0.466
0.5	0.25	3	200	8.674	1.542	5.625	13.374	26.748	#N/A	21	0.472	0.466
0.5	0.25	3	200	8.674	1.542	5.625	13.374	26.748	#N/A	23	0.486	0.466
0.5	0.25	3	200	8.674	1.542	5.625	13.374	26.748	#N/A	25	0.494	0.466
0.5	0.25	3	200	8.674	1.542	5.625	13.374	26.748	#N/A	27	0.461	0.466
0.5	0.25	3	200	8.674	1.542	5.625	13.374	26.748	#N/A	29	0.591	0.466
0.5	0.25	3	200	8.674	1.542	5.625	13.374	26.748	#N/A	30	0.737	0.466
0.5	0.25	3	200	8.674	1.542	5.625	13.374	26.748	#N/A	31	0.814	0.466
0.5	0.25	3	35	9.616	1.906	5.046	18.324	36.649	103	5	0.614	0.262
0.5	0.25	3	35	9.616	1.906	5.046	18.324	36.649	103	10	0.623	0.262
0.5	0.25	3	35	9.616	1.906	5.046	18.324	36.649	103	15	0.438	0.262
0.5	0.25	3	35	9.616	1.906	5.046	18.324	36.649	103	20	0.430	0.262
0.5	0.25	3	35	9.616	1.906	5.046	18.324	36.649	103	25	0.436	0.262
0.5	0.25	3	35	9.616	1.906	5.046	18.324	36.649	103	30	0.402	0.262
0.5	0.25	3	35	9.616	1.906	5.046	18.324	36.649	103	35	0.408	0.262
0.5	0.25	3	35	9.619	1.902	5.057	18.296	36.593	103	40	0.609	0.262
0.5	0.25	3	35	9.619	1.902	5.057	18.296	36.593	103	41	0.732	0.262
0.5	0.25	3	35	9.619	1.902	5.057	18.296	36.593	103	42	0.903	0.262
0.5	0.25	3	50	9.621	1.879	5.119	18.079	36.158	99	5	0.594	0.343
0.5	0.25	3	50	9.621	1.879	5.119	18.079	36.158	99	10	0.439	0.343
0.5	0.25	3	50	9.621	1.879	5.119	18.079	36.158	99	15	0.444	0.343
0.5	0.25	3	50	9.621	1.879	5.119	18.079	36.158	99	20	0.560	0.343
0.5	0.25	3	50	9.621	1.879	5.119	18.079	36.158	99	25	0.403	0.343
0.5	0.25	3	50	9.621	1.879	5.119	18.079	36.158	99	30	0.414	0.343
0.5	0.25	3	50	9.621	1.879	5.119	18.079	36.158	99	35	0.404	0.343
0.5	0.25	3	50	9.621	1.879	5.119	18.079	36.158	99	39	0.720	0.343
0.5	0.25	3	50	9.621	1.879	5.119	18.079	36.158	99	40	0.767	0.343
0.5	0.25	3	100	9.621	1.815	5.302	17.458	34.916	96	5	0.775	0.353
0.5	0.25	3	100	9.621	1.815	5.302	17.458	34.916	96	10	0.554	0.353
0.5	0.25	3	100	9.621	1.815	5.302	17.458	34.916	96	15	0.486	0.353

0.5	0.25	3	100	9.621	1.815	5.302	17.458	34.916	96	20	0.450	0.353
0.5	0.25	3	100	9.621	1.815	5.302	17.458	34.916	96	25	0.438	0.353
0.5	0.25	3	100	9.621	1.815	5.302	17.458	34.916	96	30	0.448	0.353
0.5	0.25	3	100	9.621	1.815	5.302	17.458	34.916	96	35	0.508	0.353
0.5	0.25	3	100	9.621	1.815	5.302	17.458	34.916	96	38	0.744	0.353
0.5	0.25	3	100	9.621	1.815	5.302	17.458	34.916	96	39	0.842	0.353
0.5	0.25	3	150	9.623	1.759	5.470	16.930	33.860	94	5	0.795	0.406
0.5	0.25	3	150	9.623	1.759	5.470	16.930	33.860	94	10	0.625	0.406
0.5	0.25	3	150	9.623	1.759	5.470	16.930	33.860	94	15	0.539	0.406
0.5	0.25	3	150	9.623	1.759	5.470	16.930	33.860	94	20	0.465	0.406
0.5	0.25	3	150	9.623	1.759	5.470	16.930	33.860	94	25	0.436	0.406
0.5	0.25	3	150	9.623	1.759	5.470	16.930	33.860	94	30	0.468	0.406
0.5	0.25	3	150	9.623	1.759	5.470	16.930	33.860	94	35	0.548	0.406
0.5	0.25	3	150	9.623	1.759	5.470	16.930	33.860	94	37	0.709	0.406
0.5	0.25	3	150	9.623	1.759	5.470	16.930	33.860	94	38	0.737	0.406
0.5	0.25	3	150	9.623	1.759	5.470	16.930	33.860	94	39	0.917	0.406
0.5	0.25	3	200	9.623	1.710	5.627	16.455	32.909	#N/A	5	0.765	0.676
0.5	0.25	3	200	9.623	1.710	5.627	16.455	32.909	#N/A	10	0.553	0.676
0.5	0.25	3	200	9.623	1.710	5.627	16.455	32.909	#N/A	15	0.551	0.676
0.5	0.25	3	200	9.623	1.710	5.627	16.455	32.909	#N/A	20	0.489	0.676
0.5	0.25	3	200	9.623	1.710	5.627	16.455	32.909	#N/A	25	0.469	0.676
0.5	0.25	3	200	9.623	1.710	5.627	16.455	32.909	#N/A	30	0.500	0.676

Table C - 18: Data from the ballistic heating testing for maximum offset. Various column dimensions [length (L.), inner diameter (I.D.)] were tested at a flow of 3 mL/min and at oven temperatures of 35 °C, 50 °C, 100 °C, 150 °C, and 200 °C. Power supply output [voltage (V), current (I)] was measured at the ²DTPS. The resistance (Ω), power (W), and power normalized to the length (W/m) were calculated from the measured values. The temperature offset achieved at 1 s, 2 s, and 3 s into the ballistic heating is shown. The maximum temperature offset was calculated from the average temperature offset between 5 s and 10 s. The data for the 0.5 m x 0.25 mm column was from the 2nd trial.

L. (m)	I.D. (mm)	Oven (°C)	V	I	Ω	W	W/m	1 s (°C)	2 s (°C)	3 s (°C)	Max (°C)
0.5	0.18	35	3.389	0.627	5.402	2.126	4.253	9	11	12	14
0.5	0.18	50	3.388	0.620	5.466	2.100	4.200	9	11	13	13
0.5	0.18	100	3.395	0.599	5.668	2.033	4.066	7	11	12	12
0.5	0.18	150	3.397	0.579	5.862	1.968	3.937	6	9	10	11
0.5	0.18	200	3.398	0.562	6.043	1.911	3.822	6	9	10	11
0.5	0.18	35	4.252	0.787	5.406	3.345	6.690	14	20	21	21
0.5	0.18	50	4.260	0.779	5.469	3.318	6.635	13	18	19	20
0.5	0.18	100	4.253	0.750	5.672	3.189	6.378	12	16	19	19
0.5	0.18	150	4.232	0.722	5.863	3.055	6.110	12	16	17	18
0.5	0.18	200	4.234	0.700	6.045	2.966	5.932	12	16	17	18
0.5	0.18	35	5.080	0.939	5.409	4.771	9.541	20	26	29	30
0.5	0.18	50	5.083	0.929	5.471	4.723	9.446	19	25	28	29
0.5	0.18	100	5.088	0.897	5.674	4.562	9.124	18	25	26	28
0.5	0.18	150	5.088	0.868	5.862	4.416	8.833	17	23	25	26
0.5	0.18	200	5.096	0.843	6.045	4.296	8.593	18	23	24	25
0.5	0.18	35	6.207	1.147	5.413	7.118	14.237	29	39	43	45
0.5	0.18	50	6.208	1.134	5.476	7.037	14.075	29	38	40	42
0.5	0.18	100	6.212	1.094	5.677	6.798	13.597	27	36	39	40
0.5	0.18	150	6.216	1.059	5.868	6.586	13.171	26	33	37	39
0.5	0.18	200	6.217	1.028	6.047	6.393	12.786	24	33	35	38
0.5	0.18	35	7.150	1.321	5.414	9.442	18.884	41	53	57	59
0.5	0.18	50	7.151	1.305	5.479	9.334	18.667	38	49	53	55
0.5	0.18	100	7.154	1.260	5.679	9.012	18.024	36	47	50	53
0.5	0.18	150	7.157	1.219	5.869	8.728	17.456	35	45	49	51
0.5	0.18	200	7.159	1.184	6.049	8.474	16.947	33	44	47	49
0.5	0.18	35	8.086	1.492	5.419	12.065	24.131	51	67	71	74
0.5	0.18	50	8.086	1.475	5.482	11.928	23.855	48	63	67	70
0.5	0.18	100	8.091	1.424	5.681	11.523	23.046	48	60	64	67
0.5	0.18	150	8.096	1.379	5.871	11.165	22.329	44	56	62	64
0.5	0.18	200	8.100	1.338	6.052	10.842	21.683	43	55	61	62
0.5	0.18	35	9.233	1.702	5.423	15.718	31.437	65	85	92	95
0.5	0.18	50	9.235	1.683	5.486	15.545	31.089	64	81	87	90
0.5	0.18	100	9.227	1.623	5.685	14.978	29.955	59	77	83	86
0.5	0.18	150	9.244	1.574	5.873	14.550	29.100	58	74	81	83
0.5	0.18	200	9.247	1.528	6.052	14.129	28.259	54	71	77	81
0.5	0.18	35	10.156	1.870	5.430	18.993	37.985	79	102	109	113
0.5	0.18	50	10.161	1.851	5.491	18.804	37.607	77	98	104	109
0.5	0.18	100	10.169	1.788	5.687	18.184	36.368	72	94	99	104
0.5	0.18	150	10.173	1.732	5.875	17.616	35.232	69	89	95	99

0.5	0.18	200	10.178	1.681	6.053	17.114	34.229	65	85	92	96
0.5	0.25	35	5.784	1.149	5.036	6.644	13.288	26	33	36	38
0.5	0.25	50	5.786	1.135	5.096	6.569	13.138	24	32	35	37
0.5	0.25	100	5.790	1.095	5.286	6.343	12.686	24	32	33	35
0.5	0.25	150	5.796	1.061	5.462	6.151	12.302	21	29	32	34
0.5	0.25	200	5.798	1.031	5.623	5.978	11.957	21	30	32	33
0.5	0.25	35	6.713	1.331	5.044	8.934	17.868	34	45	49	51
0.5	0.25	50	6.710	1.315	5.103	8.821	17.642	35	45	48	51
0.5	0.25	100	6.707	1.268	5.290	8.504	17.007	33	42	46	48
0.5	0.25	150	6.707	1.228	5.462	8.235	16.471	30	38	43	45
0.5	0.25	200	6.710	1.193	5.624	8.005	16.011	29	39	41	44
0.5	0.25	35	7.657	1.516	5.050	11.609	23.218	44	58	61	64
0.5	0.25	50	7.659	1.499	5.110	11.480	22.960	46	57	62	63
0.5	0.25	100	7.662	1.447	5.296	11.086	22.171	44	56	60	62
0.5	0.25	150	7.670	1.403	5.466	10.763	21.527	39	52	58	60
0.5	0.25	200	7.676	1.364	5.625	10.473	20.946	39	50	57	58
0.5	0.25	35	8.673	1.706	5.082	14.800	29.599	58	76	81	84
0.5	0.25	50	8.668	1.688	5.134	14.636	29.271	58	74	79	82
0.5	0.25	100	8.671	1.634	5.308	14.165	28.330	55	72	78	79
0.5	0.25	150	8.677	1.585	5.474	13.756	27.512	52	69	74	77
0.5	0.25	35	9.616	1.906	5.046	18.324	36.649	70	92	99	103
0.5	0.25	50	9.621	1.879	5.119	18.079	36.158	69	88	95	98
0.5	0.25	100	9.621	1.815	5.302	17.458	34.916	67	88	93	96
0.5	0.25	150	9.623	1.759	5.470	16.930	33.860	64	84	90	94
3.015	0.25	35	29.735	1.016	29.265	30.213	10.021	22	28	30	32
3.015	0.25	50	29.746	1.004	29.633	29.860	9.904	20	28	30	31
3.015	0.25	100	29.753	0.966	30.815	28.729	9.529	20	26	28	30
3.015	0.25	150	29.752	0.931	31.940	27.713	9.192	18	24	28	28
3.015	0.25	200	29.756	0.901	33.015	26.818	8.895	19	23	26	27
3.015	0.25	35	48.277	1.648	29.287	79.577	26.394	52	69	75	79
3.015	0.25	50	48.279	1.628	29.658	78.590	26.066	52	69	75	77
3.015	0.25	100	48.278	1.566	30.837	75.582	25.069	49	66	71	74
3.015	0.25	150	48.289	1.511	31.961	72.957	24.198	46	61	66	70

Table C - 19: Heating rate (1 s and 3 s duration) and maximum temperature offset results for the 0.5 m x 0.25 mm column, tested at a flow of 3 mL/min and at oven temperatures of 35 °C, 50 °C, 100 °C, 150 °C, and 200 °C. The power supply output [voltage (V), current (I)] was measured at the ²DTPS. The resistance (Ω) and power (W)were calculated from the measured values. The standard deviation (S.D.) was the S.D. of the Ω measurement (converted to °C) during the column calibration (temperature versus resistance) at the oven temperature. The offset (°C) was the temperature offset of the ²D temperature program. Highlighted in red was the maximum heating rate for each set of conditions.

Oven (°C)	V	I	Ω	W	Duration (s)	Offset (°C)	Rate (°C/s)	Max Offset (°C)	$\lvert\Delta T\rvert_{avg.}$ (°C)	S.D. (°C)
35	9.642	1.904	5.063	18.362	1	70	70.0	104	0.690	0.374
35	9.642	1.904	5.063	18.362	1	71	71.0	104	0.722	0.374
35	9.642	1.904	5.063	18.362	1	72	72.0	104	0.904	0.374
35	9.642	1.904	5.063	18.362	1	73	73.0	104	0.849	0.374
35	9.642	1.904	5.063	18.362	1	74	74.0	104	0.986	0.374
35	9.642	1.904	5.063	18.362	3	88	29.3	104	0.704	0.374
35	9.642	1.904	5.063	18.362	3	89	29.7	104	0.744	0.374
35	9.642	1.904	5.063	18.362	3	90	30.0	104	0.799	0.374
35	9.642	1.904	5.063	18.362	3	92	30.7	104	0.827	0.374
35	9.642	1.904	5.063	18.362	3	93	31.0	104	0.875	0.374
50	9.651	1.885	5.121	18.189	1	66	66.0	99	0.532	0.451
50	9.651	1.885	5.121	18.189	1	67	67.0	99	0.484	0.451
50	9.651	1.885	5.121	18.189	1	68	68.0	99	0.699	0.451
50	9.651	1.885	5.121	18.189	1	69	69.0	99	0.667	0.451
50	9.651	1.885	5.121	18.189	1	70	70.0	99	0.713	0.451
50	9.651	1.885	5.121	18.189	1	71	71.0	99	0.891	0.451
50	9.651	1.885	5.121	18.189	1	72	72.0	99	0.818	0.451
50	9.651	1.885	5.121	18.189	3	83	27.7	99	0.536	0.451
50	9.651	1.885	5.121	18.189	3	84	28.0	99	0.568	0.451
50	9.651	1.885	5.121	18.189	3	85	28.3	99	0.604	0.451
50	9.651	1.885	5.121	18.189	3	86	28.7	99	0.670	0.451
50	9.651	1.885	5.121	18.189	3	87	29.0	99	0.661	0.451
50	9.651	1.885	5.121	18.189	3	88	29.3	99	0.713	0.451
50	9.651	1.885	5.121	18.189	3	89	29.7	99	0.764	0.451
50	9.651	1.885	5.121	18.189	3	90	30.0	99	0.763	0.451
50	9.651	1.885	5.121	18.189	3	91	30.3	99	0.805	0.451
100	9.659	1.820	5.307	17.578	1	67	67.0	98	0.682	0.683
100	9.659	1.820	5.307	17.578	1	68	68.0	98	0.684	0.683
100	9.659	1.820	5.307	17.578	1	69	69.0	98	0.766	0.683
100	9.659	1.820	5.307	17.578	1	70	70.0	98	0.839	0.683
100	9.659	1.820	5.307	17.578	3	84	28.0	98	0.669	0.683
100	9.659	1.820	5.307	17.578	3	85	28.3	98	0.720	0.683
100	9.659	1.820	5.307	17.578	3	86	28.7	98	0.725	0.683
100	9.659	1.820	5.307	17.578	3	87	29.0	98	0.762	0.683
100	9.659	1.820	5.307	17.578	3	88	29.3	98	0.815	0.683
100	9.659	1.820	5.307	17.578	3	89	29.7	98	0.908	0.683
150	9.664	1.765	5.474	17.059	1	64	64.0	96	0.586	0.558
150	9.664	1.765	5.474	17.059	1	65	65.0	96	0.627	0.558
150	9.664	1.765	5.474	17.059	1	66	66.0	96	0.716	0.558

150	9.664	1.765	5.474	17.059	1	67	67.0	96	0.796	0.558
150	9.664	1.765	5.474	17.059	1	68	68.0	96	0.916	0.558
150	9.664	1.765	5.474	17.059	3	83	27.7	96	0.665	0.558
150	9.664	1.765	5.474	17.059	3	84	28.0	96	0.718	0.558
150	9.664	1.765	5.474	17.059	3	85	28.3	96	0.780	0.558
150	9.664	1.765	5.474	17.059	3	86	28.7	96	0.859	0.558
35	8.781	1.736	5.059	15.241	1	57	57.0	85	0.480	0.363
35	8.781	1.736	5.059	15.241	1	58	58.0	85	0.635	0.363
35	8.781	1.736	5.059	15.241	1	59	59.0	85	0.590	0.363
35	8.781	1.736	5.059	15.241	1	60	60.0	85	0.746	0.363
35	8.781	1.736	5.059	15.241	1	61	61.0	85	0.766	0.363
35	8.781	1.736	5.059	15.241	1	62	62.0	85	0.957	0.363
35	8.781	1.736	5.059	15.241	3	73	24.3	85	0.594	0.363
35	8.781	1.736	5.059	15.241	3	74	24.7	85	0.659	0.363
35	8.781	1.736	5.059	15.241	3	75	25.0	85	0.664	0.363
35	8.781	1.736	5.059	15.241	3	76	25.3	85	0.760	0.363
35	8.781	1.736	5.059	15.241	3	77	25.7	85	0.838	0.363
50	8.778	1.715	5.119	15.052	1	55	55.0	82	0.473	0.546
50	8.778	1.715	5.119	15.052	1	56	56.0	82	0.585	0.546
50	8.778	1.715	5.119	15.052	1	57	57.0	82	0.690	0.546
50	8.778	1.715	5.119	15.052	1	58	58.0	82	0.594	0.546
50	8.778	1.715	5.119	15.052	1	59	59.0	82	0.758	0.546
50	8.778	1.715	5.119	15.052	1	60	60.0	82	0.773	0.546
50	8.778	1.715	5.119	15.052	3	70	23.3	82	0.582	0.546
50	8.778	1.715	5.119	15.052	3	71	23.7	82	0.558	0.546
50	8.778	1.715	5.119	15.052	3	72	24.0	82	0.634	0.546
50	8.778	1.715	5.119	15.052	3	73	24.3	82	0.671	0.546
50	8.778	1.715	5.119	15.052	3	74	24.7	82	0.696	0.546
50	8.778	1.715	5.119	15.052	3	75	25.0	82	0.762	0.546
50	8.778	1.715	5.119	15.052	3	76	25.3	82	0.852	0.546
100	8.775	1.656	5.300	14.530	1	53	53.0	80	0.533	0.947
100	8.775	1.656	5.300	14.530	1	54	54.0	80	0.496	0.947
100	8.775	1.656	5.300	14.530	1	55	55.0	80	0.661	0.947
100	8.775	1.656	5.300	14.530	1	56	56.0	80	0.573	0.947
100	8.775	1.656	5.300	14.530	1	57	57.0	80	0.752	0.947
100	8.775	1.656	5.300	14.530	1	58	58.0	80	0.763	0.947
100	8.775	1.656	5.300	14.530	3	70	23.3	80	0.665	0.947
100	8.775	1.656	5.300	14.530	3	71	23.7	80	0.692	0.947
100	8.775	1.656	5.300	14.530	3	72	24.0	80	0.724	0.947
100	8.775	1.656	5.300	14.530	3	73	24.3	80	0.798	0.947
100	8.775	1.656	5.300	14.530	3	74	24.7	80	0.869	0.947
150	8.779	1.605	5.470	14.091	1	54	54.0	79	0.566	0.664
150	8.779	1.605	5.470	14.091	1	55	55.0	79	0.705	0.664
150	8.779	1.605	5.470	14.091	1	56	56.0	79	0.732	0.664
150	8.779	1.605	5.470	14.091	1	57	57.0	79	0.784	0.664
150	8.779	1.605	5.470	14.091	1	58	58.0	79	0.952	0.664

150	8.779	1.605	5.470	14.091	3	70	23.3	79	0.635	0.664
150	8.779	1.605	5.470	14.091	3	71	23.7	79	0.701	0.664
150	8.779	1.605	5.470	14.091	3	72	24.0	79	0.802	0.664
150	8.779	1.605	5.470	14.091	3	73	24.3	79	0.886	0.664
150	8.779	1.605	5.470	14.091	3	74	24.7	79	0.915	0.664
35	7.749	1.535	5.049	11.895	1	44	44.0	66	0.594	0.315
35	7.749	1.535	5.049	11.895	1	45	45.0	66	0.476	0.315
35	7.749	1.535	5.049	11.895	1	46	46.0	66	0.573	0.315
35	7.749	1.535	5.049	11.895	1	47	47.0	66	0.577	0.315
35	7.749	1.535	5.049	11.895	1	48	48.0	66	0.704	0.315
35	7.749	1.535	5.049	11.895	1	49	49.0	66	0.840	0.315
35	7.749	1.535	5.049	11.895	1	50	50.0	66	1.057	0.315
35	7.749	1.535	5.049	11.895	1	51	51.0	66	0.989	0.315
35	7.749	1.535	5.049	11.895	3	58	19.3	66	0.534	0.315
35	7.749	1.535	5.049	11.895	3	59	19.7	66	0.584	0.315
35	7.749	1.535	5.049	11.895	3	60	20.0	66	0.612	0.315
35	7.749	1.535	5.049	11.895	3	61	20.3	66	0.675	0.315
35	7.749	1.535	5.049	11.895	3	62	20.7	66	0.741	0.315
35	7.749	1.535	5.049	11.895	3	63	21.0	66	0.851	0.315
35	7.749	1.535	5.049	11.895	3	64	21.3	66	0.927	0.315
50	7.751	1.516	5.112	11.752	1	44	44.0	64	0.387	0.478
50	7.751	1.516	5.112	11.752	1	45	45.0	64	0.588	0.478
50	7.751	1.516	5.112	11.752	1	46	46.0	64	0.622	0.478
50	7.751	1.516	5.112	11.752	1	47	47.0	64	0.679	0.478
50	7.751	1.516	5.112	11.752	1	48	48.0	64	0.898	0.478
50	7.751	1.516	5.112	11.752	1	49	49.0	64	0.914	0.478
50	7.751	1.516	5.112	11.752	3	58	19.3	64	0.542	0.478
50	7.751	1.516	5.112	11.752	3	59	19.7	64	0.671	0.478
50	7.751	1.516	5.112	11.752	3	60	20.0	64	0.728	0.478
50	7.751	1.516	5.112	11.752	3	61	20.3	64	0.777	0.478
50	7.751	1.516	5.112	11.752	3	62	20.7	64	0.914	0.478
100	7.752	1.464	5.296	11.346	1	44	44.0	63	0.518	0.568
100	7.752	1.464	5.296	11.346	1	45	45.0	63	0.698	0.568
100	7.752	1.464	5.296	11.346	1	46	46.0	63	0.740	0.568
100	7.752	1.464	5.296	11.346	1	47	47.0	63	0.902	0.568
100	7.752	1.464	5.296	11.346	1	48	48.0	63	1.034	0.568
100	7.752	1.464	5.296	11.346	3	57	19.0	63	0.651	0.568
100	7.752	1.464	5.296	11.346	3	58	19.3	63	0.696	0.568
100	7.752	1.464	5.296	11.346	3	59	19.7	63	0.734	0.568
100	7.752	1.464	5.296	11.346	3	60	20.0	63	0.842	0.568
100	7.752	1.464	5.296	11.346	3	61	20.3	63	0.938	0.568
150	7.761	1.420	5.466	11.020	1	42	42.0	61	0.624	0.361
150	7.761	1.420	5.466	11.020	1	43	43.0	61	0.596	0.361
150	7.761	1.420	5.466	11.020	1	44	44.0	61	0.714	0.361
150	7.761	1.420	5.466	11.020	1	45	45.0	61	0.768	0.361
150	7.761	1.420	5.466	11.020	1	46	46.0	61	0.929	0.361

150	7.761	1.420	5.466	11.020	3	54	18.0	61	0.553	0.361
150	7.761	1.420	5.466	11.020	3	55	18.3	61	0.617	0.361
150	7.761	1.420	5.466	11.020	3	56	18.7	61	0.660	0.361
150	7.761	1.420	5.466	11.020	3	57	19.0	61	0.742	0.361
150	7.761	1.420	5.466	11.020	3	58	19.3	61	0.783	0.361
150	7.761	1.420	5.466	11.020	3	59	19.7	61	0.883	0.361
200	7.769	1.382	5.623	10.735	1	40	40.0	59	0.588	0.748
200	7.769	1.382	5.623	10.735	1	41	41.0	59	0.627	0.748
200	7.769	1.382	5.623	10.735	1	42	42.0	59	0.709	0.748
200	7.769	1.382	5.623	10.735	1	43	43.0	59	0.777	0.748
200	7.769	1.382	5.623	10.735	1	44	44.0	59	0.961	0.748
200	7.769	1.382	5.623	10.735	1	45	45.0	59	1.016	0.748
200	7.769	1.382	5.623	10.735	3	53	17.7	59	0.652	0.748
200	7.769	1.382	5.623	10.735	3	54	18.0	59	0.701	0.748
200	7.769	1.382	5.623	10.735	3	55	18.3	59	0.709	0.748
200	7.769	1.382	5.623	10.735	3	56	18.7	59	0.800	0.748
200	7.769	1.382	5.623	10.735	3	57	19.0	59	0.899	0.748
35	6.804	1.351	5.035	9.195	1	34	34.0	51	0.532	0.504
35	6.804	1.351	5.035	9.195	1	35	35.0	51	0.498	0.504
35	6.804	1.351	5.035	9.195	1	36	36.0	51	0.513	0.504
35	6.804	1.351	5.035	9.195	1	37	37.0	51	0.616	0.504
35	6.804	1.351	5.035	9.195	1	38	38.0	51	0.774	0.504
35	6.804	1.351	5.035	9.195	1	39	39.0	51	0.916	0.504
35	6.804	1.351	5.035	9.195	3	45	15.0	51	0.518	0.504
35	6.804	1.351	5.035	9.195	3	46	15.3	51	0.583	0.504
35	6.804	1.351	5.035	9.195	3	47	15.7	51	0.594	0.504
35	6.804	1.351	5.035	9.195	3	48	16.0	51	0.712	0.504
35	6.804	1.351	5.035	9.195	3	49	16.3	51	0.775	0.504
35	6.804	1.351	5.035	9.195	3	50	16.7	51	0.861	0.504
50	6.799	1.334	5.097	9.070	1	34	34.0	50	0.591	0.229
50	6.799	1.334	5.097	9.070	1	35	35.0	50	0.483	0.229
50	6.799	1.334	5.097	9.070	1	36	36.0	50	0.533	0.229
50	6.799	1.334	5.097	9.070	1	37	37.0	50	0.720	0.229
50	6.799	1.334	5.097	9.070	1	38	38.0	50	0.982	0.229
50	6.799	1.334	5.097	9.070	1	39	39.0	50	1.050	0.229
50	6.799	1.334	5.097	9.070	1	45	45.0	50	0.596	0.229
50	6.799	1.334	5.097	9.070	1	46	46.0	50	0.690	0.229
50	6.799	1.334	5.097	9.070	1	47	47.0	50	0.719	0.229
50	6.799	1.334	5.097	9.070	1	48	48.0	50	0.878	0.229
50	6.799	1.334	5.097	9.070	1	49	49.0	50	0.944	0.229
100	6.806	1.288	5.285	8.765	1	33	33.0	49	0.472	0.562
100	6.806	1.288	5.285	8.765	1	34	34.0	49	0.537	0.562
100	6.806	1.288	5.285	8.765	1	35	35.0	49	0.549	0.562
100	6.806	1.288	5.285	8.765	1	36	36.0	49	0.725	0.562
100	6.806	1.288	5.285	8.765	1	37	37.0	49	0.863	0.562
100	6.806	1.288	5.285	8.765	1	38	38.0	49	1.032	0.562

100	6.806	1.288	5.285	8.765	3	44	14.7	49	0.563	0.562
100	6.806	1.288	5.285	8.765	3	45	15.0	49	0.658	0.562
100	6.806	1.288	5.285	8.765	3	46	15.3	49	0.738	0.562
100	6.806	1.288	5.285	8.765	3	47	15.7	49	0.770	0.562
100	6.806	1.288	5.285	8.765	3	48	16.0	49	0.907	0.562
150	6.815	1.248	5.460	8.508	1	32	32.0	47	0.551	0.523
150	6.815	1.248	5.460	8.508	1	33	33.0	47	0.645	0.523
150	6.815	1.248	5.460	8.508	1	34	34.0	47	0.69	0.523
150	6.815	1.248	5.460	8.508	1	35	35.0	47	0.816	0.523
150	6.815	1.248	5.460	8.508	1	36	36.0	47	1.062	0.523
150	6.815	1.248	5.460	8.508	3	42	14.0	47	0.559	0.523
150	6.815	1.248	5.460	8.508	3	43	14.3	47	0.641	0.523
150	6.815	1.248	5.460	8.508	3	44	14.7	47	0.758	0.523
150	6.815	1.248	5.460	8.508	3	45	15.0	47	0.809	0.523
150	6.815	1.248	5.460	8.508	3	46	15.3	47	0.911	0.523
200	6.820	1.213	5.620	8.275	1	31	31.0	46	0.545	0.738
200	6.820	1.213	5.620	8.275	1	32	32.0	46	0.618	0.738
200	6.820	1.213	5.620	8.275	1	33	33.0	46	0.766	0.738
200	6.820	1.213	5.620	8.275	1	34	34.0	46	0.948	0.738
200	6.820	1.213	5.620	8.275	1	35	35.0	46	1.129	0.738
200	6.820	1.213	5.620	8.275	3	40	13.3	46	0.564	0.738
200	6.820	1.213	5.620	8.275	3	41	13.7	46	0.612	0.738
200	6.820	1.213	5.620	8.275	3	42	14.0	46	0.717	0.738
200	6.820	1.213	5.620	8.275	3	43	14.3	46	0.783	0.738
200	6.820	1.213	5.620	8.275	3	44	14.7	46	0.900	0.738
35	5.807	1.154	5.030	6.703	1	25	25.0	37	0.614	0.462
35	5.807	1.154	5.030	6.703	1	26	26.0	37	0.570	0.462
35	5.807	1.154	5.030	6.703	1	27	27.0	37	0.686	0.462
35	5.807	1.154	5.030	6.703	1	28	28.0	37	0.886	0.462
35	5.807	1.154	5.030	6.703	1	29	29.0	37	1.034	0.462
35	5.807	1.154	5.030	6.703	3	31	10.3	37	0.501	0.462
35	5.807	1.154	5.030	6.703	3	32	10.7	37	0.470	0.462
35	5.807	1.154	5.030	6.703	3	33	11.0	37	0.590	0.462
35	5.807	1.154	5.030	6.703	3	34	11.3	37	0.599	0.462
35	5.807	1.154	5.030	6.703	3	35	11.7	37	0.686	0.462
35	5.807	1.154	5.030	6.703	3	36	12.0	37	0.796	0.462
50	5.811	1.141	5.091	6.633	1	25	25.0	36	0.513	0.716
50	5.811	1.141	5.091	6.633	1	26	26.0	36	0.525	0.716
50	5.811	1.141	5.091	6.633	1	27	27.0	36	0.608	0.716
50	5.811	1.141	5.091	6.633	1	28	28.0	36	0.727	0.716
50	5.811	1.141	5.091	6.633	1	29	29.0	36	0.943	0.716
50	5.811	1.141	5.091	6.633	3	31	10.3	36	0.460	0.716
50	5.811	1.141	5.091	6.633	3	32	10.7	36	0.506	0.716
50	5.811	1.141	5.091	6.633	3	33	11.0	36	0.592	0.716
50	5.811	1.141	5.091	6.633	3	34	11.3	36	0.601	0.716
50	5.811	1.141	5.091	6.633	3	35	11.7	36	0.686	0.716

50	5.811	1.141	5.091	6.633	1	36	36.0	36	0.791	0.716
100	5.814	1.101	5.281	6.401	1	24	24.0	35	0.466	0.589
100	5.814	1.101	5.281	6.401	1	25	25.0	35	0.555	0.589
100	5.814	1.101	5.281	6.401	1	26	26.0	35	0.713	0.589
100	5.814	1.101	5.281	6.401	1	27	27.0	35	0.796	0.589
100	5.814	1.101	5.281	6.401	1	28	28.0	35	1.084	0.589
100	5.814	1.101	5.281	6.401	3	31	10.3	35	0.537	0.589
100	5.814	1.101	5.281	6.401	3	32	10.7	35	0.563	0.589
100	5.814	1.101	5.281	6.401	3	33	11.0	35	0.643	0.589
100	5.814	1.101	5.281	6.401	3	34	11.3	35	0.729	0.589
100	5.814	1.101	5.281	6.401	3	35	11.7	35	0.908	0.589
150	5.815	1.066	5.456	6.198	1	23	23.0	34	0.548	0.492
150	5.815	1.066	5.456	6.198	1	24	24.0	34	0.604	0.492
150	5.815	1.066	5.456	6.198	1	25	25.0	34	0.818	0.492
150	5.815	1.066	5.456	6.198	1	26	26.0	34	1.03	0.492
150	5.815	1.066	5.456	6.198	1	27	27.0	34	1.295	0.492
150	5.815	1.066	5.456	6.198	3	30	10.0	34	0.588	0.492
150	5.815	1.066	5.456	6.198	3	31	10.3	34	0.647	0.492
150	5.815	1.066	5.456	6.198	3	32	10.7	34	0.686	0.492
150	5.815	1.066	5.456	6.198	3	33	11.0	34	0.817	0.492
150	5.815	1.066	5.456	6.198	3	34	11.3	34	0.909	0.492
200	5.815	1.035	5.619	6.019	1	22	22.0	34	0.567	0.521
200	5.815	1.035	5.619	6.019	1	23	23.0	34	0.639	0.521
200	5.815	1.035	5.619	6.019	1	24	24.0	34	0.775	0.521
200	5.815	1.035	5.619	6.019	1	25	25.0	34	0.839	0.521
200	5.815	1.035	5.619	6.019	3	30	10.0	34	0.660	0.521
200	5.815	1.035	5.619	6.019	3	31	10.3	34	0.716	0.521
200	5.815	1.035	5.619	6.019	3	32	10.7	34	0.811	0.521
200	5.815	1.035	5.619	6.019	3	33	11.0	34	0.869	0.521
200	5.815	1.035	5.619	6.019	3	34	11.3	34	0.946	0.521

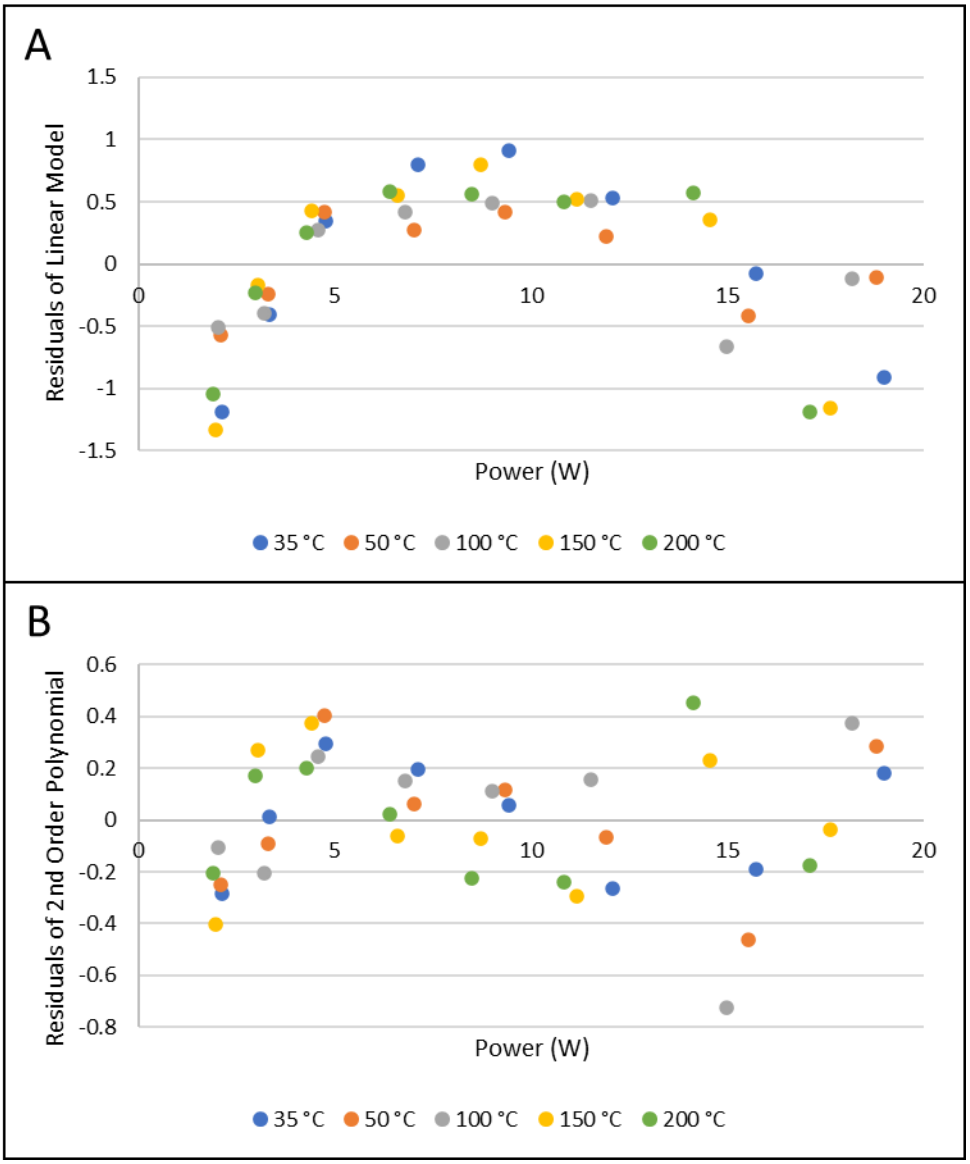

Figure C - 9: Residual plots for the maximum offset of the 0.5 m x 0.18 mm x 0.20 µm column at various PSU voltages (3.5 V, 4.5 V, 5.5 V, 6.5 V, 7.5 V, 8.5 V, 9.5 V, 10.5 V) and oven temperatures (35 °C, 50 °C, 100 °C, 150 °C, 200 °C) fitted to a linear model (A) and a second-order polynomial (B).

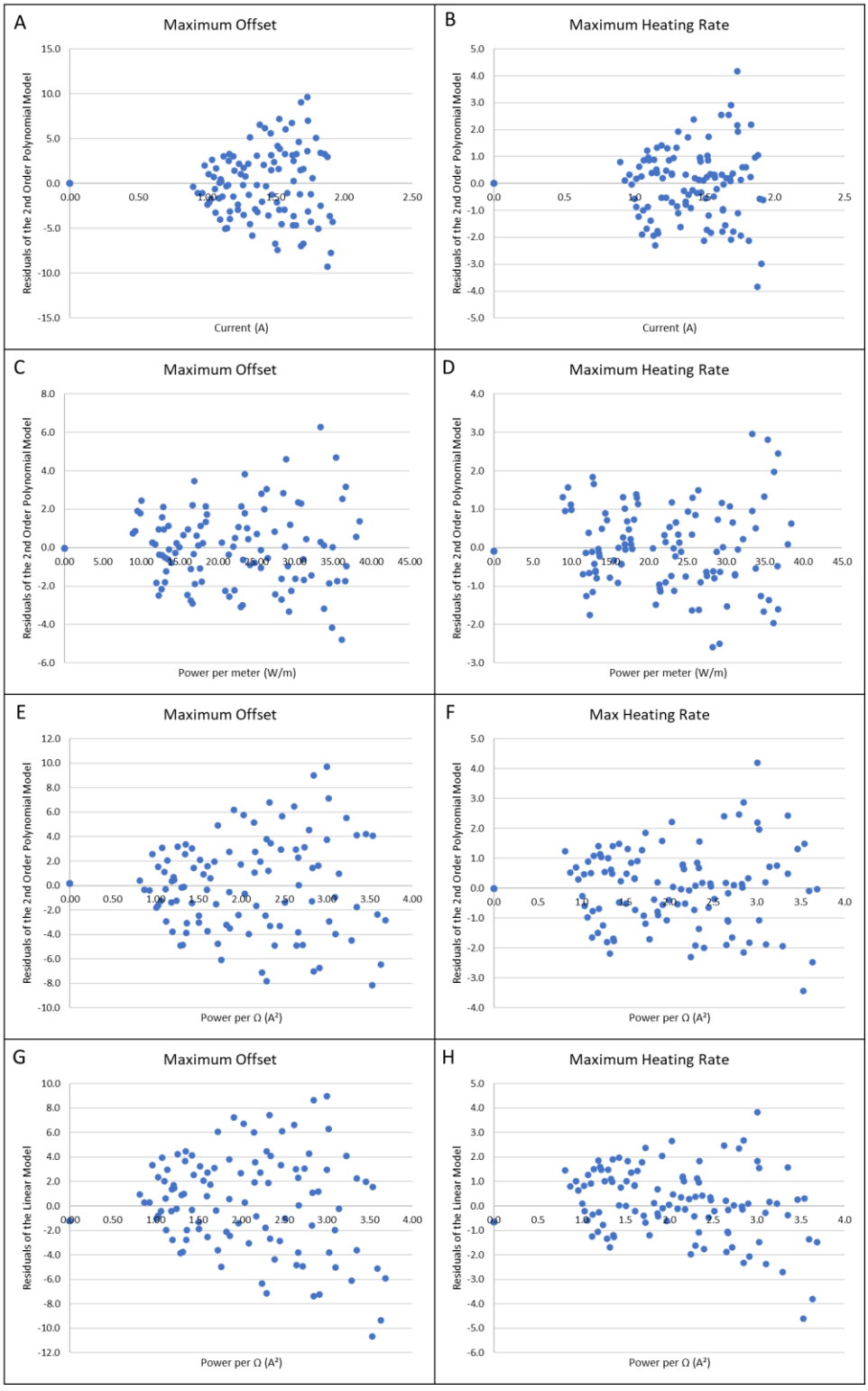

Figure C - 10: Residual plots (A to F: 2nd order polynomial, G/H: linear) for the maximum offset and heating rate of all columns (0.5 m x 0.25 mm, 1.0 m x 0.25 mm, 3.0 m x 0.25 mm, 0.5 m x 0.18 mm, 1.0 m x 0.18 mm) and oven temperatures (35 °C, 50 °C, 100 °C, 150 °C, 200 °C). Residual plots correspond to the plots found in Figure 4-35. G/H are residual plots for a linear model instead of the 2nd order polynomial model in E/F.

C: Windows Forms Application: Form1.cs

```
using System;
using Microsoft.VisualBasic.FileIO;
using System.ComponentModel;
using System.Threading;
using System.IO;
using System.IO.Ports;
using System.Windows.Forms;
using System.Data;
using System.Linq;
using System.Text;
using System.Drawing;
using System.Windows.Forms.DataVisualization.Charting;

namespace Temperature_Programming
{
    public partial class Form1 : Form
    {
        DataTable programs = new DataTable();

        //create a mirror of the dataTable which has filepaths instead of
file names
        DataTable sequenceFile = new DataTable();

        //data table to display in sequence
        DataTable sequence = new DataTable();

        Boolean constantOffsetMode = false;
        StringBuilder storeData = new StringBuilder();
        private Thread readThread = null;

        public Form1()
        {
            InitializeComponent();
            getAvailablePorts();
        }
        private void Form1_Load(object sender, EventArgs e)
        {
            DataColumn modulationStart = new DataColumn();
            modulationStart.DataType =
System.Type.GetType("System.Decimal");
            modulationStart.ColumnName = "Retention Time (min)";
            modulationStart.DefaultValue = 0;

            DataColumn tempOffset = new DataColumn();
            tempOffset.DataType = System.Type.GetType("System.Decimal");
            tempOffset.ColumnName = "Offset (°C)";
            tempOffset.DefaultValue = 50;

            DataColumn delay = new DataColumn();
            delay.DataType = System.Type.GetType("System.Decimal");
            delay.ColumnName = "Delay (ms)";
            delay.DefaultValue = 1500;

            DataColumn ramp = new DataColumn();
```

```
                ramp.DataType = System.Type.GetType("System.Decimal");
                ramp.ColumnName = "Ramp (ms)";
                ramp.DefaultValue = 1000;

                DataColumn constant = new DataColumn();
                constant.DataType = System.Type.GetType("System.Decimal");
                constant.ColumnName = "Constant (ms)";
                constant.DefaultValue = 1000;

                DataColumn cool = new DataColumn();
                cool.DataType = System.Type.GetType("System.Decimal");
                cool.ColumnName = "Cool (ms)";
                cool.DefaultValue = 500;

                DataColumn modulationPeriod = new DataColumn();
                modulationPeriod.DataType =
System.Type.GetType("System.Decimal");
                modulationPeriod.ColumnName = "Modulation Period (s)";
                modulationPeriod.Expression = "([Delay (ms)] + [Ramp (ms)] +
[Constant (ms)] + [Cool (ms)])/1000";

                programs.Columns.Add(modulationStart);
                programs.Columns.Add(tempOffset);
                programs.Columns.Add(delay);
                programs.Columns.Add(ramp);
                programs.Columns.Add(constant);
                programs.Columns.Add(cool);
                programs.Columns.Add(modulationPeriod);

                DataRow program1 = programs.NewRow();
                DataRow program2 = programs.NewRow();
                DataRow program3 = programs.NewRow();
                programs.Rows.Add(program1);
                programs.Rows.Add(program2);
                programs.Rows.Add(program3);
                ModulationProgram.DataSource = programs;
                ModulationProgram.AutoResizeColumns();
                ModulationProgram.BackgroundColor = Color.White;
                ModulationProgram.RowHeadersVisible = false;

                DataColumn FilePath = new DataColumn();
                FilePath.DataType = System.Type.GetType("System.String");
                FilePath.ColumnName = "FilePath";

                DataColumn ModProg = new DataColumn();
                ModProg.DataType = System.Type.GetType("System.String");
                ModProg.ColumnName = "Program";

                DataColumn Runs = new DataColumn();
                Runs.DataType = System.Type.GetType("System.Decimal");
                Runs.ColumnName = "Runs";
                Runs.DefaultValue = 0;

                DataColumn RunsMirror = new DataColumn();
                RunsMirror.DataType = System.Type.GetType("System.Decimal");
                RunsMirror.ColumnName = "Runs";
                RunsMirror.DefaultValue = 0;
```

```
            sequence.Columns.Add(ModProg);
            sequence.Columns.Add(Runs);
            sequenceFile.Columns.Add(FilePath);
            sequenceFile.Columns.Add(RunsMirror);
            SequenceObj.DataSource = sequence;
            SequenceObj.Columns[0].Width = 170;
            SequenceObj.Columns[1].Width = 40;
            SequenceObj.RowHeadersVisible = false;
        }
        void getAvailablePorts()
        {
            String[] ports = SerialPort.GetPortNames();
            ComPortComboBox.Items.AddRange(ports);
        }
        private void OpenPortButton_Click(object sender, EventArgs e)
        {
            try
            {
                if (ComPortComboBox.Text == "" || BaudRateComboBox.Text ==
""")
                {
                    FunctionsText.Text = "Please select serial port
settings";
                }
                else
                {
                    serialPort1.PortName = ComPortComboBox.Text;
                    serialPort1.BaudRate =
Convert.ToInt32(BaudRateComboBox.Text);
                    serialPort1.Parity = Parity.None;
                    serialPort1.StopBits = StopBits.One;
                    serialPort1.DataBits = 8;
                    serialPort1.Handshake = Handshake.None;
                    serialPort1.DtrEnable = true;
                    serialPort1.Open();

                    LoadCSV.Enabled = true;
                    SaveCSV.Enabled = true;
                    AddMethod.Enabled = true;
                    MinusMethod.Enabled = true;
                    StartSequence.Enabled = true;
                    HeatPulseSetButton.Enabled = true;
                    FinalPIDSet.Enabled = true;
                    ConstPIDSet.Enabled = true;
                    OpenPortButton.Enabled = false;
                    SetIntercept.Enabled = true;
                    StartCalibration.Enabled = true;
                    StopCalibration.Enabled = false;
                    ClosePortButton.Enabled = true;
                    ConstantOffset.Enabled = true;
                    ClearData.Enabled = true;
                    TempLimitSetButton.Enabled = true;
                    StartSequence.Enabled = true;
                    FunctionsText.Text = "Standby Mode";

                    readThread = new Thread(new ThreadStart(this.Read));
```

```
                readThread.Start();
            }
        }
        catch (UnauthorizedAccessException)
        {
            FunctionsText.Text = "Unauthorized access";
        }
    }
    private void ClosePortButton_Click(object sender, EventArgs e)
    {
        serialPort1.Close();
        HeatPulseSetButton.Enabled = false;
        FinalPIDSet.Enabled = false;
        ConstPIDSet.Enabled = false;
        OpenPortButton.Enabled = true;
        ClosePortButton.Enabled = false;
        StartCalibration.Enabled = false;
        StopCalibration.Enabled = false;
        SetIntercept.Enabled = false;
        TempLimitSetButton.Enabled = false;
        StartSequence.Enabled = false;
    }
    public void Read()
    {
        int counter = 0;
        while (serialPort1.IsOpen)
        {
            try
            {
                if (serialPort1.BytesToRead > 0)
                {
                    if (counter < 10)
                    {
                        string message = serialPort1.ReadLine();
                        counter++;
                    }
                    else
                    {
                        string message = serialPort1.ReadLine();
                        this.handleData(message);
                    }
                }
            }
            catch (Exception)
            {
            }
        }
    }
    private void handleData(string data)
    {
        this.Invoke((MethodInvoker)delegate
{ printSerialData(data); });
        DateTime datetime = DateTime.Now;
        double oaDate = datetime.ToOADate();
        string[] arrList = data.Split(new char[] { ' ' });
        if (arrList.Length == 2)
        {
```

```
                    string setpoint = arrList[0];
                    string temperature = arrList[1];
                    double setpointValue = Convert.ToDouble(setpoint);
                    double temperatureValue = Convert.ToDouble(temperature);
                    double delta = Math.Round(temperatureValue -
setpointValue, 2);
                    this.Invoke((MethodInvoker)delegate { drawGraph(datetime,
oaDate, setpointValue, temperatureValue, delta); });
                }
            }
            private void drawGraph(DateTime datetime, double oaDate, double
setpoint, double temperature, double delta)
            {
                TemperatureProgramChart.Series[0].Points.AddXY(oaDate,
setpoint);
                TemperatureProgramChart.Series[1].Points.AddXY(oaDate,
temperature);

                double removeBefore = datetime.AddSeconds((double)(10) * (-
1)).ToOADate();
                while (TemperatureProgramChart.Series[1].Points[0].XValue <
removeBefore)
                {
                    TemperatureProgramChart.Series[0].Points.RemoveAt(0);
                    TemperatureProgramChart.Series[1].Points.RemoveAt(0);
                }

                TemperatureProgramChart.ChartAreas[0].AxisX.Minimum =
TemperatureProgramChart.Series[1].Points[0].XValue;
                TemperatureProgramChart.ChartAreas[0].AxisX.Maximum =
DateTime.FromOADate(TemperatureProgramChart.Series[1].Points[0].XValue).AddSe
conds(10).ToOADate();
                TemperatureProgramChart.ChartAreas[0].RecalculateAxesScale();
                TemperatureProgramChart.Invalidate();
            }
            private void printSerialData(string data)
            {
                string[] systemReady = { "System", "Ready", "and",
"Waiting" };
                string[] stop = { "Stop" };
                string[] start = { "Start" };
                if (systemReady.Any(data.Contains))
                {
                    checkScroll.Checked = false;
                    StartSequence.Enabled = false;
                    AddMethod.Enabled = false;
                    MinusMethod.Enabled = false;
                    LoadCSV.Enabled = false;
                    SaveCSV.Enabled = false;
                    FunctionsText.Text = "GC Ready about to Run";
                }
                if (start.Any(data.Contains))
                {
                    FunctionsText.Text = "Run Started";
                }
                if (stop.Any(data.Contains))
                {
```

```
                StartSequence.Enabled = true;
                StartCalibration.Enabled = true;
                StopCalibration.Enabled = false;
                LoadCSV.Enabled = true;
                SaveCSV.Enabled = true;
                AddMethod.Enabled = true;
                MinusMethod.Enabled = true;
                checkScroll.Checked = true;
                runEnded();
                FunctionsText.Text = "Standby Mode";
            }
            if (checkScroll.Checked)
            {
                if (storeData.Length > 1)
                {
                    SerialData.AppendText(storeData.ToString());
                    storeData.Clear();
                }
                SerialData.AppendText(data + "\n");
                SerialData.ScrollToCaret();
            }
            else
            {
                storeData.Append(data + "\n");
            }
        }
        private void runEnded()
        {
            int NumberofRuns = int.Parse(sequence.Rows[0][1].ToString());
            if(NumberofRuns - 1 > 0)
            {
                sequence.Rows[0][1] = NumberofRuns - 1;
            }
            if(NumberofRuns - 1 == 0)
            {
                sequence.Rows.RemoveAt(0);
                sequenceFile.Rows.RemoveAt(0);
                nextMethod();
            }
        }
        private void nextMethod()
        {
            if(sequence.Rows.Count > 0)
            {
                int NumberofRuns =
int.Parse(sequence.Rows[0][1].ToString());
                if (NumberofRuns > 0)
                {
                    string methodpath =
sequenceFile.Rows[0][0].ToString();
                    BindData(methodpath);
                    System.Timers.Timer timer = new System.Timers.Timer();
                    timer.Interval = 1000;
                    timer.Elapsed += OnTimedEvent;
                    timer.AutoReset = false;
                    timer.Enabled = true;
                }
```

```
                    else
                    {
                        //remove all upcoming lines with 0 runs
                        while(NumberofRuns == 0)
                        {
                            sequence.Rows.RemoveAt(0);
                            sequenceFile.Rows.RemoveAt(0);
                            if (sequence.Rows.Count > 0)
                            {
                                NumberofRuns =
int.Parse(sequence.Rows[0][1].ToString());
                            }
                            //sequence completed
                            else
                            {
                                //break loop
                                NumberofRuns = 1;
                                string sequenceStop = "<Sequence F>";
                                serialPort1.WriteLine(sequenceStop);
                                FunctionsText.Text = sequenceStop;
                                checkScroll.Checked = true;
                                StartSequence.Enabled = true;
                                SerialData.AppendText("Sequence Completed" +
"\n");
                            }
                        }
                        if (sequence.Rows.Count > 0)
                        {
                            NumberofRuns =
int.Parse(sequence.Rows[0][1].ToString());
                            if (NumberofRuns > 0)
                            {
                                string methodpath =
sequenceFile.Rows[0][0].ToString();
                                BindData(methodpath);
                                System.Timers.Timer timer = new
System.Timers.Timer();
                                timer.Interval = 1000;
                                timer.Elapsed += OnTimedEvent;
                                timer.AutoReset = false;
                                timer.Enabled = true;
                            }
                        }
                    }
                }
                else
                {
                    string sequenceStop = "<Sequence F>";
                    checkScroll.Checked = true;
                    serialPort1.WriteLine(sequenceStop);
                    FunctionsText.Text = sequenceStop;
                    StartSequence.Enabled = true;
                    SerialData.AppendText("Sequence Completed" + "\n");
                }
            }
            private void setPID()
            {
```

```
            string Kp = Convert.ToString(this.Kp.Value);
            string Ki = Convert.ToString(this.Ki.Value);
            string Kd = Convert.ToString(this.Kd.Value);
            string PID = "<SetPID " + Kp + " " + Ki + " " + Kd + ">";
            serialPort1.WriteLine(PID);
            FunctionsText.Text = PID;
        }
        private void setConstPID()
        {
            string constKp = Convert.ToString(ConstKp.Value);
            string constKi = Convert.ToString(ConstKi.Value);
            string constKd = Convert.ToString(ConstKd.Value);
            string constPID = "<SetConstPID " + constKp + " " + constKi +
" " + constKd + ">";
            serialPort1.WriteLine(constPID);
            FunctionsText.Text = constPID;
        }
        private void setHeatPulse()
        {
            string heatWindow = Convert.ToString(HeatWindow.Value);
            string heatPulseWidth = "<SetHeatingPulseWidth " + heatWindow
+ ">";
            serialPort1.WriteLine(heatPulseWidth);
            FunctionsText.Text = heatPulseWidth;
        }
        private void constantOffset()
        {
            constantOffsetMode = !constantOffsetMode;
            if (constantOffsetMode)
            {
                StartCalibration.Enabled = true;
                StopCalibration.Enabled = false;
                Offset.Enabled = false;
                StartSequence.Enabled = false;
            }
            else
            {
                Offset.Enabled = true;
                StartSequence.Enabled = true;
            }
            string mode = constantOffsetMode.ToString();
            string finalOffset = Convert.ToString(this.Offset.Value);
            string ConstantOffset = "<ConstantOffset " + mode + " " +
finalOffset + ">";
            serialPort1.WriteLine(ConstantOffset);
            FunctionsText.Text = ConstantOffset;
        }
        private void endCalibration()
        {
            serialPort1.WriteLine("<StopCalibration>");
            constantOffsetMode = false;
            StartCalibration.Enabled = true;
            StopCalibration.Enabled = false;
            FunctionsText.Text = "Standby Mode";
        }
        private void beginCalibration()
        {
```

```
                serialPort1.WriteLine("<StartCalibration>");
                constantOffsetMode = false;
                StartCalibration.Enabled = false;
                StopCalibration.Enabled = true;
                FunctionsText.Text = "Calibration Mode";
            }
            private void setCalibration()
            {
                string coefficient2 =
Convert.ToString(Coefficient2Value.Value);
                string coefficient1 =
Convert.ToString(Coefficient1Value.Value);
                string coefficient0 =
Convert.ToString(Coefficient0Value.Value);
                string setCalibration = "<SC " + coefficient2 + " " +
coefficient1 + " " + coefficient0 + ">";
                serialPort1.WriteLine(setCalibration);
                FunctionsText.Text = setCalibration;
            }
            private void setColumnTempLimit()
            {
                string tempLimit = Convert.ToString(TempLimit.Value);
                string setTempLimit = "<LimitTemp " + tempLimit + ">";
                serialPort1.WriteLine(setTempLimit);
                FunctionsText.Text = setTempLimit;
            }
            private void setModulationProgram()
            {
                double runTimeValue = Convert.ToDouble(runTime.Value);
                string modulationPeriod = programs.Rows[0][6].ToString();
                double MP = Convert.ToDouble(modulationPeriod);
                double runTimeInModulations = runTimeValue * 60 / MP;
                StringBuilder ModulationProgram = new StringBuilder("<SM ");
                for (int i = 0; i < programs.Rows.Count; i++)
                {
                    for (int j = 0; j < programs.Columns.Count - 1; j++)
                    {
                        string value = programs.Rows[i][j].ToString();
                        if (j == 0)
                        {
                            double retentionTime = Convert.ToDouble(value);
                            int modulations = Convert.ToInt32(retentionTime *
60 / MP);
                            string mod = modulations.ToString();
                            ModulationProgram.Append(mod);
                        }
                        else
                        {
                            ModulationProgram.Append(value);
                        }
                        if ((i == programs.Rows.Count - 1) && (j ==
programs.Columns.Count - 2))
                        {
                            ModulationProgram.Append(" " +
runTimeInModulations.ToString() + ">");
                        }
                        else
```

```
            {
                ModulationProgram.Append(" ");
            }
        }
    }
    String command = ModulationProgram.ToString();
    FunctionsText.Text = command;
    serialPort1.WriteLine(command);
}

private void FinalPIDSet_Click(object sender, EventArgs e)
{
    setPID();
}
private void HeatPulseSetButton_Click(object sender, EventArgs e)
{
    setHeatPulse();
}
private void TempLimitSetButton_Click(object sender, EventArgs e)
{
    setColumnTempLimit();
}
private void StartCalibration_Click(object sender, EventArgs e)
{
    beginCalibration();
}
private void StopCalibration_Click(object sender, EventArgs e)
{
    endCalibration();
}
private void SetIntercept_Click(object sender, EventArgs e)
{
    setCalibration();
}
private void ConstPIDSet_Click(object sender, EventArgs e)
{
    setConstPID();
}
private void ConstantOffset_Click(object sender, EventArgs e)
{
    constantOffset();
}
private void ClearData_Click(object sender, EventArgs e)
{
    SerialData.Clear();
}
private void SaveCSV_Click(object sender, EventArgs e)
{
    //Build the CSV file data as a Comma separated string.
    string csv = string.Empty;

    //Adding the Rows
    foreach (DataGridViewRow row in ModulationProgram.Rows)
    {
        foreach (DataGridViewCell cell in row.Cells)
        {
            //Add the Data rows.
```

```
                    csv += cell.Value.ToString().Replace(",", ";") + ',';
                }

                //Add new line.
                csv += "\r\n";
            }
            csv += runTime.Value;
            //Exporting to CSV.
            saveFileDialog1.Filter = "|*.csv";
            saveFileDialog1.Title = "Save CSV File";
            //saveFileDialog1.ShowDialog();

            if (saveFileDialog1.ShowDialog() == DialogResult.OK)
            {
                    string folderPath = saveFileDialog1.FileName;
                    File.WriteAllText(saveFileDialog1.FileName, csv);
            }
        }
        private void LoadCSV_Click(object sender, EventArgs e)
        {
            openFileDialog1.ShowDialog();
            FunctionsText.Text = openFileDialog1.FileName;
            BindData(FunctionsText.Text);
        }
        private void BindData(string filePath)
        {
            string[] lines = System.IO.File.ReadAllLines(filePath);
            if (lines.Length > 0)
            {
                //For Data
                for (int i = 0; i < lines.Length; i++) //rows
                {
                    if (i<lines.Length-1)
                    {
                        string[] mod = lines[i].Split(',');
                        for (int j = 0; j < programs.Columns.Count - 1;
j++)
                        {
                            programs.Rows[i][j] = mod[j];
                        }
                    }
                    else
                    {
                        string runTimeString = lines[i];
                        runTime.Value = Convert.ToDecimal(runTimeString);
                    }
                }
            }
            if (programs.Rows.Count > 0)
            {
                ModulationProgram.DataSource = programs;
            }

        }
        private void SetModulationProgramButton_Click_1(object sender,
EventArgs e)
        {
```

```
            setModulationProgram();
        }
        private void AddMethod_Click(object sender, EventArgs e)
        {
            DataRow dr = sequenceFile.NewRow();
            DataRow mirror = sequence.NewRow();
            openFileDialog1.ShowDialog();
            dr[0] = openFileDialog1.FileName;
            mirror[0] =
Path.GetFileNameWithoutExtension(openFileDialog1.FileName);
            sequenceFile.Rows.Add(dr);
            sequence.Rows.Add(mirror);
        }
        private void StartSequence_Click(object sender, EventArgs e)
        {
            string sequenceStart = "<Sequence T>";
            serialPort1.WriteLine(sequenceStart);
            FunctionsText.Text = sequenceStart;
            nextMethod();
        }
        private void OnTimedEvent(Object source,
System.Timers.ElapsedEventArgs e)
        {
            setModulationProgram();
        }
        private void MinusMethod_Click(object sender, EventArgs e)
        {
            if(sequence.Rows.Count > 0)
            {
                sequence.Rows.RemoveAt(sequence.Rows.Count - 1);
            }
        }
    }
}
```

C: ²D Temperature Programming Sketch (Version 2.0)

```
   //https://jowood4.wordpress.com/2015/01/04/arduino-pid-temperature-
controller/
   //based on this PID Temperature Controller
   //ADS1115 Solingen library for 860sps
   static boolean recvInProgress = false;
   #include <Wire.h>
   #include <Adafruit_ADS1015.h>

   #include <SPI.h>
   #include "Adafruit_MAX31855.h"

   Adafruit_ADS1115 adsVolt(0x4A);  //addr>SDA
   Adafruit_ADS1115 adsCurrent(0x4B);  //addr>SCL
   #define DS3231_I2C_ADDRESS 0x68  //default address of DS3231

   //Pins
   const int clock32k = 2; //interrupt pin
   const int mosfet = 5;
   const int startRun = 4;
   const int stopRun = 3;
   const int systemReady = 6;

   //remote port
   int startSignal;
   int stopSignal;
   int readySignal;

   //thermocouple
   #define MAXDO   8
   #define MAXCS   9
   #define MAXCLK  10

   //Start/Stop/Standby
   boolean standby = true;
   long lastFalling = 0;
   long lastRising = 0;

   Adafruit_MAX31855 thermocouple(MAXCLK, MAXCS, MAXDO); //make sure the
library is modified for faster sample rate

   //Delay heating till modulation starts
   long modulateStamp = 0;

   //Temperature Measurement
   volatile bool continuousConversionReadyVolt = false;
   volatile bool continuousConversionReadyCurrent = false;
   double resultVolt;
   double resultCurrent;
   double resultResistance;
   int temperature;

   //Calibration
   boolean done = false;
   double x2 = 0.5466296018;
```

```
   double x1 = 9.514295802;
   double x0 = -717.6956054;

   //Constant Offset
   boolean constantOffset = false;
   boolean initialRead = true;

   //Temperature Ramp Parameters
   int state = 0; //start on state 0 (Standby)
   boolean channelDischarge = false; //false = discharge reset sequence
   boolean ramp = true; //true = linear ; false = Exponential
   float maxTemp; //in degrees C
   int tempLimit = 260;
   double constantOffsetValue = 10;
   const int program = 3; //max of 3 different programs
   const int temperatureProgram = 6; //6 parameters per program:
modulationCount, temperature offset, delay time, ramp time, const time, cool
time
   int modulationCount = 0;
   int runTime = 0;
   /* modulationCount, temperature offset, delay time, ramp time, const time,
cool time */
   int modulationProgram[program][temperatureProgram] =
   { {0, 50, 1500, 1000, 1000, 500},
     {2000, 50, 1500, 1000, 1000, 500},
     {3000, 50, 1500, 1000, 1000, 500}
   };
   int currentProgram = 0; //defines the current program being used. Ranges
from 0 - 2 (3 programs in total)
   /*
     modulationProgram[state + 1 + (program*6)]

     state 1 = delay
     state 2 = ramp
     state 3 = constant offset
     state 4 = cool

     program ranges from 0 - 2 (3 programs), starting with program 0 which is
used at the start of the GCxGC separation.
     Each program occupies the following index values in modulationProgram
[0,1,2,3,4,5], [6,7,8,9,10,11], [12,13,14,15,16,17].
     The first index value defines the modulation count (number of modulation
periods that have elapsed) before initiating the program (next 5 index
values:  temp, delay, ramp, const, cool).
     By default, the first index (0) is given a value of (0) since this
program is used by default from the start of the separation.
   */

   float rampRate;
   float startTemp;

   //Modulation Time
   long freq = 32761; // 1, 1024, 4096, 8192
   int modulation = 0; //in ms
   volatile unsigned long  count = 0;
   unsigned long ms = 0;
```

```
   ////Exponential Ramp
   //float  exponent = (log10(tempOffset)) / rampTime;
   //float rampRate = pow(10, exponent);

   //track period
   long currentTime;
   unsigned long lastTime, presentTime;
   double timeChange;
   long timeElapsed;
   long elapsedProgram;
   long windowStartTime;
   long printWindow;

   //delay temperature measurement (voltage takes time to stabilize after
turning on
   unsigned long heatOn;
   boolean heating = true;

   //PID parameters
   int window = 50;  //default: 75
   int minPulse = 4;
   int minOutput = minPulse + 1;
   double Kp = 20; //Ramp Proportional Gain
   double Ki = 1.0; //Ramp Integral Gain (reacts to difference)
   double Kd = 0.0; //Ramp Differential Gain (reduces over reaction)
   double constKp = 10; //Constant Offset Proportional Gain
   double constKi = 0.6; //Constant Offset Integral Gain (reacts to
difference)
   double constKd = 0.0; //Constant Offset Differential Gain (reduces over
reaction)
   double kp = Kp;
   double ki = Ki * window;
   double kd = Kd / window;
   double error;
   double dError;
   double iError;
   double lastError;
   double Input, Output, Setpoint;


   //delay/cooling
   int gate = LOW; //Mosfet gate LOW = OFF / HIGH = ON
   int reset = 0;

   //Oven Temperature
   int oven;

   //Temperature Filter
   double previousTemperature;

   //Stuff
   #define ARG_BUF_SIZE 24     //Maximum argument string length
   #define MAX_NUM_ARGS 20      //Maximum number of arguments

   char *args[MAX_NUM_ARGS];

   //Function declarations
```

```
   int SetPID();
   int SetConstPID();
   int SetHeatingPulseWidth();
   int SM(); //Set Modulation Program
   int StartCalibration();
   int StopCalibration();
   int SC(); //Set Calibration
   int LimitTemp();
   int ConstantOffset();

   //List of functions pointers corresponding to each command
   int (*commands_func[])()
   {
     &SetPID,
     &SetConstPID,
     &SetHeatingPulseWidth,
     &SM,
     &StartCalibration,
     &StopCalibration,
     &SC,
     &LimitTemp,
     &ConstantOffset
   };

   //List of command names
   const char *commands_str[] =
   {
     "SetPID",
     "SetConstPID",
     "SetHeatingPulseWidth",
     "SM",
     "StartCalibration",
     "StopCalibration",
     "SC",
     "LimitTemp",
     "ConstantOffset"
   };

   int num_commands = sizeof(commands_str) / sizeof(char *);

   const byte numChars = 150;
   char receivedChars[numChars];

   boolean newData = false;
   //stuff

   void setup(void)
   {
     Wire.begin();
     pinMode(clock32k, INPUT_PULLUP);
     pinMode(mosfet, OUTPUT);
     pinMode(startRun, INPUT);
     pinMode(stopRun, INPUT);
     pinMode(systemReady, INPUT);
     Serial.begin(38400);
//https://arduino.stackexchange.com/questions/296/how-high-of-a-baud-rate-
can-i-go-without-errors
```

```
    adsVolt.setGain(GAIN_TWOTHIRDS);  //Vout = (1/6)Vin : do not exceed
24.576V
    adsCurrent.setGain(GAIN_TWOTHIRDS);  //0.800V/A : do not exceed
5.12A(4.096V)

    // ads.setGain(GAIN_TWOTHIRDS);  // 2/3x gain +/- 6.144V  1 bit =
0.1875mV (default)
    // ads.setGain(GAIN_ONE);        // 1x gain   +/- 4.096V  1 bit =
0.125mV
    // ads.setGain(GAIN_TWO);        // 2x gain   +/- 2.048V  1 bit =
0.0625mV
    // ads.setGain(GAIN_FOUR);       // 4x gain   +/- 1.024V  1 bit =
0.03125mV
    // ads.setGain(GAIN_EIGHT);      // 8x gain   +/- 0.512V  1 bit =
0.015625mV
    // ads.setGain(GAIN_SIXTEEN);    // 16x gain  +/- 0.256V  1 bit =
0.0078125mV

    adsVolt.begin();
    adsCurrent.begin();
    adsVolt.setSPS(ADS1115_DR_860SPS);
    adsCurrent.setSPS(ADS1115_DR_860SPS);

    adsVolt.startContinuous_SingleEnded(0);
    adsCurrent.startContinuous_SingleEnded(0);
    attachInterrupt(digitalPinToInterrupt(clock32k), isrCount, FALLING);
    attachInterrupt(digitalPinToInterrupt(stopRun), isrStop, FALLING);
  }

  void loop(void)
  {
    //Serial Read, Parse, Execute Command
    recvWithStartEndMarkers();
    parse_line();
    execute();
    memset(args, 0, sizeof(args));  //clear the command after execution
    //Serial Read, Parse, Execute Command

    switch (state)
    {
      //-------------------------------------------------------------------
-------------------------------------------------//
      case 0: //Standby
        count = 0; //reset to prevent overflow
        timeElapsed = msec();
        windowStartTime = 0;
        while (standby && timeElapsed <= 1000) //timeElapsed is needed to
leave while loop and reach the Serial read/parse/execute functions
        {
          if (Serial.available())
          {
            recvWithStartEndMarkers();
          }
          if (timeElapsed < minPulse) //2ms is too short to get a reading
          {
```

```
            gate = HIGH;
          }
          else
          {
            gate = LOW;
          }
          digitalWrite(mosfet, gate);
          if (gate == HIGH)
          {
            resultVolt = ((double) adsVolt.getLastConversionResults()) *
adsVolt.voltsPerBit() * 11;
            resultCurrent = ((double) adsCurrent.getLastConversionResults())
* adsCurrent.voltsPerBit() / 2;
          }
          if (timeElapsed - windowStartTime >= 1000)
          {
            //thermocouple.readCelsius() slows down the program too much.
Need to reduce the number of calls to a minimum
            oven = thermocouple.readCelsius();
            windowStartTime = timeElapsed;
            resultResistance = resultVolt / resultCurrent;
            temperature = tempQuad(resultResistance);
            Serial.print(oven); Serial.print(" ");
            Serial.println(temperature);
          }
          readySignal = digitalRead(systemReady);
          // GC is ready for injection
          if (readySignal == HIGH)
          {
            Serial.println("System Ready and Waiting");
            modulationCount = 0;
            currentProgram = 0;
            modulation = 0; // reset modulation before calculation
            //assuming the modulation period will not change between
programs
            for (int i = 2; i <= (temperatureProgram - 1); i++ )
            {
              //sum the different portions of the temperature program to
determine the modulation period
              modulation += modulationProgram[currentProgram][i];
            }

            if (modulationProgram[2] > 0)
            {
              state = 1;
            }
            else if (modulationProgram[3] > 0)
            {
              state = 2;
            }
            else if (modulationProgram[4] > 0)
            {
              state = 3;
            }
            else if (modulationProgram[5] > 0)
            {
              state = 4;
```

```
            }

            startSignal = digitalRead(startRun);
            //Wait for start signal
            while (startSignal == HIGH)
            {
              startSignal = digitalRead(startRun);
            }
            Serial.println("Start");
            count = 0;
            standby = false;
          }
          timeElapsed = msec();
        }
        break;

      //-------------------------------------------------------------------
-------------------------------------------------//

      case 1: //delay
        gate = LOW;
        timeElapsed = msec();
        printWindow = 0;
        digitalWrite(mosfet, gate);
        while (timeElapsed <= modulationProgram[currentProgram][state + 1])
        {
          if (timeElapsed - printWindow >= 100)
          {
            oven = thermocouple.readCelsius();
            printWindow = timeElapsed;
            Serial.print(oven); Serial.print(" ");
            Serial.println(oven);
          }
          timeElapsed = msec() - 0;
        }
        if (standby)
        {
          state = 0;
        }
        else if (modulationProgram[(3 + (currentProgram * 6))] > 0)
        {
          state = 2;
        }
        else if (modulationProgram[(4 + (currentProgram * 6))] > 0)
        {
          state = 3;
        }
        else if (modulationProgram[(5 + (currentProgram * 6))] > 0)
        {
          state = 4;
        }
        else
        {
          //at the end of the temperature program, reset count, increment
modulation count, compare modulation count with the next temperature program
start time (modulation)
```

```
            count = 0; //reset clock here rather than at State 1 to account
for loss in time returning to state 1.
            modulationCount ++;
            if (modulationCount - runTime >= 0)
            {
              standby = true;
            }
            if (currentProgram < 2)
            {
              if (modulationProgram[currentProgram + 1][0] >
modulationProgram[currentProgram][0]) //Check if the subsequent modulation
program was set to a later timestamp, if not, can ignore all values in that
index.
              {
                if (modulationCount >= modulationProgram[currentProgram +
1][0]) //Check if the current modulation count has reached the desired
timestamp for the next modulation program
                {
                  currentProgram ++;
                }
              }
            }
            state = 1;
          }
          break;

        //-------------------------------------------------------------------
-------------------------------------------------//

        case 2: //ramp Time
          oven = thermocouple.readCelsius();

          //reset PID values
          lastError = 0;
          iError = 0;
          lastTime = msec();

          currentTime = msec();
          elapsedProgram = 0;
          for (int i = 2; i <= state; ++i)
          {
            elapsedProgram += modulationProgram[currentProgram][i];
          }
          timeElapsed = currentTime - elapsedProgram;
          printWindow = 0;
          windowStartTime = 0;
          //Serial.print("Ramp : "); Serial.println(currentTime);

          gate = HIGH;
          digitalWrite(mosfet, gate);
          while (timeElapsed <= minPulse) //provide the initial temperature to
the PID (wake as many readings for 5ms and take the latest one)
          {
            resultVolt = ((double) adsVolt.getLastConversionResults()) *
adsVolt.voltsPerBit() * 11;
            resultCurrent = ((double) adsCurrent.getLastConversionResults()) *
adsCurrent.voltsPerBit() / 2;
```

```
            timeElapsed = msec() - currentTime; //ensure a full 5ms is given
to take the temperature measurement if the start of ramp time is delayed.
          }
          resultResistance = resultVolt / resultCurrent;
          temperature = tempQuad(resultResistance);
          startTemp = temperature;
          maxTemp = oven + modulationProgram[currentProgram][1];
          rampRate = (maxTemp - startTemp) /
(modulationProgram[currentProgram][state + 1]); //set ramp rate for ramp
(C/ms)
          timeElapsed = msec() - elapsedProgram; //correct elapsed time within
the temperature ramp
          //determine the starting temperature and heating rate for the LINEAR
ramp

          //Linear Ramp
          Setpoint = (timeElapsed * rampRate) + startTemp;

          if (Setpoint > tempLimit)
          {
            Setpoint = tempLimit;
          }
          Input = temperature;
          computePID(Kp, Ki, Kd);
          while (timeElapsed <= modulationProgram[currentProgram][state + 1] )
          {
            //Linear Ramp
            Setpoint = (timeElapsed * rampRate) + startTemp;//calculate
setpoint for current time

            if (Setpoint > tempLimit) //prevent overheating
            {
              Setpoint = tempLimit;
            }
            if (timeElapsed - windowStartTime >= window)
            {
              windowStartTime = timeElapsed;
            }
            if (Output > timeElapsed - windowStartTime)
            {

              gate = HIGH;
              if (heating)
              {
                heating = false;
                heatOn = msec();
              }
            }
            else
            {
              gate = LOW;
              heating = true;
            }
            digitalWrite(mosfet, gate);
            if (gate == HIGH)
            {
```

```
            if (msec() - heatOn >  minPulse)//wait 3ms after heating starts
before taking a measurement
            {
              resultVolt = ((double) adsVolt.getLastConversionResults()) *
adsVolt.voltsPerBit() * 11;
              resultCurrent = ((double)
adsCurrent.getLastConversionResults()) * adsCurrent.voltsPerBit() / 2;
              resultResistance = resultVolt / resultCurrent;
              temperature = tempQuad(resultResistance);
              Input = temperature;
              computePID(Kp, Ki, Kd);
            }
            if (timeElapsed - printWindow >= 100)
            {
              printWindow = timeElapsed;
              Serial.print(Setpoint, 0); Serial.print(" ");
              Serial.println(temperature);
            }
          }
          //Determine time left in current phase
          timeElapsed = msec() - elapsedProgram; //using startTime resulted
in a perpetual error. 1ms was lost in the transition from one state to
another. However, the ramp still occurred for the full duration resulting in
this state taking 1ms longer.
        }
        if (standby)
        {
          state = 0;
        }
        else if (modulationProgram[(4 + (currentProgram * 6))] > 0)
        {
          state = 3;
        }
        else if (modulationProgram[(5 + (currentProgram * 6))] > 0)
        {
          state = 4;
        }
        else
        {
          count = 0; //reset clock here rather than at State 1 to account
for loss in time returning to state 1.
          modulationCount ++;
          if (modulationCount - runTime >= 0)
          {
            standby = true;
          }
          if (currentProgram < 2)
          {
            if (modulationProgram[currentProgram + 1][0] >
modulationProgram[currentProgram][0]) //Check if the subsequent modulation
program was set to a later timestamp, if not, can ignore all values in that
index.
            {
              if (modulationCount >= modulationProgram[currentProgram +
1][0]) //Check if the current modulation count has reached the desired
timestamp for the next modulation program
              {
```

```
              currentProgram ++;
            }
          }
        }
        state = 1;
      }
      break;


    //-------------------------------------------------------------------------
-------------------------------------------------//

    case 3: //Const Time
      Setpoint = maxTemp;
      if (Setpoint > tempLimit)
      {
        Setpoint = tempLimit;
      }
      currentTime = msec();
      elapsedProgram = 0;
      for (int i = 2; i <= state; ++i)
      {
        elapsedProgram += modulationProgram[currentProgram][i];
      }
      timeElapsed = currentTime - elapsedProgram;
      windowStartTime = 0;
      printWindow = 0;
      //Serial.print("Const: "); Serial.println(currentTime);

      //to provide a data point at the start of the constant offset. The
next datapoint is at the print window reset.
      //Serial.print(Setpoint,0); Serial.print(" ");
      //Serial.println(temperature);
      while (timeElapsed <= modulationProgram[currentProgram][state + 1])
      {
        if (timeElapsed - windowStartTime >= window)
        {
          windowStartTime = timeElapsed;
        }
        if (Output > timeElapsed - windowStartTime)
        {
          gate = HIGH;
          if (heating)
          {
            heating = false;
            heatOn = msec();
          }
        }
        else
        {
          gate = LOW;
          heating = true;
        }
        digitalWrite(mosfet, gate);
        if (gate == HIGH)
        {
```

```
            if (msec() - heatOn > minPulse)//wait 3ms after heating starts
before taking a measurement
            {
              resultVolt = ((double) adsVolt.getLastConversionResults()) *
adsVolt.voltsPerBit() * 11;
              resultCurrent = ((double)
adsCurrent.getLastConversionResults()) * adsCurrent.voltsPerBit() / 2;
              resultResistance = resultVolt / resultCurrent;
              temperature = tempQuad(resultResistance);
              Input = temperature;
              computePID(constKp, constKi, constKd);
            }
            if (timeElapsed - printWindow >= 100)
            {
              printWindow = timeElapsed;
              Serial.print(Setpoint, 0); Serial.print(" ");
              Serial.println(temperature);
            }
          }
          //Determine time left in current phase
          timeElapsed = msec() - elapsedProgram;
        }
        if (standby)
        {
          state = 0;
        }
        else if (modulationProgram[(5 + (currentProgram * 6))] > 0)
        {
          state = 4;
        }
        else
        {
          count = 0; //reset clock here rather than at State 1 to account
for loss in time returning to state 1.
          modulationCount ++;
          if (modulationCount - runTime >= 0)
          {
            standby = true;
          }
          if (currentProgram < 2)
          {
            if (modulationProgram[currentProgram + 1][0] >
modulationProgram[currentProgram][0]) //Check if the subsequent modulation
program was set to a later timestamp, if not, can ignore all values in that
index.
            {
              if (modulationCount >= modulationProgram[currentProgram +
1][0]) //Check if the current modulation count has reached the desired
timestamp for the next modulation program
              {
                currentProgram ++;
              }
            }
          }
          state = 1;
        }
        break;
```

```
      //-------------------------------------------------------------------------
-------------------------------------------------//

      case 4: //Cool
        gate = LOW;
        currentTime = msec();
        elapsedProgram = 0;
        for (int i = 2; i <= state; ++i)
        {
          elapsedProgram += modulationProgram[currentProgram][i];
        }
        timeElapsed = currentTime - elapsedProgram;
        printWindow = 0;
        // Serial.print("Cool : "); Serial.println(currentTime);
        heating = true;
        digitalWrite(mosfet, gate);

        while (timeElapsed <= modulationProgram[currentProgram][state + 1])
        {
          if (timeElapsed - printWindow >= 100)
          {
            oven = thermocouple.readCelsius();
            printWindow = timeElapsed;
            Serial.print(oven); Serial.print(" ");
            Serial.println(oven);
          }
          timeElapsed = msec() - elapsedProgram;
        }
        count = 0; //reset clock here rather than at State 1 to account for
loss in time returning to state 1.
        modulationCount ++;
        if (modulationCount - runTime >= 0)
        {
          standby = true;
        }
        if (currentProgram < 2)
        {
          if (modulationProgram[currentProgram + 1][0] >
modulationProgram[currentProgram][0]) //Check if the subsequent modulation
program was set to a later timestamp, if not, can ignore all values in that
index.
          {
            if (modulationCount >= modulationProgram[currentProgram + 1][0])
//Check if the current modulation count has reached the desired timestamp for
the next modulation program
            {
              currentProgram ++;
            }
          }
        }
        if (standby)
        {
          state = 0;
        }
        else if (modulationProgram[(2 + (currentProgram * 6))] > 0)
        {
```

```
          state = 1;
        }
        else if (modulationProgram[(3 + (currentProgram * 6))] > 0)
        {
          state = 2;
        }
        else if (modulationProgram[(4 + (currentProgram * 6))] > 0)
        {
          state = 3;
        }
        else
        {
          state = 4;
        }
        break;

      //-------------------------------------------------------------------------
-------------------------------------------------//

      case 5: //Constant Offset
        count = 0; //reset to prevent overflow
        timeElapsed = msec();
        windowStartTime = 0;
        printWindow = 0;
        oven = thermocouple.readCelsius();
        Setpoint = oven + constantOffsetValue;
        if (Setpoint > tempLimit)
        {
          Setpoint = tempLimit;
        }
        Input = temperature;
        while (!standby)
        {
          if (timeElapsed - windowStartTime >= window)
          {
            windowStartTime = timeElapsed;
          }
          if (Output > timeElapsed - windowStartTime)
          {
            gate = HIGH;
            if (heating)
            {
              heating = false;
              heatOn = msec();
            }
          }
          else
          {
            gate = LOW;
            heating = true;
          }
          digitalWrite(mosfet, gate);
          if (gate == HIGH)
          {
            if (msec() - heatOn > minPulse)
            {
```

```
                resultVolt = ((double) adsVolt.getLastConversionResults()) *
adsVolt.voltsPerBit() * 11;
                resultCurrent = ((double)
adsCurrent.getLastConversionResults()) * adsCurrent.voltsPerBit() / 2;
                resultResistance = resultVolt / resultCurrent;
                temperature = tempQuad(resultResistance);
                Input = temperature;
                if (Input < Setpoint)
                {
                  Output = Output + 1;
                  if (Output >= window)
                  {
                    Output = window;
                  }
                }
                if (Input > Setpoint)
                {
                  Output = Output - 1;
                  if (Output <= minPulse)
                  {
                    Output = minPulse;
                  }
                }
              }
            }
            if (timeElapsed - printWindow >= 100)
            {
              oven = thermocouple.readCelsius();
              Setpoint = oven + constantOffsetValue;
              if (Setpoint > tempLimit)
              {
                Setpoint = tempLimit;
              }

              printWindow = timeElapsed;
              Serial.print(Setpoint, 0); Serial.print(" ");
              Serial.println(temperature);
            }
            //Determine time left in current phase
            timeElapsed = msec();

            //Break loop to check for other commands every 10s
            if (timeElapsed >= 10000 )
            {
              count = 0;
              timeElapsed = 0;
              windowStartTime = 0;
              printWindow = 0;
              if (Serial.available() > 0)
              {
                state = 5;
                break;
              }
              if (standby)
              {
                state = 0;
                break;
```

```
            }
          }
        }
        break;

      //-------------------------------------------------------------------
-------------------------------------------------//

      case 6: //Calibration
        count = 0; //reset to prevent overflow
        timeElapsed = msec();
        windowStartTime = 0;
        while (timeElapsed <= 1000) //timeElapsed is needed to leave while
loop and reach the Serial read/parse/execute functions
        {
          if (Serial.available())
          {
            recvWithStartEndMarkers();
          }
          if (timeElapsed < minPulse) //2ms is too short to get a reading
          {
            gate = HIGH;
          }
          else
          {
            gate = LOW;
          }
          digitalWrite(mosfet, gate);
          if (gate == HIGH)
          {
            resultVolt = ((double) adsVolt.getLastConversionResults()) *
adsVolt.voltsPerBit() * 11;
            resultCurrent = ((double) adsCurrent.getLastConversionResults())
* adsCurrent.voltsPerBit() / 2;
          }
          if (timeElapsed - windowStartTime >= 1000)
          {
            //thermocouple.readCelsius() slows down the program too much.
Need to reduce the number of calls to a minimum
            oven = thermocouple.readCelsius();
            windowStartTime = timeElapsed;
            resultResistance = resultVolt / resultCurrent;
            temperature = tempQuad(resultResistance);
            Serial.print(oven); Serial.print(" ");
            Serial.print(resultVolt); Serial.print(" ");
            Serial.print(resultCurrent); Serial.print(" ");
            Serial.println(resultResistance);
          }
          timeElapsed = msec();
        }
        break;

        //-------------------------------------------------------------------
-------------------------------------------------//
    }
  }
  //https://github.com/soligen2010/Adafruit_ADS1X15
```

```
   double tempQuad(double value)
   {
     double temperature = x2 * value * value + x1 * value + x0;
     return temperature;
   }
   void isrStop()
   {
     readySignal = digitalRead(systemReady);
     if (readySignal == LOW)
     {
       //only stop the run if the stop signal is within 2 modulations of the
expected runTime.
       if (abs(modulationCount - runTime) < 2)
       {
         Serial.println("Stop");
         state = 0;
         standby = true;
       }
     }
   }
   void isrCount()
   {
     count++;
   }
   long msec(void)
   {
     ms = count * 1000 / freq;
     return ms;
   }
   //https://www.arduino.cc/en/Tutorial/Smoothing

   //https://forum.arduino.cc/index.php?topic=288234.0
   void recvWithStartEndMarkers()
   {

     static byte ndx = 0;
     char startMarker = '<';
     char endMarker = '>';
     char rc;
     while (Serial.available() > 0 && newData == false)
     {
       rc = Serial.read();
       if (recvInProgress == true)
       {
         if (rc != endMarker)
         {
           receivedChars[ndx] = rc;
           ndx++;
           if (ndx >= numChars)
           {
             ndx = numChars - 1;
           }
         }
         else
         {
           receivedChars[ndx] = '\0'; // terminate the string
```

```
          recvInProgress = false;
          ndx = 0;
          newData = true;
        }
      }
      else if (rc == startMarker) {
        recvInProgress = true;
      }
    }
  }
  //https://www.norwegiancreations.com/2018/02/creating-a-command-line-
interface-in-arduinos-serial-monitor/
  void parse_line()
  {
    char *argument;
    int counter = 0;
    if (newData == true)
    {
      argument = strtok(receivedChars, " ");
      while ((argument != NULL))
      {
        if (counter < MAX_NUM_ARGS)
        {
          if (strlen(argument) < ARG_BUF_SIZE)
          {
            args[counter] = argument;
            argument = strtok(NULL, " ");
            counter++;
          }
        }
        else
        {
          break;
        }
      }
      newData = false;
    }
  }
  int execute()
  {
    for (int i = 0; i < num_commands; i++) {
      if (strcmp(args[0], commands_str[i]) == 0) {
        return (*commands_func[i])();
      }
    }
    return 0;
  }
  int SetPID()
  {
    Serial.println("-----------------------------------");
    String KpValue = args[1];
    String KiValue = args[2];
    String KdValue = args[3];
    Kp = KpValue.toDouble();
    Ki = KiValue.toDouble();
    Kd = KdValue.toDouble();
```

```
     Serial.print("Ramp PID = "); Serial.print(Kp); Serial.print(" ");
Serial.print(Ki); Serial.print(" "); Serial.println(Kd);
     Serial.println("-----------------------------------");
   }
   int SetConstPID()
   {
     Serial.println("-----------------------------------");
     String conKp = args[1];
     String conKi = args[2];
     String conKd = args[3];
     constKp = conKp.toDouble();
     constKi = conKi.toDouble();
     constKd = conKd.toDouble();
     Serial.print("Constant Offset PID = "); Serial.print(constKp);
Serial.print(" "); Serial.print(constKi); Serial.print(" ");
Serial.println(constKd);
     Serial.println("-----------------------------------");
   }
   int SetHeatingPulseWidth()
   {
     Serial.println("-----------------------------------");
     String heatWindow = args[1];
     window = heatWindow.toInt();
     Serial.print("Heat Pulse Width = "); Serial.println(window);
     Serial.println("-----------------------------------");
   }
   int SM() //set modulation
   {
     int counter = 1;
     Serial.println("-----------------------------------");
     Serial.println("Modulation Program");

     for (int i = 0; i < program; i++)
     {
       for (int j = 0; j < temperatureProgram; j++)
       {
         String value = args[counter];
         Serial.print(value + " ");
         modulationProgram[i][j] = value.toInt();
         counter ++;
       }
       Serial.println();
     }
     modulation = 0; //reset modulation period value before summing the
values to calculate modulation period.
     for (int i = 2; i <= (temperatureProgram - 1); i++ )
     {
       //sum the different portions of the temperature program to determine
the modulation period
       modulation += modulationProgram[currentProgram][i];
     }
     String runValue = args[counter];
     runTime = runValue.toInt(); //in modulations
     double runTimeMin = modulation / 1000 * runTime / 60;
     Serial.print("RunTime: "); Serial.println(runTimeMin);
     Serial.println("-----------------------------------");
   }
```

```
   int StartCalibration()
   {
     standby = false;
     state = 6; //Start calibration state
     Serial.println("Start Calibration");
     Serial.println("T    V        I       R");
   }
   int StopCalibration()
   {
     standby = true;
     state = 0;
   }
   int SC() //Set Calibration
   {
     Serial.println("-----------------------------------");
     String X2Value = args[1];
     String X1Value = args[2];
     String X0Value = args[3];
     x2 = X2Value.toDouble();
     x1 = X1Value.toDouble();
     x0 = X0Value.toDouble();
     Serial.println("Calibration");
     Serial.print("X2 = "); Serial.println(X2Value);
     Serial.print("X1 = "); Serial.println(X1Value);
     Serial.print("X0 = "); Serial.println(X0Value);
     Serial.println("-----------------------------------");
   }
   int LimitTemp()
   {
     Serial.println("-----------------------------------");
     String limit = args[1];
     tempLimit = limit.toInt();
     Serial.print("Column Temp. Limit = "); Serial.print(" ");
Serial.println(tempLimit);
     Serial.println("-----------------------------------");
   }
   int ConstantOffset()
   {
     Serial.println("-----------------------------------");
     if (strcmp(args[1], "True") == 0)
     {
       String value = args[2];
       constantOffsetValue = value.toDouble();
       standby = false;
       initialRead = true;
       Output = 7;
       state = 5; //start constant offset state
       Serial.print("Constant Offset: ");
Serial.println(constantOffsetValue);
     }
     if (strcmp(args[1], "False") == 0)
     {
       standby = true;
       state = 0; //back to standby
       Serial.println("Constant Offset: OFF");
     }
   }
```

```
int computePID(double p, double i, double d)
{
  kp = p;
  ki = i;
  kd = d;

  presentTime = msec();
  timeChange = presentTime - lastTime;
  if (timeChange <= 0)
  {
    timeChange = 10;
  }

  error = Setpoint - Input;

  dError = (error - lastError) / timeChange;
  iError += error * timeChange;

  if (iError > window)
  {
    iError = window;
  }
  else if (iError < minPulse + 1)
  {
    iError = minPulse + 1;
  }

  Output = kp * error + ki * iError + kd * dError;
  if (Output > window)
  {
    Output = window;
  }
  else if (Output < minPulse + 1)
  {
    Output = minPulse + 1;
  }
  lastError = error;
  lastTime = presentTime;
}
```

Appendix D Chapter 5 Supplementary Data, Figures, and Tables

Table D - 1: GC×GC-TOFMS and GC×GC-FID conditions for the characterization of samples from the refining process meant for personal care products.

<table>
<tr><th colspan="6">Renewable Hydrocarbon Samples (L and H)</th></tr>
<tr><td></td><td colspan="3">Qualitative</td><td colspan="2">Quantitative</td></tr>
<tr><td>Inlet</td><td colspan="3">0.2 µL, 250 °C, 400:1 split</td><td colspan="2">1.0 µL, 250 °C, 100:1 split</td></tr>
<tr><td>[1]D Column</td><td colspan="5">Rxi-5Sil MS W/Integra-Guard (39.219 m × 0.242 mm × 0.25 µm)</td></tr>
<tr><td>[2]D Column</td><td colspan="5">MXT-WAX (1.00 m × 0.25 mm × 0.25 µm)</td></tr>
<tr><td>Carrier Gas</td><td colspan="3">He 99.999%, 2.0 mL/min</td><td colspan="2">He 99.999%, 4.0 mL/min</td></tr>
<tr><td rowspan="3">Oven</td><td>°C/min</td><td colspan="2">Next °C</td><td colspan="2">Hold (min)</td></tr>
<tr><td></td><td colspan="2">35</td><td colspan="2">3</td></tr>
<tr><td>3</td><td colspan="2">230</td><td colspan="2">0</td></tr>
<tr><td rowspan="6">Detector</td><td colspan="2">TOFMS</td><td colspan="3">FID</td></tr>
<tr><td>Filament (V)</td><td>1.60</td><td>Temperature (°C)</td><td colspan="2">250</td></tr>
<tr><td>Filament Delay (s)</td><td>210</td><td>H_2 (mL)</td><td colspan="2">40</td></tr>
<tr><td>Mass Range (m/z)</td><td>35 – 600</td><td>Air (mL)</td><td colspan="2">400</td></tr>
<tr><td>Data Rate (Hz)</td><td>50</td><td rowspan="3">Makeup (N_2) + Carrier (mL)</td><td colspan="2" rowspan="3">30</td></tr>
<tr><td>Transfer Line (°C)</td><td>250</td></tr>
<tr><td>Ion source (°C)</td><td>250</td></tr>
<tr><td rowspan="5">Modulator</td><td colspan="5">HV 1.07 m × 0.25 mm</td></tr>
<tr><td colspan="5">P_m: 6 s</td></tr>
<tr><td colspan="3">Entry Hot Zone</td><td colspan="2">+0 °C (320 °C cap)</td></tr>
<tr><td colspan="3">Exit Hot Zone</td><td colspan="2">+30 °C (320 °C cap)</td></tr>
<tr><td colspan="3" rowspan="2">Cold Zone</td><td colspan="2">-51 °C (oven < 150 °C)</td></tr>
<tr><td colspan="2">9 °C (oven > 150 °C)</td></tr>
<tr><td>[2]DTPS</td><td colspan="3"></td><td colspan="2"> 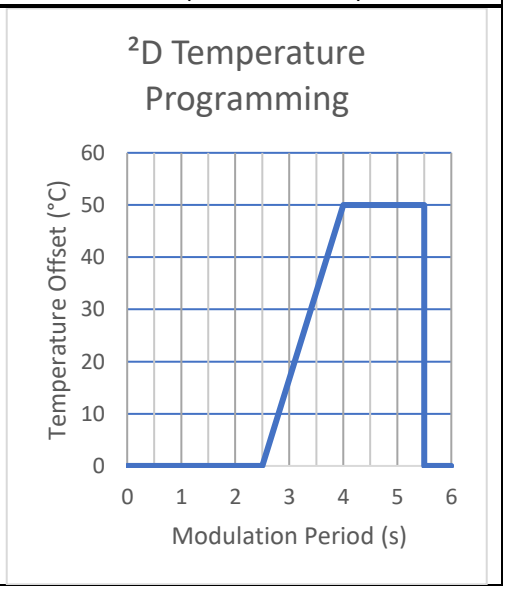
</td></tr>
</table>

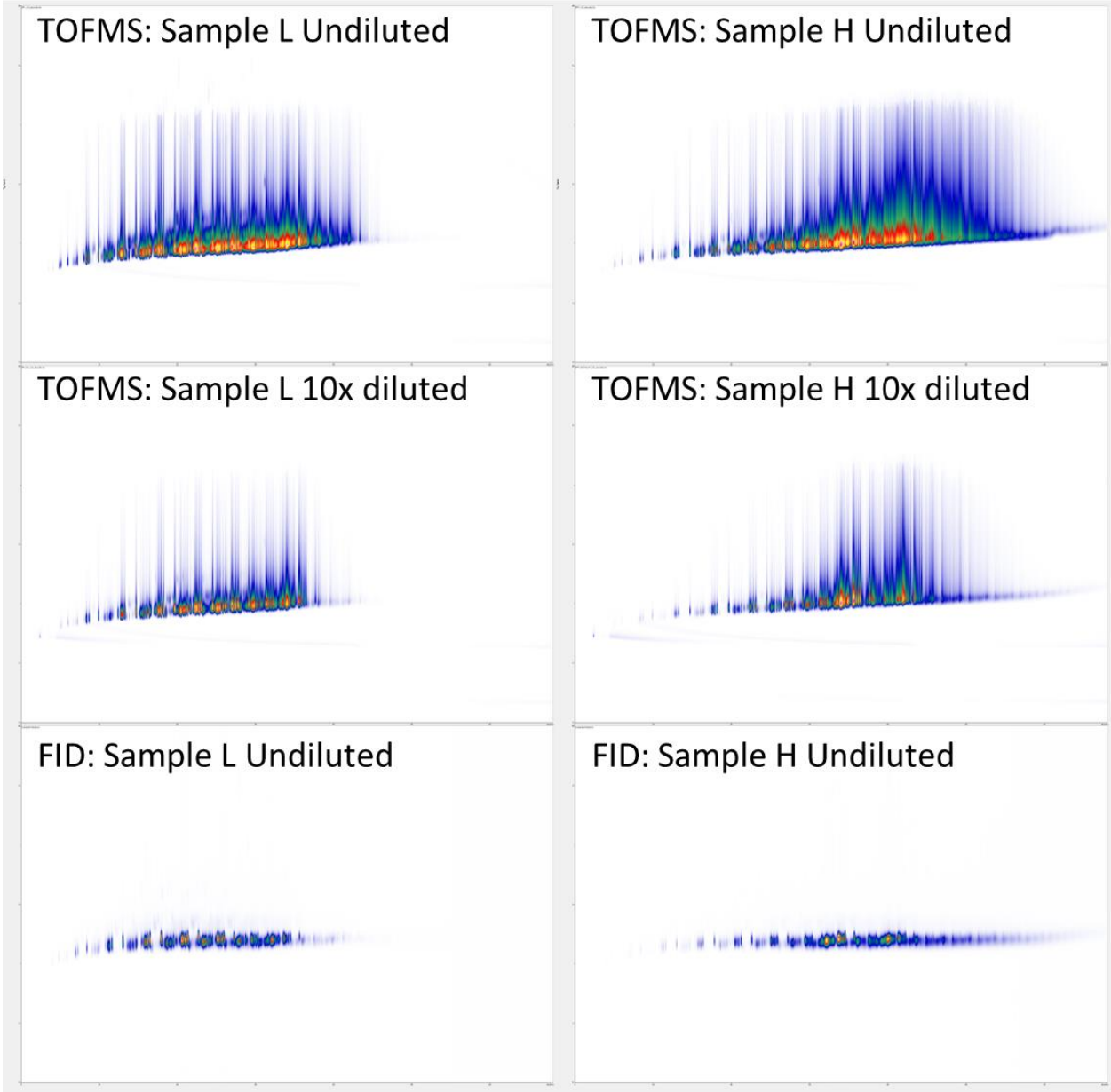

Figure D - 1: Comparison of the TOFMS and FID signal for the GC×GC separation of samples L and H. Significant ion source tailing was observed for the more concentrated compounds. A 10 times dilution of the samples using hexane reduced the tailing in the TOFMS signal. Tailing was not observed for the FID signal. Separation conditions for the TOFMS and FID chromatograms are found in Table D - 1, however, these GC×GC-FID separations did not use ²D temperature programming for a more direct comparison. ***X-axis: 0 – 68 min. Y-axis: 0 – 6 s****.*

Table D - 2: Parametric expressions used for compound class identification. Based on [255, 256, 257]

_n+i_ – Alkanes

```
(((Ordinal(43) == 1 and Intensity(57) > 0) or (Ordinal(57) == 1 and Intensity(43) > 0)
or (Ordinal(43) == 1 and Intensity(71) > 0)) and (Intensity(100)>0)) or
(((Ordinal(43) == 1 and Intensity(57) > 0) or (Ordinal(57) == 1 and Intensity(43) > 0)
or (Ordinal(43) == 1 and Intensity(71) > 0)) and (Intensity(114)>0)) or
(((Ordinal(43) == 1 and Intensity(57) > 0) or (Ordinal(57) == 1 and Intensity(43) > 0)
or (Ordinal(43) == 1 and Intensity(71) > 0)) and (Intensity(128)>0)) or
(((Ordinal(43) == 1 and Intensity(57) > 0) or (Ordinal(57) == 1 and Intensity(43) > 0)
or (Ordinal(43) == 1 and Intensity(71) > 0)) and (Intensity(142)>0)) or
(((Ordinal(43) == 1 and Intensity(57) > 0) or (Ordinal(57) == 1 and Intensity(43) > 0)
or (Ordinal(43) == 1 and Intensity(71) > 0)) and (Intensity(156)>0)) or
(((Ordinal(43) == 1 and Intensity(57) > 0) or (Ordinal(57) == 1 and Intensity(43) > 0)
or (Ordinal(43) == 1 and Intensity(71) > 0)) and (Intensity(170)>0)) or
(((Ordinal(43) == 1 and Intensity(57) > 0) or (Ordinal(57) == 1 and Intensity(43) > 0)
or (Ordinal(43) == 1 and Intensity(71) > 0)) and (Intensity(184)>0)) or
(((Ordinal(43) == 1 and Intensity(57) > 0) or (Ordinal(57) == 1 and Intensity(43) > 0)
or (Ordinal(43) == 1 and Intensity(71) > 0)) and (Intensity(198)>0)) or
(((Ordinal(43) == 1 and Intensity(57) > 0) or (Ordinal(57) == 1 and Intensity(43) > 0)
or (Ordinal(43) == 1 and Intensity(71) > 0)) and (Intensity(212)>0)) or
(((Ordinal(43) == 1 and Intensity(57) > 0) or (Ordinal(57) == 1 and Intensity(43) > 0)
or (Ordinal(43) == 1 and Intensity(71) > 0)) and (Intensity(226)>0))
```

Mononaphthene/Olefins

```
((Ordinal(55) == 1) || (Ordinal(69) == 1)) &&
(Intensity(55) > 0) && (Intensity(69) > 0) &&
(((Relative(56)>0.15) + (Relative(57)>0.15) + (Relative(70)>0.15) + (Relative(83)>0.15)
+ (Relative(97)>0.15)) >= 3)
```

Dinaphthenes

```
(Relative(124)>0.2) OR (Relative(138)>0.2) OR (Relative(152)>0.2) OR
(Relative(166)>0.2) OR (Relative(180)>0.2) OR (Relative(194)>0.2) OR
(Relative(208)>0.2) OR (Relative(222)>0.2) OR (Relative(236)>0.2) OR
(Relative(250)>0.2)
```

Monoaromatics

Alkyl-Substituted Benzenes

```
(Ordinal(78) == 1) or (Ordinal (77) == 1) or (ordinal(91) == 1) or (ordinal(92) == 1)
or (ordinal(117) == 1) or (ordinal(116) == 1) or (ordinal(105) == 1)or (ordinal(119) ==
1)or (ordinal(133) == 1)or (ordinal(147) == 1)or (ordinal(161) == 1)
```

Tetralin (1,2,3,4-tetrahydronaphthalene

```
(Ordinal(145) == 1) or (ordinal(159) == 1)or (ordinal(173) == 1)or (ordinal(187) ==
1)or (ordinal(201) == 1)or (ordinal(215) == 1)or (ordinal(229) == 1)or (ordinal(243) ==
1)or (ordinal(257) == 1)or (ordinal(271) == 1)or (ordinal(118) == 1)or (ordinal(132) ==
1)or (ordinal(146) == 1)or (ordinal(160) == 1)or (ordinal(174) == 1)or (ordinal(188) ==
1)or (ordinal(202) == 1)or (ordinal(216) == 1)or (ordinal(230) == 1)or (ordinal(244) ==
1)or (ordinal(117) == 1)
```

Naphthalenes

```
(Ordinal(128) == 1) or
(Ordinal(142) == 1) or (Ordinal(156) == 1) or (Ordinal(170) == 1) or
(Ordinal(184) == 1) or (Ordinal(198) == 1) or (Ordinal(212) == 1) or
(Ordinal(226) == 1) or (Ordinal(240) == 1) or (Ordinal(254) == 1) or
(Ordinal(268) == 1) or
```

```
(Ordinal(115) == 1) or (Ordinal(129) == 1) or (Ordinal(143) == 1) or
(Ordinal(157) == 1) or (Ordinal(171) == 1) or (Ordinal(185) == 1) or
(Ordinal(199) == 1) or (Ordinal(213) == 1) or (Ordinal(227) == 1) or
(Ordinal(241) == 1) or
(Ordinal(141) == 1) or (Ordinal(155) == 1) or (Ordinal(169) == 1) or
(Ordinal(183) == 1) or (Ordinal(197) == 1) or (Ordinal(211) == 1) or
(Ordinal(225) == 1) or (Ordinal(239) == 1) or (Ordinal(253) == 1) or
(Ordinal(267) == 1)
```

Table D - 3: Toluene calibration standard concentrations and peak areas. A correction factor of 1.07 was applied to quantify hydrocarbons. All standards were diluted using hexane.

Stock	STD.	Toluene (µL)	Final Volume (mL)	ppm	µg/L	Peak Area	Cor. Peak Area
Toluene (99.95%)	15	160	5.00	32000	27,666,160	4.165E+09	3.892E+09
	14	80	5.00	16000	13,833,080	2.056E+09	1.922E+09
	13	40	5.00	8000	6,916,540	1.062E+09	9.929E+08
	12	20	5.00	4000	3,458,270	5.422E+08	5.067E+08
	11	10	5.00	2000	1,729,135	2.718E+08	2.541E+08
	10	5	5.00	1000	864,568	1.351E+08	1.263E+08
STD 13	9	300	5.00	480	414,992	6.387E+07	5.970E+07
STD 11	8	200	5.00	80	69,165	1.064E+07	9.939E+06
	7	100	5.00	40	34,583	5.157E+06	4.820E+06
STD 10	6	40	5.00	8	6,917	1.075E+06	1.005E+06
	5	20	5.00	4	3,458	5.642E+05	5.273E+05
	4	10	5.00	2	1,729	2.956E+05	2.763E+05
	3	5	5.00	1	865	1.566E+05	1.464E+05
	2	2	5.00	0.4	346	7.993E+04	7.470E+04
	1	1	5.00	0.2	173	5.690E+04	5.318E+04

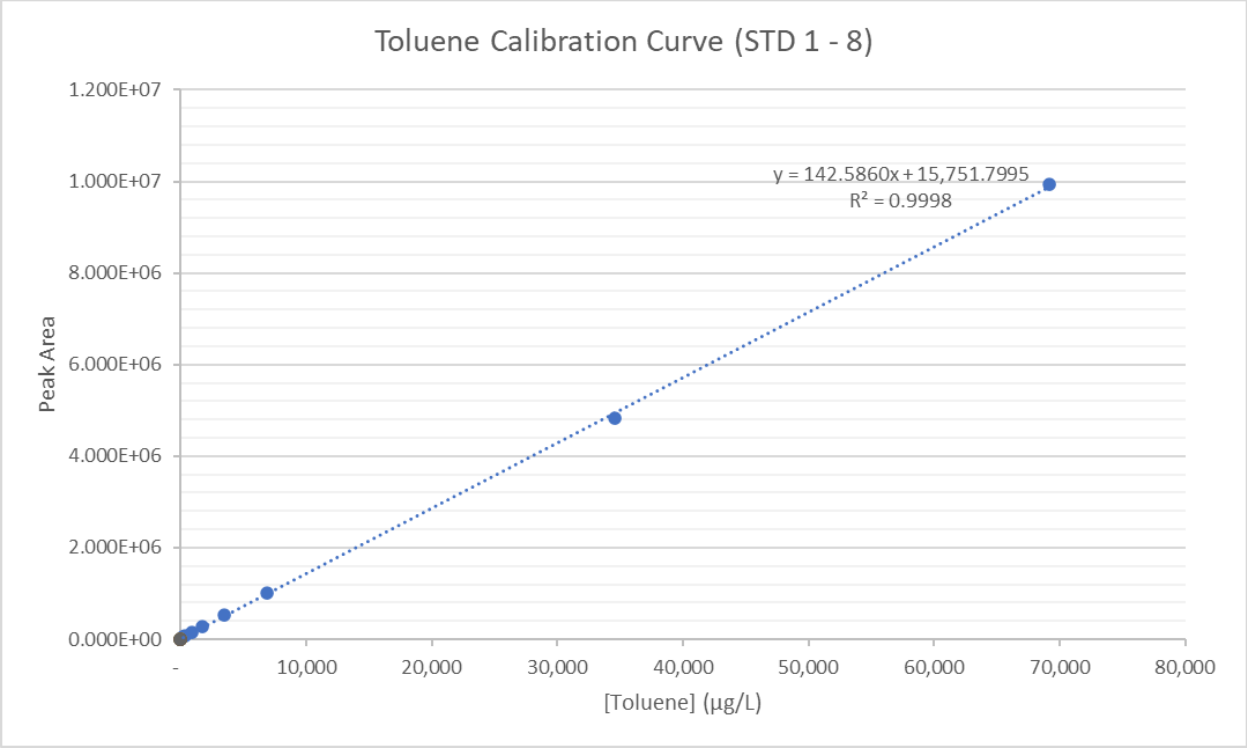

Figure D - 2: Calibration curve for toluene standards 1 to 8.Used for peak areas between 0 and 9,939,439.

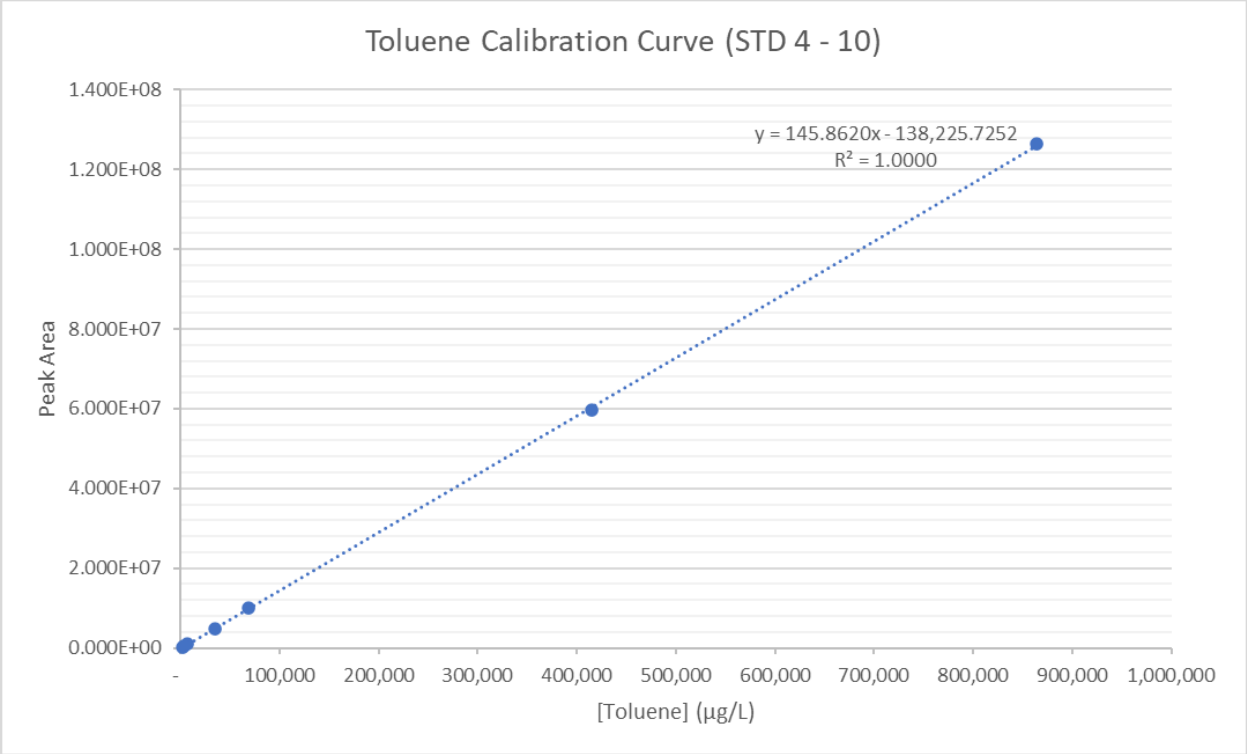

Figure D - 3: Calibration curve for toluene standards 4 to 10. Used for peak areas between 9,939,439 and 59,695607.

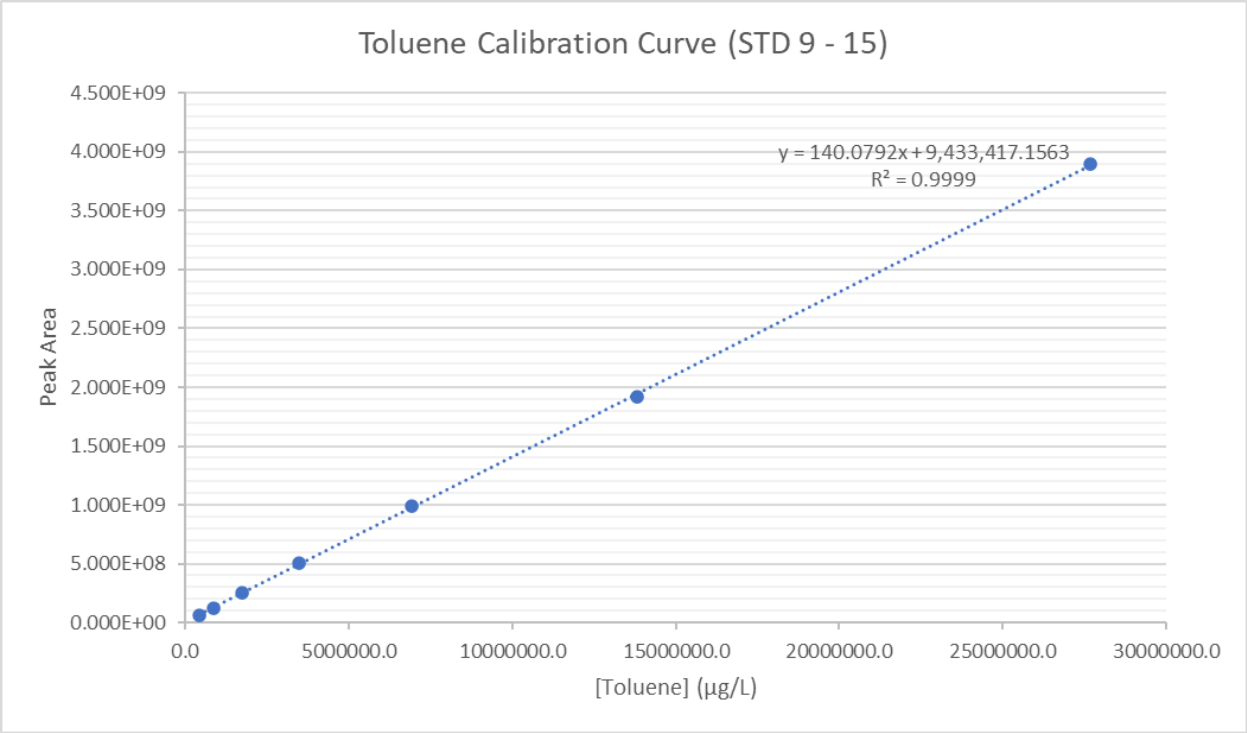

Figure D - 4: Calibration curve for toluene standards 9 to 15. Used for peak areas between 59,695607 and 3,892,336,449.

Table D - 4: Results of the hydrocarbon group type distribution of samples L and H by GC×GC-FID and ²D temperature programming. Average concentration (g/L and %), standard deviation, and RSD of three replicate runs are provided.

	Sample L		Sample H	
	Average			
	Total (g/L)	%	Total (g/L)	%
***n*-Alkane**	106.0559	12.80	104.8152	12.22
***i*-Alkane**	711.2327	85.81	750.1708	87.43
Mononaphthene/Alkene	7.854301	0.95	2.047046	0.24
Dinaphthene	2.859517	0.34	0.534731	0.06
Trinaphthene	0.079758	0.01	0.033075	0.004
Monoaromatic	0.691476	0.08	0.385174	0.04
Diaromatic	0.009506	0.001	0.015162	0.002
FAME	0.058849	0.01	0.041245	0.005
	Standard Deviation			
	Total (g/L)	%	Total (g/L)	%
***n*-Alkane**	0.3962	0.01	7.0871	0.83
***i*-Alkane**	2.6600	0.01	7.5631	0.83
Mononaphthene/Alkene	0.0301	0.01	0.0295	0.00
Dinaphthene	0.0308	0.003	0.0183	0.002
Trinaphthene	0.0038	0.0005	0.0015	0.0002
Monoaromatic	0.0153	0.002	0.0076	0.001
Diaromatic	0.00004	0.00001	0.0001	0.00001
FAME	0.0012	0.0001	0.0018	0.0002
	RSD			
	Total	% (m/m)	Total (g/L)	% (m/m)
***n*-Alkane**	0.37	0.05	6.76	6.82
***i*-Alkane**	0.37	0.01	1.01	0.95
Mononaphthene/Alkene	0.38	0.67	1.44	1.46
Dinaphthene	1.08	0.77	3.42	3.33
Trinaphthene	4.74	5.10	4.50	4.45
Monoaromatic	2.22	1.85	1.97	1.93
Diaromatic	0.44	0.76	0.74	0.81
FAME	2.01	1.64	4.35	4.44

Table D - 5: GC×GC-FID/TOFMS method for the characterization of sample L during the final refining steps of the production process.

Effect of Refining Process: Sample L			
Inlet	1.0 µL, 230 °C, 300:1 split		
^{1}D Column	MXT-Wax (20.8 m × 0.25 mm × 0.50 µm + 23.624 m × 0.25 mm × 0.25 µm)		
Modulator Column	Rxi-1ms (0.69 m × 0.25 mm × 1.0 µm) + Deactivated Fused Silica tubing (0.476 m × 0.25 mm)		
^{2}D Column	MXT-1 (0.625 m × 0.25 mm × 0.25 µm)		
^{2}D column to Splitter	Guard (0.30 m x 0.25 mm)		
Splitter to FID	Guard (0.277 m x 0.15 mm)		
Splitter to TOF	Guard (1.0 m x 0.15 mm)		
Column Flow	He 99.999%, 1.2 mL/min		
Auxiliary Pressure (splitter)	He 99.999%, 2 psi		
Oven	°C/min	Next °C	Hold (min)
		35	0
	3	98	0
	2.5	190	0
Detector (FID)	Temperature: 250 °C, H_2: 40 mL/min, Air: 400 mL/min, N_2 + Carrier: 30 mL/min, Data: 100 Hz		
Detector (TOFMS)	Filament (V)	1.6	
	Filament Delay (s)	200	
	Mass Range (m/z)	40 - 600	
	Data Rate (Hz)	100	
	Transfer Line (°C)	250	
	Ion source (°C)	250	
Modulator	Entry Hot Zone	+0 °C (320 °C cap)	
	Exit Hot Zone	+30 °C (320 °C cap)	
	Cold Zone	-51 °C (oven < 150 °C), +9 °C (oven > 150 °C)	
	Modulation Period (s)	6	
^{2}DTPS	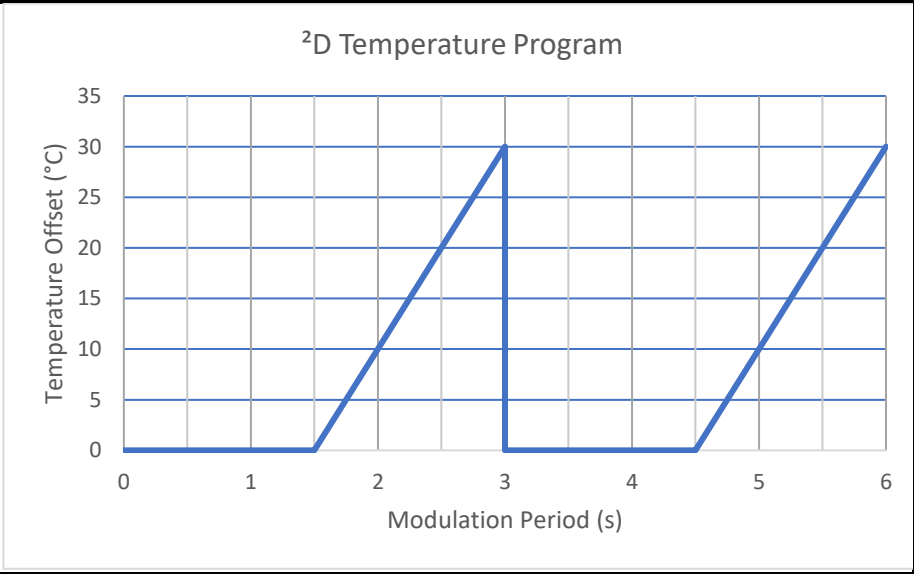		

Table D - 6: Column flow to the FID and TOFMS at the starting and final GC oven temperature with a constant auxiliary pressure of 2 psi. GC×GC column flow limit was equal to the total flow through the splitter (G3180) minus 0.5 mL/min according to the manual.

Auxiliary Pressure = 2 psi	**Oven Temperature**	
	35 °C	190 °C
Splitter to MS (mL/min)	2.369	1.195
Splitter to FID (mL/min)	1.906	0.972
Split Ratio (MS/FID)	1.242	1.229
Total Flow (mL/min)	4.275	2.167
GC×GC Column Flow Limit (mL/min)	3.775	1.667

Table D - 7: Sample concentration dissolved in CS_2.

Sample	**[g/mL]**
T1	0.0175
T2	0.1220
T3	0.0198
T4	0.0034
T5	0.1319
T26	0.0018
T27	0.0062

Table D - 8: GC-MS separation conditions for the analysis of wax samples. Detector was turned off at 29 min for the 50:1 split ratio separation to prevent damage to the electron multiplier due to the more highly concentrated hydrocarbons (> C_{30}) in the sample. This separation was for the analysis of trace compounds in the sample. The detector was on for the full separation when doing a 300:1 split. This separation was for the analysis of the overall wax sample where more than 90% of the sample were high boiling point hydrocarbons (> C_{30}). Two sets of data (50:1 and 300:1) were collected for each wax sample.

GC-MS analysis of Wax Samples			
Sample	Diesel and Perfume		
Inlet	1.0 µL, 300 °C, 50:1 split (Detector turned OFF at 29 min) or 300:1 split (Detector ON for full run)		
Column	*Zebron-5HT Inferno (31 m × 0.25 mm × 0.1 µm)*		
Carrier Gas	He 99.999%, 1.6 mL/min (Constant Flow)		
Oven	°C/min	Next °C	Hold (min)
		35	1
	7.8	400	
Detector (Quad)	Filament Delay (min)	1.32	
	Mass Range (m/z)	30-500	
	Sampling Rate (2^n)	2	
	Scans/sec	3.12	
	Quadrupole (°C)	150	
	Ion source (°C)	230	

Table D - 9: GC×GC-FID/TOFMS method for the characterization of wax samples. The FID was not turned on for the characterization of the samples.

<table>
<tr><th colspan="5">Wax Samples</th></tr>
<tr><td>Inlet</td><td colspan="4">1.0 µL, 230 °C, 300:1 split</td></tr>
<tr><td>[1]D Column</td><td colspan="4">MXT-Wax (20.8 m × 0.25 mm × 0.50 µm + 23.624 m × 0.25 mm × 0.25 µm)</td></tr>
<tr><td>Modulator Column</td><td colspan="4">Rxi-1ms (0.69 m × 0.25 mm × 1.0 µm) + Deactivated Fused Silica tubing (0.476 m × 0.25 mm)</td></tr>
<tr><td>[2]D Column</td><td colspan="4">MXT-1 (0.625 m × 0.25 mm × 0.25 µm)</td></tr>
<tr><td>[2]D column to Splitter</td><td colspan="4">Guard (0.30 m x 0.25 mm)</td></tr>
<tr><td>Splitter to FID</td><td colspan="4">Guard (0.277 m x 0.15 mm)</td></tr>
<tr><td>Splitter to TOF</td><td colspan="4">Guard (1.0 m x 0.15 mm)</td></tr>
<tr><td>Column Flow</td><td colspan="4">He 99.999%, 1.2 mL/min
Backflush at 60.45 min for 46.71 min</td></tr>
<tr><td>Auxiliary Pressure (splitter)</td><td colspan="4">He 99.999%, 2 psi (0 – 60.45 min), 18.05 psi (60.45 min – 107.16 min)</td></tr>
<tr><td rowspan="3">Oven</td><td>°C/min</td><td colspan="2">Next °C</td><td>Hold (min)</td></tr>
<tr><td></td><td colspan="2">100</td><td>0</td></tr>
<tr><td>3</td><td colspan="2">230</td><td>64.6</td></tr>
<tr><td rowspan="6">Detector (TOFMS)</td><td colspan="2">Filament (V)</td><td colspan="2">1.6</td></tr>
<tr><td colspan="2">Filament Delay (s)</td><td colspan="2">210</td></tr>
<tr><td colspan="2">Mass Range (m/z)</td><td colspan="2">50 - 600</td></tr>
<tr><td colspan="2">Data Rate (Hz)</td><td colspan="2">100</td></tr>
<tr><td colspan="2">Transfer Line (°C)</td><td colspan="2">250</td></tr>
<tr><td colspan="2">Ion source (°C)</td><td colspan="2">250</td></tr>
<tr><td rowspan="4">Modulator</td><td colspan="2">Entry Hot Zone</td><td colspan="2">+100 °C (320 °C cap)</td></tr>
<tr><td colspan="2">Exit Hot Zone</td><td colspan="2">+1200 °C (320 °C cap)</td></tr>
<tr><td colspan="2">Cold Zone</td><td colspan="2">-51 °C (oven < 150 °C), +9 °C (oven > 150 °C)</td></tr>
<tr><td colspan="2">Modulation Period (s)</td><td colspan="2">6</td></tr>
<tr><td>[2]DTPS</td><td colspan="4"> 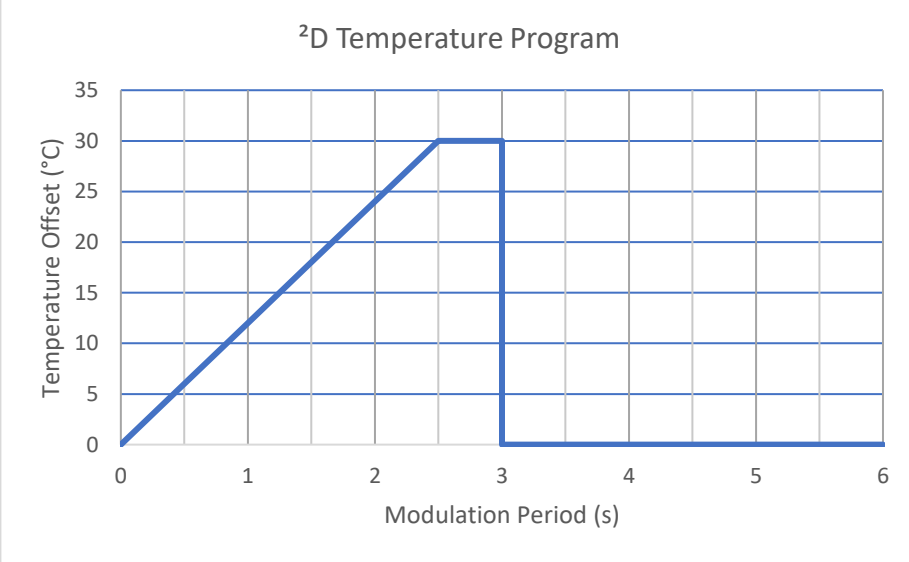
</td></tr>
</table>

Table D - 10: GC×GC columns and splitter pressure program applied. GC×GC column set was connected to the front inlet of the Agilent 6890 GC. A pressure program to run a constant flow of 1.2 mL/min of He was applied for the GC×GC separation from 0 - 60.45 min. After 60.45 min, the pressure was reduced to the minimum pressure for backflushing from 60.45 min to 107.27 min. The pressure applied to the splitter was 2 psi during the separation and 18.05 psi during the backflush. Pressure settings were restored to 1.2 mL/min (35 °C) and 2 psi for the GC×GC columns and splitter, respectively, at the end of the program.

GC×GC (Front Inlet)				Splitter (Back Inlet)			
Pressure (psi)	Ramp (psi/min)	Hold (min)	Time (min)	Pressure (psi)	Ramp (psi/min)	Hold (min)	Time
23.5				2		60.45	60.45
32.52	0.21	17.5	60.45	18.05	150	46.6	107.16
0.5	150	46.6	107.27	2	150	0	107.26
18.99	150		107.39				

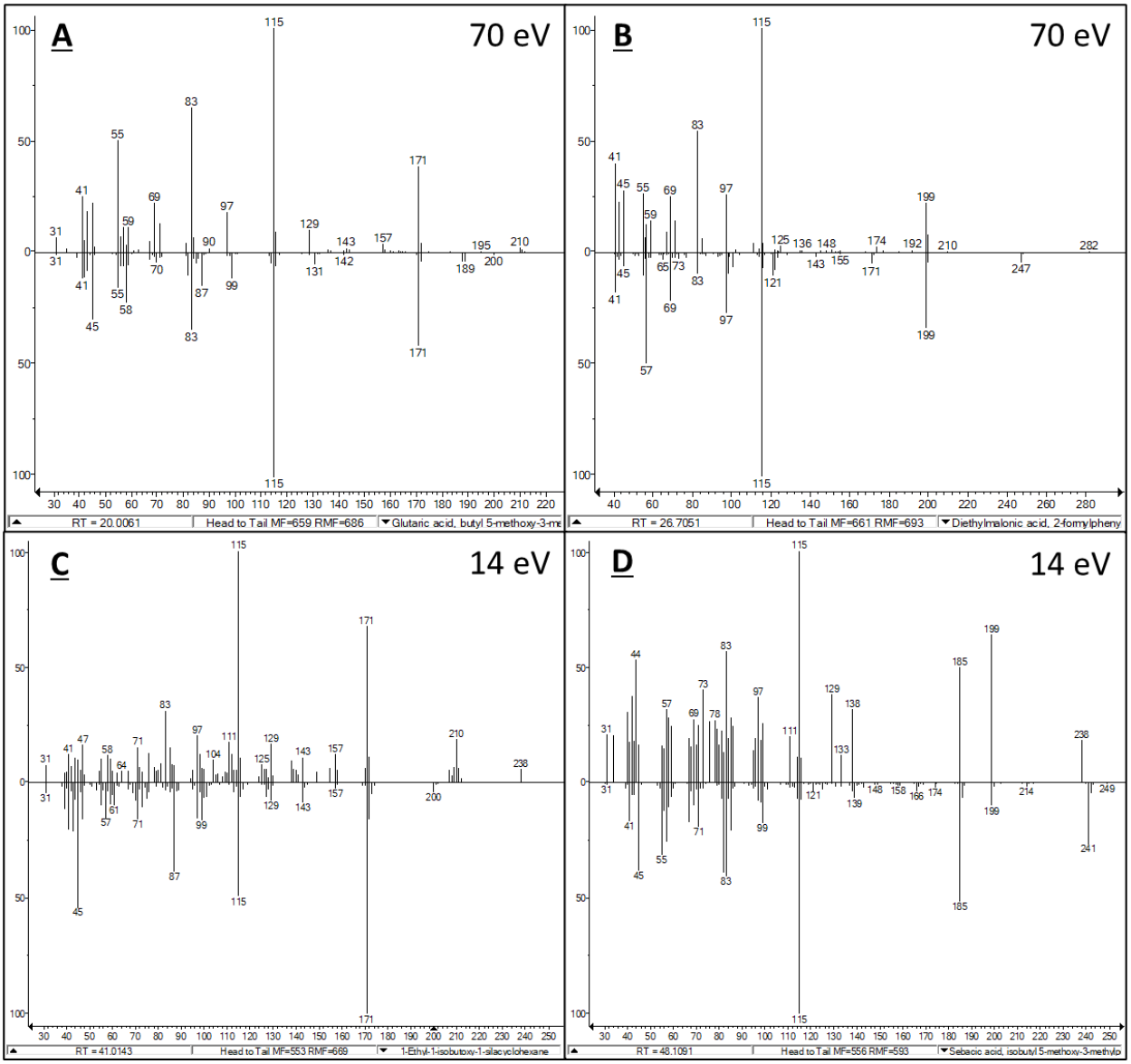

Figure D - 5: Mass spectra for unknown compound with a base peak at 115 m/z. (A) Mass spectra at 70 eV for unknown eluting with n-heptadecene in the [1]D. (B) Mass spectra at 70 eV for unknown eluting with n-nonadecene in the [1]D. (C) Mass spectra at 14 eV for the same unknown in A. (D) Mass spectra at 14 eV for the same unknown in B.

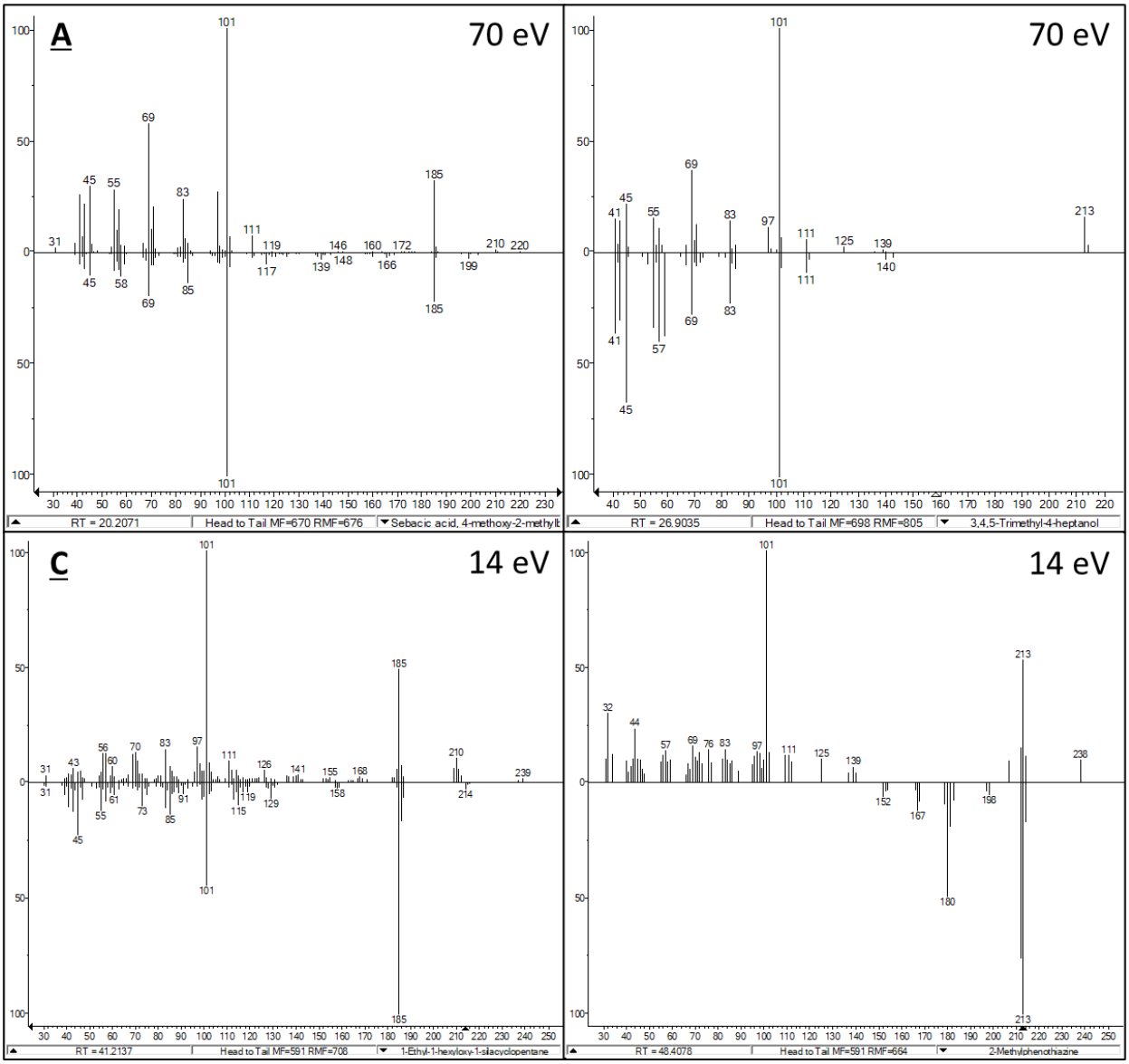

Figure D - 6: Mass spectra for unknown compound with a base peak at 101 m/z. (A) Mass spectra at 70 eV for unknown eluting with n-heptadecene in the ¹D. (B) Mass spectra at 70 eV for unknown eluting with n-nonadecene in the ¹D. (C) Mass spectra at 14 eV for the same unknown in A. (D) Mass spectra at 14 eV for the same unknown in B.

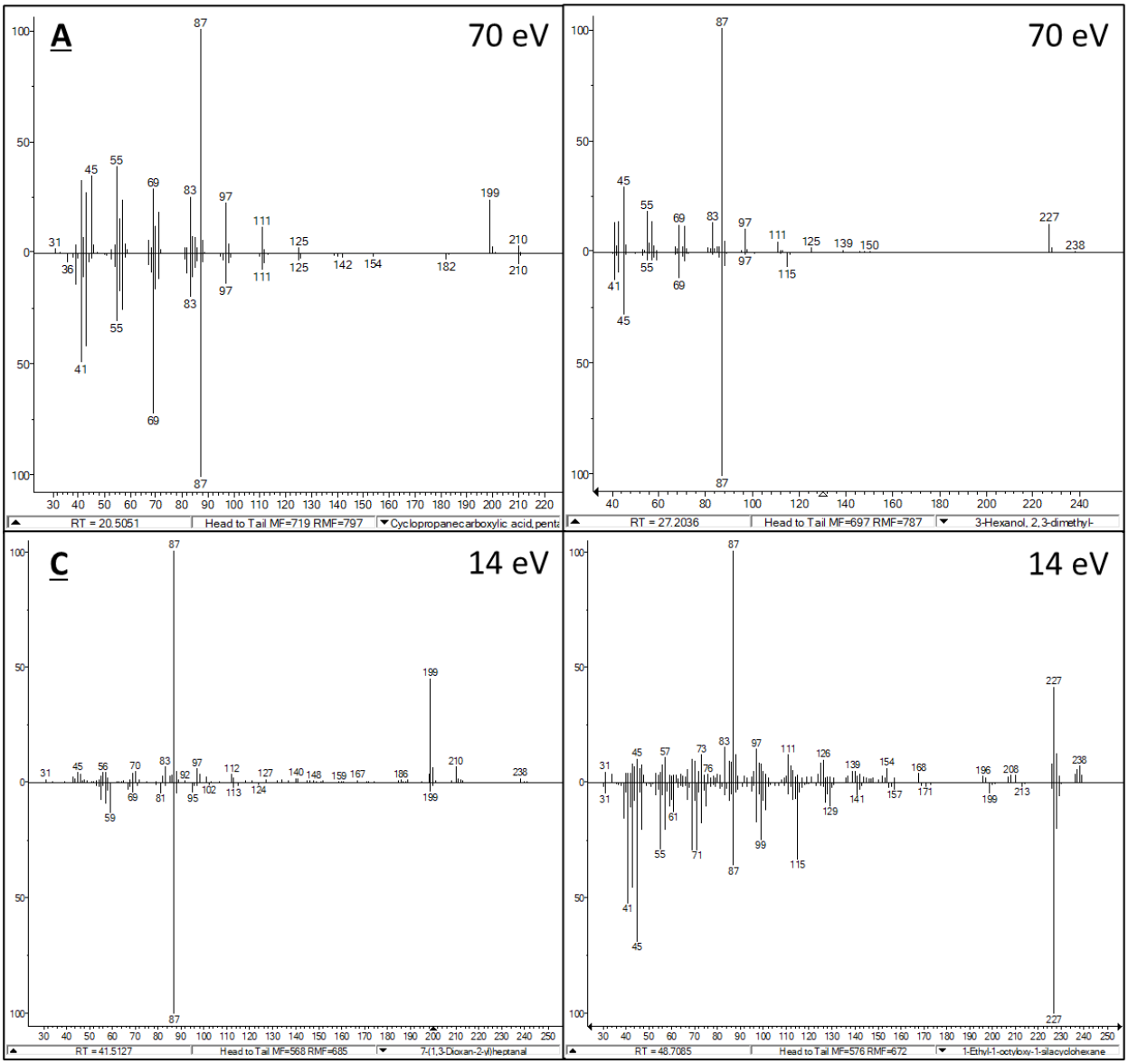

Figure D - 7: Mass spectra for unknown compound with a base peak at 87 m/z. (A) Mass spectra at 70 eV for unknown eluting with n-heptadecene in the ¹D. (B) Mass spectra at 70 eV for unknown eluting with n-nonadecene in the ¹D. (C) Mass spectra at 14 eV for the same unknown in A. (D) Mass spectra at 14 eV for the same unknown in B.

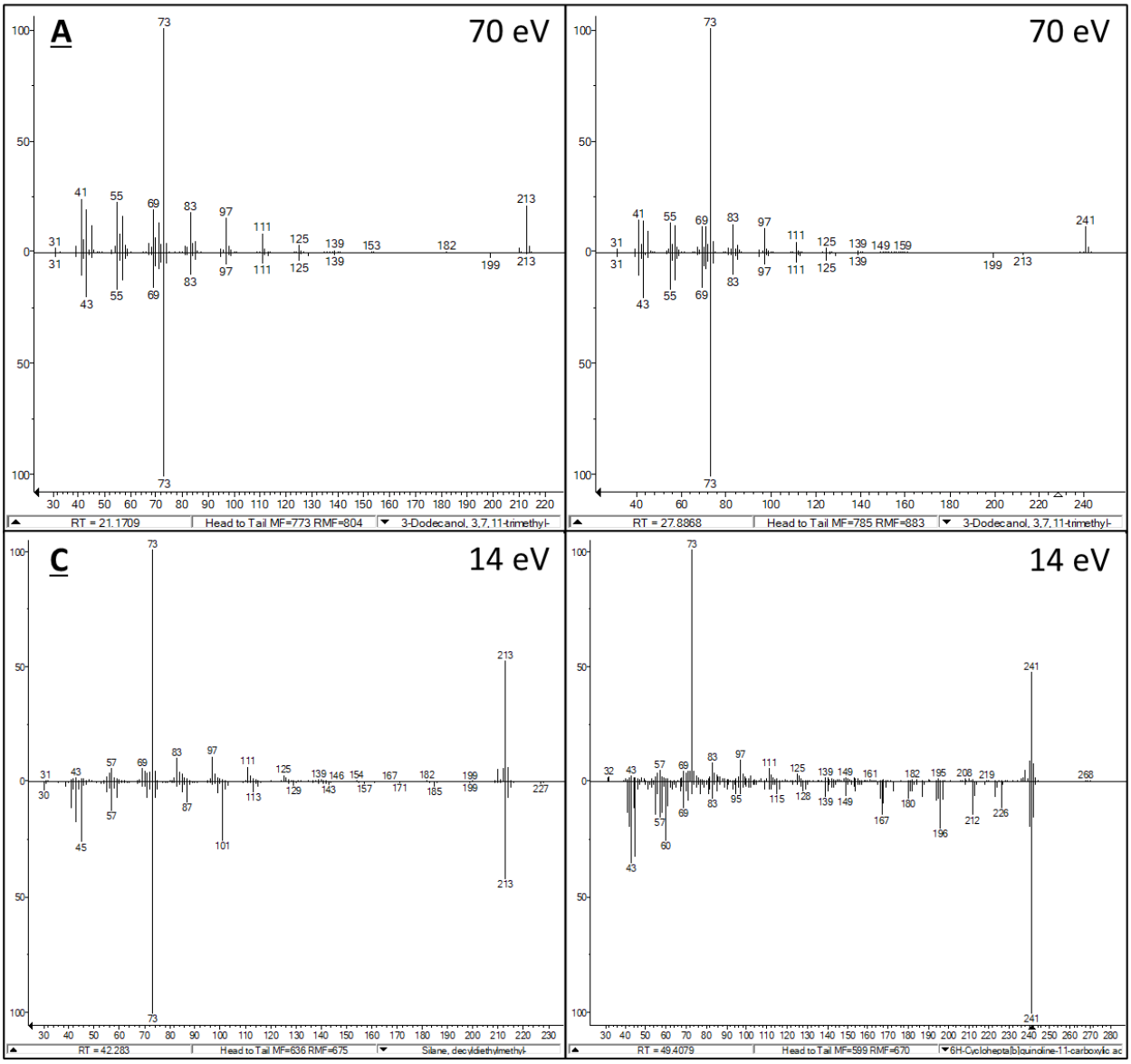

Figure D - 8: Mass spectra for unknown compound with a base peak at 73 m/z. (A) Mass spectra at 70 eV for unknown eluting with n-heptadecene in the ¹D. (B) Mass spectra at 70 eV for unknown eluting with n-nonadecene in the ¹D. (C) Mass spectra at 14 eV for the same unknown in A. (D) Mass spectra at 14 eV for the same unknown in B.

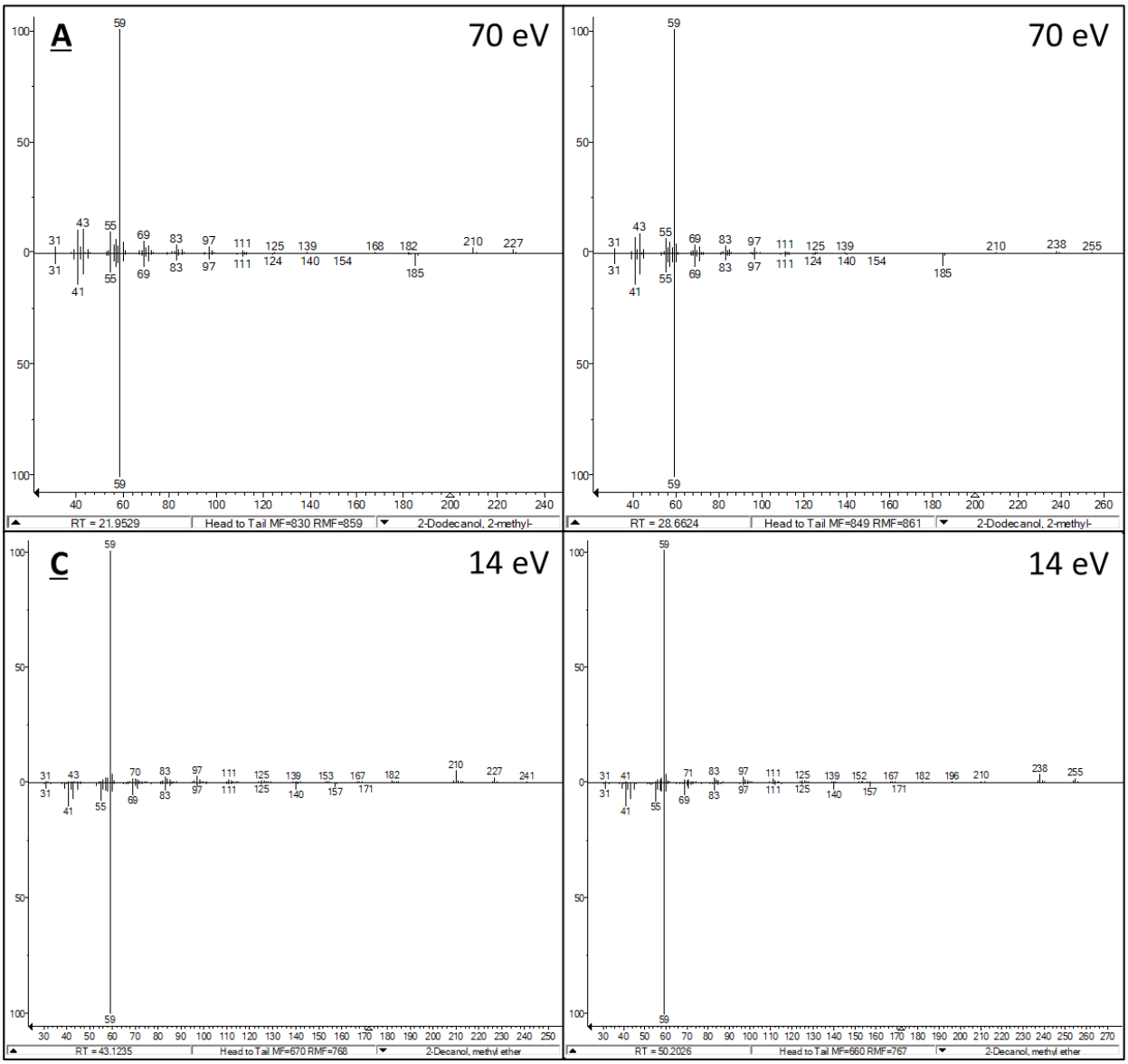

Figure D - 9: Mass spectra for unknown compound with a base peak at 59 m/z. (A) Mass spectra at 70 eV for unknown eluting with n-heptadecene in the ¹D. (B) Mass spectra at 70 eV for unknown eluting with n-nonadecene in the ¹D. (C) Mass spectra at 14 eV for the same unknown in A. (D) Mass spectra at 14 eV for the same unknown in B.

				GC×GC	GC	RT		T1		T2		T3		T4		T5		T26		T27	
Peak #	Status	Compound	Group	RI (Wax)	RI (-5)	1tr	2tr	GC×GC	GC	GC×GC2	GC3	GC×GC4	GC5	GC×GC6	GC7	GC×GC8	GC9	GC×GC16	GC17	GC×GC18	GC19
1	✔	**Nonane**	**Alkane (linear)**	**900**	**900**	**3.50**	**4.10**			**312754**						**190076**					
2	✔	1-Nonene	1-Alkene	950	886	3.70	3.97	36170													
3	?	C10 Alkane (branched)	Alkane (Branched)	950		3.72	4.24			1095305						540520					
4	✔	**Decane**	**Alkane (linear)**	**1000**	**1000**	**3.92**	**4.38**	**24472**		**787474**						**443100**					
5	?	C11 Alkane (branched)	Alkane (Branched)	1047		4.24	4.55	63587		1441609						626594					
6	✔	**Undecane**	**Alkane (linear)**	**1100**	**1100**	**4.62**	**4.74**	**35954**		**1023113**						**277144**					
7	✔	**1-Undecene**	**1-Alkene**	**1137**	**1088**	**5.00**	**4.60**			**149458**						**40126**					
8	?	C12 Alkane (branched)	Alkane (Branched)	1144		5.08	4.94	19571		643644						211762					
9	▫	1,1-dimethoxyhexane	1,1-DimethoxyAlkane	1164		5.30	4.12			14690						45147					
10	?	C12 Alkane (branched)	Alkane (Branched)	1164		5.30	5.11			126424											
11	?	C12 Alkane (branched)	Alkane (Branched)	1191		5.60	5.48			136258											
12	✔	**Dodecane**	**Alkane (linear)**	**1200**	**1200**	**5.66**	**5.37**			**332849**						**58807**					
13	?	C13 Alkane (branched)	Alkane (Branched)	**1234**		**6.29**	**5.72**			**143841**											
14	▫	1-Dodecene	1-Alkene	**1235**		**6.30**	**5.02**			**67486**											
15	?	C13 Alkane (branched)	Alkane (Branched)	**1258**		**6.70**	**5.94**			**28518**											
16	▫	1,1-dimethoxyheptane	1,1-DimethoxyAlkane	**1264**		**6.80**	**4.32**			**22825**											
17	✔	**Tridecane**	**Alkane (linear)**	**1300**	**1300**	**7.30**	**0.01**	**300351**		**2700908**	**161000**	**70000**				**621012**	**217011**				
18	▫	Tridecene	Alkene	1322	1294	7.90	5.71			70743											
19	✔	**1-Tridecene**	**1-Alkene**	**1336**	**1289**	**8.20**	**5.64**	**190958**		**2420547**	**107000**	**112703**				**406657**	**119578**				
20	▫	1,1-dimethoxyoctane	1,1-DimethoxyAlkane	1363		8.80	4.51			39517											
21	▫	Tridecene	Alkene	1363	1311	8.80	5.72			82003											
22	▫	C8:0 FAME	**FAME**	1395		9.50	4.16			15774											
23	✔	**Tetradecane**	**Alkane (linear)**	**1400**	**1400**	**9.50**	**1.22**			**649955**						**94053**	**53400**				
24	✔	**1-Tetradecene**	**1-Alkene**	**1440**	**1392**	**10.70**	**0.27**			**531699**							**44734**				
25	▫	1,1-dimehtoxynonane	1,1-DimethoxyAlkane	1463		11.33	4.71			48874											
26	▫	Pentadecene	Alkene	1488		12.00	1.29			309005											
27	✔	**Pentadecane**	**Alkane (linear)**	**1500**	**1500**	**12.15**	**1.85**	**78327863**	**7740000**	**167609564**	**51500000**	**74751271**	**10812800**	**7801490**	**2384110**	**112856182**	**63642100**	**7814500**	**1061920**	**9399587**	**3890580**
28	▫	Pentadecene	Alkene	1503	1478	12.40	1.26			1206397											
29	▫	Pentadecene	Alkene	1526	1484	13.11	1.09	3281331		29609722	345000	2788225				8991727	497952				
30	▫	Pentadecene	Alkene	1536	1493	13.41	1.00	6078773	384000	44399391		1127922	664636			2108089				24590	
31	▫	1-Pentadecene	1-Alkene	1543	1491	13.62	0.81	77728452	5440000	187721304	45000000	77799839	9982720	4885100	2160180	139445698	42531700	5244601	810115	5824495	2565890
32	▫	Pentadecene	Alkene	1555	1504	14.00	0.89	11912298	571000	58366913	4930000	10905479	964107	397258	190291	57616334	9197360	240196	64851	230200	211286
33	▫	1,1-dimethoxydecane	1,1-DimethoxyAlkane	1565		14.30	4.85			43032											
34	?	Unknown 73	Unknown	1565	1467	14.30	5.89			48518											
35	▫	Pentadecene	Alkene	1572	1513	14.52	0.79	5858396	284000	39966579	2710000	5655146	534386	123637	107785	31091012	5197370				111787
36	▫	Pentadecene	Alkene	1589	1528	15.05	0.83	2331032	119000	15086408	862000	1778451	179614			3713838	849017				
37	?	Unknown 59	Unknown	1587	1478	15.00	5.75			112927											
38	✔	**Hexadecane**	**Alkane (linear)**	**1600**	**1600**	**15.22**	**2.30**	**427222**		**2719642**	**212000**	**224822**				**547773**	**255338**				
39	▫	Cetene	1-Alkene	1643	1589	16.80	1.10	94132		1094894	98586					220809	138991				
40	▫	1,1-dimethoxyundecane	1,1-DimethoxyAlkane	1667		17.60	4.99			46758											
41	✔	**Heptadecane**	**Alkane (linear)**	**1700**	**1700**	**18.54**	**2.46**	**84970042**	**8070000**	**184641758**	**52200000**	**78186368**	**10139000**	**3355200**	**1662710**	**134712772**	**56434300**	**3739999**	**855915**	**6392631**	**3568090**
42	▫	Heptadecene	Alkene	1704		18.80	1.88			216999											
43	?	C18 Alkane (branched)	Alkane (Branched)	1711		19.03	2.12			276094											
44	▫	Heptadecene	Alkene	1727	1683	19.58	1.60	1500807		14361125	52869	758057				2789110	90888				
45	?	Unknown 115	Unknown	1734	1642	19.80	0.35	8239		839780	108000						141333				
46	▫	Heptadecene	Alkene	1736	1693	19.88	1.54	3733779		25166387		2029036				8518781	41995000				
47	?	Unknown 101	Unknown	1740	1646	20.01	0.35	117993		2606452	191000	462076				361471	223732				
48	▫	1-Heptadecene	1-Alkene	1744	1692	20.15	1.23	67745151	5720000	219029112	41000000	93018642	9667620	3086000	1600780	146610438		1895843	653894	4468665	2365590
49	?	Unknown 87	Unknown	1748	1652	20.28	0.32	701801		7431098	417000	1564368	118952	27943		1287438	477947				
50	▫	Heptadecene	Alkene	1757	1702	20.60	1.12	8115529	447000	38997715	1930000	6797661	658953	58984	70485	32586274	7421340	51106			142905
51	?	Unknown 73	Unknown	1769	1667	20.97	0.20	3301265	148000	22023714	1610000	5763127	494995	145138	125050	7807132	1760760	115734		101027	49500
52	▫	1,1-dimethoxydodecane	1,1-DimethoxyAlkane	1769		21.00	5.02			49633											
53	▫	Heptadecene	Alkene	1774	1713	21.16	1.20	3618931	218000	28013621	1930000	2947140	334148		48561	12420202	4128670				69674
54	?	Unknown 59	Unknown	1795	1678	21.87	0.18	4760533	259000	24861453	2370000	4832030	829964	381598	221606	13423113	2712530	225688	76823	248277	102047
55	▫	Heptadecene	Alkene	1793	1731	21.80	1.30	1549870	109000	10618887	684000	1463897	130505				666279				
56	✔	**Octadecane**	**Alkane (linear)**	**1800**	**1800**	**21.90**	**2.33**	**34612**		**319715**	**79734**					**67123**	**111405**				
57	▫	C12:0 FAME	**FAME**	1802	1521	22.09	4.41			58932											
58	▫	1-methoxy, pentadecane	1-MethoxyAlkane	1858	1725	23.99	5.71	1715208	128000	11618716	1290000	2418008	399308		100085	2157310	1597710			16273	63624
59	▫	1,1-dimethoxytridecane	1,1-DimethoxyAlkane	1870		24.40	5.04			47789											
60	✔	**Nonadecane**	**Alkane (linear)**	**1900**	**1900**	**25.24**	**2.26**	**512585**	**82666**	**2446056**	**610000**	**211863**	**91249**			**1041341**	**809910**				
61	?	Unknown 71	Unknown	1902		25.48	4.99			143227		13996									
62	?	Unknown 101	Unknown	1939	1844	26.70	0.30	7130		640740	123000	115348				175156	149785				
63	▫	1-Nonadecene	1-Alkene	1946	1890	26.90	1.07	132385		1585298	418000	209480	65272			566016	480793				
64	?	Unknown 87	Unknown	1949	1851	27.00	0.27	216008		2114050	284000	343026	64976			514451	325883				
65	▫	1-Dodecanol	1-Alcohol	1960	1471	27.37	3.82				75718						64053				
66	?	Unknown 73	Unknown	1970	1866	27.70	0.21	1428387	104000	8862957	1140000	1770161	295293	38313	63992	2203769	1288860	23592		34788	
67	▫	1,1-dimethoxytetradecane	1,1-DimethoxyAlkane	1970		27.70	4.96			13353											
68	?	Unknown 72	Unknown	1982		28.10	4.50			125550						120342					
69	?	Unknown 59	Unknown	1991	1877	28.39	5.91	2188245	215000	13633160	2350000	3153700	840055	151349	400956	3996711	2249300	97516		147567	
70	✔	**Eicosane**	**Alkane (linear)**	**2000**	**2000**	**28.50**	**2.20**			**33068**						**20807**	**91224**				
71	▫	C14:0 FAME	**FAME**	2003	1722	28.80	4.53			206589		67795									
72	▫	2-Pentadecanone	2-Ketone	2017		29.22	4.39			365867		80760		16935		249191		20752			
73	▫	1-methoxy, heptadecane	1-MethoxyAlkane	2060	1925	30.61	5.61	811350		5527917		1151065				1760659	1163450				
74	▫	1,1-dimethoxypentadecane	1,1-DimethoxyAlkane	2072	2071	31.00	4.99	25465		464631	67458	179810		21084				18424			
75	▫	3-Pentadecanol	3-Alcohol	2085		31.40	4.19			209465		109194		17350		82481		32220			
76	✔	**Heneicosane**	**Alkane (linear)**	**2100**	**2100**	**31.80**	**1.90**			**33927**	**143000**					**48250**	**96033**				
77	▫	C15:0 FAME	**FAME**	2107		32.10	4.52			95432		29582									
78	▫	2-Pentadecanol	2-Alcohol	2110		32.20	4.13			218651		167114				76581		93722			
79	?	Unknown 71	Unknown	2113		32.30	4.92			77659											
80	?	Unknown 55	Unknown	2189	1917	34.70	4.46	93278		929624	239000	316000									
81	?	3-Heptadecanone	Unknown	2190		34.70	1.51									83981					
82	▪	**Docosane**	**Alkane (linear)**	**2200**	**2200**	**35.02**	**1.59**	**17646**		**19806**					**80979**	**8080**	**125291**				
83	✔	**C16:0 FAME**	**FAME**	**2207**	**1923**	**35.26**	**4.54**	**11036650**	**1050000**	**67742591**	**10500000**	**42576395**	**4757730**	**3757900**	**1792670**	**6790992**	**3802810**	**3748692**	**796975**	**3423609**	**1358790**
84	▫	2-Heptadecanone	2-Ketone	2224		35.76	4.38			336499		70710				218233					
85	?	Unknown 55	Unknown	2232		36.01	4.36	368497		2933757		678692		35520							
86	▫	C16:0 FAEE	FAEE	2243	1991	36.35	4.68			1910194	362000	915418	156153	62032		3048463	1490310				
87	▫	1-pentadecanol	1-Alcohol	2262		36.92	3.93	103795		991855		527927		164435		208617		219273		110907	
88	▫	1,1-dimethoxyheptadecane	1,1-DimethoxyAlkane	2271		37.22	4.97			289544		86584									
89	?	3-Heptadecanol	Unknown	2284		37.60	4.19			144416		55954				58362					
90	✔	**Tricosane**	**Alkane (linear)**	**2300**	**2300**	**37.80**	**1.56**			**26711**						**30585**	**70141**				
91	▫	C17:0 FAME	**FAME**	2307		38.30	4.52			109460		41645									
92	▫	2-Heptadecanol	2-Alcohol	2310		38.40	4.13					107272				56714		54770			
93	▫	1-Hexadecanol	1-Alcohol	2360	1875	39.88	3.96	698957		4193627		4094575		1238260		585919		2112382	170835	856343	145655
94	?	Unknown Oxygenated Species	Unknown	2360	1999	39.90	4.22			1330670	183000										
95	▫	1,1-dimethoxyoctadecane	1,1-DimethoxyAlkane	2370		40.20	4.90			58285		18271									
96	✔	**Tetracosane**	**Alkane (linear)**	**2400**	**2400**	**41.05**	**1.40**			**52121**	**82344**				**57093**	**22606**	**78259**				
97	▫	C18:0 FAME	**FAME**	2405	2124	41.27	4.55	13267445	888000	54739041	9470000	27888859	3704770	3110800	1584380	7040701	3552410	2631945	530275	3527756	1015520
98	▫	C18:0 FAEE	FAEE	2432	2191	42.30	4.72			659881	345000	775577	147636	39955		2888879	1353570				
99	▫	1-Heptadecanol	1-Alcohol	2444		42.77	3.99	136972		826732		569657		96563		187715		181167		76229	
100	▫	2-Nonadecanol	2-Alcohol	2453		43.10	4.18	638484				260024						77501			
101	▫	1-Octadecanol	1-Alcohol	2525	2078	45.68	4.20	587262		4538716	398000	3914510	243441	966808	170823	547893	69246	1390510	69230	640290	
102	?	Unknown Oxygenated Species	Unknown	2525	2200	45.80	4.56			383246	120000										
103	▫	C20:0 FAME	**FAME**	2564	2324	47.30	5.22			362934	61061	117360				18167					
104	✔	**Hexacosane**	**Alkane (linear)**	**2600**	**2600**						**263000**						**279914**				
105	▫	C14:0 FA	FA	2626	1768	49.64	3.57													293545	
106	?	C28 Alkane (branched)	Alkane (Branched)	2762		54.78	0.09			4737241											
107	✔	**Octacosane**	**Alkane (linear)**	**2800**	**2800**				**408000**		**3730000**		**349540**		**73892**	**5995589**	**4189100**				**96891**
108	✔	**C16:0 FA**	**FA**	**2897**	**1962**	**59.88**	**3.95**	**684517**	**151000**	**7563777**	**997000**	**5192581**	**671591**	**2089020**	**491523**			**7867626**	**536331**	**405842**	**282775**

Figure D - 10: Summary of the compounds identified in the wax samples. Peak areas from the integration of the TIC chromatogram are given for each compound from the GC×GC and GC separation if found. The GC×GC retention time (^1t_r, ^2t_r) and linear ^{1}D RI from the GC×GC (MXT-WAX) and GC (ZB-5HT Inferno) separations are provided. The status column indicates the degree of confidence in the identification, where a "✔" indicates a confirmed compound using a standard, a "▫ " indicates a tentative identification based on the ^{1}D RI (Wax and/or -5HT), elution region, and mass spectra, and a "?" indicates an unknown where any identification description was a guess based on the elution region and mass spectra.